SYNTHESIS, CHARACTERIZATION, AND REACTIVITY OF RUTHENIUM(II)-DIPHOSPHINE COMPLEXES FOR CATALYTIC HOMOGENEOUS HYDROGENATION

By

KENNETH SHAWN MACFARLANE

B.Sc., University of British Columbia, 1986

M.Sc., University of British Columbia, 1990

A THESIS SUBMITTED IN PARTIAL FULFILMENT OF

THE REQUIREMENTS FOR THE DEGREE OF

DOCTOR OF PHILOSOPHY

in

THE FACULTY OF GRADUATE STUDIES

DEPARTMENT OF CHEMISTRY

We accept this thesis as conforming

to the required standard

THE UNIVERSITY OF BRITISH COLUMBIA

September 1995

© Kenneth S. MacFarlane, 1995

In presenting this thesis in partial fulfilment of the requirements for an advanced degree at the University of British Columbia, I agree that the Library shall make it freely available for reference and study. I further agree that permission for extensive copying of this thesis for scholarly purposes may be granted by the head of my department or by his or her representatives. It is understood that copying or publication of this thesis for financial gain shall not be allowed without my written permission.

Department of CHEMISTRY

The University of British Columbia
Vancouver, Canada

Date Nov. 2/95

ABSTRACT

The syntheses and reactivities of a group of ruthenium(II) diphosphine complexes were investigated, with interest specifically directed toward interactions with small gas molecules, as well as toward catalytic activity for the homogeneous hydrogenation of nitriles and imines. These potential catalyst precursors were all based on the "RuX$_2$(P–P)" core (where P–P = chelating diphosphine and X = Cl or Br). The utility of the five-coordinate complexes RuX$_2$(P–P)(PAr$_3$) (Ar = Ph or p-tolyl), which were prepared in high yield in two steps from RuCl$_3\cdot$xH$_2$O, was investigated as a precursor to complexes of the type "RuX$_2$(P–P)". These precursors reacted with a wide range of neutral, two-electron donor ligands (L) to give complexes of the formulations Ru$_2$X$_4$(P–P)$_2$(L) and RuX$_2$(P–P)(L)$_2$. These systems were mainly investigated with the precursor RuCl$_2$(DPPB)(PPh$_3$) (DPPB = Ph$_2$P(CH$_2$)$_4$PPh$_2$), which was easier to prepare than the bromo analogue and less expensive than the chiral BINAP analogue (Figure 1), both of which were investigated in a limited way.
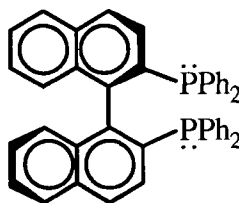
Figure 1   Structure of the chiral diphosphine (R)-BINAP.

Standard spectroscopic methods, particularly ^{1}H and ^{31}P{^{1}H} NMR, were used extensively to characterize (sometimes in conjunction with X-ray crystallography) all of the Ru-phosphine species discussed in this thesis.

The five-coordinate RuCl$_2$(DPPB)(PPh$_3$) was characterized crystallographically, and in solution is in equilibrium with the diruthenium complex [RuCl(DPPB)]$_2$(μ-Cl)$_2$ (also written as Ru$_2$Cl$_4$(DPPB)$_2$). The RuBr$_2$(PPh$_3$)$_3$ complex, was shown by X-ray

crystallography to be of a geometry similar to that of both the previously determined $RuCl_2(PPh_3)_3$ complex and $RuCl_2(DPPB)(PPh_3)$. The geometry of the three complexes is pseudo-octahedral, with a weak agostic interaction at the sixth coordination site between the Ru atom and an *ortho*-hydrogen of the PPh_3 ligand. The reactivity of $RuCl_2(DPPB)(PPh_3)$ with neutral two-electron ligands (L) is summarized in Figure 2.
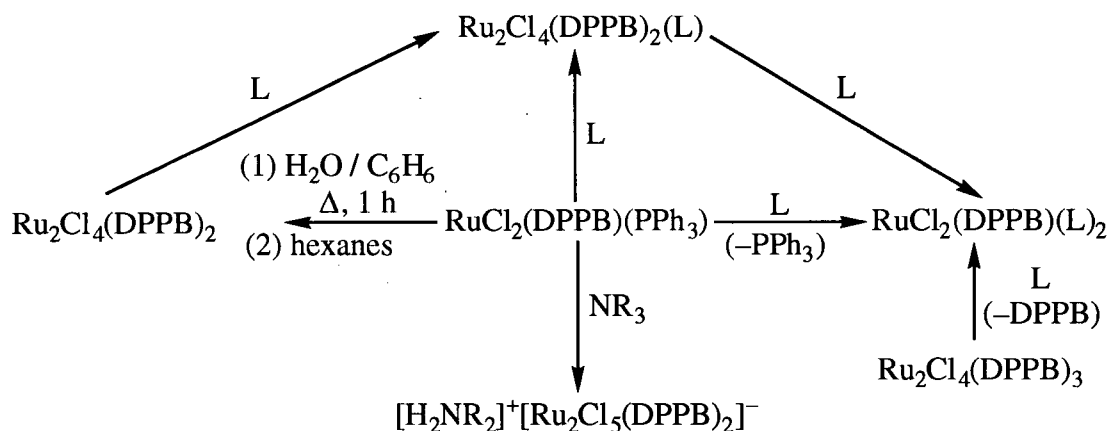

Figure 2   Summary of the reactivity of $RuCl_2(DPPB)(PPh_3)$ with neutral, two-electron donor ligands (L).

A synthetically superior route to that previously used in this laboratory to prepare $Ru_2Cl_4(DPPB)_2$ has been established. This new route from $RuCl_2(DPPB)(PPh_3)$ or $RuCl_2(DPPB)(P(p\text{-tolyl})_3)$ (see Figure 2) also allows for the preparation of the previously unknown bromo-analogue $Ru_2Br_4(DPPB)_2$ from $RuBr_2(DPPB)(PPh_3)$. $RuCl_2(DPPB)(PPh_3)$ reacts with an excess of S-donor ligands (L = DMSO, TMSO, DMS, and THT) to produce $Ru_2Cl_4(DPPB)_2(L)$ species, while the N-donor ligands L (L_2 = $2NH_3$, 2py, bipy, and phen) give mononuclear $RuCl_2(DPPB)(L)_2$ species (Figure 2). These monoruthenium complexes can also be synthesized from the phosphine-bridged species $[RuCl_2(DPPB)]_2(\mu\text{-DPPB})$ (also written as $Ru_2Cl_4(DPPB)_3$). *Cis*-$RuCl_2(DPPB)(phen)$ was characterized by X-ray crystallography.

The anionic species $[Ru_2Cl_5(P–P)_2]^-$ is produced on refluxing an excess of tertiary amine and the $RuCl_2(P–P)(PPh_3)$ complex (Figure 2), although the nature of the reaction, particularly the formation of the dialkylammonium cation, is not well understood.

Subsequently, other routes to $Ru_2X_4(DPPB)_2$ (X = Cl, Br, I) complexes were developed. All three can be prepared by the addition of two equivalents of HX to $Ru(DPPB)(\eta^3-Me-allyl)_2$, since the allyl group is protonated and cleaved off as 2-methylpropene. The bromo analogue could not be prepared by the H_2 reduction of $Ru_2Br_5(DPPB)_2$ (the established methodology for the chloro analogue) because the precursor to this complex, $RuBr_3(PPh_3)_2$, could not be isolated free of chloride contamination. $Ru_2Br_4(DPPB)_2$, however, was successfully isolated by metathesis of $Ru_2Cl_4(DPPB)_2$ with Me_3SiBr.

The solid-state reactivity of the five-coordinate complexes $RuCl_2(PPh_3)_3$, $RuCl_2(DPPB)(PPh_3)$, $Ru_2Cl_4(DPPB)_2$, and $Ru_2Cl_4(DPPB)_3$ with CO and NH_3 was investigated. Of interest, these heterogeneous (solid-gas) reactions yield octahedral complexes, sometimes via displacement of phosphine ligands.

Attempts to prepare the previously known but poorly characterized $Ru(BINAP)(\eta^3-Me-allyl)_2$ resulted in the isolation of a crystal, shown by X-ray diffraction to be half $Ru((R)-BINAP)(\eta^3-Me-allyl)_2$ and half $(R)-(+)-2,2'-$bis(diphenylphosphinoyl)-1,1'-binaphthyl, co-crystallized with two disordered deuterobenzene regions.

X-ray crystallography established the structure of $[(DMA)_2H]^+[(PPh_3)_2(H)Ru(\mu-Cl)_2(\mu-H)Ru(H)(PPh_3)_2]^-$, the anion containing both terminal and bridging hydrides. In solution, the species is in equilibrium with the previously known neutral, molecular hydrogen complex $[(\eta^2-H_2)(PPh_3)_2Ru(\mu-Cl)_2(\mu-H)Ru(H)(PPh_3)_2]\cdot2DMA$ solvate; a proton is thus transferred from the $[(DMA)_2H]^+$ cation to a terminal hydride of the anion, thereby generating the η^2-H_2 moiety.

Some of the ruthenium(II) DPPB-containing complexes were effective catalysts for the hydrogenation of the imines $PhCH_2N=C(H)Ph$ and $PhN=C(H)Ph$ at high pressures of H_2 (1000 psi) and at room temperature, while the trinuclear species $[Ru(H)Cl(DPPB)]_3$ was an effective catalyst for the hydrogenation of benzonitrile at 1 atm H_2 pressure and 70 °C.

TABLE OF CONTENTS

TABLE OF COMPOUND NUMBERS

Number	Compound	Alternative Formulations
1	$RuCl_3(PPh_3)_2(DMA) \cdot DMA$	
2	$RuCl_3(P(p\text{-tolyl})_3)_2(DMA) \cdot DMA$	
3	$RuBr_3(PPh_3)_2(MeOH)$	
4	$Ru(H)Cl(PPh_3)_3(DMA) \cdot DMA$	
5	$[RuCl_2(COD)]_x$	
6	$Ru(COD)(\eta^3\text{-allyl})_2$	
7	$Ru(COD)(\eta^3\text{-Me-allyl})_2$	
8	$RuCl_2(PPh_3)_3$	
9	$RuCl_2(P(p\text{-tolyl})_3)_3$	
10	$RuBr_2(PPh_3)_3$	
11	$RuCl_2(DPPB)(PPh_3)$	
12	$RuCl_2(DPPB)(P(p\text{-tolyl})_3)$	
13	$RuBr_2(DPPB)(PPh_3)$	
14	$RuCl_2(DCYPB)(PPh_3)$	
15	$RuCl_2((R)\text{-BINAP})(PPh_3)$	
16	$[(DMA)_2H]^+[Ru_2Cl_5(PPh_3)_4]^-$	$[(DMA)_2H]^+$ $[(PPh_3)_2ClRu(\mu\text{-Cl})_3RuCl(PPh_3)_2]^-$
17	$[(\eta^2\text{-}H_2)(PPh_3)_2Ru(\mu\text{-Cl})_2(\mu\text{-}H)Ru(H)(PPh_3)_2]$	
18	$[(DMA)_2H]^+[RuH_3Cl_2(PPh_3)_4]^-$	$[(DMA)_2H]^+[(PPh_3)_2(H)Ru(\mu\text{-Cl})_2(\mu\text{-}H)Ru(H)(PPh_3)_2]^-$
19	$Ru_2Cl_4(DPPB)_3$	$[RuCl_2(DPPB)_{1.5}]_2$ or $[RuCl_2(DPPB)]_2(\mu\text{-DPPB})$

Number	Compound	Alternative Formulation
20	$Ru_2Br_4(DPPB)_3$	$[RuBr_2(DPPB)_{1.5}]_2$ or $[RuBr_2(DPPB)]_2(\mu\text{-DPPB})$
21	$Ru_2Cl_4(DCYPB)_3$	$[RuCl_2(DCYPB)_{1.5}]_2$ or $[RuCl_2(DCYPB)]_2(\mu\text{-DCYPB})$
22	$Ru_2Cl_5(DPPB)_2$	$[RuCl(DPPB)]_2(\mu\text{-Cl})_3$ or $[(DPPB)ClRu(\mu\text{-Cl})_3RuCl(DPPB)]$
23	$Ru_2Cl_5((R)\text{-BINAP})_2$	$[((R)\text{-BINAP})ClRu(\mu\text{-Cl})_3RuCl((R)\text{-BINAP})]$
24	$Ru_2Cl_4(DPPB)_2$	$[RuCl_2(DPPB)]_2$ or $[RuCl(DPPB)]_2(\mu\text{-Cl})_2$
25	$Ru_2Br_4(DPPB)_2$	$[RuBr_2(DPPB)]_2$ or $[RuBr(DPPB)]_2(\mu\text{-Br})_2$
26	$Ru_2Cl_4((R)\text{-BINAP})_2$	$[RuCl_2((R)\text{-BINAP})]_2$ or $[RuCl((R)\text{-BINAP})]_2(\mu\text{-Cl})_2$
27	$Ru_2I_4(DPPB)_2$	$[RuI_2(DPPB)]_2$ or $[RuI(DPPB)]_2(\mu\text{-I})_2$
28	$Ru_2Cl_4(DPPB)_2(NEt_3)$	$[(NEt_3)(DPPB)Ru(\mu\text{-Cl})_3RuCl(DPPB)]$
29	$Ru_2Cl_4(DPPB)_2(py)$	$[(py)(DPPB)Ru(\mu\text{-Cl})_3RuCl(DPPB)]$
30	$Ru_2Cl_4(DPPB)_2(HNEt_2)$	$[(HNEt_2)(DPPB)Ru(\mu\text{-Cl})_3RuCl(DPPB)]$
31	$Ru_2Cl_4(DPPB)_2(acetone)\cdot acetone$	$[(acetone)(DPPB)Ru(\mu\text{-Cl})_3RuCl(DPPB)]\cdot acetone$
32	$Ru_2Cl_4(DPPB)_2(acetophenone)$	$[(acetophenone)(DPPB)Ru(\mu\text{-Cl})_3RuCl(DPPB)]$

TABLE OF COMPOUND NUMBERS (continued)

Number	Compound	Alternative Formulation
33	$Ru_2Cl_4(DPPB)_2(DMSO)$	$[(DMSO)(DPPB)Ru(\mu\text{-}Cl)_3RuCl(DPPB)]$
34	$Ru_2Cl_4(DPPB)_2(DMS)$	$[(DMS)(DPPB)Ru(\mu\text{-}Cl)_3RuCl(DPPB)]$
35	$Ru_2Cl_4(DPPB)_2(TMSO)$	$[(TMSO)(DPPB)Ru(\mu\text{-}Cl)_3RuCl(DPPB)]$
36	$Ru_2Cl_4(DPPB)_2(THT)$	$[(THT)(DPPB)Ru(\mu\text{-}Cl)_3RuCl(DPPB)]$
37	$[H_2N(n\text{-}Oct)_2]^+$ $[Ru_2Cl_5(DPPB)_2]^-$	$[H_2N(n\text{-}Oct)_2]^+$ $[(DPPB)ClRu(\mu\text{-}Cl)_3RuCl(DPPB)]^-$
38	$[H_2N(n\text{-}Bu)_2]^+$ $[Ru_2Cl_5(DPPB)_2]^-$	$[H_2N(n\text{-}Bu)_2]^+$ $[(DPPB)ClRu(\mu\text{-}Cl)_3RuCl(DPPB)]^-$
39	$[DMAH]^+$ $[Ru_2Cl_5(DPPB)_2]^-$	$[DMAH]^+$ $[(DPPB)ClRu(\mu\text{-}Cl)_3RuCl(DPPB)]^-$
40	$[H_2N(n\text{-}Bu)_2]^+$ $[Ru_2Cl_5((R)\text{-}BINAP)_2]^-$	$[H_2N(n\text{-}Bu)_2]^+[((R)\text{-}BINAP))ClRu(\mu\text{-}Cl)_3RuCl((R)\text{-}BINAP))]^-$
41	$[HNEt_3]^+[Ru_2Cl_5(DPPB)_2]^-$	$[HNEt_3]^+[(DPPB)ClRu(\mu\text{-}Cl)_3RuCl(DPPB)]^-$
42	$[Ru(H)Cl(DPPB)]_3$	
43	$RuCl_2(DPPB)(py)_2$	
44	$RuCl_2(DPPB)(bipy)$	
45	$RuCl_2(DPPB)(phen)$	
46	$RuCl_2(py)_2(PPh_3)_2$	
47	$cct\text{-}RuCl_2(CO)_2(PPh_3)_2$	
48	$cct\text{-}RuCl_2(CO)_2(P(p\text{-}tolyl)_3)_2$	
49	$RuCl_2(CO)_2(DPPB)$	
50	$RuCl_2(NH_3)_2(PPh_3)_2$	

51	$RuCl_2(DPPB)(NH_3)_2$	
52	*trans*-$RuCl_2(DPPCP)_2$	
53	*trans*-$RuCl_2(DPPB)(DPPCP)$	
54	*trans*-$RuCl_2(DPPE)_2$	
55	$Ru(DPPB)(\eta^3\text{-Me-allyl})_2$	
56	$Ru((R)\text{-BINAP})(\eta^3\text{-Me-allyl})_2$	

LIST OF TABLES

LIST OF FIGURES

LIST OF ABBREVIATIONS

Å	angstrom, 10^{-8} centimeter
AB_q	AB quartet (NMR)
Ar	argon, aryl group
atm	atmosphere (1 atm = 760 mm Hg, 101.3 kPa, 14.696 psi)
BDPP	(2*S*,4*S*)-2,4-bis(diphenylphosphino)pentane
BINAP	(*R*)- or (*S*)-2,2'-bis(diphenylphosphino)-1,1'-binaphthyl
$BINAP(O)_2$	(*R*)-(+)-2,2'-bis(diphenylphosphinoyl)-1,1'-binaphthyl
BIPHEMP	(*S*)-2,2'-dimethyl-6,6'-bis(diphenylphosphino)biphenyl
bipy	2,2'-bipyridine
BPPFA	1,1'-bis(diphenylphosphino)-2'-(1-*N*,*N*-α-dimethylamino-ethyl)ferrocene
br	broad
Bu	butyl, $CH_2(CH_2)_2CH_3$
c,c,c	*cis,cis,cis*
c,c,t	*cis,cis,trans*
$^{13}C\{^1H\}$	proton-decoupled carbon-13 (NMR)
CHIRAPHOS	2,3-bis(diphenylphosphino)butane
COD	1,5-cyclooctadiene
CP/MAS	cross polarization / magic angle spinning
Cy	cyclohexyl
CYCPHOS	1-cyclohexyl-1,2-bis(diphenylphosphino)ethane
D	configuration relative to D-glyceraldehyde
d	doublet (NMR), day(s)
dd	doublet of doublets
DCYPB	1,4-bis(dicyclohexylphosphino)butane

DCYPCP	*rac*-(±)-1,2-bis(dicyclohexylphosphino)cyclopentane; Joshi of this laboratory previously abbreviated this DPCYCP
DIOP	(2*R*,3*R*) or (2*S*,3*S*)-*O*-isopropylidene-2,3-dihydroxy-1,4-bis(diphenylphosphino)butane
DiPAMP	1,2-bis(*ortho*-anisylphenylphosphino)ethane
DMA	*N*,*N*-dimethylacetamide, $CH_3C(O)N(CH_3)_2$
DMF	*N*,*N*-dimethylformamide, $CH(O)N(CH_3)_2$
DMS	dimethyl sulfide
DMSO	dimethyl sulfoxide
DPPB	1,4-bis(diphenylphosphino)butane
DPPCP	*rac*-(±)-1,2-bis(diphenylphosphino)cyclopentane
DPPE	1,2-bis(diphenylphosphino)ethane
DPPH	1,6-bis(diphenylphosphino)hexane
DPPM	bis(diphenylphosphino)methane
DPPN	1,5-bis(diphenylphosphino)pentane
DPPP	1,3-bis(diphenylphosphino)propane
e.e.	enantiomeric excess
eq	equation
FID	flame-ionization detector (GC)
FT	Fourier transform
h	hour(s)
$^1H\{^{31}P\}$	phosphorus-decoupled proton-1 (NMR)
Hz	Hertz, cycles per second
IR	infra-red (spectroscopy)
isoPFA	1-[α-(dimethylamino)ethyl]-2-(diisopropylphosphino)ferrocene
J	coupling constant, in Hz
L	configuration relative to L-glyceraldehyde

L	ligand; litre
L-Dopa	3-(3,4-dihydroxyphenyl)-L-alanine
M	central metal atom in a complex; molarity, mols L^{-1}
m	multiplet (NMR); medium intensity (IR)
max	maximum
min	minute(s)
m.p.	melting point
NORPHOS	2,3-bis(diphenylphosphino)-bicyclo[2.2.1]hept-5-ene
NMR	nuclear magnetic resonance (spectroscopy)
N–N	chelating N-donor ligand
o	*ortho*
Oct	octyl, $CH_2(CH_2)_6CH_3$
$^{31}P\{^1H\}$	proton-decoupled phosphorus-31 (NMR)
p	*para*
PAN	1-(dimethylamino)-8-(diphenylphosphino)naphthalene
Ph	phenyl, C_6H_5
phen	1,10-phenanthroline
PHENOP	the chiral aminophosphinephosphinite ligand:, $Ph_2PN(Et)CH(CH_2Ph)CH_2OPPh_2$
PMA	*o*-diphenylphosphino-*N,N*-dimethylaniline
PROPHOS	1,2-bis(diphenylphosphino)propane
PS	proton sponge, 1,8-bis(dimethylamino)naphthalene
py	pyridine
P–P	ditertiary phosphine
q	quartet
R	alkyl group
(R)-	absolute configuration (Latin: *rectus*; right)

rac	racemic
(*S*)-	absolute configuration (Latin: *sinister*; left)
s	singlet (NMR), strong (IR), seconds
t	triplet
t-	tertiary
T_1	longitudinal relaxation time (NMR)
temp	temperature
THT	tetrahydrothiophene
TMP	1,1,3-trimethyl-2,3-dihydroperimidinium cation
TMS	tetramethylsilane
TMSO	tetramethylene sulfoxide
TOSS	total suppression of sidebands
UV-vis	ultraviolet-visible (spectroscopy)
w	weak intensity (IR)
Δ	heat
δ	chemical shift (in ppm)
ε	extinction coefficient
η	descriptor for hapticity
λ	wavelength
Λ_M	molar conductivity
μ	descriptor for bridging
ν	frequency (cm^{-1})
*	chiral centre

ACKNOWLEDGEMENTS

CHAPTER 1

INTRODUCTION

1.1   Homogeneous Catalysis

Homogeneous catalysis is used ever-increasingly by chemists to synthesize both new compounds in an academic setting, and industrially important fine chemicals. Fine chemicals ranging in use from fragrances, flavours, and perfumes to pharmaceuticals, herbicides, and pesticides can be prepared by reactions using homogeneous catalysts. Widespread interest in homogeneous systems is evident from the many books that have been published on this subject in the last fifteen years (e.g., references 1-5).

The reactions that have been catalyzed by transition metal complexes in solution include: hydrogenation, hydrosilylation, hydroformylation, hydrocyanation, epoxidation, polymerization of olefins, oxidation of hydrocarbons, oxidation of olefins to aldehydes and ketones, and carbonylation of alcohols.[2,5] Interest in the use of homogeneous catalytic systems arose out of their possible economic advantages over the established heterogeneous systems. Energy savings are realized through the use of lower temperatures and pressures, as well as the higher activity and selectivity generally observed for homogeneous catalytic systems.[5,6] The high selectivity of organic transformations offered by homogeneous systems is the result of a well-defined metal environment which is usually easily amenable to study by conventional spectroscopic and kinetic methods.[7]

Heterogeneous catalytic systems are much more difficult to study, although recent advances allow the spectroscopic examination of metal surfaces by methods such as in situ X-ray absorption[8] or magic-angle spinning NMR.[9] The reactivity of a homogenous catalyst is much easier to modify than that of a heterogeneous catalyst, and can be achieved simply by changing the ligands at the metal centre.[10] Although a

Chapter 1 References: p 14

homogeneous catalyst can be tailored toward certain properties (e.g., aqueous solubility), the matching of a particular catalyst precursor with a specific substrate is still largely empirical.[11]

On the down side, homogeneous catalysts are often expensive transition metal complexes, and are frequently difficult to separate from both the reactants and products.[1,6] They may also be sensitive to dioxygen and moisture, and are thermally sensitive.[6] The problem of separating the catalyst from the product can be overcome by either: (1) the use of insoluble supports such as silica or crosslinked polystyrene, to which the catalyst is attached;[6] (2) the use of a biphasic system;[12] or (3) the use of a phase-transfer catalytic system.[13,14]

Insoluble-supported catalysts are referred to as heterogenized homogeneous catalysts, and offer the advantages of heterogeneous catalysts in being easily separated from the product(s), while retaining the high activity and selectivity of a homogeneous system.[6]

Biphasic systems take advantage of homogeneous catalysts which are designed to be soluble in a phase different to that of the organic reactants and products.[12] Ideally, the catalyst would be designed to be soluble in an aqueous phase by the use of ligands with highly polar functional groups.[12]

Phase-transfer catalysis also takes advantage of two-phase media but employs phase-transfer agents (e.g., quaternary ammonium or phosphonium salts, crown ethers, etc.) to transfer reactants across the interface between phases.[15] A biphasic system uses no such agent.

Recent and future developments in the area of homogeneous catalysis should increase[12] the forty-odd industrial processes[5] currently using homogeneous systems. Some notable examples of industrial productions using homogeneous catalysts include the Wacker and Oxo processes, methanol carbonylation, oligomerization of dienes, some Ziegler-Natta systems, and adiponitrile synthesis.[2,5]

One emerging area is the catalysis of organic reactions in aqueous media.[12,16] The only commercial successes of homogeneous catalysis in aqueous media to date are the Wacker process for the oxidation of alkenes and the Ruhrchemie / Rhône-Poulenc oxo process for the hydroformylation of propylene to butyraldehyde.[12,16] Improvement in the catalytic activity of the above hydroformylation has been achieved on two separate occasions since the reaction was first used commercially in 1984. The improved activity was achieved by changing the water-soluble phosphine ligands on Rh to newly developed analogous phosphines. The activity is now about 100 times greater than the original catalyst.[12]

Another industrial application of homogeneous catalysts is the use of asymmetric hydrogenation of a prochiral olefin to produce the optically active L-Dopa, which is used in the treatment of Parkinson's disease.[7] The catalyst system used for this asymmetric transformation is a rhodium(I) catalyst with a chiral diphosphine ligand (eq 1.1).[17]

$$(1.1)$$

L-Dopa
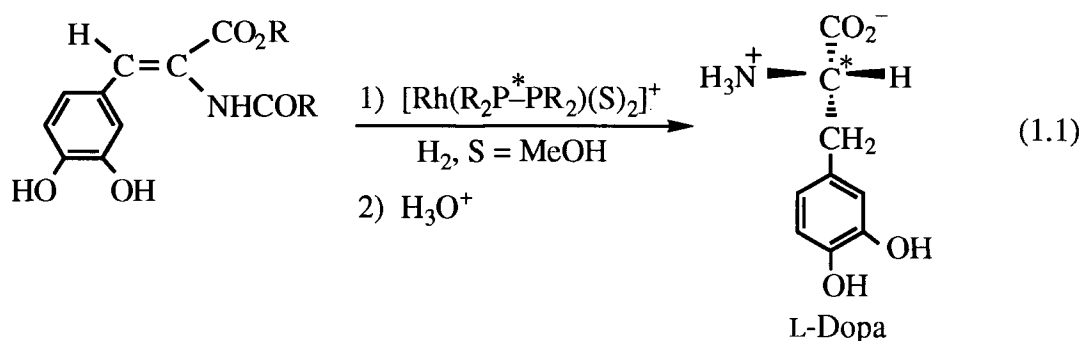
The sweetener Aspartame™, a methyl ester of a dipeptide consisting of L-phenylalanine and L-aspartic acid, also relies on homogeneous chiral catalysts for the production of the two amino acid precursors.[17] The chirality of these compounds plays an important role in determining their properties; for example, it was found that none of the other three diastereomers of Aspartame are sweet.[18] However, in the future, the production of Aspartame by asymmetric catalytic hydrogenation may be replaced by an economically more favourable fermentation process commercialized by Ajinomoto.[5,19]

1.1.1 Asymmetric Catalysis

Most of the work in asymmetric or enantioselective catalysis has been done in the area of hydrogenation (see Section 1.2.1).[17] This is probably a result of the fact that the vast majority of optically active compounds have a hydrogen atom at the asymmetric carbon atom.[20] This area of research, and asymmetric catalysis in general, have become more important in recent years, as the pharmaceutical and agrochemical industries have an increased need to produce enantiomerically (or stereochemically) pure materials.[21,22] Companies operating in these industries have both economic and regulatory reasons for wanting to prepare stereochemically pure materials of both new and existing products.

From a regulatory standpoint, the FDA's chiral drug policy[22,23] still allows for the development of drugs as racemic mixtures, but on a case by case basis it is better to develop enantiomerically pure materials.

Economically, companies have a vested interest in developing chiral drugs, not only to maintain market share,[22] but to eventually reduce manufacturing costs.[21] Manufacturers of racemic drugs run the risk of *racemic switches* by third party firms, which in the worst case scenario (at least for the firm holding a patent for the racemate) could lead to the issuing of a separate patent for the enantiomerically pure drug.[22] A racemic switch is the redevelopment of an older chiral drug currently marketed as a racemic mixture to produce the active single enantiomer. Manufacturing costs in the production of a single enantiomer over a racemic mixture, while initially higher, can eventually result in economic benefits as a result of not carrying 50% unwanted or unnecessary material (i.e., the inactive enantiomer or precursor) through the reaction pathway.[21] Savings can occur from the use of smaller amounts of reagents and solvents and their associated disposal costs.

Until recently, enantiomerism has been treated as a rather "special" type of isomerism, probably because of the difficulty in distinguishing one enantiomer from the other (with the exception of their opposite interaction with plane polarized light).[24] One

enantiomer has therefore rarely been regarded as an impurity in the presence of the other. However, in biological systems, in which the local environment is largely chiral (L-amino acids, D-sugars, chiral recognition of receptors and enzymes), the two enantiomers should be treated as very different.

New terminology that has arisen from concern over using racemic mixtures as pharmaceuticals include: *chirotechnology*, technologies combining chemistry and biology to produce enantiomeric compounds and enantioselective processes;[22,25] *racemic switches*, see above;[22] *eutomer*, the enantiomer (of the two in a racemic mixture) responsible for the desired pharmaceutical effect;[22,26] *distomer*, the inactive or unwanted isomer in a racemic mixture;[22,26] and *eudismic ratio*, the ratio of activity in any given pharmacological property of the eutomer relative to that of the distomer.[22,26]

Ariens has been one of the most vocal critics against the use of racemic pharmaceuticals.[27] From the titles of his articles alone, one gains a feel for Ariens' thoughts on the use of racemic mixtures. Some of the titles include: (1) *Racemic Therapeutics–Problems all Along the Line*;[27] (2) *Stereochemistry, a Basis for Sophisticated Nonsense in Pharmacokinetics and Clinical Pharmacology*;[28] (3) *Bias in Pharmacokinetics and Clinical Pharmacology*;[29] and (4) *Stereoselectivity of Bioactive Xenobiotics. A Pre-Pasteur Attitude in Medicinal Chemistry, Pharmacokinetics and Clinical Pharmacology*.[30]

The most frequently used example cautioning against the use of racemic pharmaceuticals is the case of thalidomide, used as a sleeping pill and remedy for morning sickness between 1957 and 1961. The result of using racemic thalidomide in the early stages of pregnancy was fetal deaths and congenital malformations in more than 8000 cases.[31-33] The teratogenicity causing the high incidence of malformations is now attributed to the S-enantiomer, while the R-isomer is believed to have the hypnotic and sedative properties that were originally desired.[34] The validity of the above statement has been argued by some workers recently and they suggest that "this conclusion should be

accepted with caution."[35,36] Also of importance is the recent evidence which suggests that thalidomide racemizes rapidly under physiological conditions.[37] Although there is now some dispute over whether the *S*-enantiomer alone is the teratogen, there is no argument that the racemate causes congenital malformations. Therefore, the case of thalidomide remains a good illustration of the potential dangers involved with using racemic drugs.

1.2   Homogeneous Hydrogenation

Although reports of homogeneous hydrogenation date back as far as 1938 when Calvin reduced quinone using a copper acetate system, it is not until more recently that homogeneous hydrogenation began to be more thoroughly investigated.[7] An increase in the intensity of research in homogeneous hydrogenation came as a direct result of the discovery by Wilkinson's group in 1965 of the highly active RhCl(PPh$_3$)$_3$ system for the hydrogenation of olefins.[38,39]

The literature in the area of homogeneous hydrogenation has become vast since the discovery of Wilkinson's catalyst. A number of comprehensive reviews,[40-43] specialized texts,[44,45] chapters in books,[3,4,7,46] and whole books[15,47] are available on this subject.

Initial studies on homogeneous hydrogenation had much of their interest directed toward the reduction of carbon-carbon double bonds. Until recently, comparatively few studies on the hydrogenation of ketones and imines appeared in the literature.[17,48] The concentration of research in the area of reducing olefins has occurred for probably two reasons: (1) carbon-carbon double bonds are more easily reduced than carbon-oxygen double bonds;[49] and (2) the substrates are readily available and there is interest in using the corresponding products.

The majority of our mechanistic understanding comes from the hydrogenation of olefins using rhodium-phosphine catalyst systems.[15] There are two general mechanisms

Chapter 1 References: p 14

of homogeneous hydrogenation of alkenes by metal complexes which initially do not contain an M–H bond. The first is referred to as the unsaturate route, which involves initial coordination of the substrate followed by activation of dihydrogen by the resulting complex. The second possibility, known as the hydride route, involves initial activation of molecular hydrogen, followed by coordination of the substrate (Figure 1.1). The hydride route is thought to be the more general of the two reaction pathways.[15]
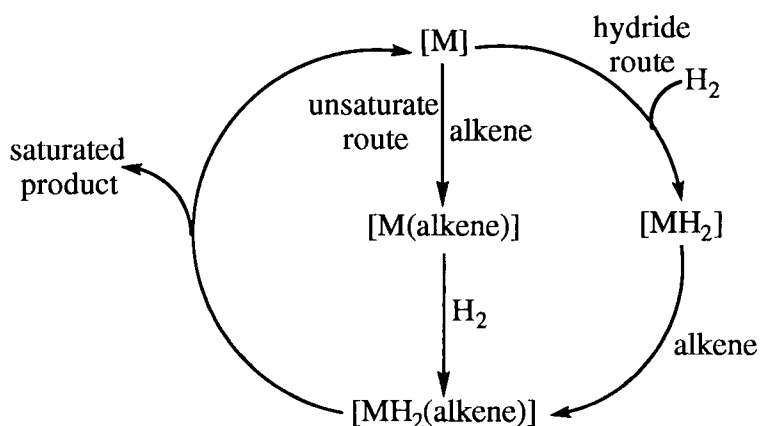
Figure 1.1   Mechanisms of homogeneous hydrogenation of alkenes catalyzed by metal species without M–H bonds.

If the catalytic species initially contains an M–H bond, the pathway shown in Figure 1.2 is thought to operate.

Figures 1.1 and 1.2 are meant to illustrate simple models, including the important steps for the homogeneous hydrogenation of alkenes. However, the actual mechanisms operating in these systems are often more complex, as they frequently contain more than one active metal species.[15] For example, the activation of dihydrogen by oxidative addition may actually include a molecular hydrogen complex as an intermediate.[50] There are many examples of isolable molecular hydrogen complexes in the literature[50] since Kubas' discovery of the first such species.[51] A brief review of this area will be given in Chapter 4.
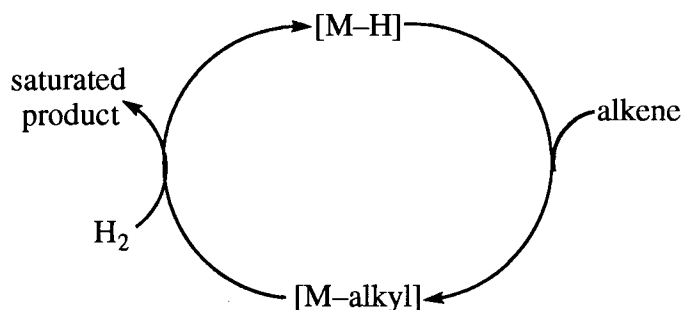
Figure 1.2　Mechanism of homogeneous hydrogenation of alkenes catalyzed by metal species containing an M–H bond.

1.2.1　Asymmetric Homogeneous Hydrogenation

A large number of the successful chiral catalysts consist of a transition metal complex containing a chiral phosphine ligand (the transition metal is usually Ir, Rh, Ru, or Os).[15] A measure of the success of asymmetric systems is given by the enantiomeric excess (e.e.) (eq 1.2).

$$\text{e.e.}(\%) = \frac{|\,[R] - [S]\,|}{[R] + [S]} \times 100 \qquad (1.2)$$

Over the past fifteen years there has been an enormous amount of work in the field of asymmetric homogeneous hydrogenation, with numerous comprehensive reviews appearing in the literature.[10,11,15,17,19,20,43,52-62]

The first chiral phosphine ligands used in asymmetric hydrogenations were chiral at the phosphorus atom (e.g., PMePrPh). However, only poor optical inductions were observed with these systems.[17] The next significant development in the synthesis of new chiral phosphines came with the preparation by Kagan's group of the diphosphine DIOP (Figure 1.3).[17,63,64] This phosphine, while containing the centre of chirality on a carbon atom in the ligand backbone, gave high optical yields with prochiral olefins. Also, the

starting material for the synthesis of DIOP is tartaric acid, and therefore, the chirality on carbon arises from natural sources, making the ligand relatively cheap to prepare.[17]

The high enantioselectivities that were observed for Rh complexes of DIOP provided the impetus for the development of new diphosphine ligands which contained their chirality on carbon. Some of the most notable diphosphines developed (see Figure 1.3) are: DiPAMP (chiral at P), which is used in Monsanto's synthesis of L-Dopa;[65] PROPHOS, prepared from lactic acid; CHIRAPHOS, which has two asymmetric centres in its backbone;[17] BPPFA, a ferrocene derivative;[17] CYCPHOS, which is effective for imine hydrogenation;[66] and BINAP, which is effective in the hydrogenation of carbonyl-containing compounds.[67] These are just a few illustrative examples of the more than a thousand chiral phosphines that have been used in asymmetric catalysis.[58] The catalysts or "precatalysts" are generally prepared by two methods: either (1) in situ, by adding one equivalent of the chelating ditertiary phosphine ligand per mol of Rh; or (2) by addition of a solid complex of the type $[Rh(diphosphine)(diene)]^+BF_4^-$, which already contains the chiral ligand.

Monophosphines generally seem to give lower optical yields than diphosphine ligands, and it should be pointed out that the rigidity of the chelate ring formed with diphosphines seems to play a key role in obtaining high enantiomeric excess.[17] Ligands that form rigid five-membered chelate rings seem to be generally more efficient than those which form more flexible six- or seven-membered chelates.[53] This is thought to be manifested through a rigid chiral array of phenyl rings in the five-membered chelates which allows a degree of discrimination of the prochiral olefinic faces in the binding step.[53]

The first prochiral substrates to be reduced with the highest enantiomeric excesses were functionalized olefins, which are believed to bind in a bidentate fashion. Therefore, it has been suggested that these substrates impose some rigidity on the system, thereby

increasing the optical yield of the product.[52] For example, some enamide substrates have been hydrogenated with up to 100% e.e.[7]

DIOP (chiral at C)

DiPAMP (chiral at P)

PROPHOS (chiral at C)

CHIRAPHOS (chiral at C)

BPPFA (planar chirality and chiral at C)

CYCPHOS (chiral at C)

BINAP (axial chirality or atropisomerism)
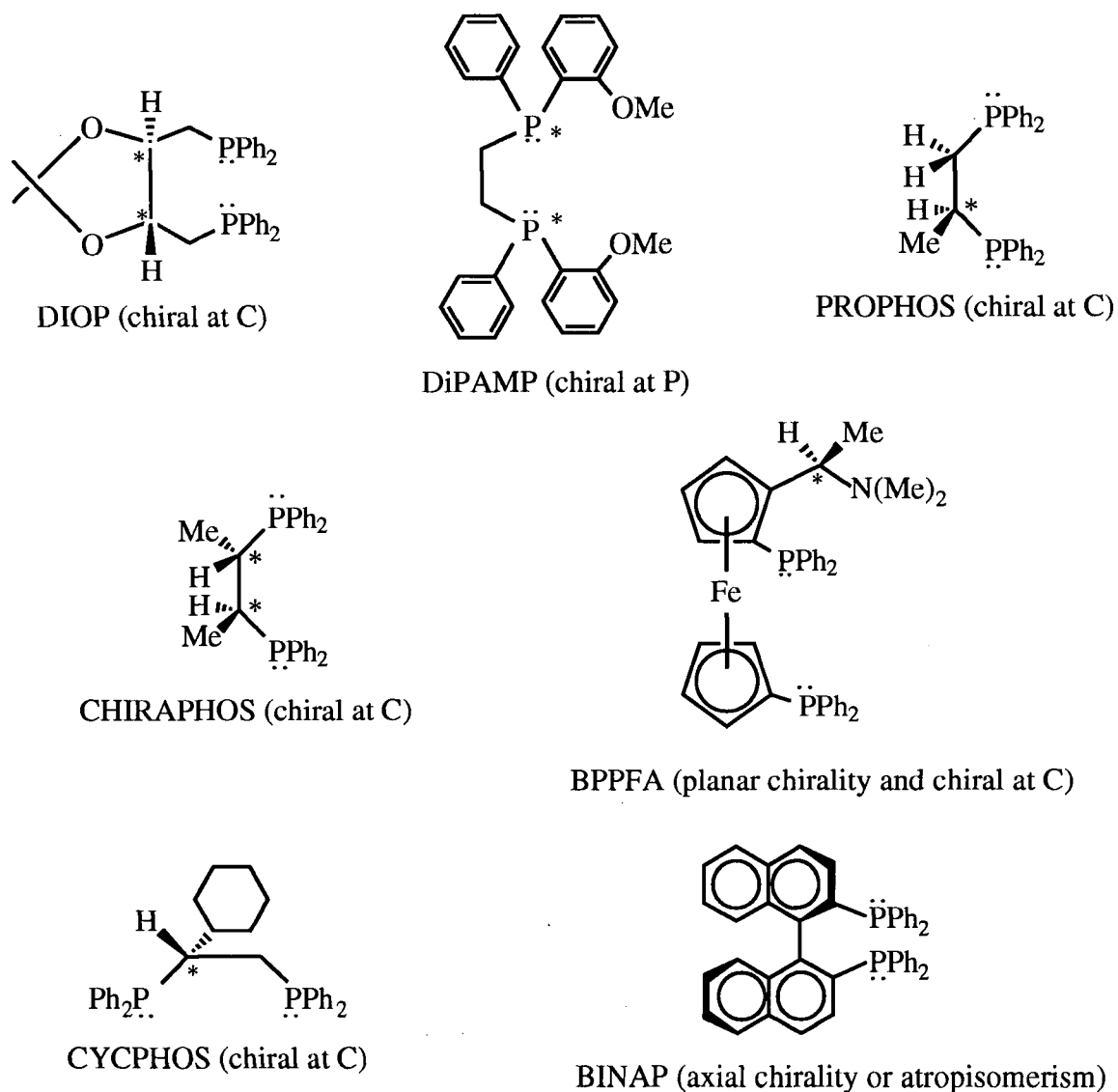
Figure 1.3   Selected chiral diphosphines used in asymmetric hydrogenation; the symbol * represents a chiral centre.

A probable mechanism for asymmetric hydrogenation of (Z)-α-acylamido-cinnamic acid derivatives has been suggested by the groups of Halpern and Brown.[7] A combination of kinetic, X-ray, and NMR techniques were used to elucidate the pathway. The mechanism shows, in contrast to what was previously believed, that the major

enantiomer obtained by asymmetric hydrogenation corresponds to the minor diastereomer of the catalyst-substrate adduct present in solution.[68-72] Thus, the hydrogenation is kinetically controlled, with the major product originating from faster reaction of the minor diastereomer of the catalyst-substrate adduct with H_2. Other studies have shown that the H_2 pressure and temperature dependences on the enantiomeric excess agree with those predicted by Halpern's mechanism.[73-75] At higher H_2 pressures, the e.e. decreases due to the increased rate of H_2 addition relative to the interconversion of major and minor diastereomers, while at lower temperatures, the e.e. is also observed to decrease.

1.3   Scope of this Thesis

The work in this thesis is directed toward the preparation of potential Ru-diphosphine catalysts for homogeneous hydrogenation. Interest in this laboratory has recently been concentrated on examining different routes to species with a single diphosphine per Ru centre. Routes to these types of complexes arose from earlier work in this laboratory on the $RuHCl(DIOP)_2$–catalyzed asymmetric hydrogenation of alkenes which indicated that "[RuHCl(DIOP)]" is the active catalytic species.[76-78]

Therefore, potential routes to Ru species containing a single chelating diphosphine (P–P) per metal were investigated in this laboratory. This work led to the discovery, by Thorburn, of a route to Ru(P–P) containing complexes of the type $[RuCl(P-P)]_2(\mu-Cl)_3$ (or $Ru_2Cl_5(P-P)_2$) and $[RuCl(P-P)]_2(\mu-Cl)_2$ (or $Ru_2Cl_4(P-P)_2$).[79-82] By 1990, Joshi had extended these series of complexes by substituting different chiral and achiral diphosphines to include 12 such $Ru_2Cl_5(P-P)_2$ and 8 $Ru_2Cl_4(P-P)_2$ complexes.[83,84] Chapter 3 will review previous work in this area from this and other laboratories, and outline new routes to complexes of the type $Ru_2X_4(P-P)_2$ (X = Cl, Br, and I) and $Ru_2Cl_4(P-P)_2(L)$. Much of the work was done with the achiral diphosphine ligand $Ph_2P(CH_2)_4PPh_2$ (DPPB), which forms a seven-membered chelate on binding to

the Ru centre. This diphosphine is a useful analogue to the expensive chiral phosphines BINAP and DIOP, which also form seven-membered chelates.

As the complexes outlined in Chapter 3 were prepared as potential hydrogenation catalysts, their reactivity with dihydrogen was investigated. Chapter 4 details the reactivity of complexes of the type $Ru_2X_4(P–P)_2$ and $RuCl_2(P–P)(PPh_3)$ with H_2 and other small gas molecules (i.e., N_2, $CH_2=CH_2$). A brief review of the literature on molecular hydrogen complexes and the relevant $Ru(\eta^2\text{-}H_2)$ complexes is presented at the beginning of Chapter 4.

A ruthenium complex formulated as $Ru_2Cl_4(BINAP)_2(NEt_3)$ has been successively used as a catalyst for the asymmetric hydrogenation of several prochiral substrates.[11,56,85,86] Therefore, ruthenium species containing both a diphosphine and a basic nitrogen-containing ligand were investigated as potential catalysts for homogeneous hydrogenation. Chapter 5 describes the reaction of $RuCl_2(P–P)(PPh_3)$ and $[RuCl_2(P–P)]_2(\mu\text{-}P–P)$ (or $Ru_2Cl_4(P–P)_3$) with nitrogen-containing ligands (NH_3, pyridine, 2,2'-bipyridine, and 1,10-phenanthroline) to generate species of the type $RuCl_2(P–P)(N)_2$, where N is the N-donor ligand.

Catalytic studies for the homogeneous hydrogenation of nitriles and imines are described in Chapter 6. The hydrogenation reactions were performed at both ambient and high pressures (1000 psi). The studies on imine hydrogenation were performed under conditions to allow comparison with work done in this laboratory by Fogg et al.[87,88] The activities of Br- and I-containing catalysts compared with that of the Cl analogues were of special interest, considering earlier reports for some Rh systems.[89] These systems showed that addition of iodide was beneficial in terms of increased enantiomeric excesses for the hydrogenation of prochiral imines. A brief review of the literature on homogeneous hydrogenation of imines will begin Chapter 6.

Chapter 7 outlines initial studies on some interesting solid state reactivity of five-coordinate complexes of the type $RuCl_2(PR_3)_3$ with CO and NH_3. Related solution reactivity is also described and discussed.

The experimental procedures used to prepare the materials used in the work described in Chapters 3–7 are given in Chapter 2. General conclusions and some recommendations for future work are found in Chapter 8.

1.4   References

(1)   Nakamura, A.; Tsutsui, M. *Principles and Applications of Homogeneous Catalysis*; Wiley-Interscience: New York, 1980.

(2)   Jennings, J. R. *Selected Developments in Catalysis*; Blackwell Scientific: Oxford, 1985; Vol. 12.

(3)   Dickson, R. S. *Homogeneous Catalysis with Compounds of Rhodium and Iridium*; D. Reidel: Dordrecht, 1985.

(4)   Masters, C. *Homogeneous Transition-Metal Catalysis: A Gentle Art*; Chapman and Hall: London, 1981.

(5)   Parshall, G.; Ittel, S. D. *Homogeneous Catalysis: The Applications and Chemistry of Soluble Transition-Metal Complexes*; 2nd ed.; Wiley: New York, 1992.

(6)   Hartley, F. R. *Supported Metal Complexes*; D. Reidel: Dordrecht, 1985; Chapter 1.

(7)   Collman, J. P.; Hegedus, L. S.; Norton, J. R.; Finke, R. G. *Principles and Applications of Organotransition Metal Chemistry*; University Science Books: Mill Valley, CA, 1987; Chapter 10.

(8)   Moggridge, G. D.; Rayment, T.; Ormerod, R. M.; Morris, M. A.; Lambert, R. M. *Nature* **1992**, *358*, 658.

(9)   Worthy, W. *Chem. Eng. News* **1991**, *69(19)*, 25.

(10)   Knowles, W. S. *Acc. Chem. Res.* **1983**, *16*, 106.

(11)   Takaya, H.; Ohta, T.; Noyori, R. In *Catalytic Asymmetric Synthesis*; Ojima, I., Ed.; VCH: Oxford, 1993, p 1.

(12)   Haggin, J. *Chem. Eng. News* **1994**, *72(41)*, 28.

(13)   Alper, H. *Adv. Organomet. Chem.* **1981**, *19*, 183.

(14)   Dehmlow, E. V.; Dehmlow, S. S. *Phase Transfer Catalysis*; 3rd ed.; VCH: New York, 1993.

(15)   Chaloner, P. A.; Esteruelas, M. A.; Joó, F.; Oro, L. A. *Homogeneous Hydrogenation*; Kluwer Academic: Dordrecht, 1994.

(16)   Herrmann, W. A.; Kohlpaintner, C. W. *Angew. Chem., Int. Ed. Engl.* **1993**, *32*, 1524.

(17)   Brunner, H. *J. Organomet. Chem.* **1986**, *39*, 300.

(18)   Hadata, M.; Jancarik, J.; Graves, B.; Kim, S. H. *J. Am. Chem. Soc.* **1985**, *107*, 4279.

(19)　Noyori, R. *CHEMTECH* **1992**, 360.

(20)　Brunner, H. *Synthesis* **1988**, 645.

(21)　Sheldon, R. *Chem. Ind. (London)* **1990**, 212.

(22)　Stinson, S. C. *Chem. Eng. News* **1993**, *71(39)*, 38.

(23)　Borman, S. *Chem. Eng. News* **1992**, *70(24)*, 5.

(24)　Hyneck, M.; Dent, J.; Hook, J. In *Chirality in Drug Design and Synthesis*; Brown, C., Ed.; Academic: London, 1990; Chapter 1.

(25)　Stinson, S. C. *Chem. Eng. News* **1994**, *72(38)*, 38.

(26)　Testa, B. In *Chirality and Biological Activity*; Holmstedt, B., Frank, H., Testa, B., Eds.; Alan R. Liss: New York, 1990, pp 15-32.

(27)　Ariens, E. J. In *Chirality in Drug Design and Synthesis*; Brown, C., Ed.; Academic: London, 1990; Chapter 2.

(28)　Ariens, E. J. *Eur. J. Clin. Pharmacol.* **1984**, *26*, 663.

(29)　Ariens, E. J.; Wuis, E. W. *Clin. Pharmacol. Ther.* **1987**, *42*, 361.

(30)　Ariens, E. J.; Wuis, E. W.; Veringa, E. J. *Biochem. Pharmacol.* **1988**, *37*, 9.

(31)　*Taber's Cyclopedic Medical Dictionary*; 17th ed.; Thomas, C. L., Ed.; F. A. Davis: Philadelphia, 1993, p 1974.

(32)　*The Columbia Encyclopedia*; 5th ed.; Chernow, B. A., Vallasi, G. A., Eds.; Columbia University: Boston, 1993, p 2725.

(33)　Selinger, B. *Chemistry in the Marketplace*; 4th ed.; Harcourt Brace Jovanovich: Sydney, 1989, p 583.

(34)　Carey, J. *Chem. Br.* **1993**, *29*, 1053.

(35)　Hunt, J. R. *Chem. Br.* **1994**, *30*, 280.

(36)　De Camp, W. H. *Chirality* **1989**, *1*, 2.

(37)　Testa, B.; Carrupt, P.-A.; Gal, J. *Chirality* **1993**, *5*, 105.

(38)　Koenig, K. E. In *Catalysis of Organic Reactions*; Kosak, J. R., Ed.; Marcel Dekker: New York, 1984, p 63.

(39)　Young, J. F.; Osborn, J. A.; Jardine, F. H.; Wilkinson, G. *J. Chem. Soc., Chem. Commun.* **1965**, 131.

(40)　Brown, J. M. *Angew. Chem., Int. Ed. Engl.* **1987**, *26*, 190.

(41)　James, B. R. *Adv. Organomet. Chem.* **1979**, *17*, 319.

(42) James, B. R. In *Comprehensive Organometallic Chemistry*; Wilkinson, G., Stone, F. G. A., Abel, E. W., Eds.; Pergamon: Oxford, 1982; Vol. 8, Chapter 51.

(43) Pino, P.; Consiglio, G. In *Fundamental Research in Homogeneous Catalysis*; Tsutsui, M., Ed.; Plenum: New York, 1979; Vol. 3, p 519.

(44) Freifelder, M. *Practical Catalytic Hydrogenation*; Wiley-Interscience: New York, 1971.

(45) Rylander, P. N. *Hydrogenation Methods*; Academic: New York, 1985.

(46) Chaloner, P. A. *Handbook of Coordination Catalysis in Organic Chemistry*; Butterworths: Toronto, 1986; Chapter 2.

(47) James, B. R. *Homogeneous Hydrogenation*; Wiley: New York, 1973.

(48) James, B. R. *Chem. Ind.* **1995**, *62*, 167.

(49) Mestroni, G.; Camus, A.; Zassinovich, G. In *Aspects of Homogeneous Catalysis*; Ugo, R., Ed.; D. Reidel: Dordrecht, 1981; Vol. 4, p 71.

(50) Jessop, P. G.; Morris, R. H. *Coord. Chem. Rev.* **1992**, *121*, 155.

(51) Kubas, G. J.; Ryan, R. R.; Swanson, B. I.; Vergamini, P. J.; Wasserman, H. J. *J. Am. Chem. Soc.* **1984**, *106*, 451.

(52) Caplar, V.; Comisso, G.; Sunjic, V. *Synthesis* **1981**, 85.

(53) Bosnich, B.; Fryzuk, M. D. In *Topics in Inorganic and Organometallic Stereochemistry*; Geoffrey, G., Ed.; Wiley: New York, 1981, p 119.

(54) Valentine, D.; Scott, J. W. *Synthesis* **1978**, 329.

(55) Blystone, S. L. *Chem. Rev.* **1989**, *89*, 1663.

(56) Noyori, R. *Science* **1990**, *248*, 1194.

(57) *Asymmetric Synthesis*; Morrison, J. D., Ed.; Academic: New York, 1985; Vol. 5.

(58) Brunner, H. In *Advances in Catalysis Design*; Graziani, M., Rao, C. N. R., Eds.; World Scientific: London, 1993; Vol. II, p 245.

(59) Arntz, D.; Schafer, A. In *Metal Promoted Selectivity in Organic Synthesis*; Noels, A. F., Graziani, M., Hubert, A. J., Eds.; Kluwer Academic: Dordrecht, 1991, p 161.

(60) *Asymmetric Catalysis*; Bosnich, B., Ed.; Martinus Nijhoff: Dordrecht, 1986.

(61) Kagan, H. B. In *Comprehensive Organometallic Chemistry*; Wilkinson, G., Stone, F. G. A., Abel, E. W., Eds.; Pergamon: Oxford, 1982; Vol. 8, Chapter 53.

(62) Noyori, R. *Asymmetric Catalysis in Organic Synthesis*; Wiley-Interscience: New York, 1994.

(63) Dang, T. P.; Kagan, H. B. *J. Chem. Soc., Chem. Commun.* **1971**, 481.

(64) Kagan, H. B.; Dang, T. P. *J. Am. Chem. Soc.* **1972**, *94*, 6429.

(65) Vineyard, B. D.; Knowles, W. S.; Sabacky, M. J.; Bachman, G. L.; Weinkauff, D. J. *J. Am. Chem. Soc.* **1977**, *99*, 5946.

(66) Kang, G.; Cullen, W. R.; Fryzuk, M. D.; James, B. R.; Kutney, J. P. *J. Chem. Soc., Chem. Commun.* **1988**, 1466.

(67) Kitamura, M.; Ohkuma, T.; Inoúe, S.; Sayo, N.; Kumobayashi, H.; Akutagawa, S.; Ohta, T.; Takaya, H.; Noyori, R. *J. Am. Chem. Soc.* **1988**, *110*, 629.

(68) Halpern, J. *Science* **1982**, *217*, 401.

(69) Chan, A. S. C.; Pluth, J. J.; Halpern, J. *J. Am. Chem. Soc.* **1980**, *102*, 5952.

(70) Brown, J. M.; Chaloner, P. A. *J. Chem. Soc., Chem. Commun.* **1980**, 344.

(71) Alcock, N. W.; Brown, J. M.; Derome, A. E.; Lucy, A. R. *J. Chem. Soc., Chem. Commun.* **1985**, 575.

(72) Brown, J. M.; Chaloner, P. A.; Morris, G. A. *J. Chem. Soc., Chem. Commun.* **1983**, 664.

(73) Ojima, I.; Kogure, T.; Yoda, N. *Chem. Lett.* **1979**, 495.

(74) Ojima, I.; Kogure, T.; Yoda, N. *J. Org. Chem.* **1980**, *45*, 4728.

(75) Sinou, D. *Tetrahedron Lett.* **1981**, *22*, 2987.

(76) Wang, D. K. W. Ph.D. Thesis, The University of British Columbia, 1978.

(77) James, B. R.; Wang, D. K. W. *Can J. Chem.* **1980**, *58*, 245.

(78) James, B. R.; McMillan, R. S.; Morris, R. H.; Wang, D. K. W. *Adv. Chem. Ser.* **1978**, *167*, 122.

(79) James, B. R.; Pacheco, A.; Rettig, S. J.; Thorburn, I. S.; Ball, R. G.; Ibers, J. A. *J. Mol. Catal.* **1987**, *41*, 147.

(80) James, B. R.; Joshi, A. M.; Kvintovics, P.; Morris, R. H.; Thorburn, I. S. In *Catalysis of Organic Reactions*; Blackburn, D. W., Ed.; Marcel Dekker: New York, 1990; Chapter 2.

(81) Thorburn, I. S. Ph.D. Thesis, The University of British Columbia, 1985.

(82) Thorburn, I. S.; Rettig, S. J.; James, B. R. *Inorg. Chem.* **1986**, *25*, 234.

(83) Joshi, A. M.; Thorburn, I. S.; Rettig, S. J.; James, B. R. *Inorg. Chim. Acta* **1992**, *198*, 283.

(84) Joshi, A. M. Ph.D. Thesis, The University of British Columbia, 1990.

(85)   Noyori, R. *Chem. Soc. Rev.* **1989**, *18*, 187.

(86)   Noyori, R. In *Modern Synthetic Methods*; Scheffold, R., Ed.; Springer-Verlag: Berlin, 1989, p 115.

(87)   Fogg, D. E.; James, B. R.; Kilner, M. *Inorg. Chim. Acta* **1994**, *222*, 85.

(88)   Fogg, D. E. Ph.D. Thesis, The University of British Columbia, 1994.

(89)   Becalski, A. G.; Cullen, W. R.; Fryzuk, M. D.; James, B. R.; Kang, G.-J.; Rettig, S. J. *Inorg. Chem.* **1991**, *30*, 5002.

CHAPTER 2

EXPERIMENTAL PROCEDURES

2.1   Materials

2.1.1   Solvents

Spectral- or analytical-grade solvents were obtained from MCB, BDH, Aldrich, Eastman, Fisher or Mallinckrodt Chemical Company. Benzene, toluene, hexanes and diethyl ether were refluxed with, and distilled from, sodium metal/benzophenone under an atmosphere of nitrogen. N,N-dimethylacetamide (DMA) was stirred with CaH_2 for at least 24 h, vacuum distilled at 35–40 °C, and stored under argon in the dark. Dichloromethane, acetone, methanol, ethanol and 2-propanol were distilled after refluxing with the appropriate drying agents (P_2O_5 or CaH_2 for CH_2Cl_2; anhydrous K_2CO_3 for acetone; and Mg/I_2 for the alcohols).[1] Dibromomethane was dried over molecular sieves prior to use. Nitromethane, used in conductivity studies, was distilled from $CaCl_2$ and stored under Ar. The solvent n-pentane was used as received. All solvents were deoxygenated prior to use.

The deuterated solvents ($CDCl_3$, CD_2Cl_2, C_6D_6, C_7D_8, $(CD_3)_2CO$, CD_3CN, $(CD_3)_2SO$, CD_3OD, $(CD_3)_2CD(OD)$ and D_2O), used in NMR spectroscopy, were obtained from Merck Frosst Canada, Cambridge Isotope Laboratories (CIL), Isotec, and Aldrich. All deuterated solvents (with the exception of D_2O) were dried if necessary over activated molecular sieves (Fisher: Type 4 Å, 4–8 mesh), deoxygenated, and stored under argon. For the preparation of sealed NMR samples, C_6D_6 and C_7D_8 were dried over Na/benzophenone and stored under vacuum, while $CDCl_3$ was stored under vacuum over CaH_2. Samples that were particularly O_2- and/or moisture-sensitive were prepared by vacuum-transferring the above solvents into sealable NMR tubes which were previously filled with the solid sample.

Chapter 2 References: p 82

2.1.2 Gases

Purified Ar (Linde), N_2 (Linde), CO (C.P.), O_2 (U.S.P) and H_2 (Research, extra dry) were obtained from Union Carbide Canada; all except H_2 and Ar were used without further purification. Hydrogen was passed through an Engelhard Deoxo catalytic hydrogen purifier to remove traces of oxygen. Argon was passed through a drying column of $CaSO_4$. Anhydrous NH_3 (Matheson) and H_2S (Matheson) were used without further purification. Deuterium (CIL and Merck Frosst Canada) was used as supplied. Ethylene (Matheson) was used without further purification.

2.1.3 Phosphines

The monodentate phosphines, PPh_3 (BDH, Aldrich, or Strem) and P(*p*-tolyl)$_3$ (Strem), were used as supplied. The bidentate phosphines, $Ph_2P(CH_2)_nPPh_2$, where n=2, DPPE, and n=4, DPPB, were purchased from Strem and used without purification. The chiral phosphine, (*R*)-BINAP, ((*R*)-2,2'-bis(diphenylphosphino)-1,1'-binaphthyl) (Strem), was a gift from Dr. S. King (Merck Research Laboratories). The phosphines, *rac*-($\pm$)-1,2-bis(diphenylphosphino)cyclopentane (DPPCP) and *rac*-($\pm$)-1,2-bis(dicyclohexylphosphino)cyclopentane (DCYPCP) were synthesized from the previously prepared *rac*-($\pm$)-1,2-bis(dichlorophosphino)cyclopentane[2] (Section 2.1.3.1) by a reported method, and used as such without resolution.[2] 1,4-Bis(dicyclohexylphosphino)butane (DCYPB) was prepared by Mr. D. Chau in this laboratory by a modified reported preparation[3,4] from dicyclohexylphosphine, *n*-butyllithium, and 1,4-dibromobutane. The purity of all of the phosphines was ascertained by $^{31}P\{^1H\}$ and ^1H NMR spectroscopy.

2.1.3.1 Preparation of $Cl_2P(C_5H_8)PCl_2$, *trans*-1,2-bis(dichlorophosphino)-cyclopentane[2]

The title bis(phosphine) was prepared with Mr. R. Schutte by modification of a published procedure.[2] Cyclopentene (205 mL, 2.33 mmol), phosphorus trichloride (298 mL, 3.42 mol), and yellow phosphorus (25.45 g, 0.21 mol P_4) were added together in a steel autoclave, which was sealed and the contents stirred at 220 °C for 69 h. The pressure reached a maximum of 27 atm after 3 h, and was 21 atm when the autoclave contents were cooled for work-up. The resulting dark-brown mixture was filtered through a Büchner funnel under a blanket of N_2, created by passing gas through an inverted funnel, to remove any solids. The brown filtrate was collected in a round-bottom flask that was then attached to a vacuum distillation apparatus. Four fractions were collected. The first two fractions contained starting cyclopentene, cyclopentane, and PCl_3 ($^{31}P\{^1H\}$ NMR (C_6D_6, 20 °C): δ = 219.0, s). The third fraction contained dichlorophosphino-cyclopentane, $(C_5H_8)PCl_2$, collected at a stillhead temperature of 80–92 °C at ~ 0.1 mm Hg. The desired product, $Cl_2P(C_5H_8)PCl_2$, was isolated in the fourth fraction as a colourless liquid at a stillhead temperature of 100–108 °C at ~ 0.1 mm Hg. Yield: 174 g (52%).

$^{31}P\{^1H\}$ NMR (C_6D_6, 20 °C): δ = 190.0, s.

^1H NMR (C_6D_6, 20 °C): δ 1.28 (2H, pentet, J = 7 Hz, H_a); 1.65 (4H, m, H_b); and 2.38 (2H, m, H_c) (Figure 2.1).
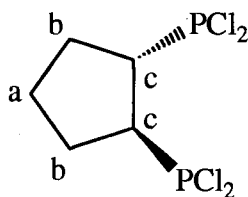
Figure 2.1   Structure of *trans*-1,2-bis(dichlorophosphino)cyclopentane indicating NMR assignments.

The physical and spectroscopic data agree with those reported.[2] The $^{31}P\{^1H\}$ NMR data have not previously been reported, but the chemical shift is in the expected region for a $PRCl_2$ compound (cf. PCl_3, see above).

dichlorophosphinocyclopentane, $(C_5H_8)PCl_2$

$^{31}P\{^1H\}$ NMR (C_6D_6, 20 °C): $\delta = 193.6$, s.

2.1.3.2 Preparation of *trans*-1,2-$(R_2P)_2C_5H_8$, where R = Ph, Cy[2]

The title racemic phosphines (DPPCP and DCYPCP) were prepared by addition of the appropriate Grignard reagent RMgBr to *trans*-1,2-$(Cl_2P)_2C_5H_8$, as outlined in the literature.[2] The spectroscopic data are shown below.

DPPCP (R = Ph) $^{31}P\{^1H\}$ NMR ($CDCl_3$, 20 °C): $\delta = -8.1$, s.

^1H NMR ($CDCl_3$, 20 °C): δ 1.65 (2H, m, CH_2 of cyclopentane), 1.90 (2H, m, CH_2 of cyclopentane), 2.26 (2H, m, CH_2 of cyclopentane), 2.75 (2H, m, CH of cyclopentane), 7.05–7.55 (20H, m, Ph).

DCYPCP (R = Cy) $^{31}P\{^1H\}$ NMR ($CDCl_3$, 20 °C): $\delta = 7.8$, s.

^1H NMR ($CDCl_3$, 20 °C): δ 1.28 (18H, br s, 2H of CH_2 of cyclopentane and 16H of Cy), 1.8 (32H, br m, 4H of cyclopentane and 28H of Cy), 2.49 (2H, br m, CH of cyclopentane).

2.1.4 Substrates

Benzonitrile (Aldrich), used as a substrate in hydrogenation studies, was purified by stirring over K_2CO_3 for several hours before decanting onto anhydrous $CaSO_4$. The nitrile was collected by vacuum distillation and stored under argon.

The imines, used as hydrogenation substrates, were prepared by Dr. D. Fogg by condensation of the appropriate amine and ketone or aldehyde.[5] The imines used were the ketimine, Ph(Me)C=NCH$_2$Ph, and the aldimine, Ph(H)C=NCH$_2$Ph. Both were used without further purification. The aldimine, *N*-benzylidene aniline (Ph(H)C=NPh), was synthesized by Dr. P. Kvintovics of this laboratory (visiting from the University of Veszprèm, Hungary).

Styrene (Aldrich) was purified by passing through a column of activated alumina (Fisher, neutral alumina, activity I, 80–200 mesh) to remove the inhibitor, 4-*t*-butylcatechol, and was stored under Ar in the refrigerator.

Authentic samples of the hydrogenation products corresponding to the above mentioned substrates were purchased from Aldrich, and used as supplied for comparison.

2.1.5   Other Materials

The amines, diethylamine (Eastman), di(*n*-butyl)amine (Mallinckrodt), tri(*n*-butyl)amine (Anachemia), benzylamine, dibenzylamine and tri(*n*-octyl)amine (Aldrich), were used without further purification. Triethylamine (MCB) was purified before use by stirring over KOH (Fisher) and collecting the amine by distillation. Poly(4-vinylpyridine), 2% cross-linked (Reillex™ 402 Polymer) (Aldrich) was used as received.

The heterocyclic compounds, pyridine (BDH), 2,2'-bipyridine (MCB), and 1,10-phenanthroline monohydrate (Fisher) were used as supplied.

The salts NH$_4$Cl (BDH), NH$_4$PF$_6$ (Ozark-Mahoning) and [15]NH$_4$Cl (MSD Isotopes) were used as supplied.

The sulfoxides, DMSO (BDH) and tetramethylene sulfoxide, TMSO (Aldrich), were used as supplied. The sulfides, dimethyl sulfide, DMS (Aldrich) and tetrahydrothiophene, THT (Aldrich) were used as supplied. 1,5-Cyclooctadiene (COD) was either used as supplied by Aldrich, or passed through an activity I neutral alumina column prior to use. Cyclopentene and allylmagnesium bromide (1.0 M in diethyl ether)

were used as supplied by Aldrich. Acetophenone (MCB) was vacuum distilled from anhydrous $CaSO_4$ and stored under argon. *Tertiary*-butanol (BDH) was used without prior purification for the Evans method[6,7] of measuring magnetic susceptibility (Section 2.5.6.1).

Phosphorus trichloride (BDH) was refluxed under N_2, and then collected by fractional distillation and stored under argon. Yellow phosphorus, P_4, (Aldrich) and 30% H_2O_2 (BDH) were used in synthetic preparations without purification. CuI (Aldrich) was used as supplied, while Zn dust (Fisher) was activated prior to use.

Zinc dust (7 g) was stirred with a 2% aq HCl solution (12 mL) for 1 min, then the solution was decanted off, and a second portion of the acid added. The Zn was collected on a filter and washed with distilled H_2O (3 x 10 mL), 95% EtOH (2 x 10 mL), and anhydrous diethyl ether (10 mL). The activated Zn was dried under vacuum and stored under Ar.[1]

LiBr (Fisher and MCB) was dried under vacuum at room temperature to remove any moisture before using it in halogen exchange reactions.

The drying agents, anhydrous $CaCl_2$ (Fisher, 4–20 mesh), CaH_2 (Fisher or BDH), anhydrous K_2CO_3 (Fisher), and anhydrous $MgSO_4$ (Fisher), were all used as supplied. Molecular sieves (4 Å, 1/16", BDH) were activated prior to use by heating overnight under dynamic vacuum. The filter aid, Celite 545® (Fisher) was used as supplied.

Neutral alumina (Fisher, Brockmann activity I, 80–200 mesh) was used as purchased or converted to activity III by adding 6% H_2O by weight.[8]

2.1.5.1   Preparation of copper(I) chloride, CuCl

CuCl was prepared from $CuCl_2 \cdot 2H_2O$ (Fisher) by a previously described method.[9,10] A solution of Na_2SO_3 (10 g in 50 mL H_2O) was slowly added to a green solution of $CuCl_2 \cdot 2H_2O$ (13.0 g, 0.0763 mol) in H_2O (20 mL). The resulting suspension was added to a solution of Na_2SO_3 (1 g) and concentrated HCl (2 mL) in H_2O (1 L). This

mixture was stirred, and then the white CuCl allowed to settle out. The supernatant was decanted, and the white solid was washed onto a sintered glass filter with an acidified Na_2SO_3 solution (same concentration as above). The solid was then washed with glacial acetic acid (5 x 20 mL), ethanol (3 x 30 mL), and diethyl ether (6 x 15 mL). Care was taken to ensure that the solid was covered by a layer of liquid at all times. After the final washing, the white product was quickly transferred to a Schlenk tube and dried under vacuum. Yield: 5.8 g (77%). The copper (I) chloride was stored in the dark under an atmosphere of argon.

2.1.5.2 Preparation of tetrameric chloro(triphenylphosphine)copper(I), $[CuCl(PPh_3)]_4$[11,12]

Triphenylphosphine (1.35 g, 5.14 mmol) and CuCl (0.53 g, 5.33 mmol) were refluxed in C_6H_6 (25 mL) for 18 h. The resulting cloudy, slightly-yellowish solution was filtered to produce a clear, colourless solution. The volume of this solution was reduced slightly at the pump until a white product precipitated; this was collected by vacuum filtration, washed with hexanes (4 x 5 mL), and dried under vacuum. Calculated for $[CuCl(PPh_3)]_4$, $[C_{18}H_{15}ClPCu]_4$: C, 59.84; H, 4.18%. Found: C, 59.73; H, 4.30%. The paper outlining the above procedure reports the product as $Cu_2Cl_2(PPh_3)_3$;[11] however, another paper reports that identical conditions give $[CuCl(PPh_3)]_4$.[12] A subsequent paper by Costa et al. reports that repeated recrystallizations of $[CuCl(PPh_3)]_4$ give $Cu_2Cl_2(PPh_3)_3$.[13]

2.1.5.3 Preparation of dibutylammonium chloride, $[H_2N(n\text{-butyl})_2]^+Cl^-$

An excess of concentrated HCl (10 mL, 0.12 mol) was added dropwise to a solution of di-n-butylamine (2.8 mL, 13 mmol) in EtOH (25 mL) at 0 °C. The clear, colourless reaction mixture was stirred at room temperature for 2 h, and then the solvent was removed with a rotary evaporator. The resulting white solid was dried at 78 °C under

vacuum. Yield: 2.1 g (97%). Calculated for [H$_2$N(n-butyl)$_2$]$^+$Cl$^-$, C$_8$H$_{20}$NCl: C, 57.99; H, 12.16; N, 8.45%. Found: C, 58.13; H, 12.29; N, 8.26%.

^{1}H NMR (CDCl$_3$, 20 °C): δ 0.93 (6H, t, J = 7.3 Hz, CH$_2$CH_3), 1.4 (4H, sextet, J = 7.5 Hz, CH$_2$CH_2 CH$_2$), 1.9 (4H, pentet, J = 7.9 Hz, CH$_3$CH$_2$CH_2CH$_2$N), 2.9 (4H, br m, CH$_2$CH_2NH$_2$), and 9.4 (2H, br s, NH_2).

2.1.5.4   Preparation of dioctylammonium chloride, [H$_2$N(n-octyl)$_2$]$^+$Cl$^-$

An excess of concentrated HCl (10 mL, 0.12 mol) was added dropwise to a solution of di-n-octylamine (3.6 mL, 12 mmol) in EtOH (25 mL) at 0 °C. The clear, colourless reaction mixture was stirred at room temperature for 2 h, and then the solvent was removed with a rotary evaporator. The resulting white solid was dried at 78 °C under vacuum. Yield: 3.3 g (98%). Calculated for [H$_2$N(n-octyl)$_2$]$^+$Cl$^-$, C$_{16}$H$_{36}$NCl: C, 69.15; H, 13.06; N, 5.04%. Found: C, 69.34; H, 13.09; N, 4.95%.

^{1}H NMR (CDCl$_3$, 20 °C): δ 0.87 (6H, t, J = 6.8 Hz, CH$_2$CH_3), 1.3 (20H, m, CH$_3$(CH_2)$_5$ CH$_2$), 1.9 (4H, pentet J = 7.5 Hz, CH$_2$CH_2CH$_2$N), 2.9 (4H, br m, CH$_2$CH_2NH$_2$), and 9.5 (2H, br s, NH_2).

2.2   Instrumentation

Infrared spectra were recorded on a Nicolet 5DX FT-IR or ATI Mattson Genesis Series FTIR spectrophotometer as KBr pellets, or as Nujol mulls between KBr plates, unless specified otherwise. UV-visible spectra were recorded on a Hewlett Packard 8452A diode array spectrophotometer with a thermostatted cell compartment, using quartz spectral cells (path length = 1.0 cm). Spectra were usually recorded in anaerobic cells (Figure 2.2) under an atmosphere of argon.
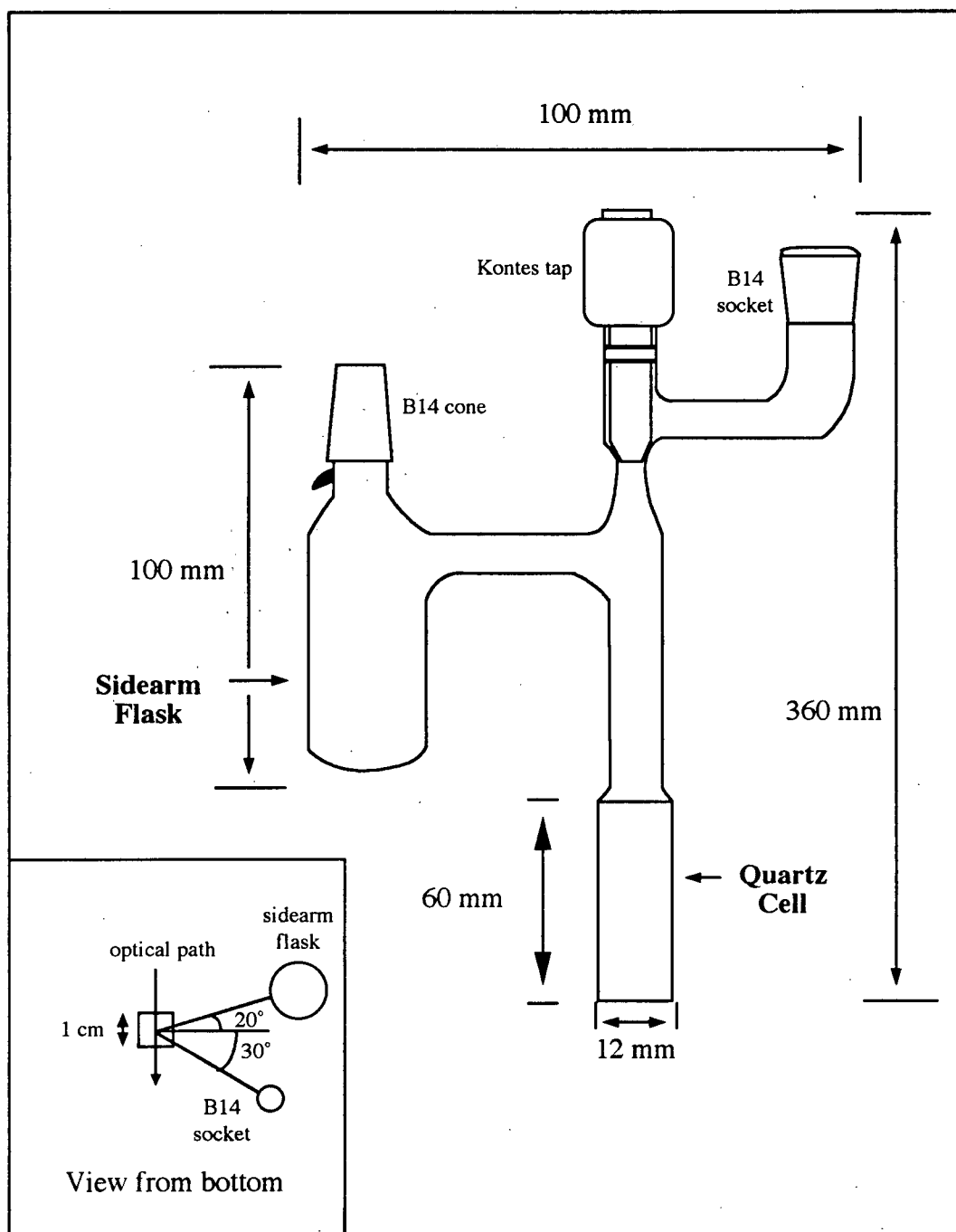
Figure 2.2   Anaerobic UV-visible cell.

The solution nuclear magnetic resonance (NMR) spectra were recorded on a Bruker AC200 (200.1 MHz for ^{1}H and 81.0 MHz for ^{31}P), a Varian XL300 (300.0 MHz for ^{1}H and 121.4 MHz for ^{31}P) and a Bruker AMX500 (500.0 MHz for ^{1}H and 202.5

MHz for ^{31}P) FT-NMR spectrometer. The ^{1}H chemical shifts are reported relative to the external standard of tetramethylsilane (TMS) at 0.0 ppm, while those measured for ^{31}P{^{1}H} NMR were externally referenced relative to trimethylphosphite, P(OMe)$_3$ (Aldrich), (141.0 ppm relative to 85% H$_3$PO$_4$).[14] All ^{31}P{^{1}H} NMR chemical shifts are reported relative to 85% H$_3$PO$_4$, with downfield shifts taken as positive.

Variable-temperature NMR spectra were measured on the Varian XL300 spectrometer.

Gas chromatographic analyses were performed on a temperature-programmable Hewlett Packard 5890A instrument equipped with a thermal conductivity detector and a flame ionization detector, using helium as the carrier gas (flow rate ~ 40 mL/min).

Gas uptakes were performed on a conventional constant-pressure, constant-temperature gas-uptake apparatus. A detailed procedure employed for gas-uptake measurements is described elsewhere,[15,16] while a brief description is given in Section 2.3.1, along with a diagram of the apparatus (Figure 2.3).

Mass spectrometry was done either by Electron Ionization (EI) or Fast Atom Bombardment (FAB). FAB was performed on an AEI MS 902 Mass Spectrometer with 3-nitrobenzylalcohol as the matrix, while EI was performed on a Kratos MS 50.

Conductivity measurements were made using a Serfass Conductance Bridge Model RCM15B1 (Arthur H. Thomas Co. Ltd.) connected to a 3403 cell from the Yellow Springs Instrument Company. The cell constant was determined by measuring the resistance of an aqueous solution of KCl (0.0100 M, σ = 0.001413 ohm^{-1} cm^{-1} at 25 °C).[17] The cell was thermostatted in a water-bath. Conductance was measured on solutions with concentrations on the order of 1 x 10^{-3} M. The solutions were prepared in air with dry solvents just prior to use.

Elemental analyses were performed by Mr. P. Borda of this department. Single crystal X-ray diffraction studies were carried out by Dr. S. Rettig of the departmental crystallographic service.

2.3   Catalytic Hydrogenation

2.3.1   Ambient Pressure Hydrogenations

A constant-pressure gas-uptake apparatus was used to study the rate of catalytic

hydrogenation of benzonitrile at a H_2 pressure of one atmosphere, and a temperature of

70 °C. The apparatus (Figure 2.3) and procedure have been described.[15,16] Degassed

solvents were used in the H_2-uptake experiments, and the solutions of nitrile and solvent

were further degassed by three freeze-pump-thaw cycles while connected to the uptake

assembly. No air was allowed into the system as the catalyst was added to the solution by

the dropping of a suspended bucket containing the catalyst.
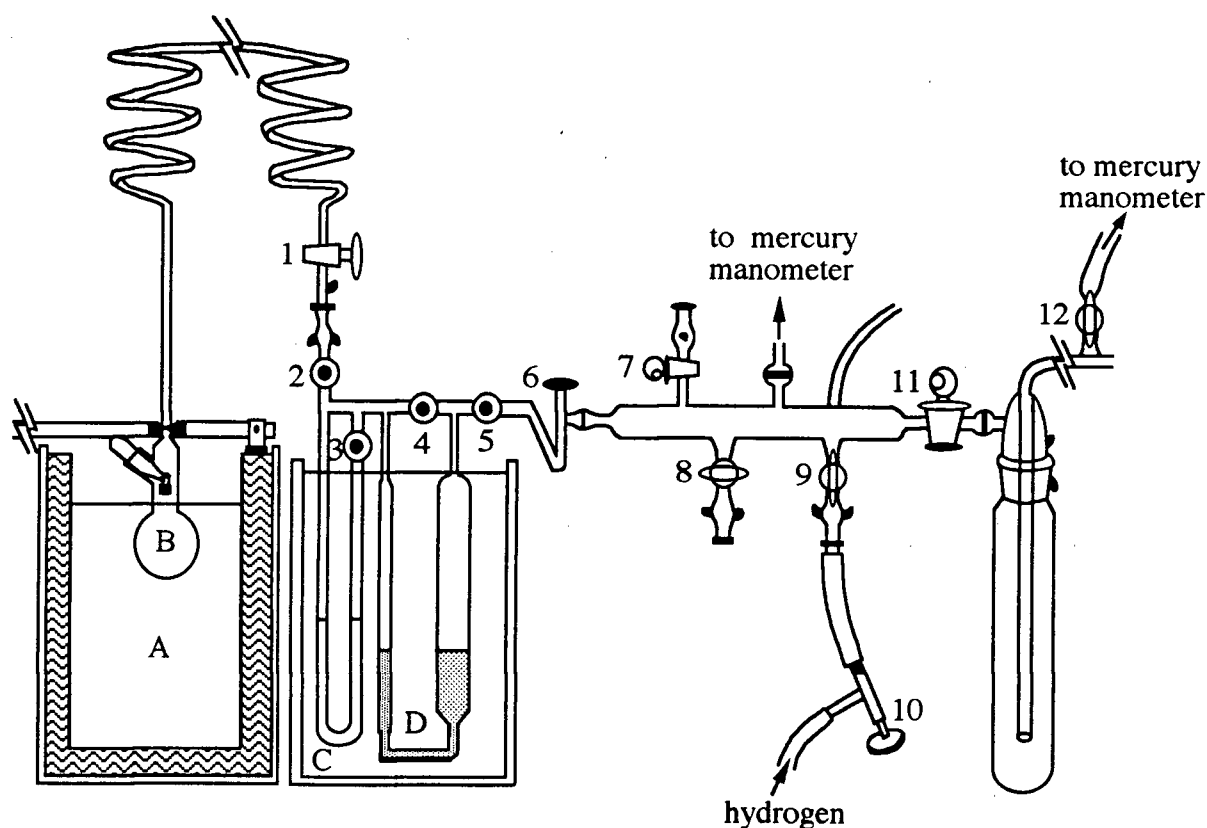
Figure 2.3   Constant-pressure gas-uptake apparatus with the key components lettered:
(A) thermostatted and insulated oil bath, (B) dimpled reaction flask, (C) oil
manometer, (D) mercury reservoir and burette. (1)–(12) label the Kontes
valves and greased taps and are described in the text.

A typical hydrogenation reaction followed by gas uptake was performed in the following manner. A flexible spiral glass capillary was used to connect the uptake flask B containing the solvent, substrate, and catalyst to the stopcock labelled 7 in Figure 2.3. While connected to this position, the solution was freeze-pump-thaw degassed at least three times, and then filled to slightly less than the required operating pressure with hydrogen. The flask B and spiral, once stopcocks 1 and 7 were closed, were then moved to Kontes valve 2. The flask and contents were allowed to equilibrate to the oil-bath temperature (A) for 30 minutes, during which time Kontes valves 2, 3, 4, and 5, and needle valve 6 were open to allow evacuation of the burette portion of the apparatus. The apparatus was then filled with the desired H_2-pressure, and stopcock 1 was opened. Kontes valve 3 was then closed to lock in the reference pressure in the small volume of the burette. Unlike previous designs of the uptake apparatus, which used greased stopcocks at positions 2, 3, 4, and 5, significant pressure changes were observed in the oil levels as Kontes valve 3 was closed, thus decreasing the volume. Therefore, an additional step of re-levelling the oil in the burette by increasing the H_2-pressure slightly with Kontes valve 10 was necessary. At this point, the H_2-pressure could be recorded from the mercury manometer. Kontes valve 4 was then closed to isolate the Hg burette, and an initial reading was made from the Hg burette with the aid of a Precision Tool Vernier Microscope Type 2158. Needle valve 6 was then closed and the reaction started by dropping the bucket containing the catalyst. The progress of the catalytic reaction was followed by introducing hydrogen through needle valve 6 in order to level the oil burette, and by reading the Hg level.

2.3.2 High Pressure Hydrogenations

Reactions at H_2 pressures of up to 1000 psi (68 atm, 6.895 MPa) for hydrogenation of imines were performed in a machined-steel autoclave equipped with glass liners. The autoclave was topped with a high-pressure regulator which was

connected to an H_2 cylinder with flexible-steel hosing. Mixing of the hydrogenation reactions was achieved with the use of a magnetic stirrer. Conversion results were found by previous workers in the laboratory[5,18] to be dependent on the method of assembly of the autoclave (see below). Therefore, a standard procedure was developed and followed to ensure reproducible results in terms of rate of conversion. This procedure is described in the following paragraph.

The empty autoclave was connected through the regulator on the H_2 cylinder to a vacuum line, then the autoclave was evacuated and filled with N_2. The glass liner containing the catalytic solution was then placed in the autoclave under a stream of N_2. The catalyst, imine substrate, and deoxygenated dry MeOH solvent had been previously placed in the glass liner under a flow of Ar. The head of the autoclave was screwed onto the assembly and tightened with a wrench. With the stirrer off, the solution was evacuated and flushed with N_2 three times, and finally evacuated again. The autoclave was then pressurized to 400 psi (2.7 MPa) H_2 and evacuated. This was repeated three times and the autoclave finally pressurized to 1000 psi (6.895 MPa) or any other desired pressure. The pressure was locked into the vessel with a needle valve and the stirrer started. The entire procedure, from the point of adding the solvent to the glass liner, to locking-in the final pressure, took just three minutes on average. This approach gave consistent results to within 3% or less from trial to trial.

The source of the inconsistent results before the adoption of this procedure was found by previous workers to be due to the presence of trace dioxygen.[5,18]

A second autoclave, acquired toward the end of this thesis, was used on a couple of occasions. This autoclave featured sampling capabilities via a liquid sampling valve and dip tube, which allowed the hydrogenation to be easily followed by gas chromatography. Pressures of up to 1000 psi H_2 could be used with this stainless steel 50 mL autoclave, which was purchased from Parr Instrument Co. (4590 Bench Top Micro

Reactor) and equipped with a glass liner and temperature controller (Parr 4843 Series 942). Stirring was overhead by use of a magnetic drive.

2.4   Analysis of Hydrogenation Products

2.4.1   Measurement of Conversion

Conversions of imine to amine in the case of the imines, PhN=C(H)Ph and PhCH$_2$N=C(H)Ph, were easily determined by removal of the MeOH solvent with a rotary evaporator, dissolution and dilution of the residue in CDCl$_3$, and ^{1}H NMR spectroscopic analysis. In the cases where *N*-phenylbenzylamine was the product, the integrations of the amine methylene and imine methyne were compared, while if dibenzylamine was the product, the integrations of methylenes of both amine and imine were used. Conversions of the ketimine, PhCH$_2$N=C(Me)Ph, to amine were also determined by ^{1}H NMR spectroscopy, but were best performed in C$_6$D$_6$, as the imine appears to exist solely as the *anti* isomer in this solvent; only one methylene, attributed to the *anti*-isomer, is apparent in C$_6$D$_6$, instead of the two singlets observed in CDCl$_3$ (in a ratio of ca. 9:1).[5]

Conversions of the imines PhCH$_2$N=C(H)Ph and PhN=C(H)Ph to the corresponding amines could also be determined by gas chromatography using a HP-20M (Carbowax 20M) column (25 m x 0.2 mm x 0.2 μm film thickness). The following conditions affected separation: initial temp 140 °C; initial time 2 min, rate 20 °C/min, final temp 220 °C, final time 20 min, FID detector temp 220 °C, and injector temp 220 °C.

The above conditions were also effective for the identification of products from PhCN hydrogenation. The remaining PhCN, benzylamine, and dibenzylamine were separated; however, another possible product, PhCH$_2$N=C(H)Ph, had the same retention time as benzylamine. The use of an OV-101 capillary column (25 m) allowed the imine PhCH$_2$N=C(H)Ph to be distinguished from benzylamine using isothermal (140 °C) conditions.

2.4.2 NMR Characterization of Imines

^{1}H NMR spectroscopic data for the imines used as substrates in catalytic hydrogenation are given below.

2.4.2.1   PhN=C(H)Ph, *N*-benzylideneaniline

^{1}H NMR (CDCl$_3$, 20 °C): δ 7.2–7.5 (8H, m, Ph), 7.8–8.0 (2H, m, Ph), 8.46 (1H, s, C*H*). The data show only the presence of one isomer, presumably the *anti*-configuration.[5]

2.4.2.2   PhCH$_2$N=C(H)Ph, *N*-benzylidene benzylamine

^{1}H NMR (CDCl$_3$, 20 °C): δ 4.83 (2H, s, C*H$_2$*), 7.22–7.45 (8H, m, Ph), 7.74–7.82 (2H, m, PhC), 8.39 (1H, s, C*H*). The data show only the presence of one isomer, presumably the *anti*-configuration.[5]

2.4.2.3   PhCH$_2$N=C(Me)Ph, *N*-(1-methylbenzylidene)benzylamine

^{1}H NMR (CDCl$_3$, 20 °C): δ 2.3–2.4 (3H total, both s, *syn* and *anti* C*H$_3$*, respectively), 4.8 and 4.4 (2H total, both s, *anti* and *syn* C*H$_2$*, respectively; 93% *anti*), 7.3–7.6 (8H, m, Ph), 7.9–8.0 (2H, m, Ph).

^{1}H NMR (C$_6$D$_6$, 20 °C): δ 1.74 (3H, s, *anti* C*H$_3$*), 4.48 (2H, s, *anti* C*H$_2$*), 7.1–7.33 (6H, m, Ph), 7.5–7.6 (2H, d, Ph), 7.85–7.95 (2H, m, Ph).

2.4.3 NMR Characterization of Reduction Products (Amines)

^{1}H NMR spectroscopic data for the amine products obtained from catalytic hydrogenation studies are given below.

2.4.3.1   PhNHCH$_2$Ph, *N*-phenylbenzylamine

^{1}H NMR (CDCl$_3$, 20 °C): δ 1.8 (1H, br s, N*H*), 4.3 (2H, s, C*H$_2$*), 6.6–6.8 (5H, m, NPh), 7.2–7.4 (5H, m, Ph).

2.4.3.2   NH(CH₂Ph)₂, dibenzylamine

¹H NMR (CDCl₃, 20 °C): δ 1.8 (1H, br s, NH), 3.82 (4H, s, CH_2), 7.2–7.4 (10H, m, Ph).

2.4.3.3   NH(CH₂Ph)(C*H(Me)Ph), *N*-(1-methylbenzyl)-*N*-benzylamine

¹H NMR (CDCl₃, 20 °C): δ 1.38 (3H, d, J = 6.6 Hz, CH_3), 1.63 (1H, br s, NH), 3.60, 3.67 (2H, ABq, J = 13.2 Hz, CH_2), 3.82 (1H, q, J = 6.6 Hz, CH), 7.21–7.39 (10H, m, Ph).

¹H NMR (C₆D₆, 20 °C): δ 1.17 (3H, d, J = 6.6 Hz, CH_3), 1.20 (1H, br s, NH), 3.43, 3.55 (2H, ABq, J = 13.2 Hz, CH_2), 3.59 (1H, q, J = 6.5 Hz, CH), 6.88–7.51 (10H, m, Ph).

2.5   Synthesis and Characterization of Ruthenium Complexes

The ruthenium was obtained on loan from Johnson Matthey Ltd. and Colonial Metals Inc. as $RuCl_3 \cdot xH_2O$; depending upon the batch, the ruthenium content varied from 41.5 to 43.96%.

All synthetic reactions, unless stated otherwise, were carried out in deoxygenated solvents under an atmosphere of argon, employing Schlenk techniques,[19] as many of the ruthenium complexes prepared in the course of this work were susceptible to oxidation on exposure to air, especially in solution.

2.5.1   Ruthenium Precursors

2.5.1.1   Preparation of trichloro(*N,N*-dimethylacetamide)bis-(triphenylphosphine)ruthenium(III) *N,N*-dimethylacetamide solvate, RuCl₃(PPh₃)₂(DMA)·DMA solvate (1)[20-24]

The title Ru(III) complex was synthesized by stirring a solution of $RuCl_3 \cdot xH_2O$ (2.0 g, 8.7 mmol) in DMA (30 mL) with two equivalents of PPh₃ (4.58 g, 17.5 mmol) for

---

* indicates chiral centre

24 h at room temperature. If the reaction was performed in MeOH instead of DMA, as done originally,[20] the product is $RuCl_3(PPh_3)_2(MeOH)$ where the sixth ligand is MeOH instead of DMA. The green solid was collected on a sintered glass filter by vacuum filtration, washed with a small amount of DMA (< 5 mL) and hexanes (2 x 5 mL), and vacuum dried. Yield: 5.5 g (73%). Calculated for $C_{44}H_{48}N_2Cl_3O_2P_2Ru$: C, 58.32; H, 5.34; N, 3.09; Cl, 11.74%. Found: C, 58.13; H, 5.21; N, 3.00; Cl, 11.73%.

IR (Nujol, CsI plates, cm^{-1}): $v_{(C=O)}$ at 1634 (m, uncoordinated DMA); $v_{(C=O)}$ at 1598 (m, coordinated DMA).

The physical and spectroscopic data for this complex agree with those reported.[21-23] The yield of this preparation could be improved (by 5–10%) by performing a second synthesis using the filtrate saved from the first reaction. The Ru(III) product is somewhat soluble in DMA, and ideally the solution should be concentrated prior to filtration in order to improve the yield of the product. However, the high boiling point of DMA (165 °C) makes this difficult.

$RuCl_3(PPh_3)_2(DMA)\cdot0.5\ H_2O$

The title complex **1** was inadvertently prepared without a DMA solvate in this work by washing the green product $RuCl_3(PPh_3)_2(DMA)\cdot DMA$ solvate with EtOH (2 x 10 mL). The solid was light brown in colour. Yield: 5.1 g (72%, starting with the same amount of materials as shown above). Calculated for $RuCl_3(PPh_3)_2(DMA)\cdot0.5\ H_2O$, $C_{40}H_{40}NCl_3O_2P_2Ru$: C, 58.01; H, 4.87; N, 1.69%. Found: C, 57.92; H, 4.86; N, 1.67%.

IR (Nujol, CsI plates, cm^{-1}): $v_{(C=O)}$ at 1601 (m, coordinated DMA). The IR spectrum showed the presence of H_2O, but this was not conclusive as the IR spectra of other materials not requiring H_2O solvates (based on elemental analysis) also show bands indicating the presence of H_2O.

2.5.1.2 Preparation of trichloro(*N,N*-dimethylacetamide)bis(tri-*p*-tolylphosphine)ruthenium(III) *N,N*-dimethylacetamide solvate, RuCl$_3$(P(*p*-tolyl)$_3$)$_2$(DMA)·DMA solvate (2)[21,22]

This Ru(III) complex was prepared in the same manner as its PPh$_3$ analogue, except that two equivalents of P(*p*-tolyl)$_3$ (5.3 g, 17.4 mmol) were used. Yield of the green solid: 5.8 g (67%). Calculated for C$_{50}$H$_{60}$N$_2$Cl$_3$O$_2$P$_2$Ru: C, 60.64; H, 6.11; N, 2.83; Cl, 10.74%. Found: C, 60.32; H, 6.11; N, 2.80; Cl, 10.79%.

IR (Nujol, CsI plates, cm^{-1}): $\nu_{(C=O)}$ at 1646 (m, uncoordinated DMA); $\nu_{(C=O)}$ at 1600 (m, coordinated DMA).

The physical and spectroscopic data for this complex agree with those reported.[21,22]

2.5.1.3 Preparation of tribromo(methanol)bis(triphenylphosphine)-ruthenium(III), RuBr$_3$(PPh$_3$)$_2$(MeOH) (3)[20,23]

An attempt to prepare the title complex made using the method given by Stephenson and Wilkinson.[20] A solution of RuCl$_3$·xH$_2$O (0.52 g, 2.3 mmol) and LiBr (3.4 g, 39 mmol; ~ 6 equiv / Cl) in methanol (100 mL) was stirred at room temperature for 24 h. Triphenylphosphine (1.1 g, 4.4 mmol; 2 equiv / Ru) was then added to the solution and stirring continued. During the next two days, a reddish-brown solid precipitated. The solid was collected by vacuum filtration, washed with methanol (3 x 10 mL) and hexanes (6 x 10 mL), and dried under vacuum. Yield: 1.3 g (64%). Calculated for C$_{37}$H$_{34}$Br$_3$OP$_2$Ru: C, 49.52; H, 3.82; Br, 26.71%. Found: C, 57.57; H, 4.16; Br, 20.49%. Repeated attempts to prepare this complex resulted in similar microanalytical data. The UV-vis spectroscopic and physical data (m.p.) did not agree with the literature values.[20,23] These data are discussed in Chapter 3, Section 3.3.1.

The synthesis of the bromo-Ru(III) complex, RuBr$_3$(PPh$_3$)$_2$(DMA)·DMA solvate also proved difficult. These difficulties are addressed in Section 3.3.1.

2.5.1.4 Preparation of chlorohydridotris(triphenylphosphine)ruthenium(II) *N,N*-dimethylacetamide solvate, Ru(H)Cl(PPh₃)₃·DMA solvate (4)[23,25-28]

N,N-Dimethylacetamide (20 mL) was pipetted into a Schlenk tube containing RuCl₂(PPh₃)₃ (1.00 g, 1.04 mmol). The resulting brown solution was immediately degassed and placed under an atmosphere of H₂. After 15 minutes, the solution began turning a bright reddish-purple colour. The solution was stirred for another 18 h at room temperature. The red-violet solid that precipitated was collected on a Schlenk filter, washed with DMA (5 mL) and hexanes (2 x 5 mL), and finally dried under vacuum. Yield: 0.82 g (78%). Calculated for $C_{58}H_{55}NClOP_3Ru$: C, 68.87; H, 5.48; N, 1.38%. Found: C, 68.70; H, 5.31; N, 1.50%.

The physical and spectroscopic data for this complex agree with those reported in the literature.[23,25-27]

2.5.1.5 Preparation of 1,5-cyclooctadieneruthenium(II) chloride polymer, [RuCl₂(COD)]ₓ (5)[29,30]

Ruthenium trichloride (RuCl₃·xH₂O; 1.03 g, 4.23 mmol based on Ru content) was dissolved in degassed ethanol (40 mL). The clear, dark-orange solution was stirred with 1,5-cyclooctadiene (5.0 mL) for five days at room temperature. A brown solid precipitated from the solution, and was collected on a sintered glass filter, washed with ethanol (3 x 10 mL), and dried under vacuum. Yield: 0.87 g (74%). Calculated for $[C_8H_{12}Cl_2Ru]_x$: C, 34.30; H, 4.32%. Found: C, 34.55; H, 4.48%.

The physical data for this polymer agree with those reported in the literature;[25] however, the yield was significantly better than the reported 30–40%.

A new preparation that reports improved yields (99%) has been published recently.[30] This new preparation was followed as described below. Ruthenium trichloride (RuCl₃·xH₂O; 2.0 g, 8.3 mmol based on Ru content) was dissolved in 95% ethanol (80 mL), and 1,5-cyclooctadiene (7.5 mL, 61 mmol) was added to the resulting solution. This mixture was heated at reflux for 3 days, at which point very little colour was left in

solution, the brown product having precipitated. The brown solid was collected by vacuum filtration, washed with ethanol (2 x 30 mL), and dried under vacuum. Yield: 2.0 g (86%).

2.5.1.6   Preparation of Ru(COD)(η^3-allyl)$_2$ (6)[31,32]

Allylmagnesium bromide (6.5 mL of 1.0 M in diethyl ether, 6.5 mmol) was added slowly to [RuCl$_2$(COD)]$_x$ (0.52 g, 1.8 mmol) in diethyl ether (30 mL). The brown suspension of the Ru starting material immediately became a pale yellow solution upon addition of the Grignard reagent. The solution was stirred at room temperature for 24 h, hydrolyzed with H$_2$O (30 mL), and the ether layer separated from the water layer. The ether washings (3 x 40 mL) were combined, dried over anhydrous CaCl$_2$, and pumped to dryness to give a dark gum, which was taken up in *n*-pentane (5 mL) and passed through a neutral alumina column (Activity III, 15 x 2.5 cm). *n*-Pentane (50 mL) was used to elute the product as a faintly yellow solution. The solvent was removed at the pump to give an off-white, waxy product. Yield: 0.30 g (56%).

^{1}H NMR (C$_6$D$_6$, 20 °C): δ –0.09 (2H, d, *J* = 10 Hz, *anti* H of allyl), 1.38 (2H, m, C*H* of COD), 1.72 (2H, d, *J* = 12 Hz, *anti* H of allyl), 1.6–2.0 (4H, m, C*H$_2$* of COD), 2.64 (2H, d, *J* = 12 Hz, *anti* H of allyl), 2.8–3.0 (4H, m, C*H$_2$* of COD), 3.1–3.4 (2H, m, central H of allyl), 3.71 (2H, dd, *J* = 2 and 8 Hz, *syn* H of allyl), 4.03 (2H, m, C*H* of COD).

The physical and spectroscopic data for this complex agree with those reported in the literature.[31,32]

2.5.1.7   Preparation of Ru(COD)(η^3-Me-allyl)$_2$ (7)[30,32]

This material was prepared by Mr. Z. Liu of this department with minor modifications to a procedure outlined by Genêt et al.[30] The Grignard reagent, 2-methylallylmagnesium chloride, was found to be fairly insoluble in diethyl ether, and therefore THF was used as the solvent. The Grignard reagent (2 M, 6 mL, 12 mmol; prepared from Mg and 3-chloro-2-methylpropene in THF) was added to a suspension of

[RuCl$_2$(COD)]$_x$ (0.28 g, 1.0 mmol) in Et$_2$O (10 mL) / THF (15 mL), and the mixture stirred at room temperature for 10 min. The excess Grignard reagent was precipitated from solution by adding more diethyl ether, and the suspension was filtered through Celite. The filtrate was hydrolyzed in ice-water and the mixture extracted with diethyl ether (2 x 20 mL). The organic layer was dried over MgSO$_4$, concentrated, filtered through a short column of neutral alumina (5 x 5 cm), and evaporated to dryness. Reprecipitation from a mixture of methanol and petroleum ether gave pure material. Yield: 0.27 g (80%). Calculated for Ru(COD)(η^3-Me-allyl)$_2$, C$_{16}$H$_{26}$Ru: C, 60.16; H, 8.20%. Found: C, 59.93; H, 8.31%. m.p. = 80–85 °C; lit. m.p. = 80–85 °C.

^{1}H NMR (C$_6$D$_6$, 20 °C): δ 0.20 (2H, s, *anti* H of Me-allyl), 1.08–1.26 (2H, m, C*H* of COD), 1.45–1.70 (4H, m, C*H$_2$* of COD), 1.56 (2H, s, *syn* H of Me-allyl), 1.70 (6H, s, C*H$_3$* of Me-allyl), 2.64–3.00 (4H, C*H$_2$* of COD), 2.88 (2H, s, *anti* H of Me-allyl), 3.52 (2H, d, *J* = 2 Hz, *syn* H of Me-allyl), 3.98 (2H, dd, *J* = 5, 9 Hz, C*H*- of COD).

^{13}C{^{1}H} NMR (C$_6$D$_6$, 20 °C): δ 24.74 (*C*H$_3$ of Me-allyl), 26.26 and 38.34 (CH$_3$C(*C*H$_2$)$_2$), 51.22 and 51.68 (*C*H$_2$ of COD), 70.63 and 88.22 (*C*H- of COD), 111.49 (CH$_3$-*C*(CH$_2$)$_2$).

The physical and spectroscopic data for this complex agree with those reported in the literature.[30,32]

2.5.2 Preparation of RuX$_2$(PAr$_3$)$_3$; X = Cl, Br; Ar = Ph, *p*-tolyl

2.5.2.1 X = Cl, Ar = Ph; Preparation of dichlorotris(triphenylphosphine)-ruthenium(II), RuCl$_2$(PPh$_3$)$_3$ (8)[20,33,34]

The Ru(II) material was prepared by refluxing a methanol solution (300 mL) of RuCl$_3$·3H$_2$O (1.95 g, 8.23 mmol) and PPh$_3$ (12.6 g, 4.82 mmol) under Ar for 3 h.[20,33,34] The dark-brown solid was collected by vacuum filtration, washed with methanol (7 x 20 mL) and diethyl ether (3 x 20 mL) to remove the remaining PPh$_3$, and dried under

vacuum. Yield: 7.3 g (93%). Calculated for $C_{54}H_{45}Cl_2P_3Ru$: C, 67.64; H, 4.73%. Found: C, 67.66; H, 4.73%.

$^{31}P\{^1H\}$ NMR (CDCl$_3$, –60 °C): δ_A = 76.1 (1P, $^2J_{AX}$ = unresolved), δ_X = 24.7 (2P, $^2J_{AX}$ = unresolved). Also, observed are δ = –6.6 (free PPh$_3$) and δ_A = 60.1, δ_B = 52.4, $^2J_{AB}$ = 41.1 Hz (Ru$_2$Cl$_4$(PPh$_3$)$_4$).

The physical and spectroscopic data for this complex agree with those reported in the literature.[20,33,34]

2.5.2.2   X = Cl, Ar = *p*-tolyl; Preparation of dichlorotris(tri-*p*-tolyl-phosphine)ruthenium(II), RuCl$_2$(P(*p*-tolyl)$_3$)$_3$ (9)[35-37]

The title compound was prepared according to the method described previously,[35-37] with some minor modifications. Ruthenium trichloride (RuCl$_3 \cdot x$H$_2$O; 1.03 g, 4.33 mmol) was refluxed in methanol (200 mL) for fifteen minutes. The dark-orange solution was cooled, excess tri-*p*-tolylphosphine (5.55 g, 18.2 mmol) added, and refluxing continued for another three hours. A dark-purple solid precipitated from the solution, and after being cooled the solution was collected on a sintered glass filter. The solid was washed thoroughly with methanol (8 x 10 mL) and diethyl ether (5 x 10 mL) to remove any excess phosphine, and dried under vacuum. Yield: 3.97 g (87%). Calculated for $C_{63}H_{63}Cl_2P_3Ru$: C, 69.74; H, 5.85%. Found: C, 69.67; H, 5.80%.

$^{31}P\{^1H\}$ NMR (C$_6$D$_6$, 20 °C): δ = 42.8 (br s); (C$_7$D$_8$, –65 °C): δ_A = 77.6 (1P, $^2J_{AX}$ = unresolved), δ_B = 28.4 (2P, $^2J_{AX}$ = unresolved). Also, observed are δ = –9.6 (free P(*p*-tolyl)$_3$) and δ_A = 60.6, δ_B = 53.7, $^2J_{AB}$ = 42.7 Hz (Ru$_2$Cl$_4$(P(*p*-tolyl)$_3$)$_4$).

The physical and spectroscopic data for this complex agree with those reported in the literature.[35-37]

2.5.2.3   X = Br, Ar = Ph; Preparation of dibromotris(triphenylphosphine)-ruthenium(II), RuBr₂(PPh₃)₃ (10)[20,23,35]

This ruthenium(II) monomer was synthesized in much the same manner as the chloro analogue (Section 2.5.2.1), except that LiBr (10.7 g, 123 mmol, 30 equiv / Ru or 10 equiv / Cl) was refluxed with $RuCl_3 \cdot xH_2O$ (1.0 g, 4.1 mmol) in MeOH (250 mL) before the addition of the PPh_3. The orange solution was refluxed for 30 min, cooled to room temperature, and PPh_3 (6.0 g, 23 mmol) was added under a flow of argon. The reddish-purple solution was refluxed for 3 h, then cooled, and the brown product that precipitated was collected by vacuum filtration. Excess triphenylphosphine was removed by washing with MeOH (6 x 30 mL) and diethyl ether (3 x 10 mL). The brown solid was dried under vacuum. Yield: 4.1 g (95%). Calculated for $C_{54}H_{45}Br_2P_3Ru$: C, 61.90; H, 4.33; Br, 15.25%. Found: C, 61.79; H, 4.26; Br, 15.11%.

$^{31}P\{^1H\}$ NMR (C_7D_8, –79 °C): δ_A = 78.2 (1P, $^2J_{AX}$ = unresolved), δ_X = 24.1 (2P, $^2J_{AX}$ = unresolved). Also, observed are δ = –6.6 (free PPh_3) and δ_A = 59.0, δ_B = 51.0, $^2J_{AB}$ = unresolved ($Ru_2Br_4(PPh_3)_4$).

The physical and spectroscopic data for this complex agree with those reported in the literature.[20,23,35]

Dark-orange crystals of **10** were isolated from a filtrate in the preparation of $RuBr_2(DPPB)(PPh_3)$ (Section 2.5.3.3). The solution consisted of CH_2Br_2 / ethanol / hexanes (~ 1:12:4), plus a large amount of PPh_3 from the substitution of $RuBr_2(PPh_3)_3$ by DPPB. The ORTEP plot, as well as selected bond lengths and angles of this complex, are shown in Section 3.3.3.1, while the full experimental parameters and details are given in Appendix I.

2.5.3 Mixed-Phosphine Complexes, RuX$_2$(P–P)(P(Ar)$_3$)

2.5.3.1 X = Cl, Ar = Ph, P–P = DPPB; Preparation of dichloro-(bis(diphenylphosphino)butane)(triphenylphosphine)ruthenium(II), RuCl$_2$(DPPB)(PPh$_3$) (11)[22,38,39]

The title complex was prepared by addition of a CH$_2$Cl$_2$ (20 mL) solution of DPPB (0.89 g, 2.09 mmol) to a CH$_2$Cl$_2$ (15 mL) solution of RuCl$_2$(PPh$_3$)$_3$ (2.0 g, 2.09 mmol) at room temperature. The dark-orange solution of the starting ruthenium complex turned green immediately upon addition of the phosphine. The reaction mixture was stirred for 2 h, and then concentrated to ~ 10 mL by removal of the solvent under dynamic vacuum. Ethanol (80 mL) was added to precipitate the green product, which was collected by vacuum filtration, washed with ethanol (3 x 20 mL) and hexanes (3 x 20 mL) to remove PPh$_3$, and dried under vacuum. Small amounts of the bridged-phosphine complex [RuCl$_2$(DPPB)$_{1.5}$]$_2$ have sometimes been reported to be present in the product.[38,39] In any case, this dinuclear complex can easily be removed by filtration prior to the concentration step, as it is quite insoluble in CH$_2$Cl$_2$ (discussed in Section 3.3.3). Yield: 1.8 g (97%). Calculated for RuCl$_2$(DPPB)(PPh$_3$), C$_{46}$H$_{43}$Cl$_2$P$_3$Ru: C, 64.19; H, 5.04%. Found: C, 64.34; H, 5.16%.

^{31}P{^{1}H} NMR: see Chapter 3, Table 3.6.

The physical and spectroscopic data for this complex agree with those reported in the literature.[22,38,39]

Green crystals of **11** were isolated from a C$_7$D$_8$ solution containing approximately 14 equivalents of added PPh$_3$. The crystals grew over several months by slow evaporation of C$_7$D$_8$ in a N$_2$ glove-box. The results of an X-ray crystallographic study are given in Chapter 3. The ORTEP plot, as well as selected bond lengths and angles of this complex, are shown in Section 3.3.3.2, while the full experimental parameters and details are given in Appendix II.

2.5.3.2   **X = Cl, Ar = *p*-tolyl, P–P = DPPB; Preparation of dichloro-
(bis(diphenylphosphino)butane)(tri-*p*-tolylphosphine)ruthenium(II),
RuCl₂(DPPB)(P(*p*-tolyl)₃) (12)**

This preparation was performed in the same manner as for the PPh₃ analogue
(Section 2.5.3.1). RuCl₂(P(*p*-tolyl)₃)₃ (1.0 g, 0.92 mmol) was dissolved in CH₂Cl₂ (20
mL), then DPPB (0.39 g, 0.92 mmol) was added under a flow of Ar, and the reaction
mixture was stirred at room temperature for 2 h. The initially orange solution changed to
dark green upon addition of the phosphine. In this preparation, unlike the above
preparation, some bridged-phosphine complex was present. Therefore, some insoluble
green complex (i.e., [RuCl₂(DPPB)₁.₅]₂) was removed by vacuum filtration (0.08 g or
about 10% of the ruthenium). The green filtrate was then reduced in volume to ~ 5 mL,
and ethanol (40 mL) was added to precipitate the green product. The complex was
isolated by vacuum filtration, washed with ethanol (2 x 10 mL) and hexanes (3 x 10 mL),
and dried under vacuum. Yield: 0.83 g (76%). Calculated for RuCl₂(DPPB)(P(*p*-tolyl)₃),
C₄₉H₄₉Cl₂P₃Ru: C, 65.19; H, 5.47; Cl, 7.85%. Found: C, 64.91; H, 5.36; Cl, 7.65%.

^{31}P{^{1}H} NMR: see Chapter 3, Table 3.6.

^{1}H NMR (C₆D₆, 20 °C): δ 1.38 (4H, br m, PCH₂C*H*₂ of DPPB), 2.02 (9H, s, C*H*₃
of *p*-tolyl), 2.92 (4H, br m, PC*H*₂ of DPPB), 6.65–7.95 (32H, m, 20H of Ph of DPPB and
12H of Ph of P(*p*-tolyl)₃).

2.5.3.3   **X = Br, Ar = Ph, P–P = DPPB; Preparation of dibromo-
(bis(diphenylphosphino)butane)(triphenylphosphine)ruthenium(II),
RuBr₂(DPPB)(PPh₃) (13)**

This bromo analogue was prepared in much the same manner as the chloro
derivative, the only difference being that the reaction was performed in methylene
bromide and on a smaller scale. RuBr₂(PPh₃)₃ (0.52 g, 0.49 mmol) and DPPB (0.20 g,
0.48 mmol) were dissolved in CH₂Br₂ (10 mL) and the mixture was stirred for 2 h at
room temperature. The originally deep-red solution changed to a yellow-orange colour

over the course of the reaction. The reaction mixture was reduced to ~ 5 mL in volume and ethanol (40 mL) was added to precipitate the product. An olive solid was collected by vacuum filtration, washed with ethanol (2 x 10 mL) and hexanes (2 x 10 mL), and finally dried under vacuum. Yield: 0.45 g (97%). Calculated for $RuBr_2(DPPB)(PPh_3)$, $C_{46}H_{43}Br_2P_3Ru$: C, 58.18; H, 4.56; Br, 16.83%. Found: C, 58.04; H, 4.64; Br, 16.76%.

$^{31}P\{^1H\}$ NMR: see Chapter 3, Table 3.6.

2.5.3.4 X = Cl, Ar = Ph, P–P = DCYPB; Preparation of dichloro-(bis(dicyclohexylphosphino)butane)(triphenylphosphine)ruthenium(II), $RuCl_2(DCYPB)(PPh_3)$ (14)

An attempt to prepare the title complex was made using the same method employed for the DPPB mixed-phosphine analogues **11-13**. The starting complex $RuCl_2(PPh_3)_3$ (0.26 g, 0.27 mmol) and DCYPB (0.12 g, 0.26 mmol) were dissolved in CH_2Cl_2 (10 mL) to give a dark-green solution. The dark-green colour was thought to be due to the formation of the desired $RuCl_2(DCYPB)(PPh_3)$ complex. However, attempts to isolate the material by adding ethanol (30 mL) after stirring the green solution for 2 h at room temperature resulted in an immediate colour change to orange-brown. Repeated attempts to isolate the green solid from a variety of solvent pairs were unsuccessful. A red solid was eventually precipitated by the addition of methanol (10 mL) to a CH_2Cl_2 solution (5 mL) of the above mixture. The solid was collected by vacuum filtration, washed with methanol (3 x 2 mL), and dried under vacuum. Calculated for $Ru_2Cl_4(DCYPB)_2 \cdot CH_2Cl_2$, C, 51.47; H, 8.03%. Found: C, 51.26; H, 8.23%.

The red solid was quite insoluble in $CDCl_3$, CD_2Cl_2, and C_6D_6, making $^{31}P\{^1H\}$ NMR spectroscopy impossible.

A subsequent in situ experiment was performed on a CH_2Cl_2 solution of a 1:1 mixture of $RuCl_2(PPh)_3$ and DCYPB. The low-temperature $^{31}P\{^1H\}$ NMR data of the resulting solution (see Chapter 3, Table 3.6) indicated the presence of the desired $RuCl_2(DCYPB)(PPh_3)$. However, within 24 h, the NMR solution had become orange. In

fact, after several weeks, red crystals deposited from the solution. However, an attempt at an X-ray diffraction study proved unsuccessful as the crystals did not diffract.

2.5.3.5   X = Cl, Ar = Ph, P–P = (*R*)-BINAP; Preparation of dichloro((*R*)-2,2'-bis(diphenylphosphino)-1,1'-binaphthyl)(triphenylphosphine)-ruthenium(II), RuCl$_2$((*R*)-BINAP)(PPh$_3$) (15)[22,39,40]

The title complex was prepared by a method similar to the one developed in this laboratory, except on a larger scale.[22,39] A CH$_2$Cl$_2$ solution (35 mL) of RuCl$_2$(PPh$_3$)$_3$ (1.0 g, 1.05 mmol) and (*R*)-BINAP (0.65 g, 1.05 mmol) was stirred at room temperature for 24 h. The resulting orange-red solution was concentrated at the pump to ~ 15 mL, and diethyl ether (60 mL) added to precipitate the product. The orange-brown solid was collected by vacuum filtration, washed with diethyl ether (3 x 10 mL) and hexanes (3 x 10 mL), and dried under vacuum. Yield: 0.99 g (89%). Calculated for C$_{62}$H$_{47}$Cl$_2$P$_3$Ru: C, 70.46; H, 4.48%. Found: C, 69.95; H, 4.54%.

^{31}P{^{1}H} NMR: see Chapter 3, Table 3.6.

The physical and spectroscopic data agree with those reported.[22,39,40] One notable exception is that the colour of the product isolated by Mezzetti et al.[40] was dark green, as opposed to the orange-brown solid obtained by the above preparation. However, the dark-green product obtained by Mezzetti et al. was isolated from toluene / ethanol, as opposed to the solvents used above, and the same dark-green colour is seen for other five-coordinate Ru(II) complexes (i.e., RuCl$_2$(DPPB)(PPh$_3$) and RuCl$_2$(DIOP)(PPh$_3$)).[22,38]

2.5.4   Preparation of [Ru$_2$X$_5$(PPh$_3$)$_4$]⁻ or [(PPh$_3$)$_2$XRu(μ-X)$_3$RuX(PPh$_3$)$_2$]⁻ Complexes; X = Cl or H

2.5.4.1   X = Cl; [(DMA)$_2$H]$^+$ [Ru$_2$Cl$_5$(PPh$_3$)$_4$]⁻ or [(DMA)$_2$H]$^+$ [(PPh$_3$)$_2$ClRu(μ-Cl)$_3$RuCl(PPh$_3$)$_2$]⁻ (16)

The ionic, title complex was prepared by modification of a route reported[35,41,42] for the neutral dimer, [Ru$_2$Cl$_4$(PPh$_3$)$_4$]. This ionic species has been observed previously

in solution but never isolated.[24,35,42] As in the preparation of the neutral dimeric complex, $RuCl_3(PPh_3)_2DMA \cdot DMA$ (0.19 g, 0.21 mmol) was stirred under an atmosphere of H_2 in DMA (10 mL) for 5 days. The green suspension/solution of the Ru(III) starting complex became a deep-red solution after ~ 30 min of stirring at room temperature under H_2. In the original preparation of the neutral complex, the solution was reduced in volume to ~ 5 mL, and MeOH (75 mL) was added to "break up" the ionic species that exists in solution. The neutral species was then isolated as an orange solid. In the case of this preparation, where the ionic Ru complex was the desired product, the solution was reduced in volume to ~ 5 mL, and diethyl ether (20 mL) was added to precipitate an orange solid. Precipitation of the product was slow. Therefore, after the addition of diethyl ether, the solution had to be left stirring overnight under H_2 for any solid to appear. The orange product was collected by vacuum filtration, washed with diethyl ether (3 x 5 mL), and dried under vacuum. Yield: 0.13 g (78%). Calculated for $[(DMA)_2H]^+$ $[Ru_2Cl_5(PPh_3)_4]^-$, $C_{80}H_{79}N_2Cl_5O_2P_4Ru_2$: C, 59.91; H, 4.96; N, 1.75; Cl, 11.05%. Found: C, 59.64; H, 5.00; N, 1.70; Cl, 10.90%.

$^{31}P\{^1H\}$ NMR (C_7D_8): δ 44.6, s from –85 to 20 °C.

^1H NMR (C_7D_8, –40 °C): δ 2.02 (6H, br s, CH_3 of DMA), 2.25 (6H, br s CH_3 of DMA), 2.68 (6H, br s, CH_3 of DMA), 6.8–7.9 (60H, m, Ph of PPh$_3$), 8.0 (1H, br s , (DMA)$_2H^+$).

2.5.4.2 X = Cl and H; Attempted Preparation of [PSH]$^+$ [Ru$_2$H$_3$Cl$_2$(PPh$_3$)$_4$]$^-$ or [PSH]$^+$ [(PPh$_3$)$_2$(H)Ru(μ-H)(μ-Cl)$_2$Ru(H)(PPh$_3$)$_2$]$^-$ Isolation of [(η^2-H$_2$)(PPh$_3$)$_2$Ru(μ-H)(μ-Cl)$_2$Ru(H)(PPh$_3$)$_2$] (17)

An excess of Proton Sponge (0.20 g, 0.93 mmol) and [(DMA)$_2$H]$^+$ [Ru$_2$Cl$_5$(PPh$_3$)$_4$]$^-$ (0.38 g, 0.24 mmol) were dissolved in C_6H_6 (5 mL) to give a deep red-brown solution. This solution was placed under an atmosphere of H_2 and stirred at room temperature for two days. The reaction mixture slowly became deep red in colour. The solution was washed through a layer of Celite with benzene (4 x 5 mL) to remove

PSH$^+$Cl$^-$, reduced in volume to ~ 5 mL, and diethyl ether (30 mL) was added to precipitate a red solid. The product was collected by vacuum filtration, washed with diethyl ether (3 x 5 mL), and dried under vacuum. Yield: 0.27 g (84%). Calculated for [PSH]$^+$ [(PPh$_3$)$_2$(H)Ru(μ-H)(μ-Cl)$_2$Ru(H)(PPh$_3$)$_2$]$^-$, C$_{86}$H$_{82}$N$_2$Cl$_2$P$_4$Ru: C, 67.05; H, 5.36; N, 1.82; Cl, 4.60%. Found: C, 65.80; H, 5.05; N, 0.00%. Calculated for [(η^2-H$_2$)(PPh$_3$)$_2$Ru(μ-H)(μ-Cl)$_2$Ru(H)(PPh$_3$)$_2$], C$_{72}$H$_{64}$Cl$_2$P$_4$Ru$_2$: C, 65.21; H, 4.86; N, 0.00%.

The product isolated is not the desired ionic complex, but rather the previously prepared molecular hydrogen complex.[24,35,41,43] Although the above elemental analysis is approximately 0.6% high in carbon, it is the best that has been reported.[41,43] The red product is reasonably difficult to handle because it turns brown on exposure to air. This may explain the elemental analysis being somewhat lower in carbon and hydrogen than the expected values.

^{31}P{^{1}H} NMR (C$_6$D$_6$, 20 °C): δ = 71.1 (br s), 45.9 (br s).

^{1}H NMR (C$_6$D$_6$, 20 °C): δ –12.8 (4H, br s, η^2-H$_2$, μ-*H*, terminal-*H*; all exchanging), 6.6–7.8 (60H, m, Ph of PPh$_3$).

2.5.4.3   X = Cl and H; [(DMA)$_2$H]$^+$ [Ru$_2$H$_3$Cl$_2$(PPh$_3$)$_4$]$^-$ or [(DMA)$_2$H]$^+$ [(PPh$_3$)$_2$(H)Ru(μ-H)(μ-Cl)$_2$Ru(H)(PPh$_3$)$_2$]$^-$ (18)

A deep-red solution containing both a pink solid and a large dark-red crystal (see below) was left by a previous worker, Dr. A. Joshi, and was worked up in the following manner. The deep-red solution and pink solid were removed from the crystal by transferring them to a sintered glass filter via a cannula under a flow of Ar. The pink solid was washed with diethyl ether (3 x 5 mL) and dried under vacuum. Yield: 0.25 g. The pink solid proved to be [DMAH]$^+$[Ru$_2$Cl$_5$(DPPB)$_2$]$^-$. The microanalytical and spectroscopic data for this complex are given in Section 2.5.9.3.

The starting materials used by Joshi for this reaction were thought to be $RuCl_3(PPh_3)_2(DMA) \cdot DMA$ solvate and one equiv of DPPB in DMA. The presence of DMA as the solvent was confirmed by ^1H NMR. Considering the nature of both the products and Ru(III) starting complex, it seems likely that the reaction was performed under an atmosphere of H_2.

The large, red crystal was submitted to Dr. S. Rettig of this department for X-ray diffraction analysis. A small crystal, cleaved from the large isolated crystal, was used for the crystallographic study. The red crystal proved to be $[(DMA)_2H]^+[(PPh_3)_2(H)Ru(\mu-H)(\mu-Cl)_2Ru(H)(PPh_3)_2]^-$. The ORTEP plot, as well as selected bond lengths and angles of this complex, are shown in Section 4.7.1, while the full experimental parameters and details are given in Appendix VI. Calculated for $[(DMA)_2H]^+[(PPh_3)_2(H)Ru(\mu-H)(\mu-Cl)_2Ru(H)(PPh_3)_2]^-$, $C_{80}H_{82}N_2Cl_2O_2P_4Ru_2$: C, 64.04; H, 5.51; N, 1.87; Cl, 4.73%. Found: C, 64.08; H, 5.44; N, 1.79; Cl, 4.50%.

IR (KBr, cm^{-1}): $v_{(C=O)}$ at 1647; v 2114, 1975, 1902, 1825 (all broad and weak).

$^{31}P\{^1H\}$ NMR (C_7D_8, 20 °C): δ = 71.3 (br s), 46.3 (br s); (C_7D_8, –89 °C): $\delta_{A,B,C,D}$ = 79.6, 63.8, 62.5, 30.2 plus δ_A = 71.9, δ_B = 68.7, $^2J_{AB}$ = 44.2 Hz.

The ABCD spin system corresponds to that observed for $[(\eta^2-H_2)(PPh_3)_2Ru(\mu-H)(\mu-Cl)_2Ru(H)(PPh_3)_2]$,[24,35,41,43] while the AB pattern, which accounts for < 15% of the integration, must correspond to the title ionic complex. At 20 °C, the AB pattern is observed at δ_A = 56.8, δ_B = 54.7, $^2J_{AB}$ ~ 30 Hz.

^1H NMR (C_7D_8, 20 °C): δ –12.8 (4H, br s, exchanging hydrides), 1.8 (6H, s, CH_3 of DMA), 2.3 (6H, s, CH_3 of DMA), 2.7 (6H, s, CH_3 of DMA), 6.6–8.1 (60H, m, Ph of PPh$_3$).

^1H NMR (C_7D_8, –89 °C): δ –8.7 (1H, br d, $^2J_{PH}$ = 66.9 Hz, μ-H), –12.6 (1H, br s, η^2-H_2), –17.3 (1H, br s, terminal-H) plus –14.9 (t, $^2J_{PH}$ = 31.1 Hz), –17.7 (br s). The first three resonances are those of $[(\eta^2-H_2)(PPh_3)_2Ru(\mu-H)(\mu-Cl)_2Ru(H)(PPh_3)_2]$, while the

remaining two resonances must belong to $[(DMA)_2H]^+[(PPh_3)_2(H)Ru(\mu-H)(\mu-Cl)_2Ru(H)(PPh_3)_2]^-$.

Attempts to measure the UV-vis spectrum of **18** in DMA or C_6H_6 were not successful, as the dark-red crystals dissolved to give green-black solutions, indicating oxidation of the complex. Chau et al. have also observed these green-black solutions for Ru(II) species in the presence of O_2.[4,44] Conductivity measurements were also impossible, as no anaerobic cell was available.

The above ionic complex had been previously prepared from $RuCl_3(PPh_3)_2(DMA)\cdot DMA$ solvate in DMA solvent in this laboratory; the product was incorrectly formulated as the neutral Ru(III) classical hydride species, $[(PPh_3)_2(H)Ru(\mu-H)(\mu-Cl)_2Ru(H)_2(PPh_3)_2]\cdot 2DMA$ solvate.[24,35] When the complex is prepared in a solvent other than DMA (i.e., C_7H_8) in the presence of Proton Sponge, the η^2-H_2 species **17** is isolated.[43,45] This complex will be described and discussed in detail in Chapter 4.

2.5.5 Synthesis of Diphosphine-Bridged Dinuclear Ruthenium(II) Complexes, $[(P–P)X_2Ru(\mu_2-(P–P))RuX_2(P–P)]$ or $[RuX_2(P–P)_{1.5}]_2$; X = Cl, Br; P–P = DPPB, DCYPB

Several diphosphine-bridged, dinuclear ruthenium complexes have previously been synthesized: $[RuCl_2(DPPB)_{1.5}]_2$,[22,46] $[RuCl_2(DIOP)_{1.5}]_2$,[23,47] $[RuCl_2(DPPN)_{1.5}]_2$,[22] and $[RuCl_2(DPPH)_{1.5}]_2$.[22] In a typical procedure, $RuCl_2(PPh_3)_3$ (0.10 g, 0.10 mmol) was stirred with two equivalents of a diphosphine in C_6H_6 (25 mL) for 1 h at room temperature under argon. The resulting dark-green solution was reduced in volume to ~ 5 mL, and hexanes (20 mL) were added to precipitate a green solid. The green product was collected by filtration, washed with hexanes (4 x 10 mL), and dried under vacuum. All of these diphosphine-bridged complexes are essentially insoluble in most non-aromatic solvents, and only sparingly soluble in aromatic solvents. The insolubility of **19**, **20**, and **21** (see below) prevented the measurement of either the ^1H or

$^{31}P\{^1H\}$ NMR spectra. These bridged species are also occasionally isolated as a side-product in the preparation of RuX$_2$(P–P)(PAr$_3$) species (Section 2.5.3).

2.5.5.1 X = Cl, P–P = DPPB; [(DPPB)Cl$_2$Ru(μ_2-(DPPB))RuCl$_2$(DPPB)] or [RuCl$_2$(DPPB)$_{1.5}$]$_2$ (19)[22,46]

The above procedure was followed, except on twice the scale. A C$_6$H$_6$ solution of RuCl$_2$(PPh$_3$)$_3$ (0.20 g, 0.21 mmol) and DPPB (0.18 g, 0.42 mmol) was used. Yield of the green solid: 0.15 g (89%). Calculated for [RuCl$_2$(DPPB)$_{1.5}$]$_2$, C$_{84}$H$_{84}$Cl$_4$P$_6$Ru$_2$: C, 62.15; H, 5.22%. Found: C, 61.86; H, 5.38%.

UV-vis (C$_6$H$_6$): λ_{max} (nm), ε_{max} (M^{-1} cm^{-1}) = 340, 4520; 450, 3950; 684, 1320.

The physical and spectroscopic data for this complex agree with those reported in the literature.[22,46]

2.5.5.2 X = Br, P–P = DPPB; [(DPPB)Br$_2$Ru(μ_2-(DPPB))RuBr$_2$(DPPB)] or [RuBr$_2$(DPPB)$_{1.5}$]$_2$ (20)

The general procedure outlined for the chloro-analogue was followed using RuBr$_2$(PPh$_3$)$_3$ (0.10 g, 0.095 mmol) and DPPB (0.081 g, 0.19 mmol). Yield of the mustard solid: 0.053 g (61%). Calculated for [RuBr$_2$(DPPB)$_{1.5}$]$_2$, C$_{84}$H$_{84}$Br$_4$P$_6$Ru$_2$: C, 56.01; H, 4.70; Br, 17.74%. Found: C, 56.27; H, 4.58; Br, 17.52%.

UV-vis (C$_6$H$_6$): λ_{max} (nm), ε_{max} (M^{-1} cm^{-1}) = 364, 2580; 466, 3620; 710, 1170.

2.5.5.3 X = Cl, P–P = DCYPB; [(DCYPB)Cl$_2$Ru(μ_2-(DCYPB))RuCl$_2$(DCYPB)] or [RuCl$_2$(DCYPB)$_{1.5}$]$_2$ (21)

The general procedure outlined in Section 2.5.5 was followed using RuCl$_2$(PPh$_3$)$_3$ (0.18 g, 0.19 mmol) and DCYPB (0.18 g, 0.40 mmol). Yield of the green solid: 0.13 g (77%). Calculated for [RuCl$_2$(DCYPB)$_{1.5}$]$_2$, C$_{84}$H$_{156}$Cl$_4$P$_6$Ru$_2$: C, 59.49; H, 9.27; Cl, 8.36%. Found: C, 59.40; H, 9.33; Cl, 8.08%.

UV-vis (C$_6$H$_6$): λ_{max} (nm), ε_{max} (M^{-1} cm^{-1}) = 340, 5080; 384, 3870 (sh); 682, 1940.

2.5.6 Dichloro-tri-µ-chloro-bis(bidentate phosphine)diruthenium(II, III) Complexes, [(P–P)ClRu(µ-Cl)₃RuCl(P–P)] or Ru₂Cl₅(P–P)₂[21,22,39,48]

A hexanes suspension (160 mL) of $RuCl_3(PAr_3)_2(DMA)\cdot DMA$ solvate (1.5 g), where Ar = phenyl or *p*-tolyl, and one equivalent of the appropriate diphosphine was refluxed under a slow flow of argon for 24 h. The red-brown solids that resulted were collected by vacuum filtration and washed thoroughly with hexanes (8 x 20 mL) to remove any PPh₃. The crude products were then reprecipitated by washing through the frit with CH_2Cl_2 (25 mL), concentrating the CH_2Cl_2 solution to ~ 5 mL, and then adding diethyl ether (40 mL). Yields of the $Ru_2^{II,III}Cl_5(P-P)_2$ complexes were typically 70-85%.

2.5.6.1 Preparation of Ru₂Cl₅(DPPB)₂ (22)[21,22,39,48]

The above general procedure was followed with $RuCl_3(PPh_3)_2(DMA)\cdot DMA$ solvate (1.7 g, 1.9 mmol) and DPPB (0.82 g, 1.9 mmol). Yield of the brick-red solid: 0.99 g (85%). Calculated for $Ru_2Cl_5(DPPB)_2$, $C_{56}H_{56}Cl_5P_4Ru_2$: C, 54.58; H, 4.58; Cl, 14.38%. Found: C, 54.60; H, 4.52; Cl, 14.50%.

The Evans method ($CDCl_3$) gives $\chi_{mol} = 1.82 \times 10^{-3}$ cgsu; $\mu_{eff} = 2.05$ μ_B / Ru₂, a 2% *t*-butanol solution in $CDCl_3$ being used for this measurement. This method is described in the literature;[6] however, one should note that the equation originally described by Evans is for a conventional magnet where the magnetic field is perpendicular to the long axis of the NMR tube. The magnets used in the spectrometers in this department are superconducting, with the polarizing magnetic field along the long axis of the NMR tube. Therefore, the first term of the equation originally described by Evans must be multiplied by –2 to obtain χ from the measured data and eventually calculate μ_{eff}. The negative sign being necessary as the shift observed with the use of a superconduting magnet is downfield while that of a conventional magnet is upfield. This is described in more detail in the literature.[7]

The physical and spectroscopic data for this complex agree with those reported in the literature.[21,22,48]

2.5.6.2 Preparation of Ru$_2$Cl$_5$((*R*)-BINAP)$_2$ (23)[5,22,39]

The above general procedure was followed with RuCl$_3$(P(*p*-tolyl)$_3$)$_2$(DMA)·DMA solvate (0.67 g, 0.68 mmol) and (*R*)-BINAP (0.44 g, 0.71 mmol). Yield of the red-brown solid: 0.43 g (76%). Calculated for Ru$_2$Cl$_5$((*R*)-BINAP)$_2$·H$_2$O, C$_{88}$H$_{66}$Cl$_5$OP$_4$Ru$_2$: C, 64.34; H, 4.05%. Found: C, 64.35; H, 4.29%. A solvate of DMA instead of H$_2$O has also been reported.[5]

The physical and spectroscopic data for this complex agree with those reported in the literature.[22,39]

2.5.7 Dihalo-di-μ-halo-bis(bidentate phosphine)diruthenium(II) Complexes, [(P–P)XRu(μ-X)$_2$RuX(P–P)] or Ru$_2$X$_4$(P–P)$_2$; X = Cl, Br, I; P–P = DPPB, BINAP

The chloro derivative, Ru$_2$Cl$_4$(P–P)$_2$, was prepared by either a previously reported route from Ru$_2$Cl$_5$(P–P)$_2$, or by a new route from the mixed phosphine complexes, RuCl$_2$(DPPB)(PAr$_3$), where Ar = phenyl or *p*-tolyl. The bromo analogue, Ru$_2$Br$_4$(P–P)$_2$, was prepared from RuBr$_2$(DPPB)(PPh$_3$), or from Ru$_2$Cl$_4$(DPPB)$_2$, by metathesis with Me$_3$SiBr. Also, the Ru$_2$X$_4$(DPPB)$_2$ species (X = Cl, Br, or I) could be prepared in situ by the reaction of HX with Ru(DPPB)(η^3-Me-allyl)$_2$. The synthetic preparations for all three compounds are outlined below. The dinuclear complexes were stored in Schlenk tubes under Ar because the species are quite air-sensitive even in the solid state. On exposure to air, the orange-brown complexes became dark green over periods of hours to days in the solid state, and within minutes in solution.

2.5.7.1 X = Cl, P–P = DPPB; Preparation of Ru$_2$Cl$_4$(DPPB)$_2$ (24)

Method 1

The ruthenium(II, II) dinuclear complex was prepared by H$_2$ reduction of the corresponding ruthenium(II, III) dinuclear complex. Typically, Ru$_2$Cl$_5$(DPPB)$_2$ (1.0 g, 0.81 mmol) was suspended in DMA (20 mL) in a large Schlenk tube under an

atmosphere of H_2, and the reaction mixture was stirred at room temperature. After 1 h, the solution was clear orange. To ensure complete reduction of the mixed-valence starting material, the Schlenk tube was refilled with H_2 after 18 h, and the mixture was stirred for another 6 h. The volume of the solution was then reduced to ~ 5 mL, and methanol (40 mL) was added to precipitate an orange-brown solid. The solid was collected by vacuum filtration, washed with methanol (2 x 5 mL) and diethyl ether (2 x 5 mL), and dried under vacuum. Yield: 0.71 g (73%).

Method 2

Alternatively, compound **24** could be prepared by a new method from $RuCl_2(DPPB)(PPh_3)$ or $RuCl_2(DPPB)(P(p\text{-tolyl})_3)$. A benzene solution (5 mL) of $RuCl_2(DPPB)(PPh_3)$ (0.19 g, 0.22 mmol) with added H_2O (5 mL) was refluxed under argon. The dark-green two-layer mixture became orange after 1 h. The mixture was cooled, the C_6H_6 layer transferred via a cannula to a Schlenk tube, and the H_2O layer washed several times with C_6H_6 (2 x 2 mL). The washings were added to the second Schlenk tube, the solution was reduced in volume to ~ 5 mL, and hexanes (30 mL) were added to precipitate a bright-orange solid. This solid was collected by vacuum filtration, washed with MeOH (2 x 5 mL) and hexanes (5 x 5 mL), and dried under vacuum. Yield: 0.099 g (75%). Calculated for $Ru_2Cl_4(DPPB)_2$, $C_{56}H_{56}Cl_4P_4Ru_2$: C, 56.20; H, 4.72%. Found: C, 56.20; H, 4.78%. The orange solid turned brown after drying under vacuum at 78 °C for 24 h. Other workers from this laboratory have noted that the product is hygroscopic.[5,21,22,39] In this case, the calculated values are for $Ru_2Cl_4(DPPB)_2 \cdot H_2O$, $C_{56}H_{56}Cl_4P_4Ru_2 \cdot H_2O$: C, 55.36; H, 4.81%. Found: C, 55.43; H, 4.89%.[5]

Subsequently, the procedure was shortened somewhat by adding hexanes (5 mL) directly to the two-phase mixture to precipitate the orange solid. The product was then simply collected by vacuum filtration and washed as above.

$^{31}P\{^{1}H\}$ NMR $(C_6D_6, 20 °C)$: $\delta_A = 64.7$, $\delta_B = 55.6$, $^2J_{AB} = 47.3$ Hz.

$(CDCl_3, 20 °C)$: $\delta_A = 63.5$, $\delta_B = 54.3$, $^2J_{AB} = 46.9$ Hz.

$(CD_2Cl_2, 20\ °C)$: $\delta_A = 64.2$, $\delta_B = 56.0$, $^2J_{AB} = 46.8$ Hz.

$(C_7D_8, 20\ °C)$: $\delta_A = 64.7$, $\delta_B = 55.5$, $^2J_{AB} = 46.9$ Hz.

The spectroscopic data agree with those for the dimer isolated by the alternative preparation from $Ru_2Cl_5(DPPB)_2$ described above.[21,22,39]

Method 3

Finally, the title complex could be prepared conveniently in situ from the reaction of HCl with $Ru(DPPB)(\eta^3\text{-Me-allyl})_2$. To a C_6D_6 or $CDCl_3$ NMR solution of $Ru(DPPB)(\eta^3\text{-Me-allyl})_2$ (0.6 mL, ~ 55 mM) was added 2.2 equiv of HCl (0.26 mL of a 0.239 M MeOH solution) at room temperature. The initially yellow solution immediately became orange on addition of HCl. After several minutes, the solution had become red. A $^{31}P\{^1H\}$ NMR spectrum showed an AB quartet corresponding to **24** and a broad singlet at 57.6 ppm in C_6D_6. No starting material was evident (see Section 3.3.4.2).

2.5.7.2 X = Br, P–P = DPPB; Preparation of $Ru_2Br_4(DPPB)_2$ (25)

Method 1

The title complex was prepared by the same method as for the above chloro dimer, but using $RuBr_2(DPPB)(PPh_3)_3$ (0.20 g, 0.21 mmol) as the starting material. An orange-brown solid was isolated. Yield: 0.12 g (86%). Calculated for $Ru_2Br_4(DPPB)_2 \cdot 3H_2O$, $C_{56}H_{56}Br_4P_4Ru_2 \cdot 3H_2O$: C, 47.07; H, 4.37%. Found: C, 47.02; H, 4.20%.

$^{31}P\{^1H\}$ NMR $(C_6D_6, 20\ °C)$: $\delta_A = 66.4$, $\delta_B = 56.8$, $^2J_{AB} = 43.7$ Hz.

$(C_7D_8, 20\ °C)$: $\delta_A = 66.7$, $\delta_B = 57.0$, $^2J_{AB} = 45.2$ Hz.

Method 2

Alternatively, the complex **25** could be prepared by metathesis of the analogous chloride dimer **24**. To a C_6H_6 solution (5 mL) of $Ru_2Cl_4(DPPB)_2$ (81 mg, 0.068 mmol) was added Me_3SiBr (200 μL, 1.52 mmol) under a flow of Ar. The originally pale-orange solution became dark orange in colour on addition of Me_3SiBr. After being stirred for

18 h at room temperature, the resulting red-brown solution was pumped to dryness. The brown solid was washed with hexanes (2 x 5 mL) and dried under vacuum. Yield: 0.050 g (54%).

The spectroscopic data were the same as those recorded for the solid isolated by method 1.

2.5.7.3   X = Cl, P–P = (*R*)-BINAP; Preparation of Ru$_2$Cl$_4$((*R*)-BINAP)$_2$ (26)[5,22,39]

A mixture of Ru$_2$Cl$_5$((*R*)-BINAP)$_2$·H$_2$O (0.19 g, 0.12 mmol) and poly(4-vinylpyridine) (0.86 g, 70 monomer equivalents) was stirred in C$_6$H$_6$ (15 mL) under an atmosphere of H$_2$ for 24 h. The orange-red suspension was filtered to remove poly(4-vinylpyridine) hydrochloride, washed with C$_6$H$_6$ (2 x 4 mL), and the filtrate reduced in volume to ~ 1 mL. Hexanes (20 mL) were added to precipitate an orange-brown solid, which was collected by vacuum filtration, washed with hexanes (3 x 5 mL), and dried under vacuum. Yield: 0.18 g (78%). Calculated for Ru$_2$Cl$_4$((*R*)-BINAP)$_2$ C$_{88}$H$_{64}$Cl$_4$P$_4$Ru$_2$: C, 66.50; H, 4.06; Cl, 8.92%. Found: C, 66.45; H, 4.11; Cl, 6.22%.

^{31}P{^{1}H} NMR (C$_6$D$_6$, 20 °C): δ_A = 75.6, δ_B = 72.3, $^2J_{AB}$ = 44.3 Hz; δ = 51.4, s.

^{1}H NMR (C$_6$D$_6$, 20 °C, hydride region): δ –14.0 (t, $^2J_{HP}$ = 29.9 Hz).

The AB quartet accounts for ~70% of the total integration. The ^{31}P{^{1}H} NMR data and chloride analysis (see Section 4.6.2) do not agree with the data determined previously for the complex Ru$_2$Cl$_4$((*R*)-BINAP)$_2$.[22,39]

2.5.7.4   X = I, P–P = DPPB; Preparation of Ru$_2$I$_4$(DPPB)$_2$ (27)

To a CDCl$_3$ NMR solution of Ru(DPPB)(η^3-Me-allyl)$_2$ (~ 47 mM) was added 2.2 equiv of HI (0.17 mL of a 0.302 M MeOH solution) at room temperature. The initial yellow solution became a red-brown suspension on addition of HI. The red-brown product was not very soluble in CDCl$_3$ / MeOH; however, a ^{31}P{^{1}H} NMR spectrum could be recorded. The complex 27 was even less soluble in C$_6$D$_6$.

$^{31}P\{^1H\}$ NMR (CDCl$_3$ / MeOH, 20 °C): $\delta_A = 70.1$, $\delta_B = 55.6$, $^2J = 39.9$ Hz.

2.5.8 Chlorotri(μ-chloro)(ligand)bis(1,4-bis(diphenylphosphino)butane)-diruthenium(II) Complexes, [(L)(DPPB)Ru(μ-Cl)$_3$RuCl(DPPB)] or Ru$_2$Cl$_4$(P–P)$_2$(L)

2.5.8.1 L = NEt$_3$: [(NEt$_3$)(DPPB)Ru(μ-Cl)$_3$RuCl(DPPB)] (28)[22,39]

The title compound was prepared by stirring RuCl$_2$(DPPB)(PPh$_3$) (0.50 g, 0.59 mmol) with an excess of NEt$_3$ (5.0 mL, 35.9 mmol) in benzene (25 mL) for 48 h at room temperature. The initially green solution slowly changed to an orange-brown solution. The work-up consisted of reducing the volume to ~ 5 mL at the pump, followed by the addition of hexanes (40 mL) to precipitate an orange solid. The solid was collected on a filter, washed with ethanol (2 x 10 mL) and hexanes (2 x 10 mL), and dried under vacuum. Yield: 0.25 g (65%). Calculated for [(NEt$_3$)(DPPB)Ru(μ-Cl)$_3$RuCl(DPPB)], C$_{62}$H$_{71}$NCl$_4$P$_4$Ru$_2$: C, 57.37; H, 5.51; N, 1.08%. Found: C, 56.78; H, 5.38; N, 0.97%.

$^{31}P\{^1H\}$ NMR (CDCl$_3$, 20 °C): 48.9, s.

^1H NMR (CDCl$_3$, 20 °C): δ 1.09 (9H, br m, C*H*$_3$CH$_2$N), 1.30 (4H, br m, C*H*$_2$ of DPPB), 1.69 (4H, br m, C*H*$_2$ of DPPB), 2.16 (4H, br m, C*H*$_2$ of DPPB), 3.00 (4H, br m, C*H*$_2$ of DPPB), 3.18 (6H, br m, CH$_3$C*H*$_2$N), 6.80–7.95 (40H, m, Ph of DPPB).

The physical and spectroscopic data for this complex agree with those reported.[22,39]

2.5.8.2 L = py: [(py)(DPPB)Ru(μ-Cl)$_3$RuCl(DPPB)] (29)

The title complex was prepared in situ by the addition of one equivalent of pyridine (0.5 μL, 6 μmol) to a CDCl$_3$ solution (0.6 mL) of Ru$_2$Cl$_4$(DPPB)$_2$ (7.58 mg, 6 μmol). The initially clear-orange solution became darker upon the addition of py.

$^{31}P\{^1H\}$ NMR (CDCl$_3$, 20 °C): $\delta_A = 54.3$, $\delta_B = 45.0$, $^2J_{AB} = 36.4$ Hz, $\delta_C = 52.6$, $\delta_D = 51.6$, $^2J_{CD} = 42.7$ Hz.

^{1}H NMR (CDCl$_3$, 20 °C): δ 1.2–3.1 (15H, m, CH_2 of DPPB), 3.98 (1H, m, CH of CH$_2$ of DPPB), 6.33–8.67 (45H, m, 40H of Ph of DPPB and 5H of py).

2.5.8.3   L = HNEt$_2$: [(HNEt$_2$)(DPPB)Ru(μ-Cl)$_3$RuCl(DPPB)] (30)

Diethylamine (5 mL) was added to a green suspension of RuCl$_2$(DPPB)(PPh$_3$) (0.20 g, 0.23 mmol) in C$_6$H$_6$ (5 mL). The resulting mixture was refluxed for 2 h. Hexanes (30 mL) were added to the cooled orange solution to precipitate the orange-brown product. The solid was collected by vacuum filtration, washed with hexanes, and dried under vacuum. Yield: 0.06 g (40%). Calculated for [(HNEt$_2$)(DPPB)Ru(μ-Cl)$_3$RuCl(DPPB)], C$_{60}$H$_{67}$NCl$_4$P$_4$Ru$_2$: C, 56.74; H, 5.32; N, 1.10%. Found: C, 56.65; H, 5.96; N, 1.46%.

^{31}P{^{1}H} NMR (CDCl$_3$, 20 °C): δ 48.9, s.

^{1}H NMR (CDCl$_3$, 20 °C): δ 1.31 (6H, t, J = 10.3 Hz, CH_3 of HNEt$_2$), 1.40 (4H, br m, CH_2 of DPPB), 1.72 (4H, br m, CH_2 of DPPB), 2.15 (4H, br m CH_2 of DPPB), 2.90 (4H, br m, CH_2 of DPPB), 2.95 (4H, q, J = 10.3 Hz, CH_2 of HNEt$_2$), 6.8–7.8 (40H, m, Ph of DPPB), 8.0 (1H, br s, HNEt$_2$).

2.5.8.4   L = acetone: [(acetone)(DPPB)Ru(μ-Cl)$_3$RuCl(DPPB)]·acetone solvate (31)[21,22,39]

The title complex was prepared by modifying a preparation previously employed in this laboratory.[21,22,39] A suspension of Ru$_2$Cl$_4$(DPPB)$_2$ (0.20 g, 0.17 mmol) in acetone (10 mL) was stirred at room temperature for 24 h. The orange solid was collected by vacuum filtration, washed with diethyl ether (2 x 5 mL), and dried under vacuum. Yield: 0.18 g (82%).

Care must be taken in degassing the solvents prior to use because the starting complex reacts with both O$_2$ and N$_2$.

^{31}P{^{1}H} NMR (C$_6$D$_6$, 20 °C): δ$_A$ = 53.7, δ$_B$ = 51.3, $^2J_{AB}$ = 42.7 Hz; δ$_C$ = 50.8, δ$_B$ = 49.6, $^2J_{AB}$ = 38.5 Hz.

. The physical and spectroscopic data for this complex agree with those reported in the literature.[21,22,39]

2.5.8.5 L = acetophenone: [(acetophenone)(DPPB)Ru(μ-Cl)₃RuCl(DPPB)] (32)

The dinuclear complex $Ru_2Cl_4(DPPB)_2$ (83 mg, 0.069 mmol) was dissolved in CH_2Cl_2 (5 mL) and acetophenone (5 mL). The dark-orange solution was stirred at room temperature for 4 h, and then diethyl ether (30 mL) and hexanes (10 mL) were added to precipitate a dark-orange solid. The solid was collected by vacuum filtration, washed with hexanes (6 x 3 mL), and dried under vacuum. Yield: 48 mg (52%). Calculated for [(acetophenone)(DPPB)Ru(μ-Cl)₃RuCl(DPPB)], $C_{64}H_{64}Cl_4OP_4Ru_2$: C, 58.37; H, 4.90%. Found: C, 57.58; H, 4.84%.

IR (KBr pellet, cm⁻¹): $\nu_{(C=O)}$ at 1679 (s); (CH_2Cl_2 solution, cm⁻¹): $\nu_{(C=O)}$ at 1683 (s).

$^{31}P\{^1H\}$ NMR (C_6D_6, 20 °C): δ_A = 53.7, δ_B = 52.7, $^2J_{AB}$ = 43.9 Hz; δ_C = 52.1, δ_D = 47.5, $^2J_{CD}$ = 37.4 Hz.

^1H NMR (C_6D_6, 20 °C): δ 2.04 (CH_3 of acetophenone).

UV-vis (C_6H_6): λ_{max} (nm), ε_{max} (M⁻¹ cm⁻¹) = 364, 3320; 484 (sh), 815; (CH_2Cl_2): 366, 3300; 484 (sh), 690.

2.5.8.6 L = DMSO: [(DMSO)(DPPB)Ru(μ-Cl)₃RuCl(DPPB)] (33)

An excess of DMSO (170 μL, 2.3 mmol) was added to a dark-green suspension of $RuCl_2(DPPB)(PPh_3)$ (0.18 g, 0.21 mmol) in C_6H_6 (5 mL). The originally green mixture became bright orange after refluxing for 1 h under argon. The solution was cooled, and hexanes (30 mL) added to precipitate a yellow-orange solid. This solid was collected on a sintered glass filter, washed with hexanes (5 x 5 mL) to remove PPh₃, and dried under vacuum. Yield: 0.12 g (87%). Calculated for [(DMSO)(DPPB)Ru(μ-Cl)₃RuCl(DPPB)] , $C_{58}H_{62}Cl_4OP_4Ru_2S$: C, 54.64; H, 4.90%. Found: C, 54.45; H, 5.10%.

IR (Nujol, cm⁻¹): $\nu_{(S=O)}$ at 1090 (s, S-bonded DMSO).

^{31}P$\{^1$H$\}$ NMR (C$_6$D$_6$, 20 °C): δ_A = 53.9, δ_B = 52.9, $^2J_{AB}$ = 43.8 Hz; δ_C = 42.5,

δ_D = 33.7, $^2J_{CD}$ = 29.6 Hz.

(CDCl$_3$, 20 °C): δ_A = 54.2, δ_B = 51.2, $^2J_{AB}$ = 42.8 Hz; δ_C =

42.2, δ_D = 29.5, $^2J_{CD}$ = 30.2 Hz.

^{1}H NMR (CDCl$_3$, 20 °C): δ 0.65–2.32 (21H, m, 15H of C*H*$_2$ of DPPB and 6H of

C*H*$_3$ of DMSO), 3.50 (1H, br m, C*H* of CH$_2$ DPPB), 6.78 (3H, m, Ph of DPPB), 6.94–

7.96 (34H, m, Ph of DPPB), 8.47 (3H, m, Ph of DPPB).

(C$_6$D$_6$, 20 °C): δ 0.50–2.50 (16H, m, 10H of C*H*$_2$ of DPPB and 6H of

C*H*$_3$ of DMSO), 2.74 (1H, m, C*H* of CH$_2$ DPPB), 3.29 (3H, m, C*H*$_2$ DPPB), 3.51 (2H,

m, C*H*$_2$ of DPPB), 6.67 (4H, t, *J* = 6.9 Hz, Ph of DPPB), 6.80 (16H, m, Ph of DPPB),

7.34 (3H, t, *J* = 8.3 Hz, Ph of DPPB), 7.47 (5H, br m, Ph of DPPB), 7.61 (2H, t, *J* = 6.8

Hz, Ph of DPPB), 7.74 (2H, t, *J* = 8.0 Hz, Ph of DPPB), 8.07 (4H, pseudo q, *J* = 8.9 Hz,

Ph of DPPB), 8.18 (2H, t, *J* = 8.3 Hz, Ph of DPPB), 8.67 (2H, t, *J* = 8.0 Hz, Ph of DPPB).

UV-vis (C$_6$H$_6$): λ_{max} (nm), ε_{max} (M^{-1} cm^{-1}) = 378, 3010; 470 (sh), 590;

(CH$_2$Cl$_2$): 376, 2900; 470 (sh), 650; (C$_7$H$_8$): 378, 3010; 472 (sh), 610.

This compound has been prepared previously from a different starting material

(*cis*-RuCl$_2$(DMSO)$_4$).[22,39] The above IR and ^{31}P$\{^1$H$\}$ NMR spectroscopic data agree

with those reported in the literature.[22,39] The UV-visible and ^{1}H NMR data have not been

reported before.

2.5.8.7   L = DMS: [(DMS)(DPPB)Ru(μ-Cl)$_3$RuCl(DPPB)] (34)

An excess of dimethyl sulfide (106 μL, 1.44 mmol) was added to a dark-green

suspension of RuCl$_2$(DPPB)(PPh$_3$) (0.17 g, 0.20 mmol) in C$_6$H$_6$ (5 mL). The resulting

mixture was stirred at room temperature (in a sealed Schlenk tube because of the smell

and volatility of DMS) under an atmosphere of Ar for 4 h; the syntheses of the other

sulfide and sulfoxide analogues were performed at reflux temperatures under a slow flow

of Ar (Sections 2.5.8.6, 2.5.8.8, and 2.5.8.9). An orange-brown product was precipitated

by the addition of hexanes (30 mL). This solid was collected by vacuum filtration, washed with hexanes (5 x 5 mL), and dried under vacuum. Yield: 0.11 g (87%). Calculated for [(DMS)(DPPB)Ru(μ-Cl)$_3$RuCl(DPPB)] , $C_{58}H_{62}Cl_4P_4Ru_2S$: C, 55.33; H, 4.96; Cl, 11.26; S, 2.55%. Found: C, 55.48; H, 4.88; Cl, 11.11; S, 2.57%.

$^{31}P\{^1H\}$ NMR   (CDCl$_3$, 20 °C): $\delta_{A,B}$ = 51.3, unresolved AB pattern; δ_C = 48.2, δ_D = 46.0, $^2J_{CD}$ = 35.6 Hz.

(C$_6$D$_6$, 20 °C): δ_A = 52.5, δ_B = 51.8, $^2J_{AB}$ = 44.1 Hz; δ_C = 48.6, δ_D = 46.2, $^2J_{CD}$ = 35.3 Hz.

^{1}H NMR   (CDCl$_3$, 20 °C): δ 0.82–2.75 (20H, m, 14H of CH_2 of DPPB and 6H of CH_3 of DMS), 3.13 (1H, m, CH of CH$_2$ DPPB), 3.70 (1H, br m, CH of CH$_2$ DPPB), 6.65–7.80 (35H, m, Ph of DPPB), 8.04 (2H, t, J = 7.8, Ph of DPPB), 8.33 (3H, m, Ph of DPPB).

(C$_6$D$_6$, 20 °C): δ 0.52–2.75 (20H, m, 14H of CH_2 of DPPB and 6H of CH_3 of DMS), 3.35 (1H, br m, CH of CH$_2$ DPPB), 4.12 (1H, br m, CH of CH$_2$ DPPB), 6.68–7.85 (32H, m, Ph of DPPB), 8.15 (4H, m, Ph of DPPB), 8.70 (4H, m, Ph of DPPB).

UV-vis (C$_6$H$_6$): λ_{max} (nm), ε_{max} (M^{-1} cm^{-1}) = 374, 3780; 460 (sh), 730; (CH$_2$Cl$_2$): 372, 3470; 460 (sh), 660.

2.5.8.8   L = TMSO: [(TM$\underline{S}$O)(DPPB)Ru(μ-Cl)$_3$RuCl(DPPB)] (35)

The title product was synthesized in the same manner as the DMSO analogue (Section 2.5.8.6). An excess of tetramethylene sulfoxide (TMSO, 210 µL, 2.32 mmol) was added to a dark-green suspension of RuCl$_2$(DPPB)(PPh$_3$) (0.190 g, 0.221 mmol) in C$_6$H$_6$ (5 mL). The originally green mixture became bright orange after refluxing for 1.5 h under argon. The solution was cooled, and hexanes (30 mL) added to precipitate a pale-orange solid. The solid was collected on a sintered glass filter, washed with hexanes (5 x 5 mL) to remove PPh$_3$, and dried under vacuum. Yield: 0.11 g (70%). Calculated for

[(TM$\underline{S}$O)(DPPB)Ru(μ-Cl)$_3$RuCl(DPPB)] , $C_{60}H_{64}Cl_4OP_4Ru_2S$: C, 55.39; H, 4.96; Cl, 10.90; S, 2.46%. Found: C, 55.11; H, 5.20; Cl, 10.71; S, 2.60%.

IR (Nujol or KBr pellet, cm^{-1}): $\nu_{(S=O)}$ at 1093 (s, $\underline{S}$-bonded TMSO).

^{31}P{^{1}H} NMR   (C$_6$D$_6$, 20 °C): δ_A = 55.1, δ_B = 52.2, $^2J_{AB}$ = 42.8 Hz; δ_C = 44.2, δ_D = 29.1, $^2J_{CD}$ = 29.0 Hz.

(CDCl$_3$, 20 °C): δ_A = 54.7, δ_B = 50.8, $^2J_{AB}$ = 41.1 Hz; δ_C = 43.4, δ_D = 26.3, $^2J_{CD}$ = 27.8 Hz.

^{1}H NMR   (CDCl$_3$, 20 °C): δ 0.65–3.10 (20H, m, 12H of CH_2 of DPPB and 8H of CH_2 of TMSO), 3.26 (3H, br m, CH_2 DPPB), 3.73 (1H, br m, CH of CH$_2$ DPPB), 6.61 (3H, br m, Ph of DPPB), 7.00–8.12 (35H, m, Ph of DPPB), 8.51 (2H, br m, Ph of DPPB).

(C$_6$D$_6$, 20 °C): δ 0.30 (23H, m, 15H of CH_2 of DPPB and 8H of CH_2 of TMSO), 3.82 (1H, br m, CH of CH$_2$ DPPB), 6.6–8.48 (39H, m, Ph of DPPB), 8.74 (1H, br m, Ph of DPPB).

UV-vis (C$_6$H$_6$): λ_{max} (nm), ε_{max} (M^{-1} cm^{-1}) = 376, 2470; 460 (sh), 830; (CH$_2$Cl$_2$): 374, 2410; 460 (sh), 600.

2.5.8.9   L = THT: [(THT)(DPPB)Ru(μ-Cl)$_3$RuCl(DPPB)] (36)

The title product was synthesized in the same manner as the DMSO analogue (Section 2.5.8.6). An excess of tetrahydrothiophene (THT, 180 µL, 2.0 mmol) was added to a dark-green suspension of RuCl$_2$(DPPB)(PPh$_3$) (0.18 g, 0.21 mmol) in C$_6$H$_6$ (5 mL). The originally green mixture became bright orange after refluxing for 1 h under argon. The solution was cooled and hexanes (30 mL) added to precipitate a orange-brown solid. The solid was collected on a sintered glass filter, washed with hexanes (5 x 5 mL) to remove PPh$_3$, and dried under vacuum. Yield: 0.12 g (90%). Calculated for [(THT)(DPPB)Ru(μ-Cl)$_3$RuCl(DPPB)] , $C_{60}H_{64}Cl_4P_4Ru_2S$: C, 56.08; H, 5.02. Found: C, 56.61; H, 5.13%.

The elemental analysis was found to be slightly high in carbon, probably as a result of using unpurified THT, which is known to commonly contain impurities. Reprecipitation of this material did not improve the elemental analysis.

$^{31}P\{^{1}H\}$ NMR (CDCl$_3$, 20 °C): δ_A = 51.9, δ_B = 51.2, $^{2}J_{AB}$ = 43.2 Hz; δ_C = 49.1, δ_D = 46.7, $^{2}J_{CD}$ = 36.1 Hz.

(C$_6$D$_6$, 20 °C): $\delta_{A,B}$ = 52.3, unresolved AB pattern; δ_C = 49.5, δ_D = 47.1, $^{2}J_{CD}$ = 36.1 Hz.

^{1}H NMR (CDCl$_3$, 20 °C): δ 0.85–2.90 (22H, m, 14H of CH_2 of DPPB and 8H of CH_2 of THT), 3.20 (1H, br m, CH of CH$_2$ DPPB), 3.69 (1H, br m, CH of CH$_2$ DPPB), 6.78–7.75 (35H, m, Ph of DPPB), 8.07 (2H, t, J = 8.8, Ph of DPPB), 8.30 (3H, m, Ph of DPPB).

(C$_6$D$_6$, 20 °C): δ 0.50–2.75 (22H, m, 14H of CH_2 of DPPB and 8H of CH_2 of THT), 3.39 (1H, br m, CH of CH$_2$ DPPB), 4.10 (1H, br m, CH of CH$_2$ DPPB), 6.72–7.80 (32H, m, Ph of DPPB), 8.20 (4H, br m, Ph of DPPB), 8.65 (4H, br m, Ph of DPPB).

UV-vis (C$_6$H$_6$): λ_{max} (nm), ε_{max} (M^{-1} cm^{-1}) = 374, 3700; 460 (sh), 605; (CH$_2$Cl$_2$): 372, 3200; 460 (sh), 440.

2.5.9 Preparation of [Ru$_2$Cl$_5$(DPPB)$_2$]$^-$ or [(DPPB)ClRu(μ-Cl)$_3$RuCl(DPPB)]$^-$ Complexes

2.5.9.1 [H$_2$N(n-Oct)$_2$]$^+$ [Ru$_2$Cl$_5$(DPPB)$_2$]$^-$ or [H$_2$N(n-Oct)$_2$]$^+$ [(DPPB)ClRu(μ-Cl)$_3$RuCl(DPPB)]$^-$ (37)

An excess of tri-n-octylamine (5 mL, 11 mmol) was added to a dark-green suspension of RuCl$_2$(DPPB)(PPh$_3$) (0.19 g, 0.22 mmol) in C$_6$H$_6$ (5 mL). After the solution was refluxed for 16 h under a slow flow of Ar, the volume of the orange suspension was reduced to ~ 5 mL, and hexanes (30 mL) were added to precipitate more product. The orange product was collected by vacuum filtration, washed with ethanol (2 x 5 mL) and hexanes (5 x 5 mL), and dried under vacuum. Yield: 0.063 g (40%, based on

Ru content). Calculated for [H$_2$N(n-Oct)$_2$]$^+$ [Ru$_2$Cl$_5$(DPPB)$_2$]$^-$, C$_{72}$H$_{92}$NCl$_5$P$_4$Ru$_2$: C, 58.64; H, 6.29; N, 0.95; Cl, 12.02%. Found: C, 58.55; H, 6.17; N, 0.90; Cl, 12.20%.

^{31}P{^{1}H} NMR   (CDCl$_3$, 20 °C): δ = 48.9, s.

(C$_6$D$_6$, 20 °C): δ = 49.2, s.

^{1}H NMR (CDCl$_3$, 20 °C): δ = 0.97 (6H, t, J = 8.8 Hz, –CH$_2$CH_3), 1.40 (24H, m, 20H for –CH$_2$(CH_2)$_5$CH$_3$ and 4H for CH_2 of DPPB), 1.70 (8H, m, 4 each of CH_2 of DPPB and H$_2$NCH$_2$CH_2CH$_2$–), 2.15 (4H, br m, CH_2 of DPPB), 2.90 (4H, m, H$_2$NCH_2CH$_2$–), 2.95 (4H, br m, CH_2 of DPPB), 6.9–7.6 (40H, m, Ph of DPPB), 7.9 (2H, br s, HN$_2$CH$_2$–).

UV-vis (CH$_2$Cl$_2$): λ$_{max}$ (nm), ε$_{max}$ (M^{-1} cm^{-1}) = 316, 5080; 374, 3190; 486, 590.

2.5.9.2   [H$_2$N(n-Bu)$_2$]$^+$ [Ru$_2$Cl$_5$(DPPB)$_2$]$^-$ or [H$_2$N(n-Bu)$_2$]$^+$ [(DPPB)ClRu(μ-Cl)$_3$RuCl(DPPB)]$^-$ (38)

The title complex was prepared in exactly the same manner as the octyl analogue, except that tri-n-butylamine (5 mL, 21 mmol) was added to RuCl$_2$(DPPB)(PPh$_3$) (0.19 g, 0.22 mmol) in C$_6$H$_6$ (5 mL). The isolated product was orange like the octyl analogue. Yield: 0.070 g (44%, based on Ru content). Calculated for [H$_2$N (n-Bu)$_2$]$^+$ [Ru$_2$Cl$_5$(DPPB)$_2$]$^-$, C$_{64}$H$_{76}$NCl$_5$P$_4$Ru$_2$: C, 56.41; H, 5.62; N, 1.03; Cl, 13.01%. Found: C, 56.47; H, 5.59; N, 0.98; Cl, 13.29%.

^{31}P{^{1}H} NMR   (CDCl$_3$, 20 °C): δ = 48.8, s.

(CD$_2$Cl$_2$, –98 °C): δ = 48.8, s.

^{1}H NMR (CDCl$_3$, 20 °C): δ = 0.97 (6H, t, –CH$_2$CH_3), 1.35 (4H, m, –CH$_2$CH_2CH$_3$), 1.40 (4H, m, CH_2 of DPPB), 1.65 (4H, m, H$_2$NCH$_2$CH_2CH$_2$–), 1.75 (4H, br m, CH_2 of DPPB), 2.15 (4H, br m, CH_2 of DPPB), 2.90 (4H, m, H$_2$NCH_2CH$_2$–), 2.95 (4H, br m, CH_2 of DPPB), 6.9–7.6 (40H, m, Ph of DPPB), 7.9 (2H, br s, HN$_2$CH$_2$–).

UV-vis (C$_7$H$_8$): λ$_{max}$ (nm), ε$_{max}$ (M^{-1} cm^{-1}) = 372, 3300; 484, 590; (CH$_2$Cl$_2$): 316, 5330; 374, 3250; 484, 590.

2.5.9.3 [DMAH]⁺ [Ru₂Cl₅(DPPB)₂]⁻ or [DMAH]⁺ [(DPPB)ClRu(μ-Cl)₃RuCl(DPPB)]⁻ (39)

A pink solid isolated from a reaction mixture left by a previous worker in this laboratory, Dr. A. Joshi, proved to be the title complex (see Section 2.5.4.3). As outlined in Section 2.5.4.3, the reaction mixture most probably contained $RuCl_3(PPh_3)_2(DMA) \cdot DMA$ solvate and 1 equiv of DPPB in DMA under an atmosphere of H_2. Yield: 0.25 g. Calculated for [DMAH]⁺ [(DPPB)ClRu(μ-Cl)₃RuCl(DPPB)]⁻, $C_{60}H_{66}NCl_5OP_4Ru_2$: C, 54.58; H, 5.04; N, 1.06; Cl, 13.42%. Found: C, 54.96; H, 5.06; N, 0.90; Cl, 13.47%.

IR (KBr, cm⁻¹): $\nu_{(C=O)}$ between 1623–1652 (br, m).

³¹P{¹H} NMR (CDCl₃, 20 °C): δ = 48.9, s.

(C₆D₆, 20 °C): δ = 49.2, s.

¹H NMR (CDCl₃, 20 °C): δ = 1.58 (4H, br m, CH_2 of DPPB), 1.65 (4H, br m, CH_2 of DPPB), 2.05 (3H, s, CH_3 of DMA), 2.15 (2H, br m, CH_2 of DPPB), 2.55 (4H, br m, CH_2 of DPPB), 2.88 (2H, br m, CH_2 of DPPB), 2.90 (3H, s, CH₃ of DMA), 3.00 (3H, s, CH₃ of DMA), 6.7–7.6 (40H, m, Ph of DPPB), 8.2 (1H, br s, DMAH).

UV-vis (CH₂Cl₂): λ_{max} (nm), ε_{max} (M⁻¹ cm⁻¹) = 316, 5990; 374, 3770; 480, 880.

The title complex has previously been prepared in this laboratory by another route.[21,49] The Ru starting material in this case was Ru₂Cl₅(DPPB)₂, and the reaction was performed in DMA solvent under an atmosphere of H₂.

2.5.9.4 [H₂N(n-Bu)₂]⁺ [Ru₂Cl₅((R)-BINAP)₂]⁻ or [H₂N(n-Bu)₂]⁺ [((R)-BINAP)ClRu(μ-Cl)₃RuCl((R)-BINAP)]⁻ (40)

An excess of tri-n-butylamine (5 mL, 21 mmol) was added to an orange suspension of RuCl₂((R)-BINAP)(PPh₃) (0.13 g, 0.12 mmol) in C₆H₆ (5 mL). After the solution was refluxed for 20 h under a slow flow of Ar, the volume of the orange solution was reduced to ~ 5 mL, and hexanes (10 mL) were added to precipitate the product. The orange solid was collected by vacuum filtration, washed with hexanes (4 x 5 mL), and

dried under vacuum. Yield: 0.080 g (70%, based on Ru content). Calculated for [H$_2$N(n-Bu)$_2$]$^+$ [Ru$_2$Cl$_5$((R)-BINAP)$_2$]$^-$·2H$_2$O, C$_{96}$H$_{88}$NCl$_5$O$_2$P$_4$Ru$_2$: C, 64.38; H, 4.95; N, 0.78%. Found: C, 64.24; H, 4.78; N, 0.68%.

^{31}P{^{1}H} NMR (CDCl$_3$, 20 °C): δ_A = 55.1, δ_B = 51.6, $^2J_{AB}$ = 37.6 Hz.

(C$_6$D$_6$, 20 °C): δ_A = 54.9, δ_B = 51.9, $^2J_{AB}$ = 38.5 Hz.

^{1}H NMR (CDCl$_3$, 20 °C): δ 1.05 (6H, t, J = 8.8 Hz, –CH$_2$CH_3), 1.45 (4H, m, –CH$_2$CH_2CH$_3$), 1.87 (4H, m, NCH$_2$CH_2CH$_2$–), 2.40 (1H, br m, H$_2$NCH_2CH$_2$–), 2.95 (2H, br m, H$_2$NCH_2CH$_2$–), 3.25 (1H, br m, H$_2$NCH_2CH$_2$–), 6.1–8.1 (64H, m, aromatic protons of BINAP), 8.5 (2H, br s, H_2NCH$_2$–). H$_2$O was observed at 1.5 ppm.

UV-vis (CH$_2$Cl$_2$): λ_{max}, ε_{max} (M^{-1} cm^{-1}) = 334 (sh), 13700; 400 (sh), 4700. The UV-visible spectrum is relatively featureless.

2.5.9.5   [HNEt$_3$]$^+$[Ru$_2$Cl$_5$(DPPB)$_2$]$^-$ or [HNEt$_3$]$^+$[(DPPB)ClRu(μ-Cl)$_3$RuCl(DPPB)]$^-$ (41)

The title complex was isolated as an orange solid, a by-product in the preparation of the trinuclear species [Ru(H)Cl(DPPB)]$_3$ (Section 2.5.10.1). Yield: 0.13 g (24%). Calculated for [HNEt$_3$]$^+$[Ru$_2$Cl$_5$(DPPB)$_2$]$^-$, C$_{62}$H$_{72}$NCl$_5$P$_4$Ru$_2$: C, 55.80; H, 5.44; N, 1.05; Cl, 13.28%. Found: C, 55.73; H, 5.49; N, 0.97; Cl, 12.95%.

^{31}P{^{1}H} NMR (CDCl$_3$, 20 °C): 49.0, s.

^{1}H NMR (CDCl$_3$, 20 °C): δ 1.05 (9H, br m, CH_3 of HNEt$_3$), 1.36 (4H, br m, CH_2 of DPPB), 1.72 (4H, br m CH_2 of DPPB), 2.15 (4H, br m, CH_2 of DPPB), 3.01 (4H, br m, CH_2 of DPPB), 3.15 (6H, br m CH_3 of HNEt$_3$), 6.8–7.7 (40H, m, Ph of DPPB), 7.85 (1H, t, J = 9 Hz, HNEt$_3$).

2.5.10   Synthesis of Chlorohydrido(bidentate phosphine)ruthenium(II) Trimers, [Ru(H)Cl(P–P)]$_3$

The title triruthenium-chlorohydrido complexes containing DPPB and S,S-CHIRAPHOS were first isolated in low yields (5–10%) by Thorburn in this laboratory.[49]

The yield of these reactions was improved (to 50%) by Joshi[22] by changing the order of addition of the reagents H_2 and NEt_3. Originally, triethylamine was added to the diruthenium starting material $Ru_2Cl_4(DPPB)_2$, followed by the addition of dihydrogen.

2.5.10.1 P–P = DPPB; [Ru(H)Cl(DPPB)]₃ (42)[22,49]

Method 1

A benzene solution (30 mL) of $Ru_2Cl_4(DPPB)_2$ (0.49 g, 0.41 mmol) was stirred under an atmosphere of H_2 for 1 h at room temperature. Triethylamine (deoxygenated, 0.11 mL, 0.86 mmol) was then added via a syringe under a blanket of H_2. The orange-red suspension/solution was stirred under H_2 for 36 h at room temperature, with the Schlenk tube being refilled with dihydrogen after the first 18 h. The $NEt_3 \cdot HCl$ produced was collected by vacuum filtration on a bed of Celite, washed with C_6H_6 (5 mL), and the red-brown filtrate was reduced in volume to ~ 10 mL. Hexanes (15 mL) was added to precipitate an orange solid $[HNEt_3]^+[Ru_2Cl_5(DPPB)_2]^-$ (Section 2.5.9.5), which was collected by filtration, washed with a 1:1 mixture of benzene/hexanes (10 mL), and finally washed with hexanes (2 x 5 mL). The hexanes washes were not added to the filtrate as were the 1:1 mixture of C_6H_6 / hexanes washings. The filtrate was then reduced in volume to ~ 5 mL, followed by addition of hexanes (15 mL) to precipitate a brown solid. The brown product, $[Ru(H)Cl(DPPB)]_3$, was collected by vacuum filtration, washed with hexanes (2 x 5 mL), and dried under vacuum. Yield of the triruthenium species, $[Ru(H)Cl(DPPB)]_3$: 0.25 g (54%). Calculated for $C_{84}H_{87}Cl_3P_6Ru$: C, 59.63; H, 5.18; Cl, 6.29%. Found: C, 59.65; H, 5.36; Cl, 6.23%.

$^{31}P\{^1H\}$ NMR (C_6D_6, 20 °C): $\delta_A = 71.7$, $\delta_B = 48.3$, $\delta_C = 68.9$, $\delta_D = 61.6$, $\delta_E = 59.5$, $\delta_F = 57.3$. All resonances show unresolved *cis*-coupling constants. The six resonances have been paired previously into AB quartets on the basis of line-shape[49] and selective phosphorus decoupled-proton NMR studies.[22] Figure 3.11 (Section 3.2) shows the molecular structure of $[Ru(H)Cl(DPPB)]_3$.

^{1}H NMR (C_6D_6, 20 °C, hydride region): δ –21.9 (1H, t, $^2J_{PH}$ = 32.1 Hz, terminal hydride coupled to P_A and P_B), –21.1 (1H, m, bridging hydride coupled to P_A, P_B, P_E, and P_F), –17.7 (1H, t, $^2J_{PH}$ = 32.1 Hz, terminal hydride coupled to P_C and P_D); see Figure 3.11 for phosphorus assignment.

T_1 measurements in C_6D_6 (300 MHz, 20.0 °C): δ –21.9 (275 ± 10 ms), –21.1 (390 ± 20 ms), –17.7 (390 ± 10 ms).

Mass spectrum (FAB, matrix: 3-nitrobenzylalcohol) [m/z]: 1692±4 [M+H]$^+$.

Method 2

An alternative route to the title triruthenium complex **42** was from $Ru_2Cl_4(DPPB)_2(NEt_3)$.

$Ru_2Cl_4(DPPB)_2(NEt_3)$ (0.33 g, 0.25 mmol) was added to a C_6H_6 solution (10 mL) which had been presaturated with H_2. One equivalent of NEt_3 (35 µL, 0.25 mmol) was then added to the resulting orange suspension. The reaction mixture which was contained in a glass liner was placed in an autoclave and pressurized to 1000 psi with H_2. The contents were stirred at room temperature for 4 days. The resulting orange-brown solution was handled under Ar following the work-up outlined above. Yield: 0.11 g (40%). The spectroscopic data were as given above.

The physical and spectroscopic data for this complex agree with those reported in the literature.[22,49] The T_1 data have not been measured previously.

2.5.11   Preparation of Ruthenium(II) Amine Complexes from RuCl₂(PPh₃)₃, RuCl₂(DPPB)(PPh₃), and [RuCl₂(DPPB)₁.₅)]₂

2.5.11.1   Preparation of dichloro(bis(diphenylphosphino)butane)-bis(pyridine)ruthenium(II), RuCl₂(DPPB)(py)₂ (43)

Method 1

An excess of pyridine (190 µL, 2.3 mmol) was added to a dark-green suspension of RuCl₂(DPPB)(PPh₃) (0.18 g, 0.21 mmol) in C_6H_6 (5 mL). The solution became orange

after refluxing for 1.5 h under a slow flow of Ar. The solution was cooled, and hexanes (30 mL) added to precipitate a mustard-coloured solid. The solid was collected on a sintered glass filter, washed with hexanes (5 x 5 mL) to remove PPh_3, and dried under vacuum. Yield: 0.13 g (82%). Solvated benzene could be removed from the solid by heating under vacuum in a Abderhalden drying apparatus at 78 °C, after the solid was finely divided in a mortar and pestle. Calculated for $RuCl_2(DPPB)(py)_2$, $C_{38}H_{38}N_2Cl_2P_2Ru$: C, 60.32; H, 5.06; N, 3.70; Cl, 9.37%. Found: C, 50.94; H, 5.10; N, 3.53; Cl, 9.20%.

$^{31}P\{^1H\}$ NMR   (C_6D_6, 20 °C): $\delta = 41.5$, s.

($CDCl_3$, 20 °C): $\delta = 40.4$, s.

(CD_2Cl_2, 20 °C): $\delta = 40.4$, s.

^1H NMR   (C_6D_6, 20 °C): δ 1.63 (4H, br m, $PCH_2CH_2CH_2$ of DPPB), 3.15 (4H, br m, $PCH_2(CH_2)_2CH_2P$ of DPPB), 6.17 (4H, t, $J = 7.9$ Hz, *meta*-py), 6.55 (2H, t, $J = 7.9$ Hz, *para*-py), 6.94 (12H, m, *meta*- and *para*-Ph protons of DPPB), 7.92 (8H, m, *ortho*-Ph protons of DPPB), and 9.40 (4H, d, $J = 5.3$ Hz, *ortho*-py).

($CDCl_3$, 20 °C): δ 1.67 (4H, br m, $PCH_2CH_2CH_2$ of DPPB), 3.03 (4H, br m, $PCH_2(CH_2)_2CH_2P$ of DPPB), 6.64 (4H, br m, *meta*-py), 6.95–7.20 (12H, m, *meta*- and *para*-Ph protons of DPPB), 7.22 (2H, br m, *para*-py), 7.61 (8H, m, *ortho*-Ph of DPPB), 8.85 (4H, br m, *ortho*-py).

UV-vis (CH_2Cl_2): λ_{max} (nm), ε_{max} (M^{-1} cm^{-1}) = 462, 430; 672, 90; (C_6H_6) = 458, 492; 678, 96.

Conductivity data in MeOH and CH_3NO_2 are given in Table 5.2 (Section 5.2).

Method 2

The title complex was also prepared from a different Ru starting material, $[RuCl_2(DPPB)_{1.5}]_2$, following a synthetic procedure by Batista et al.[50,51] To a CH_2Cl_2 suspension (10 mL) of $[RuCl_2(DPPB)_{1.5}]_2$ (0.28 g, 0.17 mmol) was added an excess of pyridine (140 µL, 1.7 mmol). The resulting mustard-coloured mixture was stirred at room

temperature for 4 h. The solution was then reduced to 1–2 mL at the pump, and diethyl ether (15 mL) added to precipitate the mustard product. The solid was collected by vacuum filtration, washed with diethyl ether (6 x 5 mL), and dried under vacuum. Yield: 0.23 g (87%). The physical and spectroscopic data are the same as those determined for the product isolated from the other preparation outlined above.

2.5.11.2 Preparation of dichloro(bis(diphenylphosphino)butane)-bipyridylruthenium(II), RuCl₂(DPPB)(bipy) (44)

Method 1

An excess of 2,2'-bipyridine (0.36 g, 2.3 mmol) was added to a dark-green suspension of RuCl₂(DPPB)(PPh₃) (0.20 g, 0.23 mmol) in C_6H_6 (5 mL). The mixture immediately turned a cloudy red colour. The solution was refluxed for 1 h under a flow of Ar. The solution was cooled, and hexanes (15 mL) added to precipitate more red solid. The solid was collected on a sintered glass filter, washed with hexanes (5 x 5 mL) to remove PPh₃, and dried under vacuum. Yield: 0.16 g (92%). Calculated for RuCl₂(DPPB)(bipy), $C_{38}H_{36}N_2Cl_2P_2Ru$: C, 60.48; H, 4.81; N, 3.71; Cl, 9.40%. Found: C, 60.57; H, 4.68; N, 3.60; Cl, 9.22%.

$^{31}P\{^1H\}$ NMR (CDCl₃, 20 °C): δ_A = 43.5, δ_B = 29.8, $^2J_{AB}$ = 32.9 Hz for the *cis* isomer and δ = 32.6, s for the *trans* isomer. The ratio of *cis* to *trans* is approximately 1:1.

^1H NMR of *trans*-**44** (CDCl₃, 20 °C): δ 1.82 (4H, br m, CH_2 of DPPB), 2.77 (4H, br m, CH_2 of DPPB), 6.67 (2H, m, H₄,₄' of bipy), 7.13 (2H, m, H₅,₅' of bipy), 7.18–7.50 (12H, m, *meta*- and *para*-Ph of DPPB), 7.77 (8H, m, *ortho*-Ph of DPPB), 7.95 (2H, d, J = 8.8 Hz, H₃,₃' of bipy), 8.60 (2H, d, J = 4 Hz, H₆,₆' of bipy).

^1H NMR of *cis*-**44** (CDCl₃, 20 °C): see Figure 5.5 (Section 5.3.1).

UV-vis (CH₂Cl₂): λ_{max} (nm), ε_{max} (M⁻¹ cm⁻¹) = 300, 12300; 346 (sh), 2600; 458, 2200; (MeOH) = 292, 15400; 436, 2600.

Conductivity data in MeOH and CH₃NO₂ are given in Table 5.2 (Section 5.2).

Method 2

The title complex was also prepared from a different Ru starting material, [RuCl$_2$(DPPB)$_{1.5}$]$_2$, following a synthetic procedure by Batista et al.[50,51] An excess of 2,2'-bipyridine (0.11 g, 0.70 mmol) was added to a CH$_2$Cl$_2$ suspension (10 mL) of [RuCl$_2$(DPPB)$_{1.5}$]$_2$ (0.26 g, 0.16 mmol). The initially green suspension, after being stirred at room temperature for 1.5 h, slowly changed to a chocolate-brown colour over a period of 1.5 h. After 4 h, the resulting red solution was reduced to 1–2 mL in volume at the pump, and diethyl ether (15 mL) was added to precipitate a brown solid, which was collected by vacuum filtration, washed with diethyl ether (6 x 5 mL), and dried under vacuum. Yield: 0.23 g (94%). The physical and spectroscopic data are the same as those determined for the product isolated from the above preparation using the starting material RuCl$_2$(DPPB)(PPh$_3$).

2.5.11.3 Preparation of dichloro(bis(diphenylphosphino)butane)(1,10-phenanthroline)ruthenium(II), RuCl$_2$(DPPB)(phen) (45)

Method 1

An excess of 1,10-phenanthroline monohydrate (0.48 g, 2.42 mmol) was added to a dark-green suspension of RuCl$_2$(DPPB)(PPh$_3$)$_3$ (0.20 g, 0.23 mmol) in C$_6$H$_6$ (5 mL). The mixture, which immediately turned a cloudy red colour, was stirred at room temperature for 1 h. The resulting red suspension was pumped to dryness, the red residue dissolved in CH$_2$Cl$_2$ (3 mL), and EtOH (40 mL) added to precipitate the red product. The solid was collected by vacuum filtration, washed with ethanol (4 x 5 mL), and dried under vacuum. Yield: 0.14 g (77%). Calculated for RuCl$_2$(DPPB)(phen), C$_{40}$H$_{36}$N$_2$Cl$_2$P$_2$Ru: C, 61.70; H, 4.66; N, 3.60; Cl, 9.11%. Found: C, 61.63; H, 4.83; N, 3.60; Cl, 9.00%.

^{31}P{^{1}H} NMR (CDCl$_3$, 20 °C): δ_A = 45.1, δ_B = 29.6, $^2J_{AB}$ = 33.7 Hz.

^{1}H NMR of *cis*-45 (CDCl$_3$, 20 °C): δ 1.25 (1H, m, C*H* of CH$_2$ of DPPB), 1.74 (1H, m, C*H* of CH$_2$ of DPPB), 1.90–2.37 (3H, m, C*H* of CH$_2$ of DPPB), 2.55 (1H, m, C*H*

of CH$_2$ of DPPB), 3.26 (1H, q, C*H* of CH$_2$ of DPPB), 4.02 (1H, m, C*H* of CH$_2$ of DPPB), 6.23–10.05 (28H, m, 20 H of Ph of DPPB and 8H of phen). A ^{1}H-^{1}H COSY spectrum in CDCl$_3$ did not allow complete assignment of the aromatic region. The ^{1}H NMR spectrum of *cis*-**45** in CDCl$_3$ is shown in Figure 5.8 (Section 5.4).

UV-vis (CH$_2$Cl$_2$): λ_{max} (nm), ε_{max} (M^{-1} cm^{-1}) = 272, 13500; 438, 3900; (MeOH) = 270, 26800; 416, 4300.

Conductivity data in MeOH and CH$_3$NO$_2$ are given in Table 5.2 (Section 5.2).

Orange crystals were isolated from an orange MeOH / CH$_2$Cl$_2$ (largely MeOH) solution which had been stored for two months in a fridge. The crystals which were suitable for X-ray diffraction studies showed *cis*-RuCl$_2$(DPPB)(phen) geometry. The ORTEP plot, as well as selected bond lengths and angles of this complex, are shown in Chapter 5, while the full experimental details and parameters are given in Appendix VII.

Method 2

The title complex was also prepared from a different Ru starting material, [RuCl$_2$(DPPB)$_{1.5}$]$_2$. An excess of 1,10-phenanthroline monohydrate (0.31 g, 1.57 mmol) and [RuCl$_2$(DPPB)$_{1.5}$]$_2$ (0.28 g, 0.17 mmol) were stirred at room temperature in CH$_2$Cl$_2$ (10 mL). The initially green suspension became cloudy red-brown over a period of 1 h. After 4 h, the clear-red solution was reduced to 1–2 mL in volume at the pump, and diethyl ether (15 mL) added to precipitate the product. The red-brown solid was collected by vacuum filtration, and washed with diethyl ether (6 x 5 mL). To completely remove the excess phenanthroline, the red-brown solid was washed through the filter with CH$_2$Cl$_2$ (5 x 5 mL), reduced in volume to 1–2 mL, and hexanes (10 mL) were added to precipitate the product. The solid, after isolation by filtration, was washed with ethanol (5 x 2 mL) and hexanes (4 x 5 mL), and dried under vacuum. Yield: 0.19 g (71%).

^{31}P{^{1}H} NMR (CDCl$_3$, 20 °C): δ_A = 45.1, δ_B = 29.6, $^2J_{AB}$ = 33.7 Hz (*cis* isomer, ~ 70%), plus δ = 32.5, s (*trans* isomer, ~30%).

2.5.11.4 Preparation of dichlorobis(pyridine)bis(triphenylphosphine)-ruthenium(II), $RuCl_2(py)_2(PPh_3)_2$ (46)[52]

Pyridine (50 μL, 0.62 mmol) was added to a suspension of $RuCl_2(PPh_3)_3$ (0.20 g, 0.21 mmol). The mixture was refluxed for 3 h. The yellow solid was collected by vacuum filtration, washed with ethanol (4 x 5 mL), and dried under vacuum. Yield: 0.16 g (88%). Calculated for $RuCl_2(py)_2(PPh_3)_2$, $C_{46}H_{40}N_2Cl_2P_2Ru$: C, 64.63; H, 4.72; N, 3.28%. Found: C, 64.52; H, 4.21; N, 2.54%.

$^{31}P\{^1H\}$ NMR (CDCl$_3$, 20 °C): δ 27.7, s (sparingly soluble).

^1H NMR (CDCl$_3$, 20 °C): δ 6.55 (4H, t, $J = 4.5$ Hz, *meta*-py), 6.87–7.56 (32H, m, 30H of Ph of PPh$_3$ and 2H of *para*-py), 8.81 (4H, d, $J = 4.5$ Hz, *ortho*-py).

The complex has been prepared previously,[52] but the NMR spectroscopic data has not been reported. The elemental analysis data are somewhat low in H and N. This may be due to the presence of a small amount of $Ru_2Cl_4(PPh_3)_4(py)$; for analogous species see Section 5.2.3.

2.5.12 Reactions of Five-Coordinate Ru(II) Complexes of the Type $RuCl_2(P)_3$ and $Ru_2Cl_4(DPPB)_2$ with Small Gas Molecules

2.5.12.1 $RuCl_2(PPh_3)_3$ with CO in the solid state

Solid $RuCl_2(PPh_3)_3$ (0.3237 g, 3.376 x 10^{-4} mol) was stirred in a vial which was placed in a large Schlenk tube (~ 190 mL in volume) under 1 atm of CO. Over a period of 1 week, the brown starting complex slowly became yellow in colour. Yield: 0.3413 g (99.63% based on $RuCl_2(CO)_2(PPh_3)_2$ + PPh$_3$; 100% should be 0.3426 g). Calculated for $RuCl_2(CO)_2(PPh_3)_2$ + PPh$_3$, $C_{56}H_{45}Cl_2O_2P_3Ru$: C, 66.27; H, 4.47; Cl, 6.97%. Found: C, 66.58; H, 4.56; Cl, 7.38%.

IR (Nujol, KBr plates; or KBr pellet, cm^{-1}): $v_{(C=O)}$ at 1944 (br, s), 1978 (br, s), 1993 (br, s) 2041 (s), 2056 (s).

cis,cis,trans (cct)-RuCl$_2$(CO)$_2$(PPh$_3$)$_2$ **(47)**

The yellow solid (~ 100 mg) obtained above was dissolved in CHCl$_3$ (5 mL) to give a yellow solution. The solution was stirred at room temperature for 1 h, at which point the solution was almost colourless. Ethanol (20 mL) was added to this solution to precipitate a white solid. The product was collected by vacuum filtration, washed with ethanol (3 x 5 mL), and dried under vacuum. The white solid was reprecipitated from CH$_2$Cl$_2$ (5 mL) and methanol (20 mL) to give an analytically pure product. Yield: ~70 mg (~70%). Calculated for RuCl$_2$(CO)$_2$(PPh$_3$)$_2$, C$_{38}$H$_{30}$Cl$_2$O$_2$P$_2$Ru: C, 60.65; H, 4.02%. Found: C, 60.68; H, 4.04%.

IR (Nujol, KBr plates, cm^{-1}): $\nu_{(C=O)}$ at 1997 (s) and 2060 (s); (CHCl$_3$ soln, NaCl cell, cm^{-1}): 1994 (s) and 2057 (s).

^{31}P{^{1}H} NMR   (CDCl$_3$, 20 °C): δ = 17.0, s.

(CD$_2$Cl$_2$, 20 °C): δ = 21.6, s.

^{1}H NMR (CDCl$_3$, 20 °C): δ 7.40 (18H, m, *ortho-* and *para*-Ph) and 7.98 (12H, m, *meta*-Ph).

The physical and spectroscopic data for this complex agree with those reported in the literature.[35,53,54]

2.5.12.2   RuCl$_2$(P(*p*-tolyl)$_3$)$_3$ with CO in the solid state

Solid RuCl$_2$(P(*p*-tolyl)$_3$)$_3$ (0.3306 g, 3.047 x 10^{-4} mol) was stirred in a vial which was placed in a large Schlenk tube (~ 190 mL in volume) under 1 atm of CO. Over several hours, the purple starting complex slowly became yellow in colour . The mixture was left stirring for 24 h, and then the product was weighed. Yield: 0.3478 g (100.0% based on RuCl$_2$(CO)$_2$(P(*p*-tolyl)$_3$)$_2$ + P(*p*-tolyl)$_3$; 100% should be 0.3477 g). Calculated for RuCl$_2$(CO)$_2$(P(*p*-tolyl)$_3$)$_2$ + P(*p*-tolyl)$_3$, C$_{65}$H$_{63}$Cl$_2$O$_2$P$_3$Ru: C, 68.41; H, 5.56%. Found: C, 68.32; H, 5.59%.

IR (KBr pellet, cm^{-1}): $\nu_{(C=O)}$ at 1944 (br, s), 1986 (br, s), and 2049 (s).

ccc- (70%) and *cct*-RuCl₂(CO)₂(P(*p*-tolyl)₃)₂ (30%) **(48)**

The above yellow solid (~ 100 mg) was stirred in CHCl₃ (5 mL) for 1 h at room temperature, and the originally yellow solution slowly faded to give an almost colourless solution. The volume of this solution was reduced at the pump to ~ 3 mL, and ethanol (20 mL) added to precipitate the product. The off-white solid was collected by vacuum filtration, washed with ethanol (3 x 5 mL), and dried under vacuum. The off-white solid was reprecipitated from CH₂Cl₂ (5 mL) and methanol (25 mL) to give an analytically pure product. Calculated for RuCl₂(CO)₂(P(*p*-tolyl)₃)₂, C₄₄H₄₂Cl₂O₂P₂Ru: C, 63.16; H, 5.06%. Found: C, 62.90; H, 5.06%.

IR (Nujol, KBr plates, cm⁻¹): $v_{(C=O)}$ at (1997 (s), 2061 (s); *cct*-isomer) and (1969 (s), 2033 (s); *ccc*-isomer); (CHCl₃ soln, NaCl cell, cm⁻¹): 1992 (s) and 2055 (s); *cct*-isomer.

³¹P{¹H} NMR (CDCl₃, 20 °C): δ = 15.5, s; *cct*-isomer.

¹H NMR (CDCl₃, 20 °C): δ 2.35 (18H, s, *para*-Me), 7.19 (12H, d, *J* = 10 Hz, *meta*-Ph), 7.82 (12H, d of d, *J* = 10 Hz and ³*J*ₕₚ = 5 Hz, *ortho*-Ph); *cct*-isomer. In CHCl₃, the *ccc*-isomer was not observed as it has isomerized to the *cct*-isomer.

2.5.12.3   RuCl₂(DPPB)(PPh₃) with CO in the solid state

This reaction was performed in the same manner as for the above mondentate triarylphosphine-containing analogues. Solid RuCl₂(DPPB)(PPh₃) (0.05984 g, 6.952 x 10⁻⁵ mol) was stirred in a vial which was placed in a large Schlenk tube under CO (1 atm). In this case, the dark-green solid became lighter as the reaction proceeded and finally (48 h) became tan. Yield: 0.06205 g (100.4% based on RuCl₂(CO)(DPPB)(PPh₃); 100% should be 0.06179 g). Calculated for RuCl₂(CO)(DPPB)(PPh₃), C₄₇H₄₃Cl₂OP₃Ru: C, 63.52; H, 4.88; Cl, 7.98%. Found: C, 63.35; H, 4.92; Cl, 7.70%.

For RuCl₂(CO)₂(DPPB) + PPh₃ (97.36%; 100% should be 0.06373 g). Calculated for C₄₈H₄₃Cl₂O₂P₃Ru: C, 62.89; H, 4.73; Cl, 7.73%.

IR (KBr pellet, cm^{-1}): $\nu_{(C=O)}$ at 1944 (br, s), 2000 (br, s), and 2070 (s).

Section 7.2.4 discusses the possible products.

2.5.12.4 Ru$_2$Cl$_4$(DPPB)$_2$ with CO in the solid state

Solid Ru$_2$Cl$_4$(DPPB)$_2$ was left stirring for 6 days under an atmosphere of CO in a large Schlenk tube. The orange starting complex slowly became lighter in colour over the 6 days, when the atmosphere of CO was removed under vacuum. The solid was then dissolved in CDCl$_3$.

IR (CDCl$_3$ soln, NaCl cell, cm^{-1}): $\nu_{(C=O)}$ at 1972 (Ru$_2$Cl$_4$(DPPB)$_2$(CO)); 2024 and 2077 (*trans*-RuCl$_2$(CO)$_2$(DPPB)).

^{31}P{^{1}H} NMR (CDCl$_3$, 20 °C): $\delta_{A,B}$ = 53.4, $^2J_{AB}$ = unresolved; δ_C = 46.6, δ_D = 34.7; $^2J_{CD}$ = 29.7 Hz (Ru$_2$Cl$_4$(DPPB)$_2$(CO)) and δ = 8.1, s (*trans*-RuCl$_2$(CO)$_2$(DPPB) **49**) plus some remaining starting dimer Ru$_2$Cl$_4$(DPPB)$_2$ at δ_A = 63.5, δ_B = 54.3, $^2J_{AB}$ = 46.9 Hz. If the starting Ru$_2$Cl$_4$(DPPB)$_2$ complex was stirred for longer periods under CO, only *trans*-RuCl$_2$(CO)$_2$(DPPB) **49** and *cis*-RuCl$_2$(CO)$_2$(DPPB) (δ_A = 32.8, δ_B = 6.9, $^2J_{AB}$ = 31.9 Hz) were evident by ^{31}P{^{1}H} NMR spectroscopy. There was ~ 42% *cis*-isomer and 58% of the *trans*-isomer present in CDCl$_3$. The IR (CDCl$_3$ soln, NaCl cell) of *cis*-RuCl$_2$(CO)$_2$(DPPB) showed $\nu_{(C=O)}$ at 2001 and 2009 cm^{-1}.

2.5.12.5 RuCl$_2$(PPh$_3$)$_3$ with NH$_3$; Preparation of diamminedichloro(triphenylphosphine)ruthenium(II), RuCl$_2$(NH$_3$)$_2$(PPh$_3$)$_2$ (50)

Anhydrous NH$_3$ was added via a small Teflon tube to a Schlenk tube containing a C$_6$H$_6$ (5 mL) solution of RuCl$_2$(PPh$_3$)$_3$ (0.23 g, 0.24 mmol). The ammonia was flushed over the solution for several minutes, then the Schlenk tube sealed, and the solution stirred at room temperature for 2 h. The cream-coloured solid that precipitated during the reaction was collected by vacuum filtration, washed with C$_6$H$_6$ (3 x 5 mL), and dried

under vacuum. Yield: 0.13 g (77%). Calculated for $RuCl_2(NH_3)_2(PPh_3)_2 \cdot 0.5\ C_6H_6$, $C_{39}H_{39}N_2Cl_2P_2Ru$: C, 60.86; H, 5.11; N, 3.64%. Found: C, 61.10; H, 5.11; N, 3.74%.

$^{31}P\{^1H\}$ NMR ($CDCl_3$, 20 °C): $\delta = 45.6$, s.

^1H NMR ($CDCl_3$, 20 °C): δ 2.15 (6H, s, NH_3), 6.95–7.62 (30H, m, Ph of PPh_3); C_6H_6 solvate was observed as a singlet at 7.36.

2.5.12.6 RuCl$_2$(DPPB)(PPh$_3$) with NH$_3$; Preparation of diamminedichloro(bis(diphenylphosphino)butane)ruthenium(II), RuCl$_2$(DPPB)(NH$_3$)$_2$ (51)

Method 1

Anhydrous NH_3 was added via a small Teflon tube to a Schlenk tube containing a C_6H_6 (5 mL) suspension of $RuCl_2(DPPB)(PPh_3)$ (0.20 g, 0.23 mmol). The ammonia was flushed over the solution for several minutes, then the Schlenk tube sealed, and the solution stirred at room temperature for 24 h. The tan solid that precipitated during the reaction was collected by vacuum filtration, washed with hexanes (3 x 5 mL), and dried under vacuum. Yield: 0.12 g (82%). Calculated for $RuCl_2(DPPB)(NH_3)_2 \cdot 1.5\ C_6H_6$, $C_{37}H_{43}N_2Cl_2P_2Ru$: C, 59.27; H, 5.78; N, 3.74%. Found: C, 59.08; H, 5.76; N, 3.81%.

$^{31}P\{^1H\}$ NMR ($CDCl_3$, 20 °C): $\delta = 46.7$, s.

^1H NMR ($CDCl_3$, 20 °C): δ 1.62 (4H, br m, CH_2 of DPPB), 2.03 (6H, s, NH_3), 2.90 (4H, br m, CH_2 of DPPB), 7.23–7.75 (20H, m, Ph of DPPB); C_6H_6 solvate was observed as a singlet at 7.36.

Conductivity data in MeOH and CH_3NO_2 are given in Table 5.2 (Section 5.2).

Method 2

An alternative preparation is from $[RuCl_2(DPPB)_{1.5}]_2$. Anhydrous NH_3 was bubbled through a green suspension of $[RuCl_2(DPPB)_{1.5}]_2$ (0.24 g, 0.15 mmol) in CH_2Cl_2 (10 mL) for 2–3 min, and the mixture stirred at room temperature. After 5 h, the volume of the blue-green solution was reduced to ~ 2–3 mL, and diethyl ether (15 mL) added to precipitate the product. The tan solid was collected by vacuum filtration, washed

with diethyl ether (4 x 5 mL) and hexanes (5 mL), and dried under vacuum. Yield: 0.16 g (86%).

The spectroscopic data were the same as those recorded for the solid isolated in Method 1.

Method 3

A third method of preparation for compound **51** was from either RuCl$_2$(DPPB)(PPh$_3$) or Ru$_2$Cl$_4$(DPPB)$_2$. Anhydrous ammonia was bubbled through a CDCl$_3$ solution (~ 10 mM) of RuCl$_2$(DPPB)(PPh$_3$) or Ru$_2$Cl$_4$(DPPB)$_2$ for 2 min. An immediate colour change from the green (RuCl$_2$(DPPB)(PPh$_3$)) or orange (Ru$_2$Cl$_4$(DPPB)$_2$) to blue-green occurred on addition of NH$_3$. The ^{1}H and ^{31}P{^{1}H} NMR spectroscopic data were as given above.

Method 4

A vial containing RuCl$_2$(DPPB)(PPh$_3$) (0.04041 g, 4.695 x 10^{-5} mol) and a stir-bar were weighed and placed in a large-mouthed Schlenk tube. The tube was evacuated and anhydrous NH$_3$ added. The starting green solid immediately became brown. The solid was left stirring under an atmosphere for 24 h, and then the product was weighed. Yield: 0.04278 g (101.8% based on RuCl$_2$(DPPB)(NH$_3$)$_2$ + PPh$_3$; 100% should be 0.04201 g). The solution spectroscopic data agree with those for the solid isolated from the reactions in solution (Methods 1–3).

2.5.13   Preparation of *trans*-RuCl$_2$(DPPCP)$_2$ (52)

Method 1

The complex *trans*-RuCl$_2$(DPPCP)$_2$ was isolated in an attempt to synthesize a mixed-phosphine complex of the formula RuCl$_2$(DPPCP)(PPh$_3$). The racemic phosphine, DPPCP (0.12 g, 0.26 mmol), and RuCl$_2$(PPh$_3$)$_3$ (0.26 g, 0.27 mmol) were dissolved in CH$_2$Cl$_2$ (10 mL) and the solution stirred at room temperature. After two hours, the brown suspension was concentrated to about 5 mL at the pump. Ethanol (10 mL) was added to

precipitate a beige solid, which was collected by vacuum filtration, washed with ethanol

(2 x 5 mL), and dried under vacuum. Yield: 0.050 g (36% based on the amount of starting

phosphine).

Method 2

Alternatively, the title complex could be prepared from $RuCl_3 \cdot xH_2O$ (0.25 g, 1.0

mmol; 41.50% Ru) and DPPCP (0.93 g, 2.1 mmol) in ethanol (25 mL). The resulting

dark-orange reaction mixture was refluxed for 5 h. A light-coloured solid, which

precipitated during the reaction, was collected by vacuum filtration, then washed with

ethanol (10 mL), and dried under vacuum. Yield: 0.72 g (67%). Calculated for

$C_{58}H_{56}Cl_2P_4Ru$: C, 66.41; H, 5.38; Cl, 6.76%. Found: C, 66.16; H, 5.36; Cl 7.03%.

$^{31}P\{^1H\}$ NMR ($CDCl_3$, 20 °C): δ = 22.8 and 23.3, s; see Section 3.10.1 for

assignment and discussion.

^1H NMR ($CDCl_3$ 20 °C): δ 0.55 (2H, br m, CH_2 of DPPCP), 1.30 (4H, br m, CH_2

of DPPCP), 1.62 (4H, br m, CH_2 of DPPCP), 1.83 (2H, br m, CH_2 of DPPCP), 3.55 (4H,

br m, CH of DPPCP), 6.80–7.90 (40H, m, Ph of DPPCP).

2.5.14 Reactions of RuCl₂(DPPB)(PPh₃) with Chelating Phosphines (P–P); Formation of RuCl₂(DPPB)(P–P)

2.5.14.1 P–P = DPPCP, *trans*-RuCl₂(DPPB)(DPPCP) (53)

One equivalent of the bidentate phosphine, *r a c*-1,2-

bis(diphenylphosphino)cyclopentane (DPPCP) (0.12 g, 0.28 mmol) was added to

$RuCl_2(DPPB)(PPh_3)$ (0.22 g, 0.25 mmol) in C_6H_6 (30 mL). The initially green solution

was stirred at room temperature for 1 h over which time it turned orange-brown in colour.

The solution was then reduced in volume to ~ 5 mL, and hexanes (35 mL) were added to

precipitate a beige solid, which was collected on a sintered glass filter, washed with

hexanes (3 x 5 mL), and dried under vacuum. Yield: 0.19 g (73%). Calculated for

$C_{57}H_{56}Cl_2P_4Ru$: C, 66.02; H, 5.44; Cl, 6.84%. Found: C, 66.23; H, 5.60; Cl, 7.00%.

$^{31}P\{^1H\}$ NMR (CDCl$_3$, 20 °C): a complicated second-order AA'BB' pattern is observed (Figure 3.27), and this will be discussed later in Section 3.9.

^1H NMR (CDCl$_3$ 20 °C): δ 0.65 (2H, br m, CH_2 of DPPCP), 1.32 (4H, br m, CH_2 of DPPB), 2.12 (2H, br m, CH_2 of DPPCP), 2.19 (2H, br m, CH_2 of DPPCP), 2.25 (2H, br m, CH_2 of DPPB), 2.69 (2H, br m, CH_2 of DPPB), 3.45 (2H, br m, CH of DPPCP), 6.42–8.02 (40H, m, Ph of DPPB and DPPCP).

2.5.14.2 P–P = DPPE, *trans*-RuCl$_2$(DPPE)$_2$ (54)

One equivalent of DPPE (0.98 g, 0.25 mmol) and RuCl$_2$(DPPB)(PPh$_3$) (0.24 g, 0.28 mmol) were dissolved in C$_6$H$_6$ (30 mL). After being stirred at room temperature for 2 h, the solution was concentrated to ~ 5 mL at the pump, and hexanes (35 mL) were added to precipitate the product. The pale yellow-green solid was collected by vacuum filtration, washed with hexanes (3 x 5 mL), and dried under vacuum. Yield: 0.10 g (40% based on Ru).

$^{31}P\{^1H\}$ NMR (CDCl$_3$, 20 °C): 45.0, s.

^1H NMR (CDCl$_3$, 20 °C): δ 2.72 (8H t, J = 7.4 Hz, CH_2 of DPPE), 6.80–7.42 (40H, m, Ph of DPPE).

The physical and spectroscopic data for this complex agree with those reported in the literature.[5,38,55] This compound, previously prepared from RuCl$_3$·xH$_2$O,[55] RuCl$_2$(PPh$_3$)$_3$,[38] and Ru$_2$Cl$_4$(C$_6$H$_6$)$_2$,[5] was recently characterized by crystallography.[56]

2.5.15 Preparation of Ru(P–P)(η^3-allyl)$_2$ Complexes

2.5.15.1 P–P = DPPB, allyl = Me-allyl; Preparation of Ru(DPPB)(η^3-Me-allyl)$_2$ (55)

The title complex was prepared from Ru(COD)(Me-allyl)$_2$ using a modified preparation of that used by Genêt et al. for the synthesis of complexes of the type Ru(P–P)(Me-allyl)$_2$, containing a wide variety of chiral phosphines.[30,57,58] One equivalent of

DPPB (0.13 g, 0.31 mmol) and Ru(COD)(Me-allyl)$_2$ (0.10 g, 0.31 mmol) were dissolved in CH$_2$Cl$_2$ (1 mL) and heated in a Schlenk tube to 40 °C under a flow of Ar. The colourless solution slowly became yellow. After the reaction mixture was heated for 18 h, the solvent was removed under vacuum. The yellow solid was transferred onto a filter, washed with hexanes (4 x 2 mL) and diethyl ether (2 x 2 mL), and dried under vacuum. Yield: 0.15 g (76%). Calculated for Ru(DPPB)(Me-allyl)$_2$, C$_{36}$H$_{42}$P$_2$Ru: C, 67.80; H, 6.64%. Found: C, 67.52; H, 6.64 %.

^{31}P{^{1}H} NMR (C$_6$D$_6$, 20 °C): 44.2, s.

(CDCl$_3$, 20 °C): 44.1, s.

^{1}H NMR (C$_6$D$_6$, 20 °C): δ 1.09 (2H, AB quartet, C*H* of Me-allyl), 1.43 (2H, s, C*H* of Me-allyl), 1.49 (2H, s, C*H* of Me-allyl), 1.55 (2H, br m, C*H*$_2$ of DPPB), 1.70 (2H, br m, C*H*$_2$ of DPPB), 2.10 (6H, s, C*H*$_3$ of Me-allyl), 2.19 (2H, br m, C*H*$_2$ of DPPB), 2.52 (2H, s, C*H* of Me-allyl), 2.59 (2H, br m, C*H*$_2$ of DPPB), 6.85–7.37 (16H, m, *ortho*- and *meta*-Ph of DPPB), 7.86 (4H, t, *J* = 8.8 Hz, *para*-Ph of DPPB).

2.5.15.2   P–P = DPPB, allyl = allyl; Attempted Preparation of Ru(DPPB)(η^3-allyl)$_2$

One equivalent of DPPB (0.37 g, 0.87 mmol) and Ru(COD)(η^3-allyl)$_2$ (0.26 g, 0.89 mmol) were refluxed in benzene / hexanes (5 mL / 10 mL) for 5 h. The yellow solution was cooled to room temperature, and an aliquot taken for a ^{31}P{^{1}H} NMR spectrum. The spectrum in CDCl$_3$ showed only the presence of free DPPB. Therefore, no reaction had taken place. This synthesis was not pursued further, as Ru(COD)(η^3-Me-allyl)$_2$ proved to be a much better starting material for the synthesis of Ru(P–P)(η^3-allyl)$_2$ type species.

As in the case of Ru(DPPB)(η^3-Me-allyl)$_2$, the synthesis of the title complex was attempted by modifying a procedure published by Genêt et al. for complexes of the type Ru(P–P)(η^3-allyl)$_2$ containing chiral diphosphines.[58]

2.5.15.3 P–P = (*R*)-BINAP, allyl = Me-allyl; Preparation of Ru((*R*)-BINAP)(η^3-Me-allyl)$_2$ (56)

The title complex was synthesized by modifying a procedure reported by Genêt et al.[30,57] One equivalent of (*R*)-BINAP (0.15 g, 0.24 mmol) and Ru(COD)(η^3-Me-allyl)$_2$ (0.078 g, 0.24 mmol) were refluxed in C_7H_8 (2 mL) for 4 h. The resulting orange-brown solution was reduced to dryness at the pump, and the dark-orange residue was placed on a filter and washed with hexanes (4 x 2 mL). The bright-orange washings were reduced to dryness at the pump. The brown solid remaining on the filter was dried under vacuum.

$^{31}P\{^1H\}$ NMR (C_6D_6, 20 °C) of the dark-orange residue: δ = 42.1, s, plus another singlet resonance at δ = –15.0 indicating some free BINAP.

$^{31}P\{^1H\}$ NMR (C_6D_6, 20 °C) of the brown solid: δ = 42.1, s, plus two other singlet resonances at δ = –15.0 (free BINAP) and δ = 26.6 (BINAP(O)$_2$).

An orange crystal suitable for X-ray diffraction studies was deposited from a C_6D_6 solution which showed singlets for BINAP, BINAP(O)$_2$, and Ru(BINAP)(η^3-Me-allyl)$_2$ in the $^{31}P\{^1H\}$ NMR spectrum. The crystal was deposited from the NMR solution over a period of several weeks, over which time the NMR solution had changed from orange to dark green in colour. The solution of the X-ray diffraction data showed the unit cell of the crystal to be composed of half of a Ru((*R*)-BINAP)(η^3-Me-allyl)$_2$ molecule and half of a (*R*)-(+)-2,2'-bis(diphenylphosphinoyl)-1,1'-binaphthyl molecule, co-crystallized with two disordered deuterobenzene regions (see Section 3.3.4.3 for discussion and Appendix IV for complete experimental details and parameters).

The $^{31}P\{^1H\}$ NMR data are in agreement with those previously reported in the literature, although no assignments were given.[30,57]

2.6 References

(1)   Perrin, D. D.; Armarego, W. L. F.; Perrin, D. R. *Purification of Laboratory Chemicals*; 2nd ed.; Pergamon: Oxford, 1980.

(2)   Allen, D. L.; Gibson, V. C.; Green, M. L. H.; Skinner, J. F.; Bashkin, J.; Grebenik, P. D. *J. Chem. Soc., Chem. Commun.* **1983**, 895.

(3)   Priemer, H. Ph.D. Thesis, der Ruhr-Universität Bochum, 1987.

(4)   Chau, D. E. K.-Y. M.Sc. Thesis, The University of British Columbia, 1992.

(5)   Fogg, D. Ph.D. Thesis, The University of British Columbia, 1994.

(6)   Evans, D. F. *J. Chem. Soc.* **1959**, 2003.

(7)   Live, D. H.; Chan, S. I. *Anal. Chem.* **1970**, *42*, 791.

(8)   Gordon, A. J.; Ford, R. A. In *The Chemist's Companion: A handbook of practical data, techniques and references*; Wiley: New York, 1972, p 374.

(9)   Jolly, W. L. In *Synthetic Inorganic Chemistry*; Prentice-Hall: Englewood Cliffs, N.J., 1960, p 142.

(10)   Keller, R. N.; Wycoff, H. D. *Inorg. Synth.* **1946**, 2, 1.

(11)   Costa, G.; Pellizer, G.; Rubessa, F. *J. Inorg. Nucl. Chem.* **1964**, *26*, 961.

(12)   Glockling, F.; Hooton, K. A. *J. Chem. Soc.* **1962**, 2658.

(13)   Costa, G.; Reisenhofer, E.; Stefani, L. *J. Inorg. Nucl. Chem.* **1965**, *27*, 2581.

(14)   Dixon, K. R. In *Multinuclear NMR*; Mason, J., Ed.; Plenum: New York, 1987; Chapter 13.

(15)   James, B. R.; Rempel, G. L. *Disc. Faraday Soc.* **1968**, *46*, 48.

(16)   James, B. R.; Rempel, G. L. *Can. J. Chem.* **1966**, *44*, 233.

(17)   Lind, J. E., Jr.; Zwolenik, J. J.; Fuoss, R. M. *J. Am. Chem. Soc.* **1959**, *81*, 1557.

(18)   Fogg, D. E.; James, B. R.; Kilner, M. *Inorg. Chim. Acta* **1994**, *222*, 85.

(19)   Shriver, D. F.; Drezdon, M. A. *The Manipulation of Air-Sensitive Compounds*; 2nd ed.; Wiley: New York, 1986.

(20)   Stephenson, T. A.; Wilkinson, G. *J. Inorg. Nucl. Chem.* **1966**, *28*, 945.

(21)   Thorburn, I. S. Ph.D. Thesis, The University of British Columbia, 1985.

(22)   Joshi, A. M. Ph.D. Thesis, The University of British Columbia, 1990.

(23) Wang, D. K. W. Ph.D. Thesis, The University of British Columbia, 1978.

(24) Dekleva, T. W.; Thorburn, I. S.; James, B. R. *Inorg. Chim. Acta* **1985**, *100*, 49.

(25) Markham, L. D. Ph.D. Thesis, The University of British Columbia, 1973.

(26) Skapski, A. C.; Troughton, P. G. H. *J. Chem. Soc., Chem. Commun.* **1968**, 1230.

(27) Hallman, P. S.; McGarvey, B. R.; Wilkinson, G. *J. Chem. Soc. (A)* **1968**, 3143.

(28) Markham, L. D.; James, B. R. *J. Catal.* **1972**, *27*, 442.

(29) Bennett, M. A.; Wilkinson, G. *Chem. Ind. (London)* **1959**, 1516.

(30) Genêt, J. P.; Pinel, C.; Ratovelomanana-Vidal, V.; Mallart, S.; Pfister, X.; Caño De Andrade, M. C.; Laffitte, J. A. *Tetrahedron: Asymmetry* **1994**, *5*, 665.

(31) Schrock, R. R.; Johnson, B. F. G.; Lewis, J. *J. Chem. Soc., Dalton Trans.* **1974**, 951.

(32) Powell, J.; Shaw, B. L. *J. Chem. Soc. (A)* **1968**, 159.

(33) Hallman, P. S.; Stephenson, T. A.; Wilkinson, G. *Inorg. Synth.* **1970**, *12*, 237.

(34) Hoffman, P. R.; Caulton, K. G. *J. Am. Chem. Soc.* **1975**, *97*, 4221.

(35) Dekleva, T. W. Ph.D. Thesis, The University of British Columbia, 1983.

(36) Knoth, W. H. *J. Am. Chem. Soc.* **1972**, *94*, 104.

(37) Armit, P. W.; Sime, W. J.; Stephenson, T. A.; Scott, L. *J. Organomet. Chem.* **1978**, *161*, 391.

(38) Jung, C. W.; Garrou, P. E.; Hoffman, P. R.; Caulton, K. G. *Inorg. Chem.* **1984**, *23*, 726.

(39) Joshi, A. M.; Thorburn, I. S.; Rettig, S. J.; James, B. R. *Inorg. Chim. Acta* **1992**, *198*, 283.

(40) Mezzetti, A.; Costella, L.; Del Zotto, A.; Rigo, P.; Consiglio, G. *Gazz. Chim. Ital.* **1993**, *123*, 155.

(41) Hampton, C. R. S. M. Ph.D. Thesis, The University of British Columbia, 1989.

(42) James, B. R.; Thompson, L. K.; Wang, D. K. W. *Inorg. Chim. Acta* **1978**, *29*, L237.

(43) Hampton, C. R. S. M.; Butler, I. R.; Cullen, W. R.; James, B. R.; Charland, J.-P.; Simpson, J. *Inorg. Chem.* **1992**, *31*, 5509.

(44) Chau, D. E. K.-Y.; James, B. R. *Inorg. Chim. Acta* in press.

(45) Hampton, C.; Dekleva, T. W.; James, B. R.; Cullen, W. R. *Inorg. Chim. Acta* **1988**, *145*, 165.

(46)   Bressan, M.; Rigo, P. *Inorg. Chem.* **1975**, *14*, 2286.

(47)   James, B. R.; McMillan, R. S.; Morris, R. H.; Wang, D. K. W. *Adv. Chem. Ser.* **1978**, *167*, 122.

(48)   Thorburn, I. S.; Rettig, S. J.; James, B. R. *Inorg. Chem.* **1986**, *25*, 234.

(49)   James, B. R.; Pacheco, A.; Rettig, S. J.; Thorburn, I. S.; Ball, R. G.; Ibers, J. A. *J. Mol. Catal.* **1987**, *41*, 147.

(50)   Batista, A. A.; Queiroz, S. L.; Oliva, G.; Santos, R. H. A.; Gambardella, M. T. d. P. 5th Int. Conf. Chemistry of Platinum Metals, St. Andrews, UK; 1993; Abstract A40.

(51)   Batista, A. A.; Queiroz, S. L.; Oliva, G.; Gambardella, M. T. d. P.; Santos, R. H. A., personal communication.

(52)   Gilbert, J. D.; Wilkinson, G. *J. Chem. Soc. (A)* **1969**, 1749.

(53)   Krassowski, D. W.; Nelson, J. H.; Brower, K. R.; Havenstein, D.; Jacobson, R. A. *Inorg. Chem.* **1988**, *27*, 4294.

(54)   Batista, A. A.; Zukerman-Schpector, J.; Porcu, O. M.; Queiroz, S. L.; Araujo, M. P.; Oliva, G.; Souza, D. H. F. *Polyhedron* **1994**, *13*, 689.

(55)   Mason, R.; Meek, D. W.; Scollary, G. R. *Inorg. Chim. Acta* **1976**, *16*, L11.

(56)   Polam, J. R.; Porter, L. C. *J. Coord. Chem.* **1993**, *29*, 109.

(57)   Genêt, J. P.; Pinel, C.; Mallart, S.; Juge, S.; Thorimbert, S.; Laffitte, J. A. *Tetrahedron: Asymmetry* **1991**, *2*, 555.

(58)   Genêt, J. P.; Mallart, S.; Pinel, C.; Juge, S.; Laffitte, J. A. *Tetrahedron: Asymmetry* **1991**, *2*, 43.

CHAPTER 3

SYNTHESIS AND REACTIVITY OF FIVE-COORDINATE RUTHENIUM(II) DITERTIARY PHOSPHINE COMPLEXES

3.1 Introduction

Interest in ruthenium(II) complexes containing a ditertiary phosphine ligand as catalysts for homogeneous hydrogenation began in the late 1970s.[1] The success of rhodium complexes containing chiral bidentate phosphines as catalysts for enantioselective hydrogenation of prochiral unsaturated substrates is evident from several commercial processes employing these systems as catalysts, as well as numerous publications in this area.[2] Enantioselectivities of up to 100% e.e. have been achieved with rhodium catalysts for various substrates. Researchers have been actively studying the effect of substituting other transition metals for Rh in these chiral ligand systems. Ruthenium is of particular interest, due to its effectiveness as an achiral hydrogenation catalyst for terminal alkenes (cf. $Ru(H)Cl(PPh_3)_3$ vs. $RhCl(PPh_3)_3$),[3-5] and because it is relatively inexpensive.

Ruthenium has developed a rich coordination and organometallic chemistry over the years. Reports on the synthesis, properties, reactivity, and catalytic applications of ruthenium complexes containing tertiary phosphine ligands are numerous.[6-11] Recently, the success of ruthenium-chiral phosphine complexes for asymmetric hydrogenation (especially Ru-BINAP systems)[12] has stimulated increased interest in the synthesis, reactivity, and catalytic activity of ditertiary phosphine ruthenium complexes.

The chemistry that will be discussed in this chapter is the result of several observations of coordinatively unsaturated species in a catalytic environment. Coordinative unsaturation is thought to be necessary at some stage of a catalytic cycle for a complex to act as an effective catalyst.[13] In this laboratory, mechanistic studies on trans-$Ru(H)Cl(DIOP)_2$, which was shown to be a "catalyst" for the asymmetric

85

hydrogenation of prochiral olefinic carboxylic acids, revealed the active catalyst to be ["Ru(H)Cl(DIOP)"].[1,14,15] More recently, a catalytic system for the enantioselective hydrogenation of similar alkenes using *trans*-Ru(H)Cl(BINAP)$_2$ as the catalyst precursor shows the probable active catalytic species to be ["Ru(H)Cl(BINAP)"].[16] The above two examples show that coordinatively unsaturated complexes are important for an active catalytic species. Similar *trans*-Ru(H)Cl(P–P)$_2$ complexes, where P–P is CHIRAPHOS or Ph$_2$P(CH$_2$)$_n$PPh$_2$ with n = 1–3, exhibit little activity as catalysts for alkene hydrogenation, possibly because the phosphines are bound to the metal centre too strongly to allow an unsaturated, and thereby active, complex to be formed.[15,17,18]

The synthetic methodology discussed in this chapter is an ongoing study to develop preparative routes to coordinatively unsaturated ruthenium complexes containing a single, chelating ditertiary phosphine per metal centre. The five-coordinate ruthenium(II) complexes containing such a diphosphine that have been reported to date are shown in Figure 3.1.

P—P = DIOP or Ph$_2$P(CH$_2$)$_n$PPh$_2$

where n = 4, DPPB; 5, DPPN; 6, DPPH

P—P = DPPB, DIOP, BINAP, or BIPHEMP

P—P = DPPP, DPPB, DPPN, BINAP*,

CHIRAPHOS, or BDPP

* of different geometry, see Figure 3.5
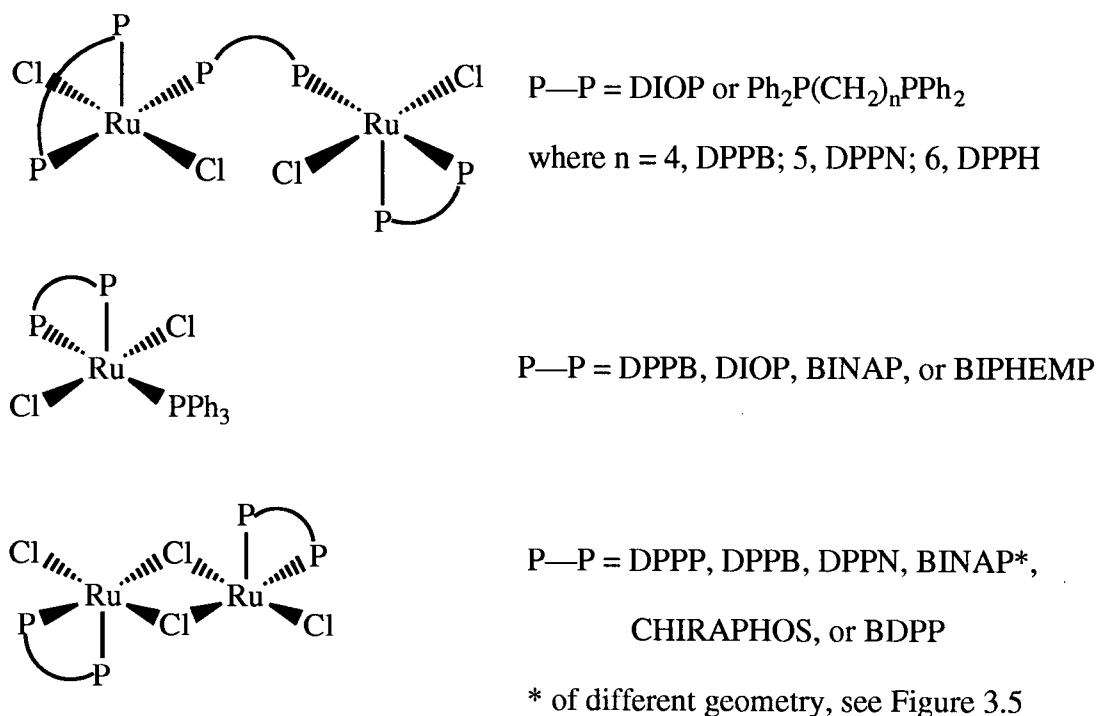
Figure 3.1   Five-coordinate ruthenium(II) complexes containing a diphosphine that have been reported to date.[15,17,19-26]

3.2 Synthesis and Characterization of $Ru_2Cl_5(P-P)_2$, $Ru_2Cl_4(P-P)_2$, and $[Ru(H)Cl(P-P)]_3$ Complexes–A Brief Review

The route to $Ru_2Cl_5(P-P)_2$, and subsequent reduction to $Ru_2Cl_4(P-P)_2$, were developed in this laboratory by Thorburn et al.,[25,26] who also developed a low-yield route (10%) from $Ru_2Cl_4(P-P)_2$ to the trinuclear species $[Ru(H)Cl(P-P)]_3$, where P–P = DPPB or CHIRAPHOS.[26]

Joshi et al. then extended the range of $Ru_2Cl_5(P-P)_2$ and $Ru_2Cl_4(P-P)_2$ complexes to include other chiral and achiral bis(phosphines).[22,23] The yield of the triruthenium complex $[Ru(H)Cl(P-P)]_3$ was improved to 50% by Joshi.[22]

Some analogous Ru chemistry involving monodentate phosphines was known before Thorburn started his work. The species $Ru_2Cl_4(PR_3)_4$, which is a monodentate analogue of $Ru_2Cl_4(P-P)_2$, could be prepared by reduction of $RuCl_3(PR_3)_2$.[27,28]

An attempt to prepare $RuCl_3(P-P)$ complexes by phosphine displacement within $RuCl_3(PR_3)_2$ species led to the isolation of the formally mixed-valence dinuclear $Ru^{II,III}$ compounds, $Ru_2Cl_5(P-P)_2$ (Figure 3.2).[23,25,29]

$$4RuCl_3(PR_3)_2 + 4P-P \xrightarrow[\text{trace } H_2O]{\text{hexanes, reflux}} \begin{array}{c} 2Ru_2Cl_5(P-P)_2 + O=PR_3 \\ + \\ 7PR_3 + 2HCl \end{array}$$
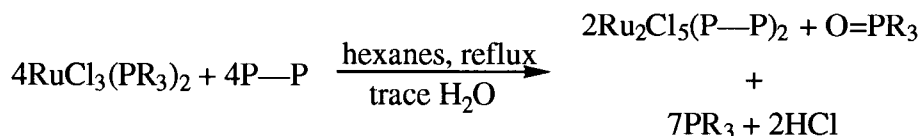
R = phenyl, *p*–tolyl

P–P = DPPP, DPPB, DIOP, CHIRAPHOS, or NORPHOS

Figure 3.2   Reaction of one equivalent of diphosphine with $RuCl_3(PR_3)_2$.

Joshi et al. subsequently extended this series of mixed-valence complexes to include: DPPN, DPPH, DPPCP, DCYPCP, BDPP, BINAP, and PHENOP.[22,23]

An X-ray diffraction analysis of $Ru_2Cl_5(CHIRAPHOS)_2$ showed the complex to be a highly symmetric trichloro-bridged species with irregular octahedral geometry around each ruthenium centre (Figure 3.3).[25,29]
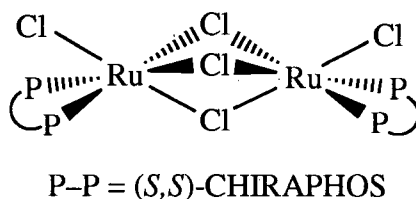
P–P = (*S,S*)-CHIRAPHOS

Figure 3.3   Geometry of the $Ru_2Cl_5((S,S)$-CHIRAPHOS$)_2$ complex.

The reduction of these mixed-valence $Ru_2Cl_5(P–P)_2$ complexes with H_2 in the presence of a base gave the target "$RuCl_2(P–P)$" species as dichloro-bridged dimers (Figure 3.4).[25,29]

P—P = DPPP, DPPB, DIOP, or CHIRAPHOS
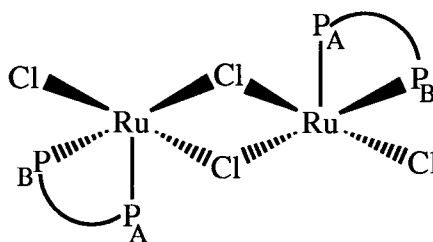
Figure 3.4   Suggested geometry for $Ru_2Cl_4(P–P)_2$ complexes.

Joshi extended the series of $Ru_2Cl_4(P–P)_2$ complexes to include: DPPN, (*R*)- and (*S*)-BINAP, and (*S,S*)-BDPP.[22,23] The BINAP species $Ru_2Cl_4(BINAP)_2$ is thought to differ slightly in geometry from the other dimers based on $^{31}P\{^1H\}$ NMR spectral evidence (Figure 3.5).[22,23]

P—P = (*R*)- and (*S*)-BINAP
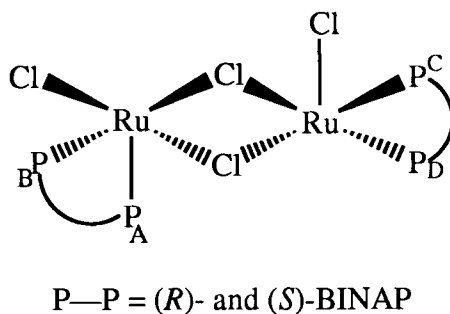
Figure 3.5 Suggested geometry for the $Ru_2Cl_4(BINAP)_2$ complex.

The preparative chemistry leading from $RuCl_3 \cdot xH_2O$ to $Ru_2Cl_5(P-P)_2$, and subsequently to $Ru_2Cl_4(P-P)_2$, is shown in Figure 3.6.

$$RuCl_3 \cdot xH_2O + 2PR_3 \xrightarrow[\text{24 h, 25 °C}]{\text{DMA}} RuCl_3(PR_3)_2(DMA) \cdot DMA \text{ solvate}$$

50–70%

DMA = *N,N*-dimethylacetamide
R = phenyl or *p*-tolyl

P–P (1 equiv / Ru^{III})

hexanes, reflux
24 h

$$Ru_2Cl_4(P-P)_2 \quad 40-85\% \xleftarrow{\text{1 atm H}_2, \text{ 16 h, 25 °C}} Ru_2Cl_5(P-P)_2 \quad 45-85\%$$

base·HCl   base

base = DMA for achiral diphosphines and
polyvinylpyridine for chiral diphosphines
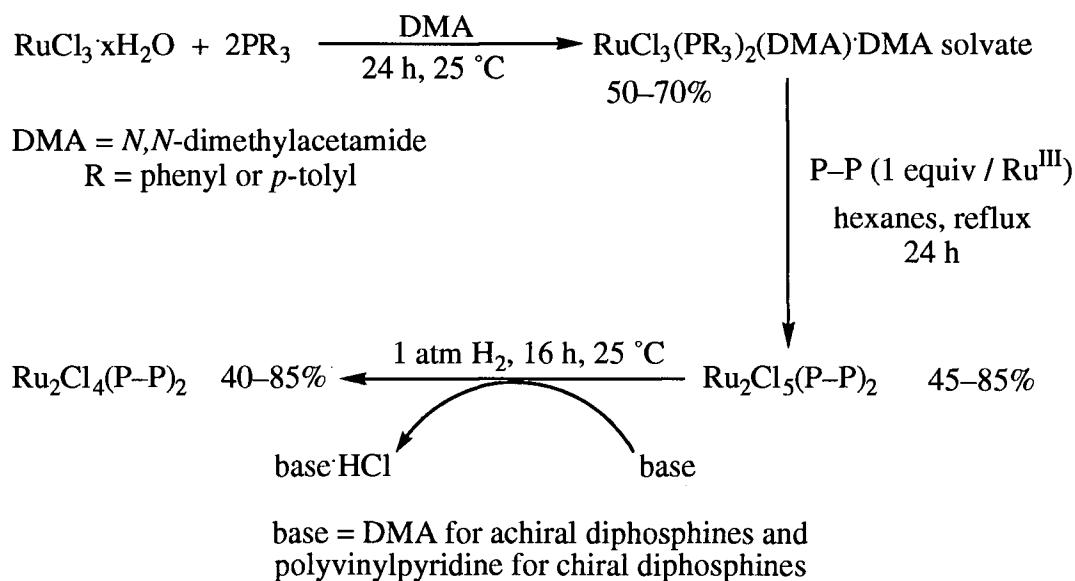
Figure 3.6 Reaction pathway from $RuCl_3 \cdot xH_2O$ to $Ru_2Cl_5(P-P)_2$ and $Ru_2Cl_4(P-P)_2$
complexes.

It is interesting to note that Thorburn was unable to prepare $Ru_2Cl_5(DPPE)_2$.[25] This was unexpected, as the CHIRAPHOS analogue was prepared by this route, and DPPE and CHIRAPHOS both form five-membered chelate rings upon binding to the metal centre. DPPE differs from CHIRAPHOS only in having hydrogens in place of

methyl groups in the carbon backbone. Recently, some preliminary experiments by Fogg produced some $Ru_2Cl_5(DPPE)_2$.[30] In these studies, the reaction was performed in CH_2Cl_2 at room temperature instead of a refluxing procedure in hexanes. However, the $Ru_2Cl_5(DPPE)_2$ was not separated from some *trans*-$RuCl_2(DPPE)_2$,[30] which was the sole product identified by Thorburn when this reaction was performed in hexanes.[25]

The neutral diruthenium complexes $Ru_2Cl_4(P–P)_2$ were initially found by Thorburn, and extended later by Joshi and Fogg, to react with a variety of neutral two-electron donors (Figure 3.7).[22,23,25,30]

$L = DMA, CO, Me_2CO, Me_2SO, MeCN, PhCN, N_2, or H_2$
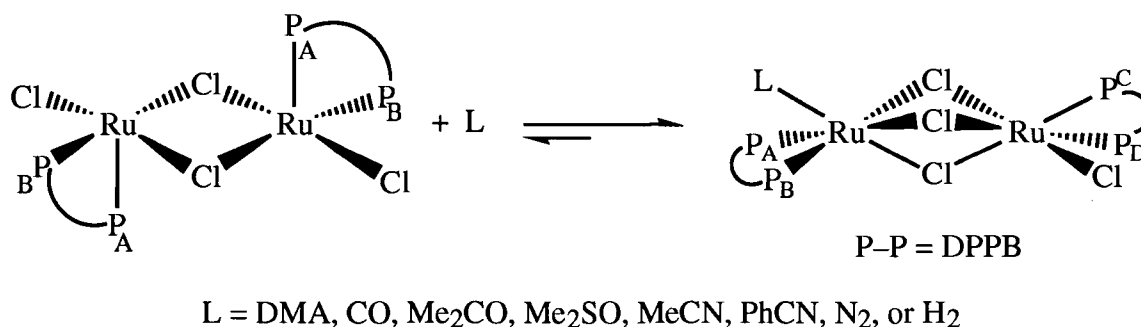
Figure 3.7   Reaction of $Ru_2Cl_4(P–P)_2$ with neutral ligand L to form $Ru_2Cl_4(P–P)_2(L)$ complexes.

Formation of the triply-chloro-bridged products was easily assessed by $^{31}P\{^1H\}$ NMR spectroscopy, as these products gave spectra consisting of two AB quartets corresponding to the two ends of the dinuclear complex. Occasionally, some species gave $^{31}P\{^1H\}$ NMR spectra which did not consist of the two AB patterns (e.g., for L = NEt_3), and the singlet observed in the phosphorus NMR spectra was thought to be due to an exchange process (see Section 3.4 for details). Some of the $Ru_2Cl_4(P–P)(L)$ species were observed in situ, while others were isolated as solids.[22,23,25,30] The isolated $Ru_2Cl_4(P–P)_2(L)$ species include: L = CO, Me_2CO, Me_2SO, NEt_3, MeCN, and PhCN. It should be noted that not all of the $Ru_2Cl_4(P–P)_2(L)$ species were formed directly from $Ru_2Cl_4(P–P)_2$. Some of the complexes were prepared from $RuCl_2(P–P)(PPh_3)$ (see Section 3.3.3).

An X-ray crystal structure determination of $Ru_2Cl_4(DPPB)_2(DM\underline{S}O)$, produced by the addition of one equivalent of DPPB to *cis*-$RuCl_2(DMSO)_4$, revealed that the geometry around each Ru centre is irregular octahedral (Figure 3.8).[22,23]

P–P = DPPB
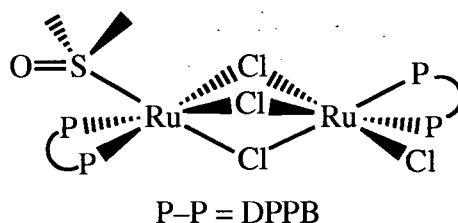
Figure 3.8   Geometry of the $Ru_2Cl_4(DPPB)_2(DM\underline{S}O)$ complex.

Comparison of this geometry with that seen for $Ru_2Cl_5(CHIRAPHOS)_2$ (Figure 3.3) shows one striking difference. Unlike the highly symmetrical CHIRAPHOS complex, the positioning of the diphosphines in the DPPB complex is unsymmetrical: one of the octahedra has been rotated by 120° around the Ru–Ru vector.[22,23]

The analogous thiocarbonyl complex $Ru_2Cl_4(PPh_3)_4(CS)$ reported by Fraser and Gould also shows a similar unsymmetrical arrangement of the PPh_3 ligands (Figure 3.9).[31]
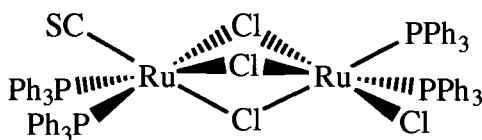
Figure 3.9   Geometry of the $Ru_2Cl_4(PPh_3)_4(CS)$ complex.

The triruthenium species $[Ru(H)Cl(P–P)]_3$ synthesized by Thorburn was initially obtained only in low yields (10%) from $Ru_2Cl_4(P–P)_2$ (Figure 3.10).[26] The $^{31}P\{^1H\}$ NMR spectrum of this $[Ru(H)Cl(DPPB)]_3$ complex first suggested a nuclearity of greater than two, and this was confirmed by an X-ray structure determination of the

CHIRAPHOS complex (Figure 3.11).[26] The placement of the hydrides is based on selective $^1\text{H}\{^{31}\text{P}\}$ NMR studies,[22] as well as on the X-ray crystallography-determined framework.[26]

$$\text{Ru}_2\text{Cl}_4(\text{P--P})_2 \xrightarrow[\text{(2) H}_2, 24 \text{ h}, 25\ ^\circ\text{C}]{\text{(1) 2NEt}_3,\ \text{C}_6\text{H}_6} \text{[Ru(H)Cl(P--P)]}_3\ \ 5\text{--}10\%$$

route (a)

$$+$$
$$\text{[HNEt}_3]^+\text{[Ru}_2\text{Cl}_4(\text{P--P})_2]^-$$
$$+$$
$$\text{NEt}_3\text{H}^+\text{Cl}^-$$

route (b)

(1) H_2, C_6H_6, 1 h, 25 °C
(2) 2NEt$_3$, 23 h

[Ru(H)Cl(P–P)]$_3$ 50%
+
[HNEt$_3$]$^+$[Ru$_2$Cl$_5$(P–P)$_2$]$^-$
+
NEt$_3$H$^+$Cl$^-$
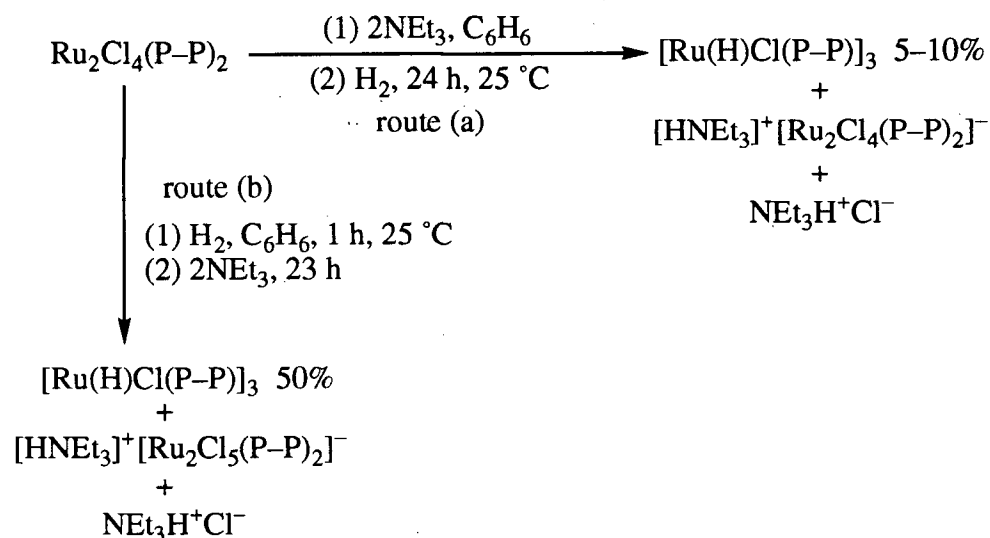
Figure 3.10   Synthesis of [Ru(H)Cl(P–P)]$_3$ from Ru$_2$Cl$_4$(P–P)$_2$, where P–P = DPPB, DIOP or CHIRAPHOS; (a) original synthetic method;[26] (b) improved synthesis developed by Joshi.[22]
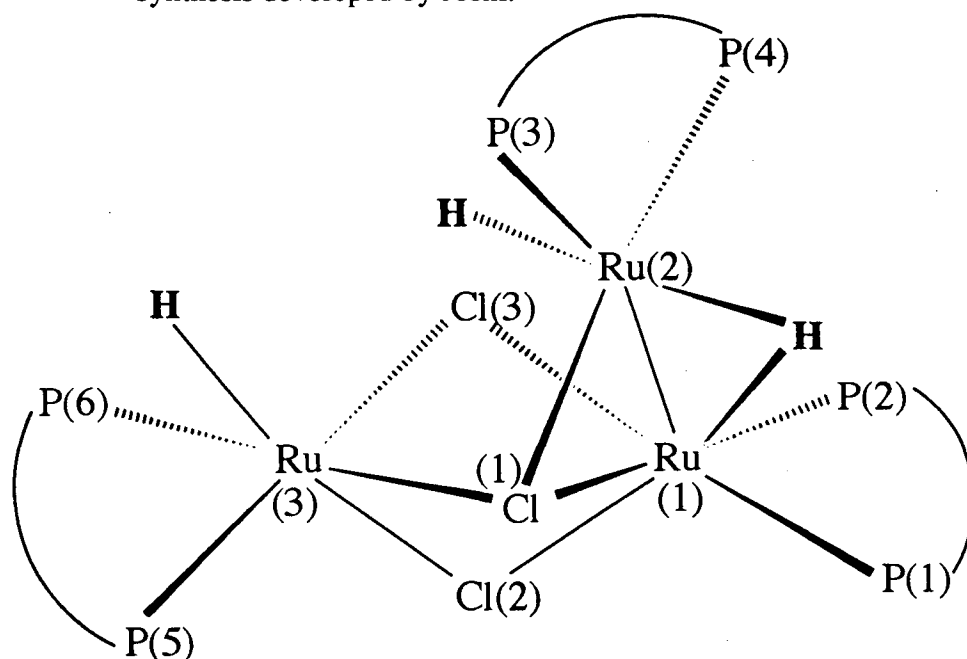
Figure 3.11   Geometry of the [Ru(H)Cl(P–P)]$_3$ complexes (based on the X-ray structure of the CHIRAPHOS derivative[26] and phosphorus-decoupled proton NMR studies).[22]

92

Joshi improved the synthesis of the trinuclear species, [Ru(H)Cl(P–P)]$_3$, to 50% by reversing the order of the addition of base and H$_2$ (Figure 3.10).[22]

The amine-containing co-product in the DPPB system was originally thought by Thorburn and Joshi to be the neutral Ru$_2$Cl$_4$(DPPB)$_2$(NEt$_3$) complex as judged by comparison of the ^{31}P{^{1}H} NMR spectrum with that of an authentic sample (Section 2.5.8.1). Also, the ^{1}H NMR spectrum showed the presence of amine. However, elemental analysis of the orange solid in this work showed that the complex is actually the ionic complex [HNEt$_3$]$^+$[Ru$_2$Cl$_5$(DPPB)$_2$]$^-$ (Section 2.5.9.5). The ^{31}P{^{1}H} and ^{1}H NMR are essentially the same as those observed earlier by Thorburn and Joshi, but the ^{31}P{^{1}H} NMR spectroscopic studies are uninformative in distinguishing between the neutral and ionic complexes.

The addition of one equivalent of NEt$_3$·HCl to Ru$_2$Cl$_4$(DPPB)$_2$ in CDCl$_3$ produced an orange solution, which after 2 h at room temperature gave a singlet in the ^{31}P{^{1}H} NMR spectrum, strongly suggesting [HNEt$_3$]$^+$[Ru$_2$Cl$_5$(DPPB)$_2$]$^-$ formation.

3.3   Routes into the Bromide Analogues and Related Chemistry

3.3.1   Ruthenium(III) Bromide Complexes, RuBr$_3$(PPh$_3$)$_2$

The logical entry point into the bromide analogues of the "RuCl(P–P)" species was to follow the route outlined in Figure 3.6 by first synthesizing the known complex RuBr$_3$(PPh$_3$)$_2$ (i.e., RuBr$_3$(PPh$_3$)$_2$(MeOH)) from RuCl$_3$·xH$_2$O, LiBr, and PPh$_3$.[32] Unfortunately, there were many problems associated with this route (outlined below). Several sets of conditions were tried in attempting to prepare pure RuBr$_3$(PPh$_3$)$_2$(DMA)·DMA solvate or RuBr$_3$(PPh$_3$)$_2$(MeOH). One such method is outlined in detail (Section 2.5.1.3). Various other conditions were attempted, and are summarized in equations 3.1–3.4.

$$\text{RuCl}_3\cdot x\text{H}_2\text{O} + \text{xs LiBr} + 2\text{PPh}_3 \xrightarrow{\text{MeOH}} \text{RuBr}_3(\text{PPh}_3)_2(\text{MeOH}) \qquad (3.1)$$

$$\text{RuCl}_3 \cdot x\text{H}_2\text{O} + \text{xs LiBr} + 2\text{PPh}_3 \xrightarrow{\text{DMA}} \text{RuBr}_3(\text{PPh}_3)_2(\text{DMA}) \cdot \text{DMA solvate} \quad (3.2)$$

$$\text{RuBr}_3 \cdot x\text{H}_2\text{O} + 2\text{PPh}_3 \xrightarrow{\text{MeOH}} \text{RuBr}_3(\text{PPh}_3)_2(\text{MeOH}) \quad (3.3)$$

$$\text{RuBr}_3 \cdot x\text{H}_2\text{O} + 2\text{PPh}_3 \xrightarrow{\text{DMA}} \text{RuBr}_3(\text{PPh}_3)_2(\text{DMA}) \cdot \text{DMA solvate} \quad (3.4)$$
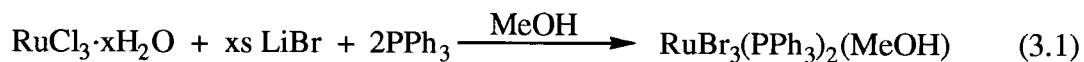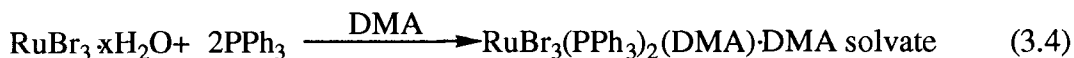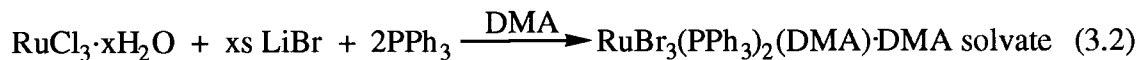
None of the above methods resulted in analytically pure material. A careful potentiometric titration§ of the red-brown solid isolated following the chemistry of equation 3.1 showed an inflection in the titration curve for the halide analysis, indicating the presence of chloride.

Other workers have had similar difficulties in preparing RuBr3(PPh3)2(MeOH)[33] and RuCl3(PPh3)2(MeOH).[34,35] These workers obtained solids which were thought to be Ru^{II} species[34] or mixtures of Ru^{II} (e.g., RuCl2(PPh3)3) and Ru^{III} species. In this thesis work, the isolated solid was also probably a mixture of Ru^{II} and Ru^{III} species, the diamagnetic species being observed in the ^{1}H NMR spectrum. An additional difficulty was that the solid contained some residual chloride (potentiometric titration).

The RuBr3·xH2O starting material (eqs 3.3–3.4) was found to be ineffective for preparing either Ru^{III} or Ru^{II} (described in Section 3.3.2) phosphine complexes. The difficulty in using this material is probably due to its limited solubility in MeOH. If, however, the "RuBr3" is produced in situ from RuCl3·xH2O and LiBr, the material seems to be more soluble. Therefore, in equation 3.1, stoichiometric quantities of PPh3 are thought to react with "RuBr3(MeOH)3."[33]

---

§   The potentiometric titration was performed carefully by Mr. P. Borda of this department using small additions of 0.02 N silver nitrate. The inflection between the titrated chloride and bromide curves showed the presence of both halides.

On the other hand, the syntheses of $RuCl_3(PAr_3)_2(DMA)\cdot DMA$ solvate (where Ar = PPh_3 or $P(p\text{-tolyl})_3$) are straightforward, and these complexes have been prepared in this work (Sections 2.5.1.1 and 2.5.1.2), as well as by numerous other workers.[22,25,33]

Some typical analytical results for the red-brown solid isolated in the attempted preparations of $RuBr_3(PPh_3)_2$ include:

(1) for equation 3.1, the best results obtained for $RuBr_3(PPh_3)_2(MeOH)$ [calculated: C, 49.52; H, 3.82%. Found: C, 54.77; H, 3.97%], may be compared with the values expected for $RuBr_2(PPh_3)_3$ [C, 61.90; H, 4.33%].

(2) for equation 3.4, calculated for $RuBr_3(PPh_3)_2(DMA)\cdot DMA$ solvate: C, 50.84; H, 4.65; N, 2.69%. Found: C, 54.29; H, 4.23; N, 1.37%.

Dekleva's analytical results were also very high (>10%) in carbon,[28,33] and were indicative of the presence of $RuBr_2(PPh_3)_3$.

Therefore, attempts to isolate materials of the composition $RuBr_3(PPh_3)_2$ were finally abandoned in favour of a ruthenium(II) precursor.

3.3.2 Ruthenium(II) Bromide Complexes; $RuBr_2(PPh_3)_3$ (10)

The complex $RuBr_2(PPh_3)_3$ **10** has been previously reported in the literature[32] and has also been prepared in this laboratory.[15,33] Two routes to **10** were attempted in this present thesis work (eqs 3.5–3.6).

$$RuCl_3\cdot xH_2O + xs\ LiBr + 6PPh_3 \xrightarrow{\text{MeOH, }\Delta} RuBr_2(PPh_3)_3 \qquad (3.5)$$

$$RuBr_3\cdot xH_2O + 6PPh_3 \xrightarrow{\text{MeOH, }\Delta} RuBr_2(PPh_3)_3 \qquad (3.6)$$
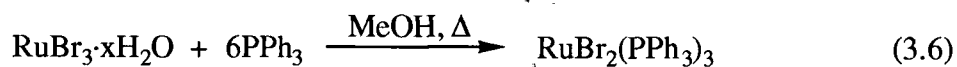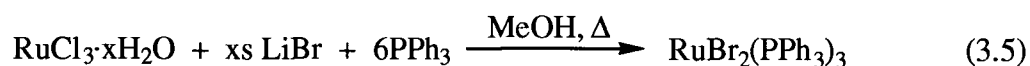
Equation 3.5 provided pure material on occasion, although quite often the isolated solid still contained chloride. The purity of this material (at least in terms of the presence or absence of chloride) could be ascertained by reaction of the isolated solid with CO in

CDCl$_3$ (eq 3.7).[33] The ^{31}P{^{1}H} NMR data for the products of the reaction with CO are shown in Table 3.1.

$$\text{RuXY(PPh}_3)_3 \ + \ \text{CO} \ \xrightarrow{\ \text{CDCl}_3\ } \ \textit{cct-}\text{RuXY(CO)}_2(\text{PPh}_3)_2 \ + \ \text{PPh}_3 \qquad (3.7)$$

$$\text{X, Y = Br or Cl}$$
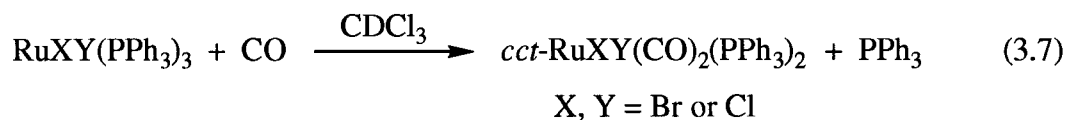
Table 3.1   The ^{31}P{^{1}H} NMR Chemical Shifts (121.42 MHz, 20 °C) for the Possible *cis, cis, trans*-Isomers of RuXY(CO)$_2$(PPh$_3$)$_2$

Complex	Chemical Shift, δ	
	CDCl$_3$	C$_6$D$_6$
*cct-*RuCl$_2$(CO)$_2$(PPh$_3$)$_2$	17.0[a]	17.0[b]
*cct-*RuBr$_2$(CO)$_2$(PPh$_3$)$_2$	13.1[a]	13.3[b]
*cct-*RuBrCl(CO)$_2$(PPh$_3$)$_2$	14.8[a]	15.0[b]

(a) this work; (b) from Dekleva's Ph.D. Thesis.[33]

Therefore, the absence of a resonance at 14.8 ppm in the ^{31}P{^{1}H} NMR spectrum (i.e., no *cct-*RuBrCl(CO)$_2$(PPh$_3$)$_2$ is present) is indicative of pure RuBr$_2$(PPh$_3$)$_3$.

Addition of an excess of pyridine to a sample of "RuBr$_2$(PPh$_3$)$_3$" was also useful in determining the presence of chloride impurity (Section 5.2).

The species RuBr$_3$·xH$_2$O was ineffective as a starting material for the preparation of RuBr$_2$(PPh$_3$)$_3$ (eq 3.6), as it was in preparing RuBr$_3$(PPh$_3$)$_2$ complexes. This is probably because of the limited solubility of RuBr$_3$·xH$_2$O in MeOH.

Other workers have experienced difficulty in completely substituting Br for Cl in preparations of RuBr$_2$(PPh$_3$)$_3$ (eq 3.5).[36] Even though pure material, free of chloride,

could be isolated on occasion, this method was inconsistent, and therefore not a good route into "RuBr$_2$(P–P)" chemistry.

The results of an X-ray diffraction study of RuBr$_2$(PPh$_3$)$_3$ will be presented in Section 3.3.3.

3.3.3 RuX$_2$(DPPB)(PAr$_3$), where X = Cl or Br and Ar = Ph or (*p*-tolyl)

The mixed-phosphine complexes RuCl$_2$(P–P)(PPh$_3$), where P–P = DPPB[21] or DIOP,[15,17] have been known for several years, and were synthesized by a simple phosphine exchange reaction (eq 3.8). More recently, the corresponding mixed-phosphine complexes of BINAP (see Figure 1.3)[22-24] and (*S*)-BIPHEMP (Figure 3.12)[24] have been prepared.

$$\text{RuCl}_2(\text{PPh}_3)_3 + \text{P-P} \xrightarrow{\text{P-P = DPPB, DIOP}} \text{RuCl}_2(\text{P-P})(\text{PPh}_3) + 2\text{PPh}_3 \qquad (3.8)$$
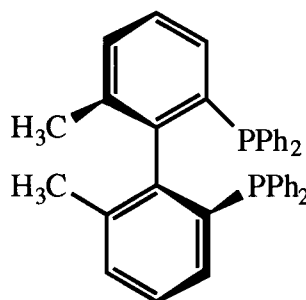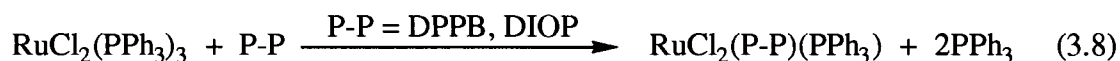
(S)-BIPHEMP

Figure 3.12 The structure of (*S*)-BIPHEMP.

The mixed-phosphine complexes are viewed as synthetically useful intermediates, largely because the following equilibrium (eq 3.9) is known to exist in solution (see below).

$$2RuCl_2(P\text{-}P)(PPh_3) \rightleftharpoons Ru_2Cl_4(P\text{-}P)_2 + 2PPh_3 \qquad (3.9)$$

Therefore, if the correct set of conditions were discovered, it may be possible to isolate the species "$RuCl_2(P\text{–}P)$" (i.e., $Ru_2Cl_4(P\text{–}P)_2$ or $Ru_2Cl_4(P\text{–}P)_2(L)$, where L is a neutral two–electron donor). Joshi of this laboratory had, in fact, synthesized $Ru_2Cl_4(P\text{–}P)_2(NEt_3)$, $Ru_2Cl_4(P\text{–}P)_2(CO)$, and $Ru_2Cl_4(P\text{–}P)_2(HN(n\text{-}Bu)_2)$ from $RuCl_2(DPPB)$-(PPh_3), although the formulation of the last mentioned complex remains in question, and will be discussed in Section 3.4.[22,23] Ideally, the so-called *naked dimer* $Ru_2Cl_4(DPPB)_2$ **24** could be isolated to allow maximum flexibility in terms of preparing additional species such as $[Ru(H)Cl(DPPB)]_3$.

Therefore, several different mixed-phosphine complexes were prepared in this work. Although the preparation of the mixed-phosphine complex was straightforward, occasionally the desired product had to be separated from the phosphine-bridged by-product, $Ru_2Cl_4(DPPB)_3$ **19** (or $[RuCl_2(DPPB)_{1.5}]_2$). This minor complication has been reported in the literature.[21-23] The bridged-phosphine species are insoluble in CH_2Cl_2, and can be separated from the mixed-phosphine complexes by washing the latter through a filter with CH_2Cl_2, leaving the former behind.

In the course of this work, it was noted in repeated preparations of $RuCl_2(DPPB)(PPh_3)$ that varying amounts of **19** were present (ranging from 0–43% based on DPPB). This was correlated with the purity of the $RuCl_2(PPh_3)_3$ **8** starting material. If excess PPh_3 was present in **8** (elemental analysis showed high C and H), then the bridged-phosphine complex was observed. However, if **8** was free of phosphine impurity, then no **19** was observed. Investigations into the origins of these observations included experiments in which free PPh_3 was added to the reaction mixture, and in which the "so-called tetrakis(phosphine) complex $RuCl_2(PPh_3)_4$" was used as the starting material.

A reaction mixture containing PPh$_3$ (0.5 equivalents per Ru, an amount which corresponded to the amount of PPh$_3$ present in an impure sample of **8**), pure RuCl$_2$(PPh$_3$)$_3$, and DPPB produced only the mixed-phosphine complex **11**. This was somewhat surprising, considering that **8** contaminated by PPh$_3$ always gave some **19**. In this experiment, the methylene chloride solvent was added to the three solids, **8**, PPh$_3$, and DPPB. The formation of increased amounts of the bridged-phosphine complex appears to require the PPh$_3$ 'impurity' to be somehow associated with the starting ruthenium complex. Therefore, a more informative experiment may have been to stir **8** and PPh$_3$ in solution for several hours before adding DPPB. Excess phosphine would affect the position of the known equilibrium (eq 3.10).[33,36]

$$2RuCl_2(PPh_3)_3 \; \rightleftharpoons \; Ru_2Cl_4(PPh_3)_4 + 2PPh_3 \qquad (3.10)$$
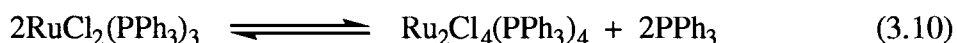
An alternative approach was to prepare RuCl$_2$(PPh$_3$)$_4$[32,37] and observe the effect of using this starting material on the ratio of mixed-phosphine to bridged-phosphine complexes. Equations 3.11 and 3.12 illustrate the published preparations for RuCl$_2$(PPh$_3$)$_3$ and RuCl$_2$(PPh$_3$)$_4$, respectively. The ratio of starting materials and concentrations are identical, as are the other reaction conditions, with the exception of temperature and reaction time. Other workers have argued that RuCl$_2$(PPh$_3$)$_4$ should be formulated as RuCl$_2$(PPh$_3$)$_3$·PPh$_3$, where the fourth PPh$_3$ is not coordinated, but is in the lattice framework.[36] The arguments are based on NMR evidence, as well as on the similarity of the colours of the two species. Hoffman and Caulton suggest that the supposed six-coordinate complex, isolated as a brown solid, should be yellow or colourless if it is in fact six-coordinate, as is observed for other six-coordinate Ru(II) phosphine-containing compounds.

$$RuCl_3 \cdot xH_2O + 6PPh_3 \xrightarrow[N_2, \, 3\,h]{MeOH, \, \Delta} RuCl_2(PPh_3)_3 \qquad (3.11)$$

$$RuCl_3 \cdot xH_2O + 6PPh_3 \xrightarrow[\text{N}_2,\, 24\,\text{h}]{\text{MeOH, 25 °C}} RuCl_2(PPh_3)_4 \tag{3.12}$$
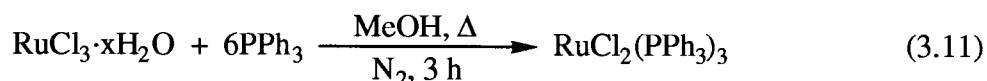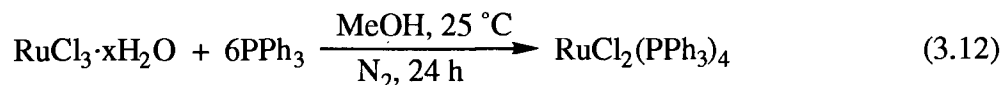
One attempt in this thesis work at preparing $RuCl_2(PPh_3)_4$ following the literature procedure[37] resulted in the isolation of a brown solid which analyzed as $RuCl_2(PPh_3)_3$. Calculated for $RuCl_2(PPh_3)_3$: C, 67.64; H, 4.73%. Found: C, 67.56; H, 4.78%. The calculated values for the tetrakis species, $RuCl_2(PPh_3)_4$ are: C, 70.82; H, 4.95%. Therefore, the effect of a fourth phosphine on the distribution of products could not be investigated.

Although nothing can be concluded about the nature of the role of PPh_3 from these studies, one can at least use reaction conditions to avoid the production of the bridged-phosphine complex in the synthesis of the mixed-phosphine complex. The reaction conditions necessary to avoid the formation of the bridged complex include the use of: (1) pure $RuCl_2(PPh_3)_3$, free of uncoordinated PPh_3, and (2) addition of exactly one equivalent of the bis(phosphine). If these conditions are employed, the $RuX_2(P-P)(PAr_3)$ species can be isolated in high yield (95%).

Interestingly, it is possible to prepare the six-coordinate ruthenium(II) antimony analogue, $RuCl_2(SbPh_3)_4$. An X-ray crystallographic study shows that the Ru–Sb bond lengths (average: 2.63 Å)[38] are significantly longer than the Ru–P bond lengths found in five-coordinate ruthenium(II) phosphine complexes (2.17–2.42 Å, see Sections 3.3.3.1 and 3.3.3.2).

3.3.3.1 Molecular Structure of RuBr$_2$(PPh$_3$)$_3$ (10)

During the course of these studies, a dark-orange crystal was isolated from the filtrate (CH_2Br_2 / EtOH / hexanes in ca. 1:6:2 ratio) of a preparation of $RuBr_2(DPPB)(PPh_3)$. This single-crystal X-ray diffraction study showed the molecular structure to be $RuBr_2(PPh_3)_3$, the starting complex. The presence of free PPh_3 in the

filtrate, resulting from the displacement of PPh3 by DPPB in the starting complex, probably aided the crystallization of the product by affecting the position of the equilibrium between **10** and $Ru_2Br_4(PPh_3)_4$ (cf. eq 3.10).[33] The ORTEP plot of $RuBr_2(PPh_3)_3$ **10** is shown in Figure 3.13; the molecular structure corresponds to that found for $RuCl_2(PPh_3)_3$ **8** by La Placa and Ibers.[39]

The geometry of **10** around the Ru centre is distorted square pyramidal, with the sixth coordination site of an octahedron blocked by an *ortho*-H (H(5)) of a PPh3 (P(1)). The Ru(1)–H(5) distance is 2.68 Å. Blocking of the sixth coordination site is also observed for both $RuCl_2(PPh_3)_3$[†] and $RuCl_2(DPPB)(PPh_3)$ (see Section 3.3.3.2 for the ORTEP plot and discussion of the DPPB complex). Hoffman and Caulton have discussed the preference of square pyramidal over trigonal bipyramidal geometries for five-coordinate Ru(II) complexes.[36] Selected bond lengths and angles for $RuBr_2(PPh_3)_3$ **10** are given in Tables 3.2 and 3.3, respectively. The structural parameters and experimental details are given in Appendix I.

---

†   Several authors (references i, ii, and iii listed below) have indicated that this compound is the first example of an agostic C–H_a metal interaction. The interaction in this case would be weak, as the M–H distance is quite long (2.59 Å).

(i)   Perera, S. D.; Shaw, B. L. *J. Chem. Comm., Chem. Commun.* **1994**, 1201.

(ii)   Crabtree, R. H. *Agnew. Chem., Int. Ed. Engl.* **1993**, *32*, 789.

(iii)   Brookhart, M.; Green, M. L. H. *J. Organomet. Chem.*, **1983**, *250*, 395.
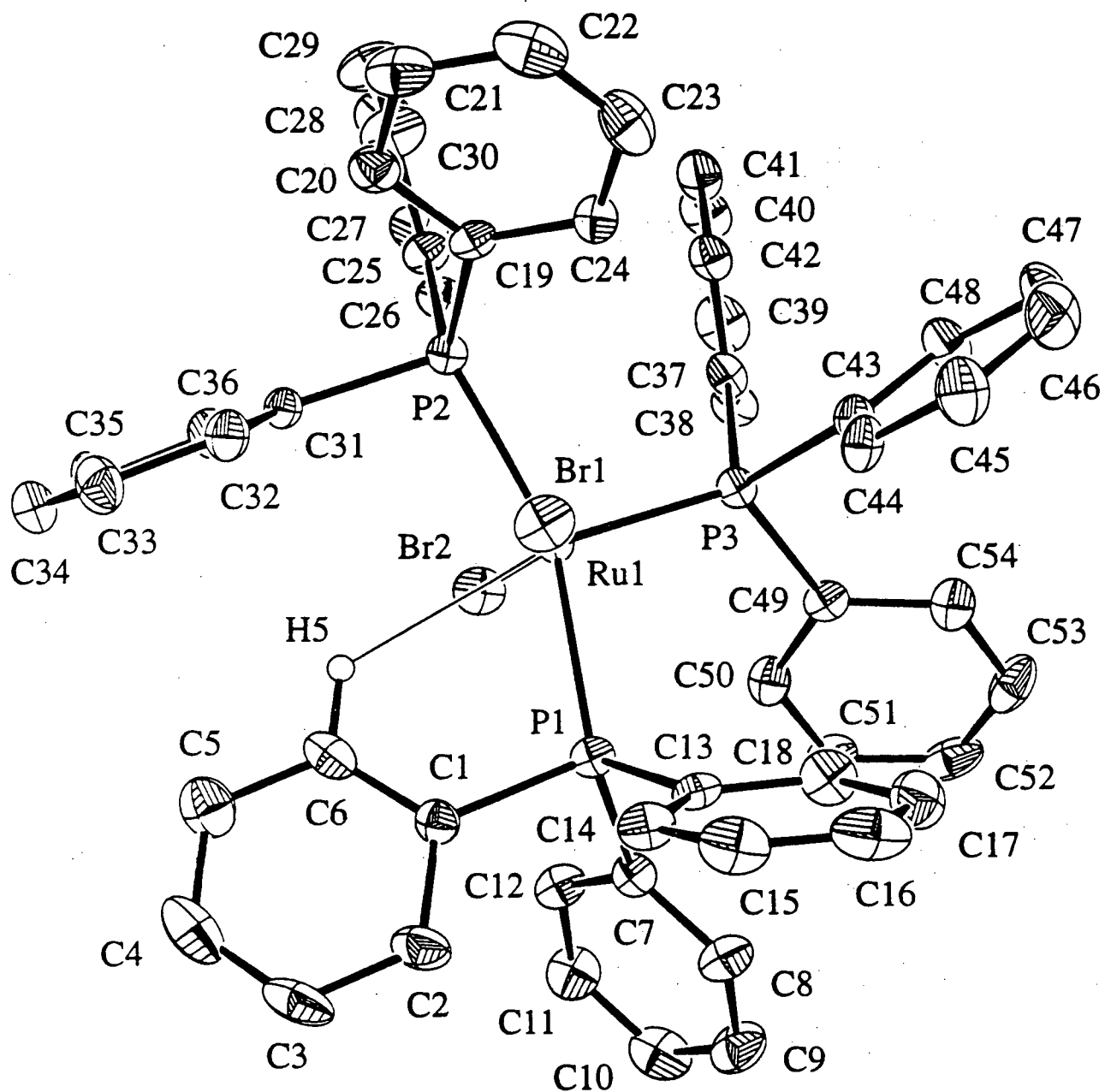
Figure 3.13 The ORTEP plot of RuBr$_2$(PPh$_3$)$_3$ **10**. Thermal ellipsoids for non-hydrogen atoms are drawn at 33% probability.

Table 3.2   Selected Bond Lengths (Å) for RuBr$_2$(PPh$_3$)$_3$ **10** with Estimated Standard
Deviations in Parentheses

Bond	Length (Å)	Bond	Length (Å)
Ru(1)—Br(1)	2.515(1)	Ru(1)—Br(2)	2.526(1)
Ru(1)—P(1)	2.423(2)	Ru(1)—P(2)	2.389(2)
Ru(1)—P(3)	2.227(2)	P(1)—C(1)	1.834(7)
P(1)—C(7)	1.844(7)	P(1)—C(13)	1.839(7)
P(2)—C(19)	1.843(7)	P(2)—C(25)	1.857(7)
P(2)—C(31)	1.837(7)	P(3)—C(37)	1.849(7)
P(3)—C(43)	1.834(7)	P(3)—C(49)	1.846(7)
Ru(1)—H(5)	2.68*		

* non-bonded contact

Table 3.3   Selected Bond Angles (°) for RuBr$_2$(PPh$_3$)$_3$ **10** with Estimated Standard
Deviations in Parentheses

Bonds	Angles (°)	Bonds	Angles (°)
Br(1)—Ru(1)—Br(2)	155.64(4)	Br(1)—Ru(1)—P(1)	82.19(5)
Br(1)—Ru(1)—P(2)	84.31(5)	Br(1)—Ru(1)—P(3)	110.39(5)
Br(2)—Ru(1)—P(1)	93.04(5)	Br(2)—Ru(1)—P(2)	91.34(5)
Br(2)—Ru(1)—P(3)	93.96(5)	P(1)—Ru(1)—P(2)	156.43(7)
P(1)—Ru(1)—P(3)	101.28(7)	P(2)—Ru(1)—P(3)	101.50(7)
Br(1)—Ru(1)—H(5)	83.2	Br(2)—Ru(1)—H(5)	72.9
P(1)—Ru(1)—H(5)	68.3	P(2)—Ru(1)—H(5)	91.0
P(3)—Ru(1)—H(5)	162.2		

3.3.3.2 Molecular Structure of RuCl$_2$(DPPB)(PPh$_3$) (11)

The solid-state structure of RuCl$_2$(DPPB)(PPh$_3$) **11** was suggested by Joshi to be square pyramidal. His comparison of the solid-state (CP/MAS) and low-temperature solution ^{31}P{^{1}H} NMR spectra of **11** with the spectra of RuCl$_2$(PPh$_3$)$_3$ **8** showed similarities that were thought to indicate a similar solid-state structure.[22] An X-ray crystallographic study of **11** in this present work confirmed this suggestion.[22] Green crystals were isolated from an NMR solution comprised of **11** and 14 equivalents of PPh$_3$ in C$_7$D$_8$, which was left under an atmosphere of N$_2$ in a glove-box for several months. The molecular structure corresponded to those found for **8** and **10** (Figure 3.13). The ORTEP of RuCl$_2$(DPPB)(PPh$_3$) **11** is shown in Figure 3.14.

The geometry of **11** around the Ru centre is distorted square pyramidal, with the sixth coordination site of an octahedron blocked by an *ortho*-H (H(29)) of a PPh$_3$ (P(3)). The Ru(1)–H(29) distance is 2.69 Å. Selected bond lengths and angles for RuCl$_2$(DPPB)(PPh$_3$) **11** are given in Tables 3.4 and 3.5, respectively. The structural parameters and experimental details are given in Appendix II.

Table 3.4 Selected Bond Lengths (Å) for RuCl$_2$(DPPB)(PPh$_3$) **11** with Estimated Standard Deviations in Parentheses

Bond	Length (Å)	Bond	Length (Å)
Ru(1)—Cl(1)	2.3796(8)	Ru(1)—Cl(2)	2.4047(9)
Ru(1)—P(1)	2.3346(9)	Ru(1)—P(2)	2.2029(9)
Ru(1)—P(3)	2.3786(9)	P(1)—C(1)	1.836(4)
P(1)—C(5)	1.820(4)	P(1)—C(11)	1.826(4)
P(2)—C(4)	1.849(3)	P(2)—C(17)	1.842(3)
P(2)—C(23)	1.834(3)	P(3)—C(29)	1.824(3)
P(3)—C(35)	1.844(3)	P(3)—C(41)	1.834(3)
Ru(1)—H(29)	2.69*		

* non-bonded contact
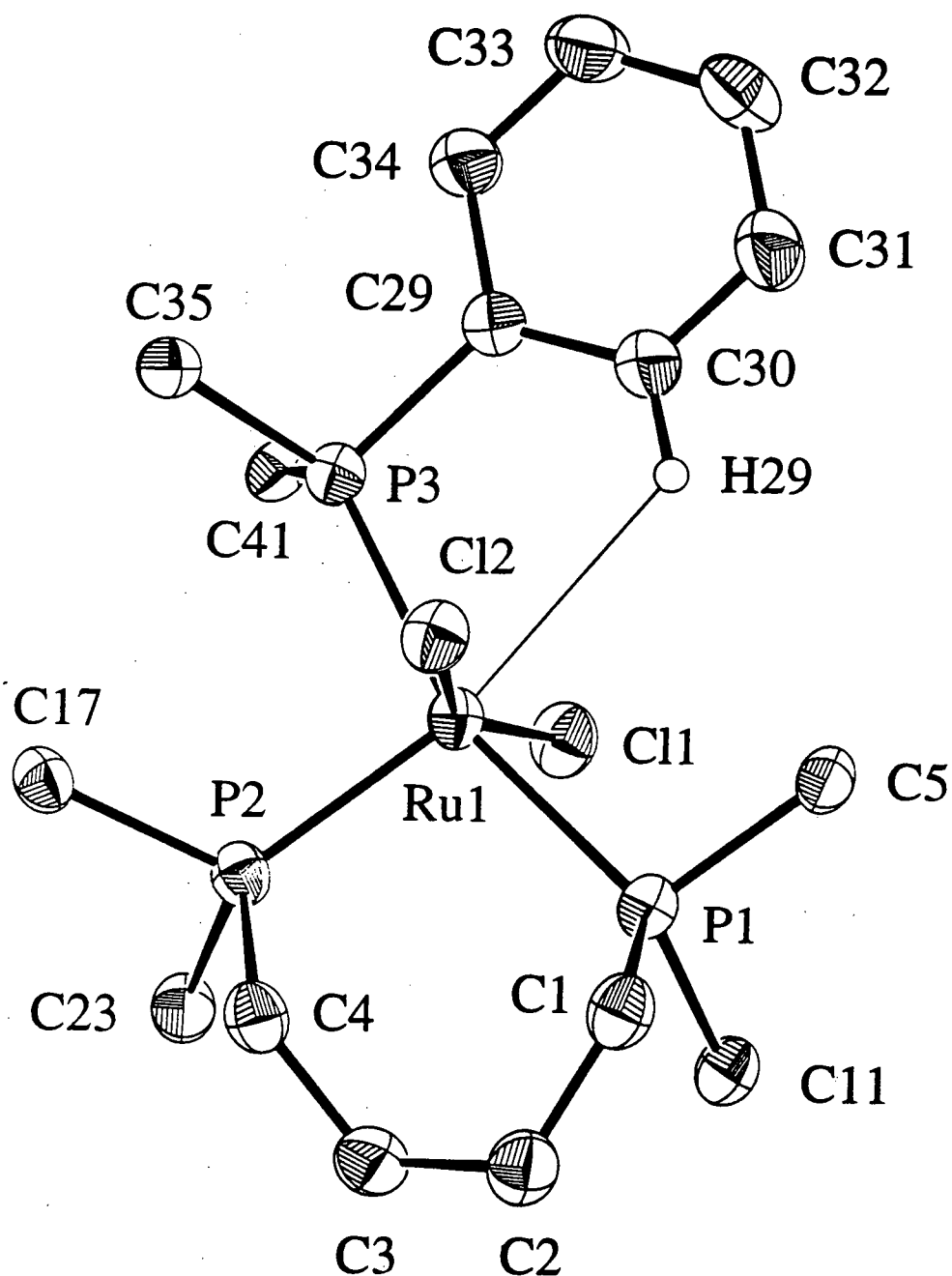
Figure 3.14   The ORTEP plot of RuCl₂(DPPB)(PPh₃) **11**. Thermal ellipsoids for non-hydrogen atoms are drawn at 33% probability (some of the phenyl carbons have been omitted for clarity).

Table 3.5   Selected Bond Angles (°) for RuCl$_2$(DPPB)(PPh$_3$) **11** with Estimated Standard Deviations in Parentheses

Bonds	Angles (°)	Bonds	Angles (°)
Cl(1)—Ru(1)—Cl(2)	158.75(3)	Cl(1)—Ru(1)—P(1)	88.61(3)
Cl(1)—Ru(1)—P(2)	109.76(3)	Cl(1)—Ru(1)—P(3)	85.82(3)
Cl(2)—Ru(1)—P(1)	87.06(3)	Cl(2)—Ru(1)—P(2)	91.42(3)
Cl(2)—Ru(1)—P(3)	91.87(3)	P(1)—Ru(1)—P(2)	97.01(3)
P(1)—Ru(1)—P(3)	161.78(3)	P(2)—Ru(1)—P(3)	101.20(3)
Cl(1)—Ru(1)—H(29)	81.2	Cl(2)—Ru(1)—H(29)	78.2
P(1)—Ru(1)—H(29)	92.6	P(2)—Ru(1)—H(29)	165.5
P(3)—Ru(1)—H(29)	69.4		

The metal centres of RuBr$_2$(PPh$_3$)$_3$ **10** and RuCl$_2$(DPPB)(PPh$_3$) **11** are best described as being near the centre of gravity of a distorted square pyramid composed of *trans* P atoms and *trans* Cl atoms in the base, with a third P atom at the apex. The main differences in the structures of RuCl$_2$(PPh$_3$)$_3$ **8, 10**, and **11** are probably due to the chelating DPPB ligand in **11**.

The Ru metal centre in each of **8, 10**, and **11** is found above the mean plane created by the two halides and two basal phosphorus atoms, the Ru atom being observed 0.456, 0.518, and 0.404 Å above the basal plane, respectively. In all three complexes, the apical Ru–P distances (2.20–2.23 Å) are shorter than the basal Ru–P distances (2.34–2.42 Å). Also, the Ru–P distances of the phosphine groups involved in the agostic hydrogen interaction (i.e., *ortho*–H of a phenyl group) are longer than the other basal Ru–P bond lengths.

Other five-coordinate ruthenium(II) phosphine complexes for which X-ray structural data have been determined include RuCl$_2$(PMA)(P(*p*-tolyl)$_3$)[40,41] and

RuCl$_2$(isoPFA)(PPh$_3$)[42,43] which both contain P–N chelates (PMA is shown in Figure 3.28, Section 3.10). Interestingly, the latter complex has an *ortho*-H of a PPh$_3$ blocking the sixth coordination site of an octahedron while the former complex does not. RuCl$_2$(PMA)(P(p-tolyl)$_3$) is known to coordinate a range of small molecules including O$_2$, CO, H$_2$O, H$_2$S, SO$_2$, and MeOH.[40,41]

The analogous mixed-phosphine complexes RuCl$_2$(DPPB)(P(p-tolyl)$_3$) **12**, RuBr$_2$(DPPB)(PPh$_3$) **13**, and RuCl$_2$((R)-BINAP)(PPh$_3$) **15** prepared in this work are believed to have the same geometry around Ru as in **11**, based on low temperature ^{31}P{^{1}H} NMR studies. Table 3.6 summarizes the room- and low temperature ^{31}P{^{1}H} NMR spectral data; those for **12** in CD$_2$Cl$_2$ are shown in Figure 3.15.

The dynamic process observed in the room temperature ^{31}P{^{1}H} NMR spectrum of **12** (and the other mixed-phosphine complexes) is due to intramolecular exchange of the DPPB (or other diphosphine) nuclei on the NMR timescale as observed for **11** by Jung et al.[21] The rate of PPh$_3$ dissociation is too slow to be responsible for the fluxional process observed at room temperature (the linewidth of the PPh$_3$ was essentially invariant over the temperature range –66–+20 °C).

The ABX pattern observed in the low temperature ^{31}P{^{1}H} NMR spectrum (see Figure 3.15 and Table 3.6) is consistent with the structure determined by X-ray crystallography for the PPh$_3$ analogue. The spectrum is consistent with two *cis*- and one *trans*-phosphorus-phosphorus interactions. The *trans* $^2J_{PP}$ coupling constants are known to be much greater in magnitude than *cis* $^2J_{PP}$ coupling constants.[44]
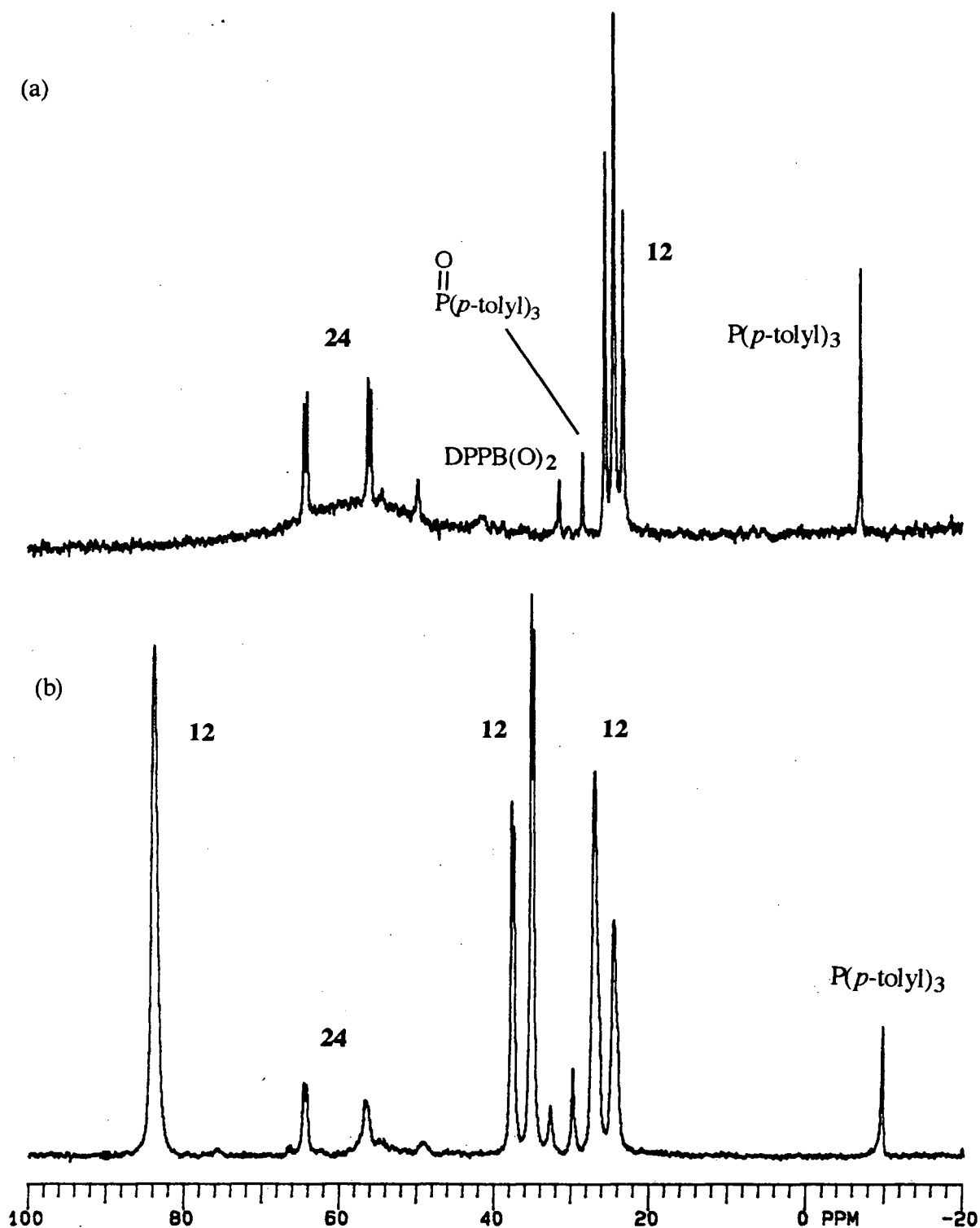
Figure 3.15 The $^{31}P\{^1H\}$ NMR spectra (121.42 MHz) of $RuCl_2(DPPB)(P(p\text{-tolyl})_3)$ **12**
in CD_2Cl_2 at: (a) 20 °C and (b) –66 °C. **24** = $Ru_2Cl_4(DPPB)_2$.

108

Table 3.6 $^{31}P\{^1H\}$ NMR Data (121.42 MHz)[a] for $RuX_2(P–P)(PAr_3)$ Complexes

Complex	Solvent	Temp (°C)	Chemical Shift, δ	$^2J_{PP}$, (Hz)
$RuCl_2(DPPB)(PPh_3)$ **11**	C_6D_6	20	$\delta_A = 25.7$	140[b]
	C_7D_8	20	$\delta_A = 26.7$	142[b]
	C_7D_8	–70	$\delta_A = 28.4$ $\delta_B = 36.2$ $\delta_X = 86.1$	$^2J_{AX}$ = unresolved $^2J_{BX} = 37.7$ $^2J_{AB} = 297.5$
	CH_2Cl_2[c]	–75	$\delta_A = 26.3$ $\delta_B = 35.2$ $\delta_X = 83.2$	$^2J_{AX} = -22.6$ $^2J_{BX} = -37.5$ $^2J_{AB} = 302.4$
$RuCl_2(DPPB)(P(p\text{-tolyl})_3)$ **12**	C_6D_6	20	$\delta_A = 25.5$	141[b]
	CD_2Cl_2	20	$\delta_A = 24.5$	141[b]
	CD_2Cl_2	–66	$\delta_A = 25.9$ $\delta_B = 36.6$ $\delta_X = 83.9$	$^2J_{AX}$ = unresolved $^2J_{BX} = -35.7$ $^2J_{AB} = 303.2$
	$CDCl_3$	–58	$\delta_A = 24.7$ $\delta_B = 34.9$ $\delta_X = 84.4$	$^2J_{AX}$ = unresolved $^2J_{BX} = -35.9$ $^2J_{AB} = 303.7$
$RuBr_2(DPPB)(PPh_3)$ **13**	C_6D_6	20	$\delta_A = 27.6$	135[b]
	CD_2Cl_2	20	$\delta_A = 27.3$	145[b]
	CD_2Cl_2	–66	$\delta_A = 29.3$ $\delta_B = 37.5$ $\delta_X = 86.8$	$^2J_{AX}$ = unresolved $^2J_{BX} = -35.8$ $^2J_{AB} = 300.4$

Chapter 3 References: p 157

Table 3.6 (continued)

Complex	Solvent	Temp (°C)	Chemical Shift, δ	$^2J_{PP}$, (Hz)
RuCl$_2$((S)-BINAP)(PPh$_3$)	CD$_2$Cl$_2$[d]	20	$\delta_A = 19.0$	151[b]
	CD$_2$Cl$_2$[d]	–60	$\delta_A = 22.6$	$^2J_{AX} = 23.2$
			$\delta_B = 26.4$	$^2J_{BX} = 39.6$
			$\delta_X = 87.4$	$^2J_{AB} = 327.5$
RuCl$_2$(DIOP)(PPh$_3$)[e]	C$_7$D$_8$[f]	–60	$\delta_A = 17.3$	$^2J_{AX} = 24$
			$\delta_B = 32.7$	$^2J_{BX} = 41$
			$\delta_X = 66.6$	$^2J_{AB} = 310$
RuCl$_2$((S)-BIPHEMP)(PPh$_3$)[e]	CD$_2$Cl$_2$[d]	20	$\delta_A = 20.1$	151[b]
	CD$_2$Cl$_2$[d]	–60	$\delta_A = 21.0$	$^2J_{AX} = 21.9$
			$\delta_B = 29.2$	$^2J_{BX} = 41.5$
			$\delta_X = 84.7$	$^2J_{AB} = 323.4$
RuCl$_2$(DCYPB)(PPh$_3$) **14**	CD$_2$Cl$_2$[g]	–50	$\delta_A = 19.5$	133[b]
	CD$_2$Cl$_2$[g]	–70	$\delta_A = 17.1$	$^2J_{AX}$ = unresolved
			$\delta_B = 24.1$	$^2J_{BX}$ = unresolved
			$\delta_X = 88.0$	$^2J_{AB} = 303.7$

(a) Spectrometer frequency used for the values measured in this work. (b) Triplet-like, three-line pattern; J value indicates line spacing. The δ_B of the AB$_2$ pattern observed at 20 °C appears as a very broad resonance between 50–60 ppm in all cases (an example is shown in Figure 3.15(a)) (c) Jung et al.[21] (d) Mezzetti et al.[24] (e) Included for completeness. (f) Wang[15] (g) Prepared in situ from RuCl$_2$(PPh$_3$)$_3$ and DCYPB.

3.3.4 Ru₂X₄(DPPB)₂ Complexes
3.3.4.1 Preparation of Ru₂Cl₄(DPPB)₂ (24) and Ru₂Br₄(DPPB)₂ (25)

The route previously employed to prepare the $Ru_2Cl_4(DPPB)_2$ **24** complex is outlined in Figure 3.6, and is shown to be via the H_2-reduction of $Ru_2Cl_5(DPPB)_2$ **22**. The inability in this work to prepare pure $RuBr_3(PPh_3)_2$ complexes prevented the preparation of $Ru_2Br_5(DPPB)_2$ complexes. Therefore, an alternative route to $Ru_2Br_4(DPPB)_2$ **25** was necessary. Generally, routes to the chloride analogues were investigated before the more difficult bromide chemistry was attempted.

Equation 3.9 shows the equilibrium between the mixed-phosphine complex $RuX_2(P-P)(PPh_3)$ and $Ru_2X_4(P-P)_2$, which suggests that the mixed-phosphine complexes are good in situ sources of $Ru_2X_4(P-P)_2$. It would be useful, however, to be able to remove the PPh_3, forcing the equilibrium to the right, and allowing the isolation of $Ru_2X_4(P-P)_2$.

It would be interesting to attempt reverse osmosis as a method of isolating $Ru_2Cl_4(DPPB)_2$. In reverse osmosis, a dissociable complex is forced against a selectively permeable membrane under pressure. The metal species is retained by the membrane, while the dissociated ligand (i.e., PPh_3) and the solvent diffuse through the membrane. Gosser et al. have made use of this method to isolate $Ru_2Cl_4(PPh_3)_4(N_2)$ from solutions of $RuCl_2(PPh_3)_4$, when N_2 was used as the pressurizing gas.[45]

Other methods of removing triphenylphosphine have been attempted. Joshi attempted to remove the PPh_3 from $RuCl_2(DPPB)(PPh_3)$ by adding MeI to produce the quaternary phosphonium salt, $PMePh_3^+I^-$.[22] This method resulted in the formation of a species, when 10 equivalents of MeI were used, that showed an AB quartet ($\delta_A = 71.1$, $\delta_B = 56.6$, $^2J_{AB} = 40.0$ Hz) in the $^{31}P\{^1H\}$ NMR spectrum.[22] Joshi suggested this species to be dinuclear, but did not suggest a structure because the $^{31}P\{^1H\}$ spectrum did not correspond to that known for **24**. In this present thesis work, $Ru_2I_4(DPPB)_2$ **27** was prepared from $Ru(DPPB)(\eta^3\text{-Me-allyl})_2$ **55** and HI, and the $^{31}P\{^1H\}$ NMR data (Table

3.9, later in this section) for this complex agree with those observed by Joshi. Therefore, the species observed on addition of 10 equivalents of MeI to the mixed-phosphine complex is actually **27**.

However, an in situ $^{31}P\{^1H\}$ NMR experiment performed by Joshi et al.[23] with the addition of 100 equivalents of MeI to $RuCl_2(DPPB)(PPh_3)$ (instead of 10 equiv), showed two AB quartets ($\delta_A = 52.6$, $\delta_B = 51.7$, $^2J_{AB} = 43.4$ Hz; $\delta_C = 48.6$, $\delta_D = 41.8$, $^2J_{CD} = 36.7$ Hz) which were attributed to $Ru_2Cl_4(DPPB)_2(MeI)$; in view of the now established formation of **27**, this MeI adduct should perhaps be reformulated as $Ru_2I_4(DPPB)_2(MeI)$.

Cu(I) halides are known to react with PPh_3 to form complexes of the type $CuX(PPh_3)_2$, $CuX(PPh_3)_3$, $Cu_2X_2(PPh_3)_3$, and $[CuX(PPh_3)]_4$.[46] Therefore, attempts were made in the course of this work to remove PPh_3 using CuCl or CuI. The use of CuI, although effective in removing PPh_3 from the $RuCl_2(P-P)(PPh_3)$ complex, resulted in complications because of halide exchange. For example, $RuCl_2(DPPB)(PPh_3)$ was found to give a mixture of chloro and iodo Ru(II) complexes, as well as $Cu_2X_2(PPh_3)_3$ species.[46] Other Cu(I)-phosphine species (listed above) may be present, but $Cu_2X_2(PPh_3)_3$ species are thought to predominate in solution.[46]

The use of 10 equivalents of CuCl was effective for the removal of PPh_3 from $RuCl_2(DPPB)(PPh_3)$ in C_6H_6 solution. The product of this reaction, however, was a mixture of $Cu^+[Ru_2Cl_5(P-P)_2]^-$ and CuCl-phosphine complex(es). The addition of CuCl to the dark-green suspension of $RuCl_2(DPPB)(PPh_3)$ produced an immediate change to a dark-orange colour. The solution was stirred at room temperature for 1 h. The excess cuprous chloride was then removed by filtering the solution through a layer of Celite, and an orange solid was obtained by concentrating the benzene solution and adding hexanes.

Although $^{31}P\{^1H\}$ NMR spectroscopy has been used to show the complexity of the solution behaviour of these $CuX-PPh_3$ species, due to the lability of the phosphine

ligands in these copper(I) complexes, no $^{31}P\{^1H\}$ NMR data for specific complexes have been reported.[46,47]

The $^{31}P\{^1H\}$ NMR spectrum of the orange solid in C_6D_6 showed a singlet for $Cu^+[Ru_2Cl_5(P-P)_2]^-$ at 53.5 ppm, and two broad resonances at 51 and -1.9 ppm for the $CuCl\text{-}PPh_3$ complex formed. These broad resonances were confirmed as belonging to a $Cu(I)\text{-}PPh_3$ complex through the preparation of such a Cu-phosphine complex. A preparation was followed which reportedly gave $Cu_2Cl_2(PPh_3)_3$.[48] In fact, the white solid isolated by this procedure gave an elemental analysis which agreed with the formation of another known complex, $CuCl(PPh_3)$ (see Section 2.1.5.2),[49] which has been shown subsequently in the literature by X-ray crystallography to be the tetramer, $[CuCl(PPh_3)]_4$, a cubane-like arrangement of copper and chlorine atoms.[50] The white solid $[CuCl(PPh_3)]_4$ gave a $^{31}P\{^1H\}$ NMR spectrum showing the broad resonances at 51 and -1.9 ppm confirming that these are associated with $CuCl\text{-}PPh_3$ species. $[CuCl(PPh_3)]_4$ is known to decompose, upon repeated recrystallizations from C_6H_6, to give $Cu_2Cl_2(PPh_3)_3$.[51] Lippard and Mayerle made use of vapour pressure osmometry to investigate the dominant CuCl-phosphine complex in solution.[46]

The anion $[Ru_2Cl_5(DPPB)_2]^-$ has been isolated previously in this laboratory with both a DMAH and TMP cation (1,1,3-trimethyl-2,3-dihydroperimidinium, see Figure 4.22, Section 4.7.2 for structure), and an X-ray structure-determination of $[TMP]^+[Ru_2Cl_5(DPPB)_2]^-\cdot2Me_2CO\cdot2H_2O$ revealed the molecular structure shown in Figure 3.16.[52,53] The molecular structure of the unusual TMP cation, generated from Proton Sponge by net hydride loss from one methyl group, has been published previously,[52] but X-ray crystallographic data for the anionic $[Ru_2Cl_5(DPPB)_2]^-$ determined by Thorburn et al.[53] have not appeared elsewhere, and will be included here for reference purposes. Selected bond lengths and angles for $[Ru_2Cl_5(DPPB)_2]^-$ are given in Tables 3.7 and 3.8, respectively. The structural parameters and experimental details are given in Appendix III. The $^{31}P\{^1H\}$ NMR spectrum of $[TMP]^+[Ru_2Cl_5(DPPB)_2]^-$ is

reported to show a singlet at 53.6 ppm in CD_2Cl_2,[52] which is the same as that observed when Cu is the cation (see above).

The ionic nature of the Cu product was further confirmed by reacting one equivalent of CuCl with $Ru_2Cl_4(DPPB)_2$ in $CDCl_3$. The $^{31}P\{^1H\}$ NMR spectrum of the orange solution after one week at room temperature showed a singlet at 48.3 ppm indicating formation of $Cu^+[Ru_2Cl_5(DPPB)_2]^-$. The reaction was slow in this solvent probably because of the limited solubility of CuCl in $CDCl_3$. The AB pattern characteristic of the starting dinuclear complex was almost completely gone after one week.

A similar ionic species, $[DMAH]^+[Ru_2Cl_5(DPPB)_2]^-$, is known to be the species produced in the H_2-reduction of $Ru_2Cl_5(DPPB)_2$ (see Figure 3.6). This ionic species is not isolated in this preparation because the complex is broken up by the addition of MeOH to generate the desired $Ru_2Cl_4(DPPB)_2$ complex and DMA·HCl.

The removal of PPh_3 by the addition of CuCl thus is a promising route. The conditions for removal of the $CuCl-PPh_3$ complex from the ionic ruthenium species, and subsequent break-up of the ionic complex to give $Ru_2Cl_4(DPPB)_2$, were not investigated further because a more straightforward route to this complex was discovered.

Table 3.7   Selected Bond Lengths (Å) for $[Ru_2Cl_5(DPPB)_2]^-$ with Estimated Standard Deviations in Parentheses

Bond	Length (Å)	Bond	Length (Å)
Ru—Cl(1)	2.4269(10)	C(1)—C(2)	1.551(7)
Ru—Cl(2)	2.4968(10)	C(2)—C(3)	1.531(7)
Ru—Cl(3)	2.4136(10)	C(3)—C(4)	1.511(6)
Ru—P(1)	2.2650(12)	P(1)—C(1)	1.858(4)
Ru—P(2)	2.2642(10)	P(2)—C(4)	1.841(4)
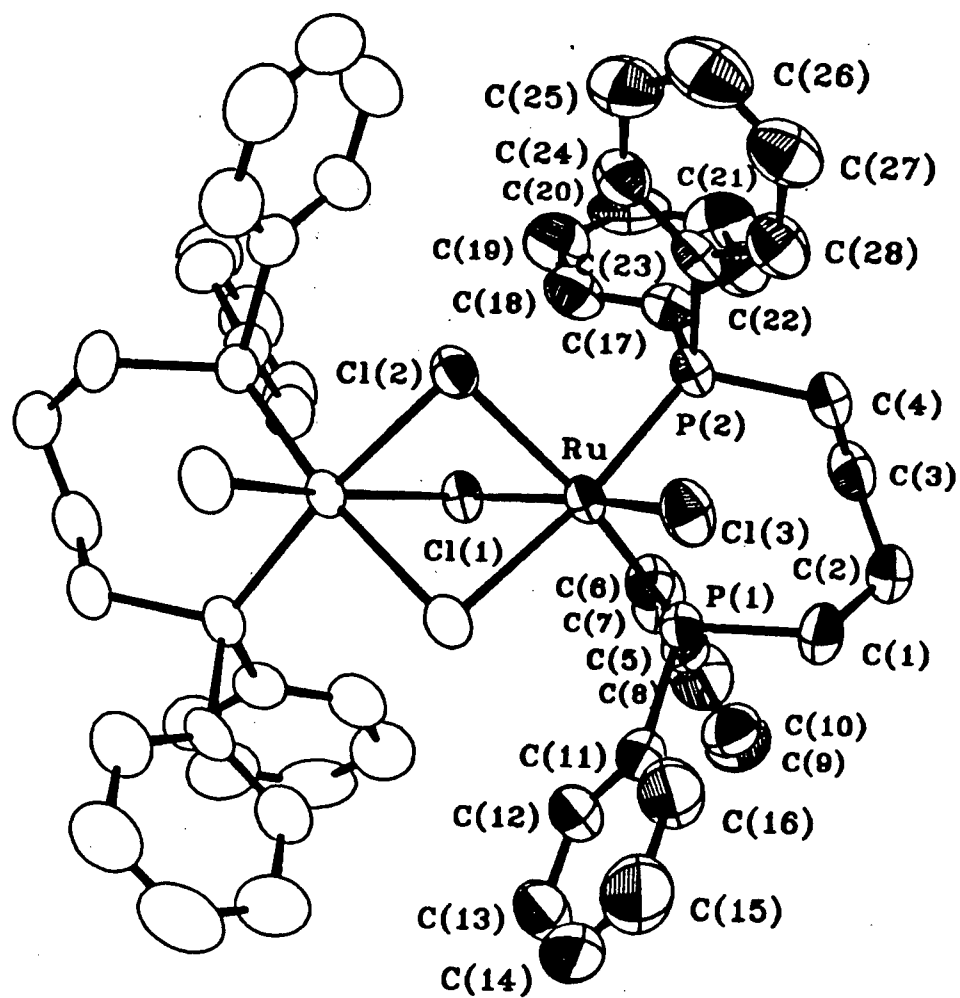
Figure 3.16 The ORTEP plot of the anionic [Ru$_2$Cl$_5$(DPPB)$_2$]$^-$ in [TMP]$^+$ [Ru$_2$Cl$_5$(DPPB)$_2$]$^-$.

115

Table 3.8   Selected Bond Angles (°) for [Ru$_2$Cl$_5$(DPPB)$_2$]$^-$ with Estimated Standard Deviations in Parentheses

Bond	Angles (°)	Bond	Angles (°)
Cl(1)—Ru—Cl(2)	78.85(3)	Cl(3)—Ru—P(1)	88.12(4)
Cl(1)—Ru—Cl(3)	167.71(3)	Cl(3)—Ru—P(2)	86.67(4)
Cl(1)—Ru—P(1)	97.50(3)	Cl(3)—Ru—Cl(2)'	90.02(4)
Cl(1)—Ru—P(2)	103.41(3)	P(1)—Ru—P(2)	96.74(4)
Cl(1)—Ru—Cl(2)'	78.77(3)	P(1)—Ru—Cl(2)'	93.52(4)
Cl(2)—Ru—Cl(3)	94.16(4)	P(2)—Ru—Cl(2)'	169.10(4)
Cl(2)—Ru—P(1)	172.04(4)	Ru—Cl(1)—Ru'	87.77(5)
Cl(2)—Ru—P(2)	91.01(4)	Ru—Cl(2)—Ru'	84.64(3)
Cl(2)—Ru—Cl(2)'	78.87(4)	Ru—P(1)—C(1)	118.8(2)
Ru—P(2)—C(4)	117.16(15)		

Refluxing RuCl$_2$(DPPB)(PPh$_3$) or RuCl$_2$(DPPB)(P(p-tolyl)$_3$) in a 1:1 mixture of C$_6$H$_6$ / H$_2$O, subsequently removing the H$_2$O layer, and adding hexanes produced in high yield an orange solid (Section 2.5.7.1) that proved to be Ru$_2$Cl$_4$(DPPB)$_2$ **24**. Alternatively, hexanes could be added directly to the two-phase system to precipitate **24**. The mechanism of PPh$_3$ (or P(p-tolyl)$_3$) removal is not understood, but H$_2$O is known to be essential for the isolation of **24**.

In the absence of H$_2$O, when the mixed-phosphine complex was refluxed in benzene in order to shift the equilibrium 3.9 to the right, the reaction mixture retained the green colour of the starting five-coordinate complex. On addition of H$_2$O, the reaction mixture quickly became orange, indicating formation of the dimer. In situ NMR experiments in C$_6$D$_6$ / D$_2$O showed that PPh$_3$, for example, had not been oxidized to phosphine oxide. The mixed-phosphine complex was also refluxed in a 1:1 benzene /

hexanes solution in an attempt to selectively precipitate the dimer as it was formed, but this also did not result in isolation of pure dimer.

The idea of adding H_2O to the mixed-phosphine complex in order to produce $Ru_2Cl_4(DPPB)_2$ came from noting that the elemental analysis of **24** determined by previous workers showed the presence of a mole of H_2O.[22,23,25,30] It is possible that in the solid-state the H_2O is actually coordinated (i.e., $Ru_2Cl_4(DPPB)_2(H_2O)$). In solution, the $^{31}P\{^1H\}$ NMR spectrum shows only a single AB pattern for **24**, while two AB quartets would be expected if the H_2O remained coordinated in solution. To date, our group has been unable to isolate crystals of $Ru_2Cl_4(P-P)_2$ which are suitable for X-ray diffraction studies, where P–P is any of the eight different phosphines used (Section 3.2). A solid-state CP/MAS $^{31}P\{^1H\}$ NMR study of the dimer, analyzing for a mole of H_2O, might provide insight into the nature of the water molecule (i.e., whether it is coordinated or solvated). In fact, on one occasion during this work the dimer was heated overnight (78 °C) under vacuum before submission for elemental analysis. The colour of the solid changed from orange to brown during the heating period, and elemental analysis showed the complex to be **24** without H_2O solvate (see Section 2.5.7.1 for micro-analytical data).

The bromo analogue, $Ru_2Br_4(DPPB)_2$ **25**, was also prepared from $RuBr_2(DPPB)(PPh_3)$ in the same manner (using H_2O) as described above (Section 2.5.7.2). The $^{31}P\{^1H\}$ NMR spectrum of **25** is shown in Figure 3.17.

Addition of $Ru_2Cl_4(DPPB)_2$ to an NMR sample of $Ru_2Br_4(DPPB)_2$ in $CDCl_3$ resulted in halide-exchange as evidenced by loss of the AB quartet for **25** in the $^{31}P\{^1H\}$ NMR spectrum and appearance of two multiple-line patterns centred at 55 and 65 ppm. These complicated patterns are indicative of the formation of $[RuBr_{2-x}Cl_x(DPPB)]_2$ species. No halide exchange is evident between **25** and the chlorinated solvents CD_2Cl_2 or $CDCl_3$.
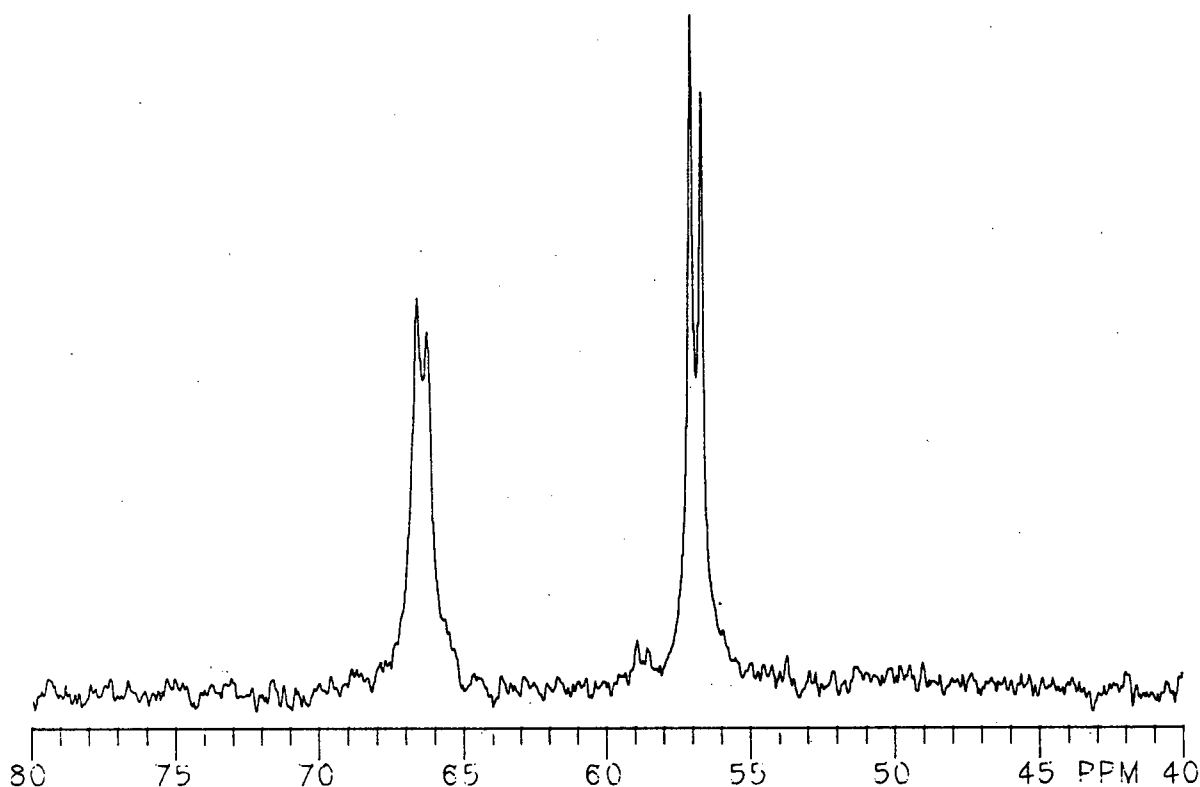
Figure 3.17 $^{31}P\{^1H\}$ NMR spectrum (121.42 MHz, 20 °C) of Ru$_2$Br$_4$(DPPB)$_2$ **25** in C$_6$D$_6$.

This "aqueous" route, although very useful for the preparation of **24** and **25** is probably not a general one for the preparation of dimers containing other chelating phosphines. Using this method, a single attempt at preparing Ru$_2$Cl$_4$((*R*)-BINAP)$_2$ **26** from RuCl$_2$(BINAP)(PPh$_3$) **15** gave material which by $^{31}P\{^1H\}$ NMR spectroscopy did not appear to be the dimer. Interestingly, Joshi et al. did not observe a mole of H$_2$O when the dimers of DIOP, CHIRAPHOS, and BINAP were submitted for micro-analysis.[22,23] The $^{31}P\{^1H\}$ NMR data for the dimers isolated in this thesis work are given in Table 3.9.

Table 3.9 $^{31}P\{^1H\}$ NMR Data (121.42 MHz, 20 °C) for $Ru_2X_4(P–P)_2$ Complexes

Complex	Solvent	Chemical Shift, δ	$^2J_{PP}$, (Hz)
$Ru_2Cl_4(DPPB)_2$ **24**	C_6D_6	$\delta_A = 64.7, \delta_B = 55.6^{(a)}$	47.3
	$CDCl_3$	$\delta_A = 63.5, \delta_B = 54.3$	46.9
	CD_2Cl_2	$\delta_A = 64.2, \delta_B = 56.0$	46.8
	C_7D_8	$\delta_A = 64.7, \delta_B = 55.5$	46.9
$Ru_2Br_4(DPPB)_2$ **25**	C_6D_6	$\delta_A = 66.4, \delta_B = 56.8$	43.7
	$CDCl_3$	$\delta_A = 65.2, \delta_B = 55.6$	44.3
	CD_2Cl_2	$\delta_A = 66.0, \delta_B = 57.3$	44.6
	C_7D_8	$\delta_A = 66.7, \delta_B = 57.0$	45.2
$Ru_2I_4(DPPB)_2$ **27**	$CDCl_3^{(b)}$	$\delta_A = 70.1, \delta_B = 55.6$	39.9
$Ru_2Cl_4((R)\text{-BINAP})_2^{(c)}$ **26**	C_6D_6	$\delta_A = 76.4, \delta_B = 6.4^{(a)}$	41.0
		$\delta_C = 59.6, \delta_D = 58.9$	41.0

(a) The chemical shifts differ somewhat from those given in the literature[22,23] due to the method of referencing (Joshi referenced $^{31}P\{^1H\}$ NMR spectra with respect to external PPh_3 and took this as –6 ppm relative to 85% H_3PO_4, regardless of solvent; while in this work, the spectra were referenced with external $P(OMe)_3$ dissolved in the solvent of interest).

(b) Small amounts of MeOH, used to add HI, are present.

(c) Observed in solution from $RuCl_2((R)\text{-BINAP})(PPh_3)$.

3.3.4.2 Preparation of $Ru_2X_4(DPPB)_2$ via $Ru(DPPB)(\eta^3\text{-Me-allyl})_2$
(X = Cl, Br, I)

Genêt and co-workers have reported routes to chiral $Ru(P-P)(\eta^3\text{-allyl})_2$ complexes, where allyl = allyl, or Me-allyl.[54-56] These are prepared from $Ru(COD)(allyl)_2$ species and are used in situ as homogeneous hydrogenation catalysts for the asymmetric reduction of β-keto esters, α,β-unsaturated acids, and allylic alcohols.[57,58]

The general preparative procedure involves refluxing a 1:1 mixture of diphosphine and $Ru(COD)(allyl)_2$ in hexanes. For some of the chiral phosphines, higher temperatures were required, and therefore the reaction mixture was refluxed in toluene.[54] The isolated $Ru(P-P)(allyl)_2$ species are then reacted with HCl and HBr to give in situ $Ru_2X_4(P-P)_2$ complexes. However, no attempts were made to isolate any of these dimeric complexes, as the interests of Genêt and co-workers concentrate on the organic syntheses using these in situ catalytic systems.[57,58]

Therefore, in this thesis work, a preparation of $Ru(P-P)(\eta^3\text{-Me-allyl})_2$ containing the achiral DPPB ligand was undertaken. Refluxing DPPB and $Ru(COD)(\eta^3\text{-Me-allyl})_2$ **7** in hexanes using the procedure outlined for the chiral phosphine analogues prepared by Genêt et al. did not prove effective. However, if the solvent was changed to CH_2Cl_2, a yellow solid analyzing as $Ru(DPPB)(\eta^3\text{-Me-allyl})_2$ **55** was obtained. The $^{31}P\{^1H\}$ NMR spectrum of this yellow solid in C_6D_6 showed a singlet at 44.2 ppm.

A similar reaction between $Ru(COD)(\eta^3\text{-allyl})_2$ **6** and DPPB was attempted in both hexanes and a hexanes / benzene mixture, but did not produce the desired $Ru(DPPB)(\eta^3\text{-allyl})_2$. This reaction was not pursued in CH_2Cl_2, as $Ru(COD)(\eta^3\text{-Me-allyl})_2$ was a better starting material than the allyl analogue, which was a waxy solid and therefore more difficult to handle (Section 2.5.1.6).

Reaction of **55** with two equivalents of dilute methanolic solutions of HX produced the corresponding $Ru_2X_4(DPPB)_2$ complexes (X = Cl, Br, and I). This was

demonstrated by $^{31}P\{^1H\}$ NMR spectroscopy, as the singlet corresponding to **55** at 44.2 ppm decreased in intensity on addition of HX, while the AB pattern corresponding to the appropriate dimer became apparent (Table 3.9). Equation 3.13 illustrates this reaction, in which the Me-allyl group is presumably removed by protonation as 2-methylpropene. The $^{31}P\{^1H\}$ NMR spectra corresponding to addition of one, two, and three equivalents of HCl (in MeOH) to a CDCl$_3$ solution of Ru(DPPB)(η^3-Me-allyl)$_2$ are shown in Figure 3.18.

$$2Ru(DPPB)(Me\text{-}allyl)_2 \ + \ 4HX \longrightarrow Ru_2X_4(DPPB)_2 \ + \ 4(CH_3)_2C=CH_2 \quad (3.13)$$

The peak at 57 ppm is known to be due to interaction of Ru$_2$Cl$_4$(DPPB)$_2$ **24** with HCl, but the nature of the complex formed remains undetermined. This resonance was substantiated as an interaction with HCl by adding HCl (in MeOH) directly to a C$_6$D$_6$ solution of **24**. An interesting possibility is that the proton could be attached to a chloro ligand (i.e., the species could be an η^1-HCl adduct; such species have been formulated within Pt(II) systems).[59]

Interestingly, the addition of NEt$_3$·HCl to Ru(DPPB)(η^3-Me-allyl)$_2$ **55** in CDCl$_3$ gave a resonance at 48.9 ppm due to Ru$_2$Cl$_4$(DPPB)$_2$(NEt$_3$) **28**, the BINAP analogue of which is a very active asymmetric homogeneous hydrogenation catalyst.[60] In essence, the Me-allyl group is protonated, causing its dissociation from the Ru centre, followed by dimerization of the remaining Ru fragment. The resulting **24** reacts with NEt$_3$ to give **28**.
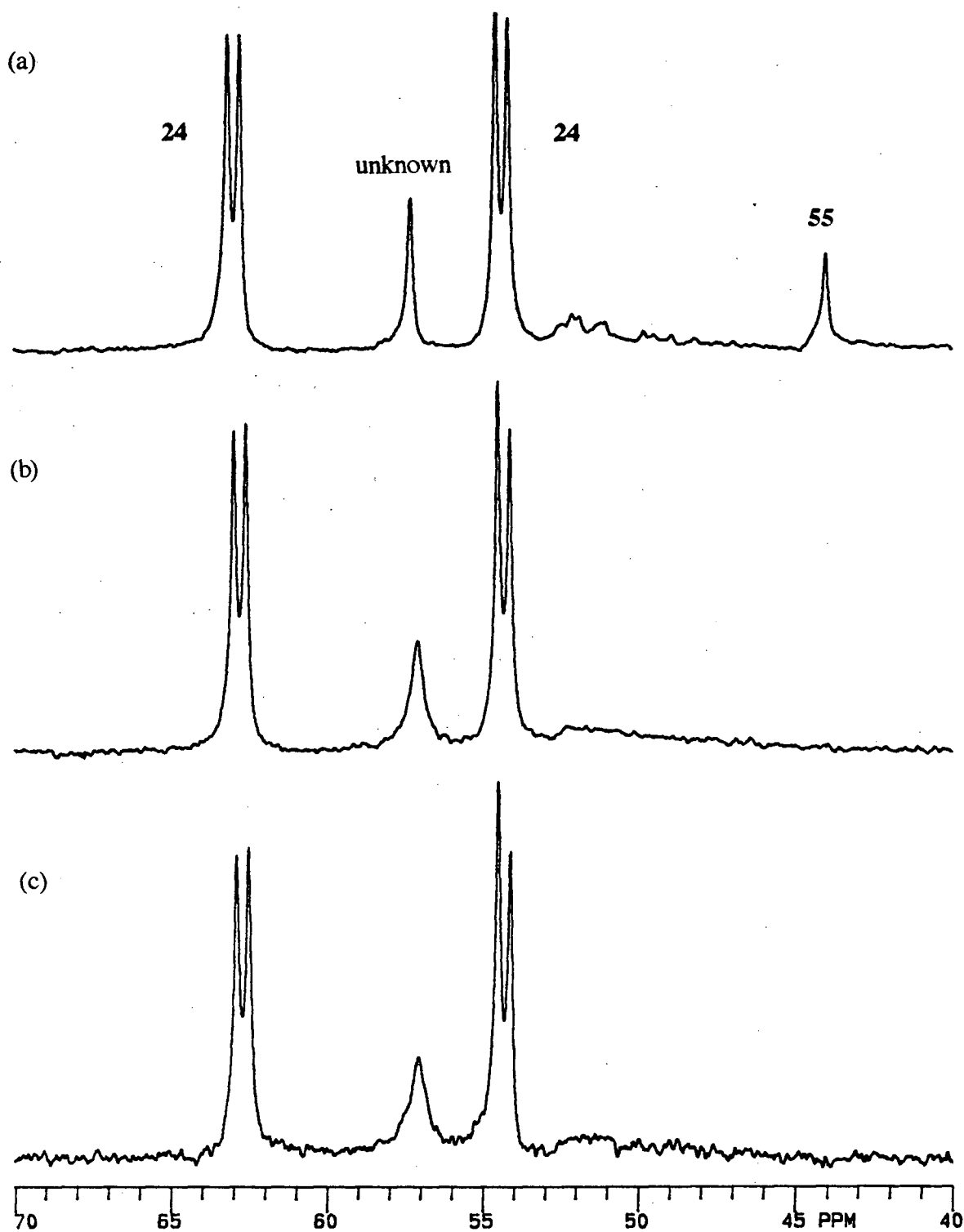
Figure 3.18 $^{31}P\{^1H\}$ NMR spectra (121.42 MHz, 20 °C) of Ru(DPPB)(η^3-Me-allyl)$_2$ **55** in CDCl$_3$ with: (a) 1 equiv HCl, (b) 2 equiv HCl, and (c) 3 equiv HCl. **24** = Ru$_2$Cl$_4$(DPPB)$_2$.

The various routes to $Ru_2Cl_4(DPPB)_2$ **24** now available are shown in Figure 3.19.

$$RuCl_3 \cdot xH_2O$$

route (a) 24 h   3 h   **route (c)** 3 days

route (b)

$RuCl_3(PPh_3)_2DMA \cdot DMA$ 73% $RuCl_2(PPh_3)_3$ 93% $[RuCl_2(COD)]_x$ 86%

24 h   2 h   10 min

$Ru_2Cl_5(DPPB)_2$ 85% $RuCl_2(DPPB)(PPh_3)$ 97% $Ru(COD)(\eta^3\text{-Me-allyl})_2$ 80%

18 h

24 h   1 h $Ru(DPPB)(\eta^3\text{-Me-allyl})_2$ 76%

5 min in situ

73% $Ru_2Cl_4(DPPB)_2$ 100%
75%
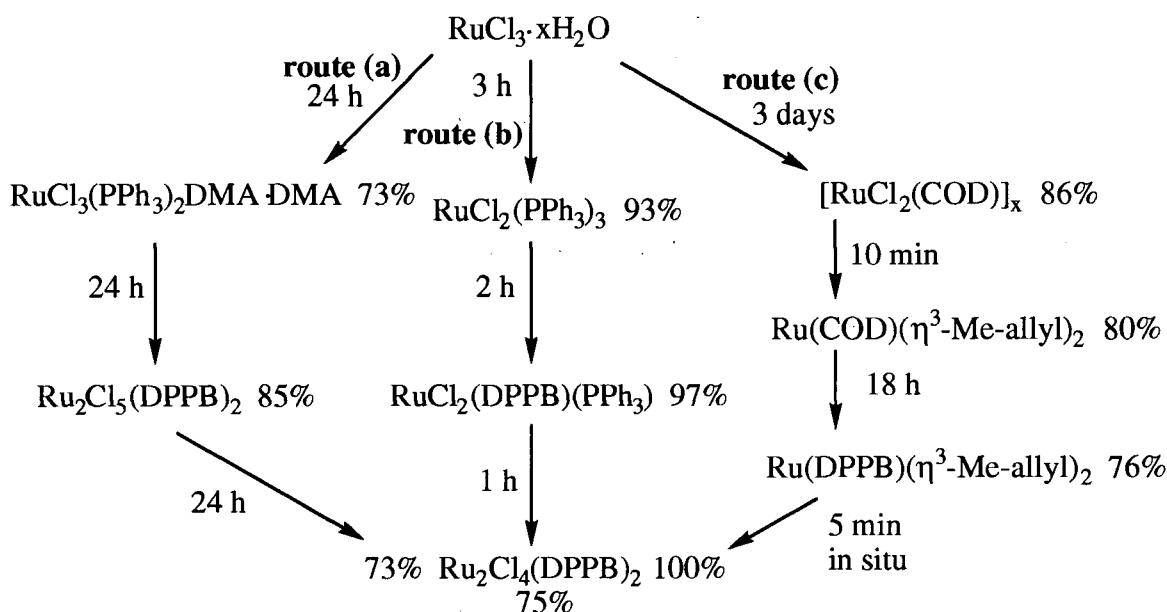
Figure 3.19   Comparison of three routes to the dimer, $Ru_2Cl_4(DPPB)_2$. The overall yields of dimer by these routes are: (a) 45%, (b) 68%, and (c) 52%. Yields of the individual steps are indicated beside the complexes.

Route (b) through the mixed-phosphine complex is the most desirable of the three routes because each of the steps has a short reaction time and is high yield. Route (a) is somewhat less desirable, as the overall yield (45%) is significantly lower than that of route (b) (68%). Also, route (a) has longer reaction times and does not allow access to the bromide analogues, as do both routes (b) and (c). The main drawbacks to route (c) are the long reaction time required in the first step, and the additional step that is needed, as compared to routes (a) and (b). However, the preparation of $Ru(DPPB)(\eta^3\text{-Me-allyl})_2$ **55** through route (c) may be desirable in certain cases because it allows for the in situ generation of the air-sensitive $Ru_2Cl_4(DPPB)_2$ without contamination by PPh_3. The dinuclear complex can also be generated in situ from $RuCl_2(DPPB)(PPh_3)$ (route (b)); however, the presence of PPh_3 in catalytic hydrogenation applications is detrimental (see Chapter 7). Although Figure 3.19 gives only an indication of the reaction time, and does

not take into account the time required in the work-up and isolation of each species, it is still representative of the advantages and disadvantages of each step. All the steps illustrated take approximately an equal amount of time for work-up, except for the step in route (c) from $[RuCl_2(COD)]_x$ to $Ru(COD)(\eta^3\text{-Me-allyl})_2$, which requires a somewhat more tedious work-up.

3.3.4.3   Preparation of Ru(BINAP)(η^3-Me-allyl)$_2$ (56)

The preparation of the title complex has been reported by Genêt et al.;[56] however, no micro-analytical data were given and the $^{31}P\{^1H\}$ NMR data[54] (singlets at 40, 27, and −15) are "ambiguous". In this work, difficulty was encountered in isolating pure Ru((*R*)-BINAP)(Me-allyl)$_2$ **56**; however, the three $^{31}P\{^1H\}$ NMR resonances could be assigned confidently to **56**, (*R*)-(+)-2,2'-bis(diphenylphosphinoyl)-1,1'-binaphthyl (BINAP(O)$_2$), and free BINAP, respectively. An authentic sample of BINAP(O)$_2$ was prepared by the H_2O_2 oxidation of BINAP in C_6D_6, and addition of the oxide to a solution of the Ru complex in C_6D_6 increased the intensity of the 26.6 ppm resonance.

An orange crystal of **56** was isolated from a C_6D_6 NMR solution. An X-ray diffraction analysis of this crystal showed the desired Me-allyl complex to be co-crystallized with (*R*)-(+)-2,2'-bis(diphenylphosphinoyl)-1,1'-binaphthyl and two C_6D_6 molecules. Figure 3.20 shows the ORTEP plot of Ru(BINAP)(η^3-Me-allyl)$_2$ **56**, while Figure 3.21 shows the ORTEP plot of (*R*)-(+)-2,2'-bis(diphenylphosphinoyl)-1,1'-binaphthyl (BINAP(O)$_2$).

Selected bond lengths and angles for Ru((*R*)-BINAP)(η^3-Me-allyl)$_2$ **56** are given in Tables 3.10 and 3.11, respectively, while those for (*R*)-(+)-2,2'-bis(diphenyl-phosphinoyl)-1,1'-binaphthyl are given in Tables 3.12 and 3.13. The experimental parameters and experimental details for both are given in Appendix IV.
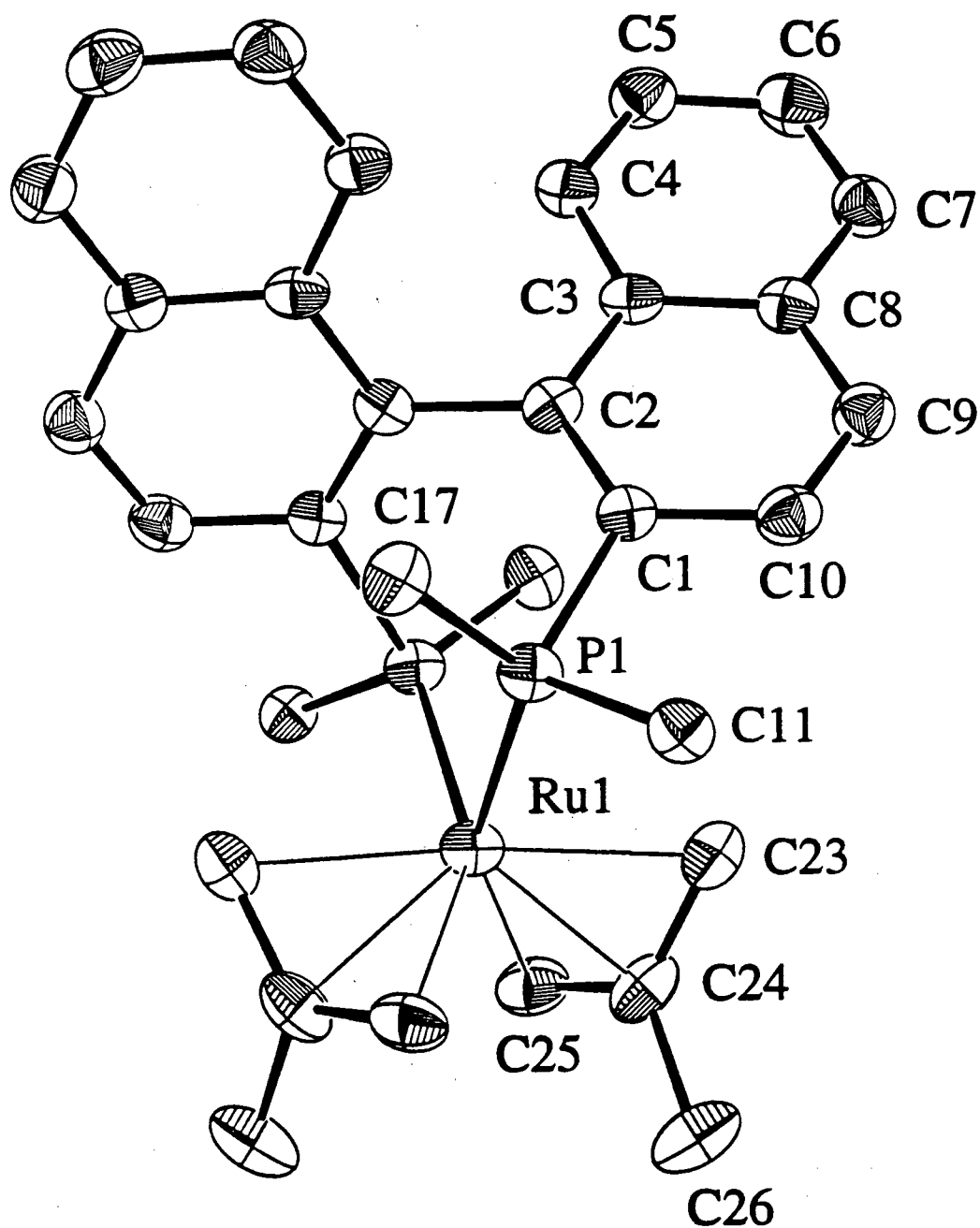
Figure 3.20   The ORTEP plot of Ru((*R*)-BINAP)(η^3-Me-allyl)$_2$ **56**. Thermal ellipsoids
for non-hydrogen atoms are drawn at 33% probability (some of the phenyl
carbons have been omitted for clarity). A C_2 axis rotates the labelled half of
the molecule into the non-labelled half (e.g., P(1) reflects into P(1)').
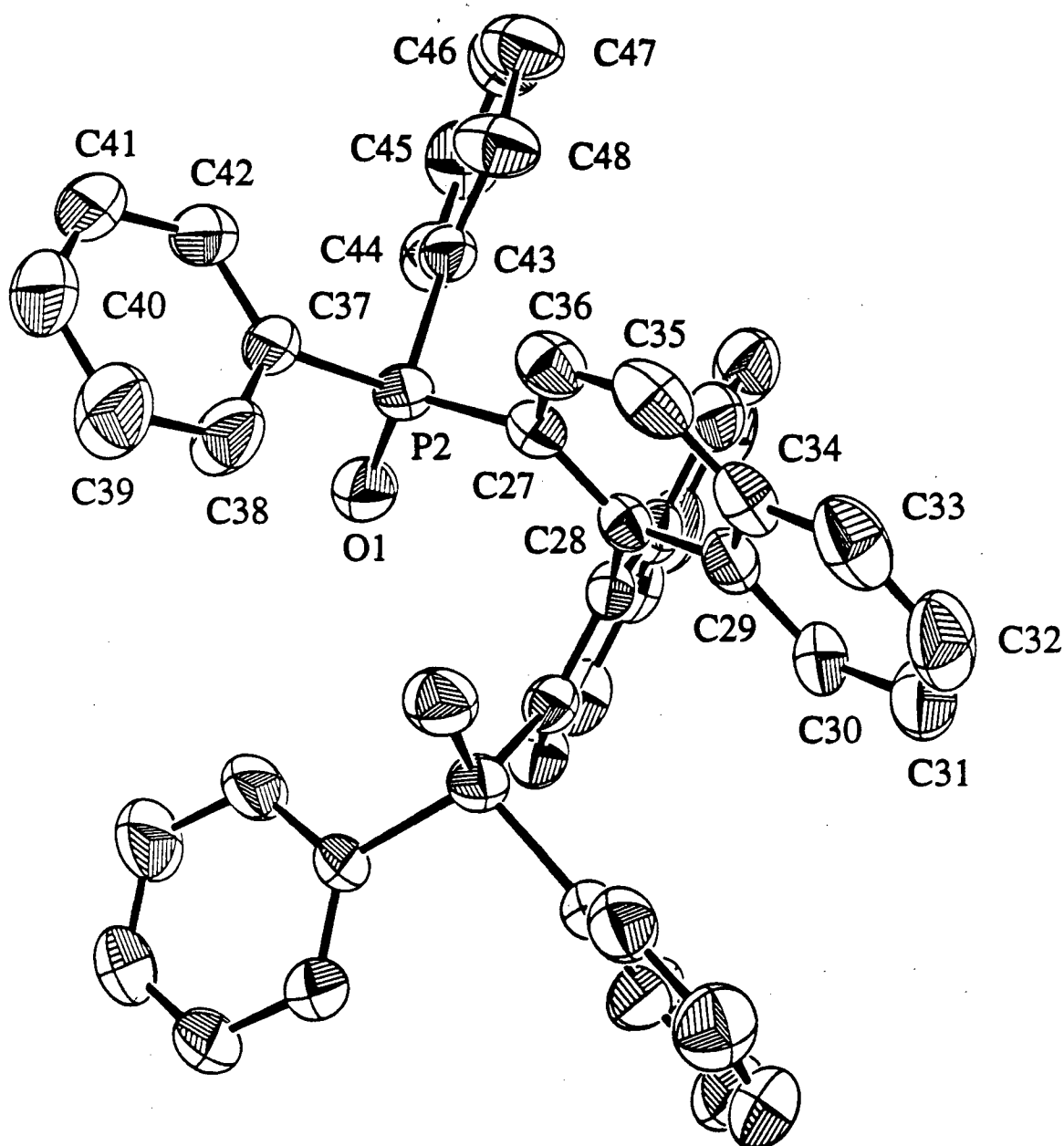
Figure 3.21 The ORTEP plot of (*R*)-(+)-2,2'-bis(diphenylphosphinoyl)-1,1'-binaphthyl (BINAP(O)₂). Thermal ellipsoids for non-hydrogen atoms are drawn at 33% probability. A C_2 axis rotates the labelled half of the molecule into the non-labelled half (e.g., P(2) reflects into P(2)').

The ORTEP of **56** (Figure 3.20) shows the complex to be chiral at the metal centre (Λ), and therefore one of the two possible diastereomers has crystallized (i.e., Λ, R; where the first designation is the metal centre, and the second is the chirality of the diphosphine). The geometry around the Ru centre of **56** can be described as strongly distorted tetrahedral, the tetrahedron being defined by the two phosphorus atoms and the two central carbons of the planar η^3-Me-allyl ligands. Distortions from tetrahedral are caused by the rigid chelating BINAP ligand (i.e., the P(1)–Ru–P(1)' angle is 91.92°).

An X-ray diffraction study of Ru(PPh$_3$)$_2$(η^3-allyl)$_2$ showed the Ru to be tetrahedrally coordinated, the P–Ru–P bond being 109.9°.[61] The Ru–P bond distance of 2.342(4) Å is identical (within experimental error) to that observed in **56**.

Two other X-ray diffraction studies have been reported on complexes of the type Ru(P–P)(η^3-Me-allyl)$_2$, where P–P = (*S*,*S*)-DIOP and (*S*,*S*)-CHIRAPHOS.[54] These structures were described as distorted octahedral, but are in fact very similar to the molecular structure of **56**. For example, the P–Ru–P bond angles are 96.8° (DIOP) and 84.96° (CHIRAPHOS), which are significantly smaller than the 109.9° seen for the monodentate PPh$_3$ analogue.

The preparation of species **56** was originally attempted by the same procedure as that found effective in the synthesis of Ru(DPPB)(η^3-Me-allyl)$_2$ **55** (i.e., in CH$_2$Cl$_2$). However, the use of CH$_2$Cl$_2$ as solvent was ineffective, as only the starting materials were isolated on work-up of the reaction. Therefore, the reaction was performed in refluxing toluene according to the procedure employed by Genêt and co-workers.[54,58]

An X-ray diffraction study has previously been performed on a 1:1:1:1 complex of (*S*)-(–)-BINAP(O)$_2$, (1*R*)-(–)-camphorsulfonic acid, acetic acid, and ethyl acetate.[62] The molecular structures of BINAP(O)$_2$ determined in this work, and those determined by Takaya et al.[62] were significantly different, probably a result of the two crystals crystallizing in different space groups (*P*1 and in this work, I422), as well as the hydrogen-bonding interactions between the phosphine oxide and the camphorsulfonic and

acetic acid groups. For example, the P(2)–O(1) bond length of 1.478 Å observed in this work is significantly shorter than one of the two P–O bond lengths of 1.506 and 1.483 Å observed by Takaya et al. The 1.506 Å P–O bond length may be lengthened by the observed hydrogen-bonding interaction of the oxygen atom with camphorsulfonic acid. Although hydrogen-bonding of the oxygen atom of the other P–O group with acetic acid is observed, this P–O bond length is within the experimental error of that observed in this work. Also of note is the angle between the least-squares planes of the two naphthyl rings, which in this work was 79.3°, while in the work of Takaya et al. it was 90.3°.[62]

Attempts to prepare $Ru_2Cl_4(BINAP)_2$ **26** by adding HCl (in MeOH) to the isolated solid containing $Ru(BINAP)(\eta^3\text{-Me-allyl})_2$ and phosphine dioxide gave a $^{31}P\{^1H\}$ NMR spectrum which did not include resonances corresponding to those reported for **26**.[22,23] The spectrum does not correspond to that recorded for any Ru(II)-BINAP species previously prepared in this laboratory (i.e., $Ru_2Cl_4(BINAP)_2)^{[22,23]}$. The spectrum showed resonances for BINAP and $BINAP(O)_2$, which are present in the starting material, as well as numerous new overlapping resonances between 50–70 ppm (which are probably AB quartets, but are impossible to assign because of the large number of overlapping peaks). The resonance at 42.1 ppm for $Ru(BINAP)(\eta^3\text{-Me-allyl})_2$ **56** was completely gone.

Table 3.10 Selected Bond Lengths (Å) for Ru((*R*)-BINAP)(η^3-Me-allyl)$_2$ **56** with Estimated Standard Deviations in Parentheses

Bond	Length (Å)	Bond	Length (Å)
Ru(1)—P(1)	2.339(1)	C(1)—C(2)	1.387(6)
Ru(1)—C(24)	2.178(5)	C(2)—C(2)'	1.524(8)
Ru(1)—C(23)	2.228(4)	C(23)—C(24)	1.403(7)
Ru(1)—C(25)	2.240(5)	C(24)—C(25)	1.388(8)
Ru(1)—A*	1.96	C(24)—C(26)	1.529(8)
P(1)—C(1)	1.845(5)		

* A refers to the unweighted centroid of the three coordinated carbon atoms of the methylallyl ligand.

Table 3.11 Selected Bond Angles (°) for Ru((*R*)-BINAP)(η^3-Me-allyl)$_2$ **56** with Estimated Standard Deviations in Parentheses

Bond	Angles (°)	Bond	Angles (°)
P(1)—Ru(1)—P(1)'	91.92(6)	P(1)—Ru(1)—C(23)	86.8(2)
P(1)—Ru(1)—C(23)'	97.1(1)	P(1)—Ru(1)—C(24)	119.2(2)
P(1)—Ru(1)—C(24)'	111.4(2)	P(1)—Ru(1)—C(25)	152.2(2)
P(1)—Ru(1)—C(25)'	89.1(2)	P(1)—Ru(1)—A*	119.8
P(1)—Ru(1)—A' *	100.2	C(23)—Ru(1)—C(23)'	174.4(3)
C(23)—Ru(1)—C(24)	37.1(2)	C(23)—Ru(1)—C(24)'	137.6(2)
C(23)—Ru(1)—C(25)	65.6(2)	C(23)—Ru(1)—C(25)'	110.7(2)
C(24)—Ru(1)—C(25)'	92.1(2)	C(24)—Ru(1)—C(24)'	104.4(3)
A—Ru(1)—A' *	122.0	C(24)—Ru(1)—C(25)	36.6(2)
C(1)—C(2)—C(2)'	119.7(3)	C(25)—Ru(1)—C(25)'	102.7(3)
P(1)—C(1)—C(2)	123.9(4)	Ru(1)—P(1)—C(1)	109.3(1)

* A and A' refers to the unweighted centroid of the three coordinated carbon atoms of the methylallyl ligand.

Table 3.12   Selected Bond Lengths (Å) for (*R*)-(+)-2,2'-bis(diphenylphosphinoyl)-1,1'-binaphthyl with Estimated Standard Deviations in Parentheses

Bond	Length (Å)	Bond	Length (Å)
P(2)—O(1)	1.478(4)	P(2)—C(27)	1.795(6)
P(2)—C(37)	1.811(6)	P(2)—C(43)	1.807(6)
C(28)—C(28)"	1.504(10)	C(27)—C(28)	1.380(7)

Table 3.13   Selected Bond Angles (°) for (*R*)-(+)-2,2'-bis(diphenylphosphinoyl)-1,1'-binaphthyl with Estimated Standard Deviations in Parentheses

Bond	Angles (°)	Bond	Angles (°)
O(1)—P(2)—C(37)	111.4(3)	O(1)—P(2)—C(27)	117.1(3)
C(27)—P(2)—C(37)	104.9(3)	O(1)—P(2)—C(43)	110.6(3)
C(37)—P(2)—C(43)	106.1(3)	C(27)—P(2)—C(43)	106.0(3)
P(2)—C(27)—C(28)	122.8(4)	C(27)—C(28)—C(28)"	119.8(5)

3.3.4.4   Metathesis of Ru₂Cl₄(DPPB)₂ by LiBr or Me₃SiBr

An alternative route into "RuBr₂(P–P)" chemistry involved substitution of Br for Cl directly on the dimer. This was accomplished most effectively by the use of Me₃SiBr, which had been reported as synthetically useful by Andersen in the preparation of some hafnium species.[63] Initial in situ ^{31}P{^{1}H} NMR studies showed Me₃SiBr to be effective in preparing Ru₂Br₄(DPPB)₂ **25** from Ru₂Cl₄(DPPB)₂ **24** in C₆D₆ (eq 3.14); an excess of Me₃SiBr was used to drive the reaction to completion. The chlorotrimethylsilane product (b.p. 57 °C) can easily be removed at the pump, as can the remaining excess Me₃SiBr (b.p. 79 °C). This reaction was scaled up and proved to be effective in preparing Ru₂Br₄(DPPB)₂ (Section 2.5.7.2).

130

$$Ru_2Cl_4(DPPB)_2 + 4Me_3SiBr \xrightarrow{C_6D_6} Ru_2Br_4(DPPB)_2 + 4Me_3SiCl \qquad (3.14)$$
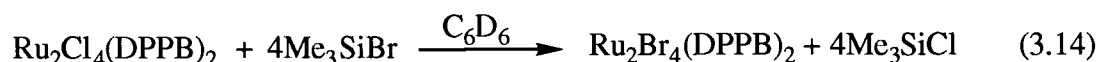
Alternatively, the addition of excess LiBr to **24** in C_6H_6 could be used to effect substitution of Cl for Br. However, the isolated product showed a singlet at 51.0 ppm (C_6D_6) in the $^{31}P\{^1H\}$ NMR spectrum, and is therefore thought to be $Li^+[Ru_2Br_5(DPPB)_2]^-$. No attempt was made to isolate the neutral dimer **25** from this ionic species, as the other methods mentioned earlier were more convenient routes to **25**. An in situ $^{31}P\{^1H\}$ NMR experiment of a CH_2Cl_2 solution of LiBr added to $Ru_2Cl_4(DPPB)_2$ (with C_6D_6 added to allow the spectrometer frequency to be locked) initially showed many overlapping AB quartets at $\delta \sim 55$ and ~ 65, indicating the presence of $Ru_2Cl_{4-x}Br_x(DPPB)_2$ complexes (n = 0–4), plus a singlet at 50 ppm for the ionic species. Precedence for the formation of these ionic species with addition of LiCl to the analogous $Ru_2Cl_4(PPh_3)_4$ complex has been shown earlier by Dekleva (eq 3.15).[33]

Interestingly, the addition of $Ru_2Cl_4(DPPB)_2$ to a solution of $Ru_2Br_4(DPPB)_2$ produced mixed-halide diruthenium species, as evidenced by the many AB quartets observed in the $^{31}P\{^1H\}$ NMR spectrum.

$$Ru_2Cl_4(PPh_3)_4 + LiCl \rightleftharpoons Li^+[Ru_2Cl_5(PPh_3)_4]^- \qquad (3.15)$$

Section 3.4 will discuss ongoing amine chemistry involving these ionic species. Recall also that an X-ray crystallographic structure (Figure 3.16) has been determined for $[TMP]^+[Ru_2Cl_5(DPPB)_2]^-$ (Section 3.3.4.1).[52]

3.4 Reaction of Tertiary Amines with $RuCl_2(P–P)(PPh_3)$ Complexes

Noyori, Takaya, and co-workers have reported on enantioselective hydrogenations catalyzed by Ru(II)–BINAP complexes,[64-66] and they have noted that a dinuclear complex formulated $Ru_2Cl_4(BINAP)_2(NEt_3)$ is a highly effective catalyst precursor for

the asymmetric reduction of functionalized substrates, including ketones.[67,68] This complex was prepared from the Ru(II) starting material, $[RuCl_2(COD)]_x$, as outlined in equation 3.16.[16,67]

$$[RuCl_2(COD)]_x + BINAP + xs\ NEt_3 \xrightarrow[\text{3 h}]{C_7H_8,\ \Delta} Ru_2Cl_4(BINAP)_2(NEt_3) \quad (3.16)$$
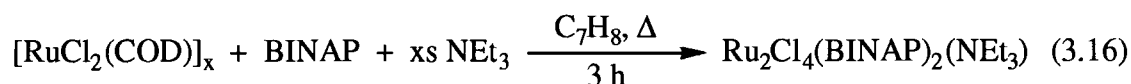
However, King and DiMichele recently discovered that on repeating the above preparation, an ionic complex $[H_2NEt_2]^+[Ru_2Cl_5(BINAP)_2]^-$ was isolated,[69] rather than the originally reported neutral species $Ru_2Cl_4(BINAP)_2(NEt_3)$.

The one difference between the reaction conditions of King and DiMichele and those of Ikariya and co-workers was the reaction temperature. The former[70] performed the reaction in a sealed vessel at 140 °C, while Ikariya and co-workers[16] ran the reaction in refluxing toluene (~110 °C). The complex was originally formulated as the neutral species on the basis of elemental analysis and $^{31}P\{^1H\}$ NMR spectroscopy (δ_A = 56, δ_B = 51; $^2J_{AB}$ = 35 Hz, the solvent was not reported);[67] however, no indication was given as to whether the elemental analysis data included Cl, or whether it was just the routine C, H, N analysis.[67] Chlorine analysis is thought to be key in distinguishing between the neutral and ionic species and this will become evident from the discussion below.

Although King and co-workers report no elemental analysis data for the ionic complex, the spectroscopic data, coupled with results from this work, provide strong evidence for their formulation.[69,70]

Work in this thesis and by other workers in this laboratory clearly illustrates the existence of both neutral and ionic ruthenium(II) amine complexes of the type described above. The majority of the work in this laboratory has been done with the achiral DPPB containing complexes.

Joshi performed the following reactions, involving tertiary amines, starting from either $RuCl_2(DPPB)(PPh_3)$ or $Ru_2Cl_4(DPPB)_2$ (eqs 3.17–3.20).[22,23]

$$Ru_2Cl_4(DPPB)_2 \;+\; xs\;NEt_3 \;\xrightarrow[\substack{25\,°C,\,6\,h}]{C_6H_6\;or\;C_7H_8}\; Ru_2Cl_4(DPPB)_2(NEt_3) \qquad (3.17)$$

$$Ru_2Cl_4(DPPB)_2 \;+\; xs\;HN(n\text{-}Bu)_2 \;\xrightarrow[\substack{25\,°C,\,6\,h}]{C_6H_6}\; Ru_2Cl_4(DPPB)_2(HN(n\text{-}Bu)_2) \quad (3.18)$$

$$RuCl_2(DPPB)(PPh_3) \;+\; xs\;N(n\text{-}Bu)_3 \;\xrightarrow[\substack{reflux,\,3\,h}]{\substack{C_6H_6\,/\,hexanes\\(1:4)}}\; Ru_2Cl_4(DPPB)_2(HN(n\text{-}Bu)_2) \quad (3.19)$$

$$RuCl_2(DPPB)(PPh_3) \;+\; xs\;NEt_3 \;\xrightarrow[\substack{25\,°C,\,48\,h}]{C_6H_6}\; Ru_2Cl_4(DPPB)_2(NEt_3) \qquad (3.20)$$
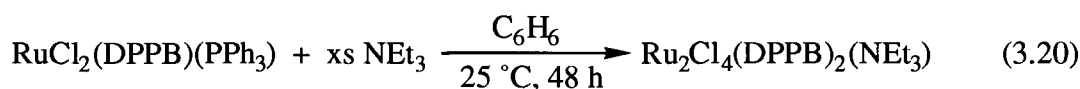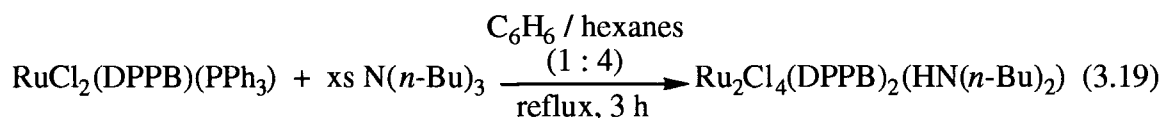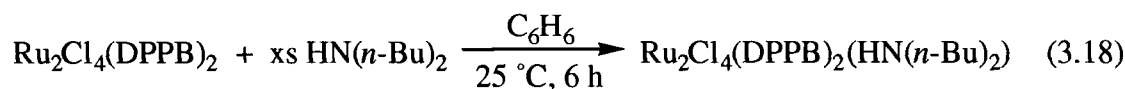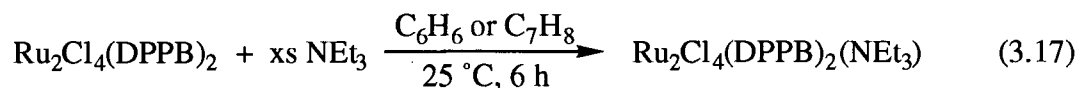
Reactions 3.17 and 3.18 are in fact known to give products of the formulation suggested by Joshi. The neutral complex $Ru_2Cl_4(DPPB)_2(NEt_3)$ analyzed well for four chlorides. The $^{31}P\{^1H\}$ NMR solution data do not distinguish between the neutral and anionic Ru–amine complexes, as both appear as singlets at ~ 49 ppm. While a singlet is expected for the anionic complex based on the structure (see Figure 4.22, Section 4.7.2), two AB quartets would be expected for a static neutral complex like that illustrated in Figure 3.22, structure A (or the enantiomer A') (L = NEt_3), or two singlets for structure B. The singlet observed for the neutral amine species has been rationalized in terms of a rapid reversible dissociation of the amine and recoordination to either Ru centre, which results in scrambling of all four P atoms, which are therefore equivalent on the NMR-timescale.[22,23] This singlet appears at 49 ppm ($CDCl_3$) at room temperature, and has been observed unchanged as low as –98 °C in this thesis work.
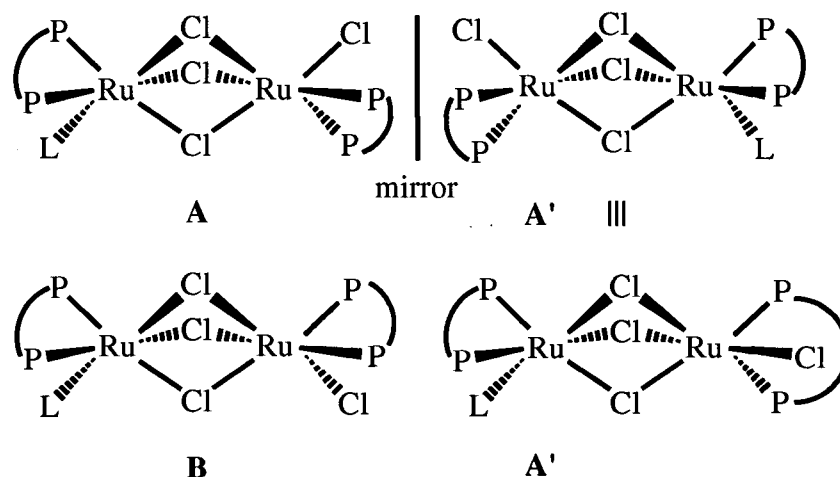
Figure 3.22 Possible structural isomers for $Ru_2Cl_4(DPPB)_2(L)$ complexes.

The patterns mentioned above for the $^{31}P\{^1H\}$ NMR spectra assume no coupling through the chloride bridges, and indeed no through-bridge P–P coupling has been observed for any of the $Ru_2Cl_4(DPPB)_2(L)$ complexes studied to date. However, through-bridge P–P coupling has been observed for the monodentate phosphine-containing species $(PPh_3)_2(H)Ru(\mu\text{-}H)(\mu\text{-}Cl)_2Ru(\eta^2\text{-}H_2)(PPh_3)$.[28,71]

Solid-state CP/MAS (TOSS) $^{31}P\{^1H\}$ NMR data for $Ru_2Cl_4(DPPB)_2(NEt_3)$ show four resonances (56.4, 54.1, 47.1, and 40.7; line broadening, $\omega_{1/2} \sim 162$ Hz, causes each of these signals to appear as singlets rather doublets), which imply structure A, where L = NEt_3.[72] It is difficult to tell from the line shape which pairs of resonances belong together (AB quartet). The same structural arrangement has been demonstrated by crystallography for L = DMSO (Figure 3.8).[22,23] Interestingly, the average chemical shifts of the four resonances observed for $Ru_2Cl_4(DPPB)_2(NEt_3)$ in the CP/MAS (TOSS) $^{31}P\{^1H]$ NMR spectrum is 49.6 ppm, while that observed for the complex in solution is a singlet at 49.4 ppm (C_6D_6).

The solid-state CP/MAS (TOSS) $^{31}P\{^1H\}$ NMR spectrum of $Ru_2Cl_4(DPPB)_2(CO)^{72}$ is a similar to that of $Ru_2Cl_4(DPPB)_2(NEt_3)$.[72] The L = CO

complex (Figure 3.22, structure A) also appears in the CP/MAS (TOSS) ^{31}P{^{1}H} NMR spectrum as four resonances ($\delta_A = 53.4$, $\delta_B = 49.1$, $\delta_B = 44.8$, $\delta_D = 29.0$; line broadening, $\omega_{1/2} \sim 405$ Hz),[72] while the solution ^{31}P{^{1}H} NMR spectrum of Ru$_2$Cl$_4$(DPPB)$_2$(CO) reveals 'the expected' two AB quartets.[23]

3.4.1 Synthesis and Characterization of [H$_2$N(n-R)$_2$]$^+$[Ru$_2$Cl$_5$(DPPB)$_2$]$^-$, R = n-Bu (38), n-Oct (37)

The title complex with R = Bu **38**, originally thought to be the neutral complex Ru$_2$Cl$_4$(DPPB)$_2$(HN(n-Bu)$_2$),[22,23] has been found in this work, at least by the higher temperature route (eq 3.19), to be [H$_2$N(n-Bu)$_2$]$^+$[Ru$_2$Cl$_5$(DPPB)$_2$]$^-$. The ^{31}P{^{1}H} NMR spectrum (a singlet at ~ 49 ppm) does not distinguish between the neutral and ionic species. The chlorine analysis (Section 2.5.9.2) was indicative of the ionic species. An X-ray crystallographic of the anion has been performed in the past (see Figure 3.16 for the ORTEP plot),[52,53] and the chemical shift for this species is in the 49 ppm region as found for [H$_2$N(n-Bu)$_2$]$^+$[Ru$_2$Cl$_5$(DPPB)$_2$]$^-$ (Table 3.14).

The reaction of tri(n-butyl)amine with the mixed-phosphine complex (eq 3.19) was originally repeated in this work in an attempt to determine the fate of the missing alkyl group. However, isolation of [H$_2$N(n-Bu)$_2$]$^+$ [Ru$_2$Cl$_5$(DPPB)$_2$]$^-$ resulted in a second problem: not only did the fate of the organic fragment need to be accounted for, but so did the requirement that a chlorine-deficient Ru species must also be formed (eq 3.21).

$$2.5\,\text{RuCl}_2(\text{DPPB})(\text{PPh}_3) + \text{NR}_3 \xrightarrow[\text{reflux}]{\text{C}_6\text{H}_6} [\text{H}_2\text{NR}_2]^+[\text{Ru}_2\text{Cl}_5(\text{DPPB})_2]^- + 0.5\text{Ru?} + \text{R'?}$$

$$(3.21)$$
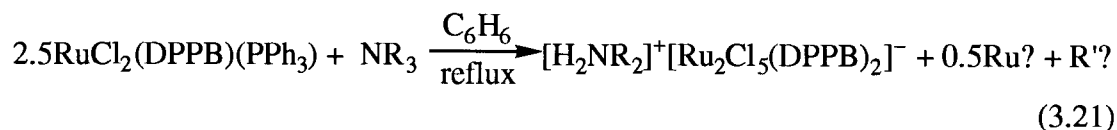
Table 3.14 $^{31}P\{^1H\}$ NMR Data (121.42 MHz)[a] for [cation]$^+$[Ru$_2$Cl$_5$(P–P)$_2$]$^-$
Complexes

Cation	P–P	Solvent	Chemical Shift, δ
TMP[b]	DPPB	CD$_2$Cl$_2$	53.6, s
DMAH **39**	DPPB	CDCl$_3$	48.9, s
		C$_6$D$_6$	49.2, s
HNEt$_3$ **41**	DPPB	CDCl$_3$	49.0, s
H$_2$N(n-Bu)$_2$ **38**	DPPB	CDCl$_3$	48.8, s
		CD$_2$Cl$_2$	48.8, s[c]
H$_2$N(n-Oct)$_2$ **37**	DPPB	CDCl$_3$	48.9, s
		C$_6$D$_6$	49.2, s
Cu	DPPB	CDCl$_3$	48.3, s
H$_2$NEt$_2$[d]	BINAP	CD$_2$Cl$_2$	δ$_A$ = 56.5, δ$_B$ = 52.3; $^2J_{PP}$ = 38.0[e]
H$_2$N(n-Bu)$_2$ **40**	BINAP	C$_6$D$_6$	δ$_A$ = 54.9, δ$_B$ = 51.9; $^2J_{PP}$ = 38.5[e]
		CDCl$_3$	δ$_A$ = 55.1, δ$_B$ = 51.6; $^2J_{PP}$ = 37.6[e]

(a) Spectrometer frequency for the values measured in this work at 20 °C; s = singlet.

(b) Refs 18,52.

(c) Measured at –98 °C.

(d) Ref 69.

(e) $^2J_{PP}$ coupling in Hz.

In situ studies provided little insight into the nature of the other products. A second crop of orange solid was isolated from the reaction (illustrated by eq 3.21 where R = *n*-Bu) by removing the solvent so that only excess amine remained. The $^{31}P\{^1H\}$ NMR spectrum of the isolated second crop showed singlets at 44.9, 49.2, 49.6, and 50.0 ppm, as well as one at 48.8 ppm for the ionic species **38** (CDCl$_3$). The first crop contained only **38**, as evidenced by a single resonance at 48.8 ppm. None of the other resonances can be assigned, although the peak at 44.9 ppm may belong to the bis(amine) ruthenium monomer, RuCl$_2$(DPPB)(amine)$_2$. This type of complex was isolated by Fogg of this laboratory on reaction of RuCl$_2$(DPPB)(PPh$_3$) and benzylamine in C$_6$H$_6$ at room temperature: the isolated complex gave a singlet in the $^{31}P\{^1H\}$ NMR spectrum at 45.7 (CDCl$_3$).[73]

No organic compounds could be identified from the ^1H NMR spectrum. Resonances were not observed between 3.2 and 6.8, and on this basis alkenes are ruled out as possible products.

Attempts were made to determine the co-product(s) of the [Ru$_2$Cl$_5$(DPPB)$_2$]$^-$ ionic species by switching to a reaction between tri(*n*-octyl)amine and RuCl$_2$(DPPB)(PPh$_3$) (Section 2.5.9.1). This was in the hope that any organic fragments produced would be less volatile than in the butylamine case. Unfortunately, nothing further could be deduced about the nature of these products from in situ NMR experiments. The main source of problems in these in situ studies was that only a small excess of amine (2 equiv) could be used in order to ensure that the aliphatic region of the ^1H NMR spectrum was not swamped by free amine signals. Under these conditions, the reaction was slow to reach completion. Even after heating the C$_6$D$_6$ solution for two days, the reaction was only approximately 50% complete.

To confirm the identity of the [H$_2$NR$_2$]$^+$[Ru$_2$Cl$_5$(DPPB)$_2$]$^-$ species **37** or **38**, D$_2$O was added to the sample, and the peaks at 7.9 ppm disappeared from the spectrum. This indicated that the resonance indeed belonged to the exchangeable N*H*$_2$ protons of the

cation. Furthermore, the methylene protons adjacent to the N atom of the alkylammonium cations were coupled to the two protons on nitrogen (see Sections 2.5.9.1–2.5.9.2). Addition of the appropriate salt (i.e., dibutyl- or dioctylammonium chloride) to an NMR sample of the ionic Ru species **38** or **37**, respectively, showed that the methyl and methylene resonances of the ammonium cations coalesce with those of the added salt. Interestingly, the NCH_2CH_2 resonance in the $[H_2N(n\text{-}Bu)_2]^+$ shifted from 1.65 to 1.85 on addition of $[H_2N(n\text{-}Bu)_2]^+Cl^-$.

3.4.2 Synthesis and Characterization of $[H_2N(n\text{-}Bu)_2]^+[Ru_2Cl_5((R)\text{-}BINAP)_2]^-$ (40)

The title complex was prepared by the same method used to prepare the ionic DPPB analogues **37** and **38**. The $^{31}P\{^1H\}$ NMR data agree with those reported by King and DiMichele[69] for $[H_2NEt_2]^+[Ru_2Cl_5((R)\text{-}BINAP)_2]^-$ and are shown in Table 3.14.

3.5 Reaction of Sulfoxides and Thioethers with $RuCl_2(DPPB)(PPh_3)$

Joshi et al. have prepared the complexes $Ru_2Cl_4(DPPB)_2(L)$, where L = CO and NEt_3 from $RuCl_2(DPPB)(PPh_3)$.[22,23] However, $Ru_2Cl_4(DPPB)_2(DMSO)$ **33** was prepared from *cis*-$RuCl_2(DMSO)_4$.[22,23] Fogg of this laboratory extended the series of complexes prepared from $RuCl_2(DPPB)(PPh_3)$ to include L = $MeCN$[30] and H_2NCH_2Ph.[73] Other such dinuclear $Ru_2Cl_4(DPPB)_2(L)$ species were prepared directly from the air-sensitive dimer $Ru_2Cl_4(DPPB)_2$.[22,25,30]

The reaction of DMSO with $RuCl_2(DPPB)(PPh_3)$ **11** was undertaken to examine the range of utility of **11** as a starting material for the preparation of $Ru_2Cl_4(DPPB)_2(L)$ species. An excess of DMSO reacted with **11** to give **33** in 87% yield (Section 2.5.8.6). This reaction is much cleaner than the one performed by Joshi using $RuCl_2(DMSO)_4$, this requiring the removal of side-products $Ru_2Cl_4(DPPB)_2$ **24** and $Ru_2Cl_4(DPPB)_3$ **19** before isolation of the product.[22,23] An X-ray crystallographic study of the complex with L = DMSO showed that the DMSO was S-bonded to ruthenium,[22,23] and the IR spectrum showed an S=O bond stretch at 1090 cm^{-1}, which is in the range reported for S-bonded

sulfoxides (1060–1130 cm^{-1}) in other ruthenium complexes,[74,75] ν_{SO} for an O-bonded

sulfoxide is generally observed at a lower wavenumber: between 920–980 cm^{-1}.[74]

Interestingly, it was not possible to prepare **33** from **19** by adding excess DMSO

(10 equiv). Chapter 5 discusses the chemistry of reactions of ammonia, py, bipy, and

phen with both **11** and **19**, where the use of either starting material gives the same

product: RuCl$_2$(DPPB)(N)$_2$ (N = a donor N-atom). The reaction of **19** with DMSO was

attempted at both room and reflux temperatures, but only the starting material was

isolated on work-up.

A reaction of **11** with TMSO was undertaken to see if the reactivity was similar to

that of DMSO. The addition of an excess of TMSO did in fact give

Ru$_2$Cl$_4$(DPPB)$_2$(TMSO) **35** (Section 2.5.8.8), again with S-bonded sulfoxide (ν_{SO} =

1093 cm^{-1}).

The analogous thioethers, DMS and THT, react with RuCl$_2$(DPPB)(PPh$_3$) to give

similar products: Ru$_2$Cl$_4$(DPPB)$_2$(L) where L = DMS **34,** or THT **36** (Section 2.5.8.7 and

2.5.8.9, respectively). Therefore, the use of the mixed-phosphine starting material is quite

general for the preparation of Ru$_2$Cl$_4$(DPPB)$_2$(L) species where L is a reasonably bulky

ligand (see Chapter 5).

The ^{31}P{^{1}H} NMR spectra of the four complexes (L = DMSO, TMSO, DMS, and

THT) are shown in Figures 3.23–3.25, while the data are compiled in Table 3.15.
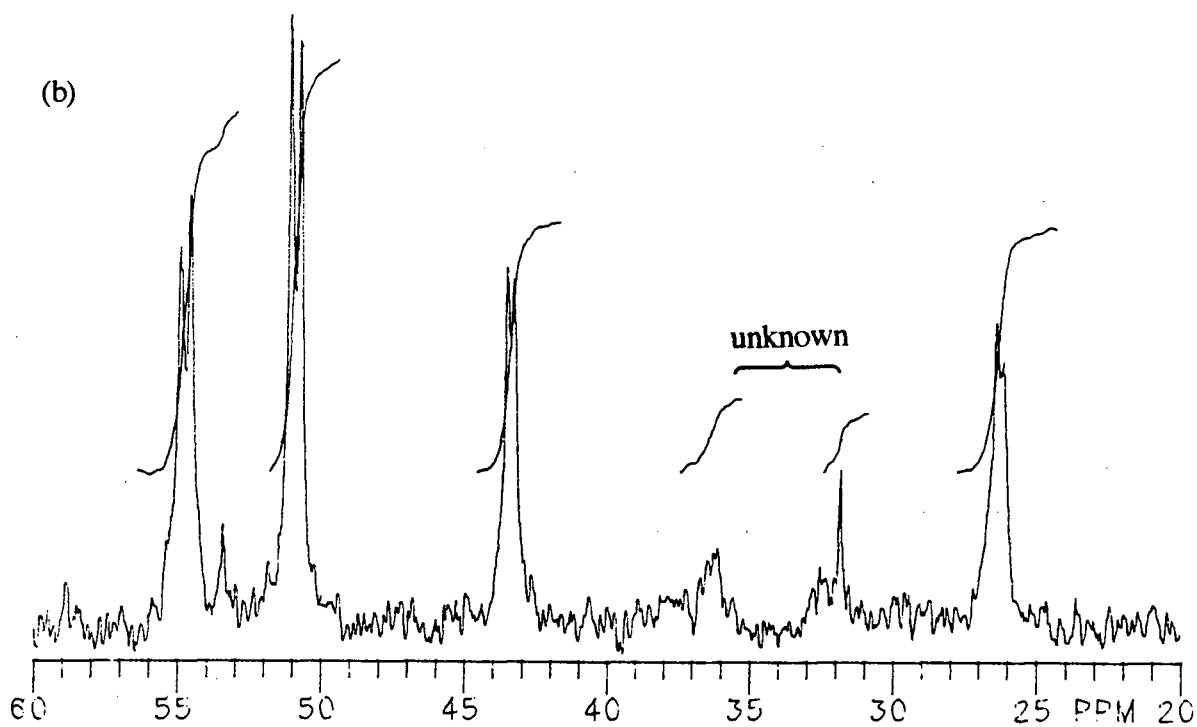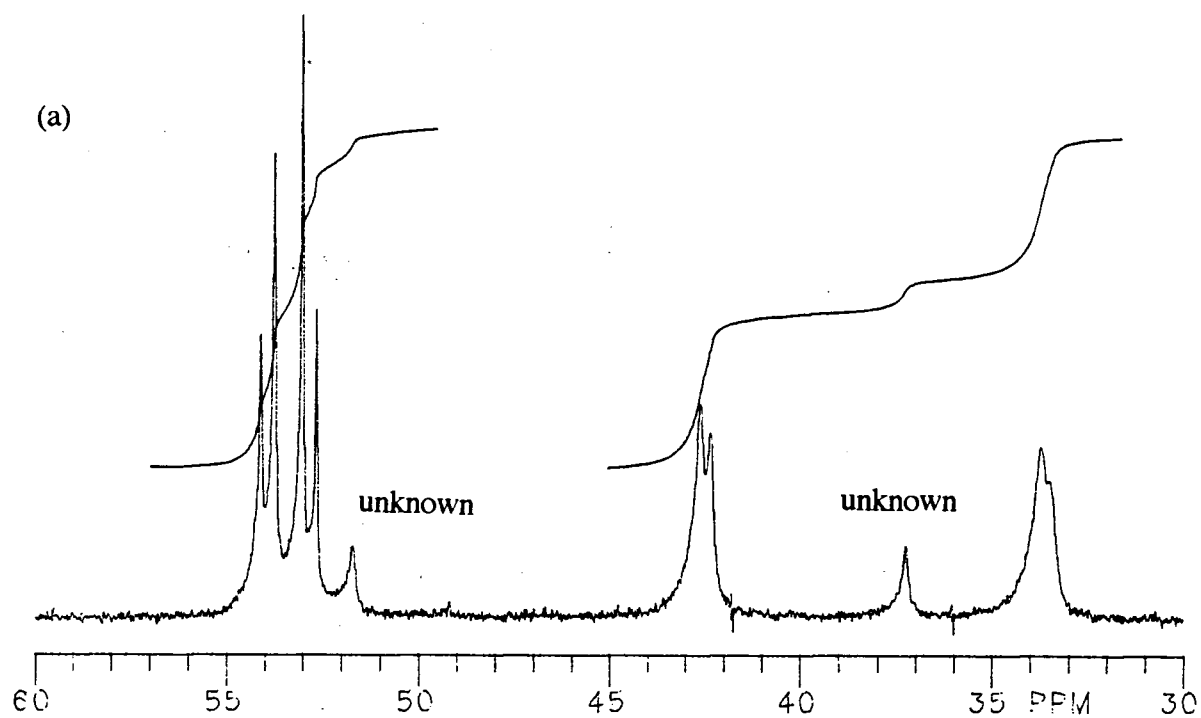
Figure 3.23 $^{31}P\{^1H\}$ NMR spectra (121.42 MHz, 20 °C) of:
(a) [(DMSO)(DPPB)Ru(μ-Cl)$_3$RuCl(DPPB)] **33** in C$_6$D$_6$ and
(b) [(TMSO)(DPPB)Ru(μ-Cl)$_3$RuCl(DPPB)] **35** in CDCl$_3$.

140
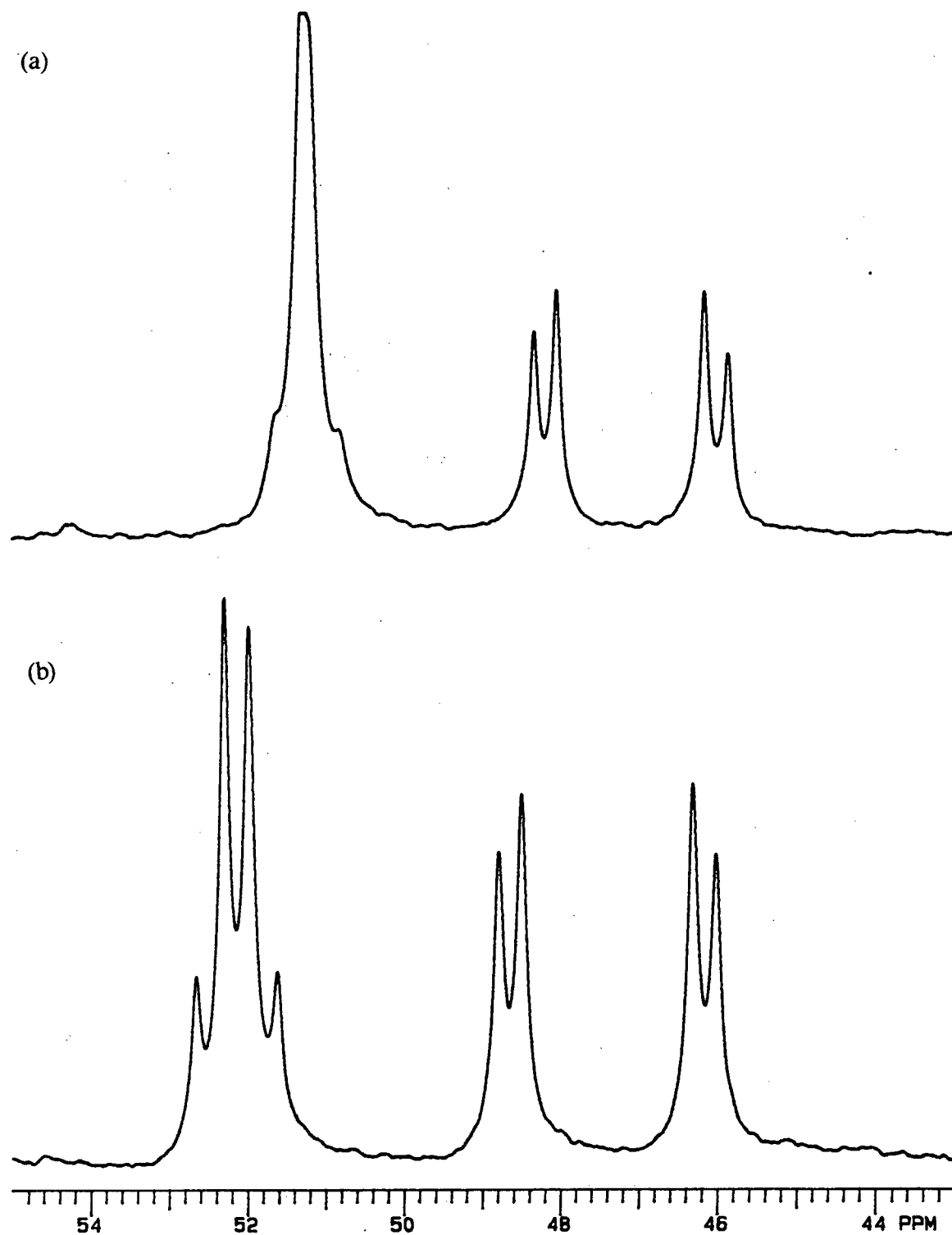
Figure 3.24 $^{31}P\{^1H\}$ NMR spectra (121.42 MHz, 20 °C) of
[(DMS)(DPPB)Ru(μ-Cl)$_3$RuCl(DPPB)] **34** in: (a) CDCl$_3$ and (b) C$_6$D$_6$.

(a)

(b)
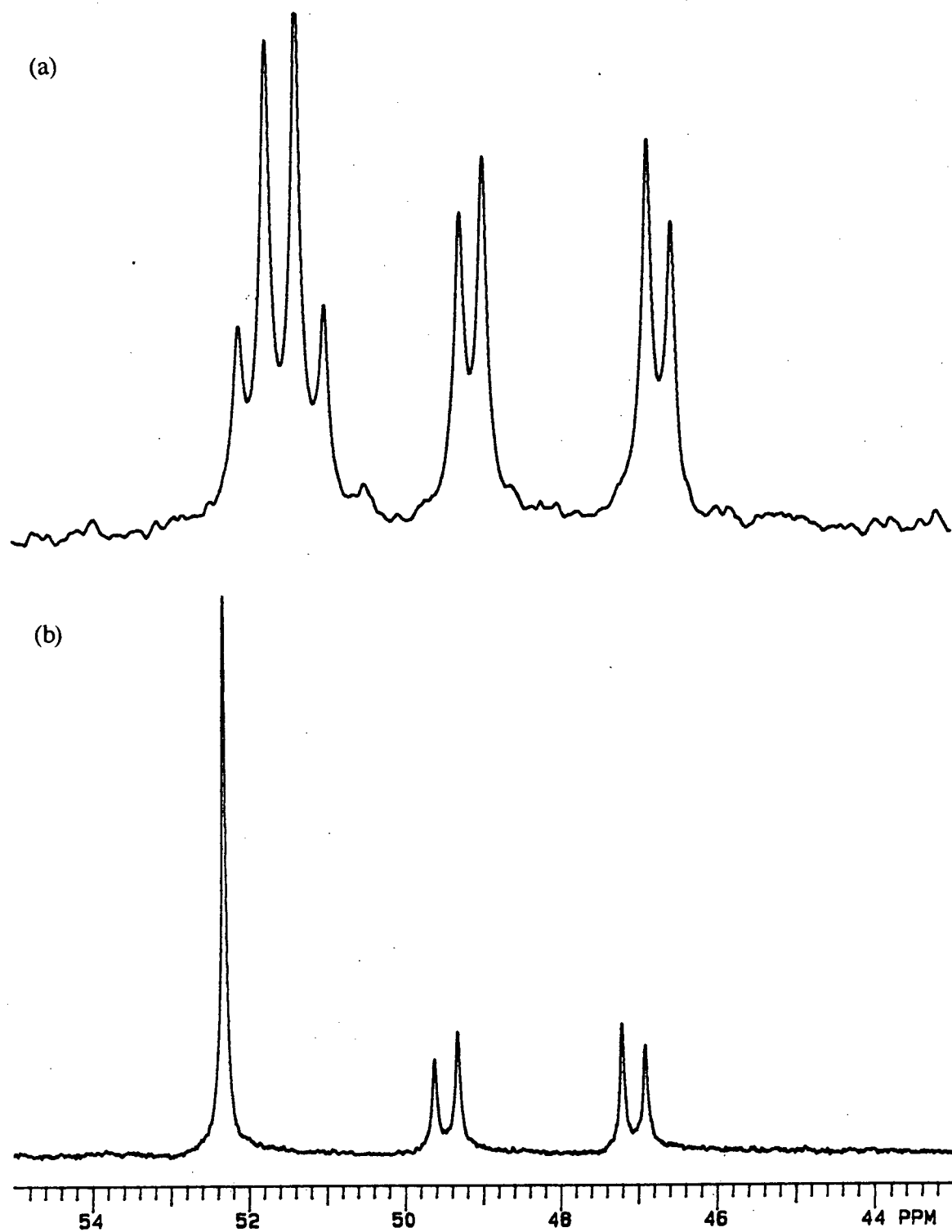
Figure 3.25 ^{31}P{^{1}H} NMR spectra (121.42 MHz, 20 °C) of
[(THT)(DPPB)Ru(μ-Cl)$_3$RuCl(DPPB)] **36** in: (a) CDCl$_3$ and (b) C$_6$D$_6$.

Table 3.15 $^{31}P\{^1H\}$ NMR Data (121.42 MHz, 20 °C) for the Dinuclear Complexes
[(L)(DPPB)Ru(μ-Cl)$_3$RuCl(DPPB)][a]

Complex	Solvent	Chemical Shift, δ	$^2J_{PP}$, (Hz)
L = DMS, Me$_2$S **34**	CDCl$_3$	$\delta_{A,B} = 51.3$[b]	----
		$\delta_C = 48.2, \delta_D = 46.0$	35.6
	C$_6$D$_6$	$\delta_A = 52.5, \delta_B = 51.8$	44.1
		$\delta_C = 48.6, \delta_D = 46.2$	35.3
DM$\underline{S}$O, Me$_2$SO **33**	CDCl$_3$	$\delta_A = 54.2, \delta_B = 51.2$	42.8
		$\delta_C = 42.2, \delta_D = 29.5$	30.2
	C$_6$D$_6$	$\delta_A = 53.9, \delta_B = 52.9$	43.8
		$\delta_C = 42.5, \delta_D = 33.7$	29.6
THT, C$_4$H$_8$S **36**	CDCl$_3$	$\delta_A = 51.9, \delta_B = 51.2$	43.2
		$\delta_C = 49.1, \delta_D = 46.7$	36.1
	C$_6$D$_6$	$\delta_{A,B} = 52.3$[b]	----
		$\delta_C = 49.5, \delta_D = 47.1$	36.1
TM$\underline{S}$O, C$_4$H$_8$SO **35**	CDCl$_3$	$\delta_A = 54.7, \delta_B = 50.8$	41.1
		$\delta_C = 43.4, \delta_D = 26.3$	27.8
	C$_6$D$_6$	$\delta_A = 55.1, \delta_B = 52.2$	42.8
		$\delta_C = 44.2, \delta_D = 29.1$	29.0
acetophenone **32** C$_6$H$_5$C(O)CH$_3$	C$_6$D$_6$	$\delta_A = 53.7, \delta_B = 52.7$	43.9
		$\delta_C = 52.1, \delta_D = 47.5$	37.4
acetone **31** CH$_3$C(O)CH$_3$	C$_6$D$_6$	$\delta_A = 53.7, \delta_B = 51.3$	42.7
		$\delta_C = 50.8, \delta_D = 49.6$	38.5

(a)   Several other complexes of this type are listed in Tables 4.1 and 5.3.

(b)   Indicates unresolved AB pattern.

143

The spectra of the L = DMS complex **34** in C_6D_6 (Fig. 3.24b) and the L = THT complex **36** in $CDCl_3$ (Fig. 3.25a) are well resolved into two AB quartets, but show strong second-order effects where the downfield resonance appears as a singlet. This is the case when the spectrum of **34** is run in $CDCl_3$ (Fig. 3.24a) and that of **36** is run in C_6D_6 (Fig. 3.25b). The difference in the appearance of this downfield signal in different solvents may be due to changes in the extent of thermal motion permitted by the solvent cage. Alternatively, the greater difference in the chemical shift between the two halves of the AB pattern in C_6D_6 (**34**) or $CDCl_3$ (**36**) may prevent averaging of the signals. It is interesting that the spectra of complexes **34** and **36** are resolved in the "opposite" solvents.

These second-order effects have been previously observed for $Ru_2Cl_4(DPPB)_2(PhCN)$ in CD_2Cl_2 by Fogg of this laboratory.[30] If the solution of the nitrile complex is cooled to –40 °C, the singlet observed in the $^{31}P\{^1H\}$ NMR spectrum begins to resolve into a tight AB pattern.[30]

The UV-visible spectra of the $Ru_2Cl_4(DPPB)_2(L)$ complexes (where L = DMSO, TMSO, DMS, and THT), although given previously with the preparation of each complex in Chapter 2, are shown in Table 3.16 to allow easy comparison.

Table 3.16   UV-Visible Data of $Ru_2Cl_4(DPPB)_2(L)$ Complexes

Complex	Solvent	λ_{max} (nm)	ε_{max} (M^{-1} cm^{-1})
L = DMSO	C_6H_6	378	3010[a]
33		470 (sh)	590
	CH_2Cl_2	376	2900
		470 (sh)	650
	C_7H_8	378	3010
		472 (sh)	610
TMSO	C_6H_6	376	2470
35		460 (sh)	830
	CH_2Cl_2	374	2410
		460 (sh)	600
DMS	C_6H_6	374	3780
34		460 (sh)	730
	CH_2Cl_2	372	3470
		460 (sh)	660
THT	C_6H_6	374	3700
36		460 (sh)	605
	CH_2Cl_2	372	3200
		460 (sh)	440
acetophenone	C_6H_6	364	3320
32		484 (sh)	815
	CH_2Cl_2	366	3300
		484 (sh)	690

(a)   Complex **33** in C_6H_6 obeyed Beer's law over the concentration range 2.2–8.6 x 10^{-4} M.

3.6 Reaction of Acetone with RuCl$_2$(DPPB)(PPh$_3$) (11)

The complex Ru$_2$Cl$_4$(DPPB)$_2$(acetone)·acetone **31** can be isolated by reaction of Ru$_2$Cl$_4$(DPPB)$_2$ **24** with an excess of acetone in methylene chloride.[23,25] In this thesis work, stirring a suspension of **24** in acetone produced **31** (i.e., no CH$_2$Cl$_2$ is necessary, Section 2.5.8.4). The ^{31}P{^{1}H} NMR spectrum of **31** in C$_6$D$_6$ shows resonances for **24** as well as **31**, indicating an equilibrium.[22] In other words, acetone is not as strongly bound to ruthenium as the sulfoxide or thioether ligands (see Figures 3.22–3.24 where no resonances for Ru$_2$Cl$_4$(DPPB)$_2$ are evident).

In fact, efforts in this work to prepare **31** from RuCl$_2$(DPPB)(PPh$_3$) **11** by adding an excess of acetone to a refluxing benzene solution failed. Likewise, refluxing **11** in acetone or EtOH did not result in any reaction. This was somewhat surprising, as Dekleva had reported the preparation of the PPh$_3$ analogue Ru$_2$Cl$_4$(PPh$_3$)$_4$(acetone)·acetone by refluxing RuCl$_2$(PPh$_3$)$_3$ **8** in acetone.[33] In contrast, the refluxing of **8** in EtOH has been reported to produce [RuCl$_2$(PPh$_3$)$_2$]$_2$.[36,76]

The inability to produce the acetone-coordinated dinuclear complex from **11** perhaps may be rationalized by comparing the donor number (DN)[77] of acetone with those of DMSO and H$_2$O (recall that **24** was isolated when **11** was reacted with H$_2$O, Section 3.3.4.1). The DN of acetone is 17.0, while those of DMSO and H$_2$O are 29.8 and 18.0, respectively. Acetone may not coordinate strongly enough to ruthenium to shift the equilibrium to the right (eq 3.9, Section 3.3.3). This is evident from the ^{31}P{^{1}H} NMR spectrum of Ru$_2$Cl$_4$(DPPB)$_2$(acetone)·acetone recorded by Joshi,[22] which showed the presence of a significant amount of **24**. At the higher reaction temperatures used, the equilibrium shown in Figure 3.7, Section 3.2 may be shifted to the left, making the isolation of the acetone adduct impossible.

The preparation of the acetone complex from RuCl$_2$(DPPB)(PPh$_3$) was also attempted in CH$_2$Cl$_2$ at room temperature. None of the desired product could be isolated

in this lower temperature reaction. The reaction was also attempted in C_6H_6 at room temperature, and again no product could be isolated.

However, an in situ reaction of $RuCl_2(DPPB)(PPh_3)$ and excess acetone (~ 200 equiv) in C_6D_6 did show formation of a small amount of $Ru_2Cl_4(DPPB)_2(acetone)$ complex, as judged by $^{31}P\{^1H\}$ NMR spectroscopy. Resonances were observed for free PPh_3 (–5.4 ppm), $RuCl_2(DPPB)(PPh_3)$ **11** (triplet-like pattern at 25.7 ppm), $Ru_2Cl_4(DPPB)_2$ **24** (see Table 3.9), and $Ru_2Cl_4(DPPB)_2(acetone)$ **31** (see Table 3.15). The ratio of naked dimer **24** to **31** observed in the $^{31}P\{^1H\}$ NMR spectrum is approximately 4:1. However, the ratio observed by Joshi when isolated **31** was dissolved in C_6D_6 was 1:7 (i.e., **24** : **31**).[22]

3.7 Reaction of Acetophenone with $Ru_2Cl_4(DPPB)_2$ (24)

Acetophenone reacts with $Ru_2Cl_4(DPPB)_2$ **24** in CH_2Cl_2 at room temperature to produce $Ru_2Cl_4(DPPB)_2(acetophenone)$, **32**. The $^{31}P\{^1H\}$ NMR spectrum of **32** is similar to that of the acetone complex, $Ru_2Cl_4(DPPB)_2(acetone)\cdot acetone$ solvate **31**[22,25] (see Table 3.13 for the NMR data). Interestingly, the elemental analysis and IR spectrum show that **32** is not solvated by a mole of ketone, as it is in **31**. A single C=O stretch for coordinated ketone is observed at 1679 cm^{-1} in the solid state, and 1683 cm^{-1} in CH_2Cl_2 solution. The CHIRAPHOS analogue, $Ru_2Cl_4(CHIRAPHOS)_2(acetone)$ also has only a coordinated acetone.[25] The UV-visible data for **32** are listed in Table 3.16.

The $^{31}P\{^1H\}$ NMR spectrum of **32** in C_6D_6 shows naked dimer as well as complex **32**, indicating that acetophenone is not strongly coordinated, as observed in the acetone complex **31** (Section 3.6).

A wide range of $Ru_2Cl_4(DPPB)_2(L)$ complexes has been prepared by Joshi et al, and in all of them (with the exception of L = amine derivatives, see Section 3.4), the four phosphorus nuclei are chemically and magnetically inequivalent.[23] The $^{31}P\{^1H\}$ NMR spectra typically show two independent AB patterns of equal integral intensity, consistent

with the unsymmetrical, trichloro-bridged dinuclear structure A shown in Figure 3.22, and confirmed for the L = DMSO complex by X-ray crystallography.[22,23] A characteristic pattern is observed, consisting of one tight AB quartet near 52 ppm, and a second, more widely separated AB quartet at higher field (the chemical shift of which varies considerably depending on the nature of L).[23,25] The latter resonance, partly because of this dependence, is assigned to the 'L-end' of the complex. The invariance of the downfield signal is attributed to the stability of the geometrical environment of the (P–P)ClRu(μ-Cl)$_3$ unit. The conformation of this end of the complex is locked, as long as the triple-chloride bridge remains intact, and is to a large extent independent of the nature of the ligand which is coordinated to the other ruthenium atom. Such discussion applies to the new complexes synthesized in this thesis work (where L = DMS, THT, TMSO, and acetophenone).

3.8 Synthesis and Characterization of Ru$_2$X$_4$(P–P)$_3$ Complexes

The bridged-phosphine species, (P–P)X$_2$Ru(μ-P–P)RuX$_2$(P–P) are prepared by reacting two equivalents of diphosphine with RuX$_2$(PAr$_3$)$_3$ complexes (Section 2.5.5). The five-coordinate, dinuclear ruthenium complexes of this type that have been synthesized previously are shown in Figure 3.1. The complex Ru$_2$Cl$_4$(DPPB)$_3$ **19** has also been prepared by adding one equivalent of DPPB to Ru$_2$Cl$_4$(DPPB)$_2$ **24**,[25] and is occasionally observed as a side-product in the preparation of RuCl$_2$(DPPB)(PPh$_3$) **11** (Section 3.3.3).

Despite the general insolubility of these phosphine-bridged species, they have been found to be useful precursors for the preparation of RuCl$_2$(P–P)(N)$_2$ species, where N is a N-donor ligand (see Chapter 5).

The five-coordinate complex **19** is known to react with CO in the solid-state to produce Ru$_2$(CO)$_2$Cl$_4$(DPPB)$_3$.[19] This was repeated in this work, and led to the

discovery of solid-state reactivity of CO with other five-coordinate complexes of the type $RuCl_2(PAr_3)_3$, $RuCl_2(DPPB)(PAr_3)$, and $Ru_2Cl_4(DPPB)_2$ (see Chapter 7).

The UV-visible spectroscopic data for complexes **19, 20**, and **21**, although given previously with the preparation of each complex in Chapter 2, are shown in Table 3.17 to allow easy comparison.

Table 3.17   UV-Visible Spectroscopic Data of $Ru_2X_4(P-P)_3$ Complexes **19, 20**, and **21** in C_6H_6

Complex	λ_{max} (nm)	ε_{max} (M^{-1} cm^{-1})
$Ru_2Cl_4(DPPB)_3$ **19**	340	4520
	450	3950
	684	1320
$Ru_2Br_4(DPPB)_3$ **20**	364	2580
	466	3620
	710	1170
$Ru_2Cl_4(DCYPB)_3$ **21**	340	5080
	384 (sh)	3870
	682	1940

The addition of an atmosphere of CO to a C_6H_6 solution of $Ru_2Br_4(DPPB)_3$ **20** resulted in the originally yellow solution immediately becoming colourless, with the UV-visible bands of **20** at 364, 466, and 710 all disappearing. This presumably is the result of the formation of $Ru_2(CO)_2Br_4(DPPB)_3$, as has been previously reported for the chloro-analogue (see above).

Despite the utility of $Ru_2Cl_4(P–P)_3$ complexes in preparing $RuCl_2(P–P)(N)_2$ complexes, the bridged-phosphine species did not react with DMSO (Section 3.5). An excess of DMSO was added to a CH_2Cl_2 solution of **19**, and the resulting mixture was stirred at room temperature. However, no reaction was observed after stirring for 24 h.

In addition, a reaction of excess H_2O with a refluxing solution of **19** was attempted in the same manner as illustrated for the preparation of $Ru_2Cl_4(DPPB)_2$ from $RuCl_2(DPPB)(PPh_3)$ (Section 3.3.4.1). However, on refluxing the resulting green suspension for three hours, no reaction was observed.

3.9 Reaction of One Equivalent of Diphosphine (P–P) with $RuCl_2(DPPB)(PPh_3)$ (11)

3.9.1 P–P = DPPCP; Synthesis and Characterization of *trans*–$RuCl_2(DPPB)(DPPCP)$ (53)

The addition of one equivalent of racemic DPPCP to a C_6H_6 solution of $RuCl_2(DPPB)(PPh_3)$ **11** at room temperature produced the six-coordinate complex *trans*-$RuCl_2(DPPB)(DPPCP)$ **53** (Section 2.5.14.1 and Figure 3.26). The $^{31}P\{^1H\}$ NMR spectrum of this complex was a complicated second-order AA'BB' pattern, as shown in Figure 3.27, along with a simulated spectrum. The chemical shift and coupling constant values used for the simulation are listed in Table 3.18.
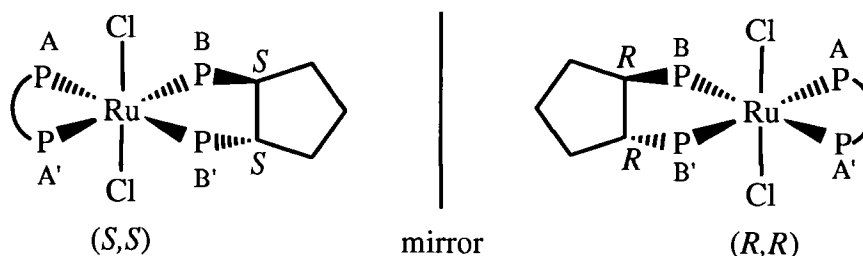
Figure 3.26 Structure of the two possible enantiomers of *trans*-$RuCl_2(DPPB)(DPPCP)$ **53**.
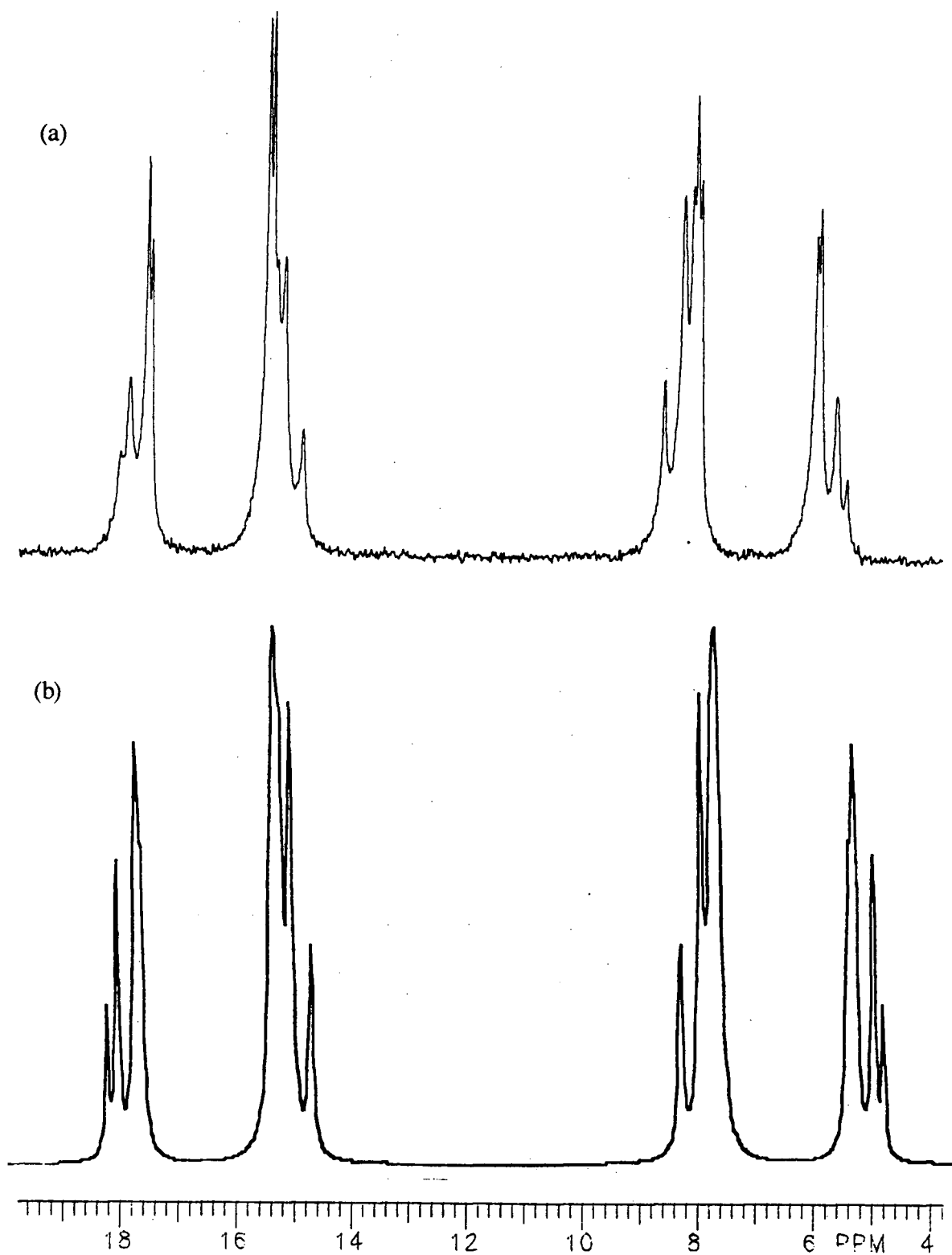
Figure 3.27 $^{31}P\{^1H\}$ NMR spectra (121.42 MHz, 20 °C) of *trans*-
RuCl$_2$(DPPB)(DPPCP) **53** in CDCl$_3$; (a) recorded spectrum and (b)
simulated spectrum (AA'BB') obtained using the parameters listed in Table
3.18.

Joshi has prepared the analogous *trans*-$RuCl_2$(DPPB)(DPPM) complex in a similar manner.[22] The $^{31}P\{^1H\}$ NMR spectrum of this complex was also a complicated second-order pattern. The higher field pattern centred at 7.1 ppm in Figure 3.27 is assigned to the P-atoms of the five-membered chelate DPPCP, while the lower field pattern centred at 16.5 ppm is assigned to those of the seven-membered chelate DPPB. This is in keeping with the reported relative deshielding of phosphorus nuclei in five- and seven-membered chelates.[21,25,44,78] For comparison, the DPPM phosphorus nuclei in the four-membered chelate of *trans*-$RuCl_2$(DPPB)(DPPM) are centred at -24.2 ppm in the $^{31}P\{^1H\}$ NMR spectrum, while those of the seven-membered chelate appear at 17.1 ppm.[22] Four-membered chelates are known to be highly shielded.[44,78]

Table 3.18 $^{31}P\{^1H\}$ NMR Spectral Parameters[a] Used to Obtain the Simulated Spectrum of *trans*-$RuCl_2$(DPPB)(DPPCP) **53** Shown in Figure 3.27

Spectral Parameter	Value[b]	Spectral Parameter	Value[b]
δ_A, $\delta_{A'}$ (DPPB)	16.5 ppm	δ_B, $\delta_{B'}$ (DPPCP)	7.1 ppm
$^2J_{A'B}$	313.8 Hz	$^2J_{AB'}$	312.1 Hz
$^2J_{AA'}$	32.0 Hz	$^2J_{BB'}$	34.8 Hz
$^2J_{A'B'}$ (or $^2J_{AB}$)	-39.6 Hz	$^2J_{AB}$ (or $^2J_{A'B'}$)	-39.1 Hz

(a)   Obtained using the program NMR" Version 1.0 by Calleo Scientific Software Publishers on a Macintosh computer, assuming an AA'BB' spin system.

(b)   The coupling constants $^2J_{AB'}$ and $^2J_{A'B}$ are due to *trans*-disposed phosphines, while the remaining coupling constants arise from mutually *cis*-phosphines. Signs of $^2J_{cis}$ are reported relative to one another while the $^2J_{trans}$ are positive.

3.9.2   P–P = DPPE; Synthesis and Characterization of *trans*-$RuCl_2$(DPPE)$_2$

The addition of one equivalent of DPPE to a C_6H_6 solution of $RuCl_2$(DPPB)(PPh$_3$) at room temperature produced the six-coordinate complex *trans*-

   Chapter 3 References: p 157

RuCl$_2$(DPPE)$_2$ **54** (Section 2.5.14.2). Unlike the case where DPPCP or DPPM were used as the diphosphines, DPPE displaced both the triphenylphosphine and DPPB from the Ru centre. Schutte of this laboratory has recently displaced triphenylphosphine from **11** with some pyridyl phosphines PPh$_{3-x}$py$_x$ to produce six-coordinate complexes of the type *trans*-RuCl$_2$(DPPB)(PPh$_{3-x}$py$_x$) where py = 2-pyridyl and x = 1, 2, and 3.[79]

Complex **54** has been prepared previously by refluxing RuCl$_3$·xH$_2$O and 2.5 equivalents of DPPE in EtOH.[21] In this thesis work, the ^{31}P{^{1}H} NMR spectrum of **54** was a singlet in CDCl$_3$ at 45.0 ppm, which is in agreement with the literature data.[21]

3.10 Reaction of One Equivalent of Diphosphine (P–P) with RuCl$_2$(PPh$_3$)$_3$ (8)

Jung et al. have shown that the mixed-phosphine complex RuCl$_2$(DPPB)(PPh$_3$) **11** is produced on reaction of one equivalent of DPPB with RuCl$_2$(PPh$_3$)$_3$ **8**.[21] This research group here at UBC has shown that it is possible to prepare the DIOP and BINAP analogues in the same manner (Section 3.3.3). All of the above mentioned diphosphines form seven-membered chelates on coordination to ruthenium. However, Jung et al. have shown that if diphosphines with smaller carbon backbones (DPPM, DPPE, and DPPP) are used, species of the type RuCl$_2$(P–P)$_2$ are isolated, instead of the desired RuCl$_2$(P–P)(PPh$_3$) complexes,[21] and this was attributed to the smaller chelate bite angle of DPPM, DPPE, and DPPP;[21] this angle results in the coordination sphere around ruthenium being less sterically crowded, and allows a second diphosphine to displace PPh$_3$ to form the coordinatively saturated products.[21]

Interestingly, Mudalige of this laboratory was able to synthesize the P–N analogues, RuCl$_2$(P–N)(PAr$_3$) using the PMA and PAN ligands (Figure 3.28) via a similar displacement reaction of PPh$_3$ from **8**.[41] Both PMA (chelate ring size of 5) and PAN (chelate ring size of 6) produce the five-coordinate Ru complexes, while the diphosphines with same length carbon backbone (i.e., DPPE and DPPP, respectively) do

not react with **8** to give $RuCl_2(P-P)(PAr_3)$ complexes. Therefore, electronic as well as steric factors must be playing an important role.
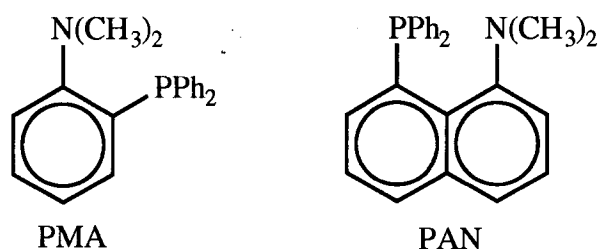
Figure 3.28 Structure of the P–N chelating ligands PMA and PAN.

3.10.1 P–P = DPPCP; Synthesis and Characterization of *trans*-$RuCl_2(DPPCP)_2$ (52)

The addition of one equivalent of racemic DPPCP to a CH_2Cl_2 of $RuCl_2(PPh_3)_3$ **8** in an attempt to prepare $RuCl_2(DPPCP)(PPh_3)$ resulted in the formation of *trans*-$RuCl_2(DPPCP)_2$ **52** (Section 2.5.13), which was subsequently prepared directly from $RuCl_3 \cdot xH_2O$ in refluxing ethanol by the addition of two equivalents of DPPCP (Section 2.5.13). The diphosphine DPPCP has the same length carbon-backbone as DPPE, which was also observed to form the *trans*-$RuCl_2(P-P)_2$ product (Section 3.9.2).

Initially, solution $^{31}P\{^1H\}$ NMR studies on the solid isolated from the reaction of **8** and DPPCP showed a singlet at 22.8 ppm, indicating a single product; however, orange crystals isolated from the filtrate gave a singlet at 23.3 ppm in $CDCl_3$. Subsequently, both resonances were observed in the solution $^{31}P\{^1H\}$ NMR spectrum of the solid isolated from the reaction of $RuCl_3 \cdot xH_2O$ with DPPCP.

The two singlets presumably result from the use of the racemic DPPCP, which produces two diastereomers of **52** (Figure 3.29).
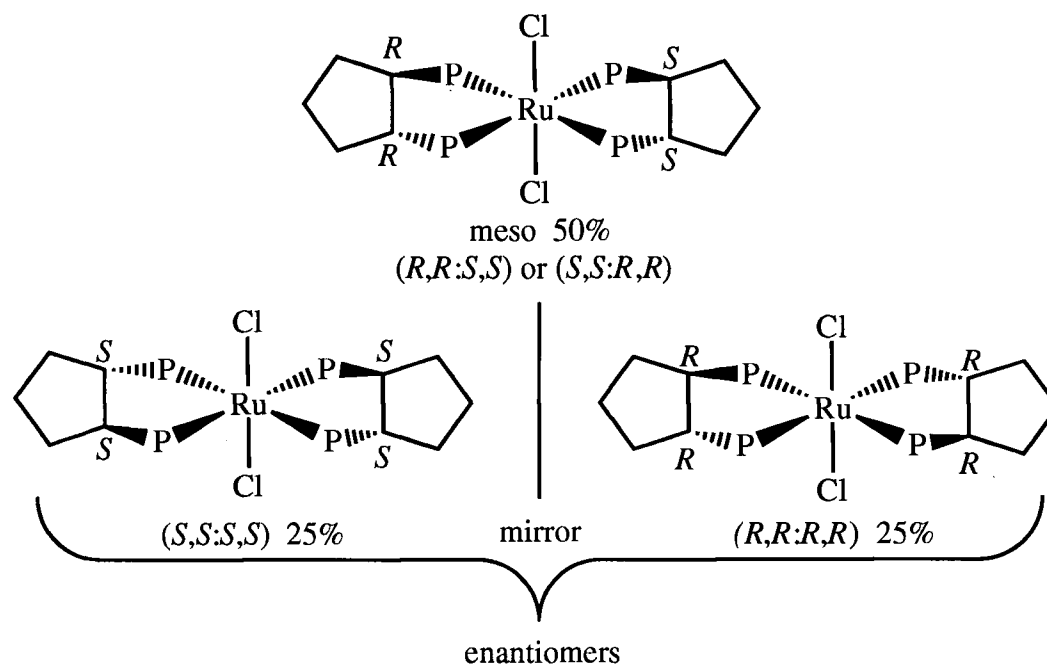
Figure 3.29   Stereoisomers of *trans*-RuCl₂(DPPCP)₂ **52**, where P represents the PPh₂ group.

The $^{31}P\{^{1}H\}$ NMR spectrum of the two diastereomers of **52** is shown in Figure 3.30. Based on a purely statistical approach, 50% of each diastereomer would be expected. However, the NMR spectrum shows an approximately 2:1 ratio of one diastereomer to the other. The difference in solubility of the two diastereomers observed on isolation of the products from the reaction of **8** and DPPCP presumably gives rise to the different ratios of diastereomers. Nothing can be deduced from the ratio of diastereomers observed (i.e., whether or not one diastereomer is kinetically or thermodynamically favoured over the other). Also, if the $^{31}P\{^{1}H\}$ NMR spectrum of the solid is measured in C₆D₆, the two resonances appear at 23.7 and 23.8 ppm, with the peak intensities reversed from those observed in Figure 3.30. This may indicate differing solubility of the two diastereomers, although another more likely possibility is that the resonance for the major diastereomer in CDCl₃ has shifted more than that of the minor diastereomer on changing solvents.

22.808

23.255

```
┌─┬─┬─┬─┬─┬─┬─┬─┬─┬─┬─┬─┬─┬─┬─┬─┬─┬─┬─┬─┬─┬─┬─┬─┬─┬─┬─┬─┬─┬─┬─┬─┬─┬─┐
50        40        30        20        10        0  PPM
```
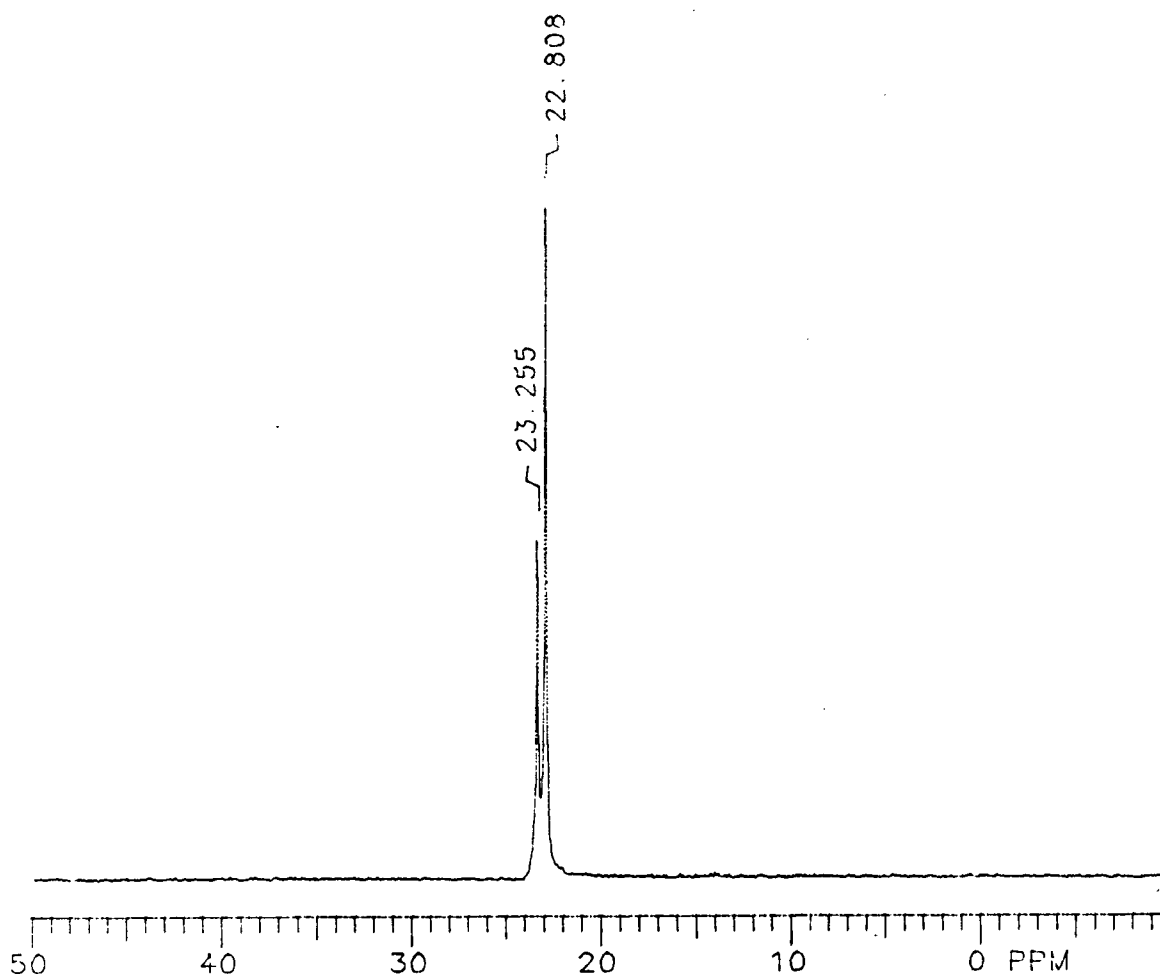
Figure 3.30 The ^{31}P{^{1}H} NMR spectrum (121.42 MHz, 20 °C) of the two diastereomers of *trans*-RuCl$_2$(DPPCP)$_2$ **52** in CDCl$_3$.

3.11 Summary

The five-coordinate complex RuCl$_2$(DPPB)(PPh$_3$) was found to be a versatile starting complex for the synthesis of Ru$_2$Cl$_4$(DPPB)$_2$ and Ru$_2$Cl$_4$(DPPB)$_2$(L) complexes, where L = DMSO, DMS, TMSO, THT, and acetophenone. During this work, it was necessary to find routes to the bromo-analogue Ru$_2$Br$_4$(DPPB)$_2$, as this complex was needed for later studies as a catalyst for imine hydrogenation (Chapter 6). Both RuBr$_2$(PPh$_3$)$_3$ and RuCl$_2$(DPPB)(PPh$_3$) were characterized in the solid state by X-ray crystallography, and were shown to be of pseudo-octahedral geometry, with a weak agostic interaction between the Ru centre and an *ortho*-hydrogen of the PPh$_3$ ligand.

3.12   References

(1)   James, B. R.; McMillan, R. S.; Morris, R. H.; Wang, D. K. W. *Adv. Chem. Ser.* **1978**, *167*, 122.

(2)   Parshall, G.; Ittel, S. D. *Homogeneous Catalysis: The Applications and Chemistry of Soluble Transition-Metal Complexes*; 2nd ed.; Wiley: New York, 1992.

(3)   Jardine, F. H. *Prog. Inorg. Chem.* **1984**, *31*, 265.

(4)   Collman, J. P.; Hegedus, L. S.; Norton, J. R.; Finke, R. G. *Principles and Applications of Organotransition Metal Chemistry*; University Science Books: Mill Valley, CA, 1987, p 545.

(5)   Chaloner, P. A.; Esteruelas, M. A.; Joó, F.; Oro, L. A. *Homogeneous Hydrogenation*; Kluwer Academic: Dordrecht, 1994.

(6)   Schröder, M.; Stephenson, T. A. In *Comprehensive Coordination Chemistry*; Wilkinson, G., Gillard, R. D., McCleverty, J. A., Eds.; Pergamon: Oxford, 1987; Vol. 4, Chapter 45.

(7)   Bruce, M. I. In *Comprehensive Organometallic Chemistry*; Wilkinson, G., Stone, F. G. A., Abel, E. W., Eds.; Pergamon: Oxford, 1982; Vol. 4, p 651.

(8)   Seddon, E. A.; Seddon, K. R. *The Chemistry of Ruthenium*; Elsevier: Amsterdam, 1984.

(9)   Jardine, F. H. *Prog. Inorg. Chem.* **1984**, *31*, 265.

(10)   Keister, J. B. *J. Organomet. Chem.* **1987**, *318*, 297.

(11)   Shapley, P. A. *J. Organomet. Chem.* **1987**, *318*, 409.

(12)   Noyori, R. *Asymmetric Catalysis in Organic Synthesis*; Wiley-Interscience: New York, 1994.

(13)   Henrici-Olivé, G.; Olivé, S. *Angew. Chem., Int. Ed. Engl.* **1971**, *10*, 105.

(14)   James, B. R.; Wang, D. K. W. *Can. J. Chem.* **1980**, *58*, 245.

(15)   Wang, D. K. W. Ph.D. Thesis, The University of British Columbia, 1978.

(16)   Kawano, H.; Ikariya, T.; Ishii, Y.; Saburi, M.; Yoshikawa, S.; Uchida, Y.; Kumobayashi, H. *J. Chem. Soc., Perkin Trans. I* **1989**, 1571.

(17)   James, B. R.; Wang, D. K. W. *Inorg. Chim. Acta* **1976**, *19*, L17.

(18)   Thorburn, I. S.; James, B. R., unpublished results.

(19)   Bressan, M.; Rigo, P. *Inorg. Chem.* **1975**, *14*, 2286.

(20) Joshi, A. M.; Batista, A. A.; James, B. R., unpublished results.

(21) Jung, C. W.; Garrou, P. E.; Hoffman, P. R.; Caulton, K. G. *Inorg. Chem.* **1984**, *23*, 726.

(22) Joshi, A. M. Ph.D. Thesis, The University of British Columbia, 1990.

(23) Joshi, A. M.; Thorburn, I. S.; Rettig, S. J.; James, B. R. *Inorg. Chim. Acta* **1992**, *198*, 283.

(24) Mezzetti, A.; Costella, L.; Del Zotto, A.; Rigo, P.; Consiglio, G. *Gazz. Chim. Ital.* **1993**, *123*, 155.

(25) Thorburn, I. S. Ph.D. Thesis, The University of British Columbia, 1985.

(26) James, B. R.; Pacheco, A.; Rettig, S. J.; Thorburn, I. S.; Ball, R. G.; Ibers, J. A. *J. Mol. Catal.* **1987**, *41*, 147.

(27) James, B. R.; Thompson, L. K.; Wang, D. K. W. *Inorg. Chim. Acta* **1978**, *29*, L237.

(28) Dekleva, T. W.; Thorburn, I. S.; James, B. R. *Inorg. Chim. Acta* **1985**, *100*, 49.

(29) Thorburn, I. S.; Rettig, S. J.; James, B. R. *Inorg. Chem.* **1986**, *25*, 234.

(30) Fogg, D. Ph.D. Thesis, The University of British Columbia, 1994.

(31) Fraser, A. J. F.; Gould, R. O. *J. Chem. Soc., Dalton Trans.* **1974**, 1139.

(32) Stephenson, T. A.; Wilkinson, G. *J. Inorg. Nucl. Chem.* **1966**, *28*, 945.

(33) Dekleva, T. W. Ph.D. Thesis, The University of British Columbia, 1983.

(34) Ruiz-Ramirez, L.; Stephenson, T. A.; Switkes, E. S. *J. Chem. Soc., Dalton Trans.* **1973**, 1770.

(35) Pez, G. P.; Grey, R. A.; Corsi, J. *J. Am. Chem. Soc.* **1981**, *103*, 7528.

(36) Hoffman, P. R.; Caulton, K. G. *J. Am. Chem. Soc.* **1975**, *97*, 4221.

(37) Hallman, P. S.; Stephenson, T. A.; Wilkinson, G. *Inorg. Synth.* **1970**, *12*, 237.

(38) Champness, N. R.; Levason, W.; Webster, M. *Inorg. Chim. Acta* **1993**, *208*, 189.

(39) La Placa, S. J.; Ibers, J. A. *Inorg. Chem.* **1965**, *4*, 778.

(40) Mudalige, D. C.; Rettig, S. J.; James, B. R.; Cullen, W. R. *J. Chem. Soc., Chem. Commun.* **1993**, 830.

(41) Mudalige, D. C. Ph.D. Thesis, The University of British Columbia, 1994.

(42) Hampton, C. R. S. M.; Butler, I. R.; Cullen, W. R.; James, B. R.; Charland, J.-P.; Simpson, J. *Inorg. Chem.* **1992**, *31*, 5509.

(43) Hampton, C. R. S. M. Ph.D. Thesis, The University of British Columbia, 1989.

(44) Dixon, K. R. In *Multinuclear NMR*; Mason, J., Ed.; Plenum: New York, 1987; Chapter 13.

(45) Gosser, L. W.; Knoth, W. H.; Parshall, G. W. *J. Am. Chem. Soc.* **1973**, *95*, 3436.

(46) Lippard, S. J.; Mayerle, J. J. *Inorg. Chem.* **1972**, *11*, 753.

(47) Muetterties, E. L.; Alegranti, C. W. *J. Am. Chem. Soc.* **1970**, *92*, 4114.

(48) Costa, G.; Pellizer, G.; Rubessa, F. *J. Inorg. Nucl. Chem.* **1964**, *26*, 961.

(49) Glockling, F.; Hooton, K. A. *J. Chem. Soc.* **1962**, 2658.

(50) Churchill, M. R.; Kalra, K. L. *Inorg. Chem.* **1974**, *13*, 1065.

(51) Costa, G.; Reisenhofer, E.; Stefani, L. *J. Inorg. Nucl. Chem.* **1965**, *27*, 2581.

(52) Gamage, S. N.; Morris, R. H.; Rettig, S. J.; Thackray, D. C.; Thorburn, I. S.; James, B. R. *J. Chem. Soc., Chem. Commun.* **1987**, 894.

(53) Thorburn, I. S.; Rettig, S. J.; James, B. R., unpublished results.

(54) Genêt, J. P.; Pinel, C.; Ratovelomanana-Vidal, V.; Mallart, S.; Pfister, X.; Caño De Andrade, M. C.; Laffitte, J. A. *Tetrahedron: Asymmetry* **1994**, *5*, 665.

(55) Gênet, J. P.; Pinel, C.; Mallart, S.; Juge, S.; Cailhol, N.; Laffitte, J. A. *Tetrahedron Lett.* **1992**, *33*, 5343.

(56) Genêt, J. P.; Mallart, S.; Pinel, C.; Juge, S.; Laffitte, J. A. *Tetrahedron: Asymmetry* **1991**, *2*, 43.

(57) Gênet, J. P.; Pinel, C.; Ratovelomanana-Vidal, V.; Mallart, S.; Pfister, X.; Bischoff, L.; Caño De Andrade, M. C.; Darses, S.; Galopin, C.; Laffitte, J. A. *Tetrahedron: Asymmetry* **1994**, *5*, 675.

(58) Genêt, J. P.; Pinel, C.; Mallart, S.; Juge, S.; Thorimbert, S.; Laffitte, J. A. *Tetrahedron: Asymmetry* **1991**, *2*, 555.

(59) Kuhlman, R.; Rothfuss, H.; Gusev, D.; Streib, W. E.; Caulton, K. G. *Abstracts of Papers,* 209th American Chemical Society National Meeting, Anaheim, CA; American Chemical Society: Washington, DC, 1995; Abstract INOR 497.

(60) Noyori, R. *Asymmetric Catalysis in Organic Synthesis*; Wiley-Interscience: New York, 1994.

(61) Smith, A. E. *Inorg. Chem.* **1972**, *11*, 2306.

(62) Takaya, H.; Mashima, K.; Koyano, K.; Yagi, M.; Kumobayashi, H.; Taketomi, T.; Akutagawa, S.; Noyori, R. *J. Org. Chem.* **1986**, *51*, 629.

(63) Andersen, R. A. *Inorg. Nucl. Chem. Lett.* **1980**, *16*, 31.

(64)   Noyori, R. *Chem. Soc. Rev.* **1989**, *18*, 187.

(65)   Noyori, R. *Science* **1990**, *248*, 1194.

(66)   Noyori, R.; Takaya, H. *Acc. Chem. Res.* **1990**, *23*, 345.

(67)   Ikariya, T.; Ishii, Y.; Kawano, H.; Arai, T.; Saburi, M.; Yoshikawa, S.; Akutagawa, S. *J. Chem. Soc., Chem. Commun.* **1985**, 922.

(68)   Noyori, R.; Ohkuma, T.; Kitamura, M.; Takaya, H.; Sayo, N.; Kumobayashi, H.; Akutagawa, S. *J. Am. Chem. Soc.* **1987**, *109*, 5856.

(69)   King, S. A.; DiMichele, L. *Chem. Ind. (Dekker)* **1994**, *62*, 157.

(70)   King, S. A.; Thompson, A. S.; King, A. O.; Verhoeven, T. R. *J. Org. Chem.* **1992**, *57*, 6689.

(71)   Hampton, C.; Dekleva, T. W.; James, B. R.; Cullen, W. R. *Inorg. Chim. Acta* **1988**, *145*, 165.

(72)   Joshi, A. M.; James, B. R., unpublished results.

(73)   Fogg, D. E.; James, B. R. *Inorg. Chem.* **1995**, *34*, 2557.

(74)   Bora, T.; Singh, M. M. *Transition Met. Chem.* **1978**, *3*, 27.

(75)   Pacheco, A.; Rettig, S. J.; James, B. R. *Inorg. Chem.* **1995**, *34*, 3477.

(76)   Caulton, K. G. *J. Am. Chem. Soc.* **1974**, *96*, 3005.

(77)   Huheey, J. E. *Inorganic Chemistry, Principles of Structure and Reactivity*; 3rd ed.; Harper & Row: New York, 1983, p 340.

(78)   Garrou, P. E. *Chem. Rev.* **1981**, *81*, 229.

(79)   Schutte, R. P., unpublished results.

CHAPTER 4

ACTIVATION OF DIHYDROGEN BY FIVE-COORDINATE RUTHENIUM(II) COMPLEXES CONTAINING CHELATING DITERTIARY PHOSPHINES

4.1   Introduction

Previous work in this laboratory has demonstrated the ability of Ru(II) five-coordinate complexes containing one chelating ditertiary phosphine ligand per Ru to react with dihydrogen to generate both classical hydride species[1] and molecular hydrogen species.[1-5] Generally, classical hydride complexes containing the moiety "Ru^{II}(H)Cl" have been isolated as the products when a dichloro Ru(II) starting complex is reacted with H$_2$ in the presence of an added base, while the molecular hydrogen complexes "Ru(H$_2$)Cl$_2$" are obtained in the absence of an added base. Our interest in the reactivity of "RuCl$_2$(P-P)" species with H$_2$ grew out of their successful use as hydrogenation catalysts.[1,2,6] Hydride complexes and their molecular hydrogen relatives are possible intermediates in catalytic hydrogenation cycles.

Some of the early work done in this area involved the generation of Ru(H)Cl(PR$_3$)$_3$ species by reacting RuCl$_2$(PR$_3$)$_3$ with H$_2$ in the presence of an appropriate base (eq 4.1).[7] Work from this group has shown the importance of the appropriate choice of base in determining the nature of the Ru species formed (eqs 4.2 and 4.3).[8-10] The highly nucleophilic character of the strongly basic trialkylamines, such as NEt$_3$, can sometimes lead to complications through the coordination and/or dehydrogenation and/or dealkylation of the amines.[11]

$$RuCl_2(PR_3)_3 + H_2 \xrightarrow{\ NEt_3\ } Ru(H)Cl(PR_3)_3 + Et_3NH^+Cl^- \qquad (4.1)$$

Chapter 4 References: p 214

$$2RuCl_3(PR_3)_2 + H_2 \xrightarrow{\text{DMA}} [RuCl_2(PR_3)_2]_2 + 2DMAH^+Cl^- \qquad (4.2)$$

$$\downarrow \text{H}_2 \text{ / Proton Sponge} \atop \text{C}_7\text{H}_8$$

$$2RuCl_3(PR_3)_2 + 4H_2 \xrightarrow[\text{DMA}]{\text{Proton Sponge}} [(\eta^2\text{-H}_2)(PR_3)_2Ru(\mu\text{-H})(\mu\text{-Cl})_2Ru(H)(PR_3)_2]$$
$$+ 4PSH^+Cl^- \qquad (4.3)$$
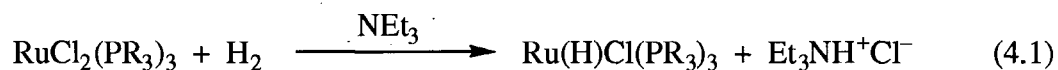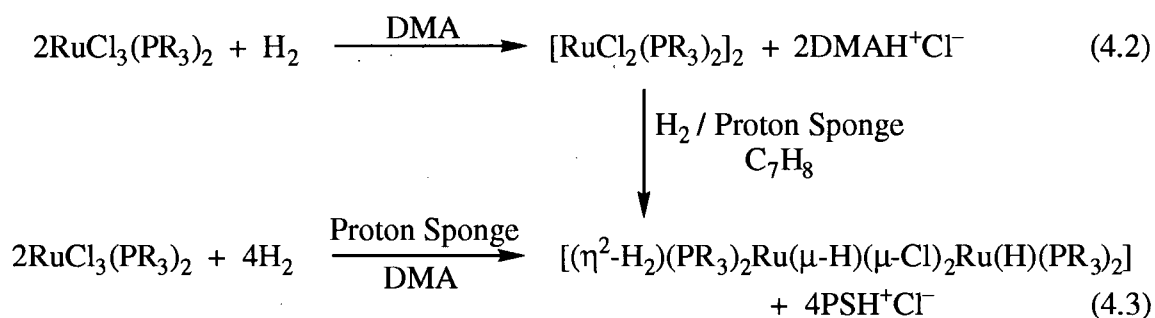
The present study focuses on the reactivity of Ru(II) species containing a single ditertiary phosphine with H_2, in both the presence and absence of an added base. Thorburn first studied the reactivity of $Ru_2Cl_5(DPPB)_2$ and $Ru_2Cl_4(DPPB)_2$ with H_2 under a variety of conditions.[1,6] The reaction of either of the above complexes with H_2 in the presence of added Proton Sponge gave the triply-chloro-bridged dinuclear anionic species $[Ru_2Cl_5(DPPB)_2]^-PSH^+$ as the major isolable product (60-65%).

4.2 A Brief Review of Molecular Hydrogen Complexes and Their Properties and Characterization

A comprehensive review by Jessop and Morris of transition metal dihydrogen complexes appeared in the literature in 1992.[12] Two other, even more recent, reviews which deal extensively with the coordination chemistry of molecular hydrogen have also appeared in the literature.[13,14] Therefore, only a brief review of the type of complexes containing the H_2 ligand and the characterization methods of these species will be discussed here.

Transition metal hydride formation by oxidative addition of dihydrogen at a metal centre has been proposed to occur by a mechanism involving the initial coordination of a hydrogen molecule, followed by cleavage (involving addition of two electrons) into two hydride ligands.[15,16] In 1976, Ashworth and Singleton proposed that neutral dihydrogen occupies a coordination site in the complexes $[RuH_4(PPh_3)_3]$ and $[RuH_3(DPPE)_2]^+$, with

little weakening of the H–H bond.[17] This was based on their observation that both complexes reacted with N_2, PPh_3, and NH_3 via the initial loss of dihydrogen,[18] which paralleled the chemistry seen for reversibly bonded molecular dioxygen compounds; however, it should be noted that the reversible O_2-carriers often exhibit the nature of coordinated peroxide. Also, in the classical reversible binding of H_2 by Vaska's compound, $IrCl(CO)(PPh_3)_2$, the H_2 is bound as two classical hydrides, and so Ashworth and Singleton's proposal was extremely speculative at best.[17]

Judging from IR spectroscopic evidence and the extreme lability of the "hydrogen ligand", Kubas suggested in 1980 that the bonding of hydrogen "may be novel" in the complexes $MH_2(CO)_3(PCy_3)_2$ (M = Mo, W).[19] Direct evidence of this "novel" binding of H_2 came from Kubas et al. in 1983 when X-ray and neutron diffraction studies of $W(CO)_3(PPr^i_3)_2(\eta^2\text{-}H_2)$ showed a side-on (η^2-) bonded H_2 ligand.[20,21] The H–H separation of the η^2-bound dihydrogen was found to be 0.75(16) Å by X-ray analysis, and 0.84 Å by neutron diffraction analysis.[22] This is in comparison with the 0.74 Å found in free H_2. Other evidence of this newly discovered mode of H_2 binding came from the ^1H NMR spectrum of the HD isotopomer of the tungsten complex (i.e., $W(CO)_3(PPr^i_3)_2(HD)$), which showed a 1:1:1 triplet with $^1J_{HD}$ = 33.5 Hz.[16,22,23] The large HD coupling constant observed is on the order of magnitude for that seen in free gaseous HD ($^1J_{HD}$ = 43.2 Hz),[24] which clearly indicates a somewhat reduced H–D bond order. On the other hand, the coupling constant seen between H/D in hydride-deuteride complexes is typically < 2 Hz.[16]

Numerous reports of molecular hydrogen complexes immediately followed these first reports by Kubas et al. In fact, by the end of 1991, more than 300 papers had been published in this area of research.[12] To date, more than 90 structural types are known. Coordination of dihydrogen to many of the transition metals is now known, the ligand environment of the majority of these complexes contain phosphorus donors, although in some cases CO (rather than a P donor) is present as a ligand.[25] More recently, a few

examples of molecular hydrogen complexes in a nitrogen donor environment have been reported.[25] Workers from this department have reported a dihydrogen complex with a P–N ligand system, where the P–N ligand is PMA (Figure 3.28, Section 3.10) and the complex is $RuCl_2(P-N)(P(p\text{-tolyl})_3)(\eta^2\text{-}H_2)$.[26,27]

The initial reports by Kubas showing $\eta^2\text{-}H_2$ binding were followed quickly by reported syntheses of $[Ir(H)(\eta^2\text{-}H_2)(bq)(PPh_3)_2]^+$ (Figure 4.1, bq = 7,8-benzoquinolate) by Crabtree and Lavin,[28,29] and $[M(H)(\eta^2\text{-}H_2)(DPPE)_2]^+$ (Figure 4.1, M = Fe, Ru) by Morris et al.[30] The latter report showed that the prediction by Ashworth and Singleton[17] was, in fact, correct.

| M = Mo, W | C–N = 7,8-benzoquinolinate | M = Fe, Ru |
| R = Pr^i, Cy | | P–P = DPPE |
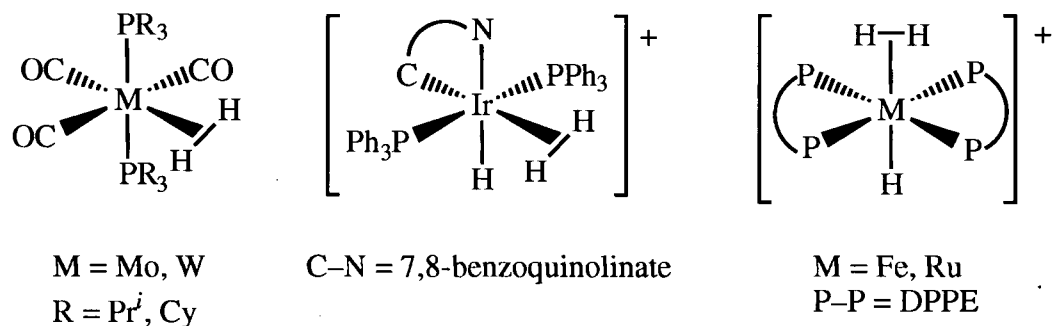
Figure 4.1   Some examples of molecular hydrogen complexes.

Several complexes originally thought to be polyhydrides have now been reformulated as molecular hydrogen complexes. For example, the complex $[RuH_4(PPh_3)_3]$ is now recognized to be $[Ru(H)_2(\eta^2\text{-}H_2)(PPh_3)_3]$,[31] while the dinuclear complex $[Ru(H)_2Cl(PPh_3)_2]_2$ is now reformulated as $[(\eta^2\text{-}H_2)(PPh_3)_2Ru(\mu\text{-}H)(\mu\text{-}Cl)_2Ru(H)(PPh_3)_2]$.[9,10,32]

Generally, ^1H NMR spectroscopy is the most useful method for characterizing molecular hydrogen complexes, and for distinguishing them from classical hydride species. The most direct evidence is structure determination by either neutron or X-ray diffraction studies. Unfortunately, suitable crystals for these types of studies are difficult

to grow. Also, because of the limited number of research institutions which have neutron-scattering and diffraction facilities, only four single-crystal studies have been reported.[12] Vibrational spectroscopy (IR, Raman) is of limited use, particularly for non-carbonyl complexes, because the $v(H_2)$ bands are often too weak to be observed.[33]

Measurement of the T_1 relaxation time of the ^1H NMR upfield resonances is perhaps the most useful and readily available method for distinguishing molecular hydrogen and classical hydride species. The T_1 criterion was introduced by Crabtree et al.[34,35] and refined by Morris and co-workers.[36] If a minimum T_1 value is determined to be less than 40 ms at 250 MHz, then the complex is likely to contain the η^2-H_2 ligand.[14] A classical hydride resonance will exhibit a T_1 relaxation value significantly larger than 100 ms.[12,14,35]

Large apparent J couplings between protons in transition-metal trihydrides have been observed, and have been explained in terms of exchange couplings between protons, which are a manifestation of quantum mechanical motion in the hydrides.[37] The couplings are not magnetic in origin; in fact, there are examples in which the couplings are larger than those reported for molecular hydrogen.[37]

The T_1 method relies on the fact that the two hydrogen atoms in an η^2-H_2 ligand are close to one another, in which case dipole-dipole or spin-lattice relaxation will dominate the modes of NMR relaxation in solution. The two protons for a classical dihydride will be greater than 1.6 Å apart, and therefore exhibit a much longer T_1 value.[12] The rate of spin-lattice relaxation, R(DD), is related to the internuclear distance by equation 4.4:

$$R(DD) = \{T_1(DD)\}^{-1} = 0.3\gamma_H^4 \left(\frac{h}{2\pi}\right)^2 (r_{HH})^{-6} \left\{\frac{\tau_c}{1+\omega^2\tau_c^2} + \frac{4\tau_c}{1+4\omega^2\tau_c^2}\right\} \qquad (4.4)$$

where,

τ_c rotational correlation time $(s\ rad^{-1})$ $= 0.62/\omega$ at $\theta_{(min)}$; θ = temperature (K)

γ gyromagnetic ratio (for ^1H, $\gamma = 2.675 \times 10^{-4}\ rad\ G^{-1}\ s^{-1}$)

ω Larmor frequency $(rad\ s^{-1})$; $\omega = 2\pi\nu$ where ν is the spectrometer frequency

h Planck's constant $(6.626 \times 10^{-34}\ J\ s)$

r_{HH} H–H internuclear distance (cm for cgs units).

The relevant units and conversion factors for both cgs and SI systems are shown in Appendix V. It is necessary to include another term in equation 4.4 if SI units are used. The right-hand side of the equation must be multiplied by $(\mu_o/4\pi)^2$, where μ_o is the permeability of a vacuum. If cgs units are employed and the T_1 measurement is performed on a 300 MHz spectrometer, equation 4.4 reduces to equation 4.5, as shown below.

$$R(DD) = \{T_1(DD)\}^{-1} = 1.291 \times 10^{-46}\ cm^6\ s^{-1} (r_{HH})^{-6} \qquad (4.5)$$

If the T_1 experiment is performed on a 300 MHz spectrometer, and SI units (and metres converted to angstroms) are used, then equation 4.6 is employed.

$$R(DD) = \{T_1(DD)\}^{-1} = 129.1\ Å^6\ s^{-1} (r_{HH})^{-6} \qquad (4.6)$$

The values for the H–H internuclear distance of a η^2-H_2 moiety range from 0.8–1.0 Å,[12] while free dihydrogen gas has an H–H bond length of 0.74 Å.[15,16] The values obtained for the H–H distance from equations 4.4–4.6 were found to be systematically longer than the distances determined by crystallography.[35] Morris et al. suggested multiplying the internuclear distance determined from equations 4.4–4.6 by a correction factor C (0.794).[36] The source of the discrepancy (and the need for the correction factor) is the fast rotation of the η^2-H_2 ligand as compared to the complex as a whole, which results in less efficient relaxation and longer T_1 values.[35,36] If the η^2-H_2 ligand were rotating slowly, then no correction factor would be necessary.[35,36]

Several reports have advised caution in the use of T_1 measurements in the characterization of molecular hydrogen complexes.[35,38-41]

The existence of an equilibrium between a dihydrogen complex and the corresponding dihydride complex in solution has been demonstrated for some complexes (eq 4.7). This observation supports the notion that dihydride complexes are produced by oxidative addition of an initially formed η^2-H_2 complex.[12,15,16,33,35]

$$L_xM{-}\!\begin{array}{c} H \\ | \\ H \end{array} \quad \rightleftharpoons \quad L_xM\!\!\begin{array}{c} \diagup H \\ \diagdown H \end{array} \qquad (4.7)$$
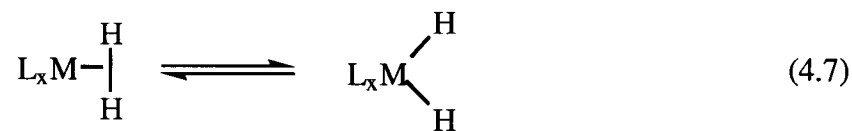
4.3 A Summary of Relevant Research Previously Done in this Laboratory on the Interaction of Dihydrogen and Other Small Molecules with Ru(II) Diphosphine Complexes

4.3.1 Interaction with H_2 in the Absence of an Added Base

Joshi et al. discovered that the dinuclear complex $Ru_2Cl_4(DPPB)_2$ **24** reacts with H_2 (1 atm) in benzene or toluene, in the absence of an added base, to produce the molecular hydrogen complex $[(\eta^2\text{-}H_2)(DPPB)Ru(\mu\text{-}Cl)_3RuCl(DPPB)].^{2,3}$ The dihydrogen complex, which is in rapid, reversible equilibrium with the $Ru_2Cl_4(DPPB)_2$

starting complex (Figure 4.2), was characterized in solution by ^{1}H and ^{31}P{^{1}H} NMR spectroscopy.[2,3]

$$[\text{RuCl(DPPB)}(\mu\text{-Cl})]_2 + H_2 \rightleftharpoons [(\eta^2\text{-}H_2)(\text{DPPB})\text{Ru}(\mu\text{-Cl})_3\text{RuCl(DPPB)}]$$

P—P = DPPB
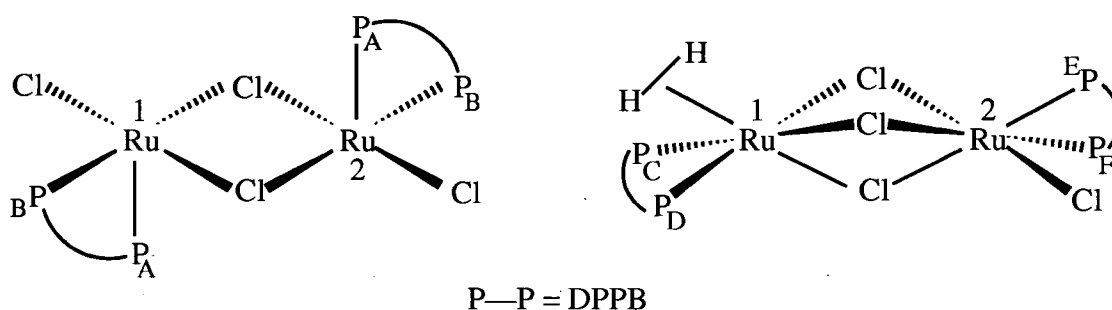
Figure 4.2   Equilibrium between $\text{Ru}_2\text{Cl}_4(\text{DPPB})_2$ **24** and $\text{Ru}_2\text{Cl}_4(\text{DPPB})_2(\eta^2\text{-}H_2)$.

A ^{1}H NMR spectrum showed the $\eta^2\text{-}H_2$ resonance as a broad peak at −11.0 ppm, with a T_1 minimum in C_7D_8 of 12 ± 1 ms at 276 K (300 MHz). If this value is entered in equation 4.6, the H–H internuclear distance of 1.08 Å is obtained.[2,3] When a correction factor C is applied (0.794 is suggested by Morris and co-workers[36]), the H–H internuclear distance was found to be 0.86 ± 0.02 Å. Crabtree and Hamilton have described the correction factor and its use.[33,35,42]

When a C_6D_6 solution of the $\text{Ru}_2\text{Cl}_4(\text{DPPB})_2$ species was placed in a mixture of H_2 (1.2 atm) and D_2 (1.8 atm) at 20 °C, an $\eta^2\text{-}HD$ isotopomer was observed in the ^{1}H NMR spectrum. Therefore, the dinuclear ruthenium complex must catalyze isotope exchange between H_2 and D_2. The ^{1}H NMR resonance was then observed at −11.0 ppm as a 1:1:1 triplet ($^1J_{HD} = 29.4$ Hz) of 1:2:1 triplets (*cis*, $^2J_{HP} = 7.5$ Hz).[2,3]

The ^{31}P{^{1}H} NMR spectra indicate that the equilibrium represented in Figure 4.2 shows about 35% conversion to the $\eta^2\text{-}H_2$ complex at 1 atm and 20 °C in C_7D_8. This was originally incorrectly reported as a 60% conversion.[2,3] However, Chau has shown by

$^{31}P\{^1H\}$ NMR spectroscopy that, in CH_2Cl_2, the constant K for the equilibrium is 1400 M^{-1} at 25 °C.[4,5,43] This corresponds to ca. 80% conversion of **24** to the molecular hydrogen complex. Therefore, the extent of conversion to the molecular hydrogen complex is probably dependent on the conditions used (especially the solvent).

4.3.2   Interaction with H_2 in the Presence of an Added Base

Thorburn et al. found that $Ru_2Cl_4(DPPB)_2$ reacted with H_2 in the presence of two equivalents of NEt_3 to produce a trinuclear complex $[Ru(H)Cl(DPPB)]_3$ in low yield.[1] Section 3.2 reviewed this work, as well as subsequent improvements made to the preparation by Joshi.

Joshi investigated the interaction of H_2 with $[Ru(H)Cl(DPPB)]_3$ in C_7D_8 by NMR spectroscopy.[2] A broad resonance was observed in the ^1H NMR spectrum at –13.1 ppm, with a T_1 of 24 ms at 293 K (300 MHz).[2] When the solution was cooled, this resonance decoalesced to show three broad signals at –7, –13 and –18 ppm at 220 K. The above data, coupled with the $^{31}P\{^1H\}$ NMR spectrum, were consistent with the structure shown in Figure 4.3, which contains a terminal and bridging hydride, as well as a η^2-H_2 moiety; such dinuclear species are well characterized within other phosphine or chelating phosphine-amine donor systems.[44,45]

P–P = DPPB
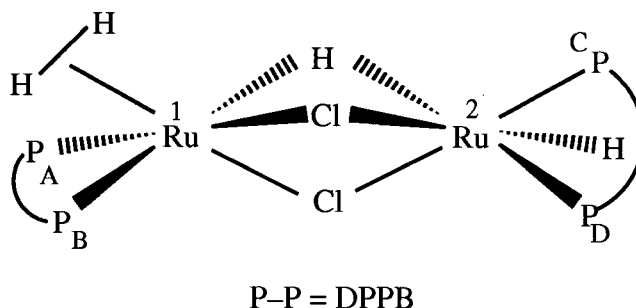
Figure 4.3   Suggested geometry of the $Ru_2(\eta^2$-$H_2)(H)_2Cl_2(DPPB)_2$ complex.

4.3.3 Interaction of Other Molecules with Ru$_2$Cl$_4$(DPPB)$_2$

Joshi also investigated the reactivity of CO and N$_2$ with Ru$_2$Cl$_4$(DPPB)$_2$ **24**.[2,3,46] In C$_6$D$_6$, complex **24** was found to form an σ-N$_2$ complex under an atmosphere of N$_2$ at 20 °C. ^{31}P{^{1}H} NMR spectroscopy indicated ca. 70% conversion to Ru$_2$Cl$_4$(DPPB)$_2$(σ-N$_2$) under the above conditions.

The analogous CO complex, Ru$_2$Cl$_4$(DPPB)$_2$(CO), could not be prepared by direct addition of carbon monoxide to **24**; however, it could be prepared from **24** by decarbonylation of formaldehyde, acetaldehyde, benzaldehyde, or Mo(CO)$_6$.[2,46] Direct addition of CO to **24** was thought to give a complex isomeric mixture of RuCl$_2$(DPPB)(CO)$_2$ and "RuCl$_2$(DPPB)(CO)" complexes.[2]

4.4 Reactivity of H$_2$ and Five-Coordinate Ruthenium(II) Diphosphine Complexes Investigated in This Thesis Work

4.4.1 Interaction with H$_2$ in the Absence of an Added Base

The molecular hydrogen complex Ru$_2$Cl$_4$(DPPB)$_2$(η^2-H$_2$) could be prepared by the reaction of RuCl$_2$(DPPB)(PPh$_3$) **11** with H$_2$ in C$_6$D$_6$. The reactivity of **11** occurs through the equilibrium established with **24** by PPh$_3$ dissociation (eq 3.9, Section 3.3.3). A ^{31}P{^{1}H} NMR spectrum of **11** under an atmosphere of H$_2$ in C$_6$D$_6$ showed **11, 24**, Ru$_2$Cl$_4$(DPPB)$_2$(η^2-H$_2$), and free PPh$_3$. Integration of the spectrum indicated ca. 28% conversion of **24** to Ru$_2$Cl$_4$(DPPB)$_2$(η^2-H$_2$) (ignoring the significant amounts of **11** present). This is similar to the 35% conversion observed previously by direct interaction of H$_2$ and **24** (Section 4.3.1). ^{1}H NMR spectroscopy showed the molecular hydrogen resonance as a broad peak at –11.0 ppm, as observed previously.[2,3]

No direct reaction of the five-coordinate **11** with H$_2$ was evident from either the ^{1}H or ^{31}P{^{1}H} NMR spectra.

A C$_6$D$_6$ solution of Ru$_2$Cl$_4$(DPPB)$_2$(acetone)·acetone solvate **31** (0.02 M) was placed under an atmosphere of H$_2$. After the orange solution was stirred for 20 h at room

temperature, a $^{31}P\{^1H\}$ NMR spectrum was recorded. The $^{31}P\{^1H\}$ NMR spectrum showed a complete loss of the two AB quartets belonging to **31** (Table 3.15). The spectrum indicated that only **24** (Table 3.9) and $Ru_2Cl_4(DPPB)_2(\eta^2-H_2)$ (Table 4.1) were present. Integration indicated ca. 33% of the ruthenium to be in the form of the molecular hydrogen complex, a value again very similar to the previously observed one for conversion of **24** to the molecular hydrogen complex (Section 4.3.1). The ^1H NMR spectrum again showed the molecular hydrogen resonance as a broad peak at -11.0 ppm. Unfortunately, the methylene protons of DPPB obscured the aliphatic region of the spectrum, making it difficult to tell whether the acetone was simply dissociated from the complex, or had actually been hydrogenated to produce isopropanol. Acetone is known by $^{31}P\{^1H\}$ NMR spectroscopy to dissociate from **31**, as evidenced by the presence of **24** in solutions of **31** (Section 3.6).

Interestingly, the reaction of $Ru_2Cl_4(DPPB)_2(DMSO)$ **33** with H_2 in C_6D_6 did not produce any molecular hydrogen complex. In fact, the $^{31}P\{^1H\}$ NMR spectrum of **33** remained unchanged. This non-reactivity may explain the poor catalytic activity of **33** observed for the hydrogenation of imines (Chapter 6). As shown by $^{31}P\{^1H\}$ NMR spectroscopy, complex **33** does not dissociate DMSO in solution, unlike complex **31** which dissociates acetone.

An atmosphere of H_2 was also added to a 0.02 M DMA solution of **24**, with a couple drops of C_6D_6 being added to allow the spectrometer to be locked. In DMA, complex **24** is known to produce $Ru_2Cl_4(DPPB)_2(DMA)$,[2,46] while the interaction of H_2 with this species was of interest, as a kinetic and mechanistic study on styrene hydrogenation by **24** has been performed in DMA.[43] $^{31}P\{^1H\}$ NMR spectroscopic studies under the conditions described above showed only $Ru_2Cl_4(DPPB)_2(DMA)$ (the $^{31}P\{^1H\}$ NMR data for this and other $Ru_2Cl_4(DPPB)_2(L)$ complexes are listed in Table 4.1) and only a small amount of $Ru_2Cl_4(DPPB)_2(\eta^2-H_2)$. Reference 43 describes this catalytic reactivity in greater detail.

Dihydrogen also reacts with the bromo analogue $Ru_2Br_4(DPPB)_2$ **25**. When a C_6D_6 solution of **25** was placed under an atmosphere of H_2 for 24 h, the resulting ^1H NMR spectrum showed a broad resonance at -13.0 ppm. A T_1 measurement at 20.1 °C on a 300 MHz spectrometer indicated that the product was a molecular hydrogen complex ($T_1 = 24.0 \pm 1$ ms). Two other T_1 measurements at 13.0 °C (21.8 ms) and 5.0 °C (20.7 ms) showed the T_1 min to lie below 5.0 °C. Unfortunately, the melting point of C_6D_6 is 5.0 °C, and therefore no T_1 measurements could be attempted below this temperature. Note that the T_1 minimum value for the chloro system is at 3 °C (Section 4.3.1). Several attempts were made to observe this molecular hydrogen complex, presumably $Ru_2Br_4(DPPB)_2(\eta^2\text{-}H_2)$ in solvents with lower melting points (CD_2Cl_2 and C_7D_8); however, surprisingly no resonances upfield of TMS were observed in these solvents. A $^{31}P\{^1H\}$ NMR spectrum of the C_6H_6 solution showed the AB pattern of the starting **25** (Section 3.3.4.1) and two broad singlets presumably belonging to $Ru_2Br_4(DPPB)_2(\eta^2\text{-}H_2)$ ($\delta = 63.4$ and 39.7). These data suggest the likelihood of the geometry shown in Figure 4.4, structure B, which is different from that of the Cl analogue of structure A.
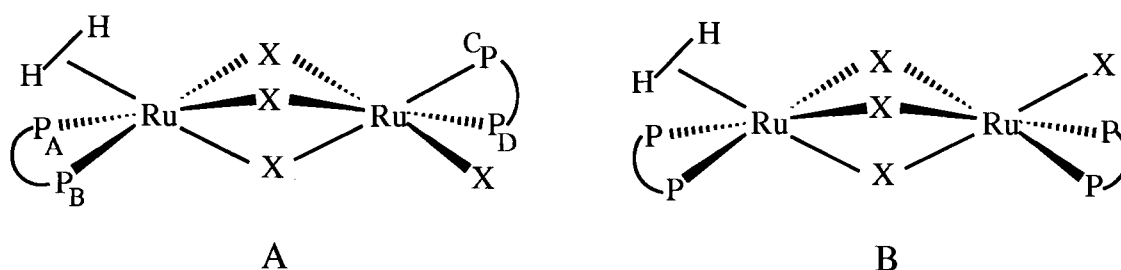
Figure 4.4   Geometry of the two possible isomers of $[(\eta^2\text{-}H_2)(P\text{-}P)Ru(\mu\text{-}X)_3RuX(P\text{-}P)]$, where P–P = DPPB or (*R*)-BINAP and X = Cl or Br.

Table 4.1 $^{31}P\{^1H\}$ NMR Data (121.42 MHz, 20 °C) for the Dinuclear Complexes
[(L)(DPPB)Ru(μ-Cl)$_3$RuCl(DPPB)]

L(Complex)	Solvent	Chemical Shift, δ	$^2J_{PP}$, (Hz)
(η^2-H$_2$)	C$_6$D$_6$	$\delta_A = 54.4$, $\delta_B = 39.0$	33.3
		$\delta_C = 53.8$, $\delta_D = 53.3$	46.6
(η^2-H$_2$)	CD$_2$Cl$_2$	$\delta_A = 54.6$, $\delta_B = 39.1$	33.9
		$\delta_C = 53.1$, $\delta_D = 52.4$	44.8
(σ-N$_2$)	C$_6$D$_6$	$\delta_A = 55.3$, $\delta_B = 53.6$	44.3
		$\delta_C = 47.2$, $\delta_D = 37.5$	32.1
CO	C$_6$D$_6$	$\delta_A = 54.5$, $\delta_B = 54.0$	44.0
		$\delta_C = 47.5$, $\delta_D = 33.8$	29.7
CO	CDCl$_3$	$\delta_{A, B} = 53.8$	46.0
		$\delta_C = 46.4$, $\delta_D = 34.6$	29.9
CO	CD$_2$Cl$_2$	$\delta_A = 53.4$, $\delta_B = 52.8$	44.6
		$\delta_C = 47.3$, $\delta_D = 34.5$	29.6
C$_2$H$_4$	C$_6$D$_6$	$\delta_A = 54.4$, $\delta_B = 53.8$	44.1
		$\delta_C = 46.8$, $\delta_D = 35.6$	34.7
DMA	DMA/C$_6$D$_6$	$\delta_A = 52.5$, $\delta_B = 51.2$	43.5
		$\delta_C = 52.0$, $\delta_D = 49.9$	40.2

The $^{31}P\{^1H\}$ NMR resonances of the bromo-ruthenium complexes studied in this work are consistently broader than those of the corresponding chloro analogues. This is probably a result of the larger electric quadrupole moment of Br compared with that of Cl, and leads to peak broadening of any nearby nuclei. The $^{31}P\{^1H\}$ NMR spectra of the bromo-ruthenium complexes studied in this work were often more difficult to interpret

than those of the chloro analogues because of loss of coupling information due to broadening of the peaks.

Another factor affecting the resolution of the $^{31}P\{^1H\}$ NMR spectra is the limited solubility of the bromo analogues in the NMR solvents commonly used.

4.4.1.1 Reaction of RuCl$_2$((*R*)-BINAP)(PPh$_3$) 15 with H$_2$ in the Absence of an Added Base

The mixed-phosphine complex RuCl$_2$((*R*)-BINAP)(PPh$_3$) **15** reacts with H$_2$ in the absence of an added base to give species which show two broad resonances in the hydride region of the ^1H NMR spectrum (Figure 4.5). These were investigated to determine whether they were classical or η^2-H$_2$ protons. Inversion-recovery experiments were used to determine the T_1 minimum. The T_1 data over the temperature range of 252–335 K are listed in Table 4.2, while a plot of T_1 versus temperature is shown in Figure 4.6.

The T_1 minimum values (measured on a 300 MHz spectrometer) of the two resonances at –8.8 and –9.6 ppm were 11 and 9 ms, respectively. Both occurred at a temperature of 32 °C, which is relatively high. T_1 values of this magnitude suggest molecular hydrogen species (see Section 4.2). If the values are substituted into equation 4.6, the H–H internuclear distances for the η^2-H$_2$ moiety are determined to be 1.06 Å and 1.03 Å for the –8.8 and –9.6 ppm resonances, respectively. If the correction factor C suggested by Morris and co-workers (0.794)[36] is applied, the H–H internuclear distances are found to be 0.84 ± 0.02 and 0.86 ± 0.06 Å. The errors are determined from the value given in Table 4.2 for the particular T_1 used.

The H–H internuclear distance is similar to that determined by Joshi of 0.86 ± 0.02 Å for (η^2-H$_2$)(DPPB)Ru(μ-Cl)$_3$RuCl(DPPB), which corresponds to a T_1 minimum of 12 ms at 4 °C.[2,3] The bond distance is similar to that determined by X-ray crystallography of 0.80(6) Å for a related diruthenium species (see Section 4.5.1, isoPFA complex).[44,45]
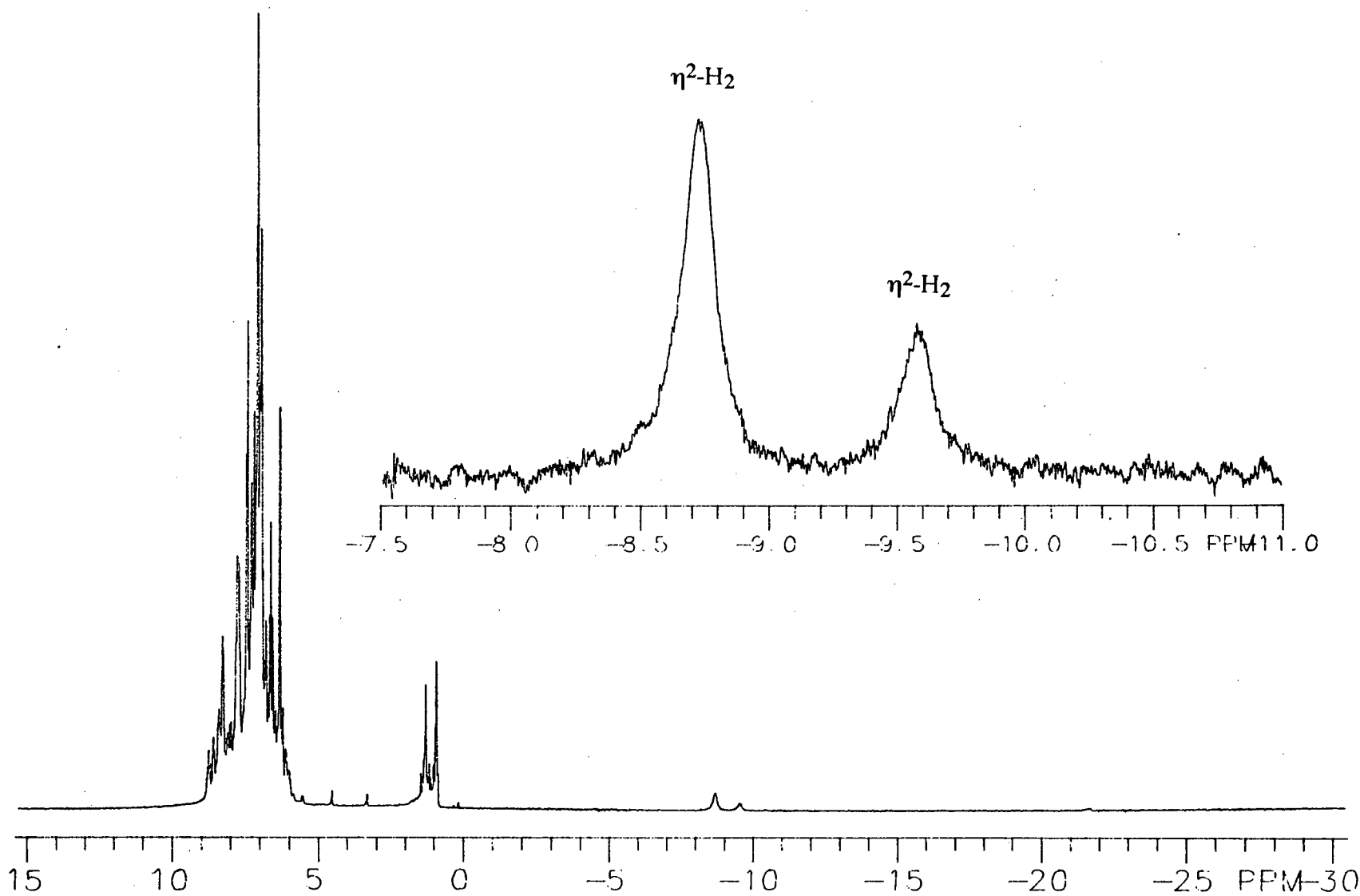
Figure 4.5 ^{1}H NMR spectrum (300 MHz, 20 °C) of RuCl$_2$((R)-BINAP)(PPh$_3$) **15** under an atmosphere of H$_2$ in C$_6$D$_6$.

Table 4.2   Temperature Dependence of the ^{1}H NMR T_1 Relaxation Time Data[a] (300 MHz, C_7D_8) for the (η^2-H_2) Resonances Observed on Reaction of H_2 and $RuCl_2((R)$-BINAP)(PPh$_3$)

Temperature	T_1 (ms)	
(K)	−8.8 ppm resonance	−9.6 ppm resonance
335	19 ± 2	21 ± 2
325	17 ± 2	20 ± 2
315	13 ± 3	17 ± 2
306	11 ± 2	9 ± 4
294	15 ± 4	14 ± 4
273	17 ± 2	14 ± 2
252	22 ± 6	17 ± 6

(a) T_1 data were obtained by the inversion-recovery method[47] using the conventional 180°–t–90° pulse sequence.
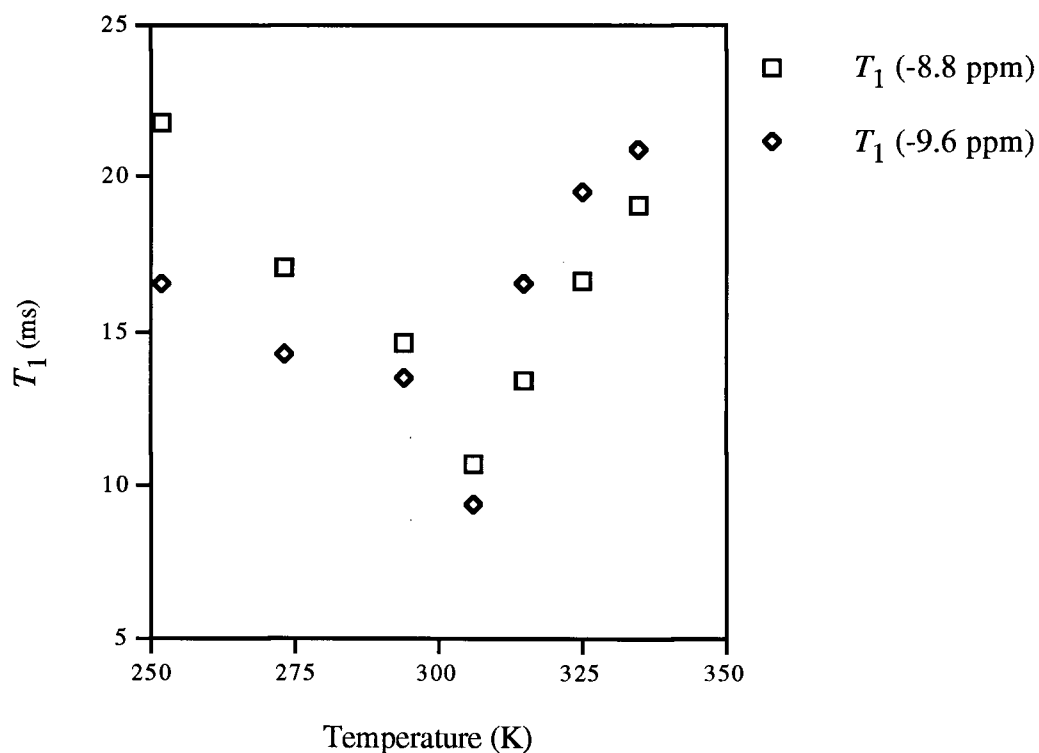
Figure 4.6   Temperature dependence of T_1 for the molecular hydrogen complexes produced on reaction of H_2 and $RuCl_2((R)$-BINAP)(PPh$_3$). Measured at 300 MHz in C_7D_8.

176

The ruthenium species catalyze isotope exchange between H_2 and D_2 in solution. The starting complex $RuCl_2((R)$-BINAP$)(PPh_3)$ or the corresponding dinuclear species (see equilibrium in equation 3.9) reversibly binds H_2. Therefore, a solution of $RuCl_2((R)$-BINAP$)(PPh_3)$ in C_6D_6 under an atmosphere of H_2 was evacuated to remove H_2 and placed under 400 torr each of H_2 and D_2. After two days under the isotopic mixture, the η^2-HD isotopomers were observed (Figure 4.7), thus confirming the existence of the molecular hydrogen species. The two upfield resonances are observed as 1:1:1 triplets of 1:2:1 triplets, with coupling constants: $^1J_{HD} = 28.4$ Hz and *cis*, $^2J_{HP} = 7.6$ Hz for the –8.8 ppm resonance, and $^1J_{HD} = 29.4$ Hz and *cis*, $^2J_{HP} = 6.6$ Hz for the –9.6 ppm resonance. Some smaller coupling is also evident in the –9.6 ppm resonance. Joshi also observed the η^2-HD isotopomer for the related DPPB system (Section 4.3.1).[2,3] The asymmetry of the η^2-HD resonances shown in Figure 4.7 is due to the underlying η^2-H_2 isotopomer, which could be avoided in similar experiments in the future by using 600 torr of D_2 and 200 torr of H_2 in order to decrease the amount of the η^2-H_2 isotopomer. The presence of the η^2-D_2 isotopomer is not important, as only the ^1H NMR spectrum is recorded.

A $^{31}P\{^1H\}$ NMR spectrum of $RuCl_2((R)$-BINAP$)(PPh_3)$ under an atmosphere of H_2 in C_6D_6 (Figure 4.8) shows three AB spin systems (two belong to one compound and one to another). Table 4.3 lists the chemical shifts and coupling constants of the two compounds.

Table 4.3 $^{31}P\{^1H\}$ NMR Data (202.5 MHz, 20 °C) for $RuCl_2((R)$-BINAP$)(PPh_3)$ **15** under an atmosphere of H_2 in C_6D_6

Complex	Chemical Shift, δ	$^2J_{PP}$, (Hz)
$(\eta^2$-$H_2)((R)$-BINAP$)Ru(\mu$-Cl$)_3RuCl((R)$-BINAP$)$	$\delta_A = 60.2$, $\delta_B = 57.6$	30.4
	$\delta_C = 57.8$, $\delta_D = 53.3$	41.5
another isomer	$\delta_A = 56.9$, $\delta_B = 56.5$	24.0

Efforts were made to define further the nature of the molecular hydrogen complexes, in particular to determine if the η^2-H_2 species were mono- or diruthenium in nature. Equilibrium between **15** and the diruthenium species $Ru_2Cl_4((R)$-BINAP$)_2$ (eq 3.9) could allow formation of either mono- or diruthenium molecular hydrogen complexes. Joshi et al. have observed the η^2-H_2 diruthenium complex where DPPB is the diphosphine (Section 4.3.1),[3] while Mezzetti and co-workers have observed a similar molecular dihydrogen complex where the diphosphine is BIPHEMP[48] (the chemical shifts and coupling constants correspond to entry 1, Table 4.3).

Excess PPh_3 (10 equiv) was added to a C_6H_6 solution of $RuCl_2((R)$-BINAP$)(PPh_3)$ (~ 0.02 M) to force the equilibrium of equation 3.9 to the left. After the solution was left for 3 h to reach equilibrium, an atmosphere of H_2 was added. After a further 3 h, ^1H and $^{31}P\{^1H\}$ NMR showed only resonances corresponding to free PPh_3, $RuCl_2((R)$-BINAP$)(PPh_3)$ **15**, and $Ru(H)Cl((R)$-BINAP$)(PPh_3)$ (described in Section 4.4.2). No η^2-H_2 resonances were evident in the ^1H NMR. These results, although complicated by the formation of $Ru(H)Cl((R)$-BINAP$)(PPh_3)$, suggest that both molecular hydrogen complexes observed are "diruthenium" in nature. The fact that some $Ru(H)Cl((R)$-BINAP$)(PPh_3)$ was formed suggests that the excess PPh_3 added is sufficiently basic to abstract HCl, which may cloud the above conclusion.

Figure 4.4 shows the geometries of two possible molecular hydrogen complexes formulated $[(\eta^2$-$H_2)((R)$-BINAP$)Ru(\mu$-Cl$)_3RuCl((R)$-BINAP$)]$. Structure A corresponds to the first entry in Table 4.3, which has been shown by selective $^1H\{^{31}P\}$ NMR spectroscopy to correspond to the η^2-H_2 resonance at -8.8 ppm. Two AB patterns are expected in the $^{31}P\{^1H\}$ NMR for a compound of structure A; the $^2J_{AB}$ coupling constant of 30.4 Hz suggests that the phosphorus chemical shifts $\delta_{A,B}$ belong to the η^2-H_2 end of the dinuclear complex (see Section 5.2.3 for discussion of $[(L)(DPPB)Ru(\mu$-Cl$)_3RuCl(DPPB)]$ $^{31}P\{^1H\}$ NMR chemical shifts and coupling constants). Broadband phosphorus decoupling at 57.7 ppm in the ^{31}P NMR while monitoring the ^1H NMR
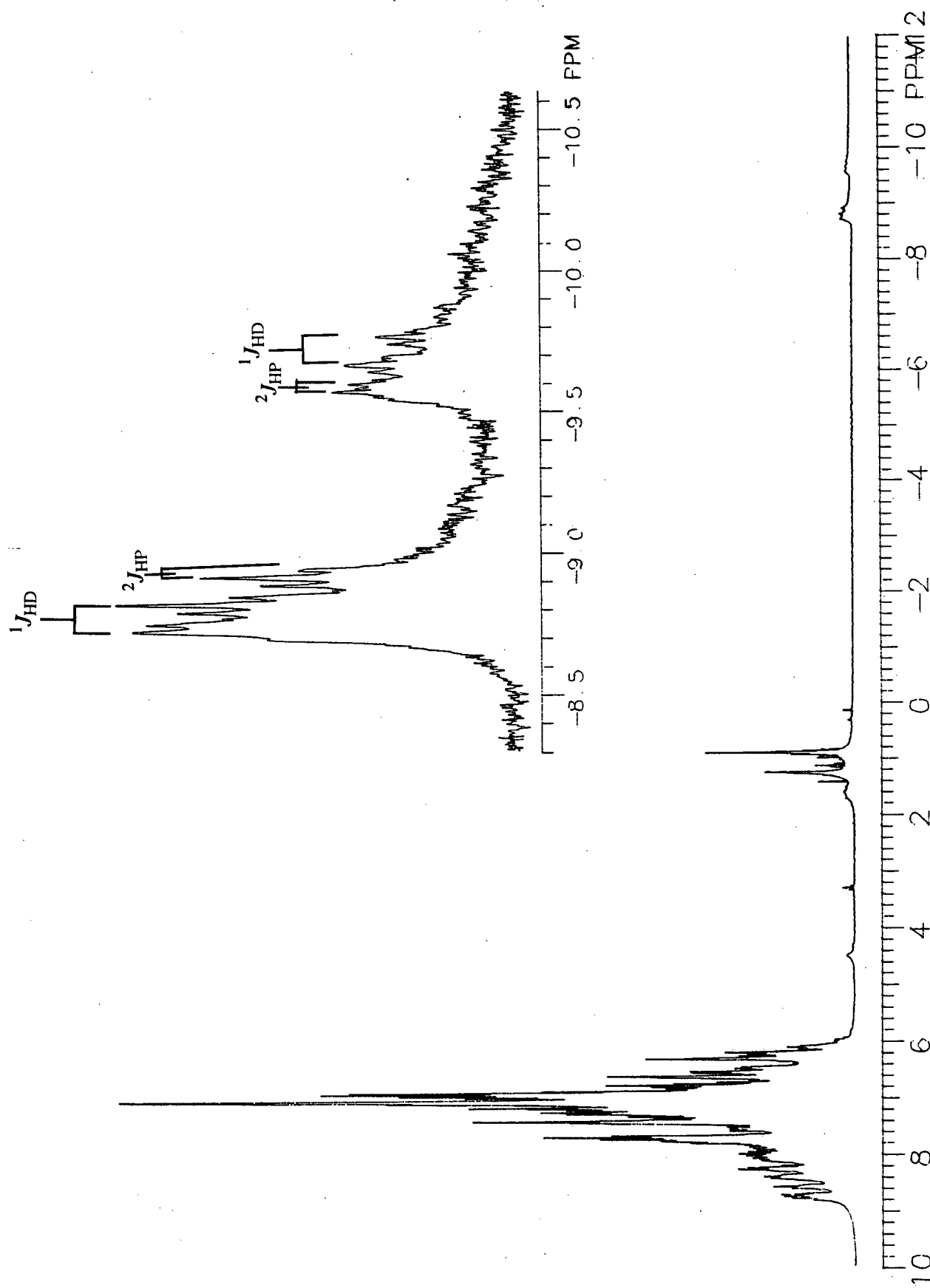
Figure 4.7 ¹H NMR spectrum of RuCl₂((R)-BINAP)(PPh₃) **15** under an atmosphere consisting of 400 torr each of D₂ and H₂ (300 MHz, C₆D₆).
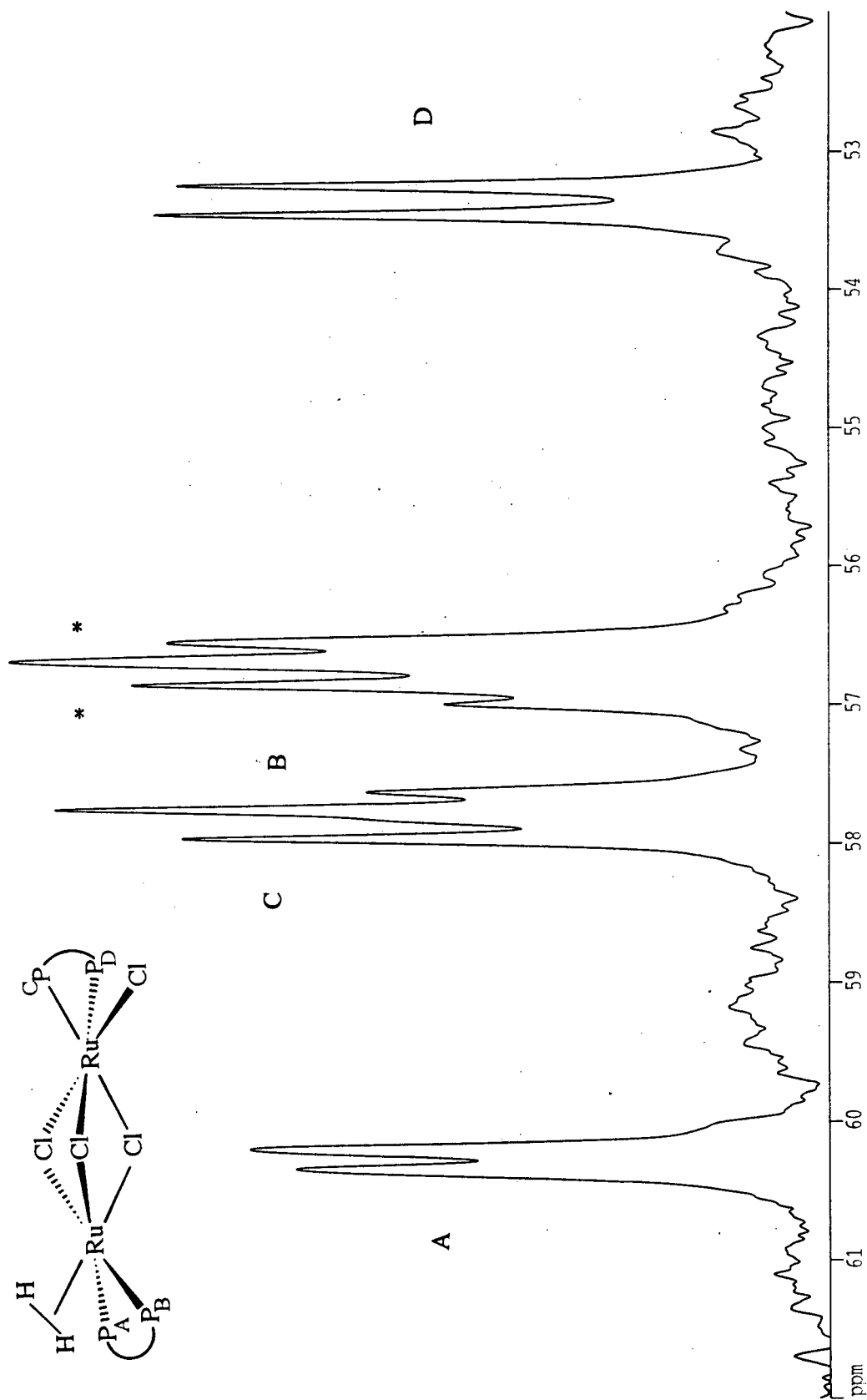
Figure 4.8   31P{1H} NMR spectrum (202.5 MHz, 20 °C) of RuCl₂((*R*)-BINAP)(PPh₃) **15** under an atmosphere of H₂ in C₆D₆; * indicates other isomer (see Table 4.3).

spectrum showed complete loss of HP coupling in both η^2-HD resonances (Figure 4.9). Selective irradiation at either 57.3 or 60.2 ppm reduced the coupling of the η^2-HD resonance at –8.8 ppm from the 1:2:1 triplet ($^2J_{HP}$) to a doublet (both peaks are still split into 1:1:1 triplets by coupling to deuterium, $^1J_{HD}$). This further confirmed that the $\delta_{A,B}$ shifts were associated with the end of the dinuclear complex containing the η^2-HD ligand. Selective irradiation at 53.3 ppm (i.e., δ_D of entry 1, Table 4.3) produced no visible change in the ^{1}H NMR spectrum. This fits the assignment, as δ_D is at the Cl-end of the dinuclear complex where phosphorus coupling to η^2-HD is not observed. Further selective irradiations of the other ^{31}P resonances were hampered by the close proximity of the peaks to one another (56.5–57.8 ppm region). Unfortunately, this made the assignment of the exact geometry of the η^2-H$_2$ resonance at –9.6 ppm more difficult.

Structure B, Figure 4.4 would be expected to give two singlets in the ^{31}P{^{1}H} NMR spectrum, one for each end of the dinuclear complex, when the diphosphine is achiral. If a chiral diphosphine is used, the singlets may each be split into AB patterns. Therefore, the ^{31}P{^{1}H} NMR spectrum would be expected to show two AB patterns for a geometry like that shown in structure B. However, the ^{31}P{^{1}H} NMR data (Table 4.3, entry 2) reveal only a single AB quartet. Second-order effects could explain this observation, as the outside resonances of the two AB quartets could be lost in the baseline, or buried under the other resonances in this region. If strong second-order effects are operating, then two "doublets" would be expected. In this case, the coupling constant listed in Table 4.3, entry 2 would actually be the line spacing of the inner two peaks of the second-order AB quartet.
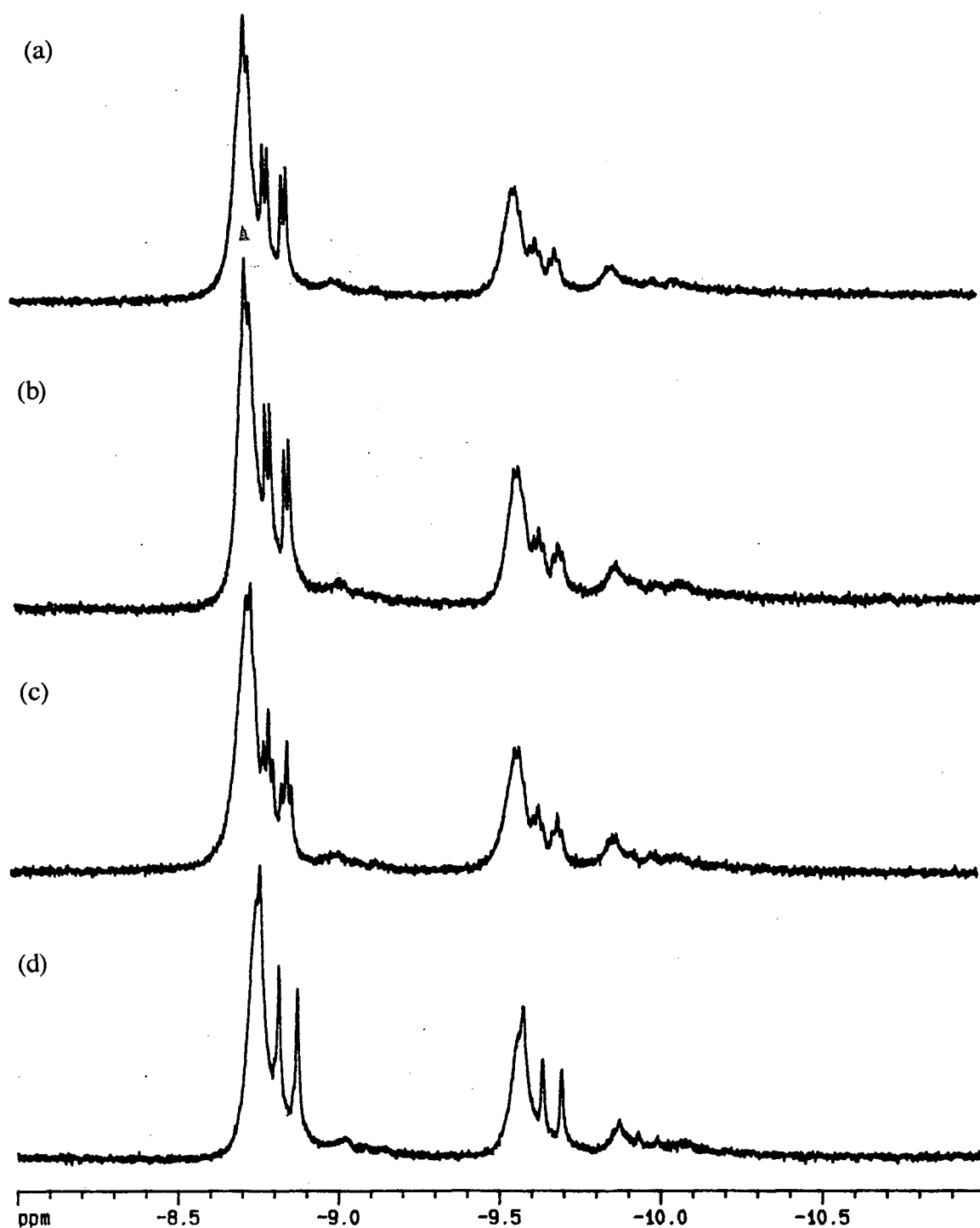
Figure 4.9 $^1H\{^{31}P\}$ high-field NMR spectra of the two isomers $[(\eta^2\text{-}H_2)((R)\text{-}BINAP)\text{-}$
Ru$(\mu\text{-}Cl)_3$RuCl$((R)\text{-}BINAP)]$ in C_6D_6 (500 MHz for ^1H, 202.5 MHz for
^{31}P, 20 °C) with selective phosphorus decoupling at: (a) 60.2, (b) 57.3,
(c) 53.3; (d) broadband at 57.7 ppm; the larger 1:1:1 $^1J_{HD}$ coupling remains
unchanged as expected.

182

4.4.2 Interaction with H_2 in the Presence of an Added Base

The mixed-phosphine complexes, $RuCl_2$(P–P)(PPh$_3$), where P–P = DPPB or BINAP, were found to react with H_2 in the presence of NEt$_3$ to give products of the formulation Ru(H)Cl(P–P)(PPh$_3$). For example, NEt$_3$ (100 μL, 50 equiv) was added to an orange solution of $RuCl_2$((*R*)-BINAP)(PPh$_3$) in CH_2Cl_2 / CD_2Cl_2 (~ 10^{-2} M). The system was evacuated, and an atmosphere of H_2 was added. The solution became red over a period of 1 h.

A $^{31}P\{^1H\}$ NMR spectrum (Figure 4.10) showed the product to be Ru(H)Cl((*R*)-BINAP)(PPh$_3$); the chemical shift and coupling constant data for two overlapping ABX patterns are listed in Table 4.4, and indicate the presence of two diastereomers. The Ru(H)Cl(P–P)(PPh$_3$) products are chiral at the metal, and contain the (*R*)-stereoisomer of the chiral diphosphine BINAP. Figure 4.11 shows the two diastereomers observed in solution.

Mezzetti et al. have observed similar chemistry with BIPHEMP, which is an analogous ligand to BINAP (Section 3.3.3).[48] Interestingly, the ABX patterns in the case of BIPHEMP were broad at room temperature, and it was necessary to cool the solution to 0 °C to resolve the resonances.[48] The dynamic process thought to be responsible for the broadness of the peaks is the interconversion of the diastereomers.[48] As this dynamic process is observed for the achiral DPPB analogue where only one stereoisomer is present (see later in this section), the process responsible for the broadness is thought to be intramolecular exchange of the phosphorus atoms of the diphosphine (Section 3.3.3.2). However, for Ru(H)Cl((*R*)-BINAP)(PPh$_3$), the ABX patterns were resolved at 20 °C (Figures 4.10).

The hydride proton was observed in the ^1H NMR spectrum (Figure 4.12) at –22.5 ppm as a doublet of triplets. The splitting is a result of coupling to the axial phosphorus (i.e., doublet, $^2J_{HP(X)}$ = 36.3 Hz) and two equatorial phosphorus atoms (i.e., triplet, $^2J_{HP(A,B)}$ = 22.7 Hz).

Mezzetti et al. isolated Ru(H)Cl((*S*)-BIPHEMP)(PPh₃) as a red solid, but further characterization was impossible, as the compound was extremely air-sensitive, even in the solid state.[48] No attempts were made in this work to isolate Ru(H)Cl((*R*)-BINAP)(PPh₃).

Table 4.4 $^{31}P\{^{1}H\}$ NMR Spectral Data (121. 42 MHz, CD_2Cl_2) of Ru(H)Cl(P–P)(PPh₃) Complexes

Complex	Temp (°C)	Chemical Shift, δ	$^2J_{PP}$, (Hz)
P–P = DPPB			
Ru(H)Cl(DPPB)(PPh₃)	20	$\delta = 42.6$	127[a], [b]
	–90	$\delta_A = 39.0$	$^2J_{AX}$ = unresolved
		$\delta_B = 45.0$	$^2J_{BX}$ = unresolved
		$\delta_A = 92.3$	$^2J_{AB} = 198.7$
P–P = (*R*)-BINAP			
Ru(H)Cl((*R*)-BINAP)(PPh₃)	20	$\delta_A = 90.3, 90.1$	$^2J_{AX} = 39.4, 36.9$
		$\delta_B = 45.0, 44.9$	$^2J_{BX} = 20.9, 18.8$
		$\delta_X = 36.0, 35.9$	$^2J_{AB} = 302.4, 303.0$

(a) triplet-like pattern; *J* value indicates line spacing.

(b) solvent is CH_2Cl_2 with a couple of drops of added CD_2Cl_2.
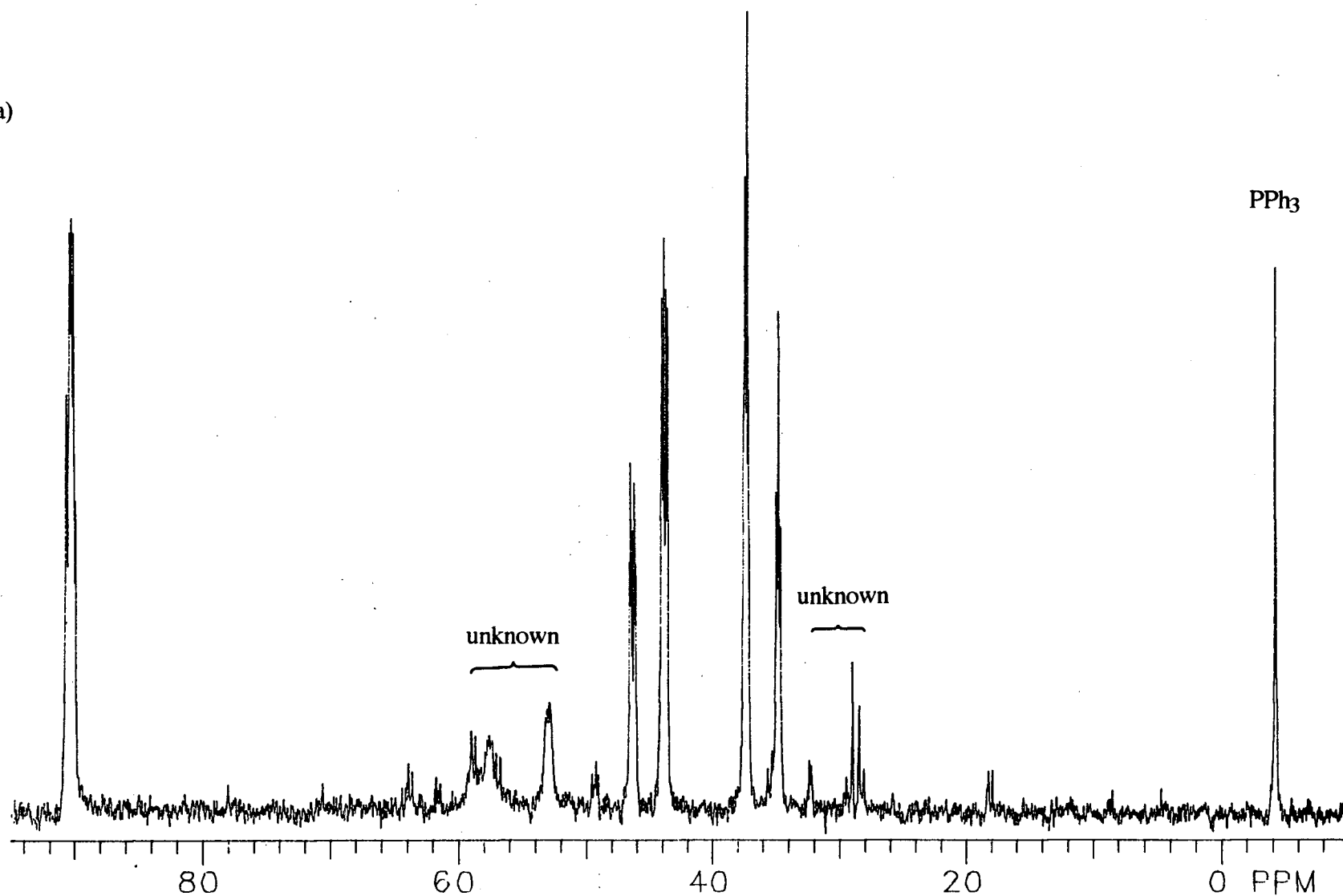
Figure 4.10 $^{31}P\{^1H\}$ NMR spectra (121. 42 MHz, CH$_2$Cl$_2$ / CD$_2$Cl$_2$) of Ru(H)Cl((*R*)-BINAP)(PPh$_3$) produced in situ from RuCl$_2$((*R*)-BINAP)(PPh$_3$) and H$_2$ at room temperature; (a) full sweep width and (b) expanded regions (see next page); • indicates resonances belonging to one diastereomer.

(b)

mirror

P–P = BINAP
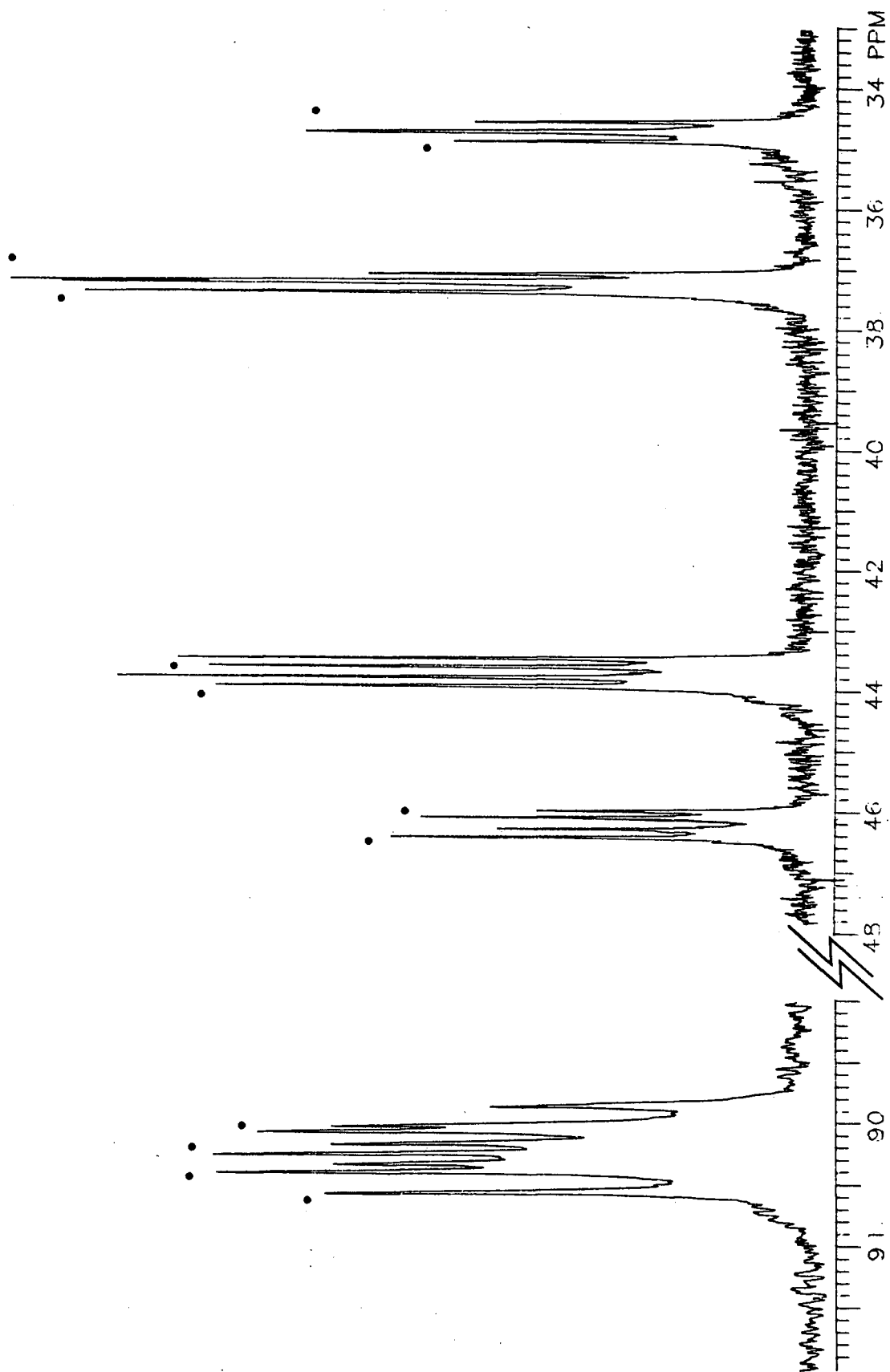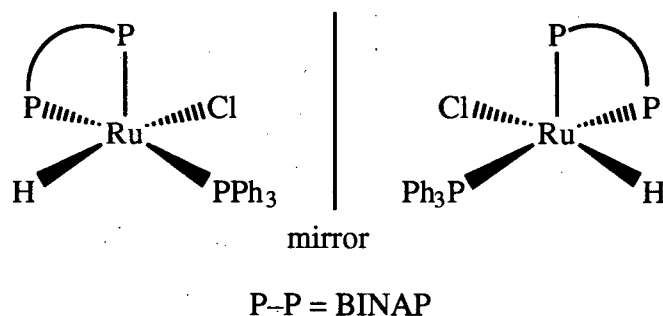
Figure 4.11   The geometry of the two diastereomers of Ru(H)Cl((*R*)-BINAP)(PPh₃).
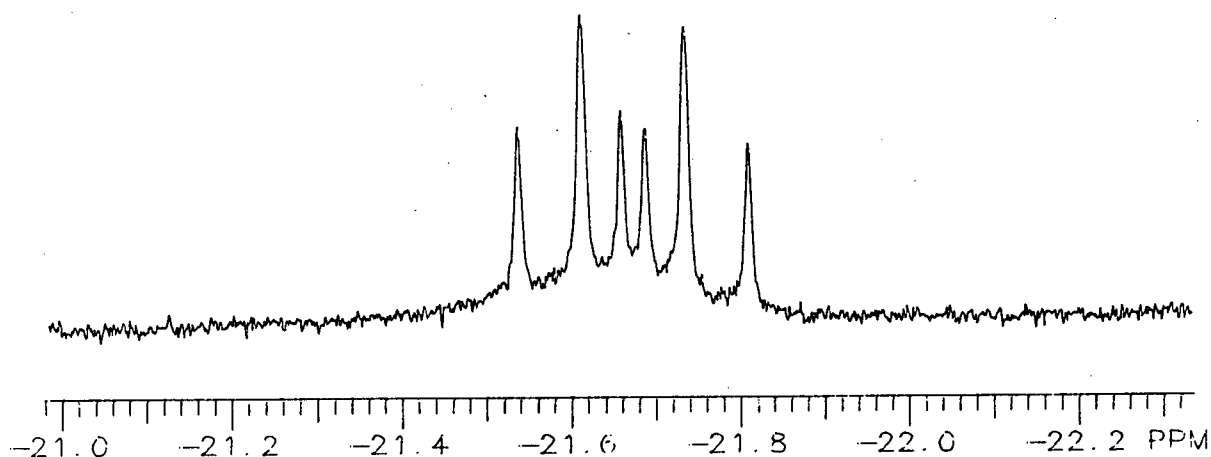
Figure 4.12   ¹H NMR spectrum (121. 42 MHz, CD₂Cl₂, 20 °C) of Ru(H)Cl((*R*)-BINAP)(PPh₃) produced in situ from RuCl₂((*R*)-BINAP)(PPh₃) **15**.

The analogous DPPB chemistry was somewhat more complicated. Triethylamine (100 µL, 30 equiv) was added to a green solution of RuCl₂(DPPB)(PPh₃) **11** (0.05 M) in CD₂Cl₂. The solution (still green) was evacuated and placed under an atmosphere of H₂. Within 1 h, the reaction solution had become orange-red. A ³¹P{¹H} NMR spectrum of the above solution at 20 °C showed starting **11**, free PPh₃, and a singlet resonance at 50.0 ppm thought to be due to [HNEt₃]⁺[Ru₂Cl₅(DPPB)₂]⁻ **41** (Table 3.14). It also showed a triplet-like pattern at 42.6 with a line-spacing of 127 Hz (Table 4.4), indicating an exchange process on the NMR-timescale. When the solution was cooled to –90 °C, the

187

spectrum was resolved into an ABX pattern (Table 4.4), indicating a meridional arrangement of phosphorus atoms; the coupling constant $^2J_{AB}$ indicates two phosphorus atoms trans-disposed to one another, while the other two coupling constants which are unresolved because of broadness, indicate *cis*-disposed phosphorus atoms. The product is therefore assigned as Ru(H)Cl(DPPB)(PPh$_3$), and the geometry is thought to be square-pyramidal, as shown for the BINAP analogue in Figure 4.11. The singlet at 50.0 ppm due to [HNEt$_3$]$^+$[Ru$_2$Cl$_5$(DPPB)$_2$]$^-$ **41** remains unchanged at –90 °C; under these reaction conditions, **41** could be produced by the reaction of Ru$_2$Cl$_4$(DPPB)$_2$ **24** and NEt$_3$·HCl, which is produced by the reaction of **11**, H$_2$ and NEt$_3$. Complex **24** is produced in situ by PPh$_3$ dissociation from **11** (eq 3.9). Triethylamine hydrochloride was shown to react with **24** to produce **41** in this work (Section 3.2). A ^{31}P{^{1}H} NMR spectrum recorded several days later showed only Ru(H)Cl(DPPB)(PPh$_3$), **41**, and free PPh$_3$, while the starting complex **11** was gone.

A ^{1}H NMR spectrum of the above sample recorded at room temperature showed a quartet upfield of TMS at –20.7 ppm ($^2J_{HP}$ = 28.8 Hz). The two middle peaks of the quartet were quite broad, and seemed to show some smaller couplings. This is probably a result of intramolecular exchange of the DPPB phosphorus atoms observed at room temperature in the phosphorus spectrum (see Section 3.3.3.2). Based on the structure (Figure 4.11), a doublet of triplets (1 axial and 2 equatorial phosphorus atoms) would be expected, as is observed for the BINAP analogue when no exchange process was involved. In fact, at –90 °C, a six-line pattern resembling the doublet of triplets seen for the BINAP analogue was observed (Figure 4.12); however, excessive noise in this spectrum made complete assignment of the coupling constants impossible.

Joshi had previously attempted to prepare Ru(H)Cl(DPPB)(PPh$_3$) from RuCl$_2$(DPPB)(PPh$_3$) **11** in DMA, but found by gas-uptake measurements that only ~ 0.20 mole equivalents of H$_2$ were used per Ru.[2] The ^{31}P{^{1}H} NMR spectrum of this solution was complicated, showing none of the ABX pattern observed in this work. Joshi also

attempted the reaction of **11** with H_2 in the presence of Proton Sponge (1.1 equiv).[2] In fact, this reaction did result in observation of the same triplet-like pattern at 42.6 ppm in the $^{31}P\{^1H\}$ NMR spectrum that was observed in this work (Table 4.4). This was one of several products observed in the reaction. Joshi did not realize that the triplet-like resonance was the result of an exchange process. In the presence of Proton Sponge, other hydride species (and possibly molecular hydrogen species) were observed by ^1H NMR spectroscopy.[2]

The importance of the choice of base (i.e., NEt$_3$ vs. DMA or Proton Sponge) in determining the product(s) is illustrated by this thesis work and Joshi's work. Joshi noted the extreme air-sensitivity of the red solutions produced by interaction of RuCl$_2$(DPPB)(PPh$_3$) with H_2 in the presence of a base.[2] This was also noted by Mezzetti et al. for the BIPHEMP analogue,[48] and in this thesis work in attempts to isolate a product from a red solution produced on reaction of RuCl$_2$(DPPB)(P(*p*-tolyl)$_3$) **12** with H_2 in the presence of NEt$_3$ (1 equiv) in C$_6$H$_6$.

One attempt was made to observe the bromo analogue of the triruthenium species (i.e., [Ru(H)Br(DPPB)]$_3$) by $^{31}P\{^1H\}$ NMR spectroscopy. Triethylamine (6 μL, 2 equiv) was added to a C$_6$D$_6$ suspension of Ru$_2$Br$_4$(DPPB)$_2$ (28 mg in 1 mL C$_6$D$_6$), and the resulting brown suspension was left stirring under an atmosphere of H_2 for 24 h. Unfortunately, the limited solubility of the complex(es) resulted in ^1H and $^{31}P\{^1H\}$ NMR spectra which were very noisy and impossible to interpret. In order to determine if the Br chemistry parallels the Cl chemistry in the formation of a trinuclear species under these conditions, a larger-scale reaction needs to be attempted, where the product could be isolated and dissolved in a better solvent (perhaps CD$_2$Cl$_2$ or CH$_2$Br$_2$) for NMR spectroscopic investigations.

4.5 **Reaction of Other Neutral Two-Electron Ligands with Five-Coordinate Ruthenium(II) Complexes**

4.5.1 **Reaction of $Ru_2Cl_4(DPPB)_2$ 24 with Ethylene**

A C_6D_6 solution of $Ru_2Cl_4(DPPB)_2$ **24** was placed under an atmosphere of ethylene for 2 h. A $^{31}P\{^1H\}$ NMR spectrum of the sample showed an equilibrium mixture of **24** (an AB pattern) and the ethylene adduct $Ru_2Cl_4(DPPB)_2(\eta^2\text{-ethylene})$ (2 AB patterns). Figure 4.13 shows the $^{31}P\{^1H\}$ NMR spectrum, while Table 4.1 lists the NMR data.

The reaction with ethylene is reversible; if the atmosphere of ethylene is replaced with argon, the resonances of the ethylene adduct disappear. Under the conditions employed (i.e., 1 atm ethylene, 20 °C, ~ 10^{-2} M Ru_2), the equilibrium is ca. 85% to the ethylene adduct side.
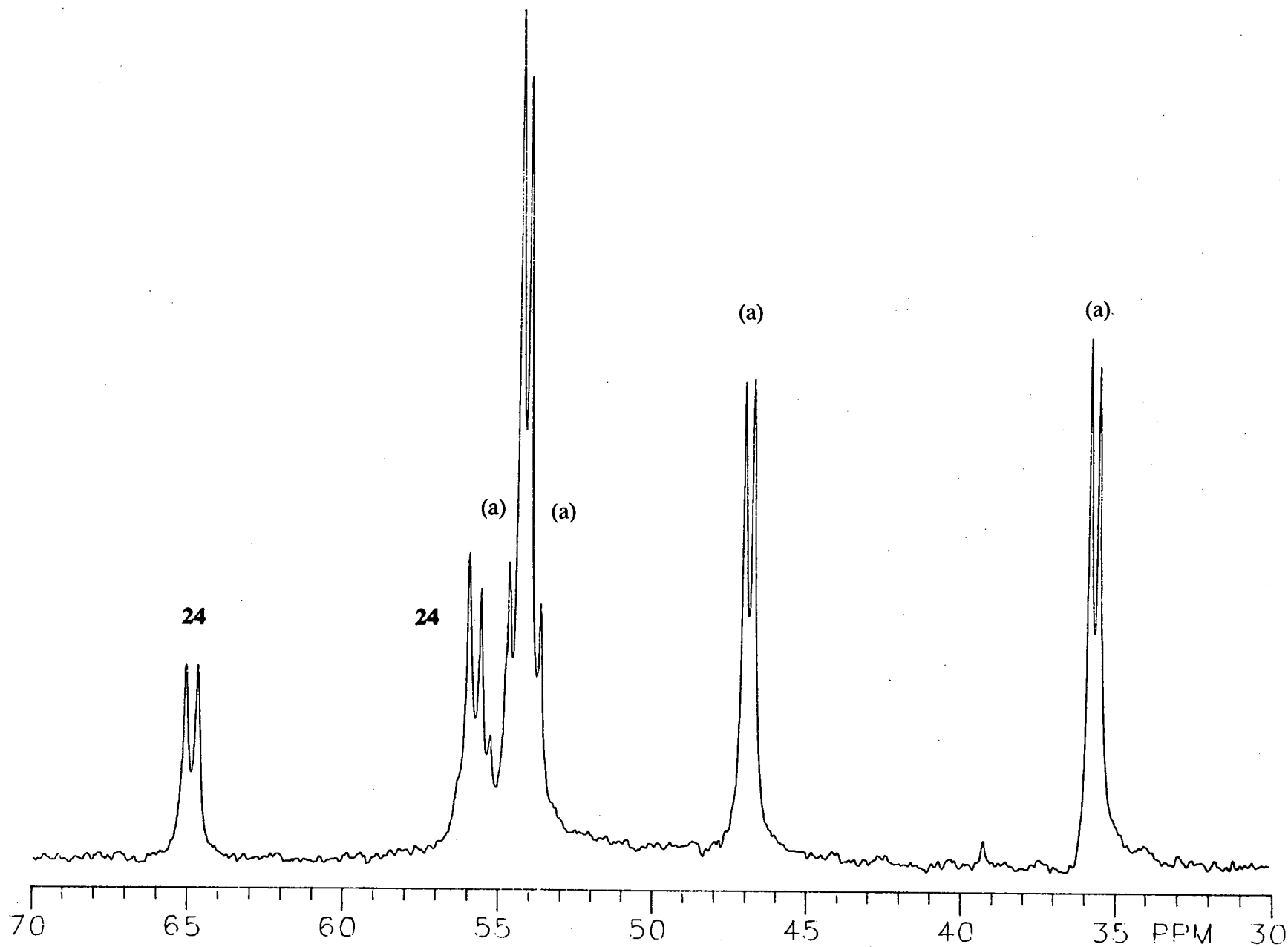
Figure 4.13 $^{31}P\{^1H\}$ NMR spectrum of $Ru_2Cl_4(DPPB)_2$ **24** under an atmosphere of ethylene in C_6D_6 (121.42 MHz, 20 °C);
(a) = $Ru_2Cl_4(DPPB)_2(\eta^2\text{-ethylene})$.

4.5.2 Reaction of Ru₂Cl₄(DPPB)₂ 24 with Styrene

Styrene (100 μL, ~ 100 equiv) was added to a C_6D_6 solution of $Ru_2Cl_4(DPPB)_2$ **24** at room temperature. After 0.5 h at room temperature, a $^{31}P\{^{1}H\}$ NMR spectrum of the orange solution showed only starting $Ru_2Cl_4(DPPB)_2$ to be present. Another experiment with 10 equivalents of styrene and 2 h reaction time also showed no styrene adduct by $^{31}P\{^{1}H\}$ NMR spectroscopy.

These results were somewhat surprising, considering that ethylene readily coordinates to **24** to produce a triply-chloro bridged adduct (Section 4.5.1). The phenyl group of styrene must provide sufficient steric bulk to force the equilibrium between **24** and any possible styrene adduct far to the side of **24**.

Styrene hydrogenation is catalyzed by **24** at 30 °C and 1 atm of H_2 in DMA, and the kinetics of this process have been investigated in some detail.[43] The mechanism is thought to occur by a hydride route, whereby **24** initially reacts with H_2 to form $Ru_2Cl_4(DPPB)_2(\eta^2\text{-}H_2)$; in some later step, styrene perhaps coordinates, and subsequently hydrogen transfer produces ethylbenzene.[43] However, other possibilities considered[43] include direct hydrogen transfer to non-coordinated styrene, which has been demonstrated for hydrogenation of α-methylstyrene with $MnH(CO)_5$ as the catalyst,[49] and cannot be ruled out as a possibility in this case. The process would involve stepwise H-atom transfers via styryl radical intermediates.[49] Of note, pairwise H_2 transfer from the molecular hydrogen complex $Ru(\eta^2\text{-}H_2)(H)_2(PPh_3)_3$ to styrene has been demonstrated by the PHIP technique (*para*-hydrogen induced polarization).[50]

Interestingly, $Ru_2Cl_5(DPPB)_2$ was also found to be an effective catalyst precursor for the hydrogenation of styrene.[51] The rate of hydrogenation to ethylbenzene, under identical conditions described above for **24**, is somewhat slower (28% of the initial rate). The active species is presumably formed via **24**, produced in situ by H_2 reduction of $Ru_2Cl_5(DPPB)_2$, and the HCl formed in the reduction process (Figure 4.14). Addition of one mole equivalent of HCl gas to a system catalyzed by **24** produced a hydrogenation

rate comparable to that of $Ru_2Cl_5(DPPB)_2$ system. The nature of the catalyst remains to be elucidated (see Section 4.6.1).

4.5.3 Reaction of $RuCl_2(DPPB)(PPh_3)$ 11 with N_2

A C_6D_6 solution of $RuCl_2(DPPB)(PPh_3)$ **11** (0.04 M) was placed under an atmosphere of N_2 for 5 h at room temperature, and a $^{31}P\{^1H\}$ NMR spectrum was recorded. The spectrum showed **11**, **24**, $Ru_2Cl_4(DPPB)_2(\eta^1\text{-}N_2)$, and free PPh_3. The NMR data (Table 4.1) for the two sets of AB patterns (designated ABCD) are the same as those observed for $Ru_2Cl_4(DPPB)_2(\eta^1\text{-}N_2)$ prepared by direct reaction of $Ru_2Cl_4(DPPB)_2$ with N_2,[2,3,46] when ca. 70% conversion to $Ru_2Cl_4(DPPB)_2(\eta^1\text{-}N_2)$ was observed under the conditions employed for the above reaction (i.e., 1 atm N_2, 20 °C). In this thesis work, N_2 reacted with **24**, which was produced in situ by PPh_3 dissociation from **11** (eq 3.9), and the $Ru_2Cl_4(DPPB)_2(\eta^1\text{-}N_2)$ complex accounted for ca. 45% of the integral intensity when compared with the amount of **24** present (i.e., the large amount of **11** present was ignored). No direct reactivity between **11** and N_2 was observed, and therefore the equilibrium between **11** and **24** is responsible for the observed reactivity (eq 3.9).

IR spectroscopy on a CH_2Cl_2 solution of **11** under an N_2 atmosphere showed a $\nu_{(N\equiv N)}$ at 2170 cm^{-1}, which agrees with that observed for $Ru_2Cl_4(DPPB)_2(\eta^1\text{-}N_2)$ prepared directly from **24**.[2]

4.5.4 Reaction of $Ru_2Cl_4(DPPB)_2$ 24 with CO

The species $Ru_2Cl_4(DPPB)_2(CO)$, whose $^{31}P\{^1H\}$ NMR spectral data are shown in Table 4.1, has been observed on several occasions in the current work. As discussed in Section 4.3.3, $Ru_2Cl_4(DPPB)_2(CO)$ had been isolated from the decarbonylation of aldehydes by $Ru_2Cl_4(DPPB)_2$ **24**.[2,46]

In the present work, $Ru_2Cl_4(DPPB)_2(CO)$ was observed in solution upon dissolving the solid produced by the reaction of CO with **24** in the solid state (see Chapter 7 for details).

Significant amounts of $Ru_2Cl_4(DPPB)_2(CO)$ were also observed in a sample of **24**, which had been prepared from $Ru_2Cl_5(DPPB)_2$ **22** in DMA (Section 2.5.7.1). This species is presumably produced by decarbonylation of DMA by **24**. The sample had been left in DMA solution for several weeks. It should be noted that DMF is known to decompose in the presence of acidic or basic materials to give dimethylamine and CO,[52] and it is therefore conceivable that DMA, in the presence of transition metal species, decomposes in the same manner, and that the CO generated reacts with **24**.

Small amounts of $Ru_2Cl_4(DPPB)_2(CO)$ were observed on one occasion when **24** was prepared in situ by the addition of HCl (in MeOH) to a $CDCl_3$ solution of **24** (Section 2.5.7.1). In this case, $Ru_2Cl_4(DPPB)_2(CO)$ was presumably produced by decarbonylation of phosgene $COCl_2$, which is known to be one of the photochemical decomposition products of chloroform.[52]

4.5.5 Reaction of $RuCl_2((R)$-BINAP)(PPh_3)$ 15 with N_2

A C_6D_6 solution of $RuCl_2((R)$-BINAP)(PPh_3)$ **15** (0.03 M) was placed under an atmosphere of N_2 for 24 h at room temperature, and a $^{31}P\{^1H\}$ NMR spectrum was recorded. The spectrum showed small amounts of several new AB patterns some of which may correspond to a $Ru_2Cl_4((R)$-BINAP)_2(\eta^1-N_2)$ complex, as previously observed for the DPPB analogue. In this BINAP case, the spectrum is difficult to interpret completely because of low conversions to the "η^1-N_2 complex" and additional resonances which may indicate the presence of more than one isomer. Nonetheless, the appearance of additional resonances in the $^{31}P\{^1H\}$ NMR spectrum when **15** is placed under an atmosphere of N_2 indicate that a reaction is occurring. When the spectrum is recorded under an atmosphere of Ar, these additional resonances are not observed.

No attempts were made to observe the $\nu_{(N\equiv N)}$ in the IR spectrum due to the low conversions to "η^1-N_2 products."

4.6 Reaction of H_2 with $Ru_2Cl_5(P\text{-}P)_2$ Complexes
4.6.1 P–P = DPPB

Bubbling H_2 gas through a C_6D_6 or CD_2Cl_2 solution of $Ru_2Cl_5(DPPB)_2$ **22** resulted in the formation of $Ru_2Cl_4(DPPB)_2$ **24** and $Ru_2Cl_4(DPPB)_2(\eta^2\text{-}H_2)$ (Figure 4.14).[53] In C_6D_6 solution, it was necessary to bubble H_2 through an NMR sample ($\sim$ 1 mL, $\sim$ 10^{-2} M) for about 1 h. In CD_2Cl_2 solution, under otherwise identical conditions, bubbling H_2 for $\sim$ 15 min was sufficient to reduce completely the starting $Ru_2Cl_5(DPPB)_2$ complex.
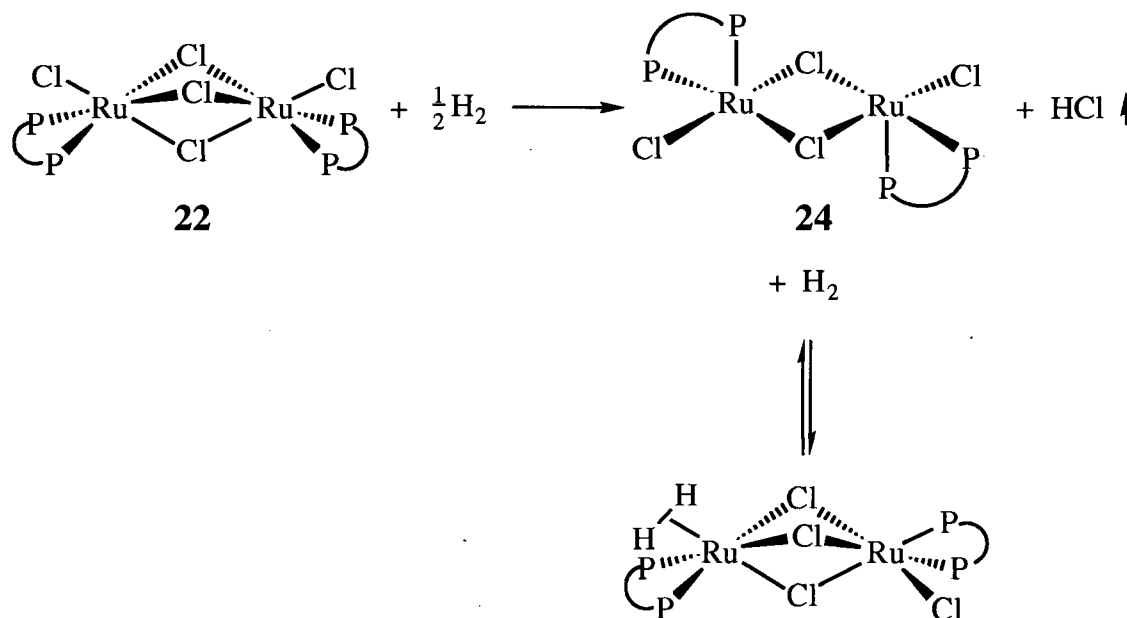
Figure 4.14 H_2-reduction of the mixed-valence complex $Ru_2Cl_5(DPPB)_2$ **22** to give $Ru_2Cl_4(DPPB)_2$ **24**, which reacts reversibly with H_2 to produce $Ru_2Cl_4(DPPB)_2(\eta^2\text{-}H_2)$; where P–P = $Ph_2P(CH_2)_4PPh_2$.

Previously, the presence of an added base was thought necessary to reduce $Ru_2^{II,III}Cl_5(DPPB)_2$ **22** to $Ru_2^{II,II}Cl_4(DPPB)_2$ **24**, because the starting complex was

reduced only in the basic solvent DMA, or in C_6H_6 or C_7H_8 with the addition of polyvinylpyridine.[2,6,46] However, clearly complex **24** can be prepared in the absence of a base if hydrogen is bubbled through a solution of **22**;[53] presumably because the HCl generated is removed from solution by the stream of H_2 gas. Indeed, when the reaction was attempted in a closed H_2 atmosphere in a large Schlenk tube, the reduction was incomplete, even after 24 h. Visual inspection was effective in determining the extent of the reaction, as the starting suspension of **22** was deep red, while the reduced products were orange. Although the reaction was slow to proceed without the bubbling procedure, some reduction was evident in the $^{31}P\{^1H\}$ NMR spectrum of the resulting solution in C_6D_6. It should be noted that the product formed on reaction of **24** with HCl (see below) is also red and insoluble in C_6D_6, and it is therefore difficult to definitely identify the red solid as either starting **22** or the product formed on reaction with HCl.

Reactions of either gaseous or aqueous HCl (as a methanolic solution) with $Ru_2Cl_4(DPPB)_2$ **24** have been attempted. Both reactions resulted in a red solid which was largely insoluble in C_6D_6. Nonetheless, when HCl was bubbled through a C_6D_6 solution of **24** for 10 min, the resulting suspension showed remaining **24**, plus a very broad peak at 48.8 ppm in the $^{31}P\{^1H\}$ NMR spectrum. The product is perhaps the ionic complex "$H^+[Ru_2Cl_5(DPPB)_2]^-$"; the anion has been observed and isolated previously with other cations (Section 3.4.1), but the formulation with a 'free proton' is probably not realistic. An interesting possibility is that the proton could be attached to a chloro ligand (i.e., the species could be an η^1-HCl adduct; such species have been formulated within Pt(II) systems).[54]

Dekleva has noted somewhat similar reactivity of $[(\eta^2-H_2)(PPh_3)_2Ru(\mu-Cl)_2(\mu-H)Ru(H)(PPh_3)_2]$ and HCl, which produced "$H^+[Ru_2Cl_5(PPh_3)_4]^-$" and H_2.[55]

When a methanolic solution of HCl was added to **24** in C_6D_6, the $^{31}P\{^1H\}$ NMR spectrum showed a broad singlet at 57 ppm (see Section 3.3.4.2). The presence of the polar solvent MeOH may effect the chemical shift (49 vs. 57 ppm). The product of this

HCl reaction needs to be isolated and further characterized, especially in terms of determining the nature of the cation in C_6D_6.

A reaction between gaseous HCl and **24** in CD_2Cl_2 was performed with Abu-Gnim of this laboratory to give the red product which was more soluble than in C_6D_6; the in situ $^{31}P\{^1H\}$ NMR spectrum showed a broad singlet at 48.8 ppm, as was observed in C_6D_6.

Red crystals were isolated on one occasion from a solution produced by the addition of 3 equivalents of HCl (methanolic solution) to Ru(DPPB)(η^3-Me-allyl)$_2$. This reaction is known to produce **24**, plus another species that gives a singlet at 57 ppm in the $^{31}P\{^1H\}$ NMR spectrum (Section 3.3.4.2). Unfortunately, X-ray diffraction studies were unsuccessful, as the crystals did not diffract.

4.6.2   P–P = (*R*)-BINAP

As for the DPPB analogue (Section 4.6.1), dihydrogen gas was bubbled through a C_6D_6 solution of $Ru_2Cl_5((R)$-BINAP)$_2$ **23** ($\sim 10^{-2}$ M) for 1 h . Over the bubbling period, the solution changed from red-brown to orange.

A $^{31}P\{^1H\}$ NMR spectrum of the above solution shows at least three products (Figure 4.15). Two of the ruthenium(II)-BINAP-containing products are thought to be dinuclear, based on the observed ABCD spin system (i.e., two AB quartets). The third product, a singlet at 13.2 ppm, is probably mononuclear. Unfortunately, none of the $^{31}P\{^1H\}$ NMR resonances (Table 4.5) correspond to those observed for $Ru_2Cl_4((R)$-BINAP)$_2$.[46] The $^{31}P\{^1H\}$ NMR spectrum reported for isolated $Ru_2Cl_4((R)$-BINAP)$_2$[46] corresponds to that observed in this work by dissociation of PPh$_3$ from $RuCl_2((R)$-BINAP)(PPh$_3$) (eq 3.9). For comparative purposes, Figure 4.16 shows the room temperature $^{31}P\{^1H\}$ NMR spectra of $RuCl_2((R)$-BINAP)(PPh$_3$) (and in situ produced $Ru_2Cl_4((R)$-BINAP)$_2$) .
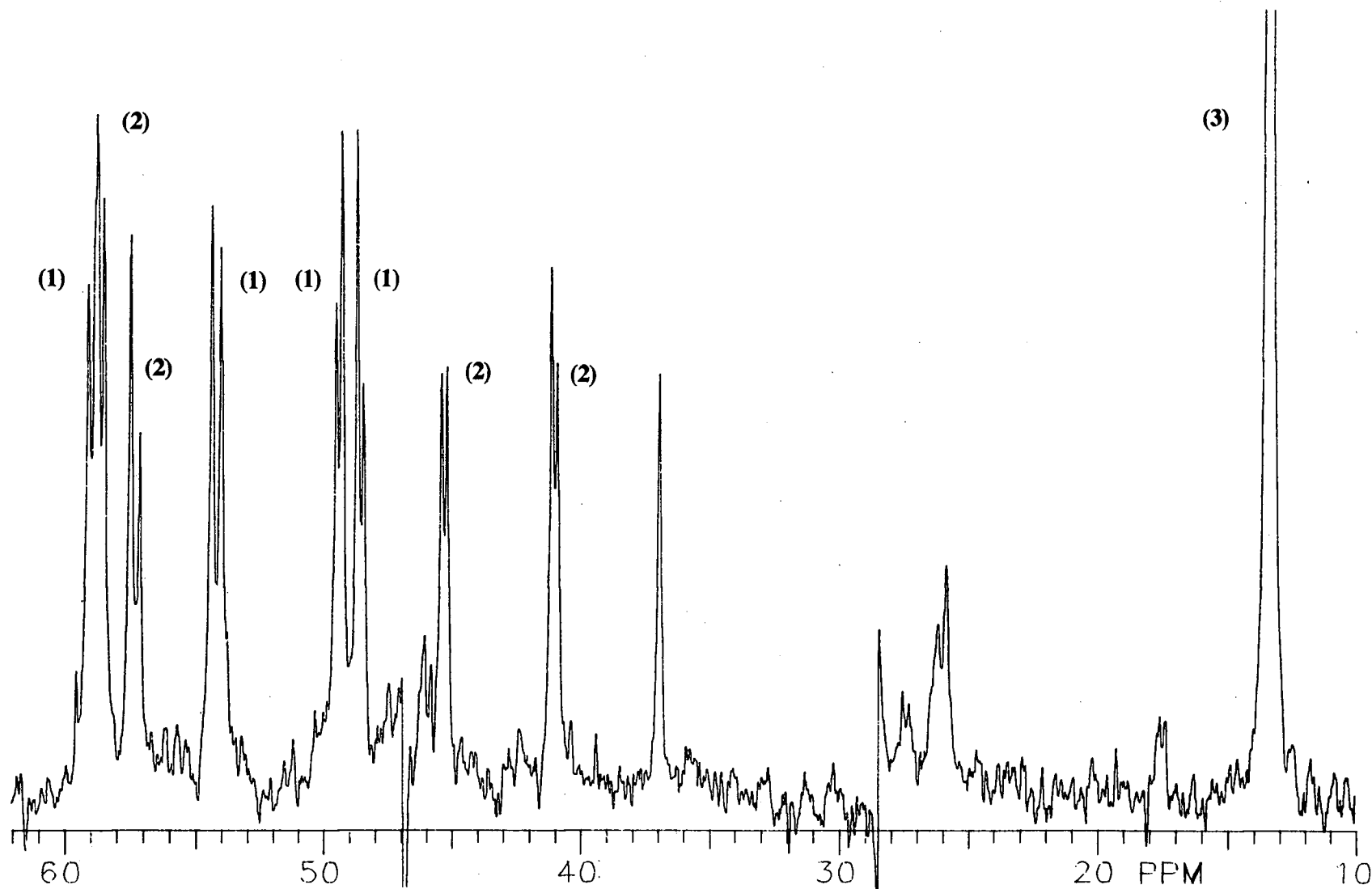
Figure 4.15 $^{31}P\{^{1}H\}$ NMR spectrum (121.42 MHz, 20 °C) of a C_6D_6 solution of $Ru_2Cl_5((R)\text{-BINAP})_2$ **23** after bubbling H_2 through the solution for 1 h. Table 4.5 lists the data for species numbered **(1)**–**(3)** on this spectrum.
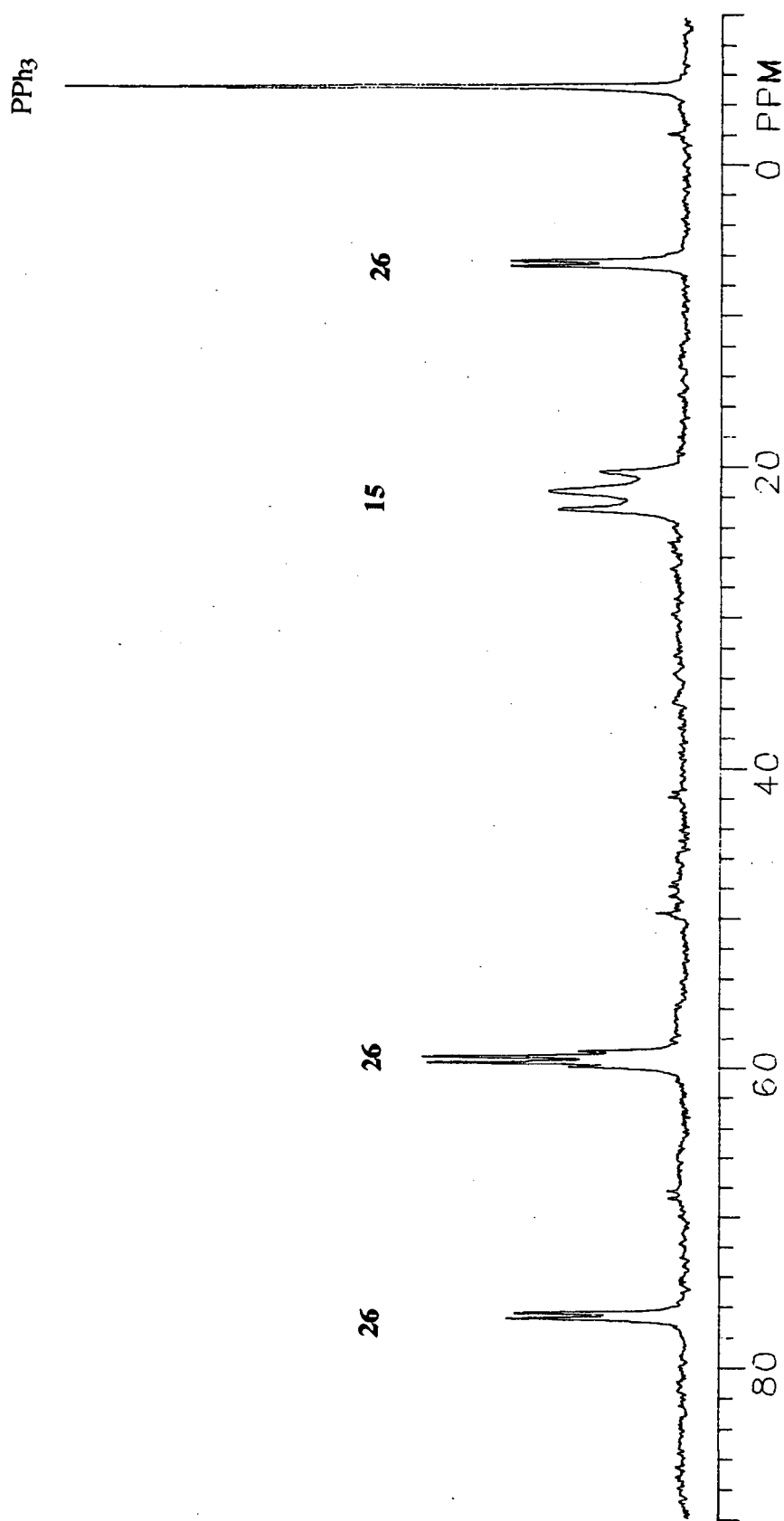
Figure 4.16 $^{31}P\{^1H\}$ NMR spectrum (121.42 MHz, 20 °C) of RuCl$_2$((R)-BINAP)(PPh$_3$) **15** in C$_6$D$_6$; **26** = Ru$_2$Cl$_4$((R)-BINAP)$_2$.

The only resonance observed upfield of TMS in the ^{1}H NMR spectrum was a triplet at –3.7 ppm ($^2J_{HP}$ = 19.4 Hz), indicating the presence of a classical hydride. No broad resonances indicating the possible presence of molecular hydrogen resonances were evident. The reduction of $Ru_2Cl_5((R)$-BINAP$)_2$ by H_2 was undertaken in the hope of observing both $Ru_2Cl_4((R)$-BINAP$)_2$ and $Ru_2Cl_4((R)$-BINAP$)_2(\eta^2$-$H_2)$, as had been previously observed for the DPPB analogue (Section 4.6.1).

Unfortunately, the exact nature of the complexes present could not be determined, and the $^{31}P\{^1H\}$ NMR data are listed in Table 4.5 for reference by future workers.

Table 4.5 $^{31}P\{^1H\}$ NMR Data (121.42 MHz, 20 °C) for the Interaction of H_2 and $Ru_2Cl_5((R)$-BINAP$)_2$ **23** in C_6D_6

Species	Chemical Shift, δ	$^2J_{PP}$ (Hz)
1	$\delta_A = 58.9, \delta_B = 54.1$	42.1
	$\delta_C = 49.3, \delta_D = 48.5$	27.2
2	$\delta_A = 58.6, \delta_B = 57.2$	40.3
	$\delta_C = 45.2 \ \delta_D = 40.9$	25.6
3	13.2, s	----

s = singlet.

When the bubbling of H_2 through the above orange solution was continued for a further 1 h, the $^{31}P\{^1H\}$ NMR spectrum showed only a single AB pattern (δ_A = 47.5, δ_B = 46.4, $^2J_{AB}$ = 30.3 Hz). Again, this species is thought to be a dinuclear Ru(II)-BINAP-containing species, but beyond this, the structure is unknown. The $^{31}P\{^1H\}$ NMR spectrum does not correspond to the resonances previously observed for either $Ru_2Cl_4(BINAP)_2$ or $Ru_2Cl_4(BINAP)_2(\eta^2$-$H_2)$.

Two attempts were made to prepare and isolate $Ru_2Cl_4((R)$-BINAP$)_2$ **26** from the mixed-valence dimer $Ru_2Cl_5((R)$-BINAP$)_2$ **23** by a procedure used previously by this

research group (Section 2.5.7.3 outlines the procedure).[2,46,56] The published procedure involves stirring $Ru_2Cl_5((R)$-BINAP$)_2$ **23** under an atmosphere of H_2 in C_6H_6 with poly(4-vinylpyridine) (70 equiv) for 24 h. However, on both occasions in this thesis work, the isolated orange-brown solid showed spectroscopic and microanalytical data different from those which had been previously determined. The C and H microanalytical data (C, 66.45; H, 4.11%) fit well for the $Ru_2Cl_4((R)$-BINAP$)_2$ formulation (C, 66.50; H, 4.06%); however, the Cl analysis was very low (6.22 vs. 8.92%).

The $^{31}P\{^1H\}$ NMR spectrum showed two species to be present. The first, accounting for ~ 70% of the total integral intensity, was an AB pattern (δ_A = 75.6, δ_B = 72.3, $^2J_{AB}$ = 44.3 Hz), while the second was a singlet (δ = 51.4); neither of these species has been observed before. The ^1H NMR spectrum showed a hydride signal at δ = –14.0 (t, $^2J_{HP}$ = 29.9 Hz), the coupling constant and splitting multiplicity indicating a hydride *cis* to two phosphorus atoms; however, the chemical shift and peak multiplicity do not correspond to those reported for Ru(H)Cl(BINAP)$_2$,[57] the presence of which would explain the low chloride analysis.

No attempts were made to separate or further characterize these reduction products, as the key goal was to isolate pure **26**, which was needed to allow for direct comparison with the molecular hydrogen complexes produced in situ by the interaction of H_2 with $RuCl_2((R)$-BINAP)(PPh$_3$) (Section 4.4.4.1).

It should be noted that Chan and Laneman have isolated and characterized a decomposition product of a Ru-BINAP species.[58] On attempting to improve the preparation of the catalyst Ru(BINAP)(OAc)$_2$, Chan and Laneman isolated a unique Ru complex in which the BINAP ligand had undergone P–C cleavage via oxidative addition of the naphthyl-phosphorus bond to the ruthenium centre. This was followed by hydrolysis to give the unusual Ru complex, the structure of which has been determined by X-ray crystallography (Figure 4.17).[58]
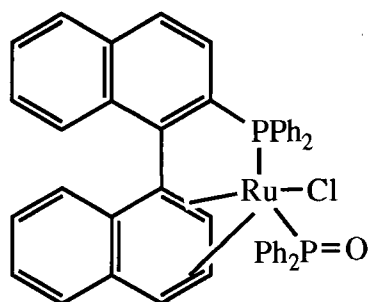
Figure 4.17 The unique ruthenium complex characterized by Chan and Laneman produced by P–C cleavage of the BINAP ligand.

4.7 A Brief Review of Ru(II)-Monodentate Phosphine Complexes Containing Molecular Hydrogen and Classical Hydride Ligands Synthesized in This Laboratory

In 1985, Dekleva et al. reported the chloride-bridged, dimeric ruthenium complexes [RuH$_2$Cl(PR$_3$)$_2$]$_2$, where PR$_3$ was either PPh$_3$ or P(p-tolyl)$_3$.[9] The structures of the above species were based on a partial single-crystal X-ray diffraction study of the P(p-tolyl)$_3$ complex, as well as on ^{31}P{^{1}H} and ^{1}H NMR spectroscopic data. Three of the hydrides were reported as terminal, while the fourth was reported as bridging.[9] The ruthenium was thought to be in oxidation state III, with a Ru–Ru bond explaining the diamagnetism. However, Hampton et al. re-investigated these systems three years later, and determined by T_1 measurements that the above complexes should be reformulated as [(PR$_3$)$_2$(H)Ru(μ-H)(μ-Cl)$_2$Ru(η^2-H$_2$)(PR$_3$)$_2$].[10] The ruthenium was now formally Ru(II), and the complex contained one η^2-H$_2$ moiety. The heavy atom skeleton of the PPh$_3$ analogue, as determined by X-ray crystallography, has also been reported, and again no hydrides were located.[45] This work was further extended by Hampton et al. to include other Ru(II) molecular hydrogen and hydrido derivatives.[32,44,45] The structure of [(η^2-H$_2$)(isoPFA)Ru(μ-Cl)$_2$(μ-H)Ru(H)(PPh$_3$)$_2$] is reported, as is the classical hydride complex Ru(H)Cl(PPh$_3$)(isoPFA), where isoPFA is the ferrocene-based ligand (η-C$_5$H$_5$)Fe(η-C$_5$H$_3$(CHMeNMe$_2$)P(i-Pr)$_2$-1,2).[32,44,45]

The species containing the classical hydride ligand (i.e., Ru(H)Cl(PPh3)(isoPFA)) was synthesized by reaction of H_2 with RuCl2(PPh3)(isoPFA) in the presence of an added base.[32,45]

4.7.1 X-ray Structure of [(DMA)₂H]⁺[(PPh₃)₂(H)Ru(μ-Cl)₂(μ-H)Ru(H)(PPh₃)₂]⁻

A dark-red prism isolated from a DMA solution of RuCl3(PPh3)2(DMA)·DMA solvate and one equivalent of DPPB left under H_2 for an extended period was proved by X-ray single-crystal crystallography to be [(DMA)2H]⁺[(PPh3)2(H)Ru(μ-Cl)2(μ-H)Ru(H)(PPh3)2]⁻ **18** (Section 2.5.4.3). The molecular structure of **18** is shown in Figure 4.18. Figure 4.19 shows the ORTEP plot, while Tables 4.6 and 4.7 list selected bond lengths and angles of **18**, respectively. Appendix VI gives the full experimental parameters and details.
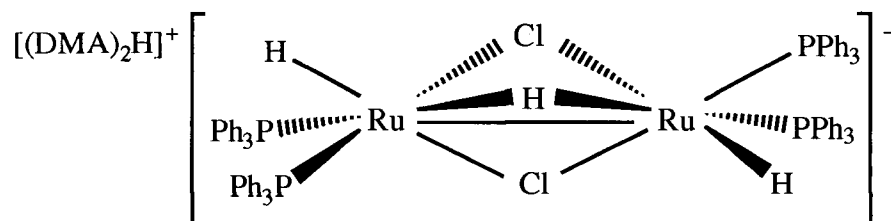
Figure 4.18 Molecular structure of [(DMA)₂H]⁺[(PPh₃)₂(H)Ru(μ-Cl)₂(μ-H)Ru(H)(PPh₃)₂]⁻ **18**.

The ORTEP plot of **18** shows the dinuclear ruthenium anion (C_2). The dinuclear anion contains two terminal and one bridging hydride. The cation [(DMA)2H]⁺, which was disordered, has been observed previously, and has been studied by X-ray and neutron diffraction.[59] The two DMA molecules are bridged by a hydrogen bond.[59]

The Ru(1)–H(1) (bridging hydride) bond length of 1.72(3) Å observed in **18** is of the same order as that observed for one side of the unsymmetrical hydride bridge in [(η²-

H$_2$)(isoPFA)Ru(μ-Cl)$_2$(μ-H)Ru(H)(PPh$_3$)$_2$] (1.71(4) Å).[44] However, the Ru–H bond length on the other side of the bridge (1.49(4) Å)[44] for the above molecular hydrogen complex is significantly shorter than that observed in **18**. The Ru(1)–H(2) (terminal hydride) bond length of 1.59(3) Å is of the order of the Ru–terminal H distance (1.50(4) Å) for the above molecular hydrogen complex.[44]

The heavy atom skeleton for [(PR$_3$)$_2$(η^2-H$_2$)Ru(μ-Cl)$_2$(μ-H)Ru(H)(PR$_3$)$_2$] **17**, where R = Ph or *p*-tolyl, has been determined by X-ray crystallography; however, the location of the hydrogen atoms was not established.[9,10,32,45] In the case of **18** and the molecular hydrogen complex containing the isoPFA ligand (see above),[44] the locations of the hydride and molecular hydrogen ligands have been determined.

The Ru–Ru bond length of 2.8251(5) Å determined for **18** is essentially identical to that determined for [(η^2-H$_2$)(PPh$_3$)$_2$Ru(μ-Cl)$_2$(μ-H)Ru(H)(PPh$_3$)$_2$] of 2.83 Å. The above values are close to the middle of the range generally found for a Ru–Ru single bond: 2.632 to 3.034 Å.[32,45] The Ru(1)–Cl(1)–Ru(1)* (69.20(3)°) and Cl(1)–Ru(1)–Cl(1)* (81.58(4)°) bond angles of **18** are also indicative of a Ru–Ru single bond.[60] Cotton and Torralba have characterized a series of Ru(II,II) and Ru(III,III) complexes with face-sharing bioctahedra of the general formula [Ru$_2$Cl$_3$(PR$_3$)$_6$][X], [Ru$_2$Cl$_5$(PR$_3$)$_4$], and [Ru$_2$Cl$_6$(PR$_3$)$_4$], respectively, and have demonstrated that longer Ru–Ru distances (3.28–3.44 Å) result in enlarged Ru–Cl$_b$–Ru angles (82.9–87.9°) and contracted Cl$_b$–Ru–Cl$_b$ angles (77.2–80.9°), where Cl$_b$ is a bridging chloride.[60]
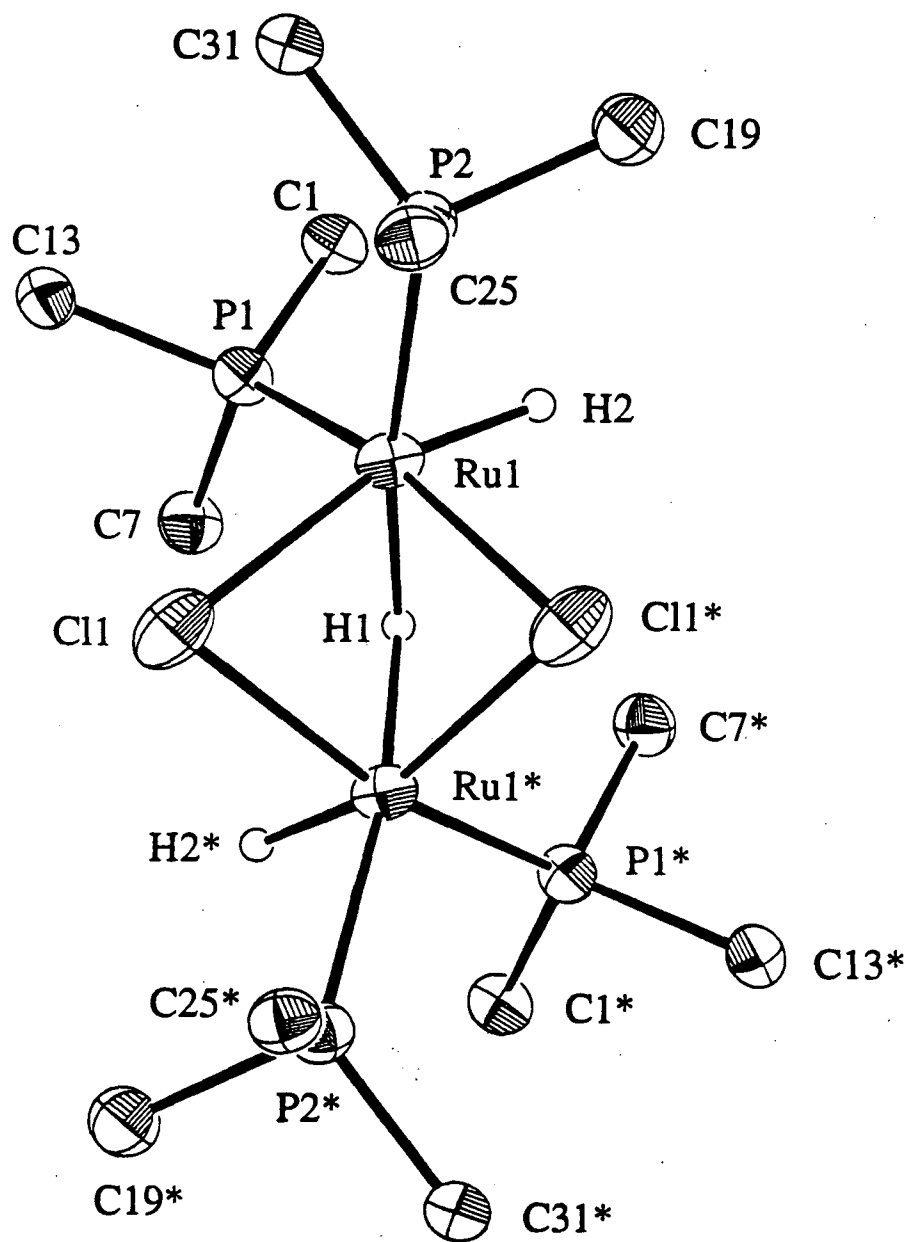
Figure 4.19 The ORTEP plot of [(DMA)₂H]⁺[(PPh₃)₂(H)Ru(μ-Cl)₂(μ-H)Ru(H)-
(PPh₃)₂]⁻ **18**. Thermal ellipsoids for non-hydrogen atoms are drawn at 33%
probability (some of the phenyl carbons have been omitted for clarity).

Table 4.6   Selected Bond Lengths (Å) for [(DMA)$_2$H]$^+$[(H)(PPh$_3$)$_2$Ru(μ-Cl)$_2$(μ-H)Ru(PPh$_3$)$_2$(H)]$^-$ with Estimated Standard Deviations in Parentheses

Bond	Length (Å)	Bond	Length (Å)
Ru(1)—Ru(1)*	2.8251(5)	Ru(1)—Cl(1)	2.510(1)
Ru(1)—Cl(1)*	2.4649(9)	Ru(1)—P(1)	2.2576(9)
Ru(1)—P(2)	2.3483(9)	P(1)—C(1)	1.850(3)
P(1)—C(7)	1.844(3)	P(1)—C(13)	1.839(3)
P(2)—C(19)	1.842(4)	P(2)—C(25)	1.845(3)
P(2)—C(31)	1.842(3)	O(1)—C(37)	1.174(8)
N(1)—C(37)	1.108(10)	N(1)—C(39)	1.370(8)
N(1)—C(40)	1.630(9)	Ru(1)—H(2)	1.59(3)
Ru(1)—H(1)	1.72(3)		

* refers to the symmetry operation: –x, y, 1/2–z

Table 4.7   Selected Bond Angles (°) for [(DMA)$_2$H]$^+$[(H)(PPh$_3$)$_2$Ru(μ-Cl)$_2$(μ-H)Ru(PPh$_3$)$_2$(H)]$^-$ with Estimated Standard Deviations in Parentheses

Bonds	Angles (°)	Bonds	Angles(°)
Ru(1)*—Ru(1)—Cl(1)	54.65(2)	Ru(1)*—Ru(1)—Cl(1)*	56.15(2)
Ru(1)*—Ru(1)—P(1)	109.64(2)	Ru(1)*—Ru(1)—P(2)	145.07(2)
Cl(1)—Ru(1)—Cl(1)*	81.58(4)	Cl(1)—Ru(1)—P(1)	96.74(3)
Cl(1)—Ru(1)—P(2)	107.71(3)	Cl(1)*—Ru(1)—P(1)	163.57(3)
Cl(1)*—Ru(1)—P(2)	94.24(3)	P(1)—Ru(1)—P(2)	101.79(3)
Ru(1)—Cl(1)—Ru(1)*	69.20(3)	Ru(1)*—Ru(1)—H(2)	109.1(9)
Ru(1)*—Ru(1)—H(1)	35(1)	Cl(1)—Ru(1)—H(2)	163.8(9)
Cl(1)—Ru(1)—H(1)	79.1(9)	Cl(1)*—Ru(1)—H(2)	88.8(9)
Cl(1)*—Ru(1)—H(1)	80.4(9)	P(1)—Ru(1)—H(2)	88.8(9)
P(1)—Ru(1)—H(1)	83.2(10)	P(2)—Ru(1)—H(2)	85.9(9)
P(2)—Ru(1)—H(1)	170.8(2)	H(1)—Ru(1)—H(2)	86(1)

* refers to the symmetry operation: –x, y, 1/2–z

4.7.2 NMR Spectroscopic Studies of [(DMA)$_2$H]$^+$[(PPh$_3$)$_2$(H)Ru(μ-Cl)$_2$(μ-H)Ru(H)(PPh$_3$)$_2$]$^-$, 18

^{31}P{^{1}H} and ^{1}H NMR spectroscopic studies of C$_7$D$_8$ solutions of the dark-red crystal of **18** show spectra almost identical to those of the neutral molecular hydrogen complex [(η^2-H$_2$)(PPh$_3$)$_2$Ru(μ-H)(μ-Cl)$_2$Ru(H)(PPh$_3$)$_2$] **17**, thus demonstrating conversion of **18** to **17** in the deuterated toluene. ^{31}P{^{1}H} NMR spectra of **18** in CDCl$_3$ at 20 °C and –89 °C are shown in Figure 4.20. The two broad singlets observed at 20 °C at 71.3 and 46.3 ppm give an ABCD spin system at –89 °C, which corresponds exactly to that previously observed for [(η^2-H$_2$)(PPh$_3$)$_2$Ru(μ-H)(μ-Cl)$_2$Ru(H)(PPh$_3$)$_2$].[9,32,45,55] No coupling constants could be obtained for the ABCD spin system observed at low temperature, as the resonances are broad and unresolved. Dekleva et al. have previously reported the coupling constants, $^2J_{AB}$ and $^2J_{CD}$, from a 32.4 MHz spectrum.[9] The ^{31}P{^{1}H} NMR spectra shown in Figure 4.20 also show a very small amount of an AB pattern (δ_A = 56.8, δ_B = 54.7, $^2J_{AB}$ = 30 Hz), which is thought to be due to **18**.

The ^{1}H NMR spectra of **18** in C$_7$D$_8$ at 20 °C and –79 °C are shown in Figure 4.21. The hydride at 20 °C shows a single broad resonance at –12.8 ppm. Cooling the above sample to –79 °C resolves the hydride and molecular hydrogen resonances. The bridging hydride is observed at –8.7 as a broad doublet, the η^2-H$_2$ ligand at –12.6 as a broad singlet, and the terminal hydride at –17.3 ppm as a broad singlet. Again, these ^{1}H resonances have been previously observed for [(η^2-H$_2$)(PPh$_3$)$_2$Ru(μ-H)(μ-Cl)$_2$Ru(H)(PPh$_3$)$_2$].[9,32,45,55] The two other resonances of lower intensity observed at –14.9 (t, $^2J_{PH}$ = 31.1 Hz) and –17.7 ppm (br s) are attributed to **18**.

The ^{1}H NMR resonance for the cation [(DMA)$_2$H]$^+$ in the complex [(DMA)$_2$H]$^+$[AuCl$_4$]$^-$ has been reported at –17.45 ppm.[59] Therefore, the –17.7 ppm resonance is assigned to the hydrogen-bonded proton of the cation, while the triplet at –14.9 is assigned to the terminal-hydrides. A third resonance expected for the bridging hydride may be buried under the broad resonances of **17**. Hampton et al. have explained

the exchange processes involved which account for the room- and low-temperature spectra observed for **17**.[32,45] An alternative assignment of the –17.7 ppm peak is possible as the resonance for the [(DMA)$_2$*H*]$^+$ may be expected to be observed in the 10–12 ppm region as has been observed for [DMA*H*]$^+$Cl$^-$.[†] Assignment of the protons of the ionic complex **18** are difficult as the equilibrium between **17** and **18** favours neutral complex **17**.

Attempts to measure the UV-visible spectrum and conductivity of **18** were unsuccessful. When some of the dark-red crystal was dissolved in either C$_6$H$_6$ or DMA, the solution became green-black, indicating oxidation of **18**, although care was taken to avoid the presence of oxygen. This behaviour contrasts with that of the stable orange-red C$_7$D$_8$ solutions observed in the NMR studies described above. Compound **18** (or **17**) may be sensitive to trace oxygen in the solvent (despite attempts to deoxygenate the solvents) at the lower concentrations used for UV-visible studies compared to those used in the NMR spectroscopic studies. Similar O$_2$ oxidation of ruthenium(II) complexes has been observed by other workers in the research group; the green products were thought to be Ru(III) species.[4,5]

[†] see Benedetti, E.; Di Blasio, B.; Baine, P. *J. Chem. Soc., Perkin II* **1980**, 500.
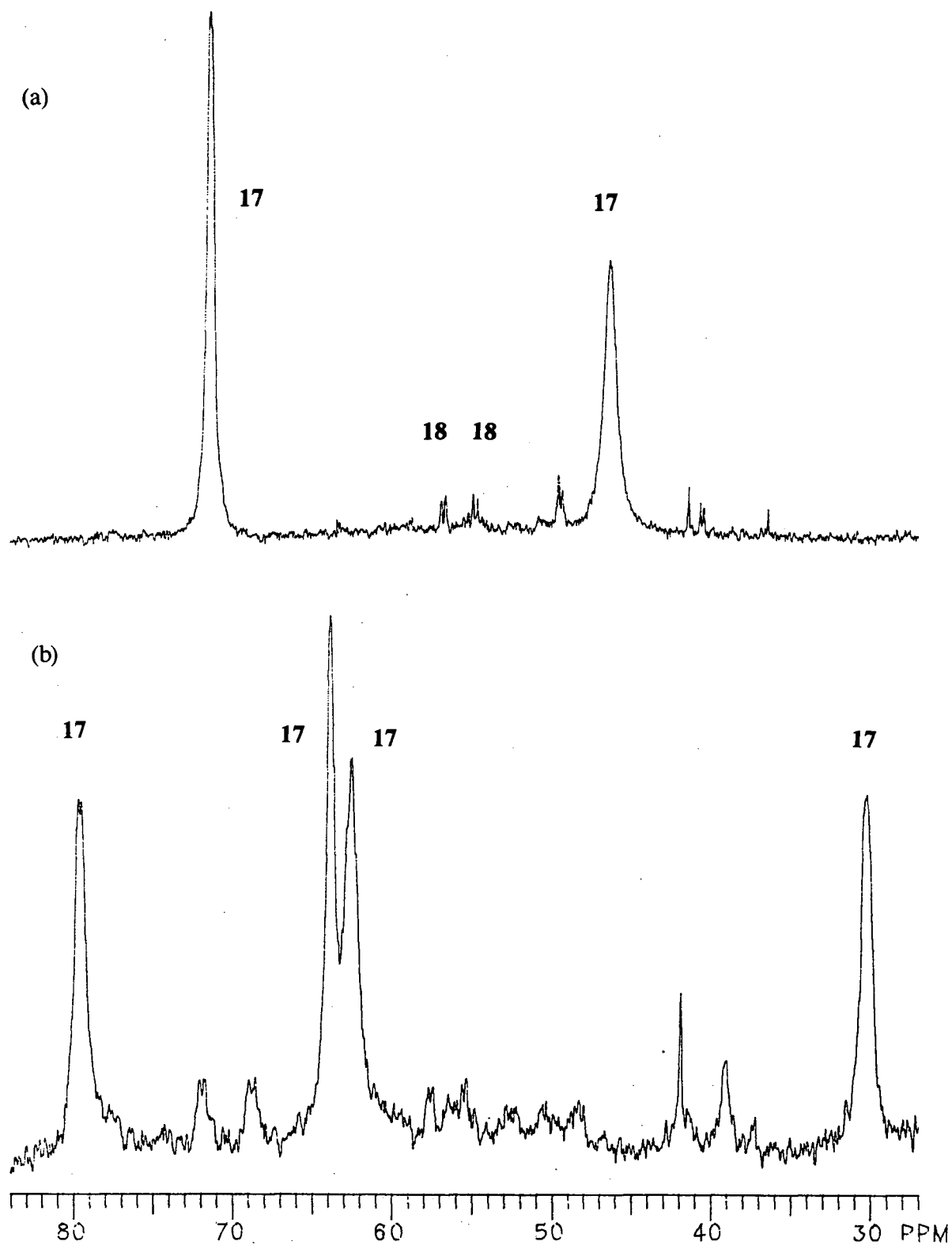
Figure 4.20 $^{31}P\{^1H\}$ NMR spectra (121.42 MHz) of **18** in C_7D_8 at: (a) 20 °C and (b) –89 °C. **17** = $[(\eta^2\text{-}H_2)(PPh_3)_2Ru(\mu\text{-}H)(\mu\text{-}Cl)_2Ru(H)(PPh_3)_2]$.

(a)

17

exchanging μ-H, terminal, and η^2-H_2

18

(b)   **17**

17

17

terminal-H

μ-H

17

18

η^2-H_2

18

18

−8   −10   −12   −14   −16   −18 PPM
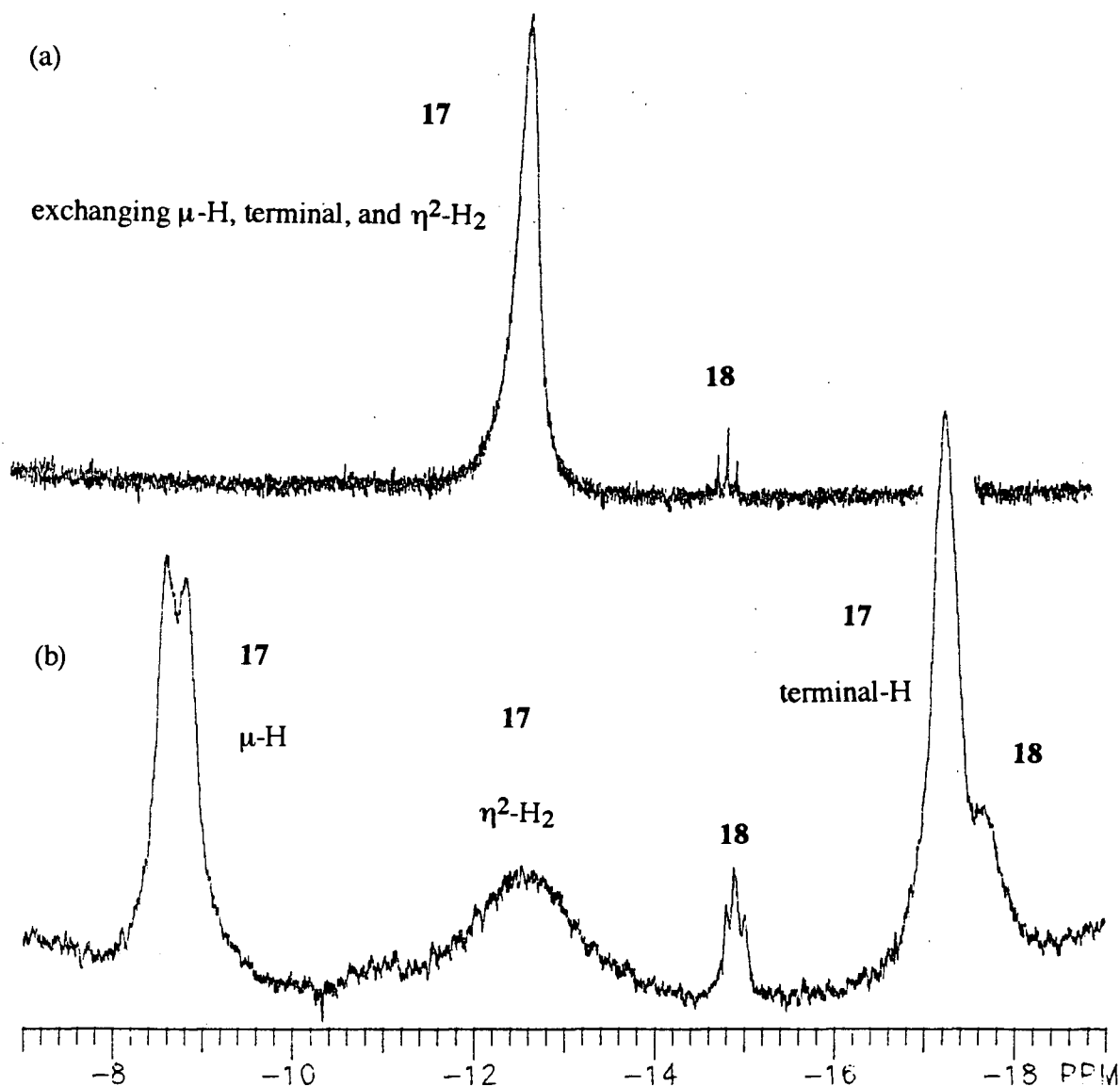
Figure 4.21 ^{1}H NMR spectra (upfield region, 300 MHz) of **18** in C_7D_8 at: (a) 20 °C and (b) −79 °C. **17** = [(η^2-H_2)(PPh_3)$_2$Ru(μ-H)(μ-Cl)$_2$Ru(H)(PPh_3)$_2$].

The spectral and X-ray structural data taken together demonstrate the existence of an equilibrium between **18** and the molecular hydrogen complex **17** (Figure 4.22).
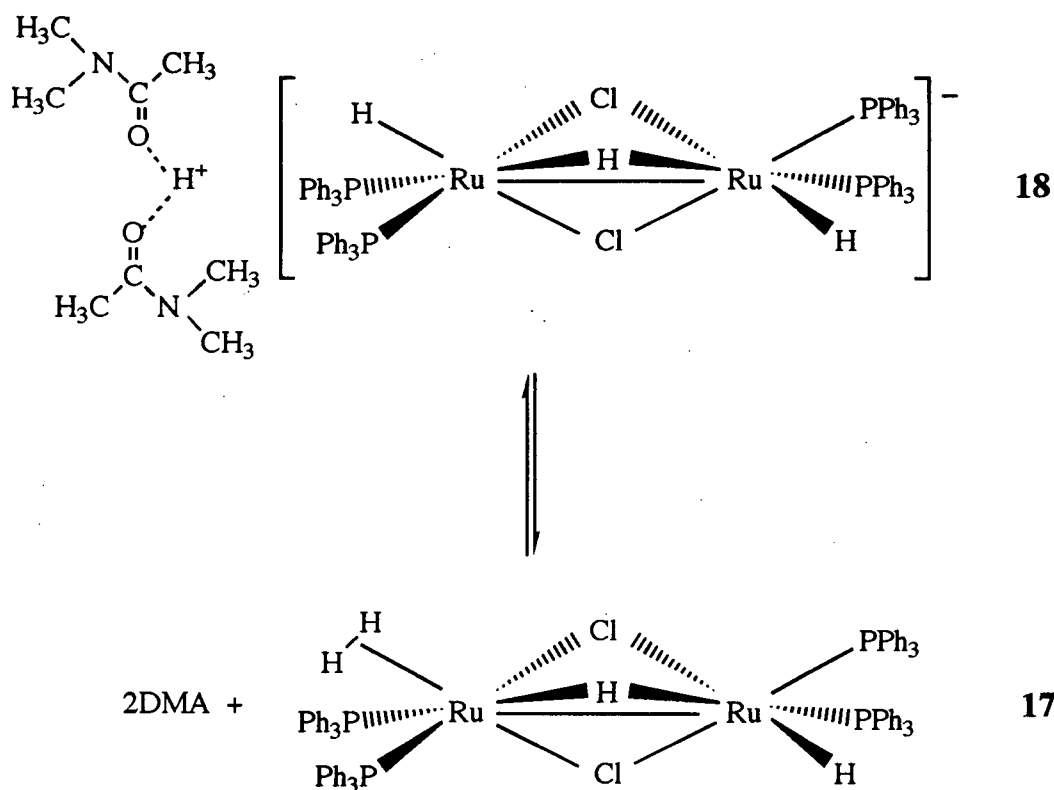
Figure 4.22 Equilibrium between [(DMA)$_2$H]$^+$[(PPh$_3$)$_2$(H)Ru(μ-Cl)$_2$(μ-H)Ru(H)-(PPh$_3$)$_2$]$^-$ **18** and [(η^2-H$_2$)(PPh$_3$)$_2$Ru(μ-Cl)$_2$(μ-H)Ru(H)(PPh$_3$)$_2$] **17**.

The T_1 measurements on **17** and the P(p-tolyl)$_3$ analogue leave little doubt that **17** is in fact a molecular hydrogen complex.[10,32,45] Also, the heavy atom skeleton determined for **17**[45] did not contain a C_2, as was seen for **18** (Section 4.5.2).

Efforts were made to develop a controlled synthetic route to the ionic complex **18**, as the crystal was isolated fortuitously after a long period of time from a reaction mixture which included the "superfluous" diphosphine DPPB (Section 2.5.4.3). Two reaction pathways to form complex **17** are shown in equations 4.2 and 4.3 (Section 4.1); one involves direct preparation from a Ru(III) starting complex (eq 4.3), while the other requires the initial preparation of a Ru(II) dinuclear species (eq 4.2). The pathway shown in equation 4.2 via Ru$_2$Cl$_4$(PPh$_3$)$_4$ was attempted, except that the work-up was changed in the hope of isolating the "ionic analogues" of the neutral species shown in equations

4.2 and 4.3. The first step was successful, in that reduction of $RuCl_3(PPh_3)_2DMA \cdot DMA$ solvate by H_2 in DMA gave $[(DMA)_2H]^+[Ru_2Cl_5(PPh_3)_4]^-$ **16** (Section 2.5.4.1). The synthesis was the same as that used previously to isolate the neutral species $Ru_2Cl_4(PPh_3)_4$; however, in this case, the work-up was changed by substituting diethyl ether for MeOH in order to precipitate the product (Section 2.5.4.1).[8,32,55]

Complex **16** has previously been observed in solution by $^{31}P\{^1H\}$ NMR spectroscopy.[9,55] The isolated orange solid in C_7D_8 gave a singlet at 44.6 over the temperature range of -85 to 20 °C, suggesting a structure similar to that shown by X-ray crystallographic studies for the DPPB analogue $[TMP]^+[Ru_2Cl_5(DPPB)_2]^-$ (Figure 3.16, Section 3.3.4.1), except with PPh_3 occupying the DPPB positions; Figure 4.23 shows the molecular structure.
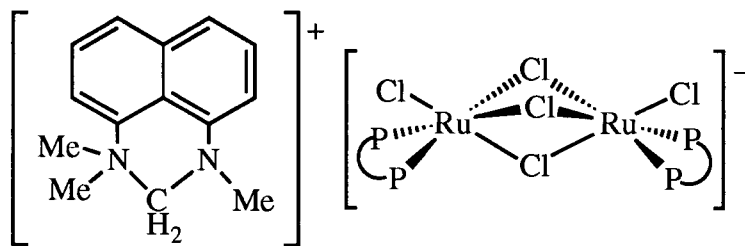
Figure 4.23   Molecular structure of $[TMP]^+[Ru_2Cl_5(DPPB)_2]^-$, where P–P = $Ph_2P(CH_2)_4PPh_2$.

The second step in the synthesis of **18** (or at least the Proton Sponge analogue, $[PSH]^+[(PPh_3)_2(H)Ru(\mu-Cl)_2(\mu-H)Ru(H)(PPh_3)_2]^-$) is the reaction of **16** with H_2 in the presence of Proton Sponge in C_6H_6. However, under work-up conditions identical to those used for the isolation of the ionic complex **16**, only the neutral molecular hydrogen complex $[(\eta^2-H_2)(PPh_3)_2Ru(\mu-Cl)_2(\mu-H)Ru(H)(PPh_3)_2]$ **17** was isolated (Section 2.5.4.2). The $^{31}P\{^1H\}$ and ^1H NMR spectra in C_6D_6 agree with those observed[9,32,45,55] previously for **17**, as well as with the resonances shown in Figure 4.20 and 4.21, where **17** was produced in solution from the equilibrium with **18** (Figure 4.22).

The neutral complex **17** has also been reported as a bis(DMA) solvate when the complex was prepared from $RuCl_3(PPh_3)_2DMA \cdot DMA$ via equation 4.3 and isolated from DMA solvent.[9,55] The preparation described above and in Section 2.5.4.2 results in the isolation of DMA-free **17**. In view of the determination of the X-ray crystal of **18** in this work, as well as the existence of the equilibrium shown in Figure 4.21, the solvated species $[(\eta^2-H_2)(PPh_3)_2Ru(\mu-Cl)_2(\mu-H)Ru(H)(PPh_3)_2] \cdot 2DMA$ should be re-formulated, at least in the solid state, as $[(DMA)_2H]^+[(PPh_3)_2(H)Ru(\mu-Cl)_2(\mu-H)Ru(H)(PPh_3)_2]^-$ **18**. The solid isolated by Dekleva from DMA was red in colour, as was the crystal analyzed in this thesis work.

The equilibrium between ionic **18** and neutral **17** shown in Figure 4.22 amounts to protonation of the anionic polyhydride complex by the acidic cation to produce the η^2-H_2 complex **17**. Jessop and Morris list protonation of a hydride complex as a common method of preparing dihydrogen complexes,[12] but there are no previous examples involving a 'proton transfer' within an ionic precursor like **18**. Essentially, formation of **18** from **17** is the reverse of intramolecular heterolytic cleavage of a molecular hydrogen complex.[12] Several examples of an equilibrium mixture of $M(H_2)$ and $M(H)_2$ have been observed.[12]

4.8   Summary

The complex $RuCl_2(BINAP)(PPh_3)$ reacted reversibly with H_2 to give two molecular hydrogen complexes which were studied in solution by NMR spectroscopy. The products were shown by a combination of NMR spectroscopic techniques to be $[(\eta^2-H_2)(BINAP)Ru(\mu-Cl)_3RuCl(BINAP)]$. In the presence of base, $RuCl_2(BINAP)(PPh_3)$ reacted with H_2 to give two diastereomers of $Ru(H)Cl(BINAP)(PPh_3)$.

The complex $[(DMA)_2H]^+[(PPh_3)_2(H)Ru(\mu-Cl)_2(\mu-H)Ru(H)(PPh_3)_2]^-$, which was characterized in the solid state by X-ray crystallography, was shown to be in equilibrium with the molecular hydrogen complex $[(\eta^2-H)(PPh_3)_2Ru(\mu-Cl)_2(\mu-H)Ru(H)(PPh_3)_2]$ in solution.

4.9 References

(1)   James, B. R.; Pacheco, A.; Rettig, S. J.; Thorburn, I. S.; Ball, R. G.; Ibers, J. A. *J. Mol. Catal.* **1987**, *41*, 147.

(2)   Joshi, A. M. Ph.D. Thesis, The University of British Columbia, 1990.

(3)   Joshi, A. M.; James, B. R. *J. Chem. Soc., Chem. Commun.* **1989**, 1785.

(4)   Chau, D. E. K.-Y.; James, B. R. *Inorg. Chim. Acta*, in press.

(5)   Chau, D. E. K.-Y. M.Sc. Thesis, The University of British Columbia, 1992.

(6)   Thorburn, I. S. Ph.D. Thesis, The University of British Columbia, 1985.

(7)   Hallman, P. S.; McGarvey, B. R.; Wilkinson, G. *J. Chem. Soc. (A)* **1968**, 3143.

(8)   James, B. R.; Thompson, L. K.; Wang, D. K. W. *Inorg. Chim. Acta* **1978**, *29*, L237.

(9)   Dekleva, T. W.; Thorburn, I. S.; James, B. R. *Inorg. Chim. Acta* **1985**, *100*, 49.

(10) Hampton, C.; Dekleva, T. W.; James, B. R.; Cullen, W. R. *Inorg. Chim. Acta* **1988**, *145*, 165.

(11) McCrindle, R.; Ferguson, G.; Arsenault, J.; McAlees, A. J. *J. Chem. Soc., Chem. Commun.* **1983**, 571.

(12) Jessop, P. G.; Morris, R. H. *Coord. Chem. Rev.* **1992**, *121*, 155.

(13) Heinekey, D. M.; Oldham, W. J. Jr. *Chem. Rev.* **1993**, *93*, 913.

(14) Crabtree, R. H. *Angew. Chem., Int. Ed. Engl.* **1993**, *32*, 789.

(15) Kubas, G. J. *Comments Inorg. Chem.* **1988**, *7*, 17; and references therein.

(16) Kubas, G. J. *Acc. Chem. Res.* **1988**, *21*, 120.

(17) Ashworth, T. V.; Singleton, E. *J. Chem. Soc., Chem. Commun.* **1976**, 705.

(18) Knoth, W. H. *J. Am. Chem. Soc.* **1972**, *94*, 104.

(19) Kubas, G. J. *J. Chem. Soc., Chem. Commun.* **1980**, 61.

(20) *Chem. Eng. News* **1983**, *61(13)*, 4.

(21) Kubas, G. J.; Ryan, R. R.; Vergamini, P. J.; Wasserman, H. J. *Abstracts of Papers,* 185th National Meeting of the American Chemical Society, Seattle, WA; American Chemical Society: Washington, DC, 1983; Abstract INOR229.

(22) Kubas, G. J.; Ryan, R. R.; Swanson, B. I.; Vergamini, P. J.; Wasserman, H. J. *J. Am. Chem. Soc.* **1984**, *106*, 451.

(23) Kubas, G. J.; Unkefer, C. J.; Swanson, B. I.; Fukushima, E. *J. Am. Chem. Soc.* **1986**, *108*, 7000.

(24) Nageswara Rao, B. D.; Anders, L. R. *Phys. Rev.* **1965**, *140*, A112.

(25) Moreno, B.; Sabo-Etienne, S.; Chaudret, B.; Rodriquez-Fernandez, A.; Jalon, F.; Trofimenko, S. *J. Am. Chem. Soc.* **1994**, *116*, 2635.

(26) Mudalige, D. C.; Rettig, S. J.; James, B. R.; Cullen, W. R. *J. Chem. Soc., Chem. Commun.* **1993**, 830.

(27) Mudalige, D. C. Ph.D. Thesis, The University of British Columbia, 1994.

(28) Crabtree, R. H.; Lavin, M. *J. Chem. Soc., Chem. Commun.* **1985**, 794.

(29) Crabtree, R. H.; Lavin, M. *J. Chem. Soc., Chem. Commun.* **1985**, 1661.

(30) Morris, R. H.; Sawyer, J. F.; Shiralian, M.; Zubkowski, J. D. *J. Am. Chem. Soc.* **1985**, *107*, 5581.

(31) Crabtree, R. H.; Hamilton, D. G. *J. Am. Chem. Soc.* **1986**, *108*, 3124.

(32) Hampton, C. Ph.D. Thesis, The University of British Columbia, 1989.

(33) Crabtree, R. H.; Hamilton, D. G. *Adv. Organomet. Chem.* **1988**, *28*, 299.

(34) Crabtree, R. H.; Lavin, M.; Bonnevoit, L. *J. Am. Chem. Soc.* **1986**, *108*, 4032.

(35) Crabtree, R. H. *Acc. Chem. Res.* **1990**, *23*, 95.

(36) Bautista, M. T.; Earl, K. A.; Maltby, P. A.; Morris, R. H.; Schweitzer, C. T.; Sella, A. *J. Am. Chem. Soc.* **1988**, *110*, 7031.

(37) Zilm, K. W.; Heinekey, D. M.; Millar, J. M.; Payne, N. G.; Neshyba, S. P.; Duchamp, J. C.; Szczyrba, J. *J. Am. Chem. Soc.* **1990**, *112*, 920.

(38) Antoniutti, S.; Albetin, G.; Amendola, P.; Bordignon, E. *J. Chem. Soc., Chem. Commun.* **1989**, 229.

(39) Cotton, F. A.; Luck, R. L. *Inorg. Chem.* **1989**, *28*, 6.

(40) Desrosiers, P. J.; Cai, L.; Lin, Z.; Richards, R.; Halpern, J. *J. Am. Chem. Soc.* **1991**, *113*, 4173.

(41) Cotton, F. A.; Luck, R. L.; Root, D. R.; Walton, R. A. *Inorg. Chem.* **1990**, *29*, 43.

(42) Hamilton, D. G.; Crabtree, R. H. *J. Am. Chem. Soc.* **1988**, *110*, 4126.

(43) Joshi, A. M.; MacFarlane, K. S.; James, B. R. *J. Organomet. Chem.* **1995**, *488*, 161.

(44) Hampton, C.; Cullen, W. R.; James, B. R.; Charland, J.-P. *J. Am. Chem. Soc.* **1988**, *110*, 6918.

(45)   Hampton, C. R. S. M.; Butler, I. R.; Cullen, W. R.; James, B. R.; Charland, J.-P.; Simpson, J. *Inorg. Chem.* **1992**, *31*, 5509.

(46)   Joshi, A. M.; Thorburn, I. S.; Rettig, S. J.; James, B. R. *Inorg. Chim. Acta* **1992**, *198*, 283.

(47)   Sanders, J. K. M.; Hunter, B. K. *Modern NMR Spectoscopy: A Guide for Chemists*; Oxford University Press: Oxford, 1987, pp 61-65.

(48)   Mezzetti, A.; Costella, L.; Zotto, A. D.; Rigo, P.; Consiglio, G. *Gazz. Chim. Ital.* **1993**, *123*, 155.

(49)   Sweany, R. L.; Halpern, J. *J. Am. Chem. Soc.* **1977**, *99*, 8335.

(50)   Kirss, R. U.; Eisenschmid, T. C.; Eisenberg, R. *J. Am. Chem. Soc.* **1988**, *110*, 8564.

(51)   Cyr, P. W. B.Sc. Thesis, The University of British Columbia, 1995.

(52)   Perrin, D. D.; Armarego, W. L. F.; Perrin, D. R. *Purification of Laboratory Chemicals*; 2nd ed.; Pergamon: Oxford, 1980.

(53)   Abu-Gnim, C.; MacFarlane, K. S.; James, B. R., unpublished results.

(54)   Kuhlman, R.; Rothfuss, H.; Gusev, D.; Streib, W. E.; Caulton, K. G. *Abstracts of Papers,* 209th American Chemical Society National Meeting, Anaheim, CA; American Chemical Society: Washington, DC, 1995; Abstract INOR 497.

(55)   Dekleva, T. W. Ph.D. Thesis, The University of British Columbia, 1983.

(56)   Fogg, D. E. Ph.D. Thesis, The University of British Columbia, 1994.

(57)   Ikariya, T.; Ishii, Y.; Kawano, H.; Arai, T.; Saburi, M.; Yoshikawa, S.; Akutagawa, S. *J. Chem. Soc., Chem. Commun.* **1985**, 922.

(58)   Chan, A. C. S.; Laneman, S. *Inorg. Chim. Acta* **1994**, *223*, 165.

(59)   Hussain, M. S.; Schlemper, E. O. *J. Chem. Soc., Dalton Trans.* **1980**, 750.

(60)   Cotton, F. A.; Torralba, R. C. *Inorg. Chem.* **1991**, *30*, 2196.

CHAPTER 5

REACTIONS OF RUTHENIUM(II) PHOSPHINE COMPLEXES WITH
N-DONOR LIGANDS

5.1   Introduction

The classical coordination chemistry of ruthenium(II) monodentate phosphine complexes was examined in some detail in the late 1960s and 1970s but structural assignments of products were generally tentative.[1] Particularly relevant to the chemistry presented in this chapter is the reaction of $RuX_2(PPh_3)_3$ complexes with pyridine, 2,2'-bipyridine, 1,10-phenanthroline, and ammonia. Gilbert and Wilkinson reacted pyridine with $RuCl_2(PPh_3)_3$ in acetone to give c,c,t-$RuCl_2(py)_2(PPh_3)_2$.[2] The tentative structural assignment was based on the observation of two Ru-Cl stretching frequencies in the far-IR.[2] Reaction of $RuBr_2(PPh_3)_3$ with neat pyridine produced $RuBr_2(py)_3(PPh_3)$, while with longer reaction times, $trans$-$RuBr_2(py)_4$ was isolated.[3] The chloro-analogue was isolated as a mixture of $trans$-$RuCl_2(py)_3(PPh_3)$ and $trans$-$RuCl_2(py)_4$.[3]

The species $RuX_2(PPh_3)_2(N\text{-}N)$, $[RuX(PPh_3)(N\text{-}N)_2]X$, and $[Ru_2X_2(PPh_3)_4(N\text{-}N)]X_2$ have all been isolated from the reaction of $RuX_2(PPh_3)_3$ with N-N ligands, where N-N is 2,2'-bipyridine or 1,10-phenanthroline, and X = Cl or Br.[3] Batista et al. have reported ruthenium(II) complexes of the formulations $RuCl_2(PPh_3)_2(N)_2$, $[RuCl(PPh_3)(N)_4]Cl$, and $[RuCl(DPPB)(N)_3]Cl$, where N is an imidazole ligand (imidazole or N-methylimidazole).[4]

Cenini et al. have shown that primary amines react with $RuCl_2(PPh_3)_3$ to give $RuCl_2(PPh_3)_2(RNH_2)_2$ complexes.[5] In particular, they have shown that bubbling ammonia through a solution of $RuCl_2(PPh_3)_3$ produces $RuCl_2(NH_3)_2(PPh_3)_2$.[5] However, the stereochemistry of the primary amine and ammine complexes has not been assigned.

Chapter 5 References: p 249

None of the amine/ammine complexes mentioned above have been structurally characterized by X-ray analysis.

The chemistry described in this chapter employs diphosphines instead of PPh_3, thereby limiting the number of isomers available, as the phosphorus atoms of the chelate must be *cis*. Therefore, of the three possible geometries available for complexes of the type $RuCl_2(L)_2(P-P)$, one (*c,c,c*) can be distinguished from the other two (*t,c,c* and *c,t,c*) by $^{31}P\{^{1}H\}$ NMR spectroscopy.

In particular, this chapter examines the reactions of five-coordinate Ru(II)-diphosphine complexes with the N-donor ligands, pyridine, 2,2'-bipyridine, 1,10-phenanthroline, and ammonia. The chemistry described here was performed under similar reaction conditions to those described in Chapter 3, in which different S- or O-donor ligands produced diruthenium products. For example, the reaction of $RuCl_2(DPPB)(PPh_3)$ with S-donors (DMSO, TMSO, DMS, and THT) produced the species $Ru_2Cl_4(DPPB)_2(L)$. However, attempts to prepare the diruthenium pyridine analogue (i.e., $Ru_2Cl_4(DPPB)_2(py)$) resulted in different reactivity, and formation of a monoruthenium species (e.g., $RuCl_2(DPPB)(py)_2$). Later attempts under different conditions using $Ru_2Cl_4(DPPB)_2$ as precursor did allow observation of $Ru_2Cl_4(DPPB)_2(py)$ in solution.

Similar monoruthenium species have been observed previously in this laboratory on reaction of $RuCl_2(DPPB)(PPh_3)$ **11** with CO,[6] RCN,[7] and RNH_2.[7] Reaction with CO produces an isomeric mixture of $RuCl_2(DPPB)(CO)_2$ and some "$RuCl_2(DPPB)(CO)$" monocarbonyl complexes;[6] reaction with benzonitrile produces $RuCl_2(DPPB)(PhCN)_2$,[7] and similarly $PhCH_2NH_2$ gives $RuCl_2(DPPB)(PhCH_2NH_2)_2$,[8] although, in these cases, the diruthenium species $Ru_2Cl_4(DPPB)_2(L)$ could be isolated if different reaction conditions were employed.[7,8]

As mentioned above, the reactions of $RuCl_2(PPh_3)_3$ with NH_3[5] and pyridine[3] to give products of the formula $RuCl_2(L)_2(PPh_3)_2$ have appeared previously in the

literature, but as no $^{31}P\{^1H\}$ NMR data were reported in these studies. These reactions were repeated in this thesis work to allow comparison between the $^{31}P\{^1H\}$ NMR data of the DPPB and PPh_3 analogues.

5.2 Reactions with Pyridine

5.2.1 Reaction of Pyridine with $RuCl_2(DPPB)(PPh_3)$ and $Ru_2Cl_4(DPPB)_3$

The reaction of excess pyridine with either of the mixed- or bridged-phosphine complexes (i.e., $RuCl_2(DPPB)(PPh_3)$ **11** and $Ru_2Cl_4(DPPB)_3$ **19**) results in the formation of *trans*-$RuCl_2(DPPB)(py)_2$ **43** species (see Section 2.5.11.1). Originally, this reaction was performed in an attempt to prepare $Ru_2Cl_4(DPPB)_2(py)$ **29** (see Figure 5.4, Section 5.2.3). The reaction conditions using **11** were the same as those used to prepare the $Ru_2Cl_4(DPPB)_2(L)$ (where L = DMSO, TMSO, DMS, and THT) species. In all cases, an excess of L was refluxed with a C_6H_6 suspension of $RuCl_2(DPPB)(PPh_3)$. However, in the case of pyridine, this produced a monomeric Ru species. The overall reaction can be written as a simple phosphine displacement (eq 5.1).

$$RuCl_2(DPPB)(PPh_3) \ + \ xs \ L \ \xrightarrow{\ C_6H_6, \ reflux\ } \ RuCl_2(DPPB)(L)_2 \ + PPh_3 \qquad (5.1)$$

The isolated $RuCl_2(DPPB)(py)_2$ species gave a singlet at 40.4 ppm in the $^{31}P\{^1H\}$ NMR spectrum (Table 5.1), indicating that the P-atoms were equivalent and ruling out the presence of the all-*cis* isomer. Unfortunately, the $^{31}P\{^1H\}$ NMR data do not distinguish between the *trans*-Cl and *trans*-py species (Figure 5.1). Other workers, one of whom (Batista) was a visiting scientist in this laboratory, have independently prepared the same $RuCl_2(DPPB)(py)_2$ complex from $Ru_2Cl_4(DPPB)_3$, the species isolated by their route giving the same singlet in the $^{31}P\{^1H\}$ NMR spectrum. An X-ray crystallographic study of **43** by these workers proved the structure to be that of the isomer with *trans* chloro ligands.[9,10] Their preparative method was repeated in this work to

ensure that the complexes isolated by the two procedures were in fact the same isomer (Section 2.5.11.1). The reaction proceeds by displacement of a molecule of DPPB from the dinuclear starting complex **19**, which breaks the bridge between the two metals (eq 5.2). The displaced DPPB was observed by $^{31}P\{^1H\}$ NMR spectroscopy as a singlet at –17 ppm when in situ reactions were performed.

Table 5.1 $^{31}P\{^1H\}$ NMR Data (121.42 MHz, 20 °C) for Some Mononuclear Complexes [RuCl$_2$(DPPB)(L)$_2$]

Complex	Solvent	Chemical Shift, $\delta^{(a)}$	$^2J_{PP}$, (Hz)
L = py			
trans-RuCl$_2$(DPPB)(py)$_2$	C$_6$D$_6$	δ = 41.5, s	----
43	CDCl$_3$	δ = 40.4, s	----
	CD$_2$Cl$_2$	δ = 40.4, s	----
(L)$_2$ = bipy			
cis-RuCl$_2$(DPPB)(bipy)	CDCl$_3$	δ_A = 43.5, δ_B = 29.8	32.9
44			
trans-RuCl$_2$(DPPB)(bipy)	CDCl$_3$	δ = 32.6, s	----
(L)$_2$ = phen			
cis-RuCl$_2$(DPPB)(phen)	CDCl$_3$	δ_A = 45.1, δ_B = 29.6	33.7
45			
trans-RuCl$_2$(DPPB)(phen)	CDCl$_3$	δ =32.5, s	----
L = NH$_3$	CDCl$_3$	δ = 46.7, s	----
trans-RuCl$_2$(DPPB)(NH$_3$)$_2$			
51			

(a) s = singlet

Figure 5.1 The two possible geometries of RuCl$_2$(DPPB)(py)$_2$ that would produce a singlet in the ^{31}P$\{^1$H$\}$ NMR spectrum, where P–P = Ph$_2$P(CH$_2$)$_4$PPh$_2$.

$$Ru_2Cl_4(DPPB)_3 + xs\ L \xrightarrow{\ CH_2Cl_2,\ room\ temp\ } 2RuCl_2(DPPB)(L)_2 + DPPB \qquad (5.2)$$
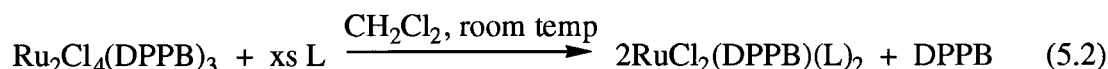
The UV-visible spectroscopic and molar conductivity data for *trans*-RuCl$_2$(DPPB)(py)$_2$ **43** are shown in Table 5.2. The complex shows molar conductivity values below the normal range in both MeOH and CH$_3$NO$_2$, where Λ_M values for 1:1 electrolytes are 80–115 and 75–95 ohm^{-1} mol^{-1} cm^2, respectively;[11] the low value measured for the conductivity presumably indicates partial dissociation of chloride from the neutral species. The molar conductivity of **43** in CH$_3$NO$_2$ increased with time, finally stabilizing after 3 h at 37.5 ohm^{-1} mol^{-1} cm^2, when the colour of the solution had changed from orange to purple. The nature of the purple species has yet to be elucidated.

The bromo analogue of **43** was prepared in situ from both RuBr$_2$(DPPB)(PPh$_3$) and Ru$_2$Br$_4$(DPPB)$_3$ by adding 10 equivalents of pyridine. The resulting orange solution showed a singlet at 39.3 ppm in the ^{31}P$\{^1$H$\}$ NMR spectrum for a presumed *trans*-RuBr$_2$(DPPB)(py)$_2$ species. A small amount of chloride impurity in the starting material results in the observation of a trace singlet at 39.8 ppm attributed to *trans*-RuBrCl(DPPB)(py)$_2$.

Of note, the resonance for the bromo analogue is observed further upfield than for that of RuBrCl(DPPB)(py)$_2$, which in turn is further upfield than that of RuCl$_2$(DPPB)(py)$_2$ (40.4 ppm). This same trend in chemical shift is observed for the RuXY(CO)$_2$(PPh$_3$)$_2$ complexes (Table 3.1, Section 3.3.2), where X, Y = Br or Cl.

221

Table 5.2   UV-visible Spectroscopic and Molar Conductivity Data for $RuCl_2(DPPB)(N)_2$ Complexes, where N represents an N-donor ligand

Complex	Solvent	λ_{max} (nm)	ε_{max} ($M^{-1}\,cm^{-1}$)	Λ_M ($ohm^{-1}\,mol^{-1}\,cm^2$)
trans-RuCl₂(DPPB)(py)₂ **43**	CH₂Cl₂	462	430	
		672	90	
	MeOH	258	7990	39.3
		342	4040	
		374 (sh)	3030	
	C₆H₆	458	492	
		678	96	
	CH₃NO₂			37.5
cis- and *trans*-RuCl₂(DPPB)(bipy) (50% of each) **44**	CH₂Cl₂	300	12300	
		346 (sh)	2600	
		458	2200	
	MeOH	292	15400	59.1
		436	2600	
	CH₃NO₂			56.5
cis-RuCl₂(DPPB)(phen) **45**	CH₂Cl₂	272	13500	
		438	3900	
	MeOH	270	26800	74.9
		416	4300	
	CH₃NO₂			69.2
trans-RuCl₂(DPPB)(NH₃)₂ **51**	CH₂Cl₂	260	5500	
		314 (sh)	1400	
	MeOH	236	4490	84.5
		330 (sh)	840	
	CH₃NO₂			19.9

Also, a presumed *trans*-RuCl$_2$((*R,R*)-DIOP)(py)$_2$ was prepared in situ by addition of 10 equivalents of pyridine to a green solution of Ru$_2$Cl$_4$(DIOP)$_3$ in CDCl$_3$. The resulting orange solution gave a singlet at 31.5 ppm in the ^{31}P{^{1}H} NMR spectrum, indicating the formation of the product. Another singlet at –23.4 ppm indicated the presence of free DIOP (cf. eq 5.2).

5.2.2 Reaction of Pyridine with RuCl$_2$(PPh$_3$)$_3$

The previously known complex formulated *c,c,t*-RuCl$_2$(py)$_2$(PPh$_3$)$_2$[2] was prepared from RuCl$_2$(PPh$_3$)$_3$ in acetone as outlined in Section 2.5.11.4. The stereochemistry of this complex was assigned as the *c,c,t*-isomer based on Ru-Cl stretching frequencies[2] (all possible geometries are illustrated in Figure 5.2). The isolated yellow solid is only sparingly soluble in CHCl$_3$, C$_6$H$_6$, and acetone.
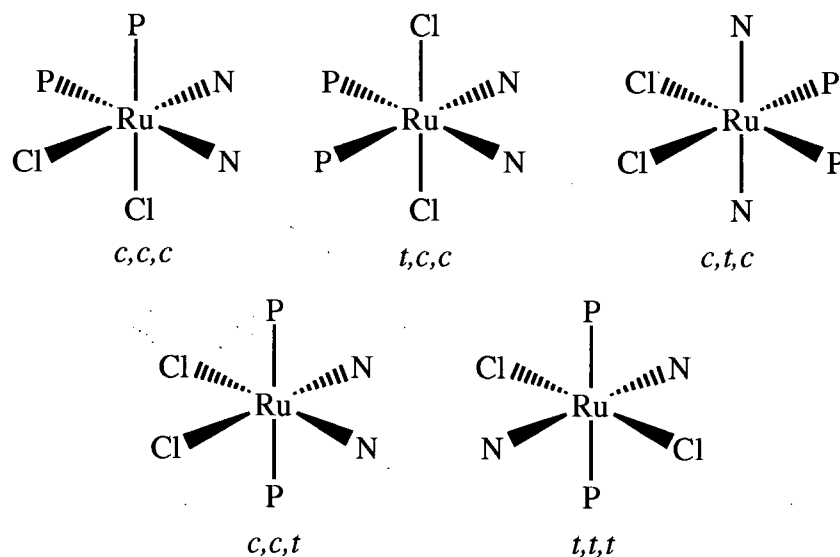
Figure 5.2 Possible geometries of the species RuCl$_2$(py)$_2$(PPh$_3$)$_2$, where P = PPh$_3$ and N = pyridine.

The ^{31}P{^{1}H} NMR spectrum of the yellow solid in CDCl$_3$ showed a singlet at 27.7 ppm, consistent with the *c,c,t*-isomer. However, all the isomers shown in Figure 5.2

would be expected to give singlets, except the *c,c,c*-isomer, which should be observed as an AB pattern.

A reaction between $RuCl_2(PPh_3)_3$ and pyridine (10 equiv) in refluxing C_6H_6 was also attempted in this work. However, the yellow solid isolated by this reaction gave a $^{31}P\{^1H\}$ NMR spectrum in $CDCl_3$ which showed singlets at 27.7 and 51.9 ppm. The resonance at 27.7 ppm is as seen for the material isolated from the acetone reaction (i.e., the presumed *c,c,t*-$RuCl_2(py)_2(PPh_3)_2$), and the other resonance at 51.9 ppm is thought to be due to *trans*-$RuCl_2(py)_3(PPh_3)$. The ^1H NMR spectrum ($CDCl_3$) supports this assignment, as a 2:1 ratio of *ortho*-py protons (doublets) are observed at 8.9 and 9.0 ppm for two sets of inequivalent pyridine ligands.

5.2.3   Reaction of Pyridine with $Ru_2Cl_4(DPPB)_2$

The addition of excess pyridine to $RuCl_2(DPPB)(PPh_3)$ **11** or $Ru_2Cl_4(DPPB)_3$ **19** produced *trans*-$RuCl_2(DPPB)(py)_2$ **43** (see Tables 5.1 and 5.2). Earlier attempts to prepare $Ru_2Cl_4(DPPB)_2(py)$ in situ by adding ~ 5 equivalents of pyridine to **11** in CD_2Cl_2 solution also produced only **43**. Even if an NMR tube containing the reactants was slowly warmed (from liquid N_2 temperature) to –65 °C in the NMR probe, no $Ru_2Cl_4(DPPB)_2(py)$ was observed.

However, the desired diruthenium complex $Ru_2Cl_4(DPPB)_2(py)$ **29** could be prepared in situ by adding one equivalent of py to $Ru_2Cl_4(DPPB)_2$ in $CDCl_3$ solution (see Section 2.5.8.2). The $^{31}P\{^1H\}$ NMR spectrum of the resulting orange-brown solution is shown in Figure 5.3, and the spectral data are listed in Table 5.3. The two AB patterns observed are characteristic of complexes of the type $Ru_2Cl_4(DPPB)_2(L)$ (see Section 3.5). This is only the second observation of such a dinuclear species that exhibits a chemical shift for the L-end of the complex further downfield than the Cl-end (the other is $Ru_2Cl_4(DPPB)_2(\eta^2-H_2)$, Chapter 4). As discussed in Section 3.5, the chemical shifts (δ_A and δ_B) of the phosphorus atoms on the Cl-end of the dinuclear complexes are

usually found with a coupling constant of $^2J_{AB} = 41$–45 Hz in the 52 ppm region, while the chemical shifts (δ_C and δ_D) of the L-end are found upfield of the Cl-end, with the $^2J_{CD}$ ranging from 28–40 Hz. In this case, where L = py, one phosphorus chemical shift of the py-end at $\delta_A = 54.3$ ppm is found downfield of the phosphorus chemical shifts of the Cl-end. The coupling constants, $^2J_{AB}$ and $^2J_{CD}$ (note that the AB and CD designations are reversed in this case by convention), are within the ranges listed above for complexes of this type.

Table 5.3 $^{31}P\{^1H\}$ NMR Data (121.42 MHz, 20 °C) for Some Dinuclear Complexes, [(L)(DPPB)Ru(μ-Cl)$_3$RuCl(DPPB)]

L(Complex)	Solvent	Chemical Shift, δ	$^2J_{PP}$, (Hz)
pyridine (py)	CDCl$_3$	$\delta_A = 54.3$, $\delta_B = 45.0$	36.4
29		$\delta_C = 52.6$ $\delta_D = 51.6$	42.7
ammonia, NH$_3$[a]	CDCl$_3$	$\delta_A = 55.6$, $\delta_B = 51.0$	39.1
		$\delta_C = 52.6$, $\delta_D = 51.9$	43.7
ammonia, NH$_3$[b]	CDCl$_3$	$\delta_A = 59.0$, $\delta_B = 53.7$	34.5
		$\delta_C = 58.5$, $\delta_D = 56.7$	39.8

(a)   Sample formed by heating *trans*-RuCl$_2$(DPPB)(NH$_3$)$_2$ **51** under vacuum (see Section 5.5.3).

(b)   The complex is more likely of formulation Ru$_2$Cl$_4$(DPPB)$_2$(NH$_3$)$_2$ (see Section 5.5.3).

Figure 5.3 shows a series of $^{31}P\{^1H\}$ NMR spectra which illustrate the effect of adding more pyridine to **29** produced in situ. Upon addition of a second equivalent of pyridine to Ru$_2$Cl$_4$(DPPB)$_2$ ((b) in Figure 5.3), the δ_C, δ_D phosphorus resonances become a broad multiplet. The δ_A, δ_B phosphorus resonances of **29** remain unchanged. As the δ_C, δ_D resonances belong to the Cl-end of **29**, the second equivalent of py is thought to coordinate to this end of the dinuclear complex en route to the monomeric *trans*-RuCl$_2$(DPPB)(py)$_2$ (observed as a singlet at 40.4 in spectra (b)–(d)). Figure 5.4 illustrates a possible route from Ru$_2$Cl$_4$(DPPB)$_2$ to Ru$_2$Cl$_4$(DPPB)$_2$(py), and eventually to *trans*-RuCl$_2$(DPPB)(py)$_2$.

(d)

43

(c)

(b)

(a)

29　**29**　**29**　　　**29**

65　　　60　　　55　　　50　　　45　　　40　PPM
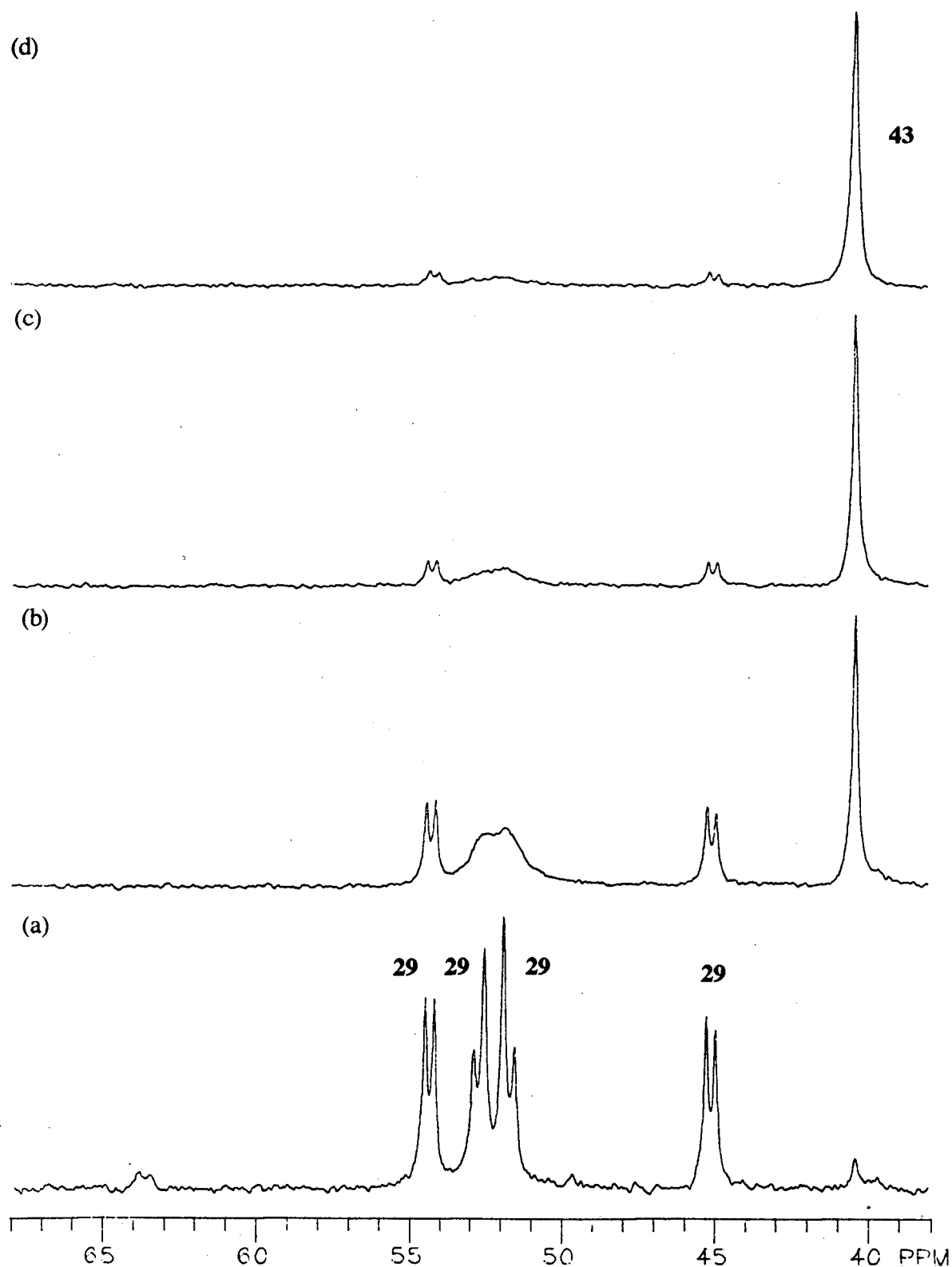
Figure 5.3　The $^{31}P\{^{1}H\}$ NMR spectra (121.42 MHz, 20 °C) of $Ru_2Cl_4(DPPB)_2$ **24** in $CDCl_3$ plus (a) one equiv of py, (b) two equiv of py, (c) four equiv of py, and (d) 10 equiv of py. **43** = *trans*-$RuCl_2(DPPB)(py)_2$.
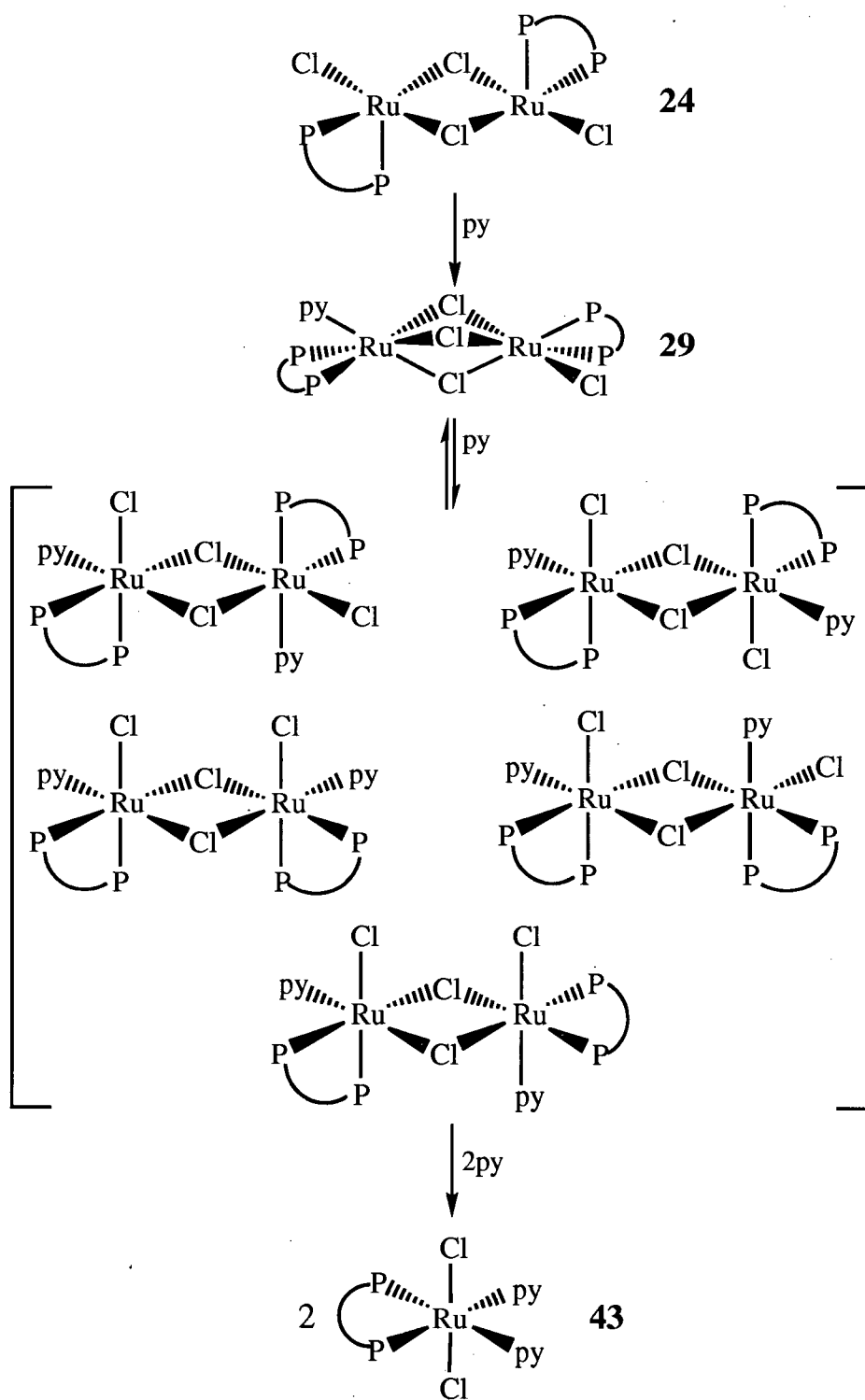
Figure 5.4   Proposed reaction pathway from Ru$_2$Cl$_4$(DPPB)$_2$ **24** through
Ru$_2$Cl$_4$(DPPB)$_2$(py) **29** to *trans*-RuCl$_2$(DPPB)(py)$_2$ **43**, where P–P =
Ph$_2$P(CH$_2$)$_4$PPh$_2$.

The addition of one equivalent of py to **29** is thought to break one of the three chloro-bridges, thereby producing any of the doubly-chloro bridged species illustrated in Figure 5.4. This intermediate isomer(s), which is not observed by $^{31}P\{^1H\}$ NMR, is thought to be in rapid equilibrium with **29** on the NMR timescale. Thus, the phosphorus resonances at the py-end, after adding one more equiv of py (i.e., total of two equiv), appear as they do in the spectrum of **29** (spectrum (a), Figure 5.3), while the resonances assigned to the Cl-end are affected by the exchange process (spectrum (b), Figure 5.3).

The addition of another two equivalents of pyridine breaks up the doubly-chloro-bridged intermediate to give complete conversion to *trans*-RuCl$_2$(DPPB)(py)$_2$. This step is fast, as indicated by the $^{31}P\{^1H\}$ NMR spectra, which were recorded immediately after the addition of pyridine.

Eventually, by adding pyridine to RuCl$_2$(DPPB)(PPh$_3$) **11**, the correct conditions to observe **29** in solution were found. The experiment was performed in CDCl$_3$ by adding 0.5 equivalents of pyridine to **11**. Three minutes after the addition of py, the two AB quartets of **29** were observed in the $^{31}P\{^1H\}$ NMR spectrum (Table 5.3). A singlet at 40.4 ppm, indicating the presence of *trans*-RuCl$_2$(DPPB)(py)$_2$, decreased in intensity relative to **29** as the reaction proceeded.

5.3 Reactions with 2,2'-Bipyridine

5.3.1 Reaction of 2,2'-Bipyridine with RuCl$_2$(DPPB)(PPh$_3$) and Ru$_2$Cl$_4$(DPPB)$_3$

The 2,2'-bipyridine analogue of the pyridine species **43** was also prepared from either RuCl$_2$(DPPB)(PPh$_3$) or Ru$_2$Cl$_4$(DPPB)$_3$ (Section 2.5.11.2). In both of these preparations, an approximately 10-fold excess of bipy was added to the starting Ru compound. Unlike the pyridine case, where only *trans*-RuCl$_2$(DPPB)(py)$_2$ was observed with no *cis*-isomer present, both isomers were observed with bipy.

The route from RuCl$_2$(DPPB)(PPh$_3$), performed in refluxing C$_6$H$_6$, produced an approximately 50:50 mixture of *cis*- and *trans*-RuCl$_2$(DPPB)(bipy) **44** (Tables 5.1 and 5.2). However, the route from Ru$_2$Cl$_4$(DPPB)$_3$, performed at room temperature in

CH_2Cl_2, produced largely *trans*-RuCl$_2$(DPPB)(bipy) (>70%), as evidenced by the singlet at 32.6 ppm in the $^{31}P\{^1H\}$ NMR spectrum. In fact, the *trans*-RuCl$_2$(DPPB)(bipy) isomer is the kinetic product in either method of preparation, while *cis*-**44** is the thermodynamic product. Heating a C_6H_6 solution of the two isomers for 18 h at reflux results in a $^{31}P\{^1H\}$ NMR spectrum showing only the AB quartet of *cis*-**44**. Likewise, a $^{31}P\{^1H\}$ NMR spectrum of a largely *trans*-**44** $CDCl_3$ solution showed almost complete isomerization to *cis*-**44** after one week at room temperature.

Table 5.1 lists the $^{31}P\{^1H\}$ NMR data recorded for both *cis*- and *trans*-**44**. The ^1H NMR spectrum of *cis*-RuCl$_2$(DPPB)(bipy) in $CDCl_3$, which is more complex than the spectrum of the *trans*-isomer (Section 2.5.11.2) because of the lower symmetry of the *cis*-geometry, is shown in Figure 5.5. Both the aliphatic and aromatic regions are quite complicated and no attempt was made to completely assign all the protons. The relative integrations of the aliphatic (8H) and phenyl regions (28H) agree with the formulation of **44**. An X-ray crystallographic study of *cis*-**44** has been performed by Batista et al.,[9,10] and is discussed in Section 5.4.

The UV-visible spectroscopic and molar conductivity data are given in Table 5.2. Complex **44** undergoes ionic dissociation in MeOH (Λ_M = 59.1 ohm^{-1} mol^{-1} cm^2; cf. Λ_M = 80–115 ohm^{-1} mol^{-1} cm^2 for a 1:1 electrolyte[11]). The Λ_M value obtained for **44** may be due either to incomplete Cl$^-$ dissociation from the neutral complex or to low mobility of the ions in solution. Similar molar conductivity values have been observed in this laboratory for other ruthenium(II) species; for example, *cis*-RuCl$_2$(PPh$_3$)(PN$_3$) in MeOH has a molar conductivity of 67.4 ohm^{-1} mol^{-1} cm^2.[12]

In fact, a $^{31}P\{^1H\}$ NMR spectrum recorded in CD_3OD showed some of the neutral *trans*-**44** as a singlet at 39.0 ppm. The mixture of *cis*- and *trans*-**44** was not very soluble in CD_3OD, and therefore, the $^{31}P\{^1H\}$ NMR spectra recorded showed poor signal-to-noise ratios. However, two AB quartets, presumably corresponding to ionic

species (see the conductivity in MeOH) were observed, along with the singlet discussed above (Table 5.4).

The two AB patterns observed in the $^{31}P\{^1H\}$ NMR spectrum indicate the presence of two isomers in deuterated methanol. There are a number of possible pairs of geometric isomers which would give an AB pattern for each member of the pair (Figure 5.6). It is difficult to predict which of the geometries is present in solution from either the $^{31}P\{^1H\}$ NMR or molar conductivity data.

In nitromethane, the molar conductivity of RuCl$_2$(DPPB)(bipy) increased over time, finally stabilizing after 18 h at 56.5 ohm^{-1} mol^{-1} cm^2, again somewhat below the values of 75–95 shown by 1:1 electrolytes.[11]

Table 5.4 $^{31}P\{^1H\}$ NMR Data of RuCl$_2$(DPPB)(N)$_2$ Complexes in CD$_3$OD, where N represents an N-donor ligand

Complex	Chemical Shift, δ	% of total integration	$^2J_{PP}$ (Hz)
cis- and *trans-* RuCl$_2$(DPPB)(bipy)	$\delta_A = 54.7$, $\delta_B = 42.9$	45	38.7
44	$\delta_A = 52.0$, $\delta_B = 47.9$	25	35.5
	$\delta = 39.0$	30	----
cis-RuCl$_2$(DPPB)(phen)	$\delta_A = 54.0$, $\delta_B = 43.0$	50	38.0
45	$\delta_A = 52.2$, $\delta_B = 48.7$	50	34.6
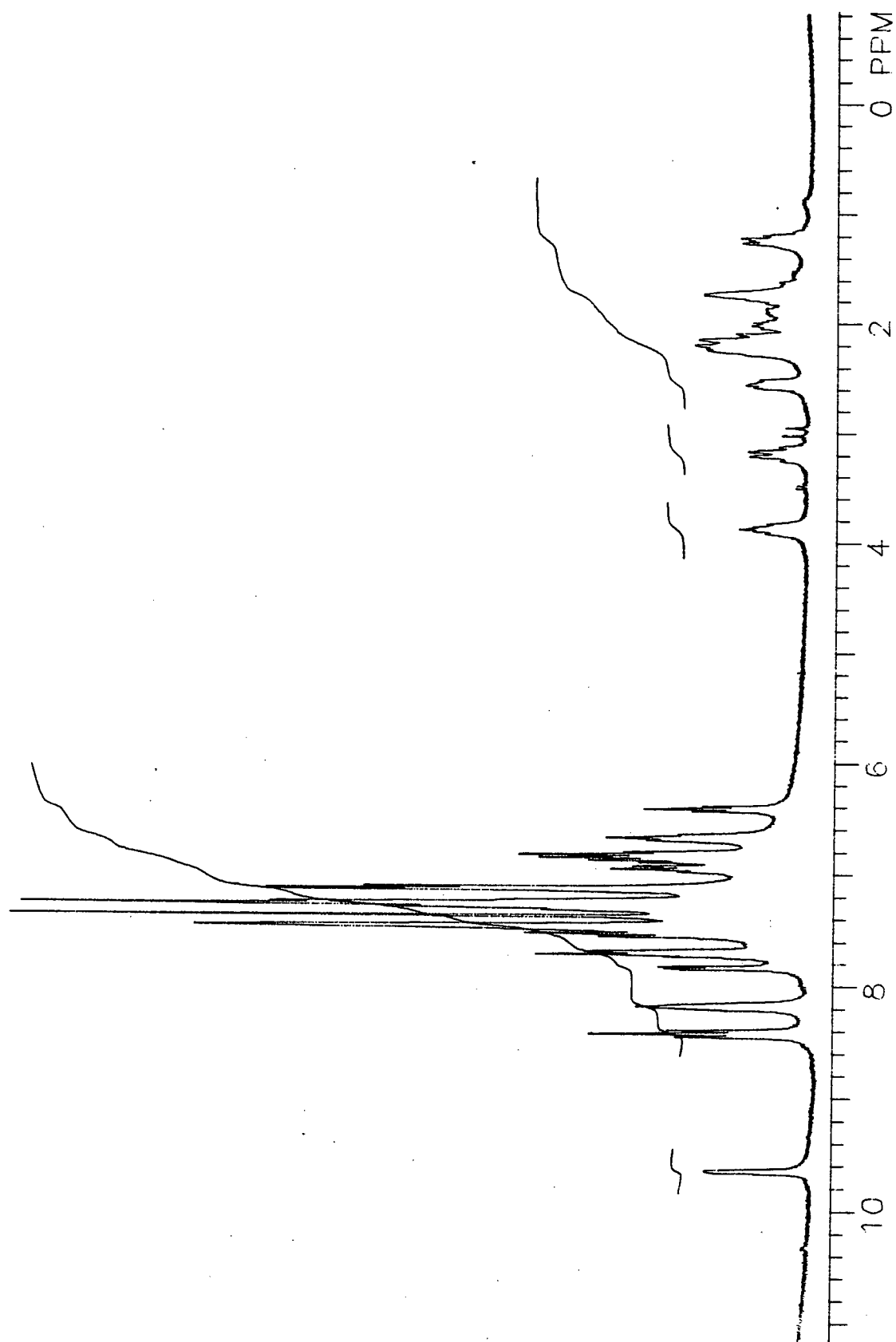
Figure 5.5   ¹H NMR spectrum of *cis*-RuCl₂(DPPB)(bipy) **44** in CDCl₃ (300 MHz, 20 °C).
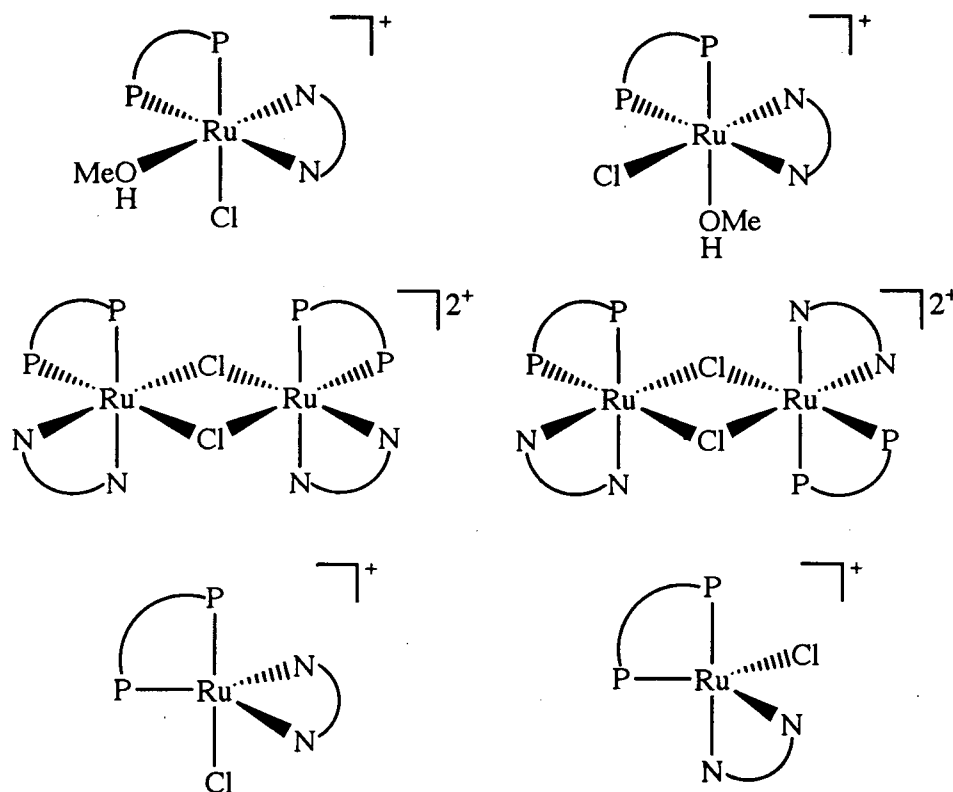
Figure 5.6   Possible geometries of "[RuCl(DPPB)(N–N)]⁺Cl⁻" which would account for
the observed $^{31}P\{^1H\}$ NMR data, where N–N = bipy or phen, and P–P =
DPPB.

5.3.2   Reaction of 2,2'-Bipyridine with $Ru_2Cl_4(DPPB)_2$

The addition of 0.5 equivalents of 2,2'-bipyridine to $Ru_2Cl_4(DPPB)_2$ **24** in $CDCl_3$

did not produce a dinuclear species of the type $Ru_2Cl_4(DPPB)_2(L)$, as was produced with

the addition of one equivalent of pyridine to **24** (Section 5.2.3). The $^{31}P\{^1H\}$ NMR

spectrum of the red solution produced by the addition of 0.5 equiv of bipy to **24** showed

only starting $Ru_2Cl_4(DPPB)_2$, as well as the mononuclear *cis*- and *trans*-

$RuCl_2(DPPB)(bipy)$ **44** (Figure 5.7).

The difference in reactivity observed on the addition of bipy and pyridine is a

result of the chelating ability of the former. Unlike the pyridine case, where the

$Ru_2Cl_4(DPPB)_2(py)$ species could be observed in solution, reaction of bipy with **24**

probably results in the initial η^1-coordination of bipy to give the non-detected Ru$_2$Cl$_4$(DPPB)$_2$(η^1-bipy), followed by rapid chelation of the bipy ligand to break-up any triply-chloro-bridged intermediate and produce *cis*- and *trans*-RuCl$_2$(DPPB)(bipy). The ratio of *cis*- to *trans*-**44** observed after 1 h at room temperature in CDCl$_3$ is ~ 30:70 (Figure 5.7).
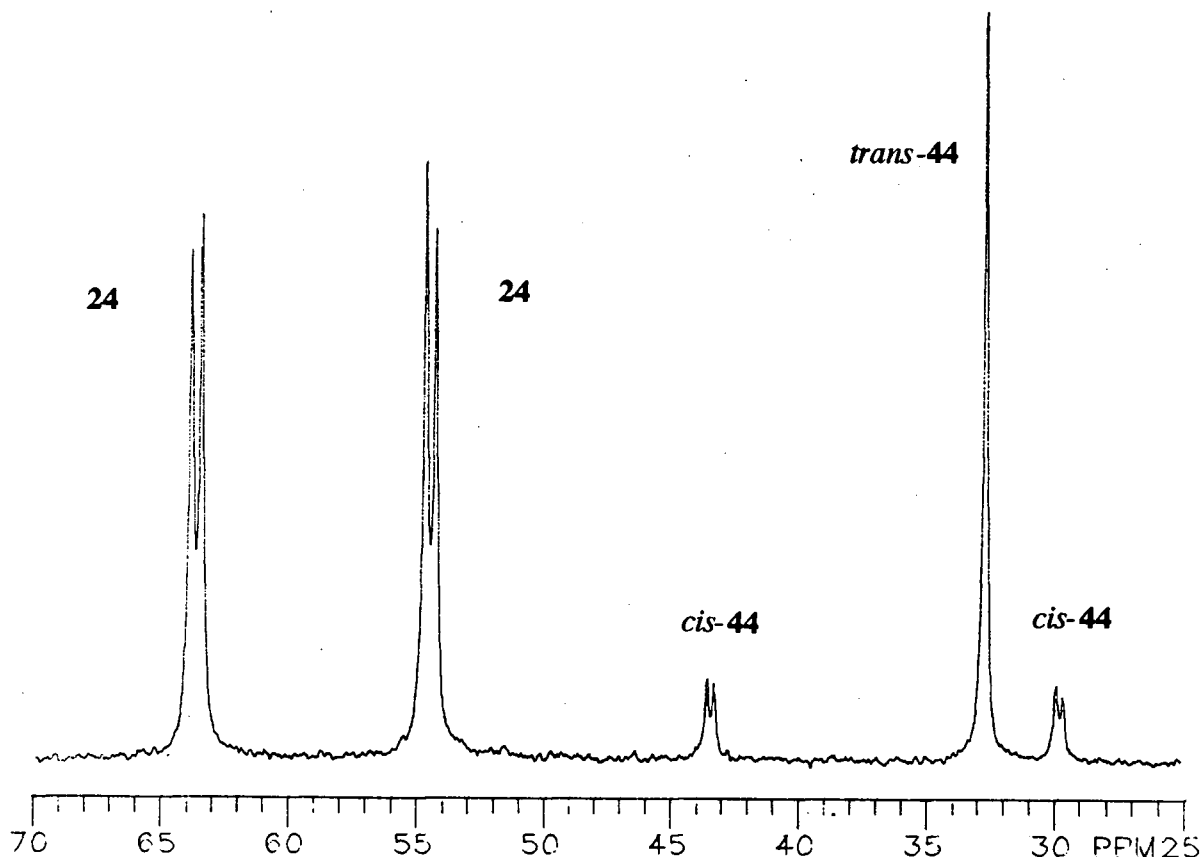
Figure 5.7   The ^{31}P{^{1}H} NMR spectrum (CDCl$_3$, 20 °C) of a red solution of **44** produced in situ by adding 0.5 equivalents of bipy to Ru$_2$Cl$_4$(DPPB)$_2$ **24**.

5.4   Reaction of 1,10-Phenanthroline with RuCl$_2$(DPPB)(PPh$_3$) and Ru$_2$Cl$_4$(DPPB)$_3$

The 1,10-phenanthroline analogue of the py and bipy species **43** and **44** was also prepared from either RuCl$_2$(DPPB)(PPh$_3$) or Ru$_2$Cl$_4$(DPPB)$_3$ (Section 2.5.11.3). In both preparations, an approximately 10-fold excess of phen was added to the starting Ru compound. Unlike the bipy system, where 50% of *trans*-**44** was isolated, almost no *trans*-

Chapter 5 References: p 249

$RuCl_2(DPPB)(phen)$ **45** (<2%) was observed when the product was prepared from $RuCl_2(DPPB)(PPh_3)$. The complex was isolated almost entirely as the *cis*-isomer from **11**. However, from $Ru_2Cl_4(DPPB)_3$, a mixture of *cis*- and *trans*-$RuCl_2(DPPB)(phen)$ was isolated (~ 70:30). Again, as observed for $RuCl_2(DPPB)(bipy)$, the *cis*-isomer is the thermodynamic product. The higher temperature route from $RuCl_2(DPPB)(PPh_3)$ (in refluxing benzene) gives the *cis*-isomer almost exclusively.

The $^{31}P\{^1H\}$ NMR spectral data for *cis*- and *trans*-$RuCl_2(DPPB)(phen)$ **45** are given in Table 5.1. The ^1H NMR spectrum of **45** in $CDCl_3$ is shown in Figure 5.8; the assignments of the aliphatic region are given in Section 2.5.11.3 but the aromatic region could not be assigned despite attempts to do so using a ^1H-^1H COSY spectrum. Table 5.2 lists the UV-visible spectroscopic and molar conductivity data.

In MeOH and CH_3NO_2, *cis*-**45** undergoes Cl^- dissociation to give a 1:1 electrolyte, as indicated by the observed Λ_M values of 74.9 and 69.2 ohm^{-1} mol^{-1} cm^2, respectively; again values are slightly below those expected for complete dissociation for simple electrolytes.[11] The molar conductivity of *cis*-**45** in CH_3NO_2 increased over time, reaching the noted value after ~ 24 h, and the colour of the solution changed from orange to yellow during the measurement period. In MeOH, the Λ_M value initially recorded remained invariant with time.
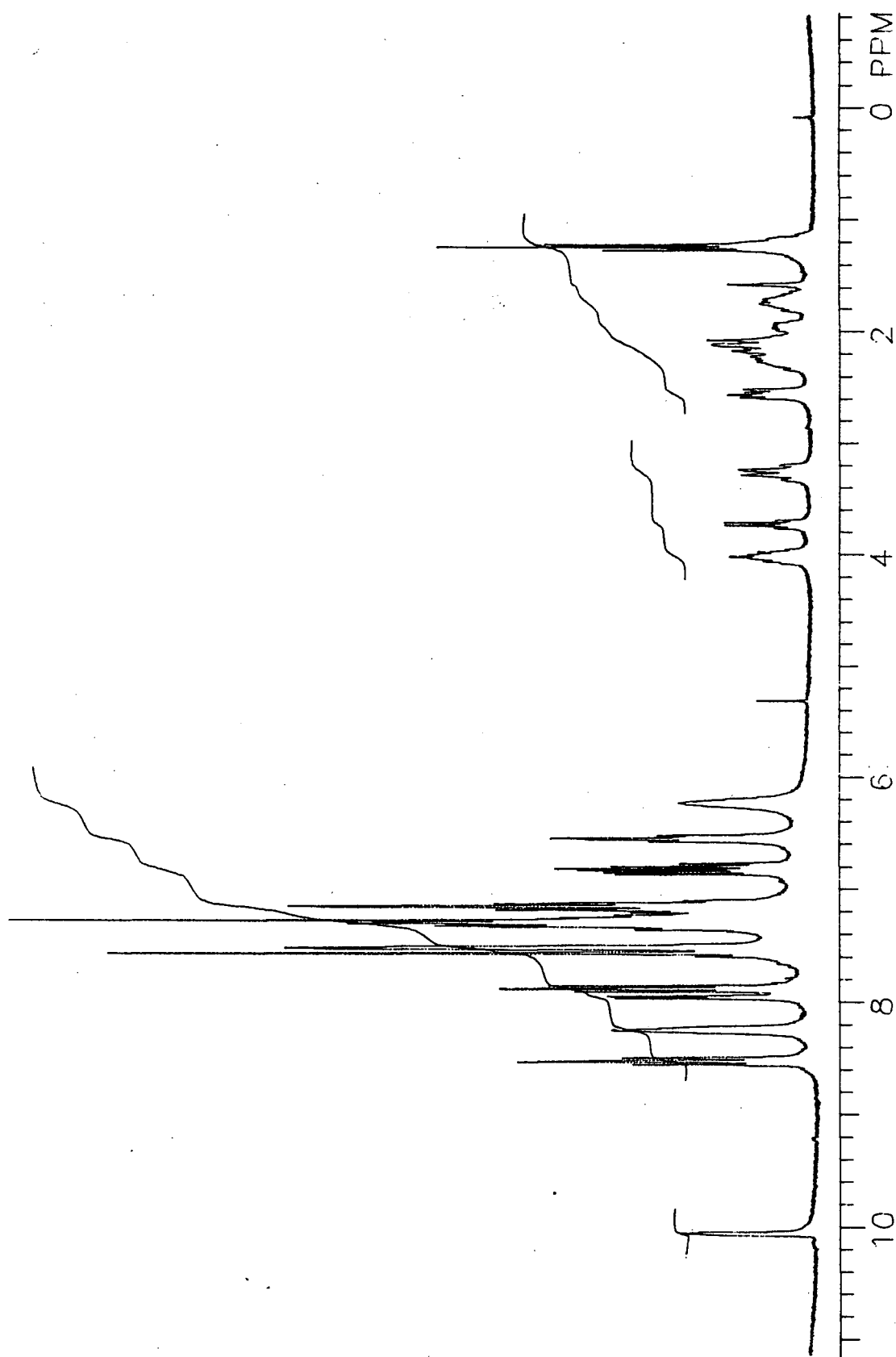
Figure 5.8   1H NMR spectrum of *cis*-RuCl₂(DPPB)(phen) **44** in CDCl₃ (300 MHz, 20 °C).

A ^{31}P{^{1}H} NMR spectrum of *cis*-**45** in CD$_3$OD showed two AB quartets (Table 5.4), the values of the chemical shifts and coupling constants being very similar to those observed for RuCl$_2$(DPPB)(bipy). However, in this case, no singlet was observed, which may explain the larger molar conductivity value observed for **45** than for **44** in MeOH (74.9 vs. 59.1 ohm^{-1} mol^{-1} cm^2), because the singlet is thought to be due to neutral RuCl$_2$(DPPB)(bipy). Possible ionic geometries which could account for the recorded data are shown in Figure 5.6.

Another explanation for the lower molar conductivity and observed singlet in the ^{31}P{^{1}H} NMR spectrum for RuCl$_2$(DPPB)(bipy) may be due to the fact that a mixture of *cis*- and *trans*-**44** were used for the measurements, while only the *cis*-isomer of **45** was used. It is possible that the *trans*-isomer does not appreciably ionize in MeOH because, for example, the molar conductivity measured for *trans*-RuCl$_2$(DPPB)(py)$_2$ is much lower than **44** or **45**.

An orange crystal of **45** was isolated from a CH$_2$Cl$_2$ / methanol solution, and an X-ray diffraction analysis showed the complex to be *cis*-RuCl$_2$(DPPB)(phen). Figure 5.9 shows the ORTEP plot , while selected bond lengths and angles are given in Tables 5.5 and 5.6, respectively. Complete experimental parameters and details are given in Appendix VII.

The geometry of *cis*-**45** is slightly distorted from octahedral. The distortions are probably due to the presence of the chelating DPPB and chelating phenanthroline. For example, the P(1)—Ru(1)—P(2) angle is 93.89°, while the N(1)—Ru(1)—N(2) angle is 78.2°. The limited chelate bite size of the rigid planar phenanthroline ligand constrains the N(1)—Ru(1)—N(2) angle to less than 90°.

The ORTEP plot arbitrarily shows the Λ-enantiomer of the two that are present in the monoclinic centrosymmetric space group P2$_1$/c.
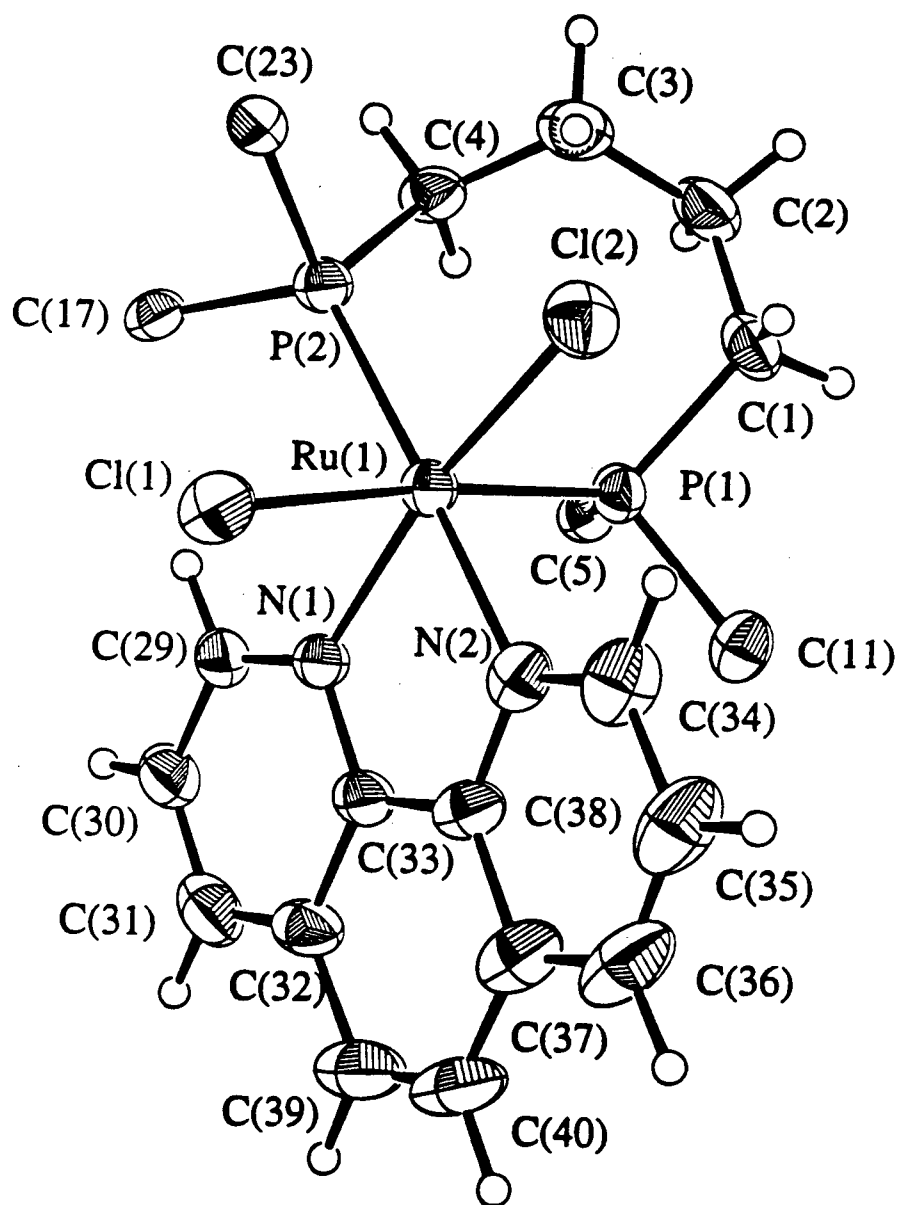
Figure 5.9   The ORTEP plot of *cis*-RuCl₂(DPPB)(phen) **45**. Thermal ellipsoids for non-hydrogen atoms are drawn at 33% probability (some of the phenyl carbons have been omitted for clarity).

The metal-ligand bond lengths show a *trans* influence phenomenon. The Ru(1)—N(1) bond length of 2.092(3), *trans* to Cl⁻, is shorter than the Ru—N(2) bond length of 2.117(4), *trans* to P. This is as expected, because PR$_3$ has a stronger *trans* influence than Cl⁻. Likewise, the Ru(1)—Cl(2) bond length of 2.417(1), *trans* to N, is shorter than the Ru—Cl(1) bond length of 2.491(1), *trans* to P. Again, this is as expected, because PR$_3$ is higher in the *trans*-directing series than py.

However, the *trans* influence is not obeyed for the two Ru—P bonds. The Ru(1)—P(1) bond length of 2.286(1), *trans* to Cl⁻, is shorter than the Ru—P(2) bond length of 2.322(1), *trans* to N. This is the reverse of that predicted by the *trans*-directing series (i.e., Cl⁻ has a stronger *trans* influence than py). The breakdown in the *trans*-influence series may be due to the fact that the series was established for monodentate ligands such as py and PPh$_3$, while in this case, the more complex bidentate ligands are present. Also, Cl⁻ and py are adjacent in the *trans*-directing series, and therefore may not be that different in their *trans*-influencing properties.

Table 5.5 Selected Bond Lengths (Å) for *cis*-RuCl$_2$(DPPB)(phen) **45** with Estimated Standard Deviations in Parentheses

Bond	Length (Å)	Bond	Length (Å)
Ru(1)—Cl(1)	2.491(1)	Ru(1)—Cl(2)	2.417(1)
Ru(1)—P(1)	2.286(1)	Ru(1)—P(2)	2.322(1)
Ru(1)—N(1)	2.092(3)	Ru(1)—N(2)	2.117(4)
P(1)—C(1)	1.837(4)	P(2)—C(4)	1.831(4)
P(1)—C(5)	1.839(4)	P(1)—C(11)	1.828(5)
P(2)—C(23)	1.852(4)	P(2)—C(17)	1.835(4)
N(2)—C(34)	1.319(6)	N(2)—C(38)	1.357(6)
N(1)—C(29)	1.326(6)	N(1)—C(33)	1.365(5)

Chapter 5 References: p 249

Table 5.6   Selected Bond Angles (°) for *cis*-RuCl₂(DPPB)(phen) **45** with Estimated
Standard Deviations in Parentheses

Bond	Angles (°)	Bond	Angles (°)
Cl(1)—Ru(1)—Cl(2)	92.46(4)	Cl(1)—Ru(1)—P(1)	174.20(4)
Cl(1)—Ru(1)—P(2)	91.86(4)	Cl(1)—Ru(1)—N(1)	84.57(9)
Cl(1)—Ru(1)—N(2)	83.16(10)	Cl(2)—Ru(1)—P(1)	88.42(4)
Cl(2)—Ru(1)—P(2)	88.60(4)	Cl(2)—Ru(1)—N(1)	167.4(1)
Cl(2)—Ru(1)—N(2)	89.3(1)	P(1)—Ru(1)—P(2)	93.89(4)
P(1)—Ru(1)—N(1)	93.34(9)	P(1)—Ru(1)—N(2)	91.12(10)
P(2)—Ru(1)—N(1)	103.7(1)	P(2)—Ru(1)—N(2)	174.5(1)
N(1)—Ru(1)—N(2)	78.2(1)		

During the course of this work, it was learned that both *trans*-RuCl₂(DPPB)(py)₂
and *cis*-RuCl₂(DPPB)(bipy) had been prepared independently from a different Ru
precursor and characterized structurally by other workers.[9,10] The structure of *cis*-
RuCl₂(DPPB)(bipy) **44** is very similar, in terms of bond lengths and angles, to that
observed for *cis*-RuCl₂(DPPB)(phen) **45** in this work.

For **44**, the bond lengths[10] for Ru—P (2.279 and 2.331 Å), Ru—N (2.088 and
2.097 Å), and Ru—Cl (2.484 and 2.428 Å) are almost identical to those observed for **45**.
The *trans*-influence series is obeyed for the Ru—Cl bond lengths, and reversed, as above,
for the Ru—P bond lengths. The two Ru—N bond lengths in **44** are essentially identical.

A plot of the Ru–P bond lengths for Ru(II)(DPPB)-containing complexes versus
their ³¹P{¹H} NMR chemical shift data is shown in Figure 5.10. The phosphorus
chemical shifts are seen to exhibit an inverse dependence on Ru–P bond length, and
similar trends have been observed for ruthenium(II) complexes containing PPh₃,[13,14]
P(*p*-tolyl)₃,[15] and the P–N ligand PMA[15] (Section 3.10, Figure 3.28).
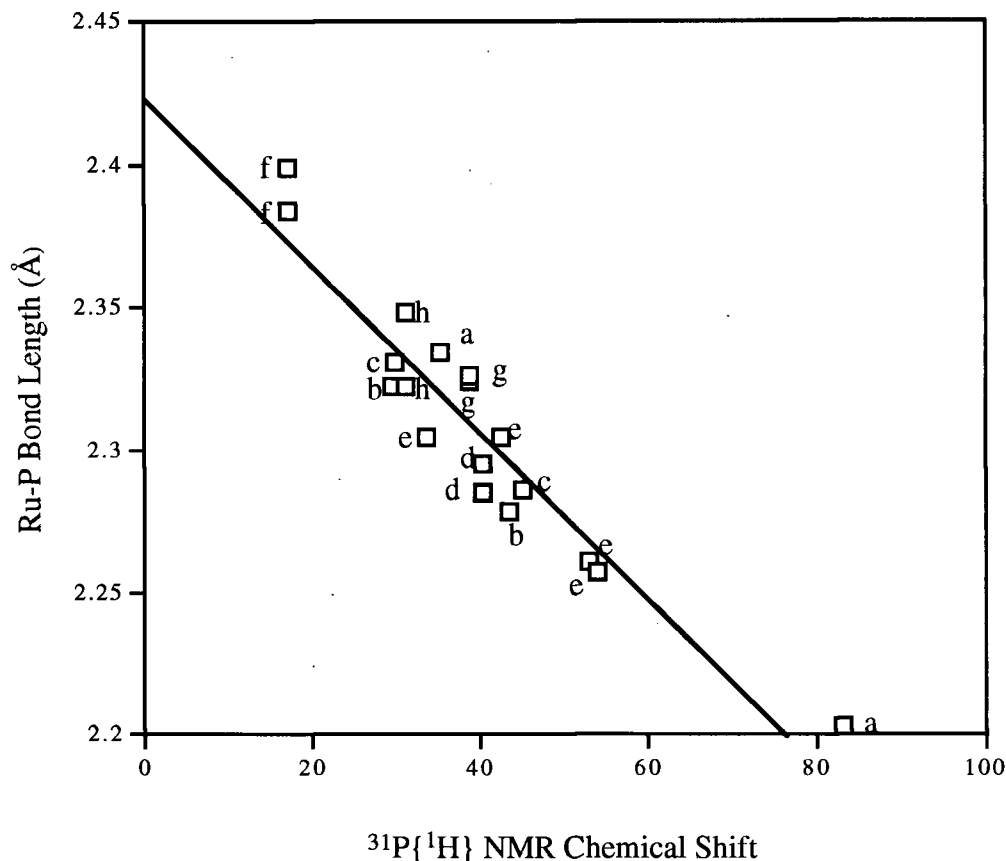
Figure 5.10 Graph of Ru–P bond length versus $^{31}P\{^1H\}$ NMR chemical shift for a series of Ru(II) complexes containing DPPB. (a) $RuCl_2(DPPB)(PPh_3)^{tw}$,
(b) *cis*-$RuCl_2(DPPB)(phen)^{tw}$, (c) *cis*-$RuCl_2(DPPB)(bipy)$,[9,10]
(d) *trans*-$RuCl_2(DPPB)(py)_2$,[9,10] (e) $Ru_2Cl_4(DPPB)_2(DMSO)$,[6,16]
(f) $RuCl_2(nbd)(DPPB)$,[17] (g) $[Ru(DPPB)(MeCN)_4][PF_6]_2$,[7]
(h) $[RuCl(DPPB)(C_7D_8)]^+PF_6^-$.[18] $^{31}P\{^1H\}$ NMR data in CD_2Cl_2 (a, f-h) or $CDCl_3$ (b–e); tw = this work.

The three X-ray structural studies performed in this work on ruthenium(II) complexes containing the ligand PPh_3 show Ru–P bond lengths and $^{31}P\{^1H\}$ NMR chemical shifts which agree with the trend observed by Dekleva[14] and Jessop et al.[13] The data which fit this trend are for $RuBr_2(PPh_3)_3$ (Chapter 3), $RuCl_2(DPPB)(PPh_3)$ (Chapter 3), and $[(DMA)_2H]^+[(PPh_3)_2(H)Ru(\mu\text{-}H)(\mu\text{-}Cl)_2Ru(H)(PPh_3)_2]^-$ (Chapter 4).

Of note, the negative slope (-2.91×10^{-3} Å ppm^{-1}) of the graph shown in Figure 5.10 for the DPPB systems is identical to that of the plot for the PPh_3 systems;[13]

Chapter 5 References: p 249

however, the intercepts are somewhat different (2.423 Å for the DPPB system and 2.465

Å for the PPh3 system).

5.5   Reactions with NH3

5.5.1   Reaction of NH3 with RuCl2(DPPB)(PPh3), Ru2Cl4(DPPB)3, and Ru2Cl4(DPPB)2

The reactions of both gaseous NH_3 and aqueous NH_3 were investigated with a variety of ruthenium(II)-phosphine complexes. The reaction of excess NH_3 with either $RuCl_2(DPPB)(PPh_3)$ or $Ru_2Cl_4(DPPB)_3$ in solution produced isolable $RuCl_2(DPPB)(NH_3)_2$ **51** (Section 2.5.12.6). This species was also prepared in situ by bubbling NH_3 through a $CDCl_3$ solution of $Ru_2Cl_4(DPPB)_2$.

The UV-visible spectroscopic and molar conductivity data for **51** are listed in Table 5.2 (Section 5.2). The molar conductivity value of 84.5 ohm^{-1} mol^{-1} cm^2 indicates that **51** is a 1:1 conductor in MeOH, while the value of 19.9 ohm^{-1} mol^{-1} cm^2 in nitromethane is below the normal range for a 1:1 conductor in this solvent (see Section 5.2 for the ranges reported in the literature).

Two possible isomers (Figure 5.11) could fit the observed $^{31}P\{^1H\}$ and ^1H NMR spectral data. The singlet observed in the $^{31}P\{^1H\}$ NMR spectrum (Table 5.1) indicated a structure with equivalent phosphorus nuclei, while the fact that only two groups of protons (δ 1.62 and 2.90, $CDCl_3$) were observed for the methylenes of DPPB (Section 2.5.12.6) also indicated a structure having a mirror plane bisecting the diphosphine.
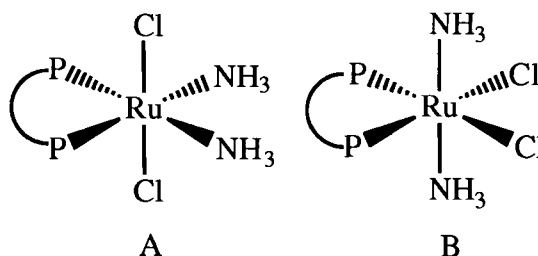
Figure 5.11   The two possible structures of $RuCl_2(DPPB)(NH_3)_2$, **51**, where P–P = $Ph_2P(CH_2)_4PPh_2$.

In order to distinguish between the two possible geometries (i.e., *trans*-Cl (A) or *trans*-NH$_3$ (B)), an NMR spectral study was undertaken on the ^{15}N analogue of **51** prepared in situ (the nuclear spin of ^{15}N is 1/2). A CDCl$_3$ solution (0.6 mL, ~ 40 mM) of RuCl$_2$(DPPB)(PPh$_3$) **11** was transferred with a cannula to an NMR tube containing ^{15}NH$_4$Cl (~ 20 mg, 0.37 mmol) and a NaOH solution (0.5 mL, 6 M). The two-phase system was mixed, giving a blue-green solution. The ^{15}NH$_3$ produced in situ reacted with the starting Ru complex to give a compound of the type RuCl$_2$(DPPB)(^{15}NH$_3$)$_2$.

A similar two-phase system was prepared with ^{14}NH$_4$Cl to prove that the same complex was produced as had been isolated with NH$_3$ gas (Section 2.5.12.6); the characteristic singlet at 46.7 ppm was observed in the ^{31}P{^{1}H} NMR spectrum.

Surprisingly, good ^{31}P{^{1}H} NMR spectra (Figure 5.12) could be recorded from these two-phase systems, as the more dense CDCl$_3$ layer was in the region of the receiver coils of the NMR spectrometer, while the lighter H$_2$O layer was above the receiver coils.

Structure A, Figure 5.11 would be expected to show an AA'XX' pattern in the ^{31}P{^{1}H} NMR spectrum, while structure B would show an A$_2$X$_2$ pattern. Therefore, a triplet should be observed in the case of structure B, while a doublet of doublets should arise from structure A. In fact, a doublet of doublets centred at 46.7 ppm is observed in the ^{31}P{^{1}H} NMR spectrum. The observed coupling constants are $^2J_{PP}$ = 21.8 and $^2J_{PN}$ = 9.5 Hz, indicating that structure A (i.e., *trans*-RuCl$_2$(DPPB)(^{15}NH$_3$)$_2$) is the isomer observed. This is consistent with the molecular structure determined by X-ray crystallography for *trans*-RuCl$_2$(DPPB)(py)$_2$ **43** by Batista et al. (Section 5.2.1).[9,10]

When a CDCl$_3$ NMR solution of **51** is left at room temperature, other isomers begin to appear in the ^{31}P{^{1}H} NMR spectrum. A singlet at 50.7 ppm becomes apparent within 30 min (Figure 5.13), and the ^{15}N-analogue of **51** slowly generates the corresponding ^{15}N-analogue as a doublet of doublets centred at 50.7 ppm ($^2J_{PP}$ = 20.5 and $^2J_{PN}$ = 8.1 Hz; Figure 5.12). This resonance is thought to be due to an ionic complex

of the type [RuCl(DPPB)(^{15}NH$_3$)$_2$]$^+$Cl$^-$, produced by Cl$^-$ dissociation from the neutral

complex **51**.
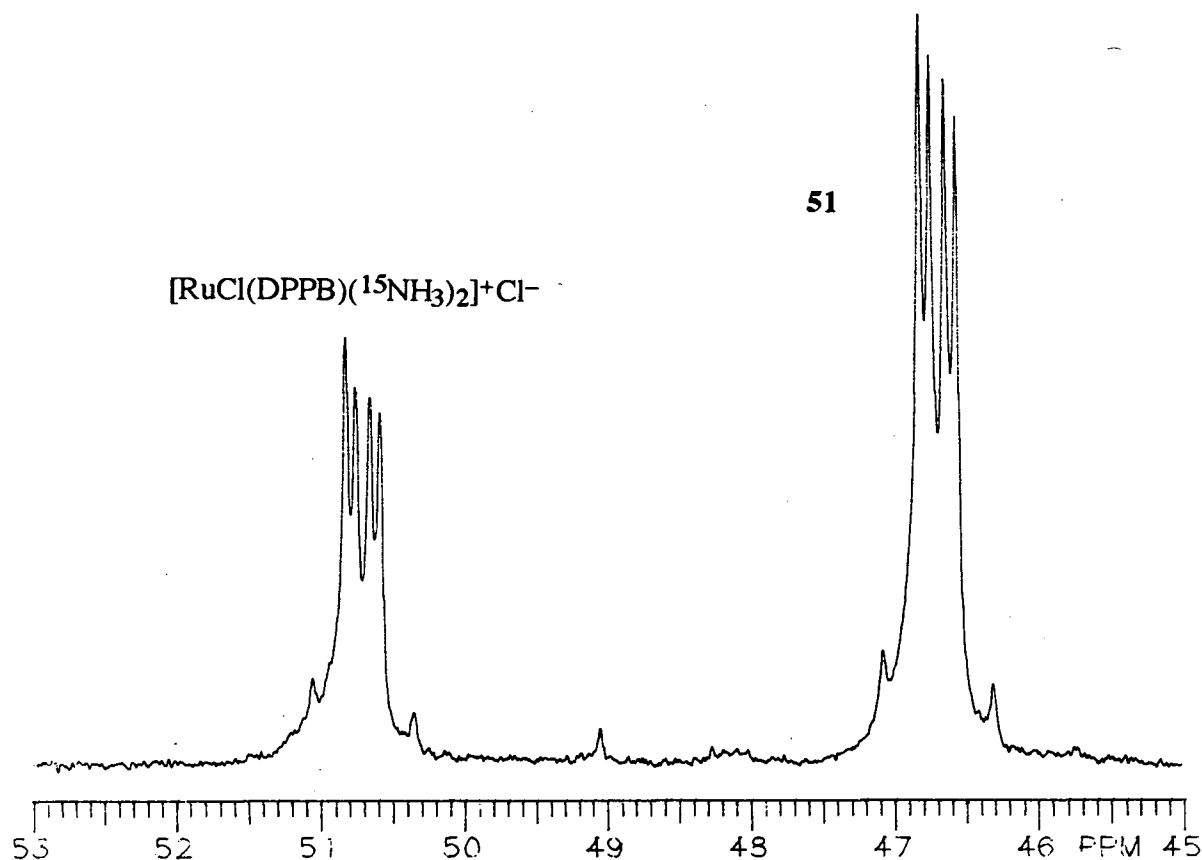
Figure 5.12 The ^{31}P{^{1}H} NMR spectrum (121.42 MHz, 20 °C) of
RuCl$_2$(DPPB)(^{15}NH$_3$)$_2$ **51** in CDCl$_3$. The sample was prepared in situ from
^{15}NH$_4$Cl, RuCl$_2$(DPPB)(PPh$_3$), and 6 M NaOH.

Under conditions of excess NH$_3$, the only two resonances observed in the

^{31}P{^{1}H} NMR spectrum are at 46.7 and 50.7 ppm (discussed above). However, when

isolated *trans*-RuCl$_2$(DPPB)(NH$_3$)$_2$ is dissolved in CDCl$_3$ and the solution left at room

temperature, other species, besides those giving the 46.7 and 50.7 ppm resonances, are

observed (Figure 5.13). An AB quartet at δ_A = 59.5, δ_B = 44.4, $^2J_{AB}$ = 38.8 Hz is

indicative of the isomerization of *trans*-RuCl$_2$(DPPB)(NH$_3$)$_2$ to the all-*cis* complex,

while a singlet generated at 54.7 ppm could be assigned to any of the structures shown in

Figure 5.14.
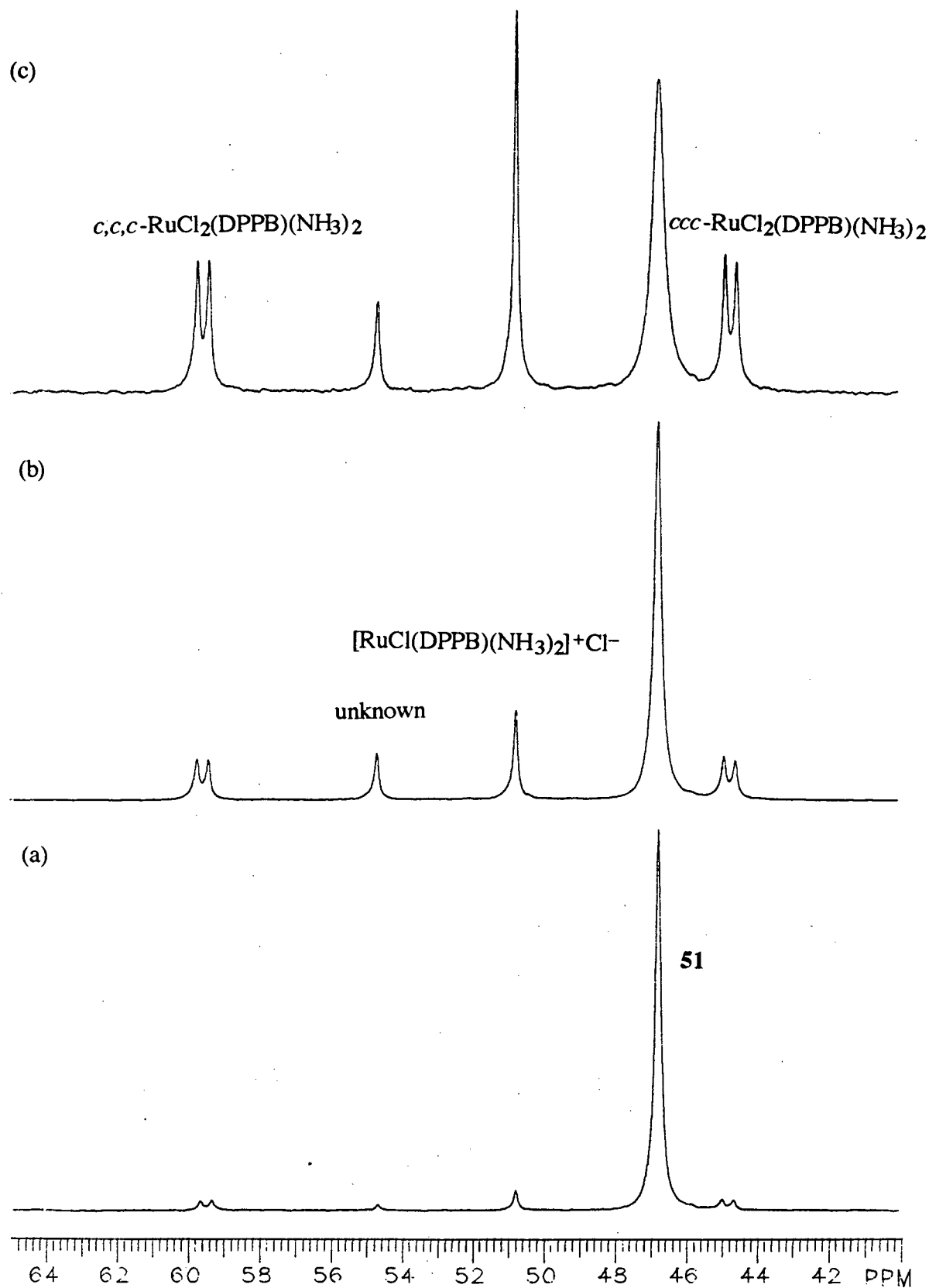
Figure 5.13 Isomerization of *trans*-RuCl₂(DPPB)(NH₃)₂ **51** in CDCl₃ (121.42 MHz, 20 °C); (a) 10 min, (b) 45 min, and (c) 2.5 h after dissolution.
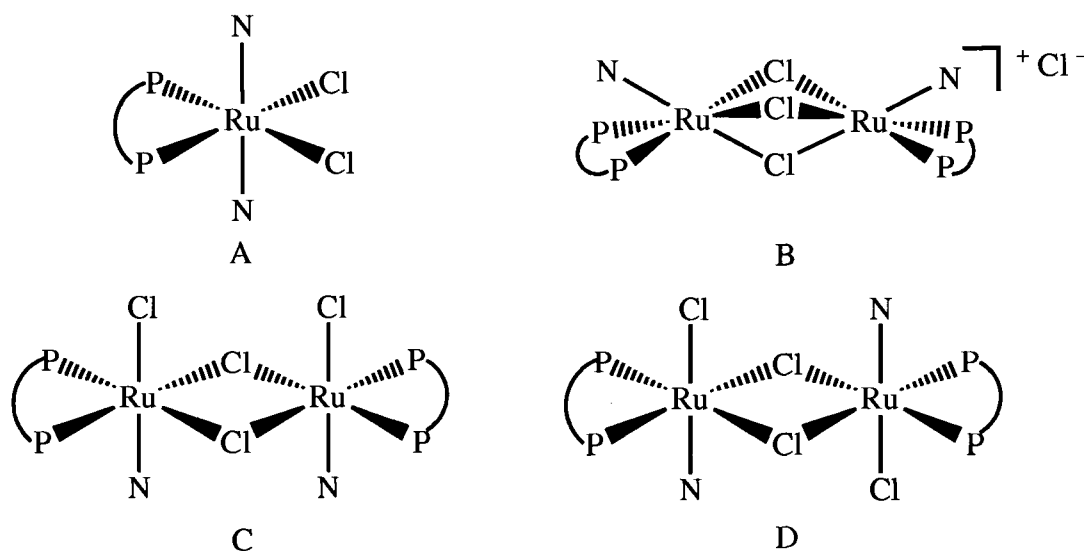
Figure 5.14 Possible structures of the type "RuCl$_2$(DPPB)(NH$_3$)$_x$" which would exhibit a singlet in the ^{31}P{^{1}H} NMR spectrum, where P–P = Ph$_2$P(CH$_2$)$_4$PPh$_2$ and N = NH$_3$.

A complex similar to B (Figure 5.14) has been previously isolated as the PF$_6^-$ salt, where N is a nitrile (i.e., MeCN or PhCN).[7] The isomer isolated in this case has the structure shown in Figure 5.15, and gives rise to an AB pattern in the ^{31}P{^{1}H} NMR spectrum, as opposed to the singlet expected for structure B. Structure A is favoured over the other three possible geometries shown in Figure 5.14, as no free NH$_3$ is observed in the ^{1}H NMR (0.4–0.6 ppm region), and the formation of structures B–D from *trans*-RuCl$_2$(DPPB)(NH$_3$)$_2$ all require the loss of a mole of NH$_3$ per Ru.
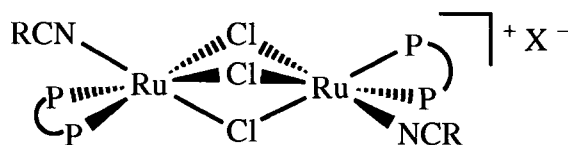
Figure 5.15 Structure of [Ru$_2$Cl$_3$(DPPB)$_2$(RCN)$_2$]$^+$X$^-$ species, where R = Me or Ph and X = PF$_6$ or Cl.

5.5.2 Reaction of NH₃ with RuCl₂(DPPB)(PPh₃) in the Solid State

The mixed-phosphine complex $RuCl_2(DPPB)(PPh_3)$ **11** (or $Ru_2Cl_4(DPPB)_2$ **24**) reacts with two moles of NH_3 (per Ru) in the solid state to give *trans*-$RuCl_2(DPPB)(NH_3)_2$ and a mole of PPh_3 (Section 2.5.12.6). The addition of an atmosphere of ammonia to **11** results in an immediate colour change from green to brown. The NH_3 atmosphere was then removed, the isolated brown solid dissolved in $CDCl_3$, and the $^{31}P\{^1H\}$ NMR spectrum recorded, showing resonances for free PPh_3 at –5.5 ppm, and *trans*-$RuCl_2(DPPB)(NH_3)_2$ **51** at 46.7 ppm.

The solid-state reaction gives the identical product to that isolated when the reaction is performed in solution. Similar solid-state reactivity of these five-coordinate Ru(II) complexes with CO is also observed and is discussed in Chapter 7.

The reaction of NH_3 gas with solid $Ru_2Cl_4(DPPB)_3$ **19** also produced **51** as evidenced by a $^{31}P\{^1H\}$ NMR spectrum of a $CDCl_3$ solution of the isolated brown solid. Also observed in the $^{31}P\{^1H\}$ NMR spectrum was a singlet at –16.2 ppm, indicating the presence of free DPPB which is displaced from **19** on reaction with NH_3 (equation 5.2 illustrates the reaction where L = NH_3 and no solvent is present). A small amount of another as yet unidentified product was evident as a resonance at 20.6 ppm.

5.5.3 Observation of Some Dinuclear Ruthenium(II)-NH₃ Containing Complexes

On heating a solid sample of *trans*-$RuCl_2(DPPB)(NH_3)_2$ **51** at 100 °C for several days under vacuum, the colour changed from tan to dark brown. A $^{31}P\{^1H\}$ NMR spectrum of this sample in $CDCl_3$ showed two AB quartets (first NH_3 entry in Table 5.3, Section 5.2.3) indicating the presence of $Ru_2Cl_4(DPPB)_2(NH_3)$, as the chemical shifts and coupling constants observed are similar to those observed for $Ru_2Cl_4(DPPB)_2(py)$ **29** (Table 5.3). The $Ru_2Cl_4(DPPB)_2(NH_3)$ complex was also observed in the two-phase system (NH_4Cl in aqueous NaOH and $CDCl_3$) used to produce *trans*-$RuCl_2(DPPB)(NH_3)_2$ in situ (Section 5.5.1). Thus, if a $RuCl_2(DPPB)(PPh_3)$ solution was

transferred onto a solution of NH_4Cl in aqueous NaOH and a $^{31}P\{^1H\}$ NMR spectrum recorded without mixing the sample, the two AB quartets corresponding to the complex $Ru_2Cl_4(DPPB)_2(NH_3)$ were observed. Also, observed were signals for free PPh_3, $RuCl_2(DPPB)(PPh_3)$, and $Ru_2Cl_4(DPPB)_2$ produced by phosphine dissociation and dimerization processes.

On one occasion, stirring the two phase mixture for 1 day before recording a $^{31}P\{^1H\}$ NMR spectrum resulted in observation of two different AB quartets (second NH_3 entry in Table 5.3). The two AB quartets again suggest a dinuclear formulation (possible structures are shown in Figure 5.16) perhaps with two coordinated NH_3 ligands (i.e., $Ru_2Cl_4(DPPB)_2(NH_3)_2$). The dinuclear species would have to be doubly-chloro bridged (edge sharing), as opposed to the first two entries in Table 5.3 which are triply-chloro bridged (face sharing).
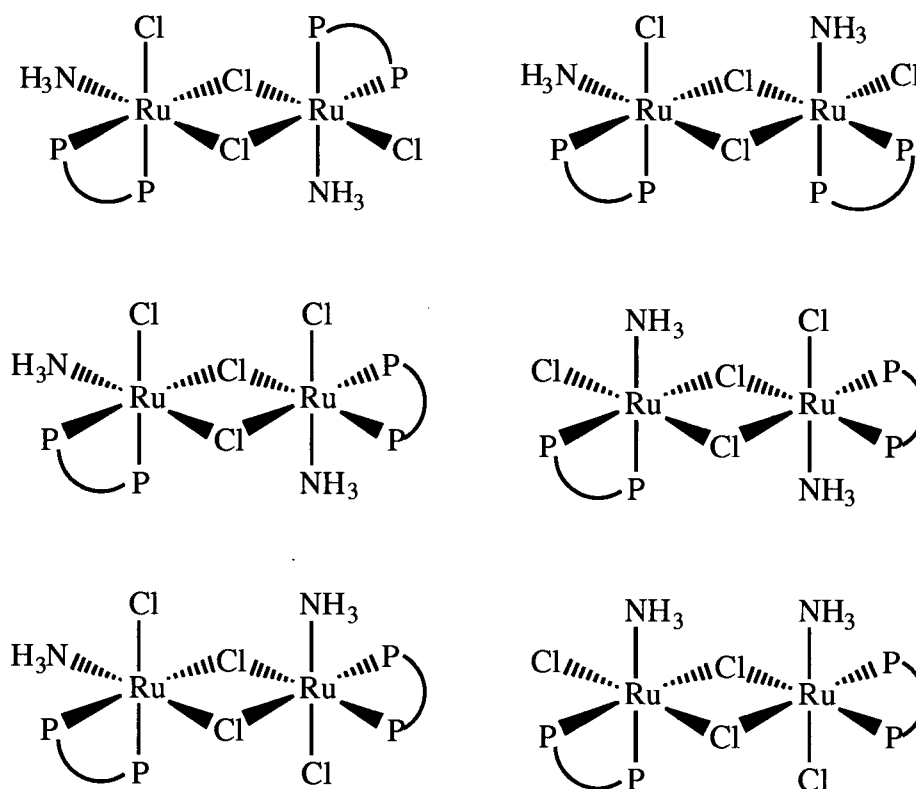
Figure 5.16 Possible doubly-chloro bridged (edge sharing) structures of the formulation $Ru_2Cl_4(DPPB)_2(NH_3)_2$ which would exhibit two AB patterns in the $^{31}P\{^1H\}$ NMR spectrum, where P–P = $Ph_2P(CH_2)_4PPh_2$.

The $^2J_{PP}$ coupling constants observed for the three entries in Table 5.3 give further support for the first two entries being triply-chloro bridged diruthenium complexes of the type (L)(DPPB)Ru(μ-Cl)$_3$RuCl(DPPB). One coupling constant of the pair observed is ~ 43 Hz which is in the range observed for the Cl-end of these dinuclear complexes (see Section 3.5 and 5.2.3).

5.6   Summary

The complex RuCl$_2$(DPPB)(PPh$_3$) reacts with an excess of the nitrogen-containing ligands. NH$_3$, py, bipy, and phen to give species of the formulation RuCl$_2$(DPPB)(L)$_2$. These complexes have been characterized in solution by UV-visible and NMR spectroscopy, as well as by conductivity. The monodentate nitrogen ligands py and NH$_3$ gave products of the *trans*-RuCl$_2$(DPPB)(L)$_2$ geometry, while the bidentate ligands bipy and phen gave both *cis*- and *trans*-RuCl$_2$(DPPB)(L)$_2$. The complex *cis*-RuCl$_2$(DPPB)(phen) was characterized in the solid state by X-ray crystallography. All of the above complexes can also be prepared from Ru$_2$Cl$_4$(DPPB)$_3$.

The addition of one equivalent of py to Ru$_2$Cl$_4$(DPPB)$_2$ produced the triply-chloro-bridged Ru$_2$Cl$_4$(DPPB)$_2$(py). The addition of further equivalents of pyridine cleaved the chloro-bridged dinuclear species to give *trans*-RuCl$_2$(DPPB)(py)$_2$.

5.7   References

(1)   Seddon, E. A.; Seddon, K. R. *The Chemistry of Ruthenium*; Elsevier: New York, 1984.

(2)   Gilbert, J. D.; Wilkinson, G. *J. Chem. Soc. (A)* **1969**, 1749.

(3)   Ruiz-Ramirez, L.; Stephenson, T. A.; Switkes, E. S. *J. Chem. Soc., Dalton Trans.* **1973**, 1770.

(4)   Batista, A. A.; Polato, E. A.; Queiroz, S. L.; Nascimento, O. R.; James, B. R.; Rettig, S. J. *Inorg. Chim. Acta* **1995**, *230*, 111.

(5)   Cenini, S.; Porta, F.; Pizzotti, M. *J. Mol. Catal.* **1982**, *15*, 297.

(6)   Joshi, A. M. Ph.D. Thesis, The University of British Columbia, 1990.

(7)   Fogg, D. Ph.D. Thesis, The University of British Columbia, 1994.

(8)   Fogg, D. E.; James, B. R. *Inorg. Chem.* **1995**, *34*, 2557.

(9)   Batista, A. A.; Queiroz, S. L.; Oliva, G.; Santos, R. H. A.; Gambardella, M. T. do. P. 5th Int. Conf. Chemistry of Platinum Metals, St. Andrews, UK; 1993; Abstract A40.

(10)   Batista, A. A.; Queiroz, S. L.; Oliva, G.; Gambardella, M. T. do. P.; Santos, R. H. A., personal communication.

(11)   Geary, W. J. *Coord. Chem. Rev.* **1971**, *7*, 81.

(12)   Schutte, R. P., unpublished results.

(13)   Jessop, P. G.; Rettig, S. J.; Lee, C.-L.; James, B. R. *Inorg. Chem.* **1991**, *30*, 4617.

(14)   Dekleva, T. W. Ph.D. Thesis, The University of British Columbia, 1983.

(15)   Mudalige, D. C. Ph.D. Thesis, The University of British Columbia, 1994.

(16)   Joshi, A. M.; Thorburn, I. S.; Rettig, S. J.; James, B. R. *Inorg. Chim. Acta* **1992**, *198*, 283.

(17)   Dekleva, T. W.; Joshi, A. M.; Thorburn, I. S.; James, B. R.; Evans, S. V.; Trotter, J. *Isr. J. Chem.* **1990**, *30*, 343.

(18)   Thorburn, I. S.; Rettig, S. J.; James, B. R. *J. Organomet. Chem.* **1985**, *296*, 103.

CHAPTER 6

HOMOGENEOUS HYDROGENATION OF IMINES AND NITRILES USING RUTHENIUM(II) PHOSPHINE COMPLEXES

6.1 Introduction

6.1.1 Homogeneous Hydrogenation of Imines

Until recently, the homogeneous hydrogenation of imines has received relatively little attention.[1] The reduction of carbon-carbon and carbon-oxygen double bonds has received much more attention and, consequently, excellent results in terms of both catalytic activity and asymmetric induction have been achieved.[2-4]

The preparation of chiral amines is synthetically useful, as many natural products contain these groups.[5] A precursor to the grass herbicide Metolachlor® (Figure 6.1), currently sold as a racemate, is a chiral amine which can potentially be prepared by asymmetric hydrogenation of the appropriate precursor imine.[1] One enantiomer (the S-enantiomer) of Metolachlor® is known to be more active than the other; therefore, selective preparation of the more active enantiomer could allow for lower applications of herbicide to be used.[6] In fact, the R-enantiomer shows better antifungal activity than the S-enantiomer. It should be noted that Metolachlor has both a chiral centre (referred to above) and a chiral axis, which is less important in determining the biological activity of the four stereoisomers.[6]
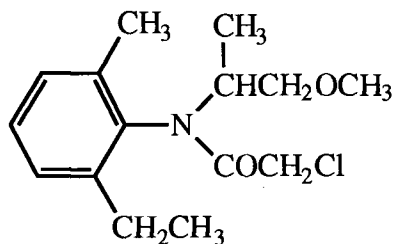
Figure 6.1   The structure of the grass herbicide Metolachlor®.

Following an early report of reduction of the carbon-nitrogen bond by a homogeneous Rh-DIOP catalytic system in 1975,[7] not much was reported until the late 1980s in this area of research. Recently, imines have been hydrogenated to the corresponding amines by homogeneous Rh,[2,8-12] Ir,[13-16] and Ru[17-19] systems. Wilkinson's Rh catalyst has also been used in the transfer hydrogenation of imines from 2-propanol in basic media.[20] Cyclic ketimines have been asymmetrically hydrogenated by a chiral titanocene catalyst to give chiral amines with excellent enantioselectivities.[5,21-24]

In terms of enantioselectivity, the rhodium phosphine systems have been the most successful, with e.e. values as high as 91% for acyclic ketimines.[1,8,10,11] The chiral titanocene system described above has been used to asymmetrically hydrogenate cyclic imines with e.e. values of up to 98%; unfortunately, these systems require high catalyst-to-substrate ratios (5 mol% catalyst) and, in some cases, high H_2 pressures (2000 psi).[5,21,22]

Burk et al. have found perhaps the most practical and useful catalytic synthesis of chiral primary amines to date.[23,25,26] This synthesis, however, is a three-step procedure referred to as reductive amination in which a prochiral ketone is converted to a functionalized imine (*N*-acylhydrazone derivative) in the first step. The second step is asymmetric hydrogenation using a Rh-chiral phosphine catalyst, followed in the third step by N–N bond cleavage of the *N*-acylhydrazine product by SmI_2 to give the final chiral amine product (Figure 6.2).[1,25] Unfortunately, these catalytic systems are not nearly as effective for the direct hydrogenation of simple imines (i.e., those which do not contain a second functional group).[25] The carbonyl group of the *N*-acylhydrazone is thought to play a key role in the asymmetric hydrogenation, allowing chelation of the substrate to the transition metal catalyst, thereby limiting the degrees of freedom of the coordinated substrate, which presumably leads to higher enantiomeric excesses.[25]

Much of the asymmetric catalytic hydrogenation of imines discussed above is covered thoroughly by a recent review.[1]

Only recently have Ru-chiral phosphine systems been used effectively to catalyze the asymmetric hydrogenation of imines. A cyclic imine (a sultam precursor) has been hydrogenated under mild conditions (4 atm H_2, 22 °C) with 99% e.e. using a catalyst formulated as $Ru_2Cl_4(BINAP)_2(NEt_3)$.[19]
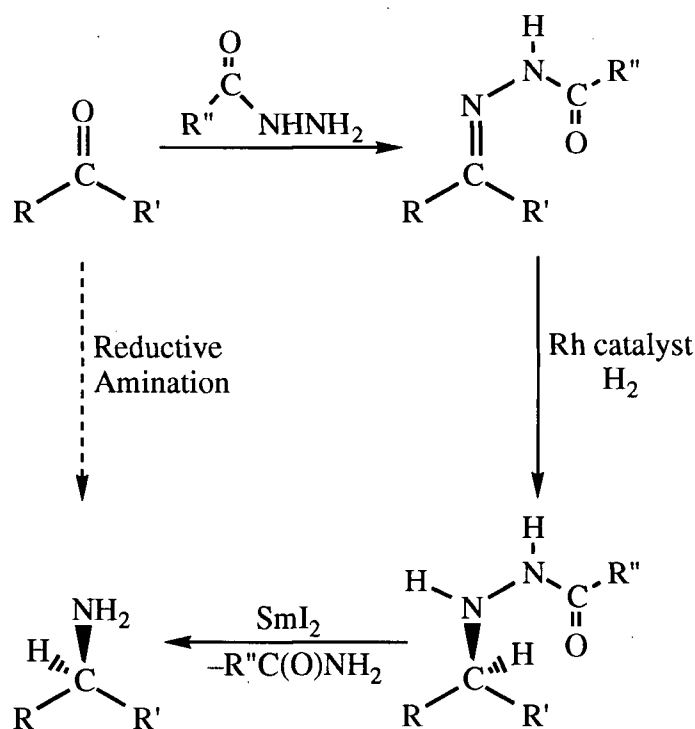
Figure 6.2   Reductive amination scheme to produce chiral amines from prochiral
ketones.

The *syn-anti* isomerization (Figure 6.3) of acyclic imines may in part be responsible for the inability to asymmetrically hydrogenate these substrates with high enantioselectivities.[1,21,24] General reviews for imines or Schiff bases discuss the *syn-anti* isomerization.[27,28] In terms of e.e. values, greater success in the reduction of cyclic imines has been suggested to be due to the fact that cyclic imines exist as a single isomer, while acyclic imines exist as an equilibrium mixture of *syn-* and *anti*-isomers which are

thought to be hydrogenated to the opposite enantiomers.[1,5,24] In fact, one report suggests that the measured enantiomeric excesses correlate roughly to the ratio of *anti* and *syn* imines.[24]
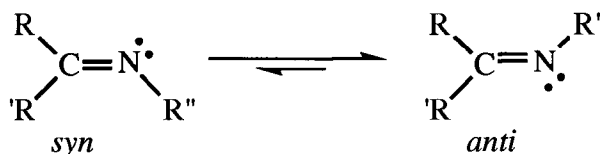
Figure 6.3   *syn-anti* Isomerization of imines (where R' is of higher priority than R).

6.1.2   Homogeneous Hydrogenation of Nitriles

The homogeneous hydrogenation of nitriles has likewise received little attention.[29] Nitrile hydrogenation is related to imine hydrogenation, as imines are produced as intermediates (eq 6.1).

$$RC\equiv N \xrightarrow{\text{H}_2} [R(H)C=NH] \xrightarrow{\text{H}_2} RCH_2NH_2 \tag{6.1}$$
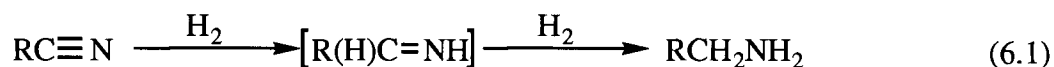
Unfortunately, the catalytic hydrogenation of nitriles often produces products which are not simply primary amines (eq 6.1), but which may be mixtures that include secondary and tertiary amines.[29-31] The secondary amine is formed because of an addition of the primary amine product to the intermediate aldimine formed in the initial step (eq 6.2).

$$RCH_2NH_2 + [R(H)C=NH] \xrightarrow{-\text{NH}_3} RCH_2N=CHR \xrightarrow{\text{H}_2} (RCH_2)_2NH \tag{6.2}$$

Most of the research on the hydrogenation of nitriles has been done using heterogeneous catalysts of the transition metals Co, Ni, and Fe.[31,32] For these heterogeneous catalytic systems, the addition of NH_3 to the nitrile hydrogenation system

253

often allows for selective production of primary amines, while the addition of primary and secondary amines yields the corresponding secondary and tertiary amines.[33]

A supported-Rh catalytic system anchored on polystyrene beads has been used in the hydrogenation of benzonitrile (1000 psi H_2, 100 °C) to give reduced products other than benzylamine (i.e., $PhCH_2N=C(H)Ph$ and $PhCH_2NHC(NH)Ph$).[34]

There have been a few reports, outside of work from the James group, of homogeneous hydrogenation of nitriles using Ir,[32] Rh,[35] Pd,[36] and Ru.[37] For example, with a Pd(II) catalytic system, benzonitrile is reduced to a mixture of dibenzylamine (90%) and benzylamine (10%).[36] Work on nitrile hydrogenation using ruthenium systems began in this laboratory upon observation of the reduction of acetonitrile ligands to ethylamine ligands (eq 6.3).[29,38] Subsequent studies showed the Ru(II) complex to be effective for the hydrogenation of CH_3CN and imine substrates under mild conditions (50 °C, 1 atm total pressure in DMA).[29,38]

$$[RuCl(DPPB)(CH_3CN)_3]^+ + 7H_2 \xrightarrow{\text{base}} [Ru(H)(DPPB)(CH_3CH_2NH_2)_3]^+ + base\cdot HCl \quad (6.3)$$
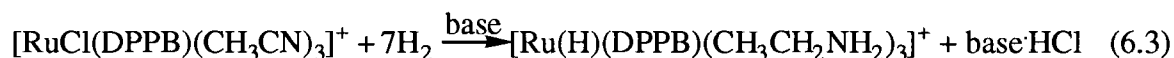
Subsequently, other Ru complexes, including the dinuclear $Ru_2Cl_4(DPPB)_2$ **24** and the triruthenium species $[Ru(H)Cl(DPPB)]_3$ **42**, were found to be effective catalysts in the hydrogenation of nitriles.[29]

It has been suggested that the difficulty in reducing nitriles may be because (a) nitriles coordinate through the nitrogen atom (but not through the π-system, usually thought necessary for a catalytic hydrogenation) and (b) the amine products may coordinate to the transition metal and "tie up" the catalyst.[32] Analogous arguments have been offered for difficulties in hydrogenating imines.[1]

6.2 H₂ Hydrogenation Catalyzed by Ruthenium(II) Diphosphine-Containing Complexes

In this thesis work, there was interest in examining ruthenium complexes containing a single chelating diphosphine per ruthenium. Previous studies by this research group and others have identified "Ru(P–P)" species as the active catalyst.[39-42] In all of the studies listed above,[40-42] the catalyst precursors contained two chelating diphosphines per ruthenium atom, but the active catalytic species in solution was shown to contain a single diphosphine.

Following on from these studies, "Ru(P–P)" species were prepared and studied in this laboratory as potential catalysts for the H₂-reduction of a variety of substrates.[43] For example, prochiral functionalized olefins (e.g., (Z)-α-acetamidocinnamic acid) were hydrogenated to 97% e.e using Ru₂Cl₄(CHIRAPHOS)₂ as the catalyst.[44,45] In related non-chiral systems, detailed kinetic and mechanistic study on styrene hydrogenation with Ru₂Cl₄(DPPB)₂ **24** has been performed.[46] Complex **24** also catalyzes the transfer hydrogenation (from 2-propanol) of acetophenone[47,48] and the H₂ hydrogenation of imines.[17,18]

6.2.1 Benzonitrile Hydrogenation Catalyzed by [Ru(H)Cl(DPPB)]₃ 42 (and Observations on Catalytic Hydrogenation of Styrene)

Preliminary experiments at atmospheric H₂ pressures by Drs. Joshi and Frediani of this laboratory showed the triruthenium species to be an effective catalyst for the hydrogenation of MeCN and PhCN.[29,30] Therefore, the hydrogenation of PhCN was monitored using a constant-pressure gas-uptake apparatus (Section 2.3.1). Convenient reaction rates were observed when the reaction was performed in DMA at 70 °C.

The solvent DMA is convenient for gas-uptake measurements because it has a low vapour pressure (23 torr at 70 °C).[49] Previous workers in this laboratory[50-55] have measured the solubility of hydrogen in this solvent over the temperature range of 15–80 °C and hydrogen pressures of 100–800 torr. The data have been collected by Joshi[48]

and shown to obey Henry's law over the temperature range and H_2 pressures stated above. The Henry's law constants K_H obtained represent an equilibrium constant for the dissolution of H_2 in DMA. Finally, a van't Hoff plot (ln K_H vs. 1/temperature) was linear, with a slope of -655 K and a y-intercept of -10.8.[48] These values can be used to calculate the H_2-solubility in DMA in the temperature range 15–80 °C.

6.2.1.1 Rate Measurements

Typical plots of H_2 uptake against time in DMA solvent for the hydrogenation of PhCN are shown in Figure 6.4. The uptake plots were S-shaped at lower [PhCN] (20 mM), and showed an "induction period" of 600–1200 s resulting from the time taken for the catalyst [Ru(H)Cl(DPPB)]$_3$ **42** to dissolve in DMA. The plot levels off at the 2:1 mole ratio of H_2:PhCN, consistent with formation of $PhCH_2NH_2$ (see below).

The shape of the uptake curve (Figure 6.4) was seen to be very different at low (20 mM) and high (192 mM) initial concentrations of PhCN, and under otherwise identical conditions. Studies were undertaken to determine the dependence of the maximum rates on the total ruthenium trimer concentration [Ru$_3$]$_T$, the initial benzonitrile concentration, and the hydrogen concentration at 70 °C. The rate data for the hydrogenation of PhCN in DMA at 70 °C are summarized in Table 6.1.

The ruthenium dependence of the hydrogenation rates was studied at an initial substrate concentration ([PhCN] = 20 mM), at H_2-pressures of 800 torr ([H_2] = 2.39 mM), and with the total ruthenium concentration ([Ru$_3$]$_T$) ranging from 0.26 to 1.4 mM. Individual rate plots are shown in Figure 6.5 (a). The plot of maximum rate against [Ru$_3$]$_T$ is shown in Figure 6.5 (b) and is linear, implying a first-order dependence on [Ru$_3$]$_T$ for the hydrogenation rate. The low PhCN concentration (20 mM) H_2 plot shows a long linear region (Figure 6.4), indicating a zero-order dependence on [PhCN]; therefore, a point which is at half the nitrile concentration (Table 6.1, entry 4) is included in Figure 6.5 (b). The fact that the rate of hydrogenation is zero-order in [PhCN], at least at low concentrations, should allow the use of this point in the metal dependence.

Chapter 6 References: p 271

(a)

Time (s)

(b)

Time (s)
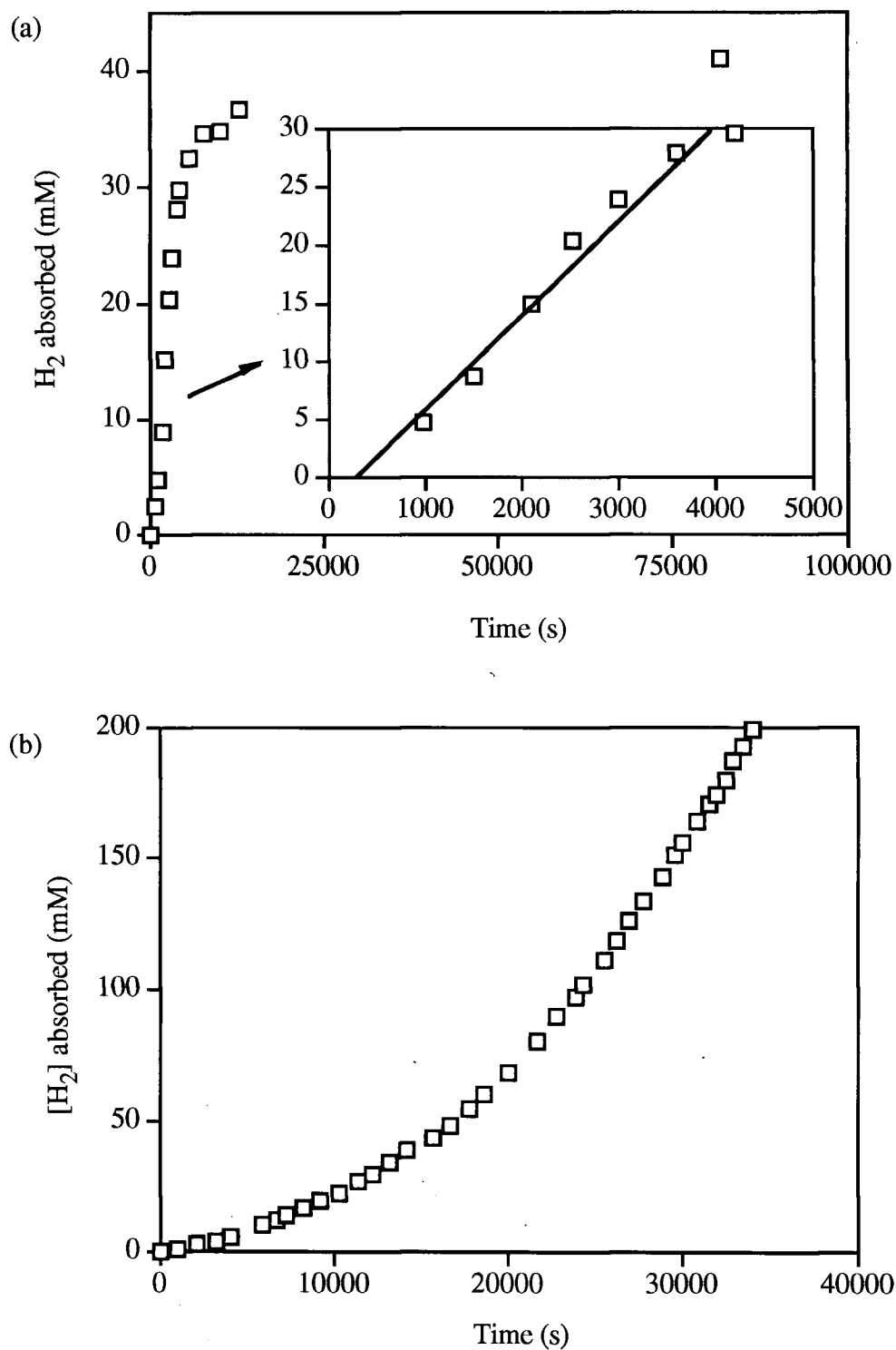
Figure 6.4   Typical H_2-uptake plots for the hydrogenation of PhCN catalyzed by [Ru(H)Cl(DPPB)]$_3$ **42** in DMA (5 mL) at 70 °C and 800 torr pressure of H_2, [Ru$_3$]$_T$ = (a) 0.80 mM and (b) 1.03 mM, [H_2] = 2.39 mM, [PhCN] = (a) 20 mM and (b) 192 mM. Inset of (a) shows initial linear portion.

257

Table 6.1   Rate Data for the Hydrogenation of PhCN Using [Ru(H)Cl(DPPB)]$_3$ **42** as the Catalyst

Entry	[Ru$_3$]$_T$ (mM)	[PhCN] (mM)	P(H$_2$)$^{(a)}$ (torr)	[H$_2$] (mM)	Max. Rate x 10^6 (M s^{-1})$^{(b)}$
1	1.03	192	800	2.39	----[c]
2	1.39	20	800	2.39	16.9
3	0.80	20	800	2.39	9.20
4	0.68	10	800	2.39	8.48
5	0.26	20	800	2.39	4.36
6	0.80	20	800	2.39	4.48
7	0.80	20	800	2.39	6.28[d]
8	0.80	20	800	2.39	4.44[d]
9	0.80	20	765	2.29	4.80[e]
10	0.80	20	703	2.10	3.98
11	0.80	20	580	1.74	38.0[f]
12	0.80	20	580	1.74	3.58
13	0.80	20	580	1.74	2.61
14	0.80	20	483	1.45	7.62
15	0.80	20	378	1.13	5.31

(a)   The vapour pressure of DMA at 70 °C is 23 torr.[49]

(b)   Error in rate values is estimated at ca. ± 5%.

(c)   Rate not included, as under these conditions the products are different (see text).

(d)   DMA solvent distilled from Ru(H)Cl(PPh$_3$)$_3$·DMA solvate prior to use.

(e)   Projector lamp was shone on the uptake flask to test for possible photochemical effects.

(f)   Very much faster than other rate data; a leak was suspected in the uptake apparatus, however, the gas uptake stopped at exactly 2 mole equivalents of H$_2$ per PhCN.
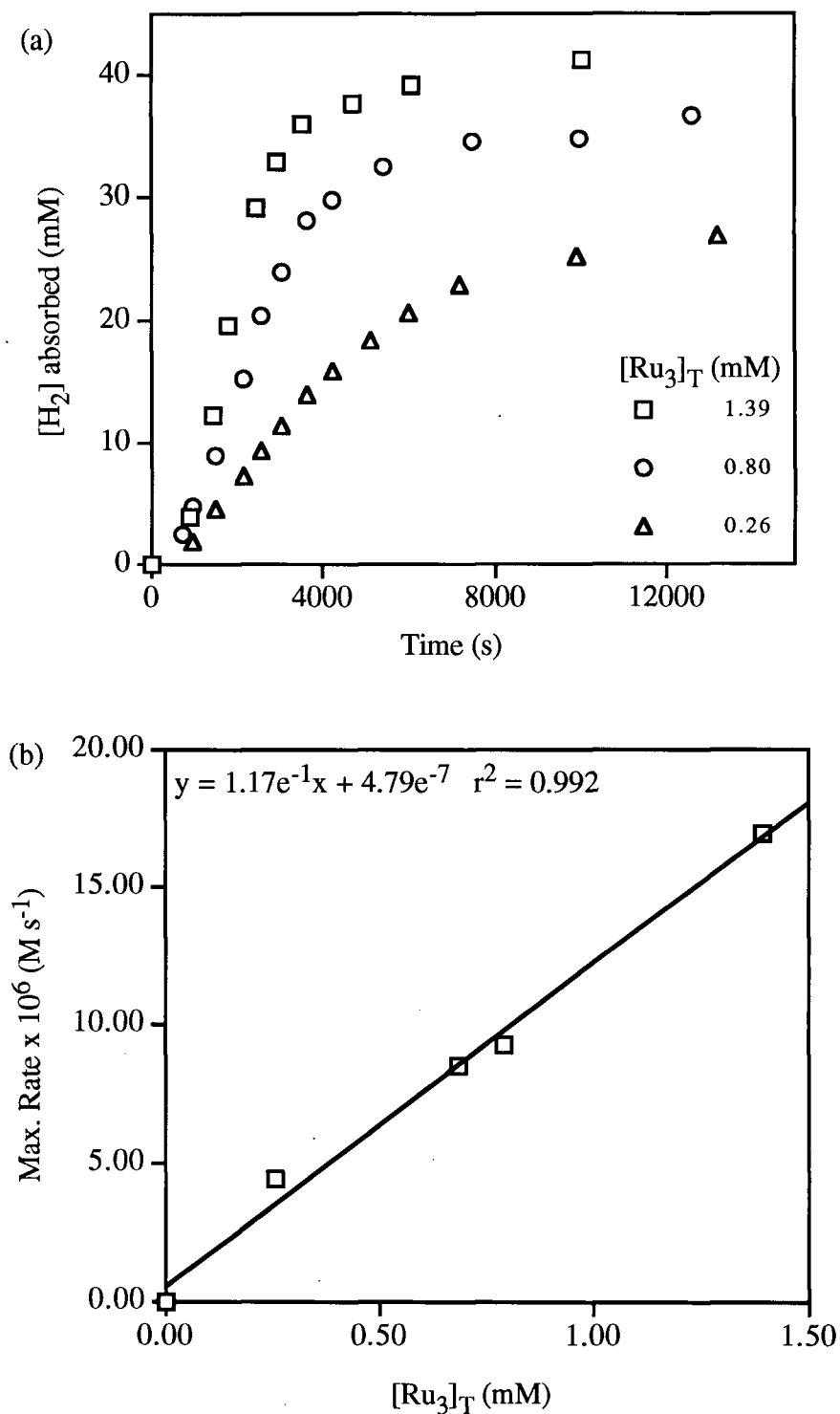
Figure 6.5   (a) Rate plots for PhCN hydrogenation catalyzed by **42** in DMA at 70 °C at various [Ru₃]ᴛ. [PhCN] = 20 mM, [H₂] = 2.39 mM. (b) Dependence of the maximum hydrogenation rate on [Ru₃]ᴛ; data from (a) plus one point (Table 6.1, entry 4) at half the [PhCN] (i.e., 10 mM).

An attempt to elucidate the PhCN dependence is complicated by the fact that different products are obtained at low (20 mM) and high (0.19–2.0 M) initial [PhCN]. Under the low [PhCN] used in this thesis work, the sole product identified by gas chromatography (Section 2.4.1) was the primary amine PhCH₂NH₂ (eq 6.1). This is in agreement with the final 2:1 H₂-uptake:PhCN stoichiometry data (see Figure 6.4(a)).

Previous workers in this laboratory also performed the benzonitrile hydrogenation under higher H_2 pressures and higher temperatures, and always at high initial [PhCN].[29,30] The product(s) formed were then secondary amine and the "coupled" imine; for example, at 110 atm H_2 and 100 °C, 85% of the PhCN was converted to $(PhCH_2)_2NH$ and $PhCH_2N=C(H)Ph$ in a 7:1 ratio (eq 6.2).

Unfortunately, inconsistent results were obtained when attempts were made to measure the [H_2] dependence (entries 3, 7–15; Table 6.1). Figure 6.6 show the large degree of scatter in the rate data. Irreproducible uptake rates have been encountered previously by this research group when DMA has been used as the solvent,[56] and similar problems have been encountered very recently in the measurement of hydrogenation rates of the imine $PhCH_2N=C(H)Ph$ as catalyzed by $Ru_2Cl_5(DPPB)_2$ in DMA.[57] Interestingly, no such problems were observed for the hydrogenation of styrene in DMA using $Ru_2Cl_5(DPPB)_2$ or $Ru_2Cl_4(DPPB)_2$ as the catalyst.[46,57]

A number of possible sources of the irreproducible results were investigated. The catalyst [Ru(H)Cl(DPPB)]₃ was changed to a new batch, the solvent DMA was distilled from Ru(H)Cl(PPh₃)₃·DMA immediately prior to use (entries 7 and 8, Table 6.1), the substrate benzonitrile was changed to a new batch (re-distilled), the uptake flask was switched, and a projector lamp was used to check for photochemical effects. The purification of DMA by distilling the solvent from the complex Ru(H)Cl(PPh₃)₃·DMA immediately prior to use has proven in the past to be effective,[56] the complex probably removing trace oxygen-containing contaminants such as hydroperoxides or peroxides. However, in this thesis work and other studies,[57] this purification procedure has not

260

alleviated the problem. In fact, none of the measures stated above resulted in the rates becoming reproducible.

It is difficult to evaluate the $[H_2]$ dependence, considering the wide scatter observed; however, considering only the three initial maximum rate data recorded (entries 3, 14, and 15 of Table 6.1 and the dashed line of Figure 6.6), the dependence seems to be first-order at low $[H_2]$, decreasing to somewhat less then first-order at higher $[H_2]$.
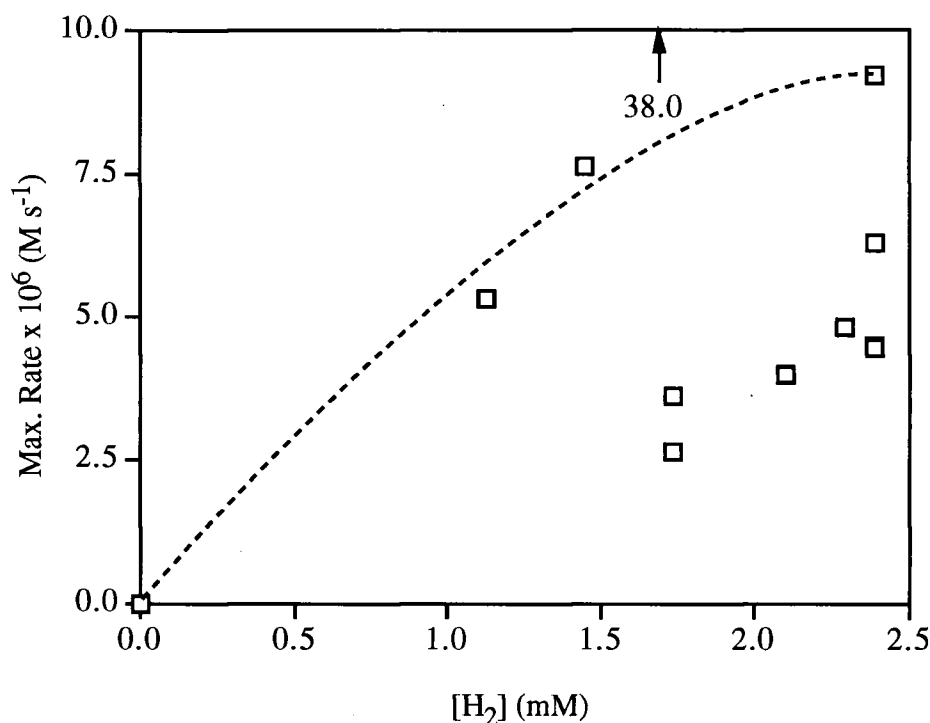
Figure 6.6   Dependence of the maximum hydrogenation rate on $[H_2]$ at 70 °C; $[Ru_3]_T = 0.80$ mM, [PhCN] = 20 mM. Entry 11 from Table 6.1 gives a much faster rate than the other entries, and is indicated by an arrow.

Ashby and Halpern have reported similar reproducibility problems for the hydrogenation of α,β-unsaturated carboxylic acids with [Ru(BINAP)(O$_2$CR)$_2$] catalysts in methanol.[58] The source of the problem was traced to the presence of a strong acid, which inhibited the hydrogenation severely, even in small amounts. The reproducibility

problems were alleviated by either treating the Pyrex glass with chlorotrimethylsilane prior to use, or by using quartz vessels.[58] Pyrex and other borasilicate glasses have been reported to react with methanol to give methylborates, which may act as Lewis acids.[58]

The hydrogenation of benzonitrile was not investigated in quartz uptake flasks in this thesis work, but should be investigated in the future. Other workers in this group are currently investigating the effect of using quartz vessels on the imine hydrogenation in DMA solvent. However, in view of Ashby and Halpern's work in tracing the reproducibility problem in their system to acidic sites in the glassware, it would seem somewhat unlikely that in the basic solvent DMA, the presence of small amounts of acid should effect the catalysis. Also, the product amines of the benzonitrile hydrogenation are themselves basic, and would be expected to neutralize any acid present.

Spectroscopically, $[Ru(H)Cl(DPPB)]_3$ **42** has been shown to react with H_2 and PhCN to form complexes of the type $[(L)(DPPB)Ru(\mu-H)(\mu-Cl)_2Ru(H)(DPPB)]$, where L = η^2-H_2 or PhCN (Figure 6.7).[29,30] The $^{31}P\{^1H\}$ NMR spectrum recorded for a sample of **42** with 3 equivalents of added PhCN shows two AB patterns, consistent with the dinuclear structure shown in Figure 6.7, while the ^1H NMR spectrum shows resonances for both a terminal and bridging hydride.[29] NMR spectroscopy showed no change in the spectrum of a C_6D_6 solution of **42** (~ 15 mg, 8.9 μmol) on addition of ~10 equivalents of DMA (10 μL, 0.11 mmol). The dinuclear species $Ru_2Cl_4(DPPB)_2$, on the other hand, is known to coordinate DMA and form $(DMA)(DPPB)Ru(\mu-Cl)_3RuCl(DPPB)$.[39,46]
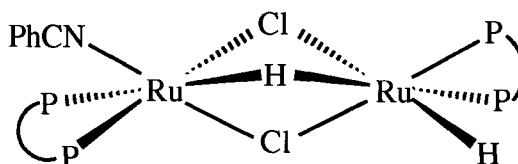
Figure 6.7   The structure of the dinuclear product produced on addition of PhCN to a C_6D_6 solution of $[Ru(H)Cl(DPPB)]_3$ **42**, where P–P = DPPB.

[Ru(H)Cl(DPPB)]$_3$ (15.6 mg, 9.21 µmol) reacted with an excess of styrene (10 µL, 87 µmol) in C$_6$D$_6$ to give, after nine days at room temperature, ethylbenzene and hydride-containing dinuclear species as judged by ^{1}H and ^{31}P{^{1}H} NMR spectroscopy. The ^{1}H NMR spectrum showed upfield resonances at –18.5 ppm (t, $^2J_{HP}$ = 33.6 Hz), –19.9 ppm (t, $^2J_{HP}$ = 33.0 Hz), and –21.6 ppm (t, $^2J_{HP}$ = 32.3 Hz), indicating classical hydrides *cis* to two equivalent phosphorus atoms plus an additional broad resonance at –19.7, possibly indicating a bridging hydride. Three of the four hydride resonances were of approximately the same integral intensity, while the fourth resonance at –19.9 ppm was about one third of the integral intensity. Ethylbenzene was evident as a triplet at 1.05 ppm (*J* = 7.5 Hz, –CH$_2$C*H*$_3$) and a quartet at 2.45 ppm (*J* = 7.5 Hz, –C*H*$_2$CH$_3$). The spectrum also showed remaining excess styrene. The exact degree of conversion of styrene to ethylbenzene is impossible to calculate because of overlap between the methylene protons of the DPPB ligand and the ethyl hydrogens of ethylbenzene. However, the conversion must certainly be less then one mole of styrene per **42**, as hydride-containing complexes remain, and no other source of H$_2$ is present.

The ^{31}P{^{1}H} NMR spectrum showed resonances indicating the presence of two main species. The first is observed as a singlet at 55.4 ppm, while the other is observed as two AB quartets (δ_A = 55.5, δ_B = 54.4, $^2J_{AB}$ = 40.2 Hz; δ_C = 52.8, δ_D = 51.8, $^2J_{CD}$ = 39.1 Hz).

From the above NMR spectroscopic data, the exact nature of the ruthenium products cannot be determined. However, one of the two species is certainly dinuclear, as indicated by the two AB quartets observed in the ^{31}P{^{1}H} NMR spectrum, and both Ru products are sure to contain hydrides, as evidenced by the many upfield resonances in the ^{1}H NMR spectrum.

A single uptake experiment showed the hydrogenation rate of styrene, as catalyzed by [Ru(H)Cl(DPPB)]$_3$ at 70 °C in DMA (under conditions comparable to the PhCN hydrogenation described above), to be very fast. The hydrogenation was performed

at [styrene] = 17.4 mM, $[Ru_3]_T$ = 1.10 mM, and $[H_2]$ = 2.33 mM in DMA (5.0 mL), and one mole equivalent of H_2 was absorbed in less than five minutes. The maximum rate determined from this single run was 9.6 x 10^{-5} M s^{-1}. This value is approximately ten times faster than the hydrogenation of benzonitrile under comparable conditions, and is approximately the same as the rate reported for the hydrogenation of styrene catalyzed by $Ru_2Cl_4(DPPB)_2$ **24** at 30 °C in DMA.[46] When the above concentration values for H_2, Ru (twice the monomer concentration was used to allow comparison to the dinuclear catalyst), and styrene are plugged into the reported rate equation,[30] the rate is calculated to be 5.5 x 10^{-5} M s^{-1}.

6.2.2 H_2 Hydrogenation of Imines at High Pressure

The hydrogenations of the imines PhCH$_2$N=C(H)Ph and PhN=C(H)Ph were investigated under conditions developed by Fogg et al.[17] It was considered useful to employ the same conditions of H_2 pressure, solvent, temperature, and substrate-to-catalyst ratio, so as to allow for comparison of the catalytic activity of various species. Conversions of imine substrate to product amine were examined by ^{1}H NMR spectroscopy, as described in Section 2.4. Table 6.2 compares the ability of various catalysts to hydrogenate PhCH$_2$N=C(H)Ph.

Although the data determined are somewhat limited in terms of the conditions used and the variety of imine substrates used, some interesting conclusions can be drawn. The activities of the potential catalysts are compared with that of the most effective Ru species found to date, namely $Ru_2Cl_5(DPPB)_2$ **22** (Table 6.2, entry 1).[17,18] Complex **22** is thought to generate $Ru_2Cl_4(DPPB)_2$ **24** under the catalytic conditions used,[17,18] and the somewhat lower activity of **24** compared to **22** is attributed to the air-sensitivity of solid **24**.

Table 6.2   Conversion Data for High-Pressure Hydrogenation of PhCH$_2$N=C(H)Ph
Using a Variety of Catalyst Precursors [a]

Entry	Catalyst	Conversion (%) [b]
1	Ru$_2$Cl$_5$(DPPB)$_2$ **22** [c]	98
2	Ru$_2$Cl$_4$(DPPB)$_2$ **24** [c], [d]	89
3	Ru$_2$Br$_4$(DPPB)$_2$ **25**	66
4	Ru$_2$Cl$_4$(DPPB)$_3$ **19** [c]	10
5	Ru$_2$Br$_4$(DPPB)$_3$ **20**	10
6	Ru$_2$Cl$_4$(DCYPB)$_3$ **21**	0
7	Ru$_2$Cl$_4$(DPPB)$_2$(DMSO) **33**	1
8	[Ru(H)Cl(DPPB)]$_3$ **42**	63
9	RuCl$_2$(DPPB)(PPh$_3$) **11**	15
10	RuCl$_2$(DPPB)(P(p-tolyl)$_3$) **12**	26
11	RuBr$_2$(DPPB)(PPh$_3$) **13**	12
12	*trans*-RuCl$_2$(DPPB)(py)$_2$ **43**	69
13	RuCl$_2$(DPPB)(bipy) **44**	3
14	RuCl$_2$(DPPB)(phen) **45**	15
15	RuCl$_2$(DPPB)(PN$_1$) [e]	32
16	[RuCl(DPPB)(PN$_2$)]$^+$Cl$^-$ [e]	5
17	Ru(DPPB)(η^3-Me-allyl)$_2$ **55**	0
18	Blank	0

(a)   Conditions: 1000 psi H$_2$, MeOH (10 mL), 0.77 mM Ru, [imine] = 0.153 M, room
temperature (~ 20 °C).

(b)   Conversion after 1 h.

(c)   Reported by Fogg[18] and repeated in this work for comparison purposes.

(d)   Reported by Fogg as 87%.[18]

(e)   A sample of the catalyst was kindly made available by Mr. R. Schutte of this
laboratory; PN$_1$ = diphenyl(2-pyridyl)phosphine, PN$_2$ = phenylbis(2-pyridyl)-
phosphine.

Chapter 6 References: p 271

The effect of substituting Br for Cl was examined by comparison of the activities of **24** and Ru$_2$Br$_4$(DPPB)$_2$ **25** (Table 6.2, entries 2 and 3, and Figure 6.8). The activity was found to be lower for the bromo analogue. This is consistent with the previous observation of lower catalytic activity when iodide is added to some in situ chloro-Rh(I)-catalyzed imine hydrogenations.[8] However, although the catalytic activity decreased with added KI, the optical activity increased when the substrate was the prochiral ketimine PhCH$_2$N=C(CH$_3$)Ph or some related *ortho-* and *para*-methoxy substituted ketimines (where the Ph substituted is that originally derived from the ketone).[8] An isolated iodo-Rh catalyst, [Rh(CHIRAPHOS)I]$_2$, also shows increased optical yields over its chloro-analogue.[8] Interestingly, the substrate PhN=C(H)Ph was hydrogenated more effectively by Ru$_2$Br$_4$(DPPB)$_2$ **25** (74%) and RuBr$_2$(DPPB)(PPh$_3$) **13** (99%) than by Ru$_2$Cl$_5$(DPPB)$_2$ **22** (24%) under identical conditions (see Table 6.4 below). Therefore, it is necessary to match a particular catalyst with a particular substrate to obtain maximum activity.

The data for Ru$_2$Cl$_4$(DPPB)$_2$ **24** in Table 6.2 (89%) are somewhat different from the 1 h data point in Figure 6.8 (77%). However, these values are considered to be in reasonable agreement, considering the slightly differing conditions used. One value was obtained from a sealed autoclave, while the other value was obtained from a sampling autoclave which required the stirring to be stopped during sampling, and which allowed the pressure to momentarily decrease. Also, both experiments were performed at room temperature, which may differ by a few degrees Celsius. The autoclave with sampling capabilities was acquired toward the end of this work, and therefore only a couple of representative plots are shown in Figure 6.8.
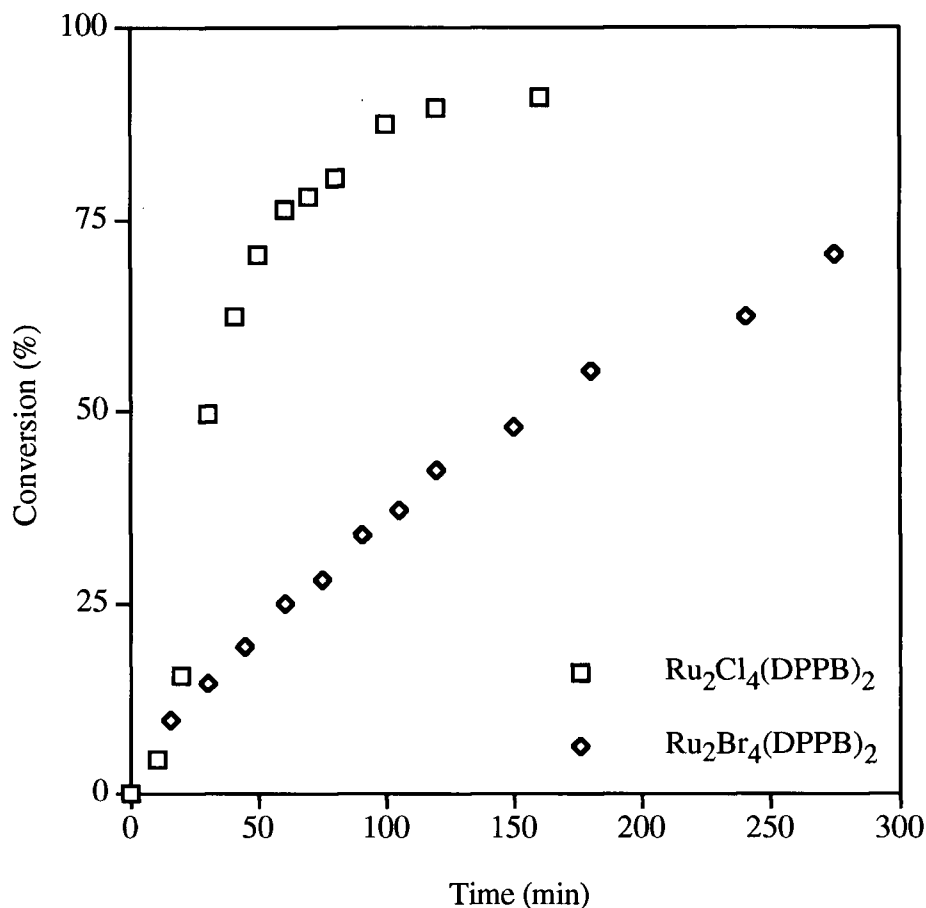
Figure 6.8   Conversion of the imine PhCH$_2$N=C(H)Ph to dibenzylamine using Ru$_2$Cl$_4$(DPPB)$_2$ **24** or Ru$_2$Br$_4$(DPPB)$_2$ **25** as the catalysts. Performed using an autoclave with sampling capabilities (Section 2.3.2) at 1000 psi H$_2$, 22 °C, MeOH (20 mL), 0.77 mM Ru monomer, [imine] = 0.153 M.

The bromo analogue **25** gave considerably lower conversions in the sampling autoclave (25.1% after 1 h) than in the sealed autoclave (66%, Table 6.2). This may be due to differences in the set-up of the two autoclaves (Section 2.3.2). The sampling autoclave could not be as rigorously deoxygenated as the sealed autoclave due to the design of the apparatus; for example, the sealed autoclave could be evacuated, while the sampling autoclave could only be purged 3–4 times with hydrogen. Evacuation was not attempted because the volume of solution necessary to allow sampling (20 mL) was very close to the top of the glass liner, and this would have caused the solution to splash out of

Chapter 6 References: p 271

the liner during evacuation. The problems with oxygen contamination have been noted previously (Section 2.3.2). The data obtained using the sampling autoclave are given in Figure 6.8, and even though the conversions may be lower than if the autoclave were deoxygenated more rigorously, at least the data show the approximate relative reactivities of the chloro **24** and bromo **25** catalysts.

The long, approximately linear portions of the curves in Figure 6.8 perhaps indicate a zero-order dependence on imine concentration.

The inactivity of Ru(DPPB)(η^3-Me-allyl)$_2$ **55** for the hydrogenation of PhCH$_2$N=C(H)Ph (Table 6.2) shows the important requirement of the presence of halide ligands. The effect on hydrogenation rates on incorporating N-donor ligands into Ru(II)-diphosphine complexes was examined. Complex **43**, *trans*-RuCl$_2$(DPPB)(py)$_2$, was a moderately effective catalyst, while the corresponding complexes **44** and **45** containing the chelating bipy and phen ligands were less effective. All three complexes (**43**, **44**, and **45**) dissociate chloride in MeOH (see Chapter 5), thus creating a vacant coordination site for possible subsequent binding of imine substrate or H$_2$. Kinetic studies by Fogg et al. on the hydrogenation of the imines RN=C(H)Ph (R = Ph or CH$_2$Ph) catalyzed by Ru$_2$Cl$_5$(DPPB)$_2$ are consistent with an unsaturate route, in which a species with coordinated imine reacts with H$_2$ in a rate-determining step.[17,18] Other complexes containing (2-pyridyl)phosphine ligands showed low to moderate catalytic activity (Table 6.2). These species were viewed as potentially good catalytic species, as the (2-pyridyl)phosphines have a number of coordination modes available, ranging from monodentate to tridentate within Ru complexes.[59,60]

The diruthenium complex Ru$_2$Cl$_4$(DPPB)$_2$(DMSO) **33** was ineffective for the hydrogenation of PhCH$_2$N=C(H)Ph, perhaps because of the strong binding of DMSO to the Ru centre, which thereby does not allow the coordination of the substrate. Dimethyl sulfoxide was found by ^{31}P{^{1}H} NMR spectroscopy to remain bound to the Ru centre in solutions of **33**,[39] while dissolution of other complexes Ru$_2$Cl$_4$(DPPB)$_2$(L), for example,

where L is a ketone, produced some catalytically active $Ru_2Cl_4(DPPB)_2$ **24** species[39] (see Chapter 3). Fogg et al. reported $Ru_2Cl_4(DPPB)_2(NH(CH_2Ph)_2)$ to be ineffective under identical conditions.[18]

Finally, the five-coordinate mixed-phosphine complexes (Table 6.2, entries 9–11) and bridged-phosphine complexes (Table 6.2, entries 4–6) have low to moderate conversions. The low activity observed for the phosphine-bridged complexes **19, 20**, and **21** may be due to the low solubility of these complexes. In fact, almost all of the complexes examined, except for the N-ligand-containing complexes, have very low solubility in MeOH. However, most of the species dissolve in MeOH after stirring under high pressures (1000 psi) of H_2. For example, after 1 h under high pressure of H_2, the red solid $Ru_2Cl_5(DPPB)_2$ dissolved in MeOH to give a yellow solution.

The mixed-phosphine species $RuX_2(DPPB)(PAr_3)$, which dissociates in solution to give $Ru_2X_4(DPPB)_2$ complexes (although this has not been established in MeOH), possibly show relatively low catalytic activity that is governed by the degree of dissociation into the active dinuclear species (but see results of the hydrogenation of the aldimine $PhN=C(H)Ph$ below). Fogg et al. have observed similarly low conversions for the hydrogenation of $PhCH_2N=C(Me)Ph$ when $RuCl_2(P-P)(PPh_3)$ complexes (P-P = DIOP or BINAP) were used as catalysts.[17]

Another aldimine, the condensation product of aniline and benzaldehyde, was reduced at 1000 psi H_2 using the variety of catalysts shown in Table 6.4. Interestingly, the complex $RuBr_2(DPPB)(PPh_3)$ **13** is a more effective catalyst for the hydrogenation of $PhN=C(H)Ph$ than $Ru_2Br_4(DPPB)_2$ **25**, thereby indicating that the catalysis is not governed by the degree of dissociation of **13**.

The hydrogenation of the prochiral ketimine $PhCH_2N=C(Me)Ph$ was performed with a single catalytic species. The trinuclear complex $[Ru(H)Cl(DPPB)]_3$, an achiral catalyst, affected 61% conversion to the amine product in 24 h under conditions that were otherwise identical to those listed in footnote (a) of Tables 6.2 and 6.3.

Table 6.3   Conversion Data for High-Pressure Hydrogenation of PhN=C(H)Ph Using a Variety of Catalyst Precursors[a]

Entry	Catalyst	Conversion (%)[b]
1	$Ru_2Cl_5(DPPB)_2$ 22[c]	24
2	$Ru_2Br_4(DPPB)_2$ 25	74
3	$RuBr_2(DPPB)(PPh_3)$ 13	99
4	$RuBr_2(DPPB)(PPh_3)$ 13[d]	77
5	$[H_2N(n\text{-}Oct)_2]^+[Ru_2Cl_5(DPPB)_2]^-$ 37[e]	15

(a)   Conditions: 1000 psi H_2, MeOH (10 mL), 0.77 mM Ru, [imine] = 0.153 M, room temperature (~20 °C).

(b)   Conversion after 3 h.

(c)   Reported by Fogg[18] and repeated in this work for comparison purposes.

(d)   Conversion after 1 h.

(e)   Conversion after 24 h.

6.3   Summary

A number of ruthenium(II) DPPB-containing complexes were found to be effective catalysts for the hydrogenation of the imines $PhCH_2N=C(H)Ph$ and $PhN=C(H)Ph$ at high pressures of H_2 (1000 psi) and at room temperature. The importance of a halide ligand for the hydrogenation of the aldimine $PhCH_2N=C(H)Ph$ was illustrated by the inactivity of $Ru(DPPB)(\eta^3\text{-}Me\text{-}allyl)_2$. Also, the bromo-containing complexes were seen to be more effective catalysts for the hydrogenation of $PhN=C(H)Ph$ than their chloro analogues, but less effective for the hydrogenation of $PhCH_2N=C(H)Ph$. This illustrates the need for the empirical matching of substrates to catalysts in order to maximize conversions of imines to amines.

The trinuclear species $[Ru(H)Cl(DPPB)]_3$ was an effective catalyst for the hydrogenation of benzonitrile at 1 atm H_2 pressure and 70 °C. At low initial substrate concentrations (20 mM), the product was benzylamine, while at high substrate concentrations (0.19–2.0 M), the products were dibenzylamine and $PhCH_2N=C(H)Ph$.

6.4 References

(1) James, B. R. *Chem. Ind.* **1995**, *62*, 167.

(2) Longley, C. J.; Goodwin, T. J.; Wilkinson, G. *Polyhedron* **1986**, *5*, 1625.

(3) Noyori, R. *Asymmetric Catalysis in Organic Synthesis*; Wiley-Interscience: New York, 1994.

(4) Chaloner, P. A.; Esteruelas, M. A.; Joó, F.; Oro, L. A. *Homogeneous Hydrogenation*; Kluwer Academic: Dordrecht, 1994.

(5) Willoughby, C. A.; Buchwald, S. L. *J. Org. Chem.* **1993**, *58*, 7627.

(6) Moser, H.; Rihs, G.; Sauter, H. *Z. Naturforsch* **1982**, *37b*, 451.

(7) Levi, A.; Modena, G.; Scorrano, G. *J. Chem. Soc., Chem. Commun.* **1975**, 6.

(8) Becalski, A. G.; Cullen, W. R.; Fryzuk, M. D.; James, B. R.; Kang, G.-J.; Rettig, S. J. *Inorg. Chem.* **1991**, *30*, 5002.

(9) Ball, G. E.; Cullen, W. R.; Fryzuk, M. D.; Henderson, W. J.; James, B. R.; MacFarlane, K. S. *Inorg. Chem.* **1994**, *33*, 1464.

(10) Cullen, W. R.; Fryzuk, M. D.; James, B. R.; Kutney, J. P.; Kang, G.-J.; Herb, G.; Thorburn, I. S.; Spogliarich, R. *J. Mol. Catal.* **1990**, *62*, 243.

(11) Kang, G.; Cullen, W. R.; Fryzuk, M. D.; James, B. R.; Kutney, J. P. *J. Chem. Soc., Chem. Commun.* **1988**, 1466.

(12) Bakos, J.; Orosz, A.; Heil, B.; Laghmari, M.; Lhoste, P.; Sinou, D. *J. Chem. Soc., Chem. Commun.* **1991**, 1684.

(13) Ng Cheong Chan, Y.; Meyer, D.; Osborn, J. A. *J. Chem. Soc., Chem. Commun.* **1990**, 869.

(14) Ng Cheong Chan, Y.; Osborn, J. A. *J. Am. Chem. Soc.* **1990**, *112*, 9400.

(15) Spindler, F.; Pugin, B.; Blaser, H.-U. *Angew. Chem., Int. Ed. Engl.* **1990**, *29*, 558.

(16) Bedford, R. B.; Chaloner, P. A.; Claver, C.; Fernandez, E.; Hitchcock, P. B.; Ruiz, A. *Chem. Ind.* **1995**, *62*, 181.

(17) Fogg, D. E.; James, B. R.; Kilner, M. *Inorg. Chim. Acta* **1994**, *222*, 85.

(18) Fogg, D. E. Ph.D. Thesis, The University of British Columbia, 1994.

(19) Oppolzer, W.; Wills, M.; Starkemann, C.; Bernardinelli, G. *Tetrahedron Lett.* **1990**, *31*, 4117.

(20) Grigg, R.; Mitchell, T. R. B.; Tongpenyai, N. *Synthesis* **1981**, 442.

(21) Willoughby, C. A.; Buchwald, S. L. *J. Am. Chem. Soc.* **1992**, *114*, 7562.

(22) Willoughby, C. A.; Buchwald, S. L. *J. Am. Chem. Soc.* **1994**, *116*, 11703.

(23) Burk, M. J.; Feaster, J. E. *J. Am. Chem. Soc.* **1992**, *114*, 6266.

(24) Willoughby, C. A.; Buchwald, S. L. *J. Am. Chem. Soc.* **1994**, *116*, 8952.

(25) Burk, M. J.; Martinez, J. P.; Feaster, J. E.; Cosford, N. *Tetrahedron* **1994**, *50*, 4399.

(26) Burk, M. J.; Gross, M. F. *Tetrahedron Lett.* **1994**, *35*, 9363.

(27) McCarty, C. G. In *The Chemistry of the Carbon-Nitrogen Double Bond*; Patai, S., Ed.; Interscience: London, 1970, p 364.

(28) Layer, R. W. *Chem. Rev.* **1963**, *63*, 489.

(29) Joshi, A. M.; MacFarlane, K. S.; James, B. R.; Frediani, P. *Chem. Ind.* **1994**, *53*, 497.

(30) Joshi, A. M.; MacFarlane, K. S.; James, B. R.; Frediani, P. *Stud. Surf. Sci. Catal.* **1992**, *73 (Progress in Catalysis)*, 143.

(31) Rylander, P. *Chem. Catal. News*, Englehard Corporation, **July 1990**.

(32) Chin, C. S.; Lee, B. *Catal. Lett.* **1992**, *14*, 135.

(33) Augustine, R. L. *Catalytic Hydrogenation: Techniques and Applications in Organic Synthesis*; Marcel Dekker: New York, 1965, p 96.

(34) Holy, N. L. *J. Org. Chem.* **1979**, *44*, 239.

(35) Yoshida, T.; Okano, T.; Otsuka, S. *J. Chem. Soc., Chem. Commun.* **1979**, 870.

(36) Bose, A.; Saha, C. R. *Indian J. Chem.* **1990**, *29A*, 461.

(37) Suarez, T.; Fontal, B. *J. Mol. Catal.* **1988**, *45*, 335.

(38) Thorburn, I. S.; Rettig, S. J.; James, B. R. *J. Organomet. Chem.* **1985**, *296*, 103.

(39) Joshi, A. M.; Thorburn, I. S.; Rettig, S. J.; James, B. R. *Inorg. Chim. Acta* **1992**, *198*, 283.

(40) James, B. R.; McMillan, R. S.; Morris, R. H.; Wang, D. K. W. *Adv. Chem. Ser.* **1978**, *167*, 122.

(41) James, B. R.; Wang, D. K. W. *Can. J. Chem.* **1980**, *58*, 245.

(42) Kawano, H.; Ikariya, T.; Ishii, Y.; Saburi, M.; Yoshikawa, S.; Uchida, Y.; Kumobayashi, H. *J. Chem. Soc., Perkin Trans. I* **1989**, 1571.

(43) James, B. R.; Joshi, A. M.; Kvintovics, P.; Morris, R. H.; Thorburn, I. S. *Chem. Ind.* **1990**, *40*, 11.

(44)   James, B. R.; Pacheco, A.; Rettig, S. J.; Thorburn, I. S.; Ball, R. G.; Ibers, J. A. *J. Mol. Catal.* **1987**, *41*, 147.

(45)   Thorburn, I. S. Ph.D. Thesis, The University of British Columbia, 1985.

(46)   Joshi, A. M.; MacFarlane, K. S.; James, B. R. *J. Organomet. Chem.* **1995**, *488*, 161.

(47)   Joshi, A. M.; James, B. R. *J. Chem. Soc., Chem. Commun.* **1989**, 1785.

(48)   Joshi, A. M. Ph.D. Thesis, The University of British Columbia, 1990.

(49)   *DMA General Information Bulletin*, Industrial and Biochemicals Department, E. I. Du Pont de Nemours and Co., Wilmington, Delware, **1962**.

(50)   Wang, D. K. W. Ph.D. Thesis, The University of British Columbia, 1978.

(51)   Chan, C.-Y. Ph.D. Thesis, The University of British Columbia, 1974.

(52)   Thorburn, I. S. M.Sc. Thesis, The University of British Columbia, 1980.

(53)   Hui, B. C. Ph.D. Thesis, The University of British Columbia, 1969.

(54)   Gamage, S. N. Ph.D. Thesis, The University of British Columbia, 1985.

(55)   Joshi, A. M. M.Sc. Thesis, The University of British Columbia, 1986.

(56)   Dekleva, T. W. Ph.D. Thesis, The University of British Columbia, 1983.

(57)   Cyr, P. W. B.Sc. Thesis, The University of British Columbia, 1995.

(58)   Ashby, M. T.; Halpern, J. *J. Am. Chem. Soc.* **1991**, *113*, 589.

(59)   Schutte, R. P.; James, B. R., unpublished results.

(60)   Newkome, G. R. *Chem. Rev.* **1993**, *93*, 2067.

CHAPTER 7

SOLID-STATE REACTIVITY OF FIVE-COORDINATE RUTHENIUM(II) COMPLEXES CONTAINING PHOSPHINE LIGANDS

7.1   Introduction

Very little attention has been given to the solid-state chemistry of transition metal complexes reacting with small gas molecules.[1] The work that is described in this chapter grew out of studies performed by Bressan and Rigo in 1975 in which CO reacted with $Ru_2Cl_4(DPPB)_3$ in the solid state to give $Ru_2Cl_4(CO)_2(DPPB)_3$.[2] James and co-workers have shown that the DIOP analogue $Ru_2Cl_4(DIOP)_3$ reacts in a similar manner in the solid state to give $Ru_2Cl_4(CO)_2(DIOP)_3$.[3,4] The fact that the five-coordinate complex $Ru_2Cl_4(DPPB)_3$ reacted in the solid state suggested that other five-coordinate ruthenium(II) complexes, such as $RuCl_2(PPh_3)_3$, $RuCl_2(DPPB)(PPh_3)$, and $Ru_2Cl_4(DPPB)_2$, may also exhibit "heterogeneous-like" chemistry.

Several groups have recently taken an interest in solid-state organometallic chemistry. Bianchini et al. have shown solid-state reactivity at both Ir and Co centres with a variety of small gas molecules, including CO, $CH_2=CH_2$, CH_2O, and H_2.[1,5-8] Siedle at al. have shown solid-state chemistry on both Rh^9 and Ir^{10-12} fragments held in a matrix comprised of anionic, molecular, metal oxide clusters. Aubart and Pignolet have catalyzed hydrogen-deuterium exchange in the solid state with platinum-gold[13-15] and palladium-gold[15] clusters. Hydrogen sulfide has been shown by Crabtree et al. to react with a five-coordinate Ir complex in the solid state, but the product (a supposed H_2S-adduct) is not well characterized.[16]

A previous worker in this group has shown some ruthenium(II) complexes to react with CO and H_2S in the solid state.[17] This chemistry will be discussed later in this

chapter, as it was performed in a similar manner and gave similar products to those described in this thesis.

7.2   Solid-State Reactivity of Five-Coordinate Ruthenium(II) Complexes with CO

To verify the authenticity of a sample of the phosphine-bridged complex $Ru_2Cl_4(DPPB)_3$ **19**, its reactivity with CO was examined in the solid state, as previously described by Bressan and Rigo.[2] Complex **19** is quite insoluble in common organic solvents, making other methods of characterization difficult (Section 2.5.5). By visual inspection of the solid, reactivity similar to that reported previously was noted (i.e., the green solid slowly became yellow under an atmosphere of CO). The yellow product $Ru_2Cl_4(CO)_2(DPPB)_3$ showed a $v_{(C=O)}$ IR band at 1994 cm^{-1}, which agreed well with the literature value of 1990 cm^{-1}.[2] This reactivity was extended to the previously unknown bromo-analogue $Ru_2Br_4(DPPB)_3$ **20**, which reacted in a similar fashion to give, presumably, $Ru_2Br_4(CO)_2(DPPB)_3$. An IR spectrum of the yellow-green product showed a $v_{(C=O)}$ band at 1995 cm^{-1}, with a shoulder at 1946 cm^{-1}. A C_6H_6 solution of **20** was placed under an atmosphere of CO, at which point the UV-vis bands of **20** at 364, 466, and 710 nm disappeared; the resulting solution was colourless.

After observing the above heterogeneous reactivity, it was decided to examine the solid-state chemistry of other five-coordinate complexes. All of the complexes studied ($RuX_2(PPh_3)_3$ X = Br or Cl, $RuCl_2(P(p\text{-tolyl})_3)_3$, $RuCl_2(DPPB)(PAr_3)$ Ar = Ph or p-tolyl, and $Ru_2Cl_4(DPPB)_2$) were seen to react in the solid state with CO. The reactions were quite slow under the ambient pressure and temperatures studied, and often gave mixtures of isomers as products. The reactions studied to date in this work (and described below) are of limited synthetic utility, as the rates of reaction are slow under the conditions employed (at least with CO) and the products often contain free phosphine created through displacement by the incoming gaseous ligand. Thus, the products often require purification, which necessitates the dissolution of the crude product, and this somewhat

lowers the utility of the preparation of these materials in the solid state. Nonetheless, the reactivity in the solid state is of considerable interest, as the potential exists to isolate kinetic products not accessible in solution because of isomerization to a thermodynamically more stable isomer.

7.2.1 Reaction of $RuCl_2(PPh_3)_3$ and CO in the Solid State

After the brown solid $RuCl_2(PPh_3)_3$ was stirred under an atmosphere of CO for one week, the colour of the solid slowly changed to yellow. Elemental analysis showed the yellow solid to be of the composition "$RuCl_2(CO)_2(PPh_3)_3$", which could possibly be a seven-coordinate complex. This was subsequently ruled out on the basis of solid-state IR data (see below).

Stoichiometric gas-uptake measurements on this system were attempted on several occasions, but the data obtained were unreliable, probably because of leaks in the system over the lengthy reaction times necessary. However, the measurement of the mass of the solid before and after the reaction with CO agreed with the calculated value for two moles of CO per mole of Ru complex (Section 2.5.12.1), although the differences in theoretical mass on changing from one to two moles of CO per complex were very small on the scale upon which the measurements were performed. Several repetitions consistently fitted the calculated mass required for the coordination of two moles of CO.

The IR spectral data, recorded both as a Nujol mull and KBr pellet, showed a number of $\nu_{(C=O)}$ bands, indicating the presence of a number of different ruthenium species (Section 2.5.12.1). On reprecipitation from chloroform and ethanol, a white solid was isolated, which was subsequently shown by elemental analysis, and IR and NMR spectroscopy to be the known complex cct-$RuCl_2(CO)_2(PPh_3)_2$ **47**,[18-20] which has recently been characterized by X-ray crystallographic studies.[20] The $\nu_{(C=O)}$ peaks observed for **47** at 1997 and 2060 cm^{-1} were also observed in the original yellow

mixture, indicating that the mixture consists of $RuCl_2(CO)_2(PPh_3)_2$ isomers and free PPh_3, not a seven-coordinate ruthenium complex.

7.2.2 Reaction of $RuCl_2(P(p\text{-tolyl})_3)_3$ and CO in the Solid State

The solid-state chemistry for the title complex is essentially the same as that described in Section 7.2.1 for the PPh_3-analogue, except that the yellow product in this case (again a mixture of at least three isomers, as evidenced by IR spectral data, Section 2.5.12.2) is obtained in 24 h. Therefore, although particle size can affect the reaction rates in the solid state, the *p*-tolyl complex reacts significantly faster than the PPh_3 analogue. It should be noted that the action of the stir bar keeps the particle size quite small and probably fairly uniform from reaction to reaction.

Again, as for the PPh_3 analogue, identifiable complexes were obtained from reprecipitation of the yellow mixture from $CHCl_3$ / EtOH. An off-white solid was isolated and consisted of *ccc*- (70%) and *cct*-$RuCl_2(CO)_2(P(p\text{-tolyl})_3)_2$ (30%), as evidenced by the $v_{(C=O)}$ bands in the solid-state IR spectrum (Section 2.5.12.2). The $^{31}P\{^1H\}$ NMR data, however, showed only the *cct*-isomer to be present in $CDCl_3$ (i.e., isomerization of the *ccc*-isomer gives the thermodynamic *cct*-product).

7.2.3 Reaction of $RuBr_2(PPh_3)_3$ and CO in the Solid State

The reactivity of the bromo-analogue was identical to the chemistry outlined in the previous two sections. The difference in mass on reaction with CO indicates an uptake of two moles per Ru. After the tan product was dissolved in $CHCl_3$, the solution IR spectrum showed only two $v_{(C=O)}$ bands at 1998 and 2058 cm^{-1}, indicating the presence of *cct*-$RuBr_2(CO)_2(PPh_3)_2$. A $^{31}P\{^1H\}$ NMR spectrum of the solid in $CDCl_3$ showed a singlet at 13.1 ppm for the *cct*-isomer, and a singlet at -5.5 ppm for free PPh_3. Therefore, the mixture of isomers produced in the solid state isomerize to a single isomer when they are dissolved in chloroform, as was the case with the chloro-analogue. No attempts were made to isolate pure isomers of the formulation $RuBr_2(CO)_2(PPh_3)_2$.

7.2.4 Reaction of RuCl₂(DPPB)(PPh₃) and CO in the Solid State

The reaction of $RuCl_2(DPPB)(PPh_3)$ **11** and CO in the solid state was slow, taking 48 h for the dark-green starting complex to become tan in colour (Section 2.5.12.3). Unfortunately, the chemistry was very complex and the nature of the product mixture, as evidenced by the number of $v_{(C=O)}$ bands in the IR spectrum (Section 2.5.12.3), has not yet been determined. A comparison of the mass gain on exposure of **11** to an atmosphere of CO fits quite well for the uptake of one mole of CO per Ru, as does the elemental analysis data. Both the IR and NMR spectral data are very complex, indicating a mixture of products.

This reaction had previously been investigated in solution, also with limited success in terms of the product characterization.[21,22] The product mixture was thought to contain both ruthenium monocarbonyl and dicarbonyl products.[21,22] In this present thesis work, only small amounts of the products encountered in the solid-state reaction of $Ru_2Cl_4(DPPB)_2$ **24** with CO (Section 7.2.5) were identified in the product mixture formed on reaction of **11** with CO.

Isomerization of the species present in the tan-solid mixture occurs on dissolution in $CHCl_3$, giving an IR spectrum with a single $v_{(C=O)}$ band at 1985 cm⁻¹. The position of the carbonyl stretch in the IR spectrum is similar to that observed by Krassowski et al. for a diruthenium complex of the formulation $Ru_2Cl_4(CO)_2(PMePh_2)_4$, which showed a carbonyl stretch at 1977 cm⁻¹.[19] Figure 7.1 shows a possible geometry for the insoluble yellow solid obtained on isomerization of the tan-coloured mixture in $CHCl_3$, which would fit the IR data. No further characterization of this product was attempted.

The complex $RuCl_2(DPPB)(P(p-tolyl)_3)$ **12** reacts with CO in the solid state in a similar manner, but with a much faster rate than **11**. The green solid **12** becomes yellow in 1 h. Both elemental analysis and mass calculations fit better for one than for two moles of CO per Ru.
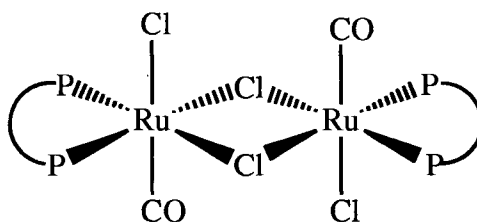
Figure 7.1   Possible geometry of the yellow solid isolated on isomerization of the product mixture obtained on reaction of RuCl$_2$(DPPB)(PPh$_3$) **11** and CO in the solid state, where P–P = DPPB.

7.2.5   Reaction of Ru$_2$Cl$_4$(DPPB)$_2$ and CO in the Solid State

The solid-state reactivity of Ru$_2$Cl$_4$(DPPB)$_2$ **24** and CO, although slow, was much cleaner than that described in the previous sections for the monoruthenium starting materials (Sections 7.2.1–7.2.4). The first product was observed after 1 day, and was identified as the previously isolated complex Ru$_2$Cl$_4$(DPPB)$_2$(CO).[21,22] Figure 7.2 shows the ^{31}P{^{1}H} NMR spectrum of a CDCl$_3$ solution of the light-orange product. The spectrum shows starting complex **24**, Ru$_2$Cl$_4$(DPPB)$_2$(CO), and *trans*-RuCl$_2$(CO)$_2$(DPPB). The chemistry is similar to the solution reaction of pyridine with **24**, which was shown initially to react with one equivalent of py to form Ru$_2$Cl$_4$(DPPB)$_2$(py), and then subsequently to produce *trans*-RuCl$_2$(DPPB)(py)$_2$ with additional equivalents of py (Section 5.2.3). With a longer reaction time between **24** and CO in the solid state (6 days), about 82% of the starting complex had reacted, giving Ru$_2$Cl$_4$(DPPB)$_2$(CO) (13%) and *trans*-RuCl$_2$(CO)$_2$(DPPB) (69%). With still longer reaction times, exclusively monomeric products were observed by ^{31}P{^{1}H} NMR spectroscopy; however, in addition to the previously observed *trans*-isomer, some *cis*-RuCl$_2$(CO)$_2$(DPPB) was also seen to be present (Figure 7.3).
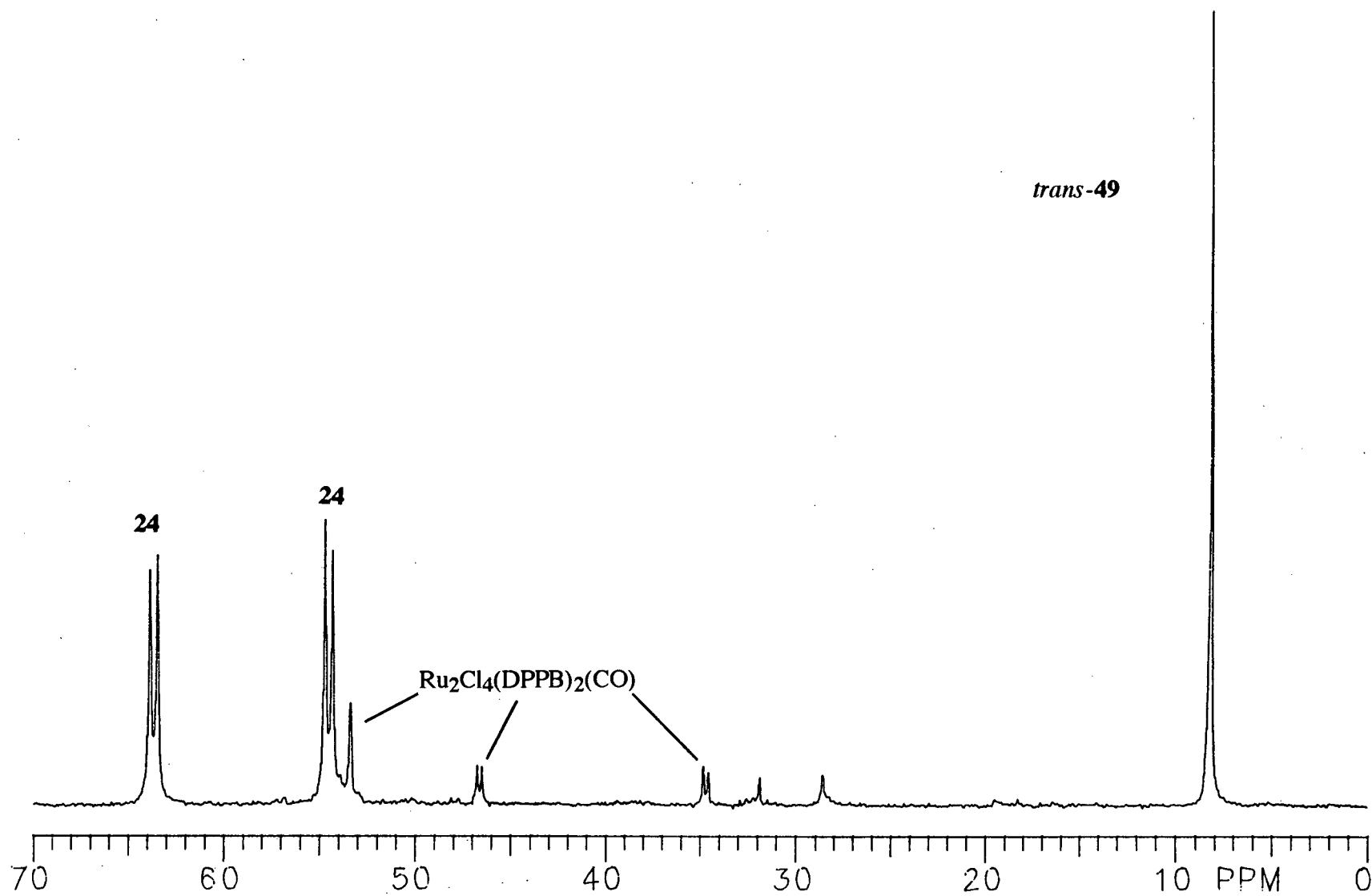
Figure 7.2 $^{31}P\{^{1}H\}$ NMR spectrum (CDCl$_3$, 121.42 MHz) of the products produced on reaction of Ru$_2$Cl$_4$(DPPB)$_2$ **24** and CO in the solid state for 24 h. **49** = RuCl$_2$(CO)$_2$(DPPB).
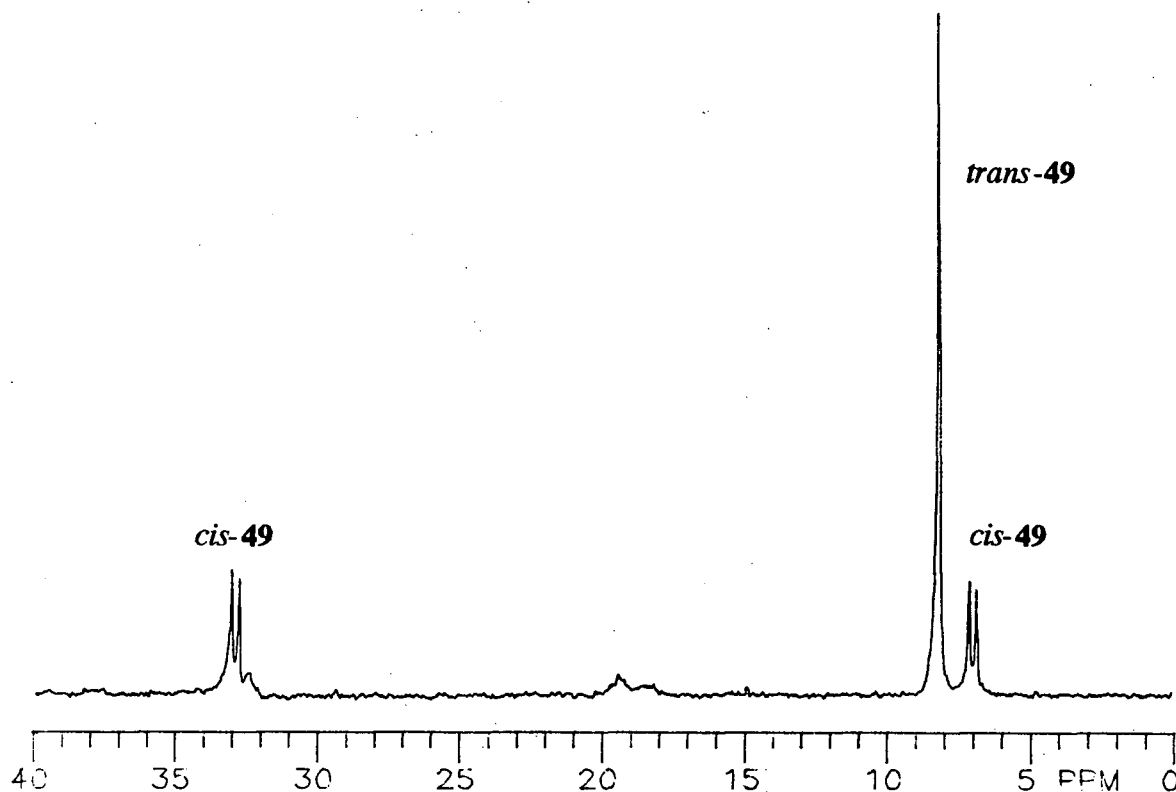
Figure 7.3 $^{31}P\{^1H\}$ NMR spectrum (CDCl$_3$, 121.42 MHz) of the products produced on reaction of Ru$_2$Cl$_4$(DPPB)$_2$ **24** and CO in the solid state for 14 days.

The ^{1}H NMR spectrum of a product [previously shown by $^{31}P\{^1H\}$ NMR spectroscopy to correspond to a singlet at 8.1 ppm, indicating the presence of largely *trans*-RuCl$_2$(CO)$_2$(DPPB)] showed two equal intensity methylene peaks (1.78 and 2.90 ppm) for the DPPB ligand, further confirming the *trans*-geometry.

The IR spectral data observed for the three carbonyl-containing complexes described above are given in Section 2.5.12.4. The diruthenium product Ru$_2$Cl$_4$(DPPB)$_2$(CO) shows a single carbonyl stretch at 1972 cm^{-1} (in CDCl$_3$ solution), in good agreement with that previously observed for the product prepared in solution ($\nu_{(C=O)}$ = 1977 cm^{-1}, Nujol mull).[21,22] The two monoruthenium complexes, which had not been prepared previously, each show two carbonyl stretches, indicating *cis*-carbonyl groups (see Section 2.5.12.4 for data).

Further evidence of the structures of *cis*- and *trans*-RuCl$_2$(CO)$_2$(DPPB), which are illustrated in Figure 7.4, comes from comparing the ^{31}P{^{1}H} NMR chemical shift data with those of known RuCl$_2$(DPPB)(L)$_2$ complexes. Figure 5.10 shows a linear relationship between the Ru–P bond lengths and the ^{31}P{^{1}H} NMR chemical shift for complexes containing the diphosphine DPPB. If the *trans*-influence series is employed to predict relative Ru–P bond lengths, the order of the ^{31}P{^{1}H} NMR chemical shifts can be predicted, and when compared to known structures, one can further substantiate proposed geometries. Compare, for example, the chemical shift of the phosphorus atoms (40.4 ppm) of *trans*-RuCl$_2$(DPPB)(py)$_2$, which are *trans* to the intermediate *trans*-influence ligands py, with the chemical shift of the P-atoms (8.1 ppm) in *trans*-RuCl$_2$(CO)$_2$(DPPB), which are *trans* to the strong *trans*-influence CO ligands. One observes a chemical shift in accord with that predicted by the plot shown in Figure 5.10 (i.e., the longer Ru–P bond expected for P-atoms *trans* to stronger *trans*-influence ligands like CO should give chemical shifts upfield from P-atoms *trans* to weaker *trans*-influencing ligands). Likewise, the chemical shifts observed for *cis*-RuCl$_2$(CO)$_2$(DPPB) come in regions predicted by Figure 5.10 and the *trans*-influence series. In fact, one can assign the downfield shift at 32.8 ppm to the P-atom *trans* to Cl, a weaker *trans*-influencing ligand, and the upfield shift at 6.9 ppm to the P-atom *trans* to CO for the complex *cis*-RuCl$_2$(CO)$_2$(DPPB).
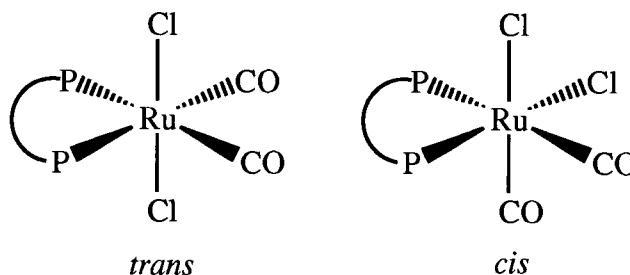
Figure 7.4   Molecular structure of *trans*-RuCl$_2$(CO)$_2$(DPPB) and *cis*-RuCl$_2$(CO)$_2$(DPPB), where P–P = DPPB.

Mudalige has discovered solid-state reactivity between CO and the ruthenium(II) complexes RuCl$_2$(PMA)(PR$_3$), where R = Ph or *p*-tolyl (the structure of PMA is shown in Figure 3.28).[17] The products were identified as the mono-carbonyl adducts RuCl$_2$(CO)(PMA)(PR$_3$), and when the chemistry was performed in solution, the product was RuCl$_2$(CO)$_2$(PMA) species.[17] The solid-state reactivity of these P–N-containing complexes with CO was significantly faster than that described above for the analogous P–P systems. The P–N systems reacted within minutes on exposure to an atmosphere of CO.[17]

There have been many studies performed on ruthenium(II) complexes of the formulation RuX$_2$(CO)$_y$(PR$_3$)$_z$ (X = Cl, Br, or I; y = 1 or 2; z = 3 or 2).[19,23-28] The chemistry can be quite complex, giving a variety of isomeric products which sometimes include dinuclear species.[19,25] Several papers have reported on the isomerization mechanisms of both RuCl$_2$(CO)$_2$(PR$_3$)$_2$ and RuCl$_2$(CO)(PR$_3$)$_3$ complexes by both thermal and photochemical routes.[19,25-28] In fact, one study investigated the solid-phase thermal isomerization of RuCl$_2$(CO)$_2$(PR$_3$)$_2$ and RuCl$_2$(CO)(PR$_3$)$_3$ complexes by thermal gravimetric analysis and differential scanning calorimetry where the complexes were found to isomerize above 135 °C.[28] The earlier studies relied heavily on the $\nu_{(C=O)}$ values, while the later studies use ^{31}P{^{1}H}, ^{13}C{^{1}H}, and ^{1}H NMR spectroscopy, as well as IR spectroscopy, to characterize the many possible isomeric products. It should be noted that the use of diphosphine ligands instead of monodentate phosphines reduces the number of possible isomers somewhat by requiring that the chelating phosphorus atoms be *cis*, although the possibility exists that the diphosphine may be 'dangling' (η^1-binding).

7.3 Solid-State Reactivity of Five-Coordinate Ruthenium(II) Complexes with NH$_3$

Although this chemistry is described briefly in Section 5.5.2 in the context of nitrogen-donor ligands and their reactivity in solution with ruthenium(II) complexes, it is discussed here in the context of solid-state reactivity. The reaction of ammonia with

$RuCl_2(DPPB)(PPh_3)$ **11**, $Ru_2Cl_4(DPPB)_2$ **24**, or $Ru_2Cl_4(DPPB)_3$ **19** is immediate, producing in all cases *trans*-$RuCl_2(DPPB)(NH_3)_2$ **51**. The reaction is amazingly fast when compared with the very slow reaction observed with CO and any of the above-mentioned ruthenium complexes in the solid state. It should be noted that the solid-state product was characterized in solution by NMR spectroscopy immediately after dissolution of the solid sample. Although unlikely, the possibility remains that the product isolated in the solid state isomerizes immediately on dissolution to the *trans*-$RuCl_2(DPPB)(NH_3)_2$ **51** observed in solution. Solid-state ^{31}P NMR spectroscopy would prove useful in ensuring that the *trans*-$RuCl_2(DPPB)(NH_3)_2$ is, in fact, the initially formed product.

Of the reactions discussed above, the most practical from a synthetic point of view is the reaction between **24** and NH_3, because no phosphine is displaced from the starting complex by incoming NH_3 and the product can therefore be isolated free of co-products.

7.4 Solid-state Reactivity of Five-Coordinate Ruthenium(II) Complexes with H_2 and H_2S

Single attempts at reacting H_2 or H_2S with $RuCl_2(DPPB)(PPh_3)$ **11** in the solid state proved unsuccessful, at least by visual inspection. The green starting material remained green under the conditions employed (1 atm of the gaseous reactant at room temperature). Increased temperatures and/or pressures may possibly allow for these solid-state reactions to proceed. While these studies were ongoing, the solid-state reactivity of the five-coordinate ruthenium complex $RuCl_2(PMA)(P(p\text{-tolyl})_3)$ and H_2S was found by Mudalige to produce $RuCl_2(PMA)(P(p\text{-tolyl})_3)(H_2S)$ (the structure of the P–N chelate PMA is shown in Figure 3.28).[17] In this case, the green solid became yellow within 1 min, but the solid was stirred for a further 2 h under an atmosphere of H_2S.[17] Interestingly, the PPh_3-analogue $RuCl_2(PMA)(PPh_3)$ did not react with H_2S under similar conditions in the solid state, but did react in solution.[17]

7.5   Summary

The five-coordinate ruthenium(II) complexes $RuCl_2(DPPB)(PAr_3)$ (Ar = Ph or p-tolyl), $Ru_2Cl_4(DPPB)_2$, and $Ru_2Cl_4(DPPB)_3$ were all found to react with CO and NH_3 in the solid state at ambient temperatures and pressures. The heterogeneous reaction of any of the above-mentioned ruthenium complexes with ammonia produced *trans*-$RuCl_2(DPPB)(NH_3)_2$. The reaction of $Ru_2Cl_4(DPPB)_2$ with CO was seen to give the dinuclear product $Ru_2Cl_4(DPPB)_2(CO)$ initially, but on longer reaction times gave *trans*- and *cis*-$RuCl_2(CO)_2(DPPB)$. The complex $RuCl_2(DPPB)(PPh_3)$ did not react in the solid state with either H_2 or H_2S at ambient temperature and pressures.

The reactivity of the $RuX_2(PAr_3)_3$ complexes (X = Br and Cl, Ar = Ph or p-tolyl) with CO was also investigated in the solid state. The products initially formed were difficult to characterize, but the *cct*-$RuX_2(CO)_2(PAr_3)_2$ species could be isolated from $CHCl_3$ solutions of the original mixtures.

7.6   References

(1)   Bianchini, C.; Peruzzini, M.; Zanobini, F. *Organometallics* **1991**, *10*, 3415.

(2)   Bressan, M.; Rigo, P. *Inorg. Chem.* **1975**, *14*, 2286.

(3)   James, B. R.; McMillan, R. S.; Morris, R. H.; Wang, D. K. W. *Adv. Chem. Ser.* **1978**, *167*, 122.

(4)   Wang, D. K. W. Ph.D. Thesis, The University of British Columbia, 1978.

(5)   Bianchini, C.; Peruzzini, M.; Vacca, A.; Zanobini, F. *Organometallics* **1991**, *10*, 3697.

(6)   Bianchini, C.; Mealli, C.; Peruzzini, M.; Zanobini, F. *J. Am. Chem. Soc.* **1992**, *114*, 5905.

(7)   Bianchini, C.; Farnetti, E.; Graziani, M.; Kaspar, J.; Vizza, F. *J. Am. Chem. Soc.* **1993**, *115*, 1753.

(8)   Bianchini, C.; Frediani, P.; Graziani, M.; Kaspar, J.; Meli, A.; Peruzzini, M.; Vizza, F. *Organometallics* **1993**, *12*, 2886.

(9)   Siedle, A. R.; Gleason, W. B.; Newmark, R. A.; Skarjune, R. P.; Lyon, P. A.; Markell, C. G.; Hodgson, K. O.; Roe, A. L. *Inorg. Chem.* **1990**, *29*, 1667.

(10)   Siedle, A. R.; Newmark, R. A.; Sahyun, M. R. V.; Lyon, P. A.; Hunt, S. L.; Skarjune, R. P. *J. Am. Chem. Soc.* **1989**, *111*, 8346.

(11)   Siedle, A. R.; Newmark, R. A. *Organometallics* **1989**, *8*, 1442.

(12)   Siedle, A. R.; Newmark, R. A. *J. Am. Chem. Soc.* **1989**, *111*, 2058.

(13)   Aubart, M. A.; Pignolet, L. H. *J. Am. Chem. Soc.* **1992**, *114*, 7901.

(14)   Kappen, T. G. M. M.; Bour, J. J.; Schlebos, P. P. J.; Roelofsen, A. M.; van der Linden, J. G. M.; Steggerda, J. J.; Aubart, M. A.; Krogstad, D. A.; Schoondergang, M. F. J.; Pignolet, L. H. *Inorg. Chem.* **1993**, *32*, 1074.

(15)   Aubart, M. A.; Chandler, B. D.; Gould, R. A. T.; Krogstad, D. A.; Schoondergang, M. F. J.; Pignolet, L. H. *Inorg. Chem.* **1994**, *33*, 3724.

(16)   Crabtree, R. H.; Davis, M. W.; Mellea, M. F.; Mihelcic, J. M. *Inorg. Chim. Acta* **1983**, *72*, 223.

(17)   Mudalige, D. C. Ph.D. Thesis, The University of British Columbia, 1994.

(18)   Dekleva, T. W. Ph.D. Thesis, The University of British Columbia, 1983.

(19)   Krassowski, D. W.; Nelson, J. H.; Brower, K. R.; Havenstein, D.; Jacobson, R. A. *Inorg. Chem.* **1988**, *27*, 4294.

(20)   Batista, A. A.; Zukerman-Schpector, J.; Porcu, O. M.; Queiroz, S. L.; Araujo, M. P.; Oliva, G.; Souza, D. H. F. *Polyhedron* **1994**, *13*, 689.

(21)   Joshi, A. M.; Thorburn, I. S.; Rettig, S. J.; James, B. R. *Inorg. Chim. Acta* **1992**, *198*, 283.

(22)   Joshi, A. M. Ph.D. Thesis, The University of British Columbia, 1990.

(23)   Jenkins, J. M.; Lupin, M. S.; Shaw, B. L. *J. Chem. Soc.* **1966**, 1787.

(24)   Lupin, M. S.; Shaw, B. L. *J. Chem. Soc. (A)* **1968**, 741.

(25)   Barnard, C. F. J.; Daniels, J. A.; Jeffery, J.; Mawby, R. J. *J. Chem. Soc., Dalton Trans.* **1976**, 953.

(26)   Barnard, C. F. J.; Daniels, J. A.; Jeffery, J.; Mawby, R. J. *J. Chem. Soc., Dalton Trans.* **1976**, 1861.

(27)   Wilkes, L. M.; Nelson, J. H.; Mitchener, J. P.; Babich, M. W.; Riley, W. C.; Helland, B. J.; Jacobson, R. A.; Cheng, M. Y.; Seff, K.; McCusker, L. B. *Inorg. Chem.* **1982**, *21*, 1376.

(28)   Krassowski, D. W.; Reimer, K.; Lemay, H. E., Jr.; Nelson, J. H. *Inorg. Chem.* **1988**, *27*, 4307.

CHAPTER 8

GENERAL CONCLUSIONS AND SOME RECOMMENDATIONS
FOR FUTURE WORK

This thesis describes routes to ruthenium complexes, both mono- and dinuclear, containing a single diphosphine per metal centre. Much of the chemistry was performed with $RuX_2(DPPB)(PPh_3)$ (where $X = Cl$ and Br, DPPB = $Ph_2P(CH_2)_4PPh_2$), which proved to be very versatile starting materials. The chloro-analogue was characterized by X-ray crystallography and proved to be pseudo-octahedral, with a weak agostic interaction at the sixth position of the octahedron between the Ru centre and an *ortho*-hydrogen of the PPh_3 ligand.

The bromo precursor ($RuBr_2(PPh_3)_3$) to the mixed-phosphine complex ($RuBr_2(DPPB)(PPh_3)$) was also characterized by X-ray crystallography and is pseudo-octahedral with a similar agostic interaction. Although the geometry is pseudo-octahedral, these complexes are considered to be five-coordinate because the agostic interaction is quite weak. The DPPB-containing mixed-phosphine complex was used to prepare the dinuclear complex $Ru_2Br_4(DPPB)_2$, which could not be synthesized via ruthenium(III) precursors because these could not be isolated free of chloride contamination.

The five-coordinate complex $RuCl_2(DPPB)(PPh_3)$ reacted with excess ligand L to form either $RuCl_2(DPPB)(L)_2$ or $Ru_2Cl_4(DPPB)_2(L)$. The planar ligands py, bipy, and phen, as well as the small NH_3, reacted to give the mononuclear complexes, while the thioethers, THT and DMS, and the sulfoxides, DMSO and TMSO, reacted to give the dinuclear complexes $Ru_2Cl_4(DPPB)_2(L)$; steric factors likely determine the reactivity pattern.

In solution, the addition of one equivalent of pyridine to $Ru_2Cl_4(DPPB)_2$, which is also formed from $RuCl_2(DPPB)(PPh_3)$ by phosphine dissociation and subsequent

dimerization, produced the triply-chloro-bridged $Ru_2Cl_4(DPPB)_2(py)$. The addition of further equivalents of pyridine cleaved the chloro-bridges to give $RuCl_2(DPPB)(py)_2$. On this basis, the reactivity of these five-coordinate $RuX_2(DPPB)(PPh_3)$ species is thought to be through the initial coordination of L to the dinuclear complex $Ru_2X_4(DPPB)_2$ thereby producing $Ru_2X_4(DPPB)_2(L)$. Then, if the ligand L is sufficiently small, additional equivalents of L react to give $RuCl_2(DPPB)(L)_2$. The equilibrium between the species $RuX_2(DPPB)(PPh_3)$ and $Ru_2X_4(DPPB)_2$ is thought to be key to the reactivity.

The synthetic chemistry of $RuCl_2(DPPB)(PPh_3)$ described above can also be performed directly from isolated $Ru_2Cl_4(DPPB)_2$. The latter, however, is air-sensitive, even in the solid state, and the chemistry is more conveniently performed from the air-stable mononuclear complex. To date, no X-ray structural studies have been performed on complexes of the formula $Ru_2X_4(P–P)_2$ (prepared with a variety of chiral and achiral diphosphines) because of a lack of success in isolating suitable, single crystals. Solid-state structural data for these diruthenium species may prove useful in determining the role of H_2O in isolation of $Ru_2Cl_4(DPPB)_2$ from a refluxing two-phase H_2O / C_6H_6 suspension of $RuCl_2(DPPB)(PPh_3)$ (a route discovered in this work). The H_2O molecule may be coordinated to the dinuclear complex in the solid state, as elemental analysis shows the presence of one mole equivalent of H_2O. In solution, however, $^{31}P\{^1H\}$ NMR spectroscopy indicates that H_2O is not coordinated. Solid-state CP / MAS $^{31}P\{^1H\}$ NMR spectroscopy may prove useful in determining if H_2O is coordinated in the solid state.

Although some studies have been done in this work on analogous BINAP ruthenium complexes, a wider range of complexes needs to be prepared in order to examine whether the BINAP systems parallel or differ from the DPPB systems. Our group has recently been given 30 g of BINAP, which should allow for examination of these systems on a reasonably large scale. Previously, the expense of the chiral ligand dictated small-scale reactions. Initial studies in this work indicate that in some instances the BINAP systems are somewhat more complex than the DPPB analogues. For example,

where $RuCl_2(DPPB)(PPh_3)$ reacts with H_2 to give a single molecular hydrogen complex, $RuCl_2(BINAP)(PPh_3)$ reacts with H_2 to give two molecular hydrogen complexes.

The complex $Ru((R)\text{-}BINAP)(\eta^3\text{-}Me\text{-}allyl)_2$ was characterized by X-ray crystallography as a crystal containing $Ru((R)\text{-}BINAP)(\eta^3\text{-}Me\text{-}allyl)_2$, the phosphine dioxide $(R)\text{-}(+)\text{-}2,2'\text{-}bis(diphenylphosphinoyl)\text{-}1,1'\text{-}binaphthyl$, and two disordered deuterobenzenes per unit cell. The $Ru((R)\text{-}BINAP)(\eta^3\text{-}Me\text{-}allyl)_2$ complex has not yet been isolated free of the dioxide. This should be pursued, as the isolated $Ru(DPPB)(\eta^3\text{-}Me\text{-}allyl)_2$ complex reacts with HX (X = Cl, Br, I) to give $Ru_2X_4(DPPB)_2$. Therefore, the Me-allyl complexes are good in situ sources of the air-sensitive $Ru_2X_4(DPPB)_2$ species.

The BINAP complexes are of special interest, as they have been shown to be successful as catalysts for asymmetric hydrogenation of a range of prochiral substrates. Much of the chemistry done to date on these systems concentrates on the organic applications, without much regard for the inorganic chemistry. In fact, some of the catalytic species are produced in situ, and are not well-defined, but are nonetheless very effective. This research group has recently acquired an autoclave with sampling capabilities, which allows for these hydrogenation reactions to be followed kinetically, thereby providing insight into possible mechanisms for these catalytic hydrogenations.

The ruthenium(II) complexes studied in this work show interesting and sometimes complex chemistry with tertiary alkyl amines. This thesis shows one of the products of the reaction of NR_3 (R = n-Bu, n-Oct) with $RuCl_2(P\text{-}P)(PPh_3)$ (P–P = DPPB, (R)-BINAP) to be an ionic species of the formulation $[H_2NR_2]^+[Ru_2Cl_5(DPPB)_2]^-$. The fate of the remaining alkyl group of the starting tertiary amine and the co-requisite chloro-deficient ruthenium product has not been determined. These co-products need to be identified, as the reactivity of amines and ruthenium(II) complexes is important with respect to imine hydrogenation since the reduction products themselves are amines.

The reactivity of $RuCl_2(DPPB)(PPh_3)$ with both NMe_3 and NPh_3 should be examined to investigate the role of the α- and β-hydrogens in the dealkylation of tertiary amines.

The solid-state reactivity of some five-coordinate ruthenium(II) complexes has been examined. The complexes $RuCl_2(DPPB)(PAr_3)$, (Ar = Ph or *p*-tolyl) $Ru_2Cl_4(DPPB)_3$, and $Ru_2Cl_4(DPPB)_2$ were found to react with the small gas molecules NH_3 and CO at ambient temperatures and pressures. The complexes $RuX_2(PAr_3)_3$ (X = Br and Cl, Ar = Ph or *p*-tolyl) were also investigated with CO in the solid state. The products were mainly characterized in solution. The heterogeneous reactivity of these ruthenium(II) species should be extended to include other small molecules such as H_2, N_2 $CH_2=CH_2$, H_2S, SO_2, and CO_2. Although H_2 and H_2S did not seem to react with $RuCl_2(DPPB)(PPh_3)$ in the solid state under the conditions employed in this thesis, at least as evidenced by visual inspection of the solid, these reactions may proceed at higher temperature or pressures. The use of solid-state NMR should prove useful for the characterization of these products.

The characterization of either of the *p*-tolyl-containing complexes $RuCl_2(P(p$-tolyl$)_3)_3$ or $RuCl_2(DPPB)(P(p$-tolyl$)_3)$ by X-ray crystallography may prove beneficial, as the *p*-tolyl species seem to react significantly faster than their PPh_3 counterparts in the solid state with CO. The molecular structures of the PPh_3-containing complexes show a weak agostic interaction between a phenyl C–H and the ruthenium centre. It would prove interesting to investigate whether the *p*-tolyl analogues have this same weak agostic interaction.

The reactivity of H_2 with $RuCl_2((R)$-BINAP$)(PPh_3)$ was examined by NMR spectroscopy and hydrogen-deuterium exchange reactions. A reversible reaction with dihydrogen was shown to give two molecular hydrogen complexes which are both thought to be dinuclear. Although selective ^{31}P-decoupled ^{1}H NMR spectra of the η^2-HD isotopomer leave little doubt as to the dinuclear nature of one of the two η^2-H$_2$

complexes, the preparation of pure $Ru_2Cl_4(BINAP)_2$, which has been obtained previously, and an examination of the reactivity with H_2 may further clarify this chemistry.

A red crystal was studied by X-ray crystallography and shown to be $[(DMA)_2H]^+[(PPh_3)_2(H)Ru(\mu\text{-}Cl)_2(\mu\text{-}H)Ru(H)(PPh_3)_2]^-$, a species containing both terminal and bridging hydrides. However, solution NMR spectroscopic studies of this crystal showed mainly the presence of the previously known molecular hydrogen complex $[(\eta^2\text{-}H_2)(PPh_3)_2Ru(\mu\text{-}Cl)_2(\mu\text{-}H)Ru(H)(PPh_3)_2]$. Therefore, an equilibrium between the ionic classical hydride-containing complex and the neutral molecular hydrogen species is evident. In solution, the latter species is favoured. This is the first example involving 'proton transfer' within an ionic complex (i.e., the transfer of a proton from a cation to an anion).

Some of the ruthenium(II) DPPB-containing complexes prepared in this work were effective catalysts for the hydrogenation of the imines $PhCH_2N=C(H)Ph$ and $PhN=C(H)Ph$ at high pressures of H_2 (1000 psi) and at room temperature, while the trinuclear species $[Ru(H)Cl(DPPB)]_3$ was an effective catalyst for the hydrogenation of benzonitrile at 1 atm H_2 pressure and 70 °C.

The recent purchase of an autoclave with sampling capabilities is now allowing these imine hydrogenations to be followed kinetically. These kinetic studies may provide insight into possible mechanisms for the catalytic hydrogenation of imines. This work needs to be extended to the asymmetric hydrogenation of prochiral ketimines by the substitution of chiral phosphines for the achiral phosphine DPPB in some of the more active ruthenium(II) complexes.

The inactivity of $Ru(DPPB)(\eta^3\text{-}Me\text{-}allyl)_2$ in this work demonstrated the importance of a halide ligand for the hydrogenation of the aldimine $PhCH_2N=C(H)Ph$. The role of halide ligands in imine hydrogenations in general should be further investigated. As the majority of catalytic hydrogenations to date have been performed

with chloro-containing complexes, substitution of other halo ligands in these complexes may increase the rate of reaction and the enantiomeric excess (in the chiral cases). The routes to the bromo-containing ruthenium(II) complexes discovered in this work should allow more detailed comparison of the reaction rates for imine hydrogenations.

APPENDICES
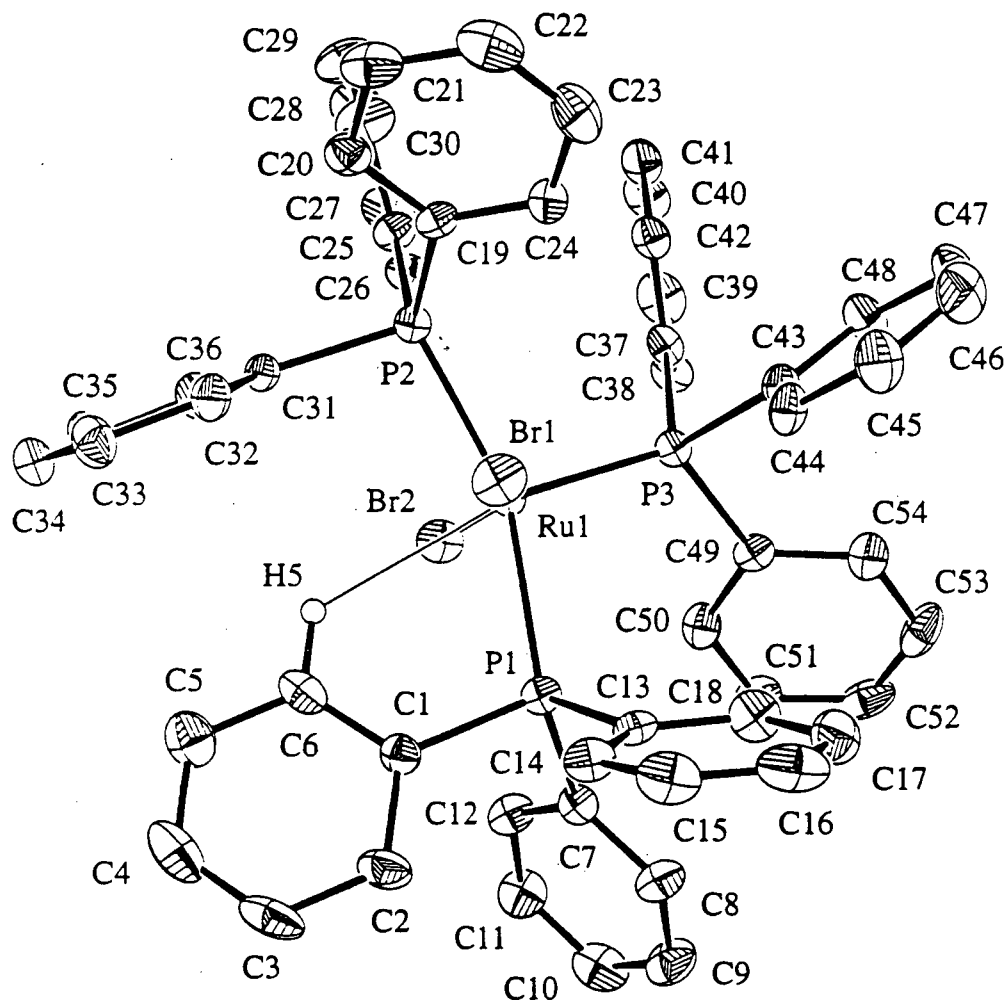
Molecular Structure of RuBr$_2$(PPh$_3$)$_3$, **10** (ORTEP Plot)
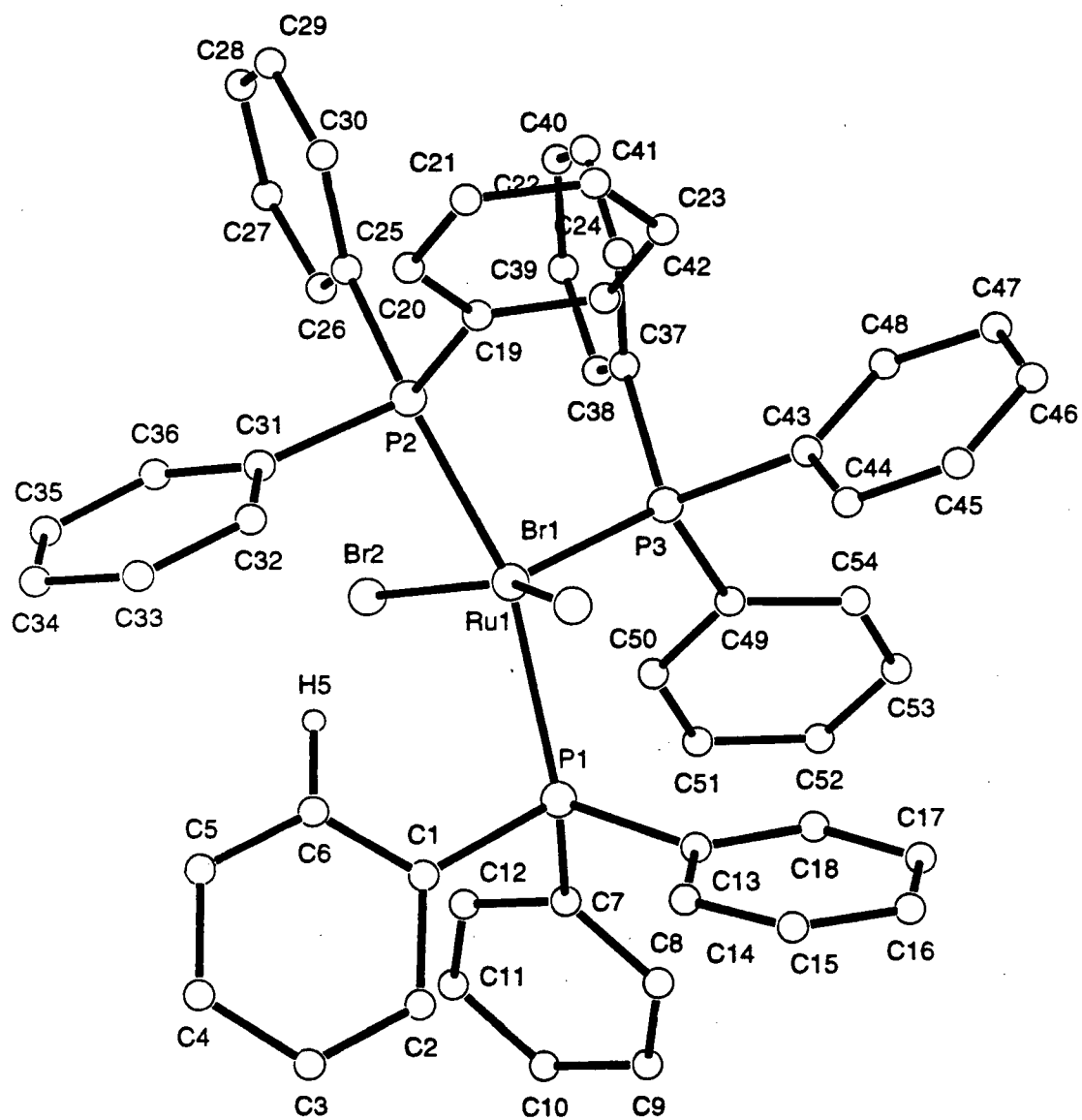
Molecular Structure of RuBr$_2$(PPh$_3$)$_3$, **10** (Pluto Plot)
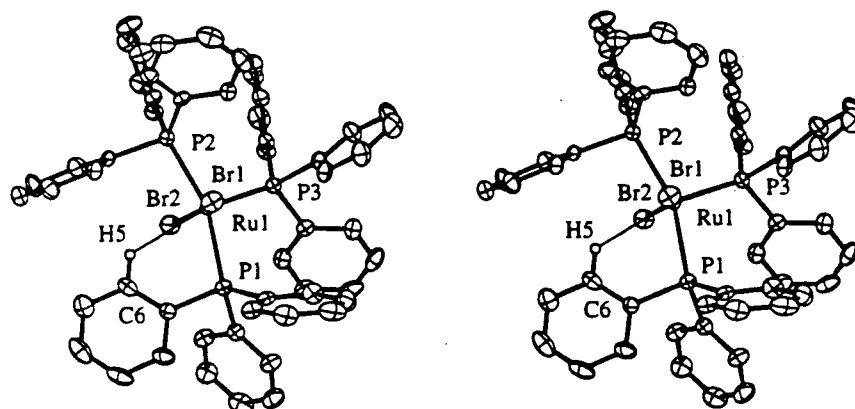
Molecular Structure of RuBr$_2$(PPh$_3$)$_3$, **10** (Stereoview)

EXPERIMENTAL DETAILS

A. Crystal Data

Empirical Formula	$C_{54}H_{45}Br_2P_3Ru$
Formula Weight	1047.75
Crystal Color, Habit	Dark-orange, prism
Crystal Dimensions	0.30 X 0.35 X 0.40
Crystal System	Monoclinic
Lattice Type	P
No. of Reflections Used for Unit Cell Determination (2θ range)	25 (22.7 - 40.3°)
Omega Scan Peak Width at Half-height	0.40°
Lattice Parameters	$a = 12.482(4)$ Å $b = 20.206(6)$ Å $c = 17.956(3)$ Å $\beta = 90.40(2)°$ $V = 4528(1)$ Å^3
Space Group	$P2_1/a$ (#14)
Z value	4
D_{calc}	1.537 g/cm^3
F_{000}	2112
$\mu(MoK\alpha)$	22.59 cm^{-1}

B. Intensity Measurements

Diffractometer	Rigaku AFC6S
Radiation	MoKα ($\lambda = 0.71069$ Å) graphite monochromated

Take-off Angle	6.0°
Detector Aperture	6.0 mm horizontal 6.0 mm vertical
Crystal to Detector Distance	285 mm
Temperature	21.0°C
Scan Type	ω-2θ
Scan Rate	32.0°/min (in omega) (8 rescans)
Scan Width	$(1.15 + 0.35 \tan \theta)°$
$2\theta_{max}$	55.0°
No. of Reflections Measured	Total: 11152 Unique: 10662 ($R_{int} = 0.067$)
Corrections	Lorentz-polarization Absorption (trans. factors: 0.73 - 1.00) Secondary Extinction (coefficient: 1.3(1) x 10^{-7})

C. Structure Solution and Refinement

Structure Solution	Direct Methods (SHELXS86)
Refinement	Full-matrix least-squares
Function Minimized	$\Sigma w(|Fo| - |Fc|)^2$
Least Squares Weights	$\frac{1}{\sigma^2(Fo)} = \frac{4Fo^2}{\sigma^2(Fo^2)}$
p-factor	0.00
Anomalous Dispersion	All non-hydrogen atoms
No. Observations ($I>3.00\sigma(I)$)	5069
No. Variables	542
Reflection/Parameter Ratio	9.35
Residuals: R; Rw	0.048 ; 0.046
Goodness of Fit Indicator	2.39
Max Shift/Error in Final Cycle	0.006
Maximum peak in Final Diff. Map	0.87 $e^-/Å^3$
Minimum peak in Final Diff. Map	-1.01 $e^-/Å^3$

Table I.1 Bond Lengths (Å) with estimated standard deviations

atom	atom	distance	atom	atom	distance
Ru(1)	Br(1)	2.515(1)	Ru(1)	Br(2)	2.526(1)
Ru(1)	P(1)	2.423(2)	Ru(1)	P(2)	2.389(2)
Ru(1)	P(3)	2.227(2)	P(1)	C(1)	1.834(7)
P(1)	C(7)	1.844(7)	P(1)	C(13)	1.839(7)
P(2)	C(19)	1.843(7)	P(2)	C(25)	1.857(7)
P(2)	C(31)	1.837(7)	P(3)	C(37)	1.849(7)
P(3)	C(43)	1.834(7)	P(3)	C(49)	1.846(7)
C(1)	C(2)	1.396(10)	C(1)	C(6)	1.367(10)
C(2)	C(3)	1.38(1)	C(3)	C(4)	1.38(1)
C(4)	C(5)	1.35(1)	C(5)	C(6)	1.38(1)
C(7)	C(8)	1.371(9)	C(7)	C(12)	1.376(10)
C(8)	C(9)	1.40(1)	C(9)	C(10)	1.36(1)
C(10)	C(11)	1.37(1)	C(11)	C(12)	1.37(1)
C(13)	C(14)	1.414(10)	C(13)	C(18)	1.381(10)
C(14)	C(15)	1.37(1)	C(15)	C(16)	1.35(1)
C(16)	C(17)	1.42(1)	C(17)	C(18)	1.38(1)
C(19)	C(20)	1.377(9)	C(19)	C(24)	1.371(9)
C(20)	C(21)	1.38(1)	C(21)	C(22)	1.38(1)
C(22)	C(23)	1.35(1)	C(23)	C(24)	1.39(1)
C(25)	C(26)	1.388(10)	C(25)	C(30)	1.38(1)
C(26)	C(27)	1.40(1)	C(27)	C(28)	1.37(1)
C(28)	C(29)	1.40(1)	C(29)	C(30)	1.35(1)
C(31)	C(32)	1.416(9)	C(31)	C(36)	1.384(9)
C(32)	C(33)	1.388(10)	C(33)	C(34)	1.37(1)
C(34)	C(35)	1.42(1)	C(35)	C(36)	1.361(10)
C(37)	C(38)	1.394(9)	C(37)	C(42)	1.376(10)
C(38)	C(39)	1.370(10)	C(39)	C(40)	1.37(1)
C(40)	C(41)	1.37(1)	C(41)	C(42)	1.377(10)
C(43)	C(44)	1.408(9)	C(43)	C(48)	1.401(9)
C(44)	C(45)	1.363(10)	C(45)	C(46)	1.33(1)
C(46)	C(47)	1.39(1)	C(47)	C(48)	1.383(10)
C(49)	C(50)	1.382(10)	C(49)	C(54)	1.398(9)
C(50)	C(51)	1.39(1)	C(51)	C(52)	1.37(1)
C(52)	C(53)	1.37(1)	C(53)	C(54)	1.38(1)

Table I.2 Bond Angles (deg) with estimated standard deviations

atom	atom	atom	angle
Br(1)	Ru(1)	Br(2)	155.64(4)
Br(1)	Ru(1)	P(2)	84.31(5)
Br(2)	Ru(1)	P(1)	93.04(5)
P(2)	Ru(1)	P(3)	93.96(5)
P(1)	Ru(1)	P(3)	101.28(7)
Ru(1)	P(1)	C(1)	104.4(2)
Ru(1)	P(1)	C(13)	115.3(2)
C(1)	P(1)	C(13)	106.9(3)
Ru(1)	P(2)	C(19)	117.4(2)
C(19)	P(2)	C(31)	100.1(2)
C(25)	P(2)	C(31)	104.7(3)
Ru(1)	P(3)	C(37)	114.1(2)
C(37)	P(3)	C(49)	117.2(2)
C(43)	P(3)	C(49)	101.6(3)
P(1)	C(1)	C(2)	121.3(6)
C(2)	C(1)	C(6)	117.4(7)
C(2)	C(3)	C(4)	119.6(8)
C(4)	C(5)	C(6)	118.8(9)
P(1)	C(7)	C(8)	125.0(6)
C(8)	C(7)	C(12)	117.8(7)
C(8)	C(9)	C(10)	120.5(8)
C(10)	C(11)	C(12)	119.8(8)
P(1)	C(13)	C(14)	121.7(6)
C(14)	C(13)	C(18)	119.4(7)
Br(1)	Ru(1)	P(1)	82.19(5)
Br(1)	Ru(1)	P(3)	110.39(5)
Br(2)	Ru(1)	P(2)	91.34(5)
P(1)	Ru(1)	P(2)	156.43(7)
P(2)	Ru(1)	P(3)	101.50(7)
Ru(1)	P(1)	C(7)	128.5(2)
C(1)	P(1)	C(7)	95.4(3)
C(7)	P(1)	C(13)	103.0(3)
Ru(1)	P(2)	C(25)	128.9(3)
C(19)	P(2)	C(25)	101.7(3)
C(25)	P(2)	C(31)	100.4(3)
Ru(1)	P(3)	C(43)	119.7(2)
C(37)	P(3)	C(43)	100.0(3)
C(43)	P(3)	C(49)	101.5(3)
P(1)	C(1)	C(6)	120.6(6)
C(1)	C(2)	C(3)	120.6(8)
C(3)	C(4)	C(5)	120.8(8)
C(1)	C(6)	C(5)	122.7(8)
P(1)	C(7)	C(12)	116.7(6)
C(7)	C(8)	C(9)	120.3(8)
C(9)	C(10)	C(11)	119.3(8)
C(7)	C(12)	C(11)	122.2(8)
P(1)	C(13)	C(18)	118.8(6)
C(13)	C(14)	C(15)	119.2(8)
C(14)	C(15)	C(16)	122.1(8)
C(16)	C(17)	C(18)	119.5(8)
P(2)	C(19)	C(20)	124.4(6)
C(20)	C(19)	C(24)	117.3(7)
C(20)	C(21)	C(22)	119.6(8)
C(22)	C(23)	C(24)	120.8(8)
P(2)	C(25)	C(26)	119.8(6)
C(26)	C(25)	C(30)	118.1(7)
C(26)	C(27)	C(28)	119.5(8)
C(28)	C(29)	C(30)	120.0(8)
P(2)	C(31)	C(32)	121.5(5)
C(32)	C(31)	C(36)	117.6(6)
C(32)	C(33)	C(34)	120.0(7)
C(34)	C(35)	C(36)	120.0(7)
P(3)	C(37)	C(38)	121.7(6)
C(38)	C(37)	C(42)	117.8(7)
C(38)	C(39)	C(40)	121.4(7)
C(40)	C(41)	C(42)	118.3(8)
P(3)	C(43)	C(44)	121.5(6)
C(44)	C(43)	C(48)	116.9(7)
C(44)	C(45)	C(46)	122.8(8)
C(46)	C(47)	C(48)	118.6(8)
P(3)	C(49)	C(50)	119.9(6)
C(50)	C(49)	C(54)	117.8(7)
C(50)	C(51)	C(52)	119.5(8)
C(52)	C(53)	C(54)	121.3(8)
C(15)	C(16)	C(17)	119.2(8)
C(13)	C(18)	C(17)	120.6(8)
P(2)	C(19)	C(24)	118.3(6)
C(19)	C(20)	C(21)	121.9(7)
C(21)	C(22)	C(23)	119.3(8)
C(19)	C(24)	C(23)	121.0(7)
P(2)	C(25)	C(30)	122.1(6)
C(25)	C(26)	C(27)	120.7(7)
C(27)	C(28)	C(29)	119.6(8)
C(25)	C(30)	C(29)	121.8(8)
P(2)	C(31)	C(36)	120.7(5)
C(31)	C(32)	C(33)	121.0(7)
C(33)	C(34)	C(35)	119.5(7)
C(31)	C(36)	C(35)	121.9(7)
P(3)	C(37)	C(42)	120.5(5)
C(37)	C(38)	C(39)	119.5(7)
C(39)	C(40)	C(41)	120.2(7)
C(37)	C(42)	C(41)	122.8(7)
P(3)	C(43)	C(48)	121.4(5)
C(43)	C(44)	C(45)	119.7(7)
C(45)	C(46)	C(47)	120.1(8)
C(43)	C(48)	C(47)	121.8(7)
P(3)	C(49)	C(54)	122.2(6)
C(49)	C(50)	C(51)	121.6(7)
C(51)	C(52)	C(53)	119.7(8)
C(49)	C(54)	C(53)	120.0(8)

Table I.3 Final Atomic Coordinates (Fractional) and B(eq)

atom	x	y	z	B_{eq}	atom	x	y	z	B_{eq}
Ru(1)	0.30818(4)	0.48785(3)	0.23966(3)	1.92(1)	C(25)	0.4784(6)	0.6271(4)	0.3248(4)	2.8(2)
Br(1)	0.24132(7)	0.53167(4)	0.11674(5)	3.99(2)	C(26)	0.5060(6)	0.5888(4)	0.3862(4)	3.2(2)
Br(2)	0.43951(7)	0.43179(4)	0.32673(5)	3.58(2)	C(27)	0.5652(7)	0.6157(4)	0.4450(5)	4.2(2)
P(1)	0.2464(2)	0.38386(10)	0.1876(1)	2.36(5)	C(28)	0.5949(7)	0.6807(5)	0.4427(5)	4.6(2)
P(2)	0.4084(1)	0.58851(9)	0.24423(10)	2.13(4)	C(29)	0.5638(8)	0.7198(5)	0.3821(5)	5.4(3)
P(3)	0.1872(1)	0.50515(10)	0.32817(9)	2.19(4)	C(30)	0.5066(7)	0.6929(4)	0.3254(4)	4.2(2)
C(1)	0.3519(6)	0.3598(4)	0.1225(4)	2.6(2)	C(31)	0.5233(5)	0.5654(3)	0.1865(4)	2.2(2)
C(2)	0.3418(7)	0.3035(4)	0.0779(4)	4.0(2)	C(32)	0.5178(6)	0.5676(4)	0.1077(4)	3.0(2)
C(3)	0.4276(9)	0.2806(4)	0.0373(5)	4.9(3)	C(33)	0.6032(7)	0.5466(4)	0.0646(4)	3.8(2)
C(4)	0.5257(8)	0.3120(5)	0.0435(5)	4.9(3)	C(34)	0.6938(7)	0.5222(4)	0.0983(5)	4.6(2)
C(5)	0.5369(7)	0.3675(5)	0.0848(5)	4.3(2)	C(35)	0.6990(6)	0.5180(4)	0.1769(5)	4.2(2)
C(6)	0.4495(7)	0.3905(4)	0.1242(4)	3.5(2)	C(36)	0.6156(6)	0.5399(4)	0.2186(4)	3.5(2)
C(7)	0.2374(6)	0.3024(4)	0.2334(4)	2.6(2)	C(37)	0.2396(5)	0.5505(4)	0.4101(4)	2.4(2)
C(8)	0.1508(6)	0.2607(4)	0.2293(4)	3.6(2)	C(38)	0.2643(6)	0.5180(4)	0.4757(4)	3.1(2)
C(9)	0.1571(7)	0.1967(4)	0.2586(5)	4.5(2)	C(39)	0.3112(7)	0.5534(5)	0.5337(4)	4.3(2)
C(10)	0.2501(8)	0.1743(4)	0.2899(5)	4.7(3)	C(40)	0.3240(7)	0.6206(5)	0.5295(5)	4.2(2)
C(11)	0.3366(7)	0.2159(5)	0.2946(4)	4.2(2)	C(41)	0.2943(6)	0.6540(4)	0.4663(5)	3.7(2)
C(12)	0.3294(6)	0.2787(4)	0.2665(4)	3.4(2)	C(42)	0.2524(6)	0.6181(4)	0.4077(4)	2.9(2)
C(13)	0.1209(6)	0.3884(3)	0.1336(4)	2.7(2)	C(43)	0.0677(5)	0.5548(4)	0.3073(4)	2.7(2)
C(14)	0.1206(6)	0.3931(4)	0.0551(4)	3.3(2)	C(44)	0.0244(5)	0.5584(4)	0.2348(4)	3.0(2)
C(15)	0.0252(7)	0.4006(4)	0.0181(4)	4.2(2)	C(45)	-0.0671(7)	0.5936(5)	0.2222(5)	4.5(2)
C(16)	-0.0696(8)	0.4021(4)	0.0541(5)	5.1(3)	C(46)	-0.1195(7)	0.6249(5)	0.2763(6)	5.0(3)
C(17)	-0.0706(7)	0.3965(4)	0.1330(5)	4.5(2)	C(47)	-0.0820(6)	0.6220(5)	0.3491(5)	4.8(3)
C(18)	0.0249(7)	0.3911(4)	0.1714(4)	3.6(2)	C(48)	0.0113(6)	0.5873(4)	0.3638(4)	3.5(2)
C(19)	0.3500(6)	0.6614(3)	0.1974(4)	2.3(2)	C(49)	0.1275(6)	0.4314(4)	0.3723(4)	2.5(2)
C(20)	0.4066(6)	0.7041(4)	0.1526(4)	3.0(2)	C(50)	0.1903(6)	0.3765(4)	0.3868(4)	3.1(2)
C(21)	0.3599(8)	0.7595(4)	0.1217(4)	4.0(2)	C(51)	0.1495(7)	0.3213(4)	0.4227(4)	3.9(2)
C(22)	0.2529(8)	0.7720(4)	0.1336(5)	4.6(3)	C(52)	0.0446(8)	0.3210(5)	0.4450(4)	4.5(3)
C(23)	0.1964(6)	0.7308(5)	0.1775(5)	4.3(2)	C(53)	-0.0187(7)	0.3749(5)	0.4313(4)	4.5(2)
C(24)	0.2435(6)	0.6747(4)	0.2079(4)	3.0(2)	C(54)	0.0205(6)	0.4296(4)	0.3945(4)	3.4(2)

X-Ray Crystallographic Analysis of RuCl$_2$(DPPB)(PPh$_3$), 11
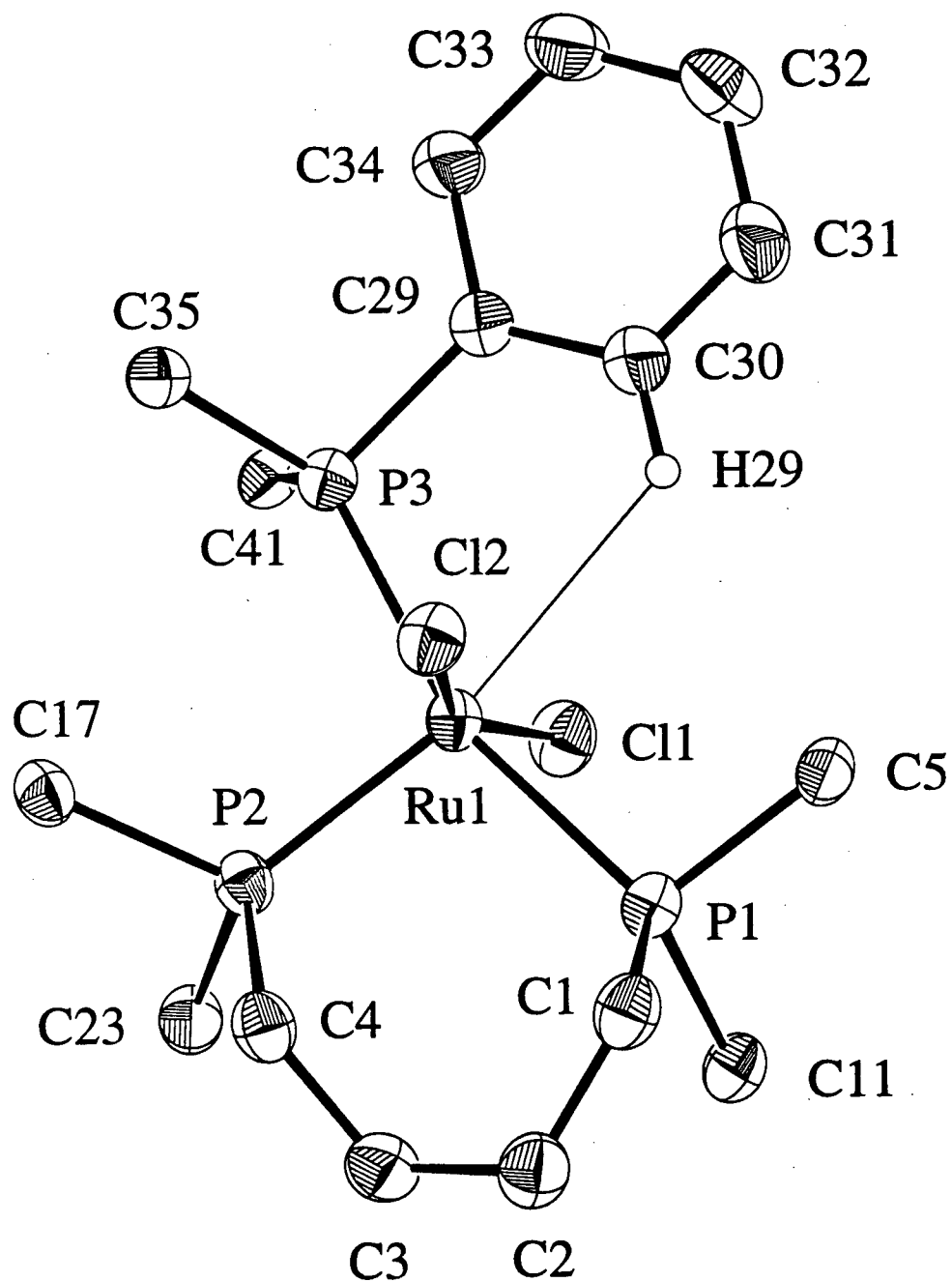
Molecular Structure of RuCl$_2$(DPPB)(PPh$_3$), **11** (ORTEP Plot)
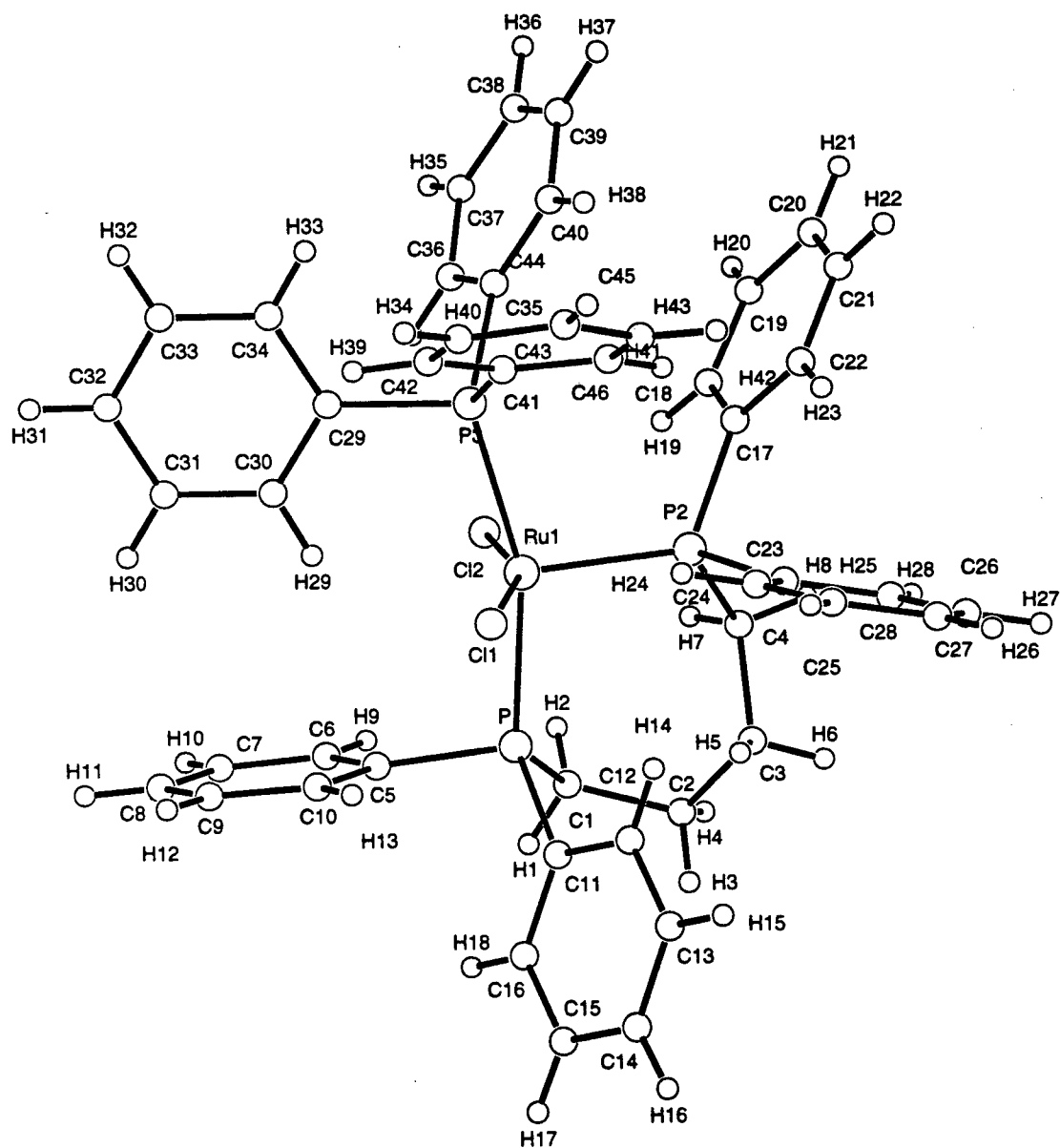
Molecular Structure of RuCl₂(DPPB)(PPh₃), **11** (Pluto Plot)
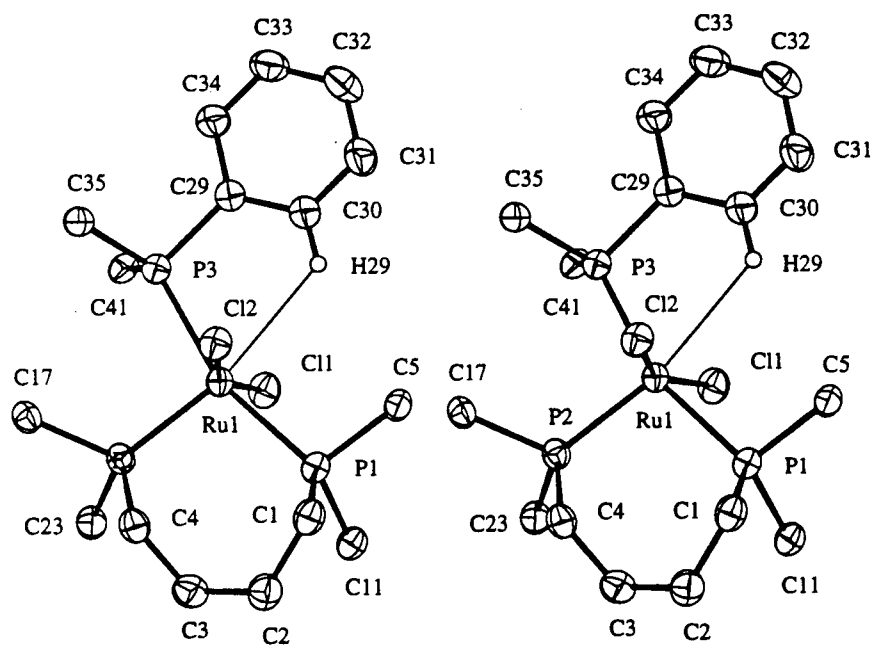
Molecular Structure of RuCl$_2$(DPPB)(PPh$_3$), **11** (Stereoview)

EXPERIMENTAL DETAILS

A. Crystal Data

Empirical Formula	$C_{46}H_{43}Cl_2P_3Ru$
Formula Weight	860.74
Crystal Color, Habit	green, plate
Crystal Dimensions	0.05 X 0.25 X 0.25 mm
Crystal System	monoclinic
Lattice Type	Primitive
No. of Reflections Used for Unit Cell Determination (2θ range)	25 (50.1 - 63.6°)
Omega Scan Peak Width at Half-height	0.38°
Lattice Parameters	a = 10.885(2) Å b = 20.477(1) Å c = 18.292(2) Å β = 99.979(9)° V = 4015.8(6) Å^3
Space Group	$P2_1/n$ (#14)
Z value	4
D_{calc}	1.424 g/cm^3
F_{000}	1768
μ(CuKα)	57.60 cm^{-1}

B. Intensity Measurements

Diffractometer	Rigaku AFC6S
Radiation	CuKα (λ = 1.54178 Å) graphite monochromated

306

Take-off Angle	6.0°
Detector Aperture	6.0 mm horizontal 6.0 mm vertical
Crystal to Detector Distance	285 mm
Temperature	21.0°C
Scan Type	ω-2θ
Scan Rate	8.0°/min (in ω) (up to 9 scans)
Scan Width	$(0.79 + 0.20 \tan \theta)°$
$2\theta_{max}$	155.4°
No. of Reflections Measured	Total: 9180 Unique: 8759 (R_{int} = 0.028)
Corrections	Lorentz-polarization Absorption (trans. factors: 0.553 - 1.000)

C. Structure Solution and Refinement

Structure Solution	Patterson Methods (DIRDIF92 PATTY)
Refinement	Full-matrix least-squares
Function Minimized	$\Sigma w(|Fo| - |Fc|)^2$
Least Squares Weights	$\frac{1}{\sigma^2(Fo)} = \frac{4Fo^2}{\sigma^2(Fo^2)}$
p-factor	0.000
Anomalous Dispersion	All non-hydrogen atoms
No. Observations (I>3.00σ(I))	5925
No. Variables	469
Reflection/Parameter Ratio	12.63
Residuals: R; Rw	0.031 ; 0.032
Goodness of Fit Indicator	1.80
Max Shift/Error in Final Cycle	0.001
Maximum peak in Final Diff. Map	0.33 $e^-/Å^3$
Minimum peak in Final Diff. Map	-0.37 $e^-/Å^3$

Table II.1 Bond Lengths (Å) with estimated standard deviations

atom	atom	distance	atom	atom	distance
Ru(1)	Cl(1)	2.3796(8)	Ru(1)	Cl(2)	2.4047(9)
Ru(1)	P(1)	2.3346(9)	Ru(1)	P(2)	2.2029(9)
Ru(1)	P(3)	2.3786(9)	P(1)	C(1)	1.836(4)
P(1)	C(5)	1.820(4)	P(1)	C(11)	1.826(4)
P(2)	C(4)	1.849(3)	P(2)	C(17)	1.842(3)
P(2)	C(23)	1.834(3)	P(3)	C(29)	1.824(3)
P(3)	C(35)	1.844(3)	P(3)	C(41)	1.834(3)
C(1)	C(2)	1.524(5)	C(2)	C(3)	1.521(5)
C(3)	C(4)	1.534(5)	C(5)	C(6)	1.390(4)
C(5)	C(10)	1.384(5)	C(6)	C(7)	1.390(5)
C(7)	C(8)	1.368(6)	C(8)	C(9)	1.366(6)
C(9)	C(10)	1.385(5)	C(11)	C(12)	1.369(5)
C(11)	C(16)	1.378(5)	C(12)	C(13)	1.380(6)
C(13)	C(14)	1.373(6)	C(14)	C(15)	1.339(6)
C(15)	C(16)	1.379(5)	C(17)	C(18)	1.392(4)
C(17)	C(22)	1.384(4)	C(18)	C(19)	1.380(5)
C(19)	C(20)	1.370(5)	C(20)	C(21)	1.357(5)
C(21)	C(22)	1.396(5)	C(23)	C(24)	1.376(5)
C(23)	C(28)	1.399(5)	C(24)	C(25)	1.374(5)
C(25)	C(26)	1.372(6)	C(26)	C(27)	1.370(6)
C(27)	C(28)	1.373(5)	C(29)	C(30)	1.388(4)
C(29)	C(34)	1.392(4)	C(30)	C(31)	1.381(5)
C(31)	C(32)	1.374(5)	C(32)	C(33)	1.373(5)
C(33)	C(34)	1.383(5)	C(35)	C(36)	1.384(5)
C(35)	C(40)	1.373(5)	C(36)	C(37)	1.380(5)
C(37)	C(38)	1.358(5)	C(38)	C(39)	1.355(6)
C(39)	C(40)	1.397(5)	C(41)	C(42)	1.384(4)
C(41)	C(46)	1.386(5)	C(42)	C(43)	1.387(5)
C(43)	C(44)	1.375(6)	C(44)	C(45)	1.372(6)
C(45)	C(46)	1.382(5)			

Table II.2 Bond Angles (deg) with estimated standard deviations

atom	atom	atom	angle
Cl(1)	Ru(1)	C(2)	158.75(3)
Cl(1)	Ru(1)	P(2)	109.76(3)
Cl(2)	Ru(1)	P(1)	87.06(3)
Cl(2)	Ru(1)	P(3)	91.87(3)
P(1)	Ru(1)	P(3)	161.78(3)
Ru(1)	P(1)	C(1)	119.7(1)
Ru(1)	P(1)	C(11)	124.1(1)
C(1)	P(1)	C(11)	101.6(2)
Ru(1)	P(2)	C(4)	112.8(1)
Ru(1)	P(2)	C(23)	119.7(1)
C(4)	P(2)	C(23)	102.6(2)
Ru(1)	P(3)	C(29)	105.3(1)
Ru(1)	P(3)	C(41)	115.4(1)
C(29)	P(3)	C(41)	104.6(2)
P(1)	C(1)	C(2)	115.1(3)
C(1)	C(2)	C(3)	116.6(3)
C(3)	C(4)	C(5)	122.2(3)
C(5)	C(6)	C(10)	118.8(3)
C(6)	C(7)	C(8)	121.0(4)
C(8)	C(9)	C(10)	120.8(4)
P(1)	C(11)	C(12)	120.6(3)
C(11)	C(16)	C(15)	118.1(3)
C(12)	C(13)	C(14)	120.7(4)
C(14)	C(15)	C(16)	120.1(4)
Cl(1)	Ru(1)	P(1)	88.61(3)
Cl(1)	Ru(1)	P(3)	85.82(3)
Cl(2)	Ru(1)	P(2)	91.42(3)
P(1)	Ru(1)	P(2)	97.01(3)
P(2)	Ru(1)	P(3)	101.20(3)
Ru(1)	P(1)	C(5)	101.3(1)
C(1)	P(1)	C(5)	103.9(2)
C(5)	P(1)	C(11)	103.3(2)
Ru(1)	P(2)	C(17)	118.2(1)
C(4)	P(2)	C(17)	99.9(2)
C(17)	P(2)	C(23)	100.7(2)
Ru(1)	P(3)	C(35)	125.0(1)
C(29)	P(3)	C(35)	99.3(2)
C(35)	P(3)	C(41)	104.4(1)
C(1)	C(2)	C(3)	115.4(3)
C(3)	C(4)	C(5)	114.6(2)
P(1)	C(5)	C(10)	118.9(3)
C(5)	C(6)	C(7)	119.7(4)
C(7)	C(8)	C(9)	119.4(4)
C(6)	C(10)	C(9)	120.4(4)
P(1)	C(11)	C(16)	121.2(3)
C(11)	C(12)	C(13)	120.1(4)
C(13)	C(14)	C(15)	119.6(4)
C(11)	C(16)	C(15)	121.3(4)
P(2)	C(17)	C(18)	119.4(3)
C(18)	C(17)	C(22)	118.4(3)
C(18)	C(19)	C(20)	121.1(4)
C(20)	C(21)	C(22)	120.6(4)
P(2)	C(23)	C(24)	122.0(3)
C(24)	C(23)	C(28)	118.3(3)
C(24)	C(25)	C(26)	120.8(4)
C(26)	C(27)	C(28)	120.0(4)
P(3)	C(29)	C(30)	120.9(3)
C(30)	C(29)	C(34)	117.7(3)
C(30)	C(31)	C(32)	120.5(4)
C(32)	C(33)	C(34)	119.7(4)
P(3)	C(35)	C(36)	117.5(3)
C(36)	C(35)	C(40)	118.0(3)
C(36)	C(37)	C(38)	120.7(4)
C(38)	C(39)	C(40)	121.4(4)
P(3)	C(41)	C(42)	123.8(3)
C(42)	C(41)	C(46)	118.0(3)
C(42)	C(43)	C(44)	120.0(4)
C(44)	C(45)	C(46)	120.0(4)
P(2)	C(17)	C(22)	122.0(3)
C(17)	C(18)	C(19)	120.0(4)
C(19)	C(20)	C(21)	119.5(4)
C(17)	C(22)	C(21)	120.3(3)
P(2)	C(23)	C(28)	119.5(3)
C(23)	C(24)	C(25)	120.4(4)
C(25)	C(26)	C(27)	119.6(4)
C(23)	C(28)	C(27)	120.8(4)
P(3)	C(29)	C(34)	121.4(3)
C(29)	C(30)	C(31)	120.8(3)
C(31)	C(32)	C(33)	119.9(4)
C(29)	C(34)	C(33)	121.4(4)
P(3)	C(35)	C(40)	124.5(3)
C(35)	C(36)	C(37)	121.0(3)
C(37)	C(38)	C(39)	119.0(4)
C(35)	C(40)	C(39)	119.8(4)
P(3)	C(41)	C(46)	118.0(3)
C(41)	C(42)	C(43)	120.9(4)
C(43)	C(44)	C(45)	119.9(4)
C(41)	C(46)	C(45)	121.1(3)

Table II.3 Final Atomic Coordinates (Fractional) and B(eq)

atom	x	y	z	B_{eq}
Ru(1)	0.02253(2)	0.15180(1)	0.18643(1)	3.014(5)
C(1)	-0.13484(8)	0.07364(4)	0.14280(5)	4.10(2)
C(2)	0.21056(8)	0.21463(4)	0.19206(5)	3.97(2)
P(1)	0.14806(8)	0.06646(4)	0.24064(5)	3.34(2)
P(2)	-0.01437(8)	0.19589(4)	0.29032(5)	3.25(2)
P(3)	-0.09011(8)	0.22343(4)	0.09658(5)	3.27(2)
C(1)	0.2848(3)	0.0844(2)	0.3121(2)	4.13(8)
C(2)	0.2593(3)	0.0860(2)	0.3914(2)	4.66(9)
C(3)	0.1406(4)	0.1214(2)	0.4018(2)	4.57(9)
C(4)	0.1201(3)	0.1896(2)	0.3671(2)	3.86(8)
C(5)	0.2161(3)	0.0376(2)	0.1622(2)	3.67(8)
C(6)	0.3313(4)	0.0593(2)	0.1489(2)	4.46(9)
C(7)	0.3758(4)	0.0377(2)	0.0864(3)	5.7(1)
C(8)	0.3069(5)	-0.0036(2)	0.0366(3)	6.0(1)
C(9)	0.1928(5)	-0.0241(2)	0.0489(2)	5.9(1)
C(10)	0.1474(4)	-0.0044(2)	0.1116(2)	4.61(9)
C(11)	0.0894(3)	-0.0081(2)	0.2769(2)	3.75(8)
C(12)	-0.0241(4)	-0.0085(2)	0.2995(3)	5.3(1)
C(13)	-0.0623(4)	-0.0630(2)	0.3338(3)	7.7(2)
C(14)	0.0119(5)	-0.1175(2)	0.3451(3)	7.1(1)
C(15)	0.1209(4)	-0.1185(2)	0.3206(3)	5.7(1)
C(16)	0.1605(4)	-0.0641(2)	0.2868(2)	4.86(10)
C(17)	-0.0432(3)	0.2845(2)	0.2918(2)	3.56(7)
C(18)	0.0541(4)	0.3276(2)	0.2874(2)	4.57(9)

atom	x	y	z	B_{eq}
C(19)	0.0368(4)	0.3939(2)	0.2948(3)	5.6(1)
C(20)	-0.0766(4)	0.4187(2)	0.3037(2)	5.2(1)
C(21)	-0.1729(4)	0.3773(2)	0.3066(2)	4.84(10)
C(22)	-0.1568(3)	0.3099(2)	0.3019(2)	4.20(9)
C(23)	-0.1436(3)	0.1652(2)	0.3330(2)	3.73(8)
C(24)	-0.2435(3)	0.1329(2)	0.2925(2)	4.26(9)
C(25)	-0.3424(4)	0.1141(2)	0.3253(3)	5.7(1)
C(26)	-0.3441(4)	0.1278(2)	0.3985(3)	6.6(1)
C(27)	-0.2454(4)	0.1601(2)	0.4398(2)	6.6(1)
C(28)	-0.1459(4)	0.1788(2)	0.4077(2)	5.6(1)
C(29)	-0.0396(3)	0.2027(2)	0.0094(2)	3.56(7)
C(30)	0.0459(3)	0.1531(2)	0.0062(2)	4.60(9)
C(31)	0.0820(4)	0.1366(2)	-0.0602(2)	5.5(1)
C(32)	0.0331(4)	0.1690(2)	-0.1244(2)	5.5(1)
C(33)	-0.0501(4)	0.2191(2)	-0.1225(2)	5.3(1)
C(34)	-0.0851(3)	0.2362(2)	-0.0559(2)	4.57(9)
C(35)	-0.0697(3)	0.3128(2)	0.0951(2)	3.58(8)
C(36)	0.0464(3)	0.3363(2)	0.0870(2)	4.58(9)
C(37)	0.0676(4)	0.4024(2)	0.0817(2)	4.90(10)
C(38)	-0.0248(4)	0.4462(2)	0.0854(2)	5.2(1)
C(39)	-0.1391(4)	0.4240(2)	0.0932(3)	6.1(1)
C(40)	-0.1627(4)	0.3573(2)	0.0990(2)	4.98(10)
C(41)	-0.2596(3)	0.2116(2)	0.0779(2)	3.47(7)
C(42)	-0.3239(3)	0.1843(2)	0.0132(2)	4.21(8)
C(43)	-0.4516(4)	0.1740(2)	0.0039(2)	5.2(1)
C(44)	-0.5161(4)	0.1909(2)	0.0594(3)	5.4(1)
C(45)	-0.4630(4)	0.2154(2)	0.1252(2)	5.0(1)
C(46)	-0.3258(3)	0.2258(2)	0.1342(2)	4.32(9)

$$B_{eq} = \frac{8}{3}\pi^2(U_{11}(aa^*)^2 + U_{22}(bb^*)^2 + U_{33}(cc^*)^2 + 2U_{12}aa^*bb^*\cos\gamma + 2U_{13}aa^*cc^*\cos\beta + 2U_{23}bb^*cc^*\cos\alpha)$$

X-Ray Crystallographic Analysis of

[TMP]$^+$[(DPPB)ClRu(μ-Cl)$_3$RuCl(DPPB)]$^-$
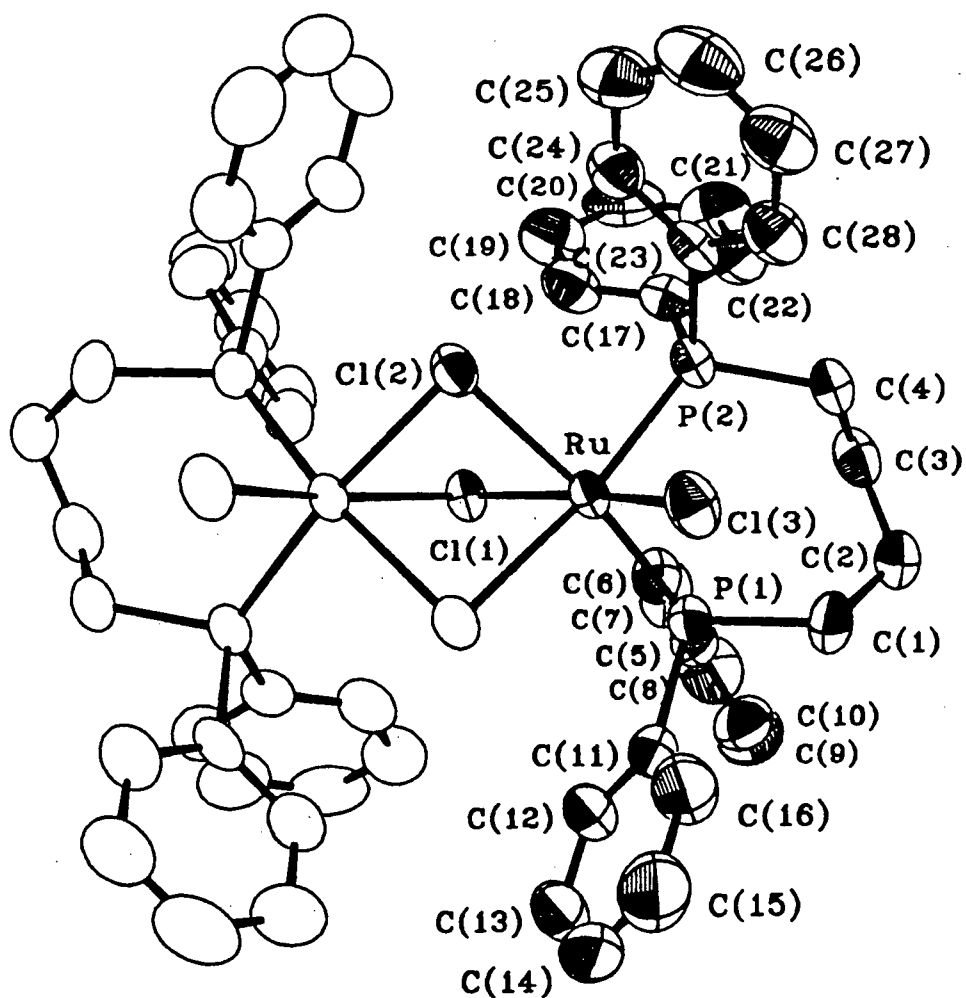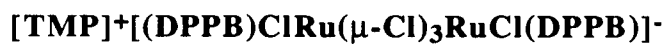
Molecular Structure of [TMP]$^+$[(DPPB)ClRu(μ-Cl)$_3$RuCl(DPPB)]$^-$ (ORTEP Plot)

Table III.1 Bond Lengths (Å) with estimated standard deviations

Bond	Length(Å)	Bond	Length(Å)
Ru -Cl(1)	2.4269(10)	C(17)-C(18)	1.381(6)
Ru -Cl(2)	2.4968(10)	C(17)-C(22)	1.396(6)
Ru -Cl(3)	2.4136(10)	C(18)-C(19)	1.379(7)
Ru -P(1)	2.2650(12)	C(19)-C(20)	1.360(8)
Ru -P(2)	2.2642(10)	C(20)-C(21)	1.355(8)
Ru -Cl(2)'	2.5007(9)	C(21)-C(22)	1.386(7)
P(1)-C(1)	1.858(4)	C(23)-C(24)	1.388(6)
P(1)-C(5)	1.840(5)	C(23)-C(28)	1.400(6)
P(1)-C(11)	1.841(5)	C(24)-C(25)	1.385(7)
P(2)-C(4)	1.841(4)	C(25)-C(26)	1.405(8)
P(2)-C(17)	1.841(4)	C(26)-C(27)	1.343(9)
P(2)-C(23)	1.840(4)	C(27)-C(28)	1.376(7)
C(1)-C(2)	1.551(7)	N -C(29)	1.443(6)
C(2)-C(3)	1.531(7)	N -C(35)	1.358(12)
C(3)-C(4)	1.511(6)	N -C(36)	1.460(6)
C(5)-C(6)	1.388(6)	N -C(37)	1.691(11)
C(5)-C(10)	1.397(6)	N -C(35)'	1.437(11)
C(6)-C(7)	1.375(7)	C(29)-C(30)	1.372(7)
C(7)-C(8)	1.361(8)	C(29)-C(34)	1.414(5)
C(8)-C(9)	1.358(8)	C(30)-C(31)	1.394(8)
C(9)-C(10)	1.378(7)	C(31)-C(32)	1.341(9)
C(11)-C(12)	1.381(7)	C(32)-C(33)	1.429(7)
C(11)-C(16)	1.382(7)	C(33)-C(34)	1.423(10)
C(12)-C(13)	1.396(9)	O(1)-C(38)	1.257(15)
C(13)-C(14)	1.405(12)	C(38)-C(39)	1.24(3)
C(14)-C(15)	1.351(13)	C(38)-C(40)	1.61(3)
C(15)-C(16)	1.377(9)		

Table III.2 Bond Angles (deg) with estimated standard deviations

Bonds	Angle(deg)	Bonds	Angle(deg)
Cl(1)-Ru -Cl(2)	78.85(3)	C(13)-C(14)-C(15)	120.4(7)
Cl(1)-Ru -Cl(3)	167.71(3)	C(14)-C(15)-C(16)	120.4(8)
Cl(1)-Ru -P(1)	97.50(3)	C(11)-C(16)-C(15)	121.1(7)
Cl(1)-Ru -P(2)	103.41(3)	P(2)-C(17)-C(18)	119.5(3)
Cl(1)-Ru -Cl(2)'	78.77(3)	P(2)-C(17)-C(22)	123.3(4)
Cl(2)-Ru -Cl(3)	94.16(4)	C(18)-C(17)-C(22)	117.0(4)
Cl(2)-Ru -P(1)	172.04(4)	C(17)-C(18)-C(19)	121.6(5)
Cl(2)-Ru -P(2)	91.01(4)	C(18)-C(19)-C(20)	120.1(5)
Cl(2)-Ru -Cl(2)'	78.87(4)	C(19)-C(20)-C(21)	120.3(5)
Cl(3)-Ru -P(1)	88.12(4)	C(20)-C(21)-C(22)	120.3(5)
Cl(3)-Ru -P(2)	86.67(4)	C(17)-C(22)-C(21)	120.8(5)
Cl(3)-Ru -Cl(2)'	90.02(4)	P(2)-C(23)-C(24)	121.6(3)
P(1)-Ru -P(2)	96.74(4)	P(2)-C(23)-C(28)	120.6(4)
P(1)-Ru -Cl(2)'	93.52(4)	C(24)-C(23)-C(28)	117.7(4)
P(2)-Ru -Cl(2)'	169.10(4)	C(23)-C(24)-C(25)	121.1(5)
Ru -Cl(1)-Ru'	87.77(5)	C(24)-C(25)-C(26)	119.0(5)
Ru -Cl(2)-Ru'	84.64(3)	C(25)-C(26)-C(27)	120.4(5)
Ru -P(1)-C(1)	118.8(2)	C(26)-C(27)-C(28)	120.6(5)
Ru -P(1)-C(5)	122.69(15)	C(23)-C(28)-C(27)	121.1(5)
Ru -P(1)-C(11)	111.15(15)	C(29)-N -C(35)	116.5(5)
C(1)-P(1)-C(5)	100.0(2)	C(29)-N -C(36)	117.2(4)
C(1)-P(1)-C(11)	99.4(2)	C(29)-N -C(37)	108.4(5)

Table III.2 Continued

C(5)-P(1)-C(11)	101.1(2)	C(29)-N -C(35)'	113.6(5)
Ru -P(2)-C(4)	117.16(15)	C(35)-N -C(36)	126.3(5)
Ru -P(2)-C(17)	120.06(13)	C(35)-N -C(37)	68.9(5)
Ru -P(2)-C(23)	114.02(13)	C(35)-N -C(35)'	37.6(7)
C(4)-P(2)-C(17)	103.1(2)	C(36)-N -C(37)	96.1(5)
C(4)-P(2)-C(23)	99.8(2)	C(36)-N -C(35)'	113.9(5)
C(17)-P(2)-C(23)	99.5(2)	C(37)-N -C(35)'	105.3(6)
P(1)-C(1)-C(2)	116.2(3)	N -C(29)-C(30)	121.3(5)
C(1)-C(2)-C(3)	115.2(4)	N -C(29)-C(34)	116.3(4)
C(2)-C(3)-C(4)	114.5(4)	C(30)-C(29)-C(34)	122.3(5)
P(2)-C(4)-C(3)	113.6(3)	C(29)-C(30)-C(31)	118.9(6)
P(1)-C(5)-C(6)	122.1(3)	C(30)-C(31)-C(32)	121.0(6)
P(1)-C(5)-C(10)	119.8(4)	C(31)-C(32)-C(33)	122.3(6)
C(6)-C(5)-C(10)	117.9(4)	C(32)-C(33)-C(34)	117.3(4)
C(5)-C(6)-C(7)	120.5(5)	C(32)-C(33)-C(32)'	125.3(8)
C(6)-C(7)-C(8)	120.7(5)	C(34)-C(33)-C(32)'	117.3(4)
C(7)-C(8)-C(9)	120.0(5)	C(29)-C(34)-C(33)	118.2(3)
C(8)-C(9)-C(10)	120.6(5)	C(29)-C(34)-C(29)'	123.6(6)
C(5)-C(10)-C(9)	120.2(5)	C(33)-C(34)-C(29)'	118.2(3)
P(1)-C(11)-C(12)	121.3(4)	N -C(35)-N'	118.5(7)
P(1)-C(11)-C(16)	119.7(4)	O(1)-C(38)-C(39)	126(3)
C(12)-C(11)-C(16)	118.9(5)	O(1)-C(38)-C(40)	95(2)
C(11)-C(12)-C(13)	120.5(7)	C(39)-C(38)-C(40)	138.5(14)
C(12)-C(13)-C(14)	118.7(7)		

X-Ray Crystallographic Analysis of Ru(BINAP)(η^3-Me-allyl)$_2$ 56
Co-Crystallized with
(*R*)-(+)-2,2'-bis(diphenylphosphinoyl)-1,1'-binaphthyl (BINAP(O)$_2$)
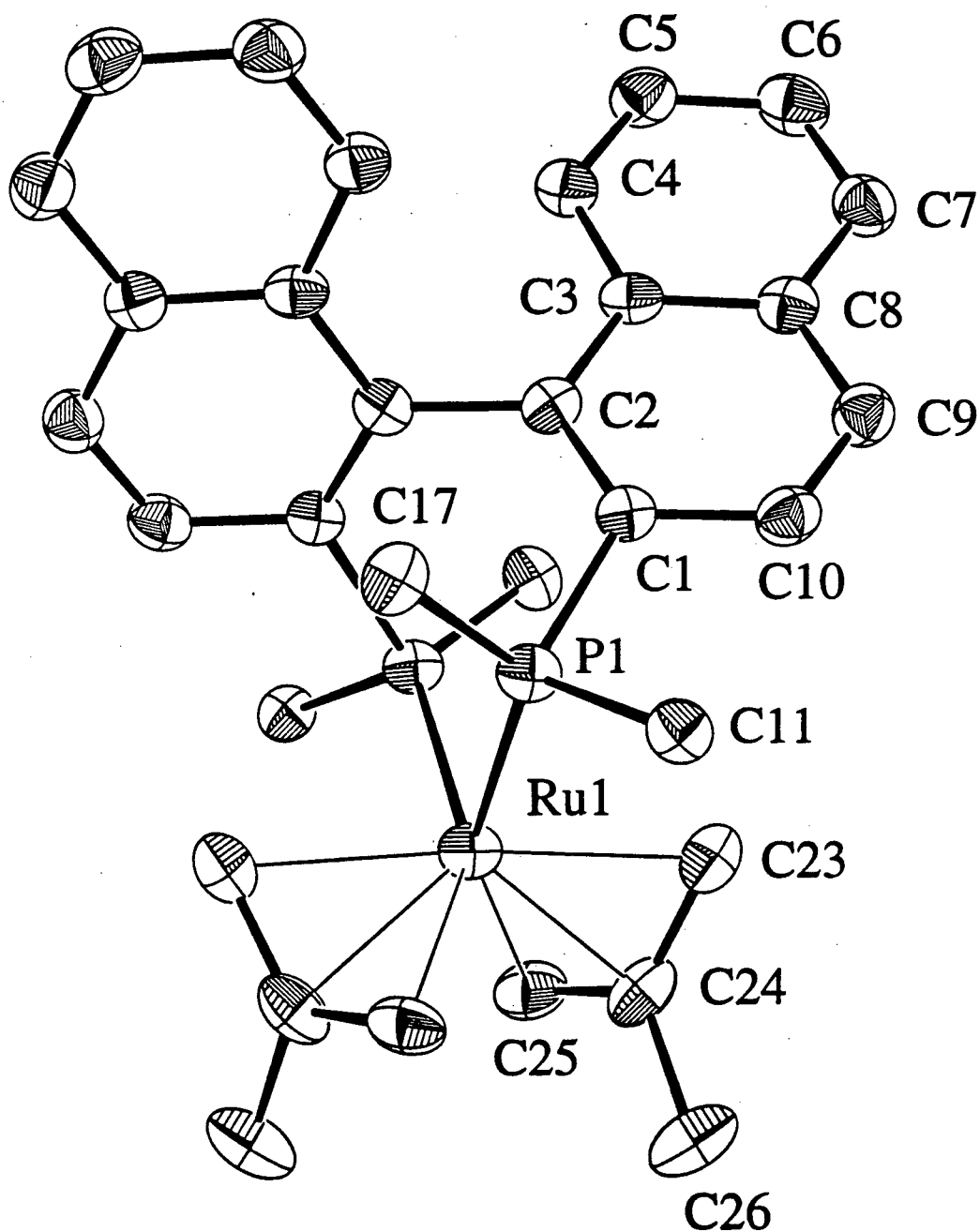
Molecular Structure of Ru(BINAP)(η^3-Me-allyl)$_2$, **56** (ORTEP Plot)
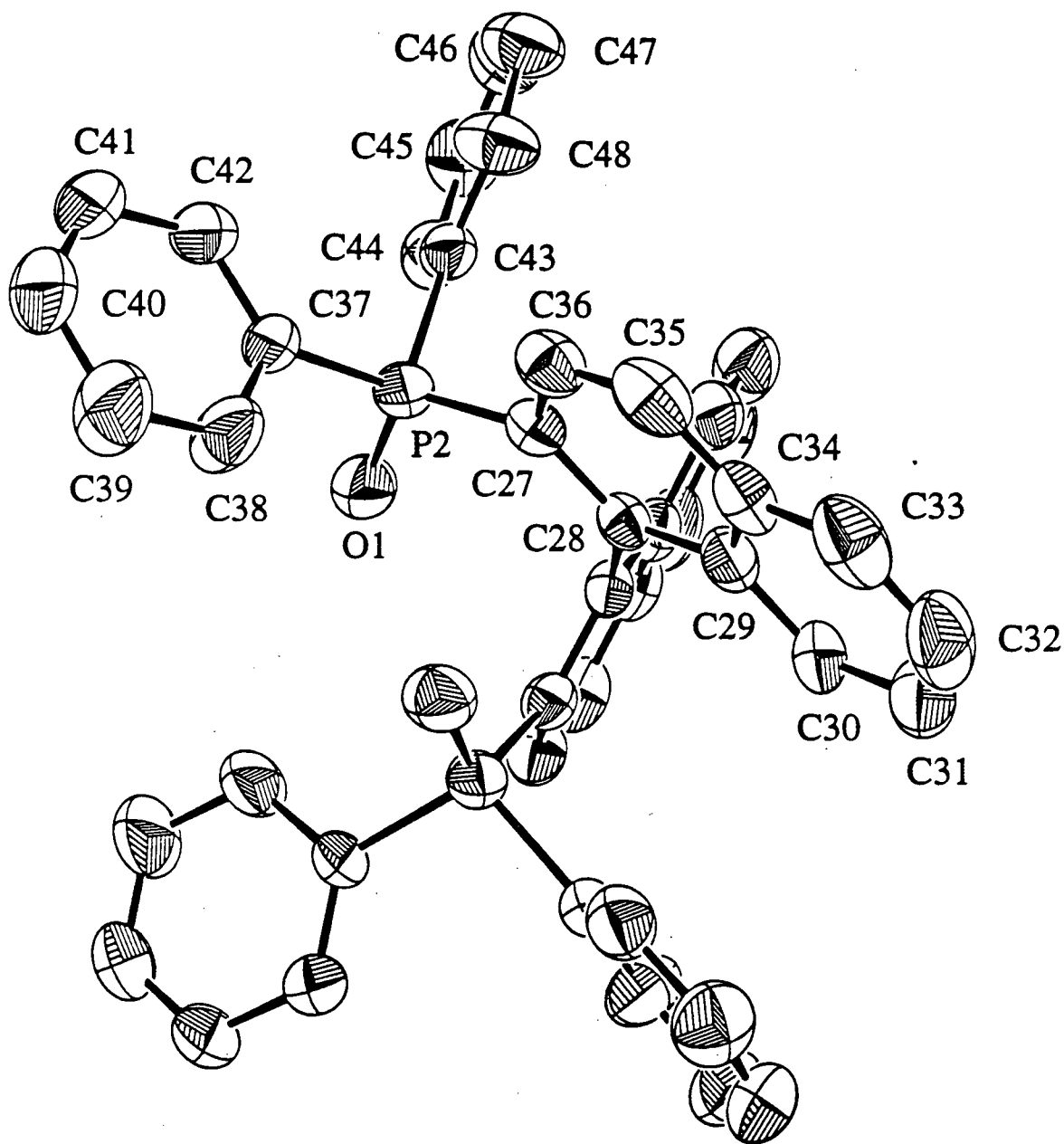
Molecular Structure of (*R*)-(+)-2,2'-bis(diphenylphosphinoyl)-1,1'-binaphthyl

(BINAP(O)$_2$) (ORTEP Plot)
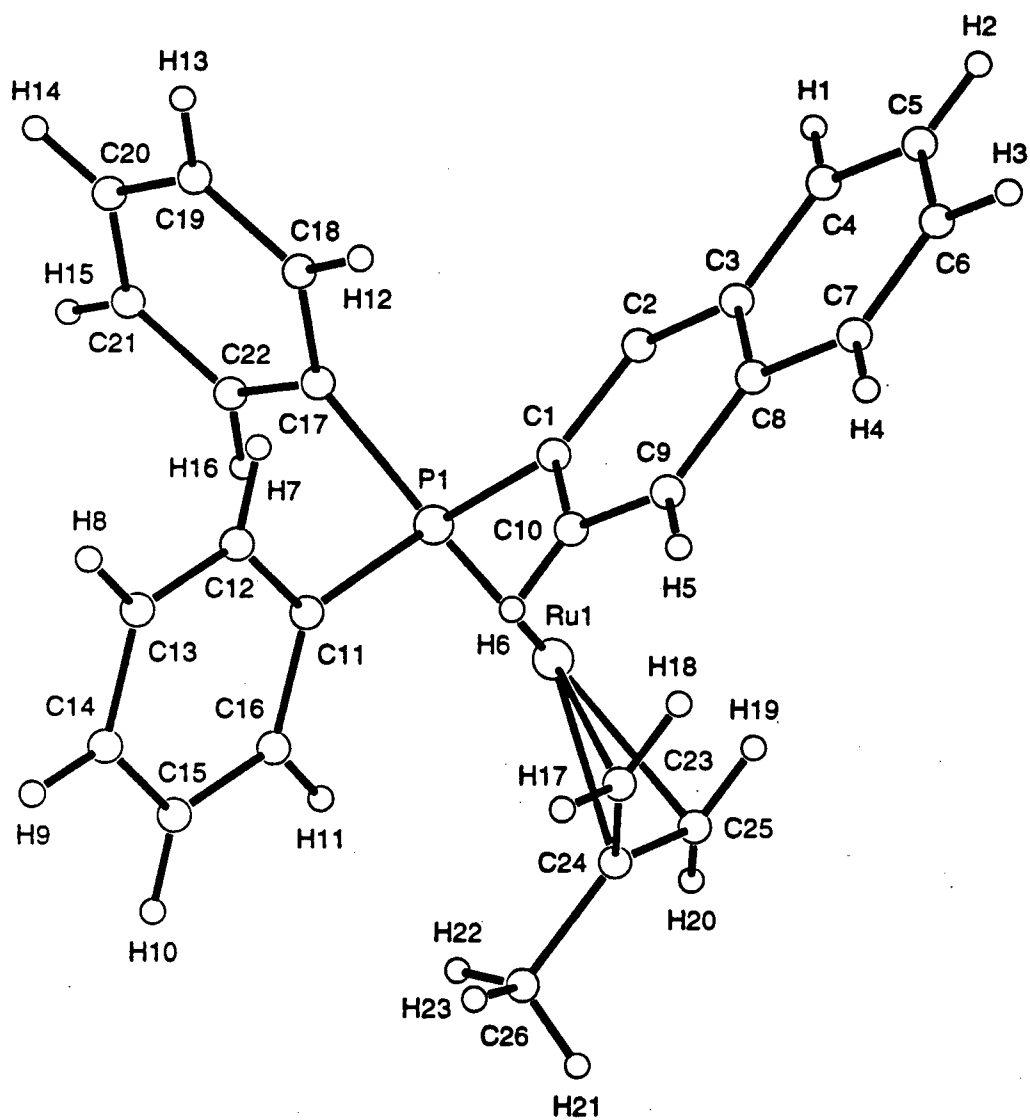
Molecular Structure of Ru(BINAP)(η^3-Me-allyl)$_2$, **56**

(Pluto Plot)
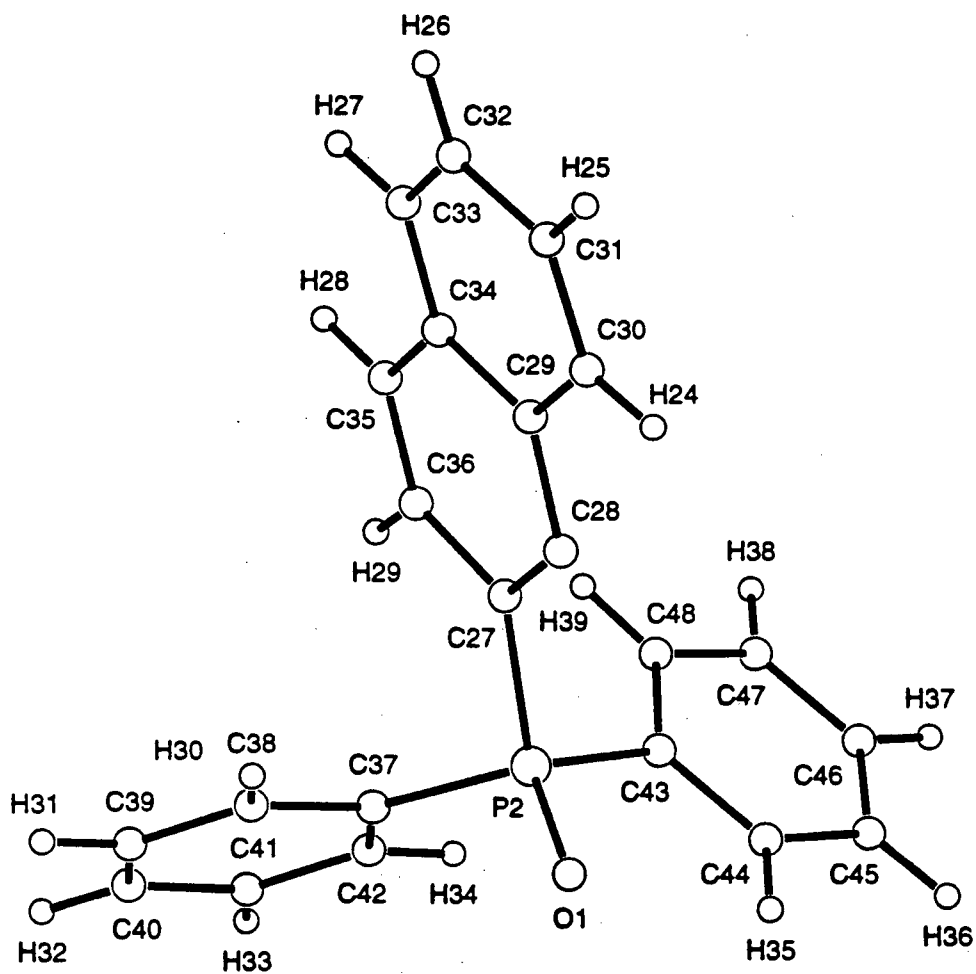
Molecular Structure of (*R*)-(+)-2,2'-bis(diphenylphosphinoyl)-1,1'-binaphthyl

(BINAP(O)$_2$) (Pluto Plot)
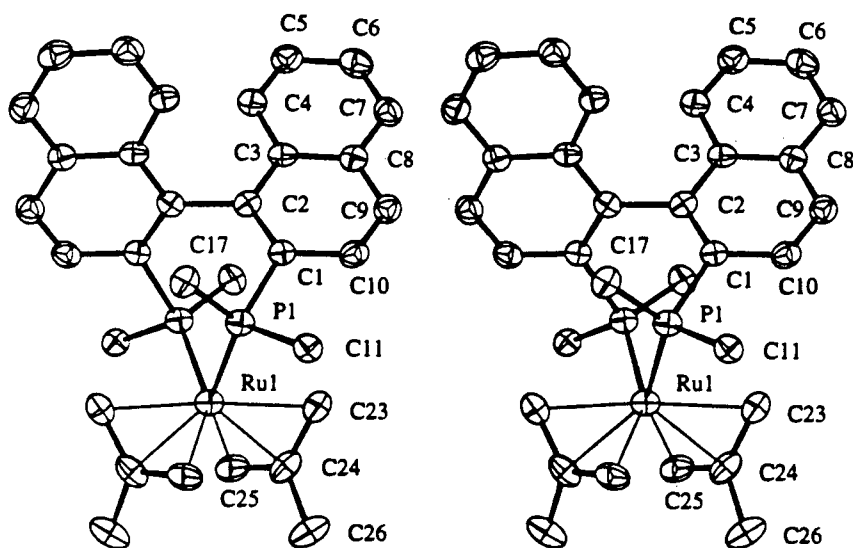
Molecular Structure of Ru(BINAP)(η^3-Me-allyl)$_2$, **56** (Stereoview)
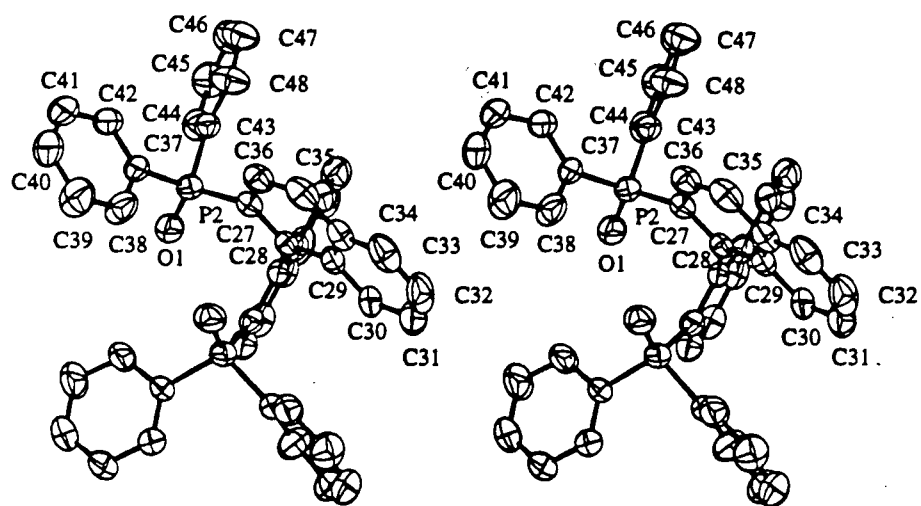
Molecular Structure of (*R*)-(+)-2,2'-bis(diphenylphosphinoyl)-1,1'-binaphthyl

(BINAP(O)$_2$) (Stereoview)
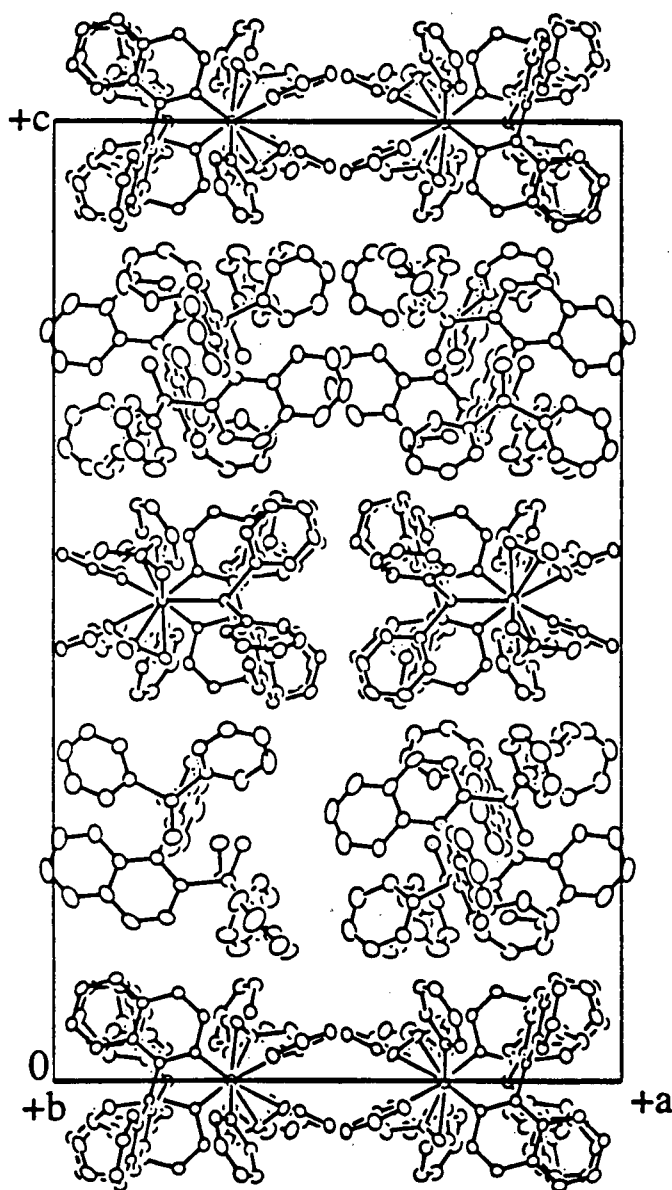
Unit cell of Ru(BINAP)(η^3-Me-allyl)$_2$ **56** co-crystallized with

(*R*)-(+)-2,2'-bis(diphenylphosphinoyl)-1,1'-binaphthyl (BINAP(O)$_2$)

EXPERIMENTAL DETAILS

A. Crystal Data

Empirical Formula	$C_{105.52}H_{87.52}O_2P_4Ru$
Formula Weight	1612.58
Crystal Color, Habit	orange, prism
Crystal Dimensions	0.25 X 0.35 X 0.35 mm
Crystal System	tetragonal
Lattice Type	I-centered
No. of Reflections Used for Unit Cell Determination (2θ range)	25 (66.6 - 82.9°)
Omega Scan Peak Width at Half-height	0.37°
Lattice Parameters	$a = 21.344(1)$ Å $c = 36.453(2)$ Å $V = 16606.0(9)$ Å^3
Space Group	I422 (#97)
Z value	8
D_{calc}	1.290 g/cm^3
F_{000}	6725.12
μ(CuKα)	26.61 cm^{-1}

B. Intensity Measurements

Diffractometer	Rigaku AFC6S
Radiation	CuKα ($\lambda = 1.54178$ Å) graphite monochromated
Take-off Angle	6.0°

Detector Aperture	6.0 mm horizontal
	6.0 mm vertical
Crystal to Detector Distance	285 mm
Temperature	21°C
Scan Type	ω-2θ
Scan Rate	32°/min (in ω) (up to 9 scans)
Scan Width	$(0.94 + 0.20 \tan \theta)°$
$2\theta_{max}$	155°
No. of Reflections Measured	Total: 4918
Corrections	Lorentz-polarization
	Absorption
	(trans. factors: 0.639 - 1.000)
	Secondary Extinction
	(coefficient: 9.89(14) x 10^{-8})

C. Structure Solution and Refinement

Structure Solution	Direct Methods (SIR92)
Refinement	Full-matrix least-squares
Function Minimized	$\Sigma w(|Fo| - |Fc|)^2$
Least Squares Weights	$\frac{1}{\sigma^2(Fo)} = \frac{4Fo^2}{\sigma^2(Fo^2)}$
p-factor	0.000
Anomalous Dispersion	All non-hydrogen atoms
No. Observations (I>3σ(I))	3431
No. Variables	510
Reflection/Parameter Ratio	6.73
Residuals: R; Rw	0.034 ; 0.032
Goodness of Fit Indicator	1.85
Max Shift/Error in Final Cycle	0.02
Maximum peak in Final Diff. Map	0.27 $e^-/\text{Å}^3$
Minimum peak in Final Diff. Map	-0.29 $e^-/\text{Å}^3$

323

Table IV.1 Bond Lengths (Å) with estimated standard deviations

atom	atom	distance	atom	atom	distance
Ru(1)	P(1)	2.339(1)	Ru(1)	C(23)	2.228(4)
Ru(1)	C(24)	2.178(5)	Ru(1)	C(25)	2.240(5)
Ru(1)	A	1.96	P(1)	C(1)	1.845(5)
P(1)	C(11)	1.857(5)	P(1)	C(17)	1.844(5)
P(2)	O(1)	1.478(4)	P(2)	C(27)	1.795(6)
P(2)	C(37)	1.811(6)	P(2)	C(43)	1.807(6)
C(1)	C(2)	1.387(6)	C(1)	C(10)	1.429(7)
C(2)	C(2)'	1.524(8)	C(2)	C(3)	1.423(6)
C(3)	C(4)	1.418(7)	C(3)	C(8)	1.426(6)
C(4)	C(5)	1.342(7)	C(5)	C(6)	1.413(7)
C(6)	C(7)	1.354(8)	C(7)	C(8)	1.413(7)
C(8)	C(9)	1.401(7)	C(9)	C(10)	1.349(7)
C(11)	C(12)	1.398(7)	C(11)	C(16)	1.375(7)
C(12)	C(13)	1.379(7)	C(13)	C(14)	1.373(7)
C(14)	C(15)	1.371(7)	C(15)	C(16)	1.387(7)
C(17)	C(18)	1.403(7)	C(17)	C(22)	1.398(7)
C(18)	C(19)	1.397(7)	C(19)	C(20)	1.360(8)
C(20)	C(21)	1.375(9)	C(21)	C(22)	1.383(7)
C(23)	C(24)	1.403(7)	C(24)	C(25)	1.388(8)
C(24)	C(26)	1.529(8)	C(27)	C(28)	1.380(7)
C(27)	C(36)	1.427(8)	C(28)	C(28)"	1.504(10)
C(28)	C(29)	1.434(8)	C(29)	C(30)	1.418(8)
C(29)	C(34)	1.422(8)	C(30)	C(31)	1.39(1)
C(31)	C(32)	1.41(1)	C(32)	C(33)	1.34(1)
C(33)	C(34)	1.39(1)	C(34)	C(35)	1.394(9)
C(35)	C(36)	1.360(9)	C(37)	C(38)	1.389(9)
C(37)	C(42)	1.345(8)	C(38)	C(39)	1.373(10)
C(39)	C(40)	1.36(1)	C(40)	C(41)	1.35(1)
C(41)	C(42)	1.383(9)	C(43)	C(44)	1.362(9)
C(43)	C(48)	1.386(8)	C(44)	C(45)	1.40(1)
C(45)	C(46)	1.33(1)	C(46)	C(47)	1.33(1)
C(47)	C(48)	1.379(10)			

* Here and elsewhere, A refers to the unweighted centroid of the
three coordinated carbon atoms of the methylallyl ligand. Symmetry
operations: (') y, x, 1-z (") 1/2-y, 1/2-x, 1/2-z.

Table IV.2 Bond Angles (deg) with estimated standard deviations

atom	atom	atom	angle
P(1)	Ru(1)	P(1)'	91.92(6)
P(1)	Ru(1)	C(23)'	97.1(1)
P(1)	Ru(1)	C(24)'	111.4(2)
P(1)	Ru(1)	C(25)'	89.1(2)
P(1)	Ru(1)	A'	100.2
C(23)	Ru(1)	C(24)	37.1(2)
C(23)	Ru(1)	C(25)	65.6(2)
C(24)	Ru(1)	C(24)'	104.4(3)
C(24)	Ru(1)	C(25)'	92.1(2)
A	Ru(1)	A'	122.0
Ru(1)	P(1)	C(11)	116.8(2)
C(1)	P(1)	C(11)	100.8(2)
C(11)	P(1)	C(17)	94.3(2)
O(1)	P(2)	C(37)	111.4(3)
C(27)	P(2)	C(37)	104.9(3)
C(37)	P(2)	C(43)	106.1(3)
P(1)	C(1)	C(10)	117.5(4)
C(1)	C(2)	C(2)'	119.7(3)
C(2)'	C(2)	C(3)	119.6(3)
C(2)	C(3)	C(8)	119.1(5)
C(3)	C(4)	C(5)	122.7(5)
C(5)	C(6)	C(7)	119.4(5)
C(3)	C(8)	C(7)	119.7(5)
C(7)	C(8)	C(9)	121.3(5)

atom	atom	atom	angle
P(1)	Ru(1)	C(23)	86.8(2)
P(1)	Ru(1)	C(24)	119.2(2)
P(1)	Ru(1)	C(25)	152.2(2)
P(1)	Ru(1)	A	119.8
C(23)	Ru(1)	C(23)'	174.4(3)
C(23)	Ru(1)	C(24)'	137.6(2)
C(23)	Ru(1)	C(25)'	110.7(2)
C(24)	Ru(1)	C(25)	86.6(2)
C(25)	Ru(1)	C(25)'	102.7(3)
Ru(1)	P(1)	C(1)	109.3(1)
Ru(1)	P(1)	C(17)	128.1(2)
C(1)	P(1)	C(17)	103.7(2)
O(1)	P(2)	C(27)	117.1(3)
O(1)	P(2)	C(43)	110.6(3)
C(27)	P(2)	C(43)	106.0(3)
P(1)	C(1)	C(2)	123.9(4)
C(2)	C(1)	C(10)	118.3(4)
C(1)	C(2)	C(3)	120.6(4)
C(2)	C(3)	C(4)	124.4(5)
C(4)	C(3)	C(8)	116.4(4)
C(4)	C(5)	C(6)	120.5(5)
C(6)	C(7)	C(8)	121.3(5)
C(3)	C(8)	C(9)	118.9(5)
C(8)	C(9)	C(10)	121.2(5)

atom	atom	atom	angle
C(1)	C(10)	C(9)	121.7(5)
P(1)	C(11)	C(16)	121.1(4)
C(11)	C(12)	C(13)	121.6(5)
C(13)	C(14)	C(15)	119.5(5)
C(11)	C(16)	C(15)	121.3(5)
P(1)	C(17)	C(22)	118.7(4)
C(17)	C(18)	C(19)	119.9(5)
C(19)	C(20)	C(21)	119.5(6)
C(17)	C(22)	C(21)	121.3(6)
C(23)	C(24)	C(26)	120.5(5)
P(2)	C(27)	C(28)	122.8(4)
C(28)	C(27)	C(36)	117.1(5)
C(27)	C(28)	C(29)	121.9(5)
C(28)	C(29)	C(30)	122.2(6)
C(30)	C(29)	C(34)	118.9(6)
C(30)	C(31)	C(32)	121.1(9)
C(32)	C(33)	C(34)	123.2(8)
C(29)	C(34)	C(35)	118.0(6)
C(34)	C(35)	C(36)	122.2(6)
P(2)	C(37)	C(38)	117.2(5)
C(38)	C(37)	C(42)	119.0(6)
C(38)	C(39)	C(40)	120.6(8)
C(40)	C(41)	C(42)	120.4(8)
P(2)	C(43)	C(44)	117.4(5)
C(44)	C(43)	C(48)	118.3(6)
C(44)	C(45)	C(46)	118.8(9)
C(46)	C(47)	C(48)	120.6(8)

atom	atom	atom	angle
P(1)	C(11)	C(12)	121.6(4)
C(12)	C(11)	C(16)	117.2(5)
C(12)	C(13)	C(14)	120.0(5)
C(14)	C(15)	C(16)	120.4(5)
P(1)	C(17)	C(18)	123.1(4)
C(18)	C(17)	C(22)	117.5(5)
C(18)	C(19)	C(20)	121.4(6)
C(20)	C(21)	C(22)	120.4(6)
C(23)	C(24)	C(25)	120.2(5)
C(25)	C(24)	C(26)	119.4(5)
P(2)	C(27)	C(36)	120.0(5)
C(27)	C(28)	C(28)"	119.8(5)
C(28)"	C(28)	C(29)	118.3(6)
C(28)	C(29)	C(34)	119.0(6)
C(29)	C(30)	C(31)	119.2(8)
C(31)	C(32)	C(33)	119.0(8)
C(29)	C(34)	C(33)	118.8(8)
C(33)	C(34)	C(35)	123.2(8)
C(27)	C(36)	C(35)	121.8(6)
P(2)	C(37)	C(42)	123.5(5)
C(37)	C(38)	C(39)	119.8(7)
C(39)	C(40)	C(41)	119.5(8)
C(37)	C(42)	C(41)	120.7(7)
P(2)	C(43)	C(48)	124.3(6)
C(43)	C(44)	C(45)	120.9(7)
C(45)	C(46)	C(47)	121.8(9)
C(43)	C(48)	C(47)	119.5(8)

Table IV.3 Final Atomic Coordinates (Fractional) and B(eq)

atom	x	y	z	B_{eq}	pop.
Ru(1)	0.19060(2)	0.19060	0.50000	3.344(5)	0.50
P(1)	0.30019(4)	0.18877(5)	0.49963(5)	3.28(2)	
P(2)	0.20691(8)	0.19387(9)	0.29135(4)	5.08(4)	
O(1)	0.2091(2)	0.1682(2)	0.2537(1)	6.9(1)	
C(1)	0.3295(2)	0.2523(2)	0.4699(1)	3.04(10)	
C(2)	0.3331(2)	0.3146(2)	0.4806(1)	2.94(9)	
C(3)	0.3533(3)	0.3614(3)	0.4554(1)	3.2(1)	
C(4)	0.3616(2)	0.4255(2)	0.4645(1)	3.7(1)	
C(5)	0.3792(3)	0.4686(2)	0.4397(2)	4.3(1)	
C(6)	0.3909(3)	0.4513(3)	0.4030(2)	4.7(1)	
C(7)	0.3841(3)	0.3906(3)	0.3928(1)	4.3(1)	
C(8)	0.3656(2)	0.3443(2)	0.4183(1)	3.4(1)	
C(9)	0.3593(2)	0.2814(3)	0.4079(1)	4.0(1)	
C(10)	0.3427(2)	0.2371(2)	0.4325(1)	3.9(1)	
C(11)	0.3381(2)	0.1197(2)	0.4780(1)	3.5(1)	
C(12)	0.4029(3)	0.1165(3)	0.4730(2)	4.8(1)	
C(13)	0.4312(3)	0.0644(3)	0.4580(2)	5.2(2)	
C(14)	0.3955(3)	0.0136(2)	0.4481(2)	4.8(2)	
C(15)	0.3318(3)	0.0157(2)	0.4527(1)	4.6(1)	
C(16)	0.3034(3)	0.0684(2)	0.4675(1)	3.9(1)	
C(17)	0.3539(2)	0.1902(2)	0.5392(1)	3.8(1)	
C(18)	0.4139(3)	0.2170(2)	0.5379(2)	4.3(1)	
C(19)	0.4558(3)	0.2076(3)	0.5668(2)	5.6(2)	
C(20)	0.4399(3)	0.1725(3)	0.5965(2)	5.8(2)	
C(21)	0.3810(3)	0.1466(3)	0.5986(2)	5.4(2)	
C(22)	0.3384(3)	0.1554(3)	0.5705(2)	4.4(1)	
C(23)	0.1957(3)	0.1784(2)	0.4394(1)	4.2(1)	
C(24)	0.1397(3)	0.1530(3)	0.4531(1)	4.2(1)	
C(25)	0.0975(2)	0.1910(3)	0.4717(1)	4.7(1)	
C(26)	0.1250(3)	0.0834(3)	0.4482(2)	6.5(2)	
C(27)	0.2165(3)	0.2770(3)	0.2963(2)	4.6(1)	
C(28)	0.2051(2)	0.3186(3)	0.2681(1)	4.3(1)	
C(29)	0.2173(3)	0.3844(3)	0.2718(2)	5.3(2)	
C(30)	0.2066(3)	0.4273(3)	0.2428(2)	6.9(2)	
C(31)	0.2228(4)	0.4900(4)	0.2475(3)	9.1(3)	
C(32)	0.2489(5)	0.5114(4)	0.2808(3)	9.3(3)	
C(33)	0.2580(4)	0.4705(4)	0.3080(2)	8.3(3)	
C(34)	0.2430(3)	0.4072(3)	0.3052(2)	5.8(2)	
C(35)	0.2533(3)	0.3644(4)	0.3335(2)	6.7(2)	
C(36)	0.2411(3)	0.3022(3)	0.3296(2)	5.9(2)	
C(37)	0.2673(3)	0.1599(3)	0.3200(2)	5.1(2)	
C(38)	0.3289(3)	0.1758(4)	0.3121(2)	8.4(2)	
C(39)	0.3770(4)	0.1483(5)	0.3313(3)	10.8(3)	
C(40)	0.3647(4)	0.1050(4)	0.3577(3)	8.5(3)	
C(41)	0.3047(4)	0.0884(4)	0.3548(2)	8.1(2)	
C(42)	0.2559(3)	0.1162(4)	0.3457(2)	6.6(2)	
C(43)	0.1333(3)	0.1750(3)	0.3131(2)	5.1(2)	
C(44)	0.0925(4)	0.1381(4)	0.2941(2)	6.8(2)	
C(45)	0.0344(4)	0.1215(4)	0.3090(3)	8.6(3)	
C(46)	0.0199(4)	0.1414(5)	0.3426(3)	9.2(3)	
C(47)	0.0591(4)	0.1708(5)	0.3622(2)	8.7(3)	
C(48)	0.1158(3)	0.1955(4)	0.3477(2)	7.8(2)	
C(49)	0.4790(9)	-0.015(1)	0.1480(4)	7.4(6)	0.50
C(50)	0.529(1)	0.029(1)	0.1602(7)	10.0(7)	0.50
C(51)	0.5644(10)	0.027(1)	0.1825(7)	9.4(6)	0.50
C(52)	0.557(1)	-0.012(1)	0.2101(6)	11.3(6)	0.50
C(53)	0.512(2)	-0.054(1)	0.2120(7)	15.1(8)	0.50
C(54)	0.471(2)	-0.058(1)	0.1846(9)	14.5(9)	0.50
C(55)	-0.060(2)	0.003(3)	0.2017(5)	9.7(8)	0.61(7)
C(56)	-0.051(1)	-0.035(1)	0.2035(4)	6.9(7)	0.58(6)
C(57)	-0.032(3)	-0.080(3)	0.2060(10)	7(1)	0.33(8)
C(58)	-0.055(4)	0.104(5)	0.209(2)	22(3)	0.24(3)

$$B_{eq} = \frac{8}{3}\pi^2(U_{11}(aa^*)^2 + U_{22}(bb^*)^2 + U_{33}(cc^*)^2 + 2U_{12}aa^*bb^*\cos\gamma + 2U_{13}aa^*cc^*\cos\beta + 2U_{23}bb^*cc^*\cos\alpha)$$

APPENDIX V

A summary of the units and constants required for the calculation of r_{HH} (the H–H internuclear distance) from the measured $T_1(min)$ value of an η^2-H_2 ligand bound to a transition metal is presented below for both (a) cgs and (b) SI units. This summary is presented because dimensional analysis of electromagnetic quantities involves unfamiliar units and can be troublesome.[1] Some useful equations, numerical constants and units were found in the literature.[1,2] Listed below are some useful conversion factors:

Henry (H) = m^2 kg s^{-2} A^{-2} (inductance)

Tesla (T) = kg s^{-2} A^{-1} = 10^4 Gauss (magnetic flux)

Gauss (Gs) = Mx cm^{-2} (magnetic flux density)

Maxwell (Mx) = 1 x 10^{-8} V s (magnetic flux)

erg (erg) = 1 x 10^{-7} J (energy)

(a) cgs Units

The internuclear H–H distance, r_{HH}, can be calculated from Woessner's equation (equation 1) if the $T_1(min)$ value of the molecular hydrogen ligand is measured.

$$R(DD) = \{T_1(DD)\}^{-1} = 0.3\gamma_H^4\left(\frac{h}{2\pi}\right)^2 (r_{HH})^{-6}\left\{\frac{\tau_c}{1+\omega^2\tau_c^2} + \frac{4\tau_c}{1+4\omega^2\tau_c^2}\right\} \qquad (1)$$

(1) Sudmeier, J. L.; Anderson, S. E., Frye; J. S. *Concepts in Magnetic Resonance*, **1990**, *2*, 197.

(2) Gaboury, J. A. M., *Introduction to the International System of Units [SI]*, Montreal, Canada, J. A. M. Gaboury, 1990.

where $\quad$ R(DD) = the reciprocal of the spin-lattice relaxation time, T_1, when ^{1}H–^{1}H

dipole-dipole interaction is the only mechanism of relaxation (s^{-1})

T_1(DD) = spin-lattice relaxation time (s)

γ_H = gyromagnetic ratio of a ^{1}H and has the value of 2.675 x 10^4 rad G^{-1} s^{-1}

$h/2\pi$ = 1.0546 x 10^{-27} erg s

r_{HH} = H–H internuclear distance (cm)

ω = resonance or Larmor frequency (rad s^{-1}) = $2\pi\nu = \gamma_H B_o$
(B_o is the static magnetic field in Gauss; ν is the operating frequency of the spectrometer)

τ_c = rotational correlation time (s rad^{-1}) = 0.6158/ω.

The term $\left\{\dfrac{\tau_c}{1+\omega^2\tau_c^2} + \dfrac{4\tau_c}{1+4\omega^2\tau_c^2}\right\}$ equals 7.561 x 10^{-10} s rad^{-1} for a 300 MHz

spectrometer (which is the most frequently used spectrometer for T_1(min) measurements in this department).

Equation 1 reduces to:

$$R(DD) = \{T_1(DD)\}^{-1} = 1.708 \times 10^{-37}\, \text{rad cm}^6\, \text{s}^{-2}(r_{HH})^{-6}\left\{\frac{\tau_c}{1+\omega^2\tau_c^2} + \frac{4\tau_c}{1+4\omega^2\tau_c^2}\right\} \qquad (2)$$

when the values for the constants are substituted into the equation.[3]

If the T_1 measurement is performed on a 300 MHz spectrometer, equation 2 reduces to:

---

(3) Bautista, M. T.; Earl, K. A.; Maltby, P. A.; Morris, R. H.; Schweitzer, C. T.; Sella, A. *J. Am. Chem. Soc.*, **1988**, *110*, 7031.

$$R(DD) = \{T_1(DD)\}^{-1} = 1.291 \times 10^{-46} \text{ cm}^6 \text{ s}^{-1} (r_{HH})^{-6} \qquad (3)$$

In order to cancel out the cgs units and arrive at equation 3, one needs Planck's constant h and the gyromagnetic ratio γ in fundamental terms (i.e., cgs units):

(1) dimensions of Planck's constant h (erg s) in fundamental terms (g cm^2 s^{-1}); and (2) the gyromagnetic ratio $\gamma = \omega/B$ in fundamental terms (cm$^{-1/2}$ g$^{-1/2}$). Therefore, the dimensions of γ^4 are cm^2 g^{-2}.

(b) SI Units

If SI units are used, an extra term of $\left(\dfrac{\mu_o}{4\pi}\right)^2$ must be included in equation 1. The equation is then:

$$R(DD) = \{T_1(DD)\}^{-1} = 0.3 \left(\frac{\mu_o}{4\pi}\right)^2 \gamma_H^4 \left(\frac{h}{2\pi}\right)^2 (r_{HH})^{-6} \left\{ \frac{\tau_c}{1+\omega^2\tau_c^2} + \frac{4\tau_c}{1+4\omega^2\tau_c^2} \right\} \qquad (4)$$

where μ_o = the permeability of a vacuum = $4\pi \times 10^{-7}$ Henry m^{-1}.

The remaining terms of equation 4 should now be in the following units:

γ_H = 2.675 x 10^8 rad T^{-1} s^{-1}

h = 6.626 x 10^{-34} J s (or $h/2\pi$ = 1.054 x 10^{-34} J s)

r_{HH} = (m).

If the terms are collected, equation 4 reduces to:

$$R(DD) = \{T_1(DD)\}^{-1} = 1.706 \times 10^{-49} \text{ rad m}^6 \text{ s}^{-2} (r_{HH})^{-6} \left\{ \frac{\tau_c}{1 + \omega^2 \tau_c^2} + \frac{4\tau_c}{1 + 4\omega^2 \tau_c^2} \right\} \quad (5)$$

and for a 300 MHz spectrometer becomes:

$$R(DD) = \{T_1(DD)\}^{-1} = 1.291 \times 10^{-58} \text{ m}^6 \text{ s}^{-1} (r_{HH})^{-6} \quad (6)$$

If equation 6 is converted from m to Å, equation 7 results:

$$R(DD) = \{T_1(DD)\}^{-1} = 129.1 \text{ Å}^6 \text{ s}^{-1} (r_{HH})^{-6} \quad (7)$$

X-Ray Crystallographic Analysis of

$[(DMA)_2H]^+[(PPh_3)_2(H)Ru(\mu\text{-}Cl)_2(\mu\text{-}H)Ru(H)(PPh_3)_2]^-$, 18
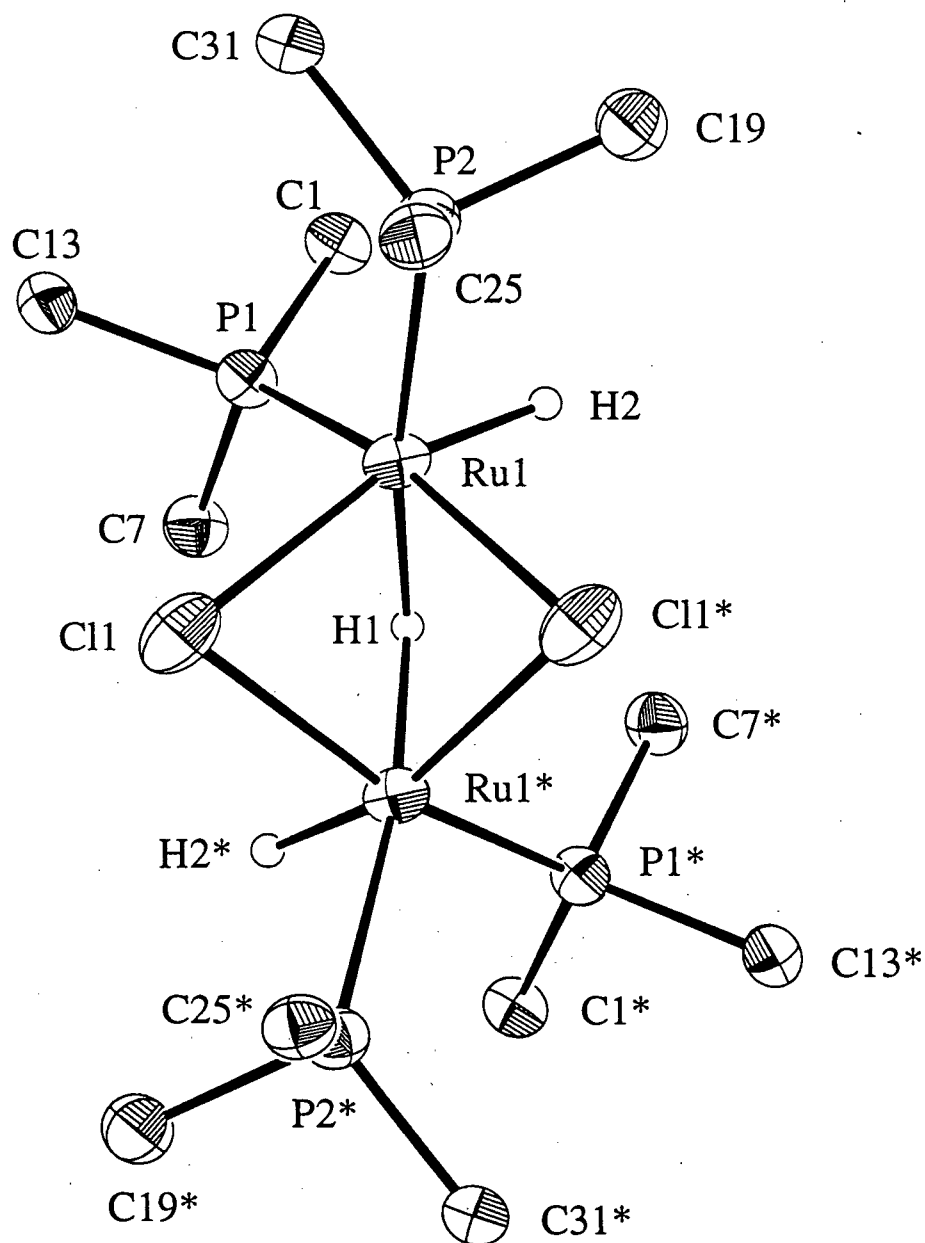
Molecular Structure of $[(DMA)_2H]^+[(PPh_3)_2(H)Ru(\mu\text{-}Cl)_2(\mu\text{-}H)Ru(H)(PPh_3)_2]^-$, 18

(ORTEP Plot)
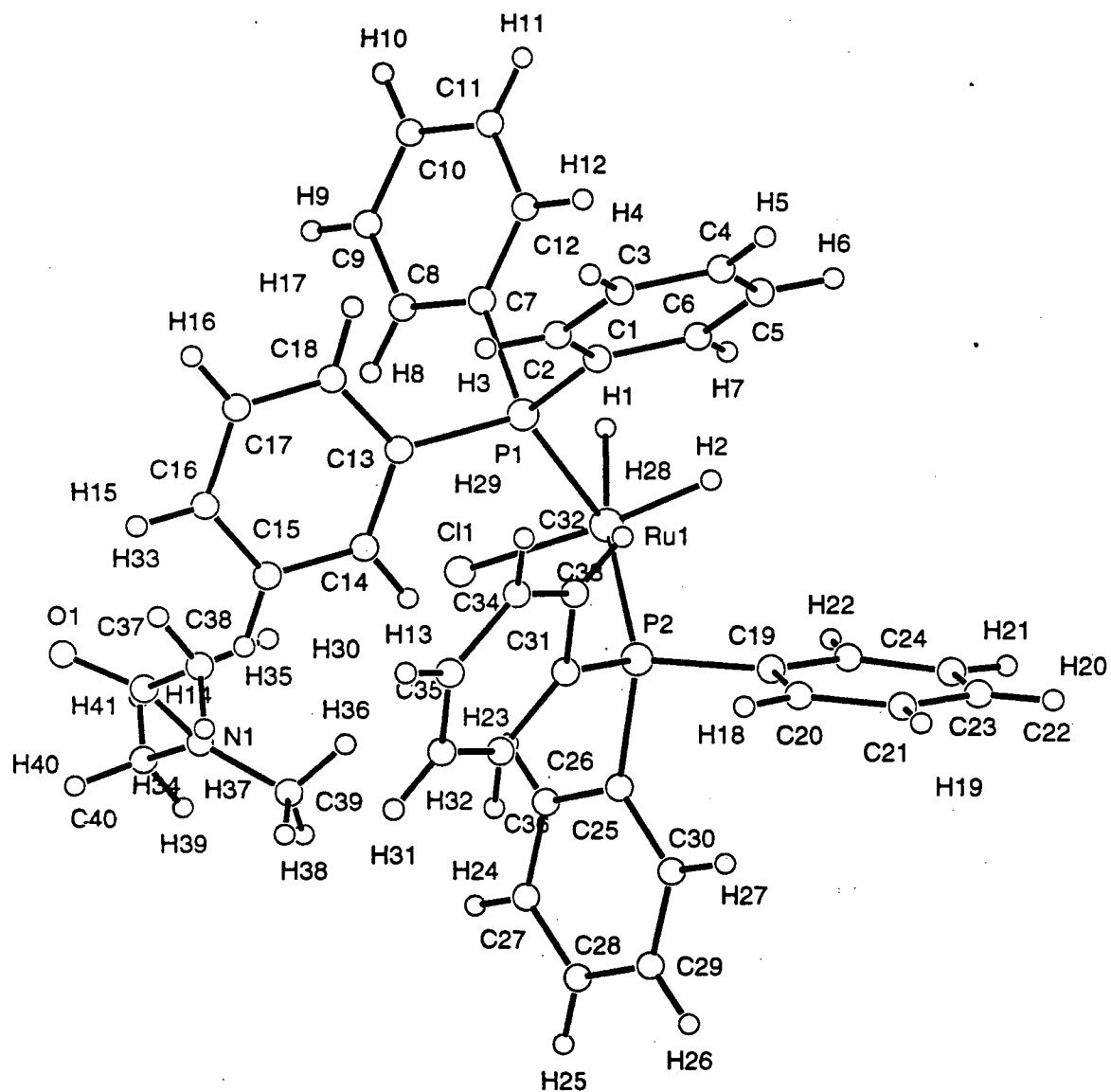
Molecular Structure of $[(DMA)_2H]^+[(PPh_3)_2(H)Ru(\mu\text{-}Cl)_2(\mu\text{-}H)Ru(H)(PPh_3)_2]^-$, **18**

(Pluto Plot)
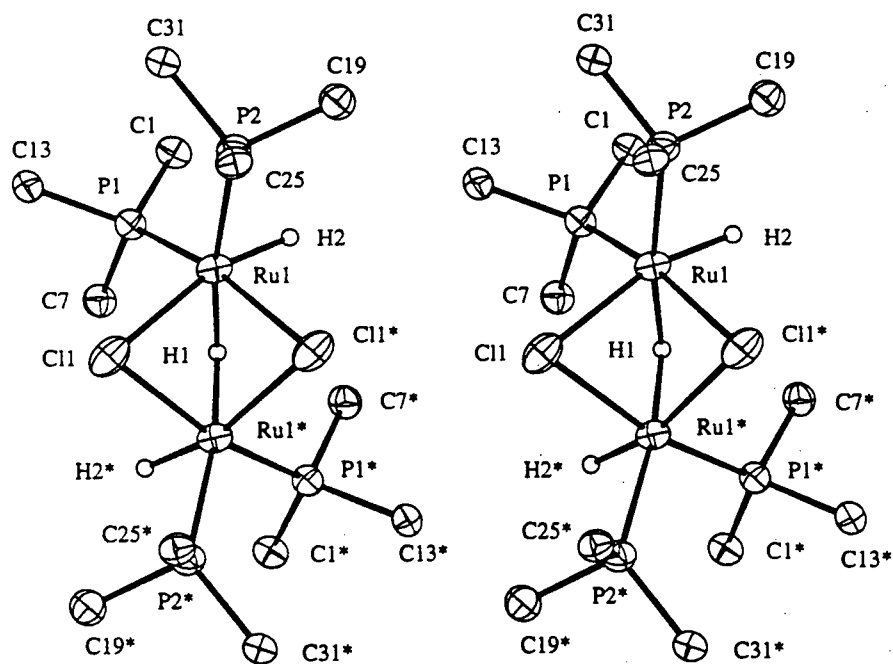
Molecular Structure of [(DMA)$_2$H]$^+$[(PPh$_3$)$_2$(H)Ru(μ-Cl)$_2$(μ-H)Ru(H)(PPh$_3$)$_2$]$^-$, **18**

(Stereoview)

EXPERIMENTAL DETAILS

A. Crystal Data

Empirical Formula	$C_{80}H_{82}Cl_2N_2O_2P_4Ru_2$
Formula Weight	1500.48
Crystal Color, Habit	red, prism
Crystal Dimensions	0.30 X 0.40 X 0.40 mm
Crystal System	monoclinic
Lattice Type	C-centered
No. of Reflections Used for Unit Cell Determination (2θ range)	25 (35.0 - 38.9°)
Omega Scan Peak Width at Half-height	0.36°
Lattice Parameters	$a = 23.762(3)$ Å $b = 13.372(2)$ Å $c = 25.937(3)$ Å $\beta = 119.575(7)°$ $V = 7167(1)$ Å^3
Space Group	C2/c (#15)
Z value	4
D_{calc}	1.390 g/cm^3
F_{000}	3096
$\mu(MoK\alpha)$	6.34 cm^{-1}

B. Intensity Measurements

Diffractometer	Rigaku AFC6S
Radiation	MoKα ($\lambda = 0.71069$ Å) graphite monochromated

Take-off Angle	6.0°
Detector Aperture	6.0 mm horizontal 6.0 mm vertical
Crystal to Detector Distance	285 mm
Temperature	21.0°C
Scan Type	ω
Scan Rate	32.0°/min (in ω) (up to 9 scans)
Scan Width	$(1.13 + 0.35 \tan \theta)°$
$2\theta_{max}$	59.9°
No. of Reflections Measured	Total: 11068 Unique: 10820 (R_{int} = 0.029)
Corrections	Lorentz-polarization Absorption (trans. factors: 0.87 - 1.00) Decay (13.1% decline)

C. Structure Solution and Refinement

Structure Solution	Patterson Methods (DIRDIF92 PATTY)
Refinement	Full-matrix least-squares
Function Minimized	$\Sigma w(|Fo| - |Fc|)^2$
Least Squares Weights	$\frac{1}{\sigma^2(Fo)} = \frac{4Fo^2}{\sigma^2(Fo^2)}$
p-factor	0.000
Anomalous Dispersion	All non-hydrogen atoms
No. Observations (I>3.00σ(I))	5504
No. Variables	421
Reflection/Parameter Ratio	13.07
Residuals: R; Rw	0.036 ; 0.033
Goodness of Fit Indicator	1.88
Max Shift/Error in Final Cycle	0.0006
Maximum peak in Final Diff. Map	0.42 $e^-/Å^3$
Minimum peak in Final Diff. Map	-0.37 $e^-/Å^3$

Table VI.1 Bond Lengths (Å) with estimated standard deviations

atom	atom	distance	atom	atom	distance
Ru(1)	Ru(1)*	2.8251(5)	Ru(1)	Cl(1)	2.510(1)
Ru(1)	Cl(1)*	2.4649(9)	Ru(1)	P(1)	2.2576(9)
Ru(1)	P(2)	2.3483(9)	P(1)	C(1)	1.850(3)
P(1)	C(7)	1.844(3)	P(1)	C(13)	1.839(3)
P(2)	C(19)	1.842(4)	P(2)	C(25)	1.845(3)
P(2)	C(31)	1.842(3)	O(1)	C(37)	1.174(8)
N(1)	C(37)	1.108(10)	N(1)	C(39)	1.370(8)
N(1)	C(40)	1.630(9)	C(1)	C(2)	1.362(4)
C(1)	C(6)	1.361(5)	C(2)	C(3)	1.385(5)
C(3)	C(4)	1.362(6)	C(4)	C(5)	1.333(5)
C(5)	C(6)	1.391(5)	C(7)	C(8)	1.376(5)
C(7)	C(12)	1.379(5)	C(8)	C(9)	1.381(5)
C(9)	C(10)	1.357(6)	C(10)	C(11)	1.357(6)
C(11)	C(12)	1.383(5)	C(13)	C(14)	1.372(4)
C(13)	C(18)	1.392(4)	C(14)	C(15)	1.390(5)
C(15)	C(16)	1.364(6)	C(16)	C(17)	1.362(6)
C(17)	C(18)	1.382(5)	C(19)	C(20)	1.384(5)
C(19)	C(24)	1.368(5)	C(20)	C(21)	1.390(5)
C(21)	C(22)	1.344(6)	C(22)	C(23)	1.376(7)
C(23)	C(24)	1.395(6)	C(25)	C(26)	1.375(4)
C(25)	C(30)	1.382(4)	C(26)	C(27)	1.392(5)
C(27)	C(28)	1.353(5)	C(28)	C(29)	1.363(5)
C(29)	C(30)	1.376(5)	C(31)	C(32)	1.389(4)
C(31)	C(36)	1.379(4)	C(32)	C(33)	1.392(5)
C(33)	C(34)	1.360(6)	C(34)	C(35)	1.362(6)
C(35)	C(36)	1.386(5)	C(37)	C(38)	1.64(1)

* Here and elsewhere refers to symmetry operation: -x, y, 1/2-z.

Table VI.2 Bond Angles (deg) with estimated standard deviations

atom	atom	atom	angle	atom	atom	atom	angle
Ru(1)*	Ru(1)	Cl(1)	54.65(2)	Ru(1)*	Ru(1)	Cl(1)*	56.15(2)
Ru(1)*	Ru(1)	P(1)	109.64(2)	Ru(1)*	Ru(1)	P(2)	145.07(2)
Cl(1)	Ru(1)	Cl(1)*	81.58(4)	Cl(1)	Ru(1)	P(1)	96.74(3)
Cl(1)	Ru(1)	P(2)	107.71(3)	Cl(1)*	Ru(1)	P(1)	163.57(3)
Cl(1)*	Ru(1)	P(2)	94.24(3)	P(1)	Ru(1)	P(2)	101.79(3)
Ru(1)	Cl(1)	Ru(1)*	69.20(3)	Ru(1)	P(1)	C(1)	116.1(1)
Ru(1)	P(1)	C(7)	114.3(1)	Ru(1)	P(1)	C(13)	119.8(1)
C(1)	P(1)	C(7)	100.5(1)	C(1)	P(1)	C(13)	105.2(1)
C(7)	P(1)	C(13)	97.8(1)	Ru(1)	P(2)	C(19)	114.1(1)
Ru(1)	P(2)	C(25)	115.8(1)	Ru(1)	P(2)	C(31)	121.4(1)
C(19)	P(2)	C(25)	100.4(2)	C(19)	P(2)	C(31)	101.5(2)
C(25)	P(2)	C(31)	100.6(2)	C(37)	N(1)	C(39)	145(1)
C(37)	N(1)	C(40)	98.0(9)	C(39)	N(1)	C(40)	116.4(8)
P(1)	C(1)	C(2)	124.5(3)	P(1)	C(1)	C(6)	118.2(3)
C(2)	C(1)	C(6)	117.3(3)	C(1)	C(2)	C(3)	120.6(4)
C(2)	C(3)	C(4)	121.1(4)	C(3)	C(4)	C(5)	118.9(4)
C(4)	C(5)	C(6)	120.1(4)	C(1)	C(6)	C(5)	122.0(4)
P(1)	C(7)	C(8)	119.2(3)	P(1)	C(7)	C(12)	123.3(3)
C(8)	C(7)	C(12)	117.5(3)	C(7)	C(8)	C(9)	121.3(4)
C(8)	C(9)	C(10)	120.1(4)	C(9)	C(10)	C(11)	119.8(4)
C(10)	C(11)	C(12)	120.3(4)	C(7)	C(12)	C(11)	120.9(4)
P(1)	C(13)	C(14)	120.2(3)	P(1)	C(13)	C(18)	122.2(3)
C(14)	C(13)	C(18)	117.5(3)	C(13)	C(14)	C(15)	121.2(3)
C(14)	C(15)	C(16)	120.4(4)	C(15)	C(16)	C(17)	119.4(4)
C(16)	C(17)	C(18)	120.5(4)	C(13)	C(18)	C(17)	120.9(4)
P(2)	C(19)	C(20)	123.2(3)	P(2)	C(19)	C(24)	118.8(3)
C(20)	C(19)	C(24)	117.8(4)	C(19)	C(20)	C(21)	121.5(4)
C(20)	C(21)	C(22)	119.8(4)	C(21)	C(22)	C(23)	120.2(4)
C(22)	C(23)	C(24)	120.0(5)	C(19)	C(24)	C(23)	120.7(5)
P(2)	C(25)	C(26)	119.4(3)	P(2)	C(25)	C(30)	122.8(3)
C(26)	C(25)	C(30)	117.6(3)	C(25)	C(26)	C(27)	121.0(3)
C(26)	C(27)	C(28)	120.3(4)	C(27)	C(28)	C(29)	119.4(4)
C(28)	C(29)	C(30)	120.8(4)	C(25)	C(30)	C(29)	120.8(4)
P(2)	C(31)	C(32)	118.2(3)	P(2)	C(31)	C(36)	123.6(3)
C(32)	C(31)	C(36)	118.1(3)	C(31)	C(32)	C(33)	121.0(4)
C(32)	C(33)	C(34)	119.4(4)	C(33)	C(34)	C(35)	120.6(4)
C(34)	C(35)	C(36)	120.4(4)	C(31)	C(36)	C(35)	120.5(4)
O(1)	C(37)	N(1)	140(1)	O(1)	C(37)	C(38)	118(1)
N(1)	C(37)	C(38)	100.0(8)				

Table VI.3 Final Atomic Coordinates (Fractional) and B(eq)

atom	x	y	z	B_{eq}
Ru(1)	0.01037(1)	0.24396(2)	0.20086(1)	3.184(5)
Cl(1)	0.07741(4)	0.15081(6)	0.29601(4)	4.80(2)
P(1)	0.08551(4)	0.35979(6)	0.21448(4)	3.15(2)
P(2)	0.00666(4)	0.14734(7)	0.12363(4)	3.45(2)
O(1)	0.2995(3)	-0.0050(6)	0.4717(2)	19.9(3)
N(1)	0.2096(3)	-0.0742(5)	0.4093(3)	13.0(2)
C(1)	0.0635(2)	0.4484(2)	0.1526(1)	3.54(8)
C(2)	0.1058(2)	0.4854(3)	0.1363(2)	5.7(1)
C(3)	0.0851(2)	0.5522(4)	0.0896(2)	7.5(1)
C(4)	0.0225(2)	0.5837(3)	0.0595(2)	5.9(1)
C(5)	-0.0194(2)	0.5480(3)	0.0751(2)	6.2(1)
C(6)	0.0012(2)	0.4809(3)	0.1219(2)	5.7(1)
C(7)	0.1048(2)	0.4478(2)	0.2757(1)	3.78(8)
C(8)	0.1397(2)	0.4144(3)	0.3333(2)	5.4(1)
C(9)	0.1563(2)	0.4779(4)	0.3806(2)	7.0(1)
C(10)	0.1387(3)	0.5757(4)	0.3709(2)	7.3(1)
C(11)	0.1024(3)	0.6098(3)	0.3146(2)	7.8(1)
C(12)	0.0856(2)	0.5466(3)	0.2670(2)	5.9(1)
C(13)	0.1689(2)	0.3206(2)	0.2373(1)	3.35(8)
C(14)	0.1832(2)	0.2211(2)	0.2375(2)	4.12(9)
C(15)	0.2460(2)	0.1897(3)	0.2554(2)	5.7(1)
C(16)	0.2948(2)	0.2578(4)	0.2728(2)	6.2(1)
C(17)	0.2820(2)	0.3556(4)	0.2747(2)	5.9(1)
C(18)	0.2200(2)	0.3883(3)	0.2582(2)	4.92(10)
C(19)	-0.0657(2)	0.1690(3)	0.0510(2)	4.33(9)
C(20)	-0.0642(2)	0.1721(3)	-0.0016(2)	4.94(10)
C(21)	-0.1203(2)	0.1842(3)	-0.0559(2)	6.5(1)
C(22)	-0.1778(3)	0.1907(5)	-0.0580(2)	9.2(2)
C(23)	-0.1813(2)	0.1838(6)	-0.0067(3)	12.1(2)
C(24)	-0.1248(2)	0.1748(5)	0.0479(2)	9.2(2)
C(25)	0.0012(2)	0.0109(2)	0.1306(1)	3.50(8)
C(26)	0.0310(2)	-0.0321(3)	0.1860(2)	4.83(10)
C(27)	0.0317(2)	-0.1354(3)	0.1928(2)	5.7(1)
C(28)	0.0029(2)	-0.1956(3)	0.1446(2)	5.6(1)
C(29)	-0.0269(2)	-0.1541(3)	0.0894(2)	6.0(1)
C(30)	-0.0281(2)	-0.0521(3)	0.0821(2)	5.4(1)
C(31)	0.0715(2)	0.1539(3)	0.1044(1)	3.61(8)
C(32)	0.0833(2)	0.2453(3)	0.0851(1)	4.42(8)
C(33)	0.1346(2)	0.2571(3)	0.0750(2)	5.8(1)
C(34)	0.1739(2)	0.1779(4)	0.0826(2)	7.4(2)
C(35)	0.1624(2)	0.0871(4)	0.0993(2)	6.9(1)
C(36)	0.1113(2)	0.0746(3)	0.1102(2)	5.2(1)
C(37)	0.2513(4)	-0.0222(8)	0.4275(4)	13.3(3)
C(38)	0.2383(4)	0.0341(7)	0.3663(4)	16.7(3)
C(39)	0.1550(4)	-0.1054(6)	0.3594(4)	15.2(3)
C(40)	0.2240(6)	-0.1261(7)	0.4715(4)	21.5(5)

$$B_{eq} = \frac{8}{3}\pi^2[U_{11}(aa^*)^2 + U_{22}(bb^*)^2 + U_{33}(cc^*)^2 + 2U_{12}aa^*bb^*\cos\gamma + 2U_{13}aa^*cc^*\cos\beta + 2U_{23}bb^*cc^*\cos\alpha]$$

X-Ray Crystallographic Analysis of

cis-RuCl₂(DPPB)(phen), 45
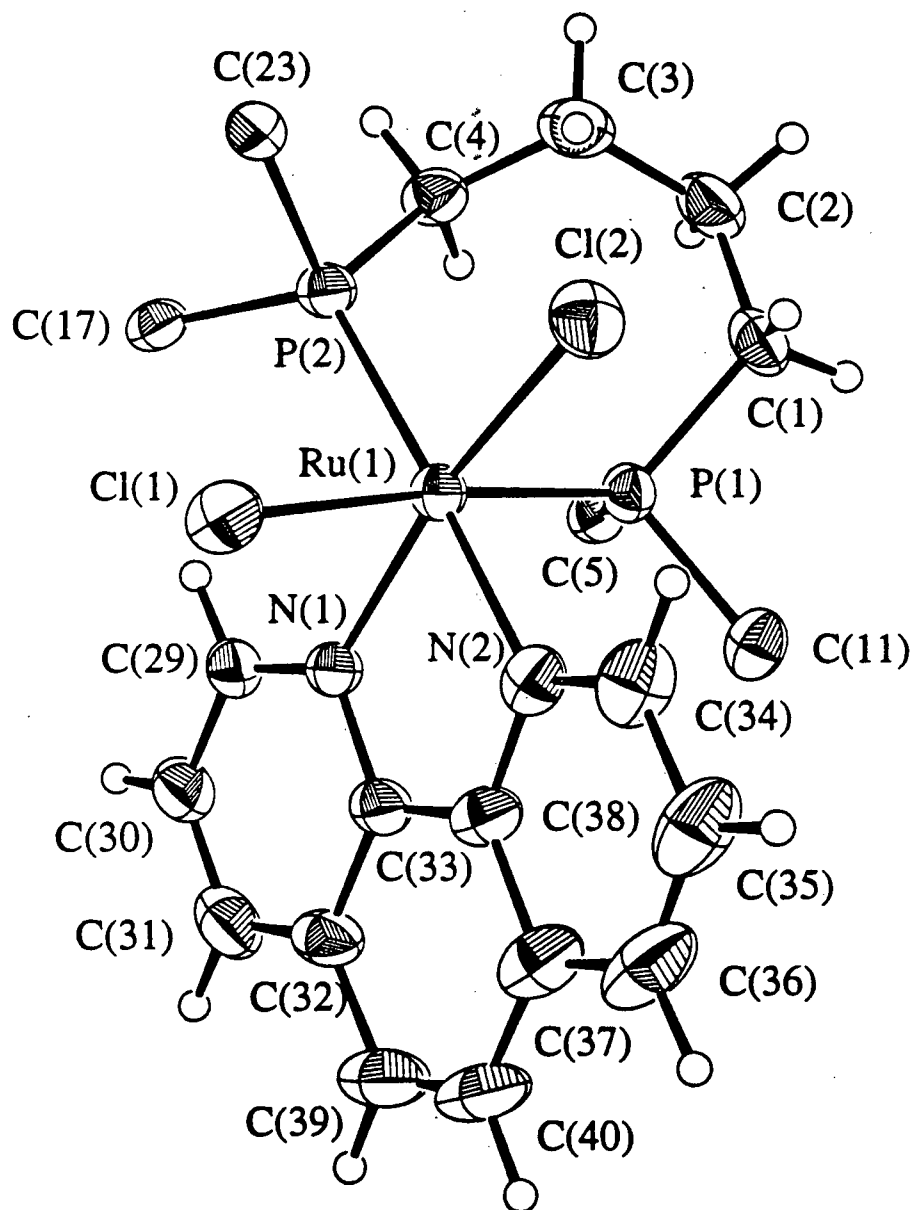
Molecular Structure of *cis*-RuCl₂(DPPB)(phen), **45** (ORTEP Plot)
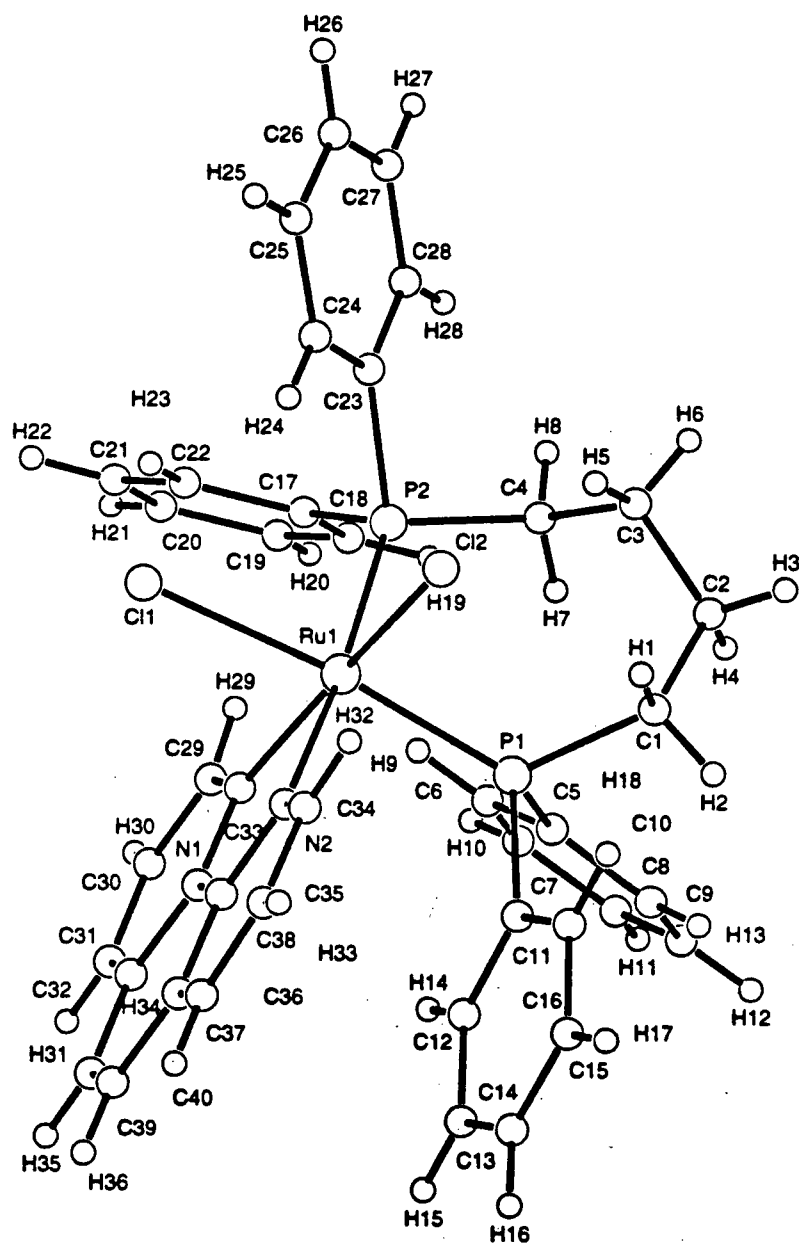
Molecular Structure of *cis*-RuCl$_2$(DPPB)(phen), **45**

(Pluto Plot)
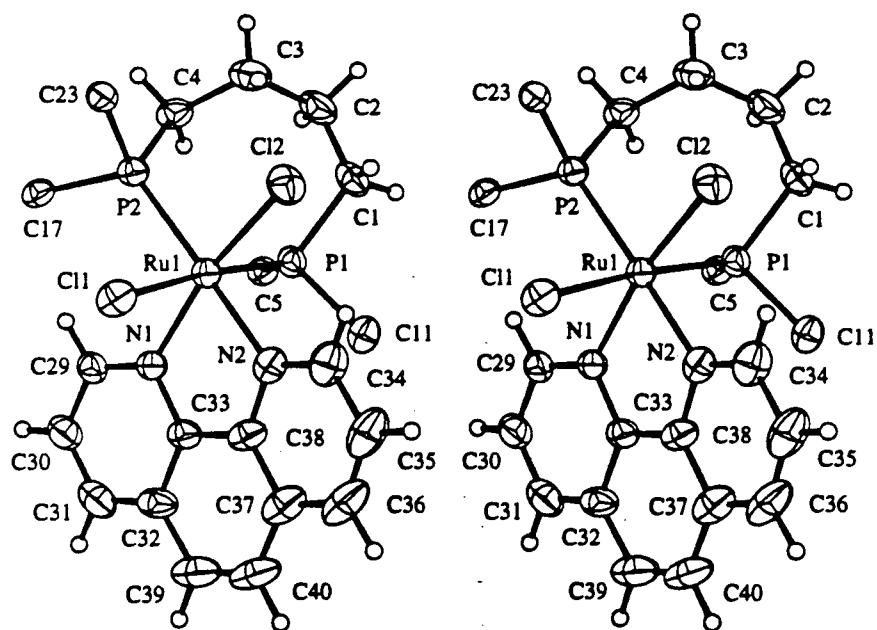
Molecular Structure of *cis*-RuCl$_2$(DPPB)(phen), **45**

(Stereoview)
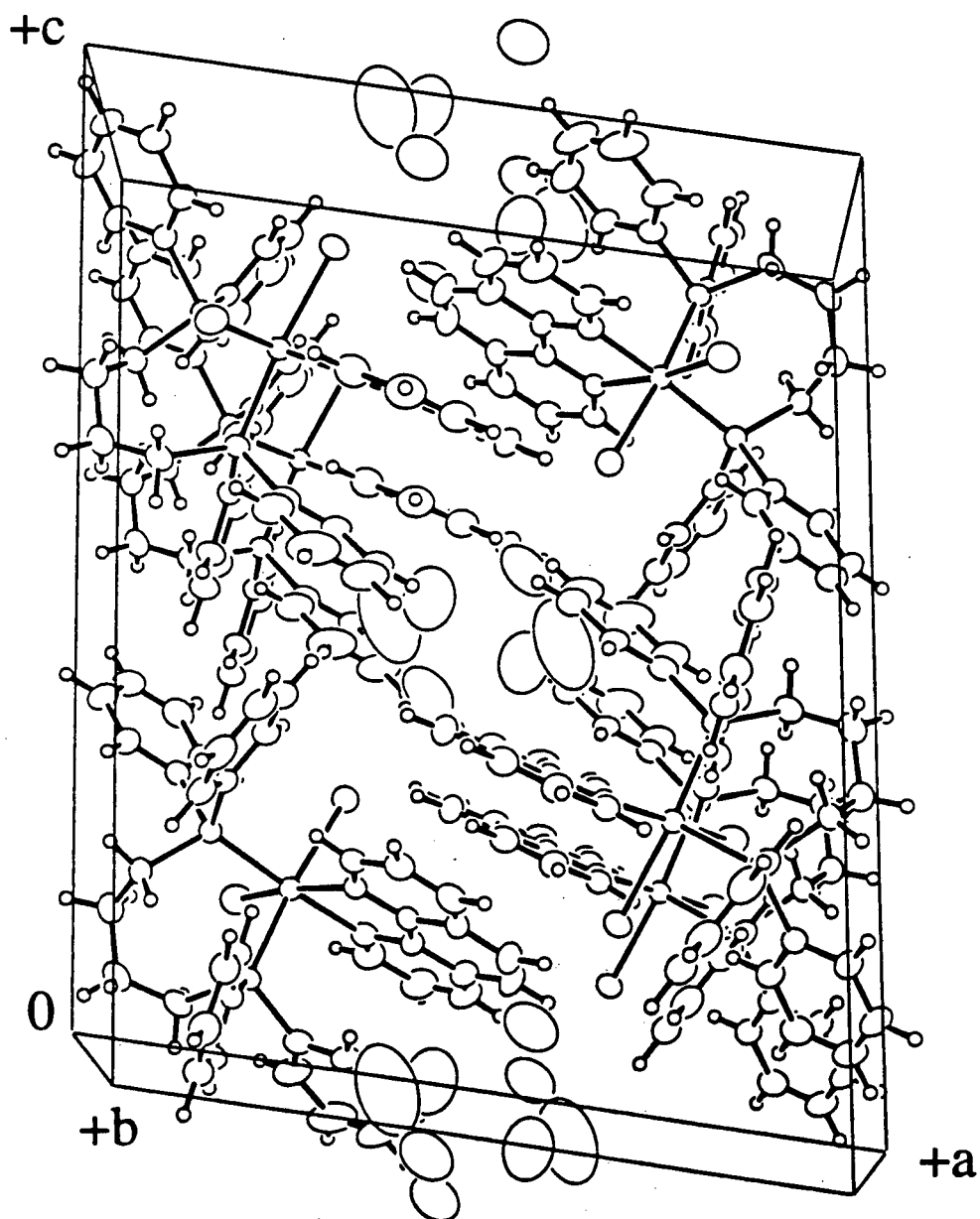
Unit cell of *cis*-RuCl$_2$(DPPB)(phen), **45**

EXPERIMENTAL DETAILS

A. Crystal Data

Empirical Formula	$C_{40.50}H_{40}Cl_2N_2P_2RuO_{1.50}$
Formula Weight	812.70
Crystal Color, Habit	orange, needle
Crystal Dimensions	0.08 X 0.08 X 0.35 mm
Crystal System	monoclinic
Lattice Type	Primitive
No. of Reflections Used for Unit Cell Determination (2θ range)	25 (42.0 - 61.9°)
Omega Scan Peak Width at Half-height	0.38°
Lattice Parameters	$a = 17.094(1)$ Å
	$b = 9.923(2)$ Å
	$c = 21.905(2)$ Å
	$\beta = 98.883(6)°$
	$V = 3670.9(7)$ Å^3
Space Group	$P2_1/c$ (#14)
Z value	4
D_{calc}	1.470 g/cm^3
F_{000}	1668.00
$\mu(CuK\alpha)$	59.12 cm^{-1}

B. Intensity Measurements

Diffractometer	Rigaku AFC6S
Radiation	CuKα ($\lambda = 1.54178$ Å) graphite monochromated

343

Take-off Angle	6.0°
Detector Aperture	6.0 mm horizontal 6.0 mm vertical
Crystal to Detector Distance	285 mm
Temperature	21°C
Scan Type	ω-2θ
Scan Rate	8°/min (in ω) (up to 9 scans)
Scan Width	$(0.84 + 0.20 \tan \theta)°$
$2\theta_{max}$	155°
No. of Reflections Measured	Total: 8766 Unique: 7919 (R_{int} = 0.054)
Corrections	Lorentz-polarization Absorption (trans. factors: 0.889 - 1.000)

C. Structure Solution and Refinement

Structure Solution	Patterson Methods (DIRDIF92 PATTY)
Refinement	Full-matrix least-squares
Function Minimized	$\Sigma w(|Fo| - |Fc|)^2$
Least Squares Weights	$\frac{1}{\sigma^2(Fo)} = \frac{4Fo^2}{\sigma^2(Fo^2)}$
p-factor	0.000
Anomalous Dispersion	All non-hydrogen atoms
No. Observations (I>3σ(I))	4824
No. Variables	453
Reflection/Parameter Ratio	10.65
Residuals: R; Rw	0.036 ; 0.039
Goodness of Fit Indicator	2.23
Max Shift/Error in Final Cycle	0.003
Maximum peak in Final Diff. Map	0.38 $e^-/Å^3$
Minimum peak in Final Diff. Map	-0.58 $e^-/Å^3$

Table VII.1 Bond Lengths (Å) with estimated standard deviations

atom	atom	distance	atom	atom	distance
Ru(1)	Cl(1)	2.491(1)	Ru(1)	Cl(2)	2.417(1)
Ru(1)	P(1)	2.286(1)	Ru(1)	P(2)	2.322(1)
Ru(1)	N(1)	2.092(3)	Ru(1)	N(2)	2.117(4)
P(1)	C(1)	1.837(4)	P(1)	C(5)	1.839(4)
P(1)	C(11)	1.828(5)	P(2)	C(4)	1.831(4)
P(2)	C(17)	1.835(4)	P(2)	C(23)	1.852(4)
N(1)	C(29)	1.326(6)	N(1)	C(33)	1.365(5)
N(2)	C(34)	1.319(6)	N(2)	C(38)	1.357(6)
C(1)	C(2)	1.538(7)	C(2)	C(3)	1.524(7)
C(3)	C(4)	1.547(7)	C(5)	C(6)	1.380(6)
C(5)	C(10)	1.402(5)	C(6)	C(7)	1.370(6)
C(7)	C(8)	1.386(7)	C(8)	C(9)	1.363(7)
C(9)	C(10)	1.381(7)	C(11)	C(12)	1.378(7)
C(11)	C(16)	1.386(7)	C(12)	C(13)	1.391(7)
C(13)	C(14)	1.36(1)	C(14)	C(15)	1.37(1)
C(15)	C(16)	1.399(8)	C(17)	C(18)	1.391(6)
C(17)	C(22)	1.398(6)	C(18)	C(19)	1.381(7)
C(19)	C(20)	1.377(8)	C(20)	C(21)	1.376(8)
C(21)	C(22)	1.373(7)	C(23)	C(24)	1.370(6)
C(23)	C(28)	1.395(6)	C(24)	C(25)	1.390(6)
C(25)	C(26)	1.374(7)	C(26)	C(27)	1.366(8)
C(27)	C(28)	1.383(6)	C(29)	C(30)	1.392(6)
C(30)	C(31)	1.349(7)	C(31)	C(32)	1.392(8)
C(32)	C(33)	1.426(6)	C(32)	C(39)	1.430(7)
C(33)	C(38)	1.410(7)	C(34)	C(35)	1.399(7)
C(35)	C(36)	1.355(9)	C(36)	C(37)	1.378(9)
C(37)	C(38)	1.412(6)	C(37)	C(40)	1.428(9)
C(39)	C(40)	1.321(9)			

Table VII.2 Bond Angles (deg) with estimated standard deviations

atom	atom	atom	angle		atom	atom	atom	angle
C(1)	Ru(1)	Cl(2)	92.46(4)		C(1)	Ru(1)	P(1)	174.20(4)
Cl(1)	Ru(1)	P(2)	91.86(4)		Cl(1)	Ru(1)	N(1)	84.57(9)
Cl(1)	Ru(1)	N(2)	83.16(10)		Cl(1)	Ru(1)	P(1)	88.42(4)
Cl(2)	Ru(1)	P(2)	88.60(4)		Cl(2)	Ru(1)	N(1)	167.4(1)
Cl(2)	Ru(1)	N(2)	89.3(1)		Cl(2)	Ru(1)	P(2)	93.89(4)
P(1)	Ru(1)	N(1)	93.34(9)		P(1)	Ru(1)	N(2)	91.12(10)
P(2)	Ru(1)	N(1)	103.7(1)		P(2)	Ru(1)	N(2)	174.5(1)
N(1)	Ru(1)	N(2)	78.2(1)		N(1)	Ru(1)	C(1)	118.6(2)
Ru(1)	P(1)	C(5)	122.4(1)		Ru(1)	P(1)	C(11)	111.4(1)
C(1)	P(1)	C(5)	101.5(2)		C(1)	P(1)	C(11)	100.1(2)
C(5)	P(1)	C(11)	99.1(2)		C(1)	P(1)	C(11)	117.0(1)
Ru(1)	P(2)	C(17)	117.0(1)		Ru(1)	P(2)	C(4)	119.3(2)
C(4)	P(2)	C(17)	102.0(2)		C(4)	P(2)	C(23)	100.7(2)
C(17)	P(2)	C(23)	97.3(2)		Ru(1)	P(2)	C(29)	130.2(3)
Ru(1)	N(1)	C(33)	113.8(3)		Ru(1)	N(1)	C(33)	116.0(4)
Ru(1)	N(2)	C(34)	128.3(4)		C(29)	N(1)	C(38)	113.6(3)
C(34)	N(2)	C(38)	118.1(4)		Ru(1)	N(2)	C(2)	118.0(3)
C(1)	C(2)	C(3)	116.6(4)		C(1)	C(1)	C(4)	113.6(4)
C(2)	C(3)	C(3)	113.9(4)		C(2)	C(3)	C(6)	122.5(3)
P(2)	C(3)	C(10)	119.5(3)		C(1)	C(5)	C(6)	118.1(4)
P(1)	C(5)	C(7)	121.6(4)		C(6)	C(5)	C(10)	120.0(5)
C(5)	C(6)	C(9)	119.2(5)		C(6)	C(7)	C(8)	121.3(4)
C(7)	C(8)	C(9)	119.8(5)		C(8)	C(9)	C(10)	119.2(5)
C(5)	C(10)	C(16)	121.2(4)		C(10)	C(11)	C(12)	119.5(4)
P(1)	C(11)				C(12)	C(11)	C(16)	119.2(5)

atom	atom	atom	angle		atom	atom	atom	angle
C(11)	C(12)	C(13)	120.4(6)		C(12)	C(13)	C(14)	119.8(7)
C(13)	C(14)	C(15)	120.9(7)		C(14)	C(15)	C(16)	119.6(7)
C(11)	C(16)	C(15)	120.0(6)		P(2)	C(17)	C(18)	124.4(4)
P(2)	C(17)	C(22)	117.6(3)		C(18)	C(17)	C(22)	118.0(4)
C(17)	C(18)	C(19)	120.7(5)		C(18)	C(19)	C(20)	120.5(5)
C(19)	C(20)	C(21)	119.5(5)		C(20)	C(21)	C(22)	120.5(5)
C(17)	C(22)	C(21)	120.8(5)		P(2)	C(23)	C(24)	124.1(4)
P(2)	C(23)	C(28)	117.9(4)		C(24)	C(23)	C(28)	118.0(4)
C(23)	C(24)	C(25)	121.8(5)		C(24)	C(25)	C(26)	119.2(5)
C(25)	C(26)	C(27)	120.1(5)		C(26)	C(27)	C(28)	120.6(5)
C(23)	C(28)	C(27)	120.4(5)		N(1)	C(29)	C(30)	124.7(4)
C(29)	C(30)	C(31)	119.8(5)		C(30)	C(31)	C(32)	118.7(5)
C(31)	C(32)	C(33)	118.4(5)		C(31)	C(32)	C(39)	124.3(5)
N(1)	C(33)	C(32)	117.3(6)		N(1)	C(33)	C(32)	122.3(5)
N(1)	C(33)	C(38)	117.5(4)		C(32)	C(33)	C(38)	120.3(4)
N(2)	C(34)	C(35)	121.8(6)		C(34)	C(35)	C(36)	120.2(6)
C(35)	C(36)	C(37)	119.9(6)		C(36)	C(37)	C(38)	117.0(6)
C(36)	C(37)	C(40)	125.0(6)		C(38)	C(37)	C(40)	118.0(6)
N(2)	C(38)	C(33)	116.9(4)		N(2)	C(33)	C(37)	122.9(5)
C(33)	C(38)	C(37)	120.2(5)		C(32)	C(39)	C(40)	122.2(6)
C(37)	C(39)	C(40)	122.0(6)					

Table VII.3 Final Atomic Coordinates (Fractional) and B(eq)

atom	x	y	z	B_{eq}
C(15)	0.3021(6)	0.7448(8)	-0.0121(3)	9.5(3)
C(16)	0.2510(4)	0.6953(6)	0.0267(3)	6.7(2)
C(17)	0.1771(2)	0.2761(5)	0.2856(2)	3.86(10)
C(18)	0.1516(3)	0.1600(5)	0.2640(2)	4.8(1)
C(19)	0.1775(3)	0.0342(5)	0.2958(3)	6.0(2)
C(20)	0.2286(3)	0.0418(6)	0.3508(3)	6.0(2)
C(21)	0.2535(3)	0.1659(6)	0.3741(2)	5.3(1)
C(22)	0.2287(3)	0.2816(5)	0.3427(2)	4.1(1)
C(23)	0.1058(2)	0.5192(5)	0.3069(2)	3.9(1)
C(24)	0.1329(3)	0.6366(5)	0.3356(2)	4.8(1)
C(25)	0.0990(3)	0.6910(6)	0.3838(2)	5.7(1)
C(26)	0.0358(3)	0.6265(6)	0.4028(2)	5.8(2)
C(27)	0.0079(3)	0.5090(6)	0.3751(2)	5.6(1)
C(28)	0.0421(3)	0.4547(5)	0.3273(2)	4.7(1)
C(29)	0.3399(3)	0.2679(5)	0.2241(2)	4.0(1)
C(30)	0.4003(3)	0.1764(6)	0.2192(2)	5.2(1)
C(31)	0.4661(3)	0.2178(6)	0.1976(2)	5.9(1)
C(32)	0.4720(3)	0.3525(6)	0.1812(2)	5.1(1)
C(33)	0.4070(2)	0.4399(5)	0.1851(2)	4.0(1)
C(34)	0.3503(3)	0.7845(5)	0.1651(2)	5.6(1)
C(35)	0.4166(4)	0.8428(6)	0.1453(3)	7.0(2)
C(36)	0.4794(4)	0.7654(8)	0.1371(3)	7.4(2)
C(37)	0.4790(3)	0.6295(7)	0.1498(2)	5.8(1)
C(38)	0.4108(3)	0.5773(5)	0.1705(2)	4.3(1)
C(39)	0.5393(3)	0.4100(8)	0.1594(3)	6.8(2)
C(40)	0.5425(3)	0.5388(9)	0.1447(3)	6.9(2)

atom	x	y	z	B_{eq}	occ.
Ru(1)	0.25295(2)	0.54449(4)	0.20552(1)	3.219(6)	
Cl(1)	0.32326(7)	0.5998(1)	0.31087(5)	4.97(3)	
Cl(2)	0.17544(8)	0.7491(1)	0.20020(8)	5.28(3)	
P(1)	0.19941(7)	0.5020(1)	0.10527(5)	3.51(2)	
P(2)	0.15194(6)	0.4355(1)	0.24581(5)	3.46(2)	
O(1)	0.4342(10)	0.515(2)	0.4295(6)	15.3(5)	0.62(1)
O(2)	0.3848(9)	0.411(3)	0.493(12)	31.7(10)	
O(3)	0.438(1)	0.332(2)	0.5108(8)	19.7(7)	0.67(1)
N(1)	0.3399(2)	0.3959(4)	0.2066(1)	3.49(8)	
N(2)	0.3470(2)	0.6544(4)	0.1770(2)	4.21(9)	
C(1)	0.1049(3)	0.5825(5)	0.0739(2)	4.8(1)	
C(2)	0.0283(3)	0.5188(6)	0.0892(2)	5.7(1)	
C(3)	0.0200(3)	0.5105(6)	0.1574(2)	5.8(1)	
C(4)	0.0638(2)	0.3890(5)	0.1913(2)	4.4(1)	
C(5)	0.1841(2)	0.3299(5)	0.0746(2)	3.56(9)	
C(6)	0.1955(3)	0.2173(5)	0.1119(2)	4.0(1)	
C(7)	0.1837(3)	0.0898(5)	0.0882(2)	5.0(1)	
C(8)	0.1591(3)	0.0717(5)	0.0254(3)	5.5(1)	
C(9)	0.1476(3)	0.1817(6)	-0.0122(2)	5.3(1)	
C(10)	0.1603(3)	0.3106(5)	0.0110(2)	4.5(1)	
C(11)	0.2622(3)	0.5671(5)	0.0516(2)	4.4(1)	
C(12)	0.3244(3)	0.4903(6)	0.0380(2)	5.2(1)	
C(13)	0.3755(4)	0.5406(8)	0.0000(3)	7.8(2)	
C(14)	0.3639(5)	0.667(1)	-0.0242(3)	9.5(3)	

$$B_{eq} = \frac{8}{3}\pi^2(U_{11}(aa^*)^2 + U_{22}(bb^*)^2 + U_{33}(cc^*)^2 + 2U_{12}aa^*bb^*\cos\gamma + 2U_{13}aa^*cc^*\cos\beta + 2U_{23}bb^*cc^*\cos\alpha)$$